Does SIRT1 or cytostasis underlie the anti-ageing activity of *trans*-stilbenes?

Vishal Chandrakumar Birar

A thesis submitted in partial fulfilment of the requirements of the University of Brighton and for the degree of Doctor of Philosophy

March 2016

Table of contents

GLOSSARY OF ABBREVIATIONS **7**

GLOSSARY OF TABLES **9**

GLOSSARY OF FIGURES **11**

DECLARATION **17**

ACKNOWLEDGEMENTS **19**

DEDICATION **21**

ABSTRACT **23**

CHAPTER 1. INTRODUCTION **25**

1.1. WHAT IS AGEING? 25
1.2. WHY DOES AGEING EXIST? 25
1.3. HEALTH SPANS MAINTENANCE MECHANISMS: AGEING MECHANISMS 26
1.3.1. Cell Senescence: 28
1.3.2. Nutrient sensing pathways: 32
1.4. RELATIONSHIP BETWEEN AGEING AND AGE-RELATED DISEASES: 35
1.5. POTENTIAL INTERVENTION TARGETING AGEING MECHANISMS: 36
1.5.1. SIRT1 activation: 38
1.5.1.1. SIRT1 activating compounds: 40
1.5.1.2. Mechanism of SIRT1 activating compounds 42
1.5.1.3. Beneficial effects of SIRT1 activation: 43
1.5.1.4. SIRT1 and lifespan increase: 43
1.5.1.5. Anti-diabetic effect: 45
1.5.1.6. SIRT1 and cardiovascular effects: 46
1.5.1.7. SIRT1 and neuroprotective effects: 46
1.5.1.8. Importance of SIRT1 activation to existing potential anti-ageing molecules: 46
1.5.2. Current potential anti-ageing compunds 48
1.5.2.1. Rapamycin: 48
1.5.2.1. Resveratrol: 48
1.6. BIOLOGICAL ACTIVITIES OF RESVERATROL DERIVATIVES: 50
1.7. SYNTHESIS OF RESVERATROL DERIVATIVES: 54
1.8. DETRIMENTAL ACTIVITY OF RESVERATROL AND TRANS-STILBENES: 59
1.9. DESIGN STRATEGIES FOR NOVEL RESVERALOGUES: 60
1.9.1. 4'-hydroxy substituted analogues of resveratrol: 60
1.9.2. Design of amino derivatives based on resveratrol: 62
1.9.3. Design of heterocyclic substituted analogues of resveratrol: 63
1.9.4. 4'-substituted benzimidazole analogues of resveratrol: 66
1.10. PROJECT AIMS: 68

CHAPTER 2. CHEMISTRY METHODS **69**

2.1. MATERIALS: 69
2.2. SYNTHESIS OF 'RESVERALOGUES': 71
2.2.1. Attempted synthesis using organozinc reagent methods: 71
2.3. METHOD DEVELOPMENT FOR ONE-POT SYNTHESIS: 71
2.3.1. Stoichiometric use of $P(OEt)_3$: 71
2.3.2. Effect of Base: 75
2.4. SYNTHESIS OF RESVERALOGUES USING ONE-POT SYNTHESIS: 76
2.4.1. Synthesis of (*E*)-1,3-dimethoxy-5-(4-nitrostyryl)benzene (V1) 76

2.4.2. Synthesis of (*E*)-1-(2-fluorostyryl)-3,5-dimethoxybenzene (V2) 77
2.4.3. Synthesis of Synthesis of (*E*)-1,3-dimethoxy-5-(4 methoxystyryl)benzene (V3) 78
2.4.4. Synthesis of (*E*)-1-(3,5-dimethoxystyryl)-3,5-dimethylbenzene (V4) 79
2.4.5. Synthesis of (*E)*-2-(3,5-dimethoxystyryl)-1,3-difluorobenzene (V5) 80
2.4.6. Synthesis of (*E*)-1-(3,5-dimethoxystyryl)-2,4-difluorobenzene (V6) 81
2.4.7. Synthesis of (*E*)-1-chloro-3-(4-methoxystyryl)benzene (V7) 82
2.4.8. Synthesis of (*E*)-N,N-dimethyl-4-(3-(trifluoromethyl)styryl)aniline (V8) 83
2.4.9. Synthesis of methyl (*E*)-4-(3,5-dimethoxystyryl)benzoate (V9) 84
2.4.10. Synthesis of (*E*)-2-(3,5-dimethoxystyryl)benzonitrile (V10) 85
2.4.11. Synthesis of (*E*)-1,3-dimethoxy-5-(4-methylstyryl)benzene (V14) 86
2.4.12. Synthesis of (*E*)-2,2'-(ethene-1,2-diyl)dibenzonitrile (V16) 87
2.4.13. Synthesis of (*E*)-4-(3-chlorostyryl)-N,N-dimethylaniline (V17) 87
2.4.14. Synthesis of (*E*)-1-(4-methoxystyryl)-2-nitrobenzene (V18) 88
2.4.15. Synthesis of (*E*)-2-(4-methoxystyryl)benzonitrile (V19) 89
2.4.16. Synthesis of (*E*)-1-(4-methoxystyryl)-3-nitrobenzene (V20) 90
2.4.17. Synthesis of (*E*)-1,3-dichloro-2-(3,5-dimethoxystyryl)benzene (V21) 91
2.4.18. Synthesis of (*E*)-1,3-dimethoxy-5-(2-nitrostyryl)benzene (V22) 92
2.4.19. Synthesis of (*E*)-2-(2-nitrostyryl)benzonitrile (V25) 93
2.4.20. Synthesis of (*E*)-1,3-dimethoxy-5-(3-nitrostyryl)benzene (V27) 94
2.4.21. Synthesis of (*E*)-2,4-dimethoxy-1-(4-nitrostyryl)benzene (V28) 95
2.4.22. Synthesis of (*E*)-1,2-diphenylethene (V29) 95
2.4.23. Synthesis of (*E*)-4-(3,5-dimethoxystyryl)benzonitrile (V33) 96
2.4.24. Synthesis of (*E*)-1,3-dimethoxy-5-styrylbenzene (V42) 97
2.4.25. Synthesis of (*E*)-1-(3-chlorostyryl)-3,5-dimethoxybenzene (V43) 98
2.5. DEMETHYLATION: SYNTHESIS OF DIHYDROXY DERIVATIVES OF RESVERALOGUES: 99
2.5.1. Attempted demethylation using pyridine hydrochloride: 99
2.5.2. Demethylation using BBr_3 in dichloromethane: 99
2.5.3. Synthesis of (*E*)-5-(4-methylstyryl)benzene-1,3-diol (V13) 101
2.5.4. Synthesis of (*E*)-2-(3,5-dihydroxystyryl)benzonitrile (V23) 101
2.5.5. Synthesis of (*E*)-5-(3,5-dimethylstyryl)benzene-1,3-diol (V26) 102
2.5.6. Synthesis of (*E*)-N-(4-(3,5-dihydroxystyryl)phenyl)acetamide (V31) 103
2.5.7. Synthesis of (*E*)-N-(4-(3,5-dihydroxystyryl)phenyl)benzamide (V37) 104
2.5.8. Synthesis of (*E*)-5-(2,4-difluorostyryl)benzene-1,3-diol (V40) 104
2.5.9. Synthesis of (*E*)-N-(2-(3,5-dihydroxystyryl)phenyl)benzamide (V41) 105
2.6. SYNTHESES OF 4'-AMINO SUBSTITUTED RESVERATROL DERIVATIVES: 107
2.6.1. Attempted reduction reaction using $SnCl_2$/MeOH: 108
2.6.2. Change of solvent for reduction reaction: 108
2.6.3. Reduction reaction using zinc metal: 108
2.6.4. Synthesis of (*E*)-4-(3,5-dimethoxystyryl)aniline (V12): 109
2.6.5. Synthesis of (*E*)-N-(4-(3,5-dimethoxystyryl)phenyl)acetamide (V11): 110
2.6.6. Synthesis of (*E*)-N-(4-(3,5-dimethoxystyryl)phenyl)methanesulfonamide (V30) 111
2.6.7. Synthesis of (*E*)-N-(4-(3,5-dimethoxystyryl)phenyl)isobutyramide (V32) 111
2.6.8. Synthesis of (*E*)-N-(4-(3,5-dimethoxystyryl)phenyl)benzamide (V36): 112
2.7. SYNTHESES OF 2-AMINO SUBSTITUTED RESVERATROL DERIVATIVES: 113
2.7.1. Synthesis of (*E*)-2-(3,5-dimethoxystyryl)aniline (V39) 114
2.7.2. Synthesis of (*E*)-N-(2-(3,5-dimethoxystyryl)phenyl)benzamide (V39): 115
2.8. SYNTHESIS OF HETEROCYCLIC BASED RESVERALOGUES: 115
2.8.1. Attempted synthesis of target molecule TM4: 116
2.8.2. Synthesis of Intermediate IN11: 116

2.8.3. Synthesis of intermediate IN10 using oxalyl chloride: 117
2.8.4. Synthesis of intermediate IN10 using thionyl chloride: 117
2.9. ATTEMPTED SYNTHESIS OF 2-SUBSTITUTED BENZIMIDAZOLE (TM2) DERIVATIVE OF RESVERATROL: 118
2.9.1. Attempted synthesis of intermediate IN13 using lithium hydroxide: 118
2.9.2. Attempted intermediate IN13 using sodium hydroxide: 118
2.10. MODIFIED MOLECULES: SYNTHESIS OF TETRAZOLE BASED RESVERATROL MOLECULES: 118
2.10.1. Synthesis of (*E*)-5-(4-(3,5-dimethoxystyryl)phenyl)-2H-tetrazole (V24): 119
2.10.2. Synthesis of Synthesis of (E)-5-(4-(3,5-dimethoxystyryl)phenyl)-2H-tetrazole (V34): 120
2.11. SYNTHESIS OF DIHYDRORESVERATROL DERIVATIVES: 120
2.11.1. Synthesis of 1,3-dimethoxy-5-(4-methylphenethyl)benzene (V15): 121

CHAPTER 3. BIOLOGICAL MATERIAL AND METHODS: 123

3.1. MATERIALS, CHEMICALS AND GLASSWARE: 124
3.2. INSTRUMENTS: 124
3.3. PREPARATION OF STANDARD BUFFERS AND ASSAY KITS: 124
3.4. CELL STRAIN AND STANDARD MAINTENANCE: 126
3.4.1. Cell passage: 126
3.4.2. Cryopreservation: 126
3.5. CYTOTOXICITY ASSAY: 126
3.5.1. MTT: 127
3.5.1.1. Introduction: 127
3.5.1.2. Protocol: 127
3.5.2. LDH: 128
3.5.2.1. Introduction: 128
3.5.2.2. Protocol: 128
3.5.3. Neutral red: 129
3.5.3.1. Introduction: 129
3.5.3.2. Protocol: 129
3.6. CELL CYTOSTASIS STUDY: 129
3.6.1. Ki-67 immunofluorescence assay: 129
3.6.1.1. Introduction: 129
3.6.1.2. Protocol: 130
3.6.2. Senescence associated-β-galactosidase assay (SA-β-gal assay): 130
3.6.2.1. Introduction: 130
3.6.2.2. Protocol: 130
3.7. SIRT1 ASSAY: 131
3.7.1. Introduction: 131
3.7.2. Protocol and optimisation of assay kits: 131
3.8. EFFECT ON SENESCENCE-ASSOCIATED SECRETORY PHENOTYPE (SASP): 133
3.8.1. Introduction: 133
3.8.2. IL-6 assay protocol: 133
3.9. DATA AND STATISTICAL ANALYSIS: 133

CHAPTER 4. BIOLOGICAL RESULTS: 135

4.1. EFFECT OF DMSO ON CELLS VIABILITY: 135
4.2. MORPHOLOGICAL CHANGES IN MRC5 CELLS: 136
4.3. CYTOTOXICITY OF RESVERALOGUES: 148
4.3.1. MTT assay and Neutral red assay: 148
4.3.2. LDH assay: 150
4.4. EFFECT OF RESVERALOGUES ON CELLS CYTOSTASIS: 152
4.4.1. Effects on proliferation marker ki-67: 152

4.4.2. Effect on SA-β-gal activity:....156
4.5. SIRT1 activity of resveralogues:....161
4.6. Effect on Senescence associated secretory phenotype (SASP):....165

CHAPTER 5. CHEMISTRY DISCUSSION....167

5.1. One-pot synthesis of resveralogues:....167
5.2. Proto-demethylation of resveralogues:....170
5.3. Synthesis of bioisostere amino-resveralogues of resveratrol:....171
5.4. Heterocyclic based resveralogues:....173
5.5. Alternative heterocyclic substitution:....176
5.6. Spectroscopic details of resveralogues:....177

CHAPTER 6. BIOACTIVITY DISCUSSION:....179

6.1. Cytotoxicity of resveralogues:....179
6.2. Cytotoxicity and lipophilicity:....181
6.3. Resveralogues effect on cytostasis:....182
6.4. Structural requirement of resveralogues for cell cytostasis activity....183
6.5. SIRT1 activation:....185
6.6. Relationship between SIRT1 activation, cytotoxicity (using LDH assay) and proliferation:....186
6.7. SIRT1 activation and IL-6 relation:....188
6.8. Lead compound:....189

CHAPTER 7. CONCLUSION:....191

CHAPTER 8. FUTURE WORK:....195

8.1. Application of One-pot Synthesis of Resveratrol metabolites:....195
8.2. Development of new Senolytes:....195

PUBLICATION AND PATENT:....197

CHAPTER 9. REFERENCES:....199

APPENDIX-A....213

APPENDIX B....225

APPENDIX C....353

Glossary of Abbreviations

AAK-1 adaptor-associated protein kinase 1

AAK-2 adaptor-associated protein kinase 2

AD alzheimer's disease

ADP/ATP adenosine diphosphate/ Adenosine triphosphate

AMPK adenosine monophosphate-activated protein kinase

AP20187 a synthetic, cell-permeable ligand used for homodimerization of fusion proteins.

ApoA-1 apolipoprotein A1

ATP adenosine triphosphate

BRASTO brain-specific Sirt1-overexpressing transgenic mice

CDK proteins cyclin-dependent kinase

COX cyclooxygenase enzyme

COX1 cyclooxygenase enzyme 1

COX2 cyclooxygenase enzyme 2

CR Calorie restriction

DHRSV dihydroresveratrol

FOXO Forkhead box proteins

HDL high-density lipoprotein

IC50 half maximal inhibitory concentration

IGF insulin-like growth factors

IGF1 Insulin-like growth factor 1

IL-6 Interleukin 6

LXR liver X receptor

MRC5 human primary lung fibroblast cells

mTOR mammalian target of rapamycin

mTOR1 mammalian target of rapamycin complex 1

mTOR2 mammalian target of rapamycin complex 2

NFκB nuclear factor kappa-light-chain-enhancer of activated B cells

PGC-1-α peroxisome proliferator-activated receptor gamma coactivator 1-alpha

rDNA ribosomal DNA

ROS reactive oxygen species

RSV resveratrol

S6 ribosomal protein

SASP- senescence-associated secretory phenotype

SH-SY5Y human neuroblastoma cell line

Sir2 silent information regulator gene found in budding yeast

SIRT1 mammal homolog of Sir2

SRT1460 synthetic drug activator of SIRT1

SRT1760 synthetic drug activator of SIRT1

SRT2183 synthetic drug activator of SIRT1

STAC sirtuin-activating compounds

TNF-α tumor necrosis factor

TOR target of rapamycin

UV ultraviolet

Glossary of Tables

Chapter 01

Table 1-1 Comparison of existing therapies for anti-ageing strategies and their side effects compared with SIRT1 activators. 47

Chapter 02

Table 2-1 Effect of varying equivalents on triethyl phosphite on reaction time. 73

Table 2-2 Effect of base in one pot synthesis 75

Chapter 05

Table 5-1 Resveralogues synthesis using one-pot synthesis..... 169

Table 5-2 Synthesis of dihydroxy resveralogues using BBr_3 in dichloromethane. 171

Table 5-3 4-substituted and 2-substituted amino resveralogues: 172

Table 5-4 Attempted hydrolysis of V10 and conditions used..... 174

Chapter 06

Table 6-1 Role of 4-substitution on resveratrol on cell cytostasis. 185

Glossary of Figures

Chapter 01

Figure 1-1 Health span maintanance mechanisms (ageing mechanisms)..... 27

Figure 1-2 Schematic representation of triggers of cell senescence, biological consequences..... 29

Figure 1-3 Clearance of senescent cells delays the age-related dysfunctions in transgenic mice INK-ATTAC upon drug treatment AP20187 31

Figure 1-4 Nutrient sensing pathways and their role in longevity. 33

Figure 1-5 Concept of biogerontology and anti-ageing strategies. 37

Figure 1-6 Overall reaction of SIRT1 deacetylation..... 39

Figure 1-7 Existing SIRT1 activators, including resveratrol and other structurally different potent, selective SIRT1 activators..... 41

Figure 1-8 Reported increase in lifespan of various organisms through SIRT1 activation. 44

Figure 1-9 Potential antiageing molecules and resveratrol related discovery. 49

Figure 1-10 Reported beneficial biological activities of *trans*-stilbenes such as anti-cancer through inhibition of COX-II, aromatase reductase and anti-diabetes through AMPK activation. 51

Figure 1-11 Neuroprotective and cardioprotective effects of resveratrol derivatives and their structures. 54

Figure 1-12 Important synthetic routes for synthesis of *trans*-stilbene derivatives..... 56

Figure 1-13 Exsisting one-pot synthesis of *trans*-stilbenes and their limitations. 58

Figure 1-14 Effect of structural changes such as fluorinated, methoxy derivatives of resveratrol on anti-cancer activity. 61

Figure 1-15 Retrosynthetic analysis for 4′-substituted resveratrol derivatives. 62

Figure 1-16 Retrosynthetic analysis of substituted amino resveratrol derivatives. 63

Figure 1-17 Design strategies for development of novel resveratrol based potential SIRT1 activators. 64

Figure 1-18 Design strategies behind novel resveratrol based molecules. 65

Figure 1-19 Retrosynthetic analysis of 4′-substituted benzimidazole resveratrol derivatives. 66

Figure 1-20 Retrosynthetic analysis of 2′-substituted heterocyclic resveratrol derivatives. 67

Chapter 03

Figure 3-1 Overall summery of biological screening study for resveralogues. 123

Figure 3-2 Formation of formazan reaction. 127

Figure 3-3 LDH assay principle modified from Pierce LDH assay protocol. 128

Figure 3-4 Enzymatic SIRT1 Fluorescent activation assay. 131

Chapter 04

Figure 4-1 Effect of DMSO on MRC5 cells viability after 48 hours incubation time. 135

Figure 4-2 Morphological changes that were observed when cells were treated with resveralogues, V1 and V2 on primary human lung fibroblasts (MRC-5) at CPD 36-40.. 137

Figure 4-3 Morphological changes that were observed when cells were treated with resveralogues V3, V4, V5 and V6 on primary human lung fibroblasts (MRC-5) at CPD 36-40. 138

Figure 4-4 Morphological changes that were observed when cells were treated with resveralogues V7, V8, V9 and V10 on primary human lung fibroblasts (MRC-5) at CPD 36-40. 139

Figure 4-5 Morphological changes that were observed when cells were treated with resveralogues V11, V12, V13 and V14 on primary human lung fibroblasts (MRC-5) at CPD 36-40. 140

Figure 4-6 Morphological changes that were observed when cells treated with resveralogues V15, V16, V17 and V18 on primary human lung fibroblasts (MRC-5) at CPD 36-40. 141

Figure 4-7 Morphological changes that were observed when cells were treated with resveralogues V19, V20, V21 and V22 on primary human lung fibroblasts (MRC-5) at CPD 36-40. 142

Figure 4-8 Morphological changes that were observed when cells were treated with resveralogues V23, V24, V25 and V26 on primary human lung fibroblasts (MRC-5) at CPD 36-40. 143

Figure 4-9 Morphological changes that were observed when cells were treated with resveralogues V27, V28, V29 and V30 on primary human lung fibroblasts (MRC-5) at CPD 36-40.. 144

Figure 4-10 Morphological changes that were observed when cells were treated with resveralogues V31, V32, V33 and V34 on primary human lung fibroblasts (MRC-5) at CPD 36-40. 145

Figure 4-11 Morphological changes that were observed when cells were treated with resveralogues V36, V37, V38 and V39 on primary human lung fibroblasts (MRC-5) at CPD 36-40.. 146

Figure 4-12 Morphological changes that were observed when cells were treated with resveralogues V40, V41, V42 on primary human lung fibroblasts (MRC-5) at CPD 36-40. 147

Figure 4-13 Effect of Resveralogue on percentage cell viability of primary human lung fibroblast (MRC-5) at CPD 36-40 was determined by using MTT assay. 148

Figure 4-14 Effect of Resveralogue on cell viability of primary human lung fibroblasts (MRC-5) at CPD 36-40 was determined by using Neutral red uptake assay. 149

Figure 4-15 Effect of resveralogues V1-V42 on percentage LDH release of primary human lung fibroblasts (MRC-5) at CPD 36-40 was determined by using LDH assay.151

Figure 4-16 Representation images of ki-67 immuno-histochemistry in MRC5 cells when treated with A) control untreated cells B) resveratrol C) V24 and D) V34 at 100 μM.153

Figure 4-17 Effect of resveralogues (10 μM) on cell proliferation of primary human lung fibroblasts (MRC-5) at CPD 36-40 determined by using ki-67 immunocytochemistry.154

Figure 4-18 Effect of resveralogues (25 μM) on cell proliferation of primary human lung fibroblasts (MRC-5) at CPD 36-40 was determined by using ki-67 assay..... 154

Figure 4-19 Effect of resveralogues (50 μM) on cell proliferation of primary human lung fibroblasts (MRC-5) at CPD 36-40 was determined by using ki-67 assay..... 155

Figure 4-20 Effect of resveralogues on cell proliferation of primary human lung fibroblasts (MRC-5) at CPD 36-40 was determined by using ki-67 assay..... 156

Figure 4-21 Effects of resveralogues on the fraction of SA-β-galactosidase positive cells in MRC5 fibroblasts cultures at a 36-40 CPD. deviation).. 157

Figure 4-22 Effects of resveralogues on the fraction of SA-β-galactosidase positive cells in MRC5 fibroblasts cultures at a 36-40 CPD. 158

Figure 4-23 Effects of resveralogues on the fraction of SA-β-galactosidase positive cells in MRC5 fibroblasts cultures at a 36-40 CPD. 159

Figure 4-24 Typical images of senescence-associated β-galactosidase (SA-β-Gal) positive cells in MRC5 cells using catalytic immunocytochemistry technique at pH6 when treated with A) control untreated cells, B) resveratrol, C) V24 and D) V34 at 25, 50 and 100 μM. 160

Figure 4-25 Activation of SIRT1 by resveratrol (RSV), sirtinol, NAM (nicotinamide) and DHRSV. 161

Figure 4-26 Activation of SIRT1 by resveratrol and synthesized resveralogues plus sirtinol and nicotinamide..... 163

Figure 4-27 Fold activation of SIRT1 by resveratrol and synthesized resveralogues plus sirtinol and nicotinamide..... 164

Figure 4-28 Effect of resveralogues on IL-6 release were analysed by a human specific IL6 antibody. 165

Chapter 05

Figure 5-1 Effect of solvent polarity on olefinic proton peak separation in V4. 178

Chapter 06

Figure 6-1 Effect of resveralogues V1-V42 on percentage LDH release (in increasing order) of primary human lung fibroblast (MRC-5) at CPD 36-40 was determined by using LDH assay. 181

Figure 6-2 Correlation plot between Log P and percentage cell death using LDH assay for resveralogue at 100 μM concentration..... 182

Figure 6-3 Correlation analysis of SIRT1 activation with a) toxicity (using LDH assay) and b) with proliferation ki-67 marker..... 187

Figure 6-4 IL-6 release was independent of SIRT1 activation using collaborator data, Prof. Lynne Cox, University of Oxford. 188

Figure 6-5 Development of non-toxic, non- growth inhibitory resveralogues with SIRT1 activity..... 189

Chapter 07

Figure 7-1 Overall effect of structural modification in resveratrol on its bio-activitites such as toxicity (using LDH assay), senescence, SIRT1 activation and IL-6 inhibition (using collaborators data provided by Prof. Cox and co-worker)..... 194

Chapter 08

Figure 8-1 Development of resveratrol based senolytes. 196

Declaration

I declare that the research contained in this thesis, unless otherwise formally indicated within the text, is the orginal work of author. The thesis has not been previoiusly submitted to this or any other university for a degree, and does not incorporate any material already submitted for a degree.

Acknowledgements

By the grace of Lord **Gorakshanatha**, my academic career so far has indeed been such a journey, full of exciting challenges. My research carrier in the last three and half years, in particular, have been filled with exhilarating intellectual experiences, to which many people have greatly contributed. I joyfully take this opportunity to express my gratitude towards them.

First & foremost, I would like to thank my Ph. D. mentor, **Dr E. Ostler**, who is always a pleasant scientist and willing to discuss any topics reminiscent of science. She taught me to look at problems and challenges from multiple angles & to always look at the bright side of life. Her hands off approach enabled me to grow as a researcher and as a person and she was always there to extend a helping hand. As a researcher, I have learned a lot from her about scientific knowledge, communication skills, and the most important one 'motivation', which has been the endless source for new ideas. I greatly appreciate her from the bottom of my heart.

Special thanks extended to **Dr A. Sheerin**, my co-advisor, who guided me through scientific as well as management skills and, and provided constant support that made my journey completed lot easier than it would have been. Despite her busy schedule, she would always find the time to discuss anything from intriguing experimental results to an issue of being survived in the scientific world.

My sincere gratitude is reserved for **Professor Richard Faragher** for his invaluable insights and suggestions. I really appreciate his willingness to meet me at short notice every time and going through several drafts of my thesis. He is the person who took a large interest in my project to extend my research in terms of collaborations. I remain amazed that despite all my mentors busy schedule, they were able to go through the final draft of my thesis and meet me in less than a week with comments and suggestions on almost every page. They are an inspiration.

I have been fortunate from the postgraduate study as I met really genius mentor **Professor Chaudhary** who taught me and inspired me time to time. During this time, apart from my mentor, there are two friends because of whom I feel I can pursue my PhD study; they are **Dr Amol Gupte** (Tata consultancy) and **Dr Ravindra Jadhav** (Purdue University). I could never have reached this goal without the help of them. They fully

understood my struggles with this endeavour, they were there for the minor victories and defeats, and they always helped me press forward. They instilled in me the value of education. Thank you for encouraging me to go all the way to the top and for believing in me more than I believed in myself.

Most importantly I would like to thank my family: my **father, mother and sister.** They were instilling in me the qualities that have made me what I am today. Without them I could not have succeeded, I would be no one and nowhere. Also, special thanks to my sister, **Dipali** and brother-in-law **Bhushan** for their strong support through these years to help me achieve what I set out to do. Moreover, I am grateful more than I express to for their constant help throughout from my academic life. They were essential in making the man I am today. I also would like to thank my uncle **Mahendra** and cousin **Ankush** for their support during this period.

Many of my PhD friends have not only been helpful but also made this experience more enjoyable. I would like to mention special thanks to **Ganesh, Yishan,** and **Sandeep** with whom I spend a lot time, especially at tea and Friday dinner. Apart from the laboratory, there is a list of friends who are well-wishers who always encouraged and supported me. To mention few are,

I am greatly indebted to **Dr Howard Dodd** for help in Nuclear magnetic resonance spectroscopy, without which this work would not be possible. It was a great moment when we discuss science, art, philosophy and human race. I thank my collaborators, **Prof. Lynne Cox** (University of Oxford), **Dr James Brown** (Aston University) for biological study. I also would like to thanks, **Dr. Flavia**, chemistry technician **Mr Baker** and tissue culture technician **Chris**. Special thanks to **Steve Johns** who provide great computer and IT supports throughout my PhD studies.

I wish to thank **Dr. Susan Sandiman**, Dean of doctoral college, **Alice Parkes** and **Daniel** for the permission to submit this work in the form of a thesis.

Finally, I really thank from my bottom of heart to the University of Brighton for the award of fellowship during the period of this work without which I could not start and complete my study.

Vishal Chandrakumar Birar

Dedication

This thesis, as well as my career, is all dedicated to my lovely parents Chandrakumar and Ranjana for their unconditional love, supports and blessing throughout my life. I also would like to dedicate my thesis to my late grandfather Murlidhar and late grandmother Bhagirathi to whom I could not meet her in her last time.

Abstract

Resveratrol and compounds related to it, known as resveralogues, have been shown to extend healthy lifespan in a number of species. A diverse set of molecular mechanisms have been proposed to account for these effects, including the activation of the NAD^+-dependent histone deacetylase SIRT1. However, both resveratrol and some of its derivatives also display potentially detrimental activities including direct DNA damage, toxicity and the induction of cellular senescence. Accordingly, the overall aim of this thesis was to enable the generation of better compounds with minimal detrimental activity and maximum beneficial activity. The data presented in this thesis show my development of a new, convenient, one-pot stereo-selective synthesis of resveratrol and other *trans*-stilbene derivatives. This synthesis has been used to prepare more than 40 compounds, of which 20 are completely novel and a further 12 previously uncharacterised with regard to their biological effects. This study have evaluated these resveralogues with respect to their cytotoxicity in human fibroblasts using a range of widely-recognised assays. Data on the compounds' toxicity are presented, together with evidence that two of the assays commonly used to measure cytotoxicity *in vitro* (the MTT and neutral red assays) are unsuited for cytotoxicity testing with this class of compound. Twenty-two of the (lowest toxicity) compounds have also been assayed for their effects on growth and senescence using indirect immunostaining for the proliferation marker pki-67 and catalytic histochemical visualisation of SA-β-galactosidase activity, respectively. The results indicate that the growth inhibitory activity of resveratrol is abrogated by the removal of the *trans*-stilbene double bond (no reduction of growth fraction in dihydroresveralogues at 100 μM). Interestingly, at low doses (5-10 μM), many resveralogues induce a significant increase in proliferation compared to control untreated cells. SIRT1 activity in the presence of each compound was measured using an *in-vitro* deacetylation assay and, whilst most resveralogues are SIRT1 activators, none of the compounds examined produced a significant increase in SIRT1 activation compared to the parent compound. SIRT1 activation was, for the first time, found to be independent of the presence of a *trans*-stilbene double bond. Some initial characterisation of the ability of the resveralogues to alter pro-inflammatory cytokine expression was also undertaken by using ELISA for interleukin 6. Some difficulties with this assay, with respect to background signal interference, were encountered but parallel data from collaborator

(Professor Lynne Cox, University of Oxford) using a human specific IL6 antibody are available. Collabrator data, evaluating a selection of resveralogues, indicate that inhibition of IL6 release is independent of SIRT1 activation, demonstrating that not all potential beneficial effects are SIRT1 mediated. Finally, this work has identified three novel lead compounds (V24, V31, and V34) that have less detrimental activities with retention in SIRT1 activity.

Chapter 1. Introduction

1.1. What is ageing?

Ageing is a feature of organisms and populations of such organisms. In populations, the defining feature of ageing is the presence an exponential increase in the intrinsic chance of sickness and death (*morbidity* and *mortality* respectively) with advancing chronological age (the Gompertz relationship). Gompertz relationships have been found to exist in the overwhelming majority of the species studied to date. However, a minority of species show a fixed chance of all-cause mortality with advancing chronological age (sometimes colloquially referred to as a 'Gompertz flatline'). These species are non-ageing, although individual members are not immortal. Ageing is thus not a universal feature of life on Earth.

A Gompertz relationship does not require that the causes of morbidity and mortality be catalogued as distinct pathological entities. However, in practice, this does happen. Thus, in humans, diseases such as cancer, diabetes, cardiovascular diseases and others show a Gompertz relationship [1]. In developed countries, such age-linked pathologies are the leading causes of death and morbidity and even in the poorest countries they comprise three of the top ten causes of death, a proportion which is set to increase [2]. Thus, there is an urgent need for interventions that will maintain the healthy life (or healthspan) of people in the middle to late life. In order to produce such interventions, it is necessary to understand the causes and mechanisms of ageing and age-related diseases and also the relationship between them. Presently, therapeutic strategies tend to be focussed on either specific age-related diseases or targets selected for their potential relevance to individual 'disease' entities. In the light of our emerging understanding of the mechanisms controlling the ageing process this may be a less than optimal strategy for the rapid achievement of healthy later life.

1.2. Why does ageing exist?

Ageing is a complex process and many theories have been proposed now in order to explain why ageing exists. The proposed theories explained the process of ageing, but none of them were fully acceptable [3]. The potential reason was complex or multiclausal nature of human ageing and interestingly individual theories were based on individual

maintenance mechanism. For example, free radical theories explained that radicals generally cause cellular damage and damage in mitochondria [4]. However, presently, evolutionary theories such as mutation accumulation theory and the antagonistic pleiotropy theory are widely considered as a basis for defining theories of ageing [4]. These theories tried to explain why the ageing process exists in various different organisms on the basis of mutation and natural selection process. Mutation accumulation theory was proposed by Medawar in 1952 [5]. According to this theory, the force of natural selection decreases with age as the greatest contribution of organisms is to create a next generation from young ones and not from old ones [6]. A lethal mutation that is harmful or destructive post the reproductive period is not selected against during early life and so late-acting deleterious genes are retained in the population [7]. Later in 1957, a theory was developed by George Williams. According to this theory, a mutation that increases early life fecundity will be strongly selected even if the same mutation produces lethal effects later on in the life course. As a result, a mutation with beneficial effects at an early stage of life but harmful at later ones will be favoured by natural selection [8]. This type of gene action is termed antagonistic pleiotropy from which the theory gets its name [8].

1.3. Health spans maintenance mechanisms: ageing mechanisms

Ageing remained an introductory problem for much of the later 20th century despite notable advances in other biological fields. The dissertation that no human has survived longer than 120 years suggested that there are certain causal mechanisms (such as cell senescence and nutrient sensing pathway) that operate in humans leading to ageing and degeneration. Recent research outcomes in biology, especially in the field of biogerontology, suggested that these have a major effect on the duration of healthy life. see **Figure 1-1**.

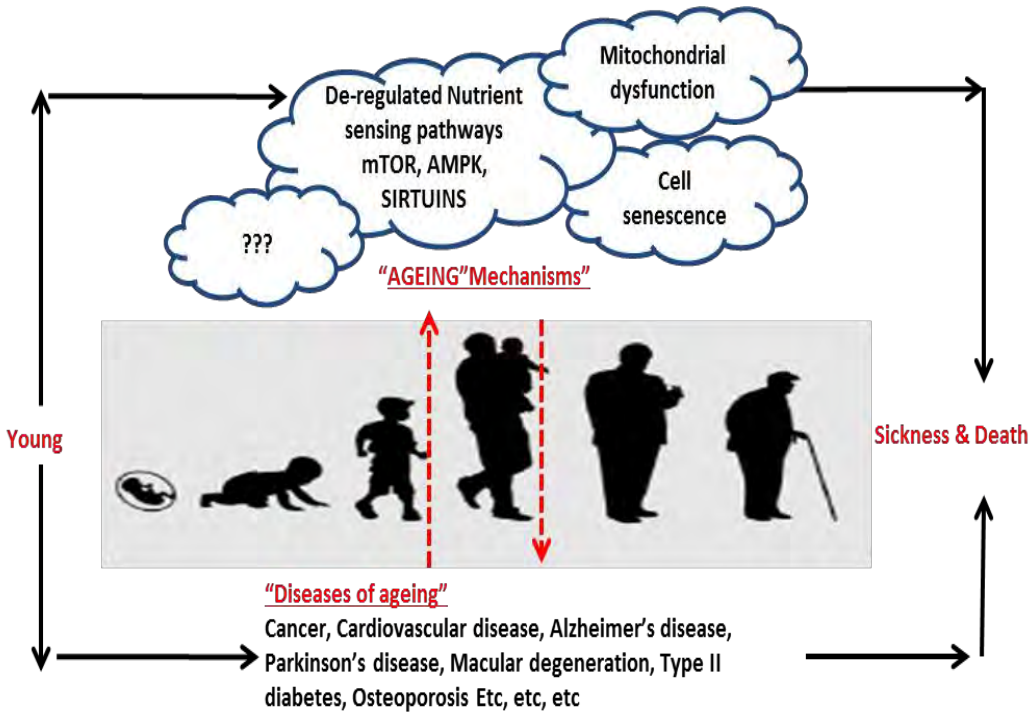

Figure 1-1 Health span maintanance mechanisms (ageing mechanisms) [9]. The scheme enumerates hallmarks of ageing mechanisms described in Section 1.3.1 and 1.3.2 that potentially lead to age-related diseases and pathology.

1.3.1. Cell Senescence:

Hayflick and Moorhead in 1961, showed that normal cells had a finite proliferative life span in cultures [10]. Proliferation decreased with each passage and finally the ability to divide was lost. However, these cells remained metabolically active but failed to enter the cell cycle. The irreversible growth arrest of the cell is termed as cellular senescence and these metabolically active cells are called senescent cells. The causes of senescence are large in number and also complex in nature. However, the limited cell proliferation capacity of many types of human cells results from the gradual loss of telomere DNA [11]. This gradual loss of telomere with every stage of DNA replication eventually results in telomere uncapping and generates DNA damage response. This damage response initiates replicative senescence and growth arrest [12, 13]. Additionally, mechanisms have been reported that cause senescence such as histone deacetylase inhibitors [14], and activation of the p53 tumour suppressor [15]. There are some additional stimuli such as oxidative stress [16]; ectopic expression of CDK inhibitors p21 and p16 [11, 17] also contribute towards senescence growth arrest (reviewed in **Figure 1-2)**. However, in these cases, the growth arrest was observed to be independent of telomere shortening. The distinctive characteristic of senescent cells is permanent growth arrest coupled with sustained metabolic activity [18]. When cells became senescent there is observed an increase in size (about two-fold increase) compare to normal cells [10]. This change in cell morphology is readily observed under the microscope. The Senescence-associated β-galactosidase (SA β-gal) assay is a widely accepted method for detecting senescent cells in a range of situations [19]. The assay relies on elevated lysosomes mass and increased β –galactosidase activity in senescent cells [20, 21]. p16 is a tumour suppressor gene which controls cell cycle and cell senescence through retinoblastoma protein. It controls the cell cycle arrest at G1 phase by inhibiting cyclin dependent kinases [22]. It has been found that it is mainly expressed in senescent cells rather than quiescent cells [23] and can be induced by stress [24], telemeric DNA damage [25].

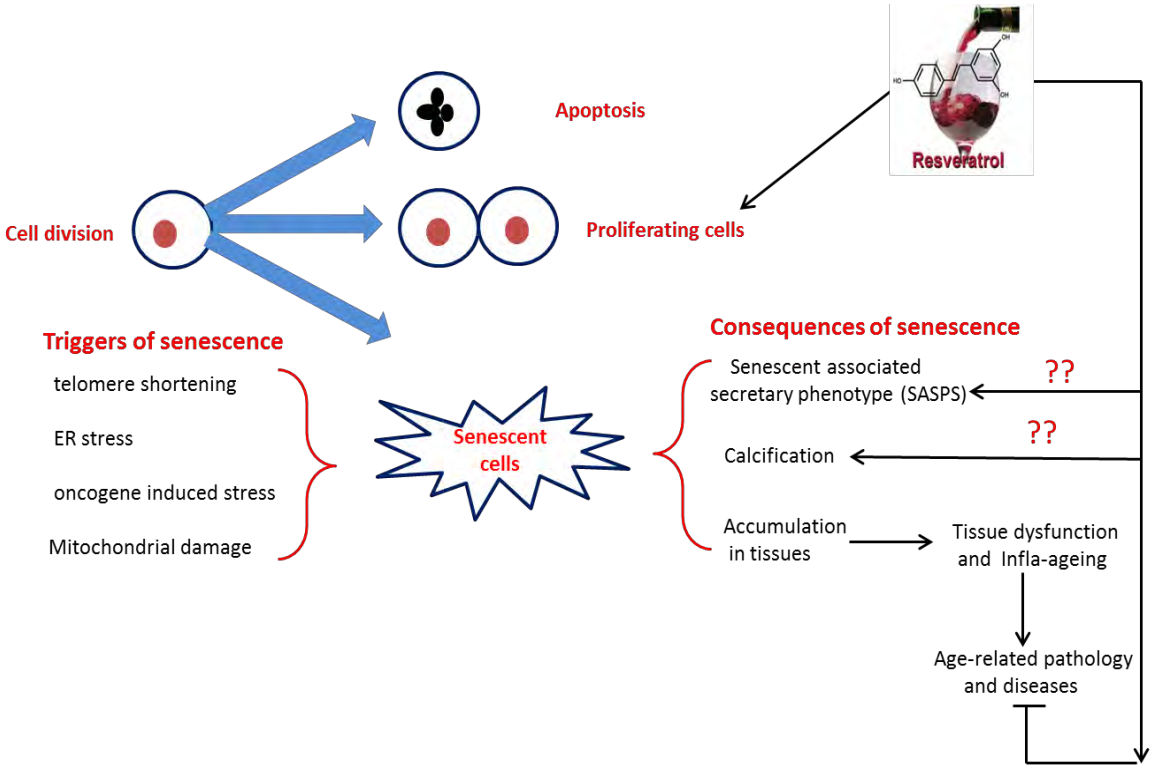

Figure 1-2: Schematic representation of triggers of cell senescence, biological consequences and explanation of potential mechanisms behind resveratrols anti-ageing properties.

During ageing, senescent cells increase in various tissue. These are also observed in some premature ageing disease (progeroid syndromes such as Werner's, Hutchinson-Gilford) [26]. Senescent cells secrete cytokines, chemokines and growth factors [11]. This phenomenon is known as the senescence-associated secretory phenotype (SASP) and probably play a major role in ageing and the development of chronic inflammation which characterises age-related diseases [26].

The primitive source of SASP is the DNA damage response [27]. The primary SASP molecules are TNF-α, IL-6 and other proteins. Additionally, these component expressions were found to be increased in senescent cells compare to non-senescent cells [28]. If these elevated pathways such as IL-6 or TNF-α are targeted through pharmacological ways, then it might be a beneficial way to target age-related inflammation and diseases. Further, this increased component altered the neighbouring tissue function and developed chronic inflammation which helps to accelerate the age-related dysfunctions [29]. For example, the presence of senescent epithelial cells affects alveolar and branching morphogenesis, as well as milk protein production [30, 31]. Additionally, indirect evidence suggested a role of senescent cells and SASP in accelerating the age-related neurodegeneration linked to cognitive impairment, and disease such as Alzheimer's and Parkinson's diseases [32]. A selective elimination of senescent cells could be one of the strategies to reduce age-related inflammation. Recently, a transgenic mouse model (called as INK-ATTAC) was developed in which senescent cells were selectively eliminated by treatment apoptosis-inducing drug AP20187, see **Figure 1-3** [33]. Selective elimination of senescent cells in this mouse model also helped to protect it against the development of cataracts and blocked the age-related decline in kidney function [33].

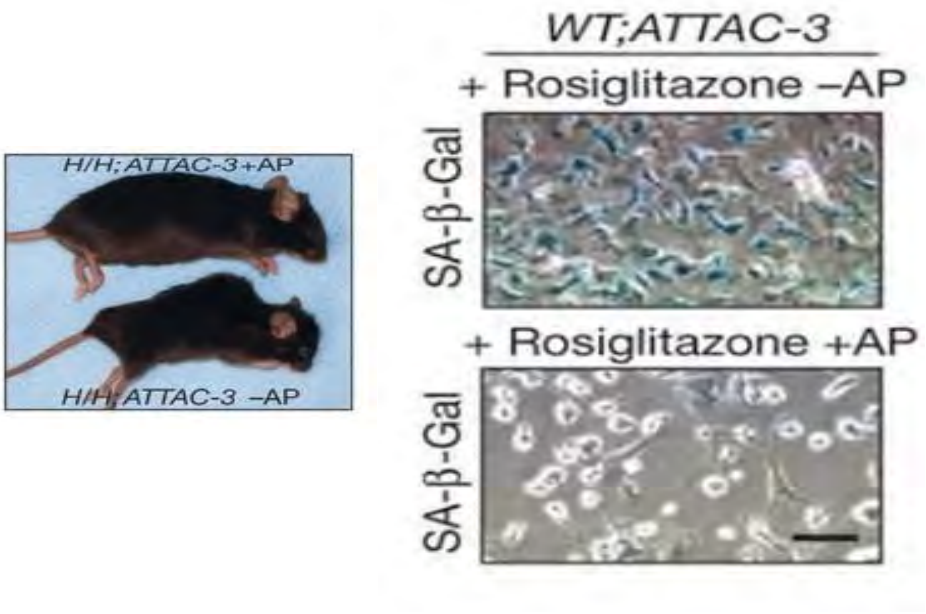

Figure 1-3: Clearance of senescent cells delays the age-related dysfunctions in transgenic mice INK-ATTAC upon drug treatment AP20187 and it also increases their median lifespans by 17% to 42%, depending on sex, diet, and genetic background [33].

1.3.2. Nutrient sensing pathways:

Nutrient sensing mechanisms and pathways are responsible for maintaining the nutrient or energy homoeostasis at cellular and thus at the organism level. These pathways include insulin/insulin-like growth factors (IGF), the target of rapamycin (TOR), AMPK and SIRTUINS. It has been shown that these pathways are important in the ageing process and many genes related to these pathways were identified that controls lifespan and nutrient sensing. e.g. insulin/IGF pathway and its involvement in life extension have been well studied in a small organism such as *C.elegans*, Drosophila [34] and the mutation in genes namely, daf2 and age-1 which encodes the insulin /IGF1 receptor were found to increase the lifespan of *C.elegans* [35]. This suggested the importent role of nutrient sensing and ageing, see **Figure 1-4**. Further, a reduction in nutrients or calorie intake has been found to reduce the ageing and age-related mortality. Calorie restriction has been to cause shown an increase in lifespan in various species including humans. Dietary restriction or Calorie restriction (CR) in which the total food intake is reduced was found to delay the onset of age-related diseases and thereby increase the lifespan of various organisms [36]. The beneficial health effects conferred by CR have been extensively studied and several potential pathways were identified. This includes changing growth hormone/IGF signalling, mTOR inhibition, reducing ROS species and AMPK and SIRT1 activation. In 2010, C. Wang and co-workers first discovered short-term dietary restriction reduces the cell senescence in mice. This reduction was associated with improving telomere maintenance (but without increasing telomerase activity) and decrease in progressive oxidative stress [37].

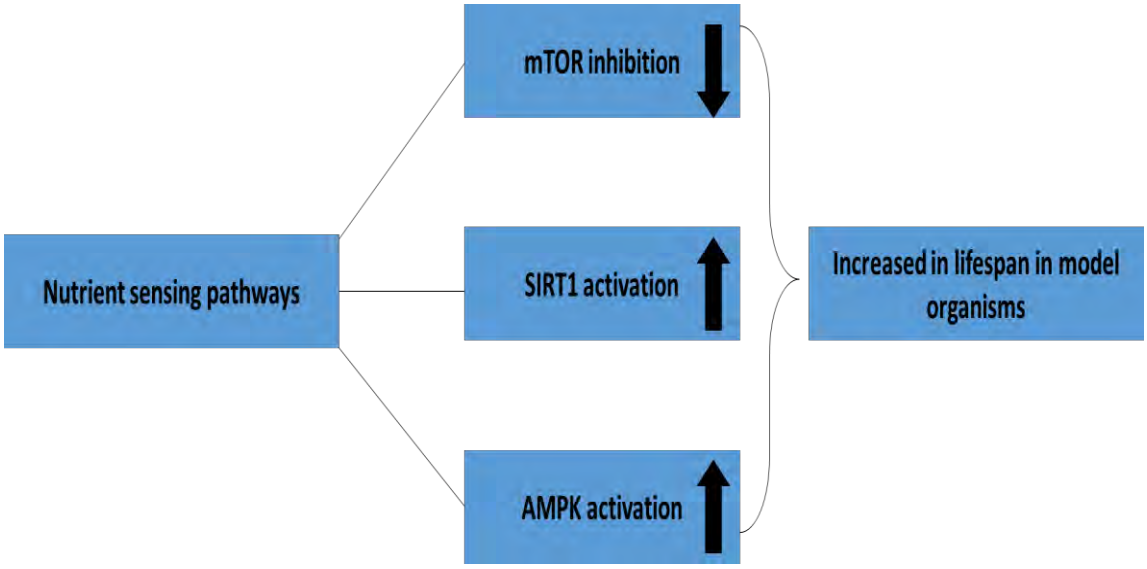

Figure 1-4: Nutrient sensing pathways and their role in longevity. For example, Inhibiting mTOR pathway using genetic mutation or pharmacological interventions has been found to increase healthy life span model organisms such as *S. cerevisiae*, *C. elegans*, *D. melanogaster*, *M. musculus* [38].

The second important pathway is mTOR; a mammalian target of rapamycin named after the drug Rapamycin, used as immunosuppressant [39]. It is a protein kinase and exists in two distinct protein form mTOR1 and mTOR2 [40]. This is involved in the various cellular processes such as cell growth and metabolism [41]. The first link between the target of rapamycin and longevity was established in *Caenorhabditis elegans* [42]. Further study on this molecule demonstrated life extension in various model organisms such as *Drosophila melanogaster* [43], and *S. cerevisiae* [44]. The role of mTOR inhibition, and increased mean life span in mammals, was reported in genetically heterogeneous mice. In this experiment, mice were fed with Rapamycin at later in life and found to have increased lifespan [45]. The inhibition of mTOR through the genetic knockout experiment such as deletion of ribosomal protein S6 kinase 1 (part of mTOR1 complex) [46] and low level of mTOR1 [47] also shows the effect on mammalian life span.

Another important pathway involved in life extension studies is AMPK (adenosine monophosphate-activated protein kinase) which is a serine/threonine protein kinase present in unicellular organisms as well as in mammals [48]. It majorly regulates the metabolic homoeostasis, stress resistance and cell housekeeping processes such as autophagy [49]. It consists of three subunits namely α, β and γ which control the regulation of this enzyme. During nutrient deficiency or in exercise there is a depletion in ATP and thereby increase in ADP/AMP (Adenosine diphosphate/Adenosine monophosphate) [50]. This elevated ADP/AMP ratio activates AMPK. One of the hallmarks of the ageing process involved the enhancement in metabolic stress, linked to decreasing AMPK activation in advancing age [51].

AMPK activation either through pharmacological or genetic experiments showed an increase in the lifespan of various model organisms. In the case of *C. elegans,* there were two related homologues found to be related to AMPKα subunit, AAK-1 and AAK-2. This experimental further showed that AAK-2 played an important role in longevity compared to AAK-1. In the case of a genetically knockout AAK-1 animal, it showed a decrease in lifespan by 12% compare to control wild type. However, a transgenic animal with overexpressing AAK-2 was found to live longer compared to wild type [52]. A similar type of genetic result showed the role of AMPK activation in life extension [53]. Recent outcomes also suggested that AMPK activation was not only limited to regulation of energy metabolism but also helped cell housekeeping processes such as autophagy [54]

and also a reduction in inflammation [55]. Additionally, chemical induced oxidative stress induced by palmitic acid in human aortic endothelial cells was found to be suppressed using AMPK activation [56]. 5-aminoimidazole-4-carboxamide ribonucleotide (AICAR) was used as a pharmacological activator for AMPK activation. The pharmacological activation of AMPK was found to decrease inflammation and conversely a reduction its activity lead to an increase in inflammation [57]. In one clinical study in humans, using AMPK antagonist Metformin, the level of C-reactive protein (CRP), a biomarker of pro-inflammation, was significantly reduced in diabetic patients [58].

Sirtuins are a deacetylase conserved proteins present in a various organisms including humans and they first identified through genetic modification experiments in *S. cerevisiae*. The last fifteen years studies in the ageing field and especially in life-longevity of various model organisms including mammals demonstrated the role of single protein activation of SIRT1.The first report on the increase in lifespan was reported in budding yeast using overexpression of SIRT1. The increase in the replicative life of yeast was found by reducing the rDNA circle formation, a factor responsible for ageing in budding yeast [59]. Similarly, increased copy of sir 2 genes in *C. elegans* increased the life by 50% compared to control *C. elegans* [60]. A similar result was recorded in mammals such as in transgenic mice (BRASTO-brain specific overexpression of SIRT1) which show a significant increase in lifespan both in males and females [61].

1.4. Relationship between ageing and age-related diseases:

Ageing is associated with a wide range of pathological and physiological changes that affect the normal function of the organism and make the organism more susceptible to death [62]. However, it's still unclear whether the diseases are an integral part of the ageing process or not. In order to understand ageing and the related age-related pathology, it is essential first to define the link between them. This was clearly described by Faragher [63]. Ageing was considered as a natural process that was distinct from abnormal diseases. This difference did not come through an exact understanding of ageing but instead of simple logic. The reason behind this was everyone gets old but not everyone who gets old suffer from age-related disease. In 1986, Brody and Schneider classified diseases such that age-related and age-dependent [64]. Age-dependent diseases are diseases, whose appearance depends on age, such as atherosclerosis. cancer, multiple

sclerosis are an examples of age-related diseases whose appearance is independent of the age of the organism. The most common deleterious effects that occur with increasing age are cardiovascular, neurodegenerative diseases and diabetes.

However, there are now common health span maintenance mechanisms such as cell senescence which could cause both ageing and age-related diseases. Cellular senescence not mediates the development and/or progression of age-related diseases but also other diseases or tissue dysfunction independent of age [65]. Additionally, it may help to progress age-related diseases due to progressive accumulation of senescent cells, while other diseases that are independent of age, may be accelerated due to the presence of senescent cells [65]. e.g. intervertebral disc degeneration which is considered as a major cause of low back pain may be accelerated due to the formation of senescence disc cells *in vivo* [66].

1.5. Potential intervention targeting ageing mechanisms:

The above sections mentioned that healthy lifespan could be increased through targeting ageing mechanisms. Biogerontology is the study of the basic biology of ageing to understand the ageing process, mechanisms and preventing age-related dysfunctions and diseases. One role of biogerontologists is to investigate the ageing mechanisms and develop anti-ageing strategies in order to increase healthy lifespan, see **Figure 1-5** [67]. Accordingly, Gems (2014) summarised the practical meaning of anti-ageing strategies. Designed strategies should focus on developing a drug that mimics calorie restriction inhibits age-related pathology or targets a single age-related pathology [68]. To address these points, a meeting was held under the sponsorship of NIH (national institute of health, USA) to address and make strategies towards healthy ageing concepts. The outcome of this meeting was collectively called the Intervention testing programme (ITP). This involvesd the study of treatments or study candidate such as hormones, diet and dietary supplements, peptides, amino acids and nutraceuticals in animal models to extend the lifespan and delay age-related dysfunctions and disability. However, the overall goal of this programme was to identify treatments that could potentially useful to humans [69]. According to literature and existing research data be potential anti-ageing or healthy ageing strategies are summerised in **Section 1.5.1 and 1.5.2**;

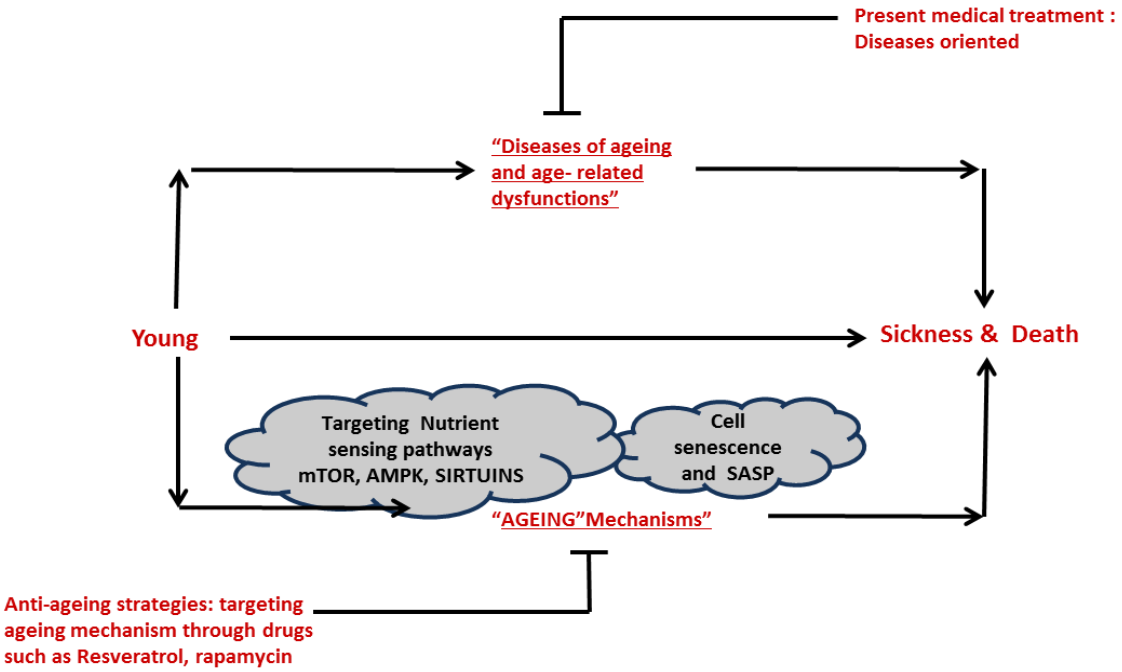

Figure 1-5: Concept of biogerontology and anti-ageing strategies [68].

1.5.1. SIRT1 activation:

SIRT1 Silent information regulator protein 1 in human, localised in the nucleus [70] belongs to the Sirtuin family of proteins. SIRT1 is present in the nucleus and cytosol and has received the most attention after the discovery of life extension effects in various model organisms. It is a class III histone deacetylase and as such requires NAD (nicotinamide adenine dinucleotide) as a cofactor for its deacetylation activity [71] (see overall deacetylase reaction in **Figure 1-6)**. This involves a reaction between the NAD^+ and acetylated protein substrate to produce nicotinamide and 2-O-acetyl-adenosine diphosphate-ribose and deacetylated protein. The overall reaction is shown in **Figure 1-6**,

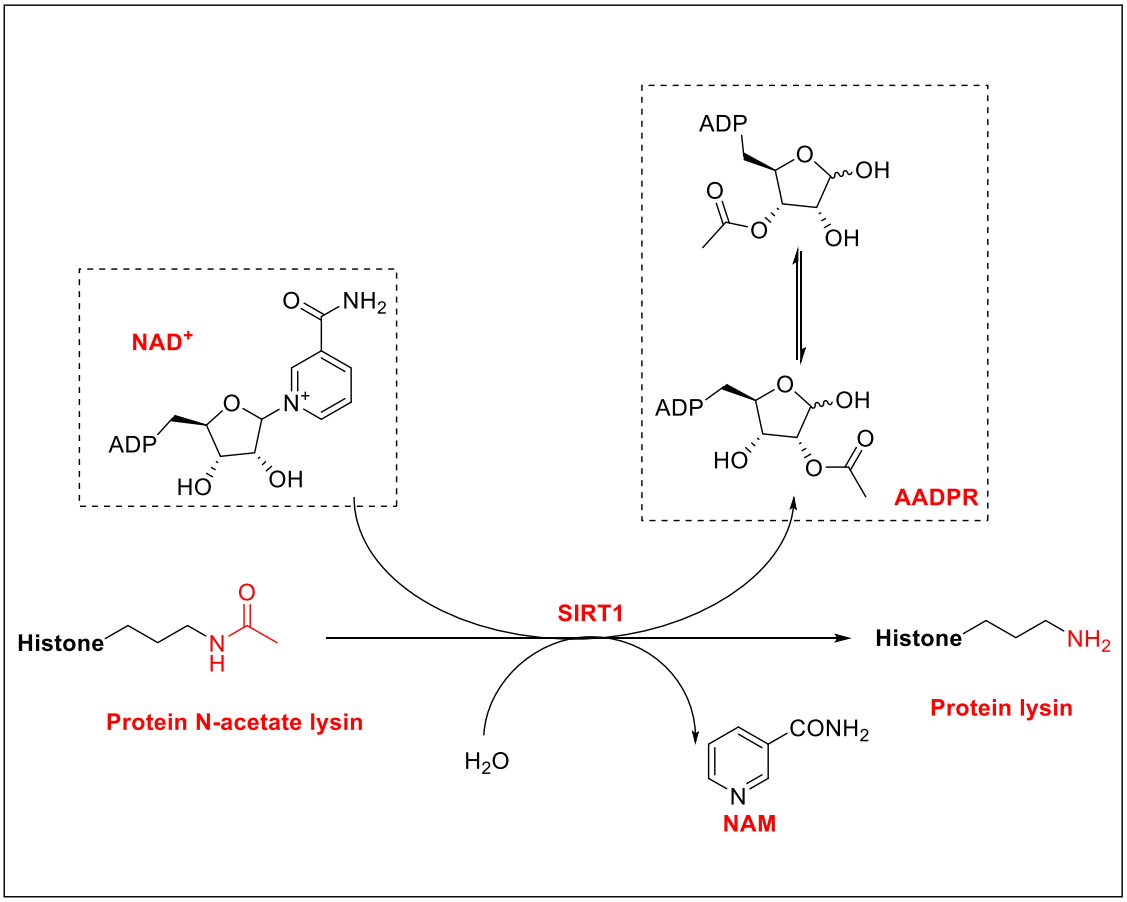

Figure 1-6 : Overall reaction of SIRT1 deacetylation which hydrolyses the acetyl group of protein substrate using nicotinamide adenine dinucleotide (NAD^+) and releases nicotinamide (NAM), o-acetyl-adenine diphosphate-ribose (AADPR) and deacetylase protein substrate [72]. This result in the deacetylation of numerous transcription factors and co-factors that includes p53, NFκB, FOXO, PGC-1α, TORC2, as well as several nuclear receptors. Therefore, SIRT1 is directly linked to the cellular metabolic status to gene expression, playing an important role in cell survival and longevity [73].

1.5.1.1. SIRT1 activating compounds:

The discovery of SIRT1 activation has been implicated in various beneficial effects to human health and hence it is considered as a drug target for treating age-related diseases. Resveratrol (**1**, see **Figure 1-7**), a polyphenol naturally occurring compound and constituent of wine, is considered as a potent SIRT1 activator compared to other polyphenols [74]. Resveratrol showed a 13-fold increase in deacetylase activity of SIRT1 protein [74]. In the year 2007, more potent molecules as SIRT1 activators were identified through *in-vitro* fluorescence polarisation assay [75]. These molecules were structurally distinct from resveratrol but 1000 times more potent than resveratrol, (**Figure 1-7)**. The screening was carried out by a pharmaceuticals company called Sirtris which was named after the sirtuin family of proteins. In these primary high throughput screening, 290000 small molecules were tested using this fluorescence assay. This screening identified three small molecules that were structurally similar to one another namely SRT1460, SRT1760 and SRT 2183 (**2, 3 and 4**, see **Figure 1-7**) [76]. Further, these molecules mimicked dietary restriction phenomenon and improved insulin sensitivity, increasing the mitochondrial activity and lowering the blood glucose levels in obese mice [75]. All these SIRT1 activating compounds (STAC) were found to activate SIRT1 at very low concentrations compared to resveratrol. e.g. SRT1720 shows increased in deacetylase activity of SIRT1 protein by 781% at 0.16 μM compared to untreated SIRT1 protein. Later, In 2009, a new series of imidazo[*1,2-b*]thiazole derivatives (**5 and 6**, see **Figure 1-7**) were reported as SIRT1 activators and these molecules were also more potent than resveratrol [77]. For example, a benzimidazole series showed 820% increase in deacetylase activity of SIRT1 protein at 0.4 μM. In addition a similar series of derivatives, novel oxazolo[*4,5-b*]pyridines (**7**, see **Figure 1-7**) and their heterocyclic analogues were also shown to be SIRT1 activators [78], See **Figure 1-7.**

The overall reports on SIRT1 activating compounds (STAC) are shown in the following **Figure 1-7**. These molecules are considered as potent activators of SIRT1. The design strategies for SIRT1 activating compounds based on resveratrol are also shown in **Figure 1-7**.

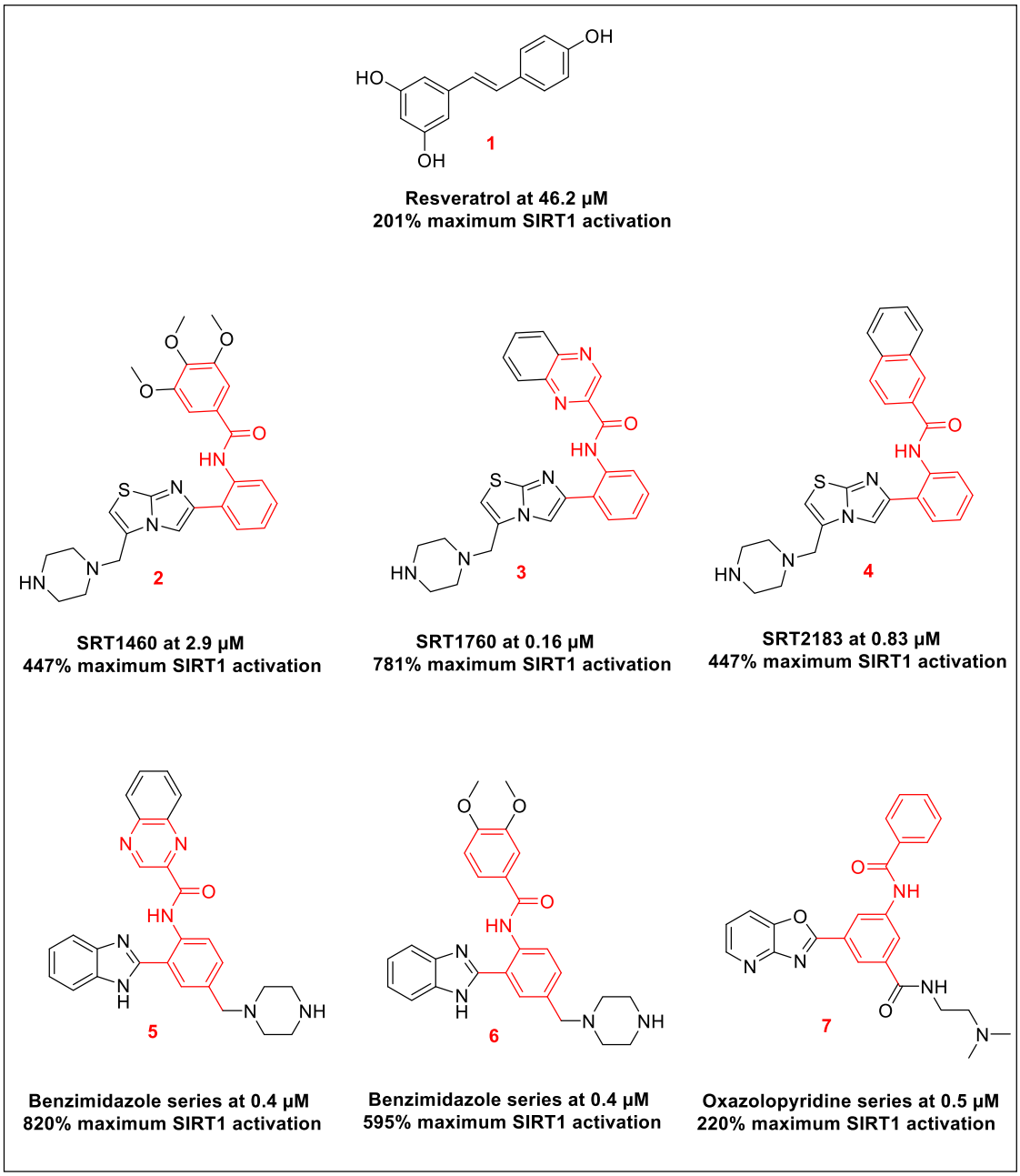

Figure 1-7: Existing SIRT1 activators, including resveratrol and other structurally different potent, selective SIRT1 activators developed by Sirtris biotech company [79].

1.5.1.2. Mechanism of SIRT1 activating compounds

High throughput screening using an enzymatic assay identified a number of SIRT1 activating compounds. This assay involves an enzymatic deacetylase reaction between SIRT1 substrate and SIRT1 enzyme. The substrate used in this assay was attached with a fluorescently tagged peptide substrate. Initially, it was considered that the STACs increased the rate of reaction of SIRT1 deacetylase by lowering the Michaelis constant [76]. Further, all the reported STACs followed a similar mechanism for SIRT1 activation [75].

However, this assay used for the determination of SIRT1 activation was challenged in 2005, suggesting that the SIRT1 activation assay was an artefact [80]. In this experiment, resveratrol was tested using three different enzymes Sir2 (the yeast homolog of human SIRT1), human SIRT1, and human SIRT2 in order to understand the mechanism of enzymatic activation. Interestingly, only SIRT1 (human homolog) was shown significant fold activation in the enzyme (approximately 8-fold) using the commercially available Fluor de Lys kit. This kit was developed by Enzo-life Sciences Company and uses SIRT1 substrate tagged fluorophore (such as 7-amino-4-methylcoumarin and rhodamine). However, when the same experiment was repeated with native p53 substrate (equivalent to assay substrate without fluorophore), resveratrol failed to activate SIRT1. This study confirmed that the presence of covalently attached fluorophore was necessary to show the enzymatic activity of STACs. Additionally, Resveratrol and second generation STACs were unable to show enzymatic activation of a SIRT1 substrate having no fluorescence moieties. It further reported that all of these molecules directly interact with fluorophore substrate as shown by NMR and other techniques [81].

Recently, two major experimental pieces of evidence suggested that STACs mediate SIRT1 activation via an allosteric activator mechanism which is substrate selective [82]. SIRT1 activation and deacetylase activity of resveratrol is totally dependent on substrate and its peptide sequence. In the first experimental evidence, a mammalian microarray was used to investigate whether endogenous deacetylase of proteins can follow through resveratrol and SIRT1 dependent manner. It involved nearly 7000 peptides in a microarray analysis and interestingly, only a few substrates, containing large hydrophobic moieties (similar to fluorophore) showed increase in deacetylase activity [83]. This result gave support for the use of fluorescence-tagged peptide as a substrate in Fluor de

Lys assay kit. The second and strong evidence for the assay was provided by Hubbard and colleagues. This finding suggested that a fluorescence tagged peptide is necessary as the substrate and might mimic the endogenous protein substrate. Further, in support to this, the presence of bulky and hydrophobic moieties might mimic the actual amino acid sequence in the natural substrate [84]. The two native peptide sequence of SIRT1 substrate PGC-1α-K778 and FOXO3a-K290 showed dose dependent activation similar to Fluor de Lys assay kit [84]. These two findings together suggested that SIRT1 activation by resveratrol and other STACs is substrate dependent and required the presence of a fluorophore or bulky hydrophobic groups that mimic the native substrate.

1.5.1.3. Beneficial effects of SIRT1 activation:

SIRT1 protein is an intensely interesting target for anti-ageing research. It is also a deacetylase enzyme for non histone proteins like PGF-α, FOXO proteins and many others. The SIRT1 activation can be achieved in one of two ways; either genetic modifications, meaning overexpressing the SIRT1 gene or using genetically modified animals such as BRASTO mice. In a second way, pharmacological activation can be achieved by using small molecules called as SIRT1 activating compounds (STACs). The most studied and easily available natural activator of SIRT1 is resveratrol. Here, the beneficial effects of SIRT1 activation is summarised below

1.5.1.4. SIRT1 and lifespan increase:

The genetic experiment in *S.Cerevisie* discovered the origin and an important role of SIRT1 proteins especially in longevity [85]. SIRT1 protein activation also mimics various beneficial aspects of dietary restriction such as an increase in mitochondrial biogenesis, or reduction in age-related disease such as diabetes, cardiovascular and neurodegenerative disease [86]. Similarly, overexpression of SIRT1 either through genetic modification or through pharmacological treatment provided life-extension of various model organisms such as *Drosophila melanogaster, Caenorhabditis elegans*, short-lived fish and honey bees [79]. The details are shown in **Figure 1-8.**

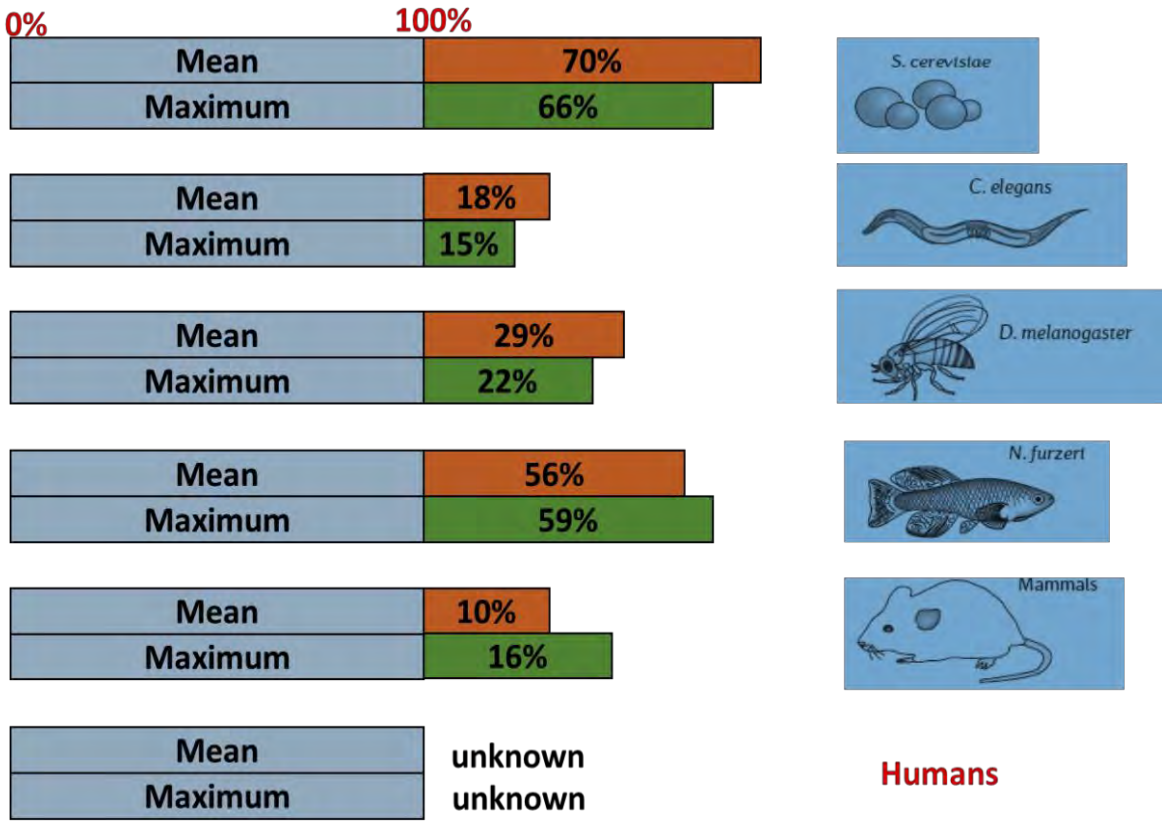

Figure 1-8 Reported increase in lifespan of various organisms through SIRT1 activation. Lifespan extensions in *Saccharomyces cerevisiae*, *Caenorhabditis elegans*, *Drosophila melanogaster*, *Nothobranchius furzeri* and in mice upon treatment with resveratrol. However, the role of resveratrol in lifespan extension of humans has yet to be investigated [87].

However, some of these life extension studies were challenged but later shown to occur in a SIR2 (yeast homolog of SIRT1) dependent manner [88]. In the case of a higher organism, such as mammals there has been no increase in life span observed but treatment with SIRT1 activating compounds such as resveratrol and others reduced the onset of age-related diseases. Recently, a BRASTO mice (brain specific overexpression of SIRT1 activation through genetic modification), was shown to cause a 16% increase in lifespan of mice. Additionally, this increase in lifespan was found to be independent of the sex of mice as both male and female mice were shown to increase the lifespan [61].

1.5.1.5. Anti-diabetic effect:

Metabolic diseases such as diabeties are caused by a disturbance in glucose and lipid homeostasis, insulin resistance, mitochondrial dysfunctions, and oxidative or environmental stress. The deacetylation and activation of peroxisome proliferation activating receptor (PPAR)-gamma co-activator-1-α (PGC-α) are mediated through SIRT1 activation which results in an increase of mitochondrial activity [89]. Thereby this improves glucose metabolism and insulin sensitivity [90]. When resveratrol, SIRT1 activator, was fed to high fat diet mice this improved the insulin sensitivity, reduction in glucose levels and led to a 20% increase in lifespan compared to untreated or vehicle-treated mice [91]. Similarly, SIRT1 activation leads to a similar kind of genetic profile which is seen in the case of dietary restriction. Resveratrol treatment of normal mice does not extend the lifespan of mice but gave improved gene expression patterns that similar to what was observed in dietary restriction [92]. It is still unclear whether the beneficial effects of resveratrol are mediated through SIRT1 or independent of SIRT1. A low dose of resveratrol (25 μM) treatment was found to improve the mitochondrial biogenesis in a SIRT1 dependent manner. However, at a higher dose (50 and 100 μM), the effect was independent of SIRT1 and observed to be mediated via AMPK activation [93]. Resveratrol did not show an increase in the lifespan of mice [94]. Similar kinds of beneficial results were reported in the case of other STACs. SRT 1720 treatment of high fat induced obese mice has been shown to give improvements in insulin sensitivity, mitochondrial activity and maintain glucose homoeostasis [75]. Recently, SRT1720 has shown to improve the life span of mice fed with a normal diet [95]. An 8.8% increase in mean lifespan of mice was noted in this case. Further, liver and muscle protein extract analysis of mice suggested that the reduction in pro-inflammatory markers was important.

1.5.1.6. SIRT1 and cardiovascular effects:

Cardiovascular disease such as atherosclerosis, endothelial dysfunction and hypertension are disorders related to blood and heart vessels. SIRT1 activation shows protective effects in atherosclerosis and improves endothelial dysfunction [96]. The overexpression of SIRT1 positively regulates the nuclear receptor LXR, liver E receptor [75]. This prevents the formation of foam cells and thereby reduces the chances of atherosclerosis and heart disease [97]. Thus, the action of SIRT1 to regulate and maintain fat and cholesterol homoeostasis may be important in preventing cardiovascular effects [98].

1.5.1.7. SIRT1 and neuroprotective effects:

Mitochondrial damage or dysfunctions have been suggested as one of the causes of neurodegenerative diseases such as Alzheimer's disease [99] and Huntington's disease [100]. Beta-amyloid protein deposition in brain is considered as a biomarker of Alzheimer's disease [101]. Experiments in a mouse model of Alzheimer's disease suggested a crucial role of SIRT1 activation and its deletion. In a similar experimental study, the beta-amyloid protein deposition was found to be reduced in cases of mouse model overexpressing SIRT1 protein while the levels were increased in SIRT1 knockout mice [102]. Similarly, a mouse study was performed to determine the role of SIRT1 activation in various neurodegenerative disease models of Huntington's disease [103, 104], and Parkinson's disease [105].

1.5.1.8. Importance of SIRT1 activation to existing potential anti-ageing molecules:

Ageing is a complex phenomenon and involves activation of complex biochemical pathways resulting in the incidence of various diseases, mentioned earlier. The discovery of SIRT1 and its activation indicates a crucial role in regulating a broad range of biochemical pathways thereby giving beneficial effects. Presently, much research is focuses on disease specific targets such as diabetes, Alzheimer's and many others. This research strategy is quite successful for developing drugs but can exhibit some side effects. The comparison is shown below in the form of **Table 1-1**.

Table 1-1 Comparison of existing therapies for anti-ageing strategies and their side effects compared with SIRT1 activators [106].

Compounds	Effects on				Drawbacks		
	Glucose homeostasis	Insulin sensitivity	Mitochondrial activity	Dietary mimetic			
SIRT1 activators	Yes	Yes	Yes	Yes			
Metformin	Yes	Yes			lactic acidosis	Kidney dysfunction	Renal/ Hepatic
Rapamycin				Yes	glucose intolerance	insulin resistance	
Insulin	Yes				Increase in weight	Increase in weight	

1.5.2. Current potential anti-ageing compounds

1.5.2.1. Rapamycin:

Rapamycin (**8**, see **Figure 1-9**) is a macrolide molecule produced by *Streptomyces hygroscopicus* and used as an immunosuppressant and anti-cancer drug [38]. Rapamycin was found to increase the lifespan of various model organisms such as yeast, worms as well as genetically modified mice [38]. The potential mechanism behind the anti-ageing effects of rapamycin may be due to its anti-cancer role, induction of autophagy, or role in translation process [38]. It has been found that autophagy activity decreased with increased age and involved impairment in the cellular cleaning process. In a transgenic aged mouse, increased activity at the lysosome receptor of the autophagy process was found to maintain the protein damage and cellular cleaning function [107].

1.5.2.1. Resveratrol:

Resveratrol is a stilbenoid natural product found in various plants, fruits and also in some foods. It was first isolated in 1940 from the root of the plant hellebore [108]. Resveratrol is a phytoalexin, that is produced by the plant in response to stress such as fungal infection or UV radiation. It is also found in Polygonum cupsidatum, which is used in Japanese and Chinese medicine [109]. However, in 1992, termed the "French paradox" phenomenon, the first beneficial effects to human health of resveratrol treatment were discovered [110]. According to this phenomenon, French people showed a low incidence of cardiovascular disease, despite their high fat diet. Further, in 1997, the anti-cancer activity of resveratrol was reported and it was found that this molecule inhibited skin cancer in mice [111]. The structure and overall discovery related to resveratrol is shown in **Figure 1-9**.

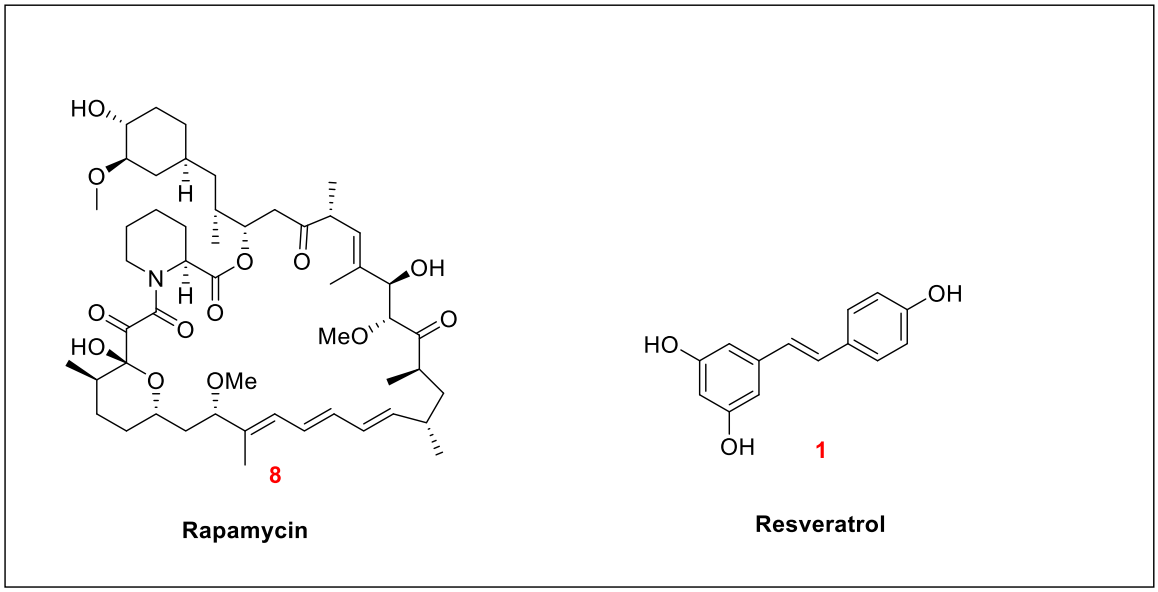

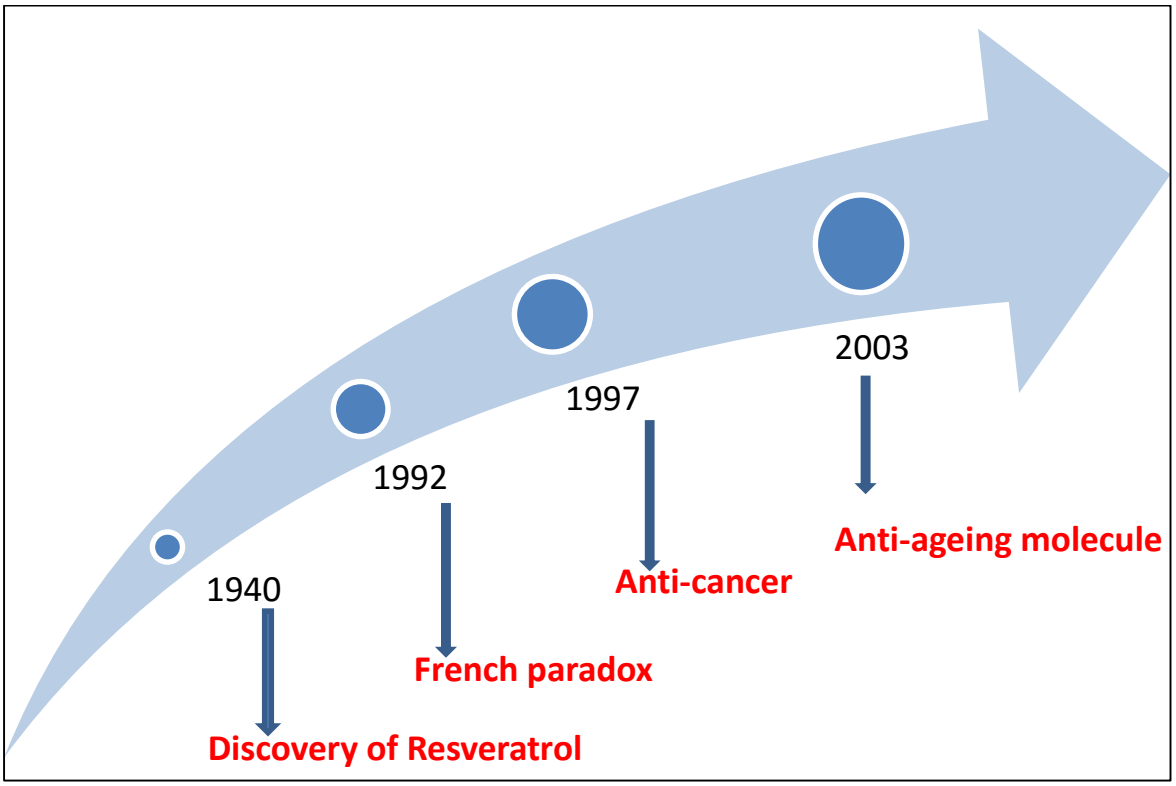

Figure 1-9: Potential antiageing molecules and resveratrol related discovery [112].

The most significant discovery regarding resveratrol was its use in extending life span in a model organism through activation of SIRT1 considered as a mimic of the calorie restriction process [59]. Furthermore, this molecule extended the lifespan of a lower organism such as yeast, worms, and flies in a SIRT1 dependent manner. However, the increase in lifespan in small organisms was further challenged in several studies [113, 114]. In the case of mammals, such as mice, it improved the health span and increased the lifespan in combination with a high fat diet [91]; however in the case of mice with a normal diet, the health span was improved with no increase in lifespan [94]. This result suggested that resveratrol does not increase the lifespan of mice but would appear to delay or slow down age-related chronic diseases.

Resveratrol has an effect on various biochemical pathways and cellular targets, like inhibiting cyclooxygenase and ornithine decarboxylase [115-117] which reduces the risk of cancer. In various cancer cell lines, it inhibited the angiogenesis process [118, 119]. The anti-inflammation activity of resveratrol was studied *in-vivo* and *in-vitro* by its prevention of platelet aggregation [120, 121] [87]. It also helped in the reduction of insulin growth factor1 level, increase in AMPK activation [91] , mTOR inhibition in cancer cell lines [123, 124], and reduction in oxidative stress [125, 126]. The mechanism of resveratrol's action is not yet clear for its beneficial health effects. Thus, it will give further room to investigate and know the mechanism of resveratrol beneficial activity. This will lead to the development of either stilbene-resveratrol based or novel molecules that can mimic the effects of resveratrol whilist improving the physicochemical properties. Presently there is no known mechanism for resveratrol's beneficial effects but it is thought that it may operate through SIRT1 enzyme activation [127].

1.6. Biological activities of resveratrol derivatives:

Resveratrol anti-cancer activity was first reported by Jang and co-worker [128] where resveratrol was found to protect mice from skin cancer. Numerous *in-vitro* study reports on resveratrol have shown that it prevents cancer by producing cell cycle arrest in the cancer cell. The mechanism for its anti-cancer activity is still unclear and found to be executed through various pathways such as COX inhibition, aromatase and quinone reductase, nuclear factor kappa B (NFκB) activation and nitric oxidase inhibition [129]. Recently, resveratrol derivatives were found to be exhibit higher anticancer activity than

resveratrol, See **Figure 1-10**. These *trans*-stilbene derivatives inhibit growth of various cancer cells through mediating similar pathways to resveratrol [130].

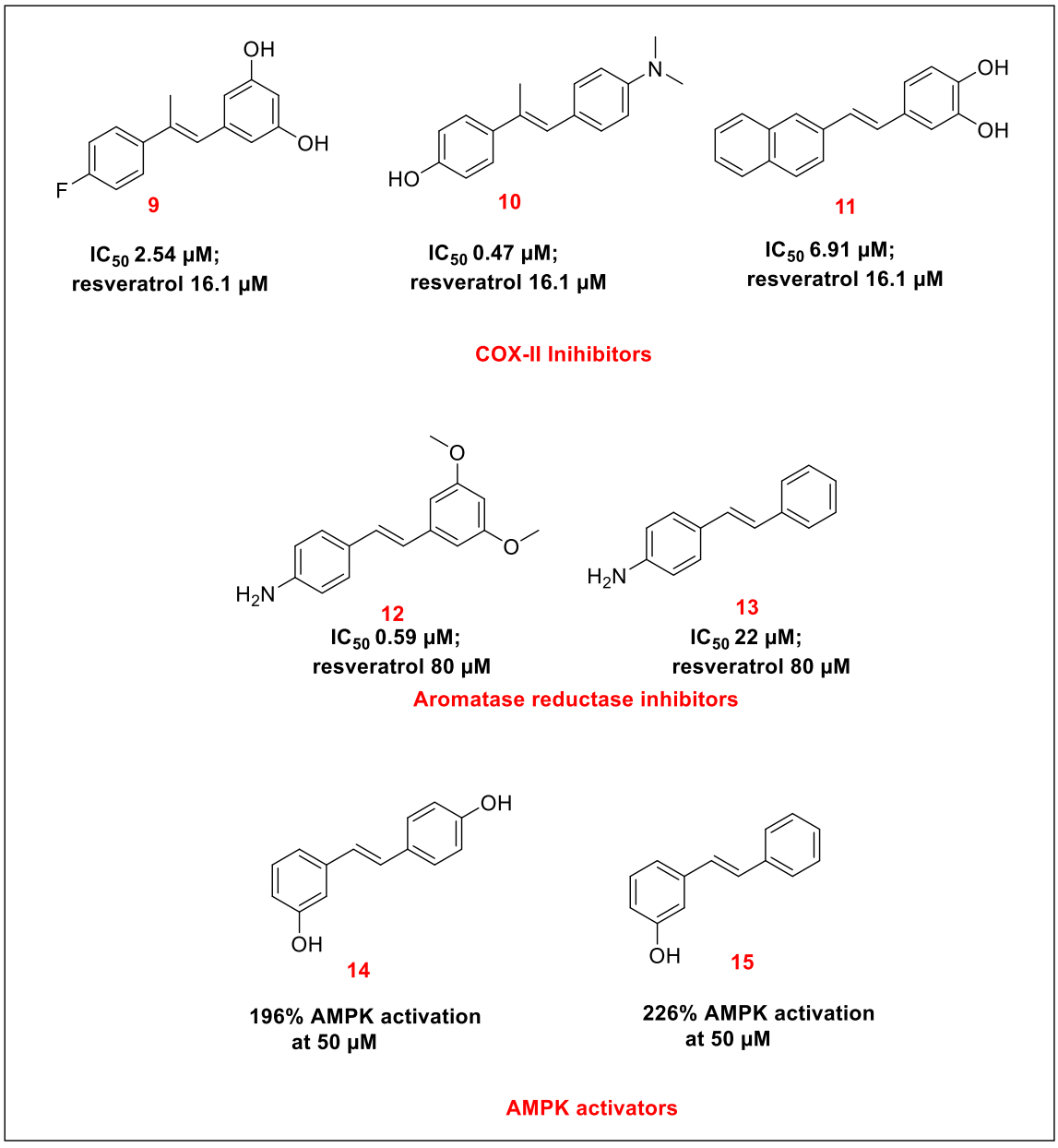

Figure 1-10: Reported beneficial biological activities of *trans*-stilbenes such as anti-cancer through inhibition of COX-II, aromatase reductase and anti-diabetes through AMPK activation.

COX are cyclooxygenase enzymes that catalyse the biotransformation of prostaglandins (PGs) from arachidonic acid. It exists in two isoforms COX-I and COX-II. COX activity was found to be increased in various cancer cells and its inhibition is considered as a target for anticancer drug development. *trans*-Stilbene based resveratrol derivatives were shown to inhibit both isoforms of COX. These derivatives were designed and synthesised either by replacing the 4′-hydroxy group of resveratrol, substituting the double bond or replacing one of the phenyl rings by a bicyclic ring, (**9**, **10**, **11**, see **Figure 1-10)**. The biological evaluation of these resveratrol derivatives has shown that some of them exhibit higher activity than resveratrol [131]. However, the evaluated derivatives were not isomerically (distereo-isomerically) pure as they were a mixture of *trans* and *cis* isomers. (90:10). Furthermore, some hydroxylated derivatives of resveratrol exhibited selectivity towards COX-II compared to COX-I. Aromatase and Quinone reductase were other possible pathways inhibited by resveratrol and its derivatives. Aromatase is an enzyme involved in the conversion of androgen to oestrogen, which is an important target for breast cancer [132]. The enzyme Quinone reductase is involved in the reduction of Quinone and recently it has been found that it might cause intracellular damage through reactive species generated during Quinone reduction [133]. Resveratrol derivatives were designed, synthesised and evaluated towards this target and found to be more potent inhibitors than resveratrol. The reported molecules were either substituted *trans*-stilbenes or amino *trans*-stilbenes, (**12**, **13**, see **Figure 1-10)** [132].

Other important age-related diseases includes diabetes and obesity. Insulin resistance is one of the physiological conditions that is observed in both of these. Resveratrol based molecules were synthesised both with and without a 4′-hydroxy group. These *trans*-stilbene resveratrol based molecules were investigated to study the inhibition of cell differentiation in 3T3-L1 cells and it was found that some of these molecules conferred higher protective effects than resveratrol. These analogues were further shown to improve the insulin resistance via AMPK activation (**14**, **15**, **Figure 1-10**). The *in-vivo* study of one analogue of resveratrol, called 3(OH) ST (**15**, **Figure 1-10**), was more effective than Resveratrol [134]. This study indicated that the position of the hydroxyl group on the *trans*-stilbene core played an important role in its activity. Additionally, *trans*-stilbene based urea derivatives were found to be inhibitors of glucosidase which is a useful target for the treatment of type II diabetes and obesity [135]. This study further suggested that

4′-substituted amino urea derivatives were found to be potent α-glucosidase inhibitors compared to resveratrol. (IC-50=8.4 μM; resveratrol IC50=26.4 μM).

The diseases related to dysfunction of brain or neurones are called neurodegenerative diseases. Neurodegenerative diseases such as Alzheimer's and Parkinson's diseases are well known pathological disorders associated with increased age. The histopathological evidence of AD showed the excessive accumulation two proteins called tau proteins and β-amyloid peptide (β-AB). This protein accumulation exerts inflammation that leads to dysfunctions of neurone cells. The imine derivatives of resveratrol, a modification of resveratrol double bond into imine bond (**16**, **Figure 1-11**), exerted neuroprotection. This imine derivatives more potent than resveratrol inhibited *in-vitro* beta-amyloid aggregation formation and showed neuroprotection in human SH-SY5Y neuroblastoma cells. Resveratrol was also found to reduce the risk of cardiovascular diseases. This might be mediated through increasing the induction of high-density protein (HDL)/ApoA-I gene expression [136]. Recently, Hansen and co-workers found that the *trans*-stilbene core bearing 4′-hydroxy group was found to be nearly 5 times more potent than resveratrol, (**17**, **18**, see **Figure 1-11).**

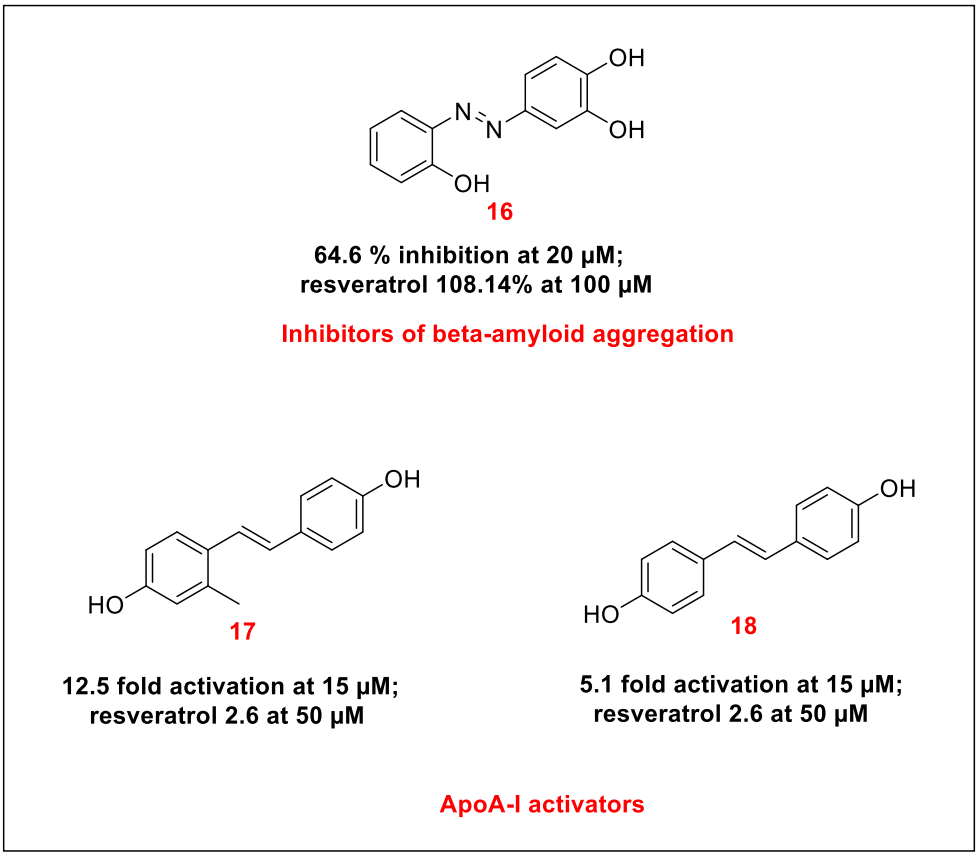

Figure 1-11: Neuroprotective and cardioprotective effects of resveratrol derivatives and their structures.

1.7. Synthesis of resveratrol derivatives:

Beneficial polyphenols such as resveratrol, pterostilbene, pinosylvin and piceid are belong to a class of stilbenoid polyphenols with *trans*-stilbene as the basic structural core. This core has attracted increasing attention over the past decade due to various beneficial biological properties. In addition, a large number of reports on resveratrol have suggested that its anti-ageing properties were due to reduction cancer, diabeties, neurodegenerative diseases and other age-related diseases and pathology [137]. Additionally, synthetic analogues of resveratrol were found to be more potent than resveratrol and found to exert similar beneficial effects to that of resveratrol. Further, naturally occurring *trans*-stilbenes such as resveratrol and its synthetic analogues have now been considered as potential anti-ageing molecules [137].

Althought existing research data on *trans*-stilbene resveratrol based molecules show they can inhibit the growth of a range of cancer cells. There have only been limited studies in

normal human cells. In addition, low bioavailability and fast metabolism are considered as major drawbacks of resveratrol [138]. To overcome these drawbacks further development of novel resveralogues could overcome the detrimental features. But, one major problem with developing new analogues is the existing synthetic methods.

trans-1,2-diphenylethene is the basic structural unit in a wide variety of naturally-occurring molecules. These, and synthetic analogues, have been deployed in photochemical dyes and fluorescent whitening agents [139], polymeric materials [140], [141], and are the subject of intense interest as potential leads for drug discovery as a consequence of their anticancer [142], [143] anti-inflammatory [144] and antioxidant properties [145]. Perhaps the best known of these is *trans*-3,5,4′-trihydroxystilbene (resveratrol), which has shown potential clinical value as a dietary restriction mimetic. Such mimetics are thought to slow down the rate of deleterious processes associated with ageing and thus have the potential to prevent, or even remediate, multiple age-associated degenerative pathologies, including cognitive impairment, arthritis, cardiovascular disease and immune dysfunction [87], [59]. However, the synthesis of new analogues were found to be inconvenient due to the use of catalytic methods and inert conditions in synthesis. *trans*-stilbene derivatives are generally synthesised utilising Wittig (**IN1** and **IN2**, **Figure 1-12**) or Horner- Wadsworth- Emmons (HWE) reactions (**IN3** and **IN2**, **Figure 1-12**) and through catalytic methods such as Heck (**IN5** and **IN6**, **Figure 1-12**), Suzuki (**IN7** and **IN8**, **Figure 1-12**) and Negishi coupling reactions or through the use of organozinc reagents (**IN4** and **IN2**, **Figure 1-12**) [146].

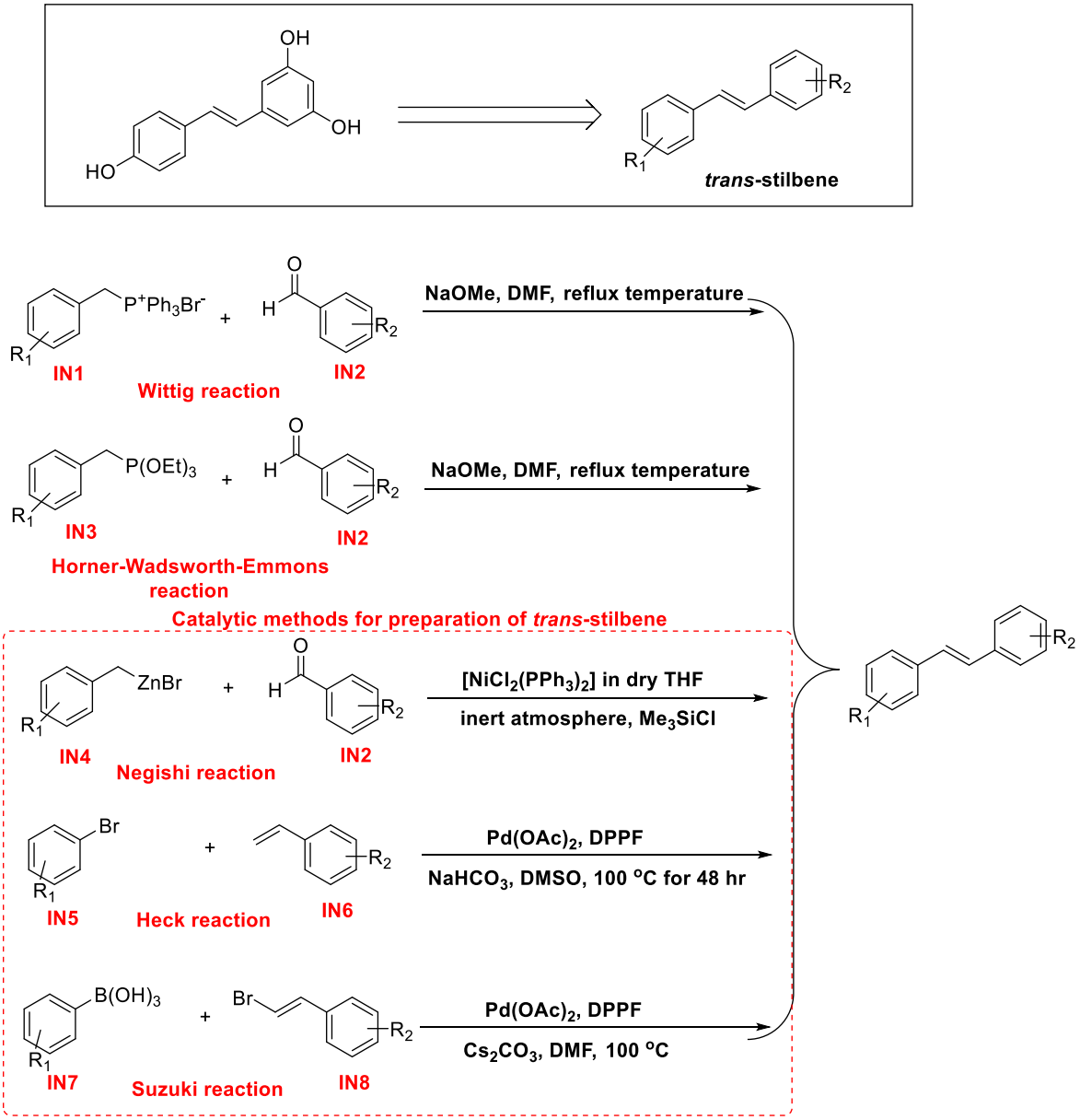

Figure 1-12 Important synthetic routes for synthesis of *trans*-stilbene derivatives includes Wittig, Horner-Wadsworth-Emmons reaction and catalytic methods such as Negishi, Heck and Suzuki reaction.

Many of the examples in the literature suffer from incomplete conversion and low yields, or poor stereoselectivity. Of the existing methods, three have been previously modified to one-pot syntheses. These utilised the oxidative Wittig-Heck reaction [147] [148] two sequential Heck-type reactions of aryl bromide [149] and organozinc reagents [146] (see, **Figure 1-13**). Although some of these protocols provide good yields, they tend to require costly organometallic catalysts, inert reaction conditions, large excesses of reagents [149], long reaction times (>40 hours in some instances) and/or complex solvent mixtures.

trans-stilbenes thus represent attractive scaffolds for future compound development. However, resveratrol itself has been shown to have a range of activities, some of which may actually be detrimental to health. Equally, resveratrol is very limited in its bioavailability and, taken together, these issues leave uncertainties about its likely *in vivo* modes of action and consequent clinical utility. There is, therefore, a need for simple and versatile syntheses of a wide variety of structural analogues of resveratrol, or resveralogues, in order to facilitate detailed investigation of stilbenoid structure-activity relationships, and to allow development of potential therapeutic compounds with improved bioavailability.

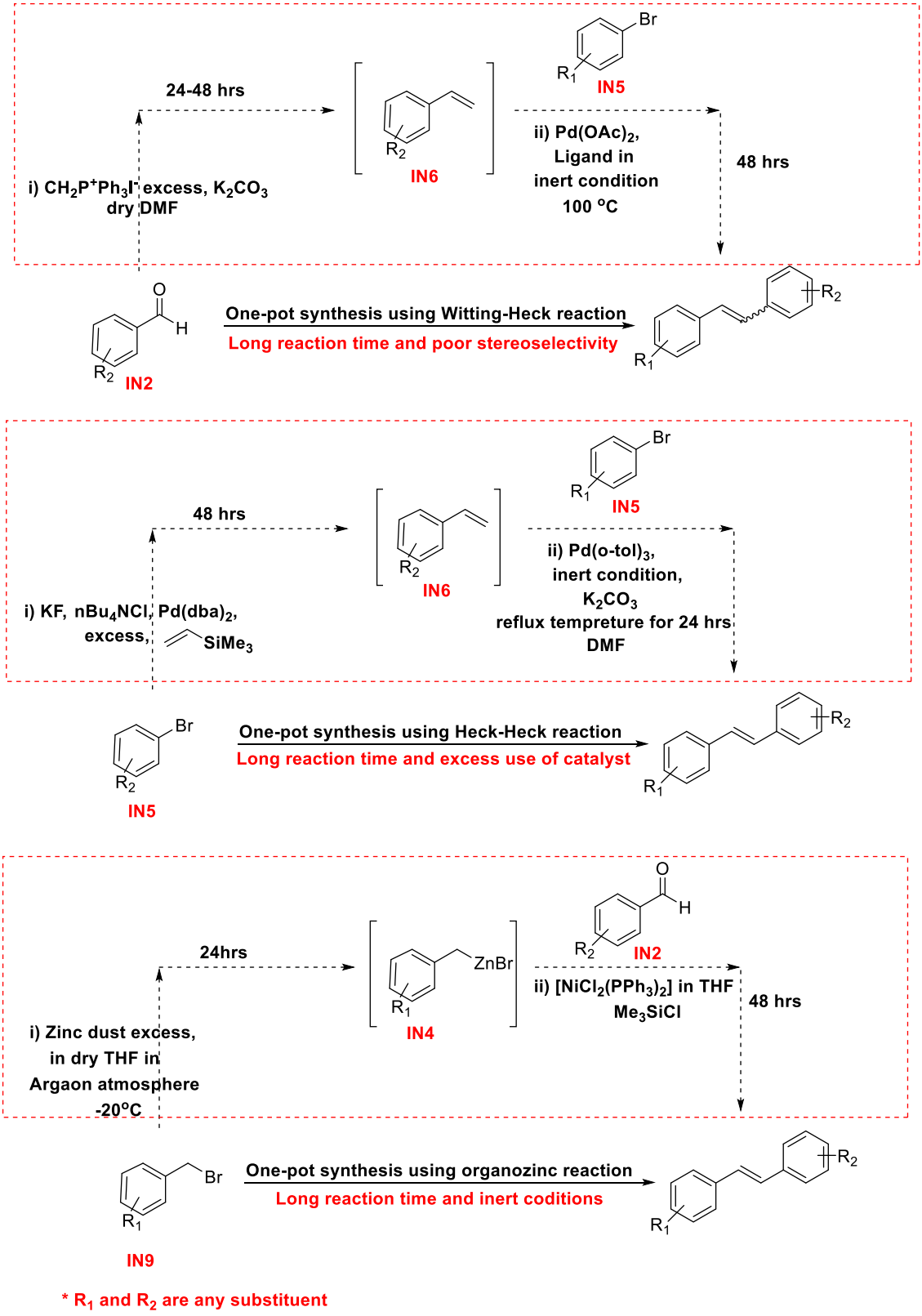

Figure 1-13 Exsisting one-pot synthesis of *trans*-stilbenes and their limitations.

1.8. Detrimental activity of resveratrol and *trans*-stilbenes:

The existing *in-vitro* and *in-vivo* research data suggested that resveratrol and *trans*-stilbenes show beneficial health effects. However, these derivatives have been found to exert detrimental activities such toxicity, premature senescence and DNA damage, fast metabolism and low bioavailability. The literature supports putative anti-cancer properties of resveratrol and these might be one of the features of resveratrol to be considered as anti-ageing. However, the concentration required to inhibit tumour cell growth (IC_{50}=13-43 μM) was much higher than that which inhibited normal cell growth. (IC_{50}=8 μM). Resveratrol was suggested as an anticancer agent as it inhibits growth in a range of cancer cell lines effectively. However, this growth suppressive effect was observed *in-vitro* using an immortal cell line. Unfortunately, very rare data are available on primary cell strains which could be a bettermodel for normal *in-vivo* study. Resveratrol has been found to induce senescence in primary human cells at and above 25 μM concentration. Resveratrol and its synthetic stilbenes are very well known for their anti-oxidant activity. However, these stilbene analogues including resveratrol exert a pro-oxidant effect at higher concentrations such as 50 μM and above. It has been observed that antioxidant molecules mediate pro-oxidant effects at higher concentration due to generating reactive oxygen species. Resveratrol has been reported to show beneficial effects at low concentration and detrimental effects at higher concentration. Recently, resveratrol was found to induce senescence in normal primary human cells at and above 25 μM concentration [150]. This might be due to some structural features in resveratrol that could induce a pro-oxidant effect at higher concentration. Furthermore, *in-vitro* studies of 4′-hydroxy analogues and stilbenes bearing two *ortho*-hydroxyl groups were found to increase the genotoxic stress in various cancer cells. The major cause of genotoxic stress involves damage to cellular DNA through generation of reactive oxygen species. Therefore, similar pathways might be observed in normal human cells. SIRT1 activation is thought to be considered as an anti-ageing target for resveratrol which was found to increase the SIRT1 activation 13-fold at 50 μM concentration. However, the concentration of resveratrol that activates SIRT1 also triggers human cells in culture to undergo premature senescence. Therefore, this conflicts with the anti-ageing properties of resveratrol as senescent cells contribute to ageing.

1.9. Design strategies for novel resveralogues:

The goal of this project was to design and synthesise a range of molecules that were bioavailable, non-toxic and not cytostatic maintaining SIRT1 activity and potentially reducing IL-6 release. In addition, an attempt would be made to probe structure-activity relationships of resveralogues. The overall designs based on resveratrol are discussed in **Section 1.9.1, 1.9.2**, **1.9.3** and **1.9.4**.

1.9.1. 4′-hydroxy substituted analogues of resveratrol:

One of the strategies to develop more potent analogues of resveratrol was to produce analogues, replacing the free hydroxyl group with a corresponding methyl ether or with fluoro groups (**19** and **20**, **Figure 1-14**); alternatively increasing the number of hydroxyl groups (**22**, **Figure 1-14**) on a *trans*-stilbene core and replacing the double bond by an amide which has shown promising results, see **Figure 1-14** [130]. The methoxylated resveratrol derivatives were found to be more cytotoxic to numerous cancer cells than resveratrol e.g. the trimethoxy analogues of resveratrol (**21**, **Figure 1-14**) exhibited more potent growth inhibitory activity than the parent resveratrol with close IC_{50} value to the anticancer drug vinorelbine (22.7 μM, 2.9 μM, 2.5 μM GI_{50} value in case of resveratrol, methoxy analogues of resveratrol and Vinorelbine respectively) [151]. In addition to this, several other substituted methoxy derivatives of resveratrol have also shown great inhibitory potential in various carcinogenic cells line [130]. Further, an increased number of hydroxyl or respective methoxy substituted resveratrol derivatives (**21**, **22**, **Figure 1-14**) resulted in more potent anti-tumor activity than resveratrol. An *in-vitro* study suggested that these molecules induce apoptosis and cell cycle arrest in various cancer cell lines [152]. Furthermore, the 3,5 dihydroxy *trans*-stilbene moiety of resveratrol is crucial for its biological activity and therefore, this structural feature was retained while designing new resveratrol based molecules [130, 153].

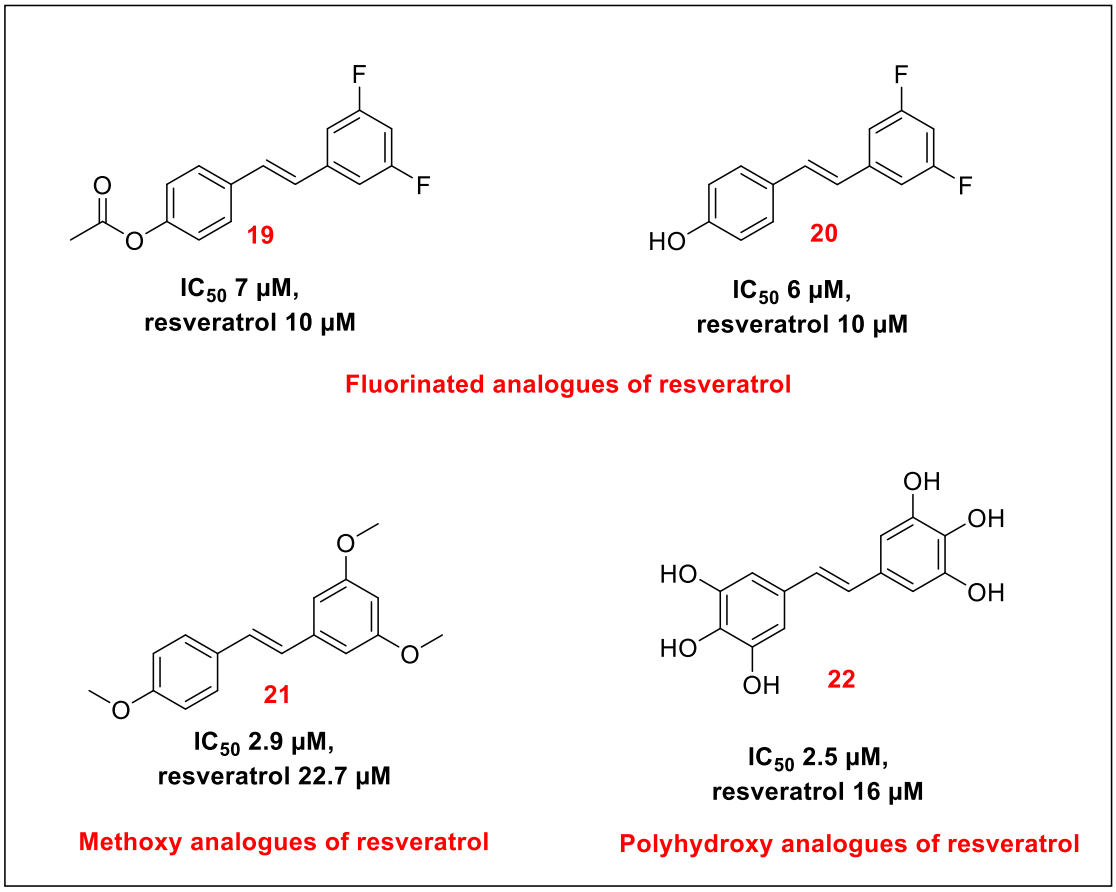

Figure 1-14 Effect of structural changes such as fluorinated, methoxy derivatives of resveratrol on anti-cancer activity.

Fast metabolism and low bioavailability is a major drawback of resveratrol and hence methylated derivatives would be designed in order to overcome the existing problems with resveratrol. Furthermore, substituents on the *trans*-stilbene core are known to increase biological activity, especially anti-cancer activity [130]. In this project various electron-donating and electron-withdrawing substituted resveratrol derivatives would be designed in order to investigate the steric and electronic effects on function particularly the relationship between SIRT1 activity and toxicity. The synthesis of designed molecules was planned as per the retrosynthetic analysis shown in **Figure 1-15** and suggested that the stilbene core could be synthesised from corresponding benzyl bromide and aldehyde.

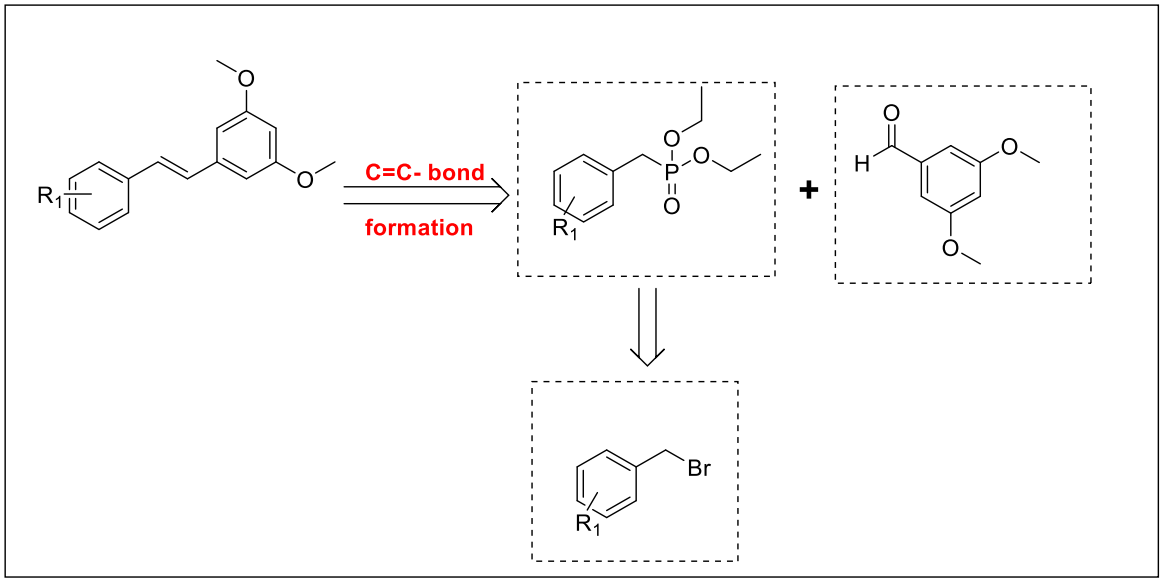

Figure 1-15: Retrosynthetic analysis for 4′-substituted resveratrol derivatives.

1.9.2. Design of amino derivatives based on resveratrol:

The second synthetic strategy was to design novel amino resveralogues in order to better understand the bioisosteric replacement of hydroxyl group. The *trans*-stilbene core and 3- and 5-hydroxl groups of resveratrol have been shown to be crucial for SIRT1 activation [74]. Therefore, the 4′-hydroxy group modification is amenable for novel and informative functionalisation of resveratrol. Additionally, *trans*-stilbenes bearing 4′-hydroxy groups have been found to induce genotoxic stress by damaging DNA at higher concentrations [154, 155]. One of the plausible mechanisms behind this toxicity might be the stability of the radicals formed. There is almost no literature on amino isosteric resveratrol derivatives. Various amino substituted derivatives of resveratrol (4′- and 2′- substituted) were synthesised to evaluate the role of substitution in cell growth and SIRT1 activation. The amino resveratrol derivatives will be used to investigate the effect of the hydroxyl replacement on SIRT1 activation. Further, 2′-substituted amino-derivatives were planned in order to understand the role of planarity of the molecule and role of the amide bond towards the SIRT1 activation.

The retrosynthetic analysis of amino resveratrol is shown in **Figure 1-16.** The 4′- and 2′-substituted amino resveralogues could be prepared from the corresponding nitro-resveratrol. This part of the project was based on the bioisosteric replacement of 4′-hydroxy with an amino group to further understand the role of functional group substitution. There is almost no literature available on amino derivatives of resveratrol and no literature reports on their SIRT1 activity and effects on cell cycle. Novel amino

derivatives of resveratrol were designed to provide replacement of the 4′-hydroxyl group by a bioisosteric group amine group (NH).

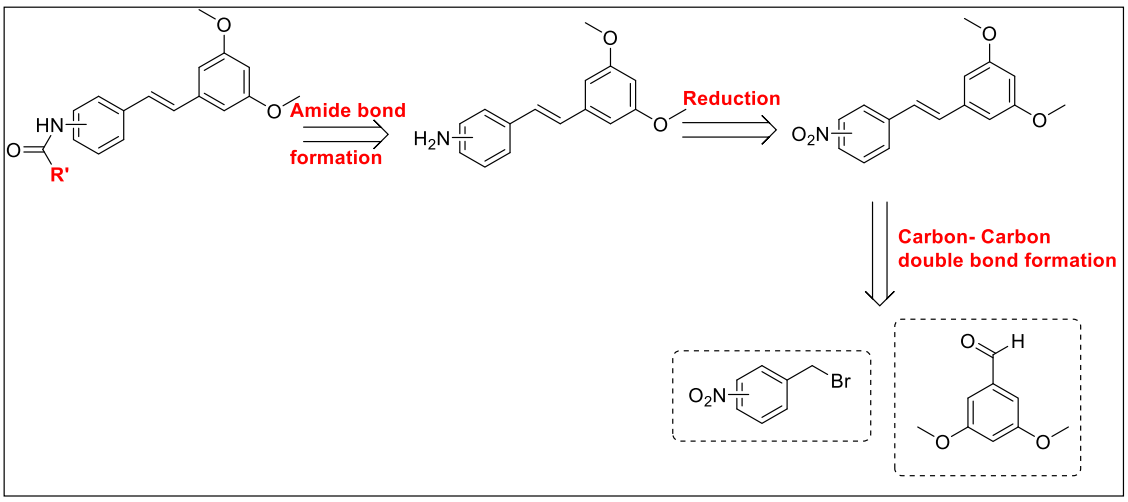

Figure 1-16: Retrosynthetic analysis of substituted amino resveratrol derivatives.

1.9.3. Design of heterocyclic substituted analogues of resveratrol:

In 2007, small molecules which were structurally very closely related to resveratrol were identified as potent SIRT1 activators (**6**, **7**, **23** in **Figure 1-17**). These molecules were found to be up to 1000 times more potent than resveratrol [79]. The most potent activators are shown below in **Figure 1-17** highlighting the basic structure core required for SIRT1 activation.

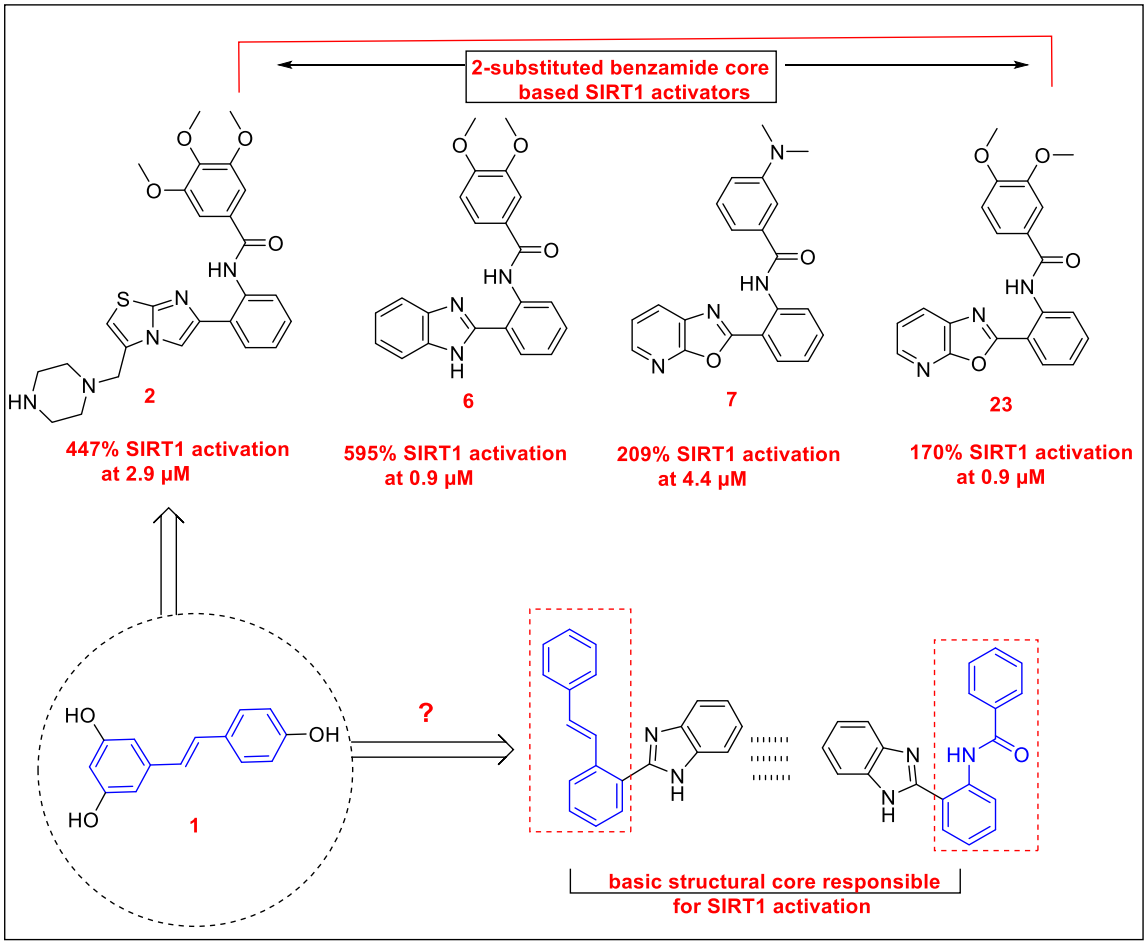

Figure 1-17 Design strategies for development of novel resveratrol based potential SIRT1 activators.

Resveratrol was shown to increase SIRT1 activation 13 fold at 100 µM. However, at and above 25 µM concentration resveratrol induced permanent cell growth arrest and premature senescence in primary human cells [150]. The design strategy is described in **Figure 1-18.** The most potent SIRT1 activators are substituted phenyl substituted benzamide core derivatives with five-membered or fused five member heterocycle at either 2′-position or 3′-position .(see **Figure 1-18**) This forms the basis for designing novel resveratrol based non-planar molecules. Additionally, it will help to investigate substitution at 2′-position of *trans*-stilbene core causing torsional strain which will force the two aromatic rings to twist out of the plane and potentially reduce the toxicity or premature senescence of resveratrol by preventing DNA intercalation. The novel resveratrol derivatives could be synthesised by heterocyclic substitution at 2′-position of a *trans*-stilbene core. The novel 2′-substituted resveratrol based molecule with benzimidazole heterocyclic ring (**TM1, see Figure 1-18**) will be synthesised, as this heterocyclic core was found in potent activator of SIRT1. Similarly, novel 2′ and 4′-

substituted amide derivatives of amino resveratrol could be synthesised to understand the role of non-planarity as well as isosteric replacement off 4′-hydroxy in SIRT1 activation. **(TM2, see Figure 1-18).**

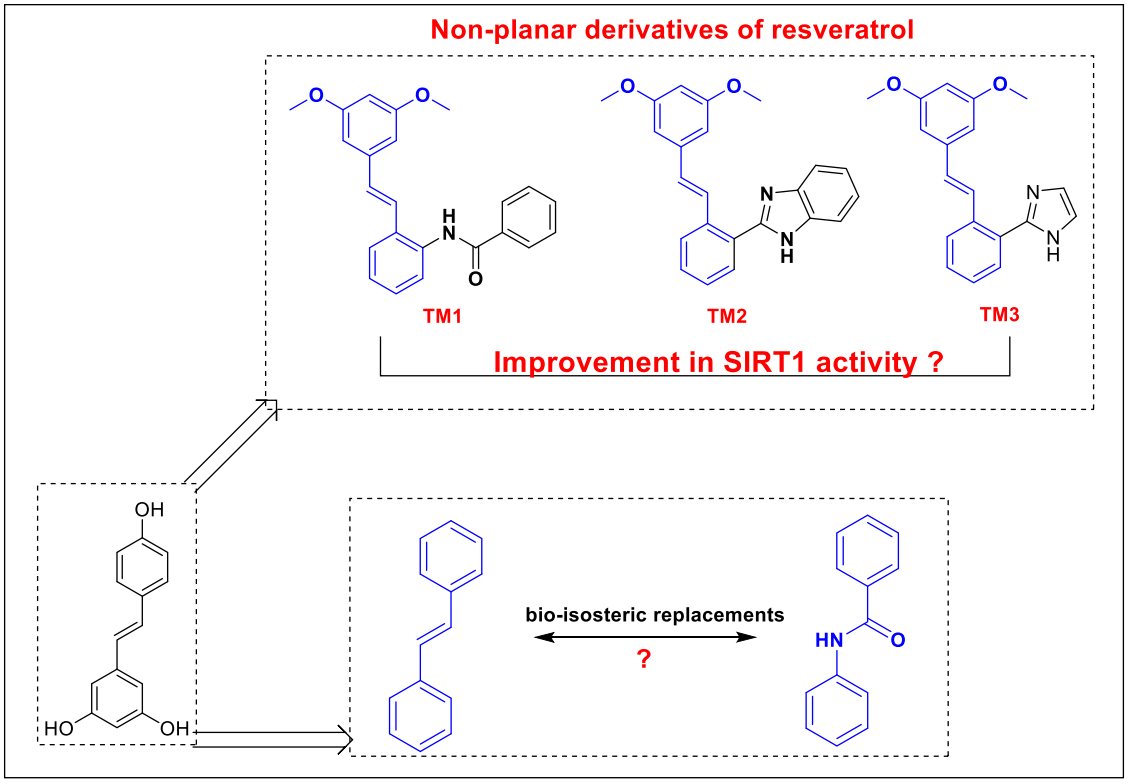

Figure 1-18: Design strategies behind novel resveratrol based molecules.

1,2-dihydroxy benzene group or 4′-hydroxy group on *trans*-stilbenes core was found to induce DNA damage and exert a pro-oxidant effect [154, 155]. Further, 3, 5 dihydroxy-catechol core of resveratrol was found to be important for SIRT1 activity. Hence, it was proposed that novel designed molecules retained the 3,5-dihydroxy catechol core of resveratrol but the 4′-hydroxy group of should be replaced by other substituents including both electron withdrawing and electron donating groups. In addition, novel heterocyclic based analogues were designed in order to investigate the role of five-membered imidazole ring substitution at 2′- and 4′-position of resveratrol. The designed was based on reported selective SIRT1 activators and secondly, to assay the role of planarity of resveratrol on SIRT1 activation.

1.9.4. 4′-substituted benzimidazole analogues of resveratrol:

The designed target molecule was based on earlier SIRT1 activators. The designed molecules had not been reported previously and there was no synthetic scheme available for these molecules. The retrosynthetic analysis is shown in **Figure 1-19** for the 4′-substituted benzimidazole derivatives (**TM4, Figure 1-19**). The stilbene core in target molecule **TM4** was planned from synthon 4′-substituted benzimidazole phosphonate (**IN10** see **Figure 1-19**) and 3,5-dimethoxy benzaldehyde. The benzimidazole phosphonate intermediate (**IN10**, **Figure 1-19**) was planned from corresponding intermediate (**IN11**, **Figure 1-19**) and the 1,2-diaminobenezene using the coupling and cyclisation reaction reported in earlier reports.

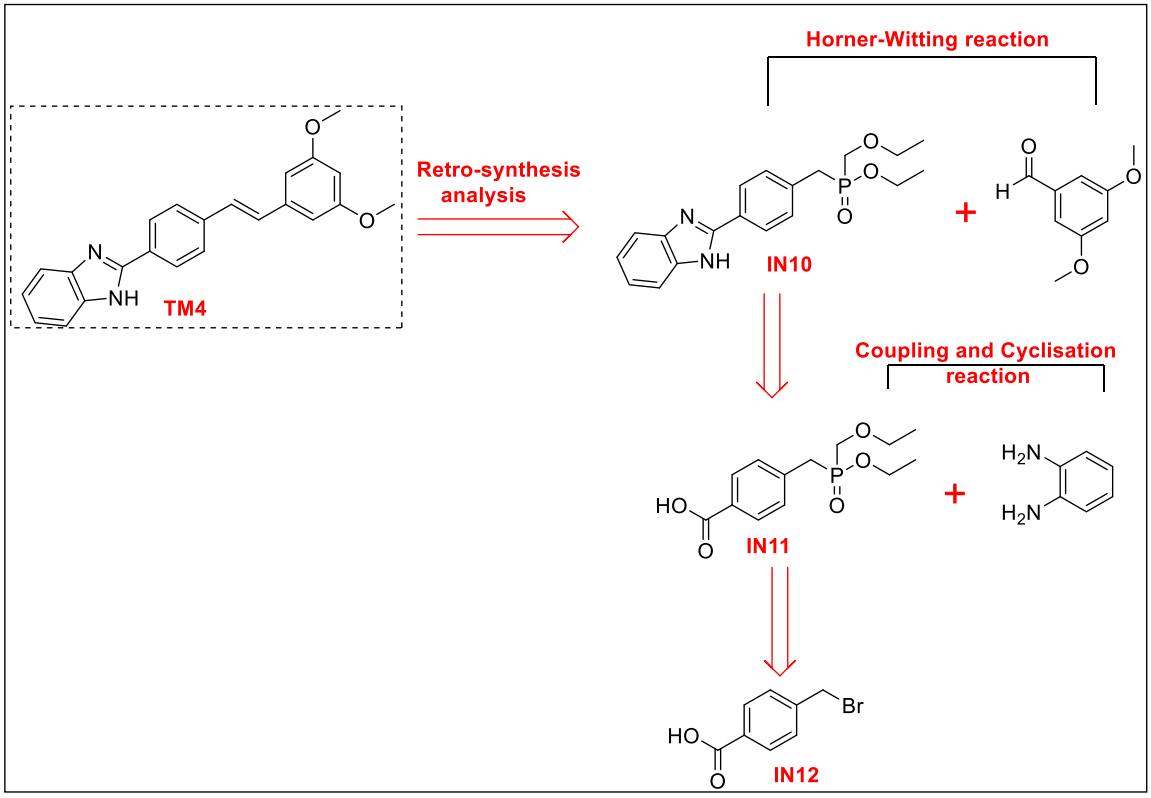

Figure 1-19: Retrosynthetic analysis of 4′-substituted benzimidazole resveratrol derivatives.

Similarly, the 2′-substituted benzimidazole resveratrol (**TM2, Figure 1-20**) derivatives were planned using the retrosynthetic scheme described in **Figure 1-20**. The retrosynthetic analysis was planned from corresponding acid derivatives and the 1,2-diaminobenezene. The intermediate acid (**IN13**) shown in **Figure 1-20** could be prepared from 2′-cyano resveratrol derivatives which were prepared from initial carbon-carbon double bond formation reaction.

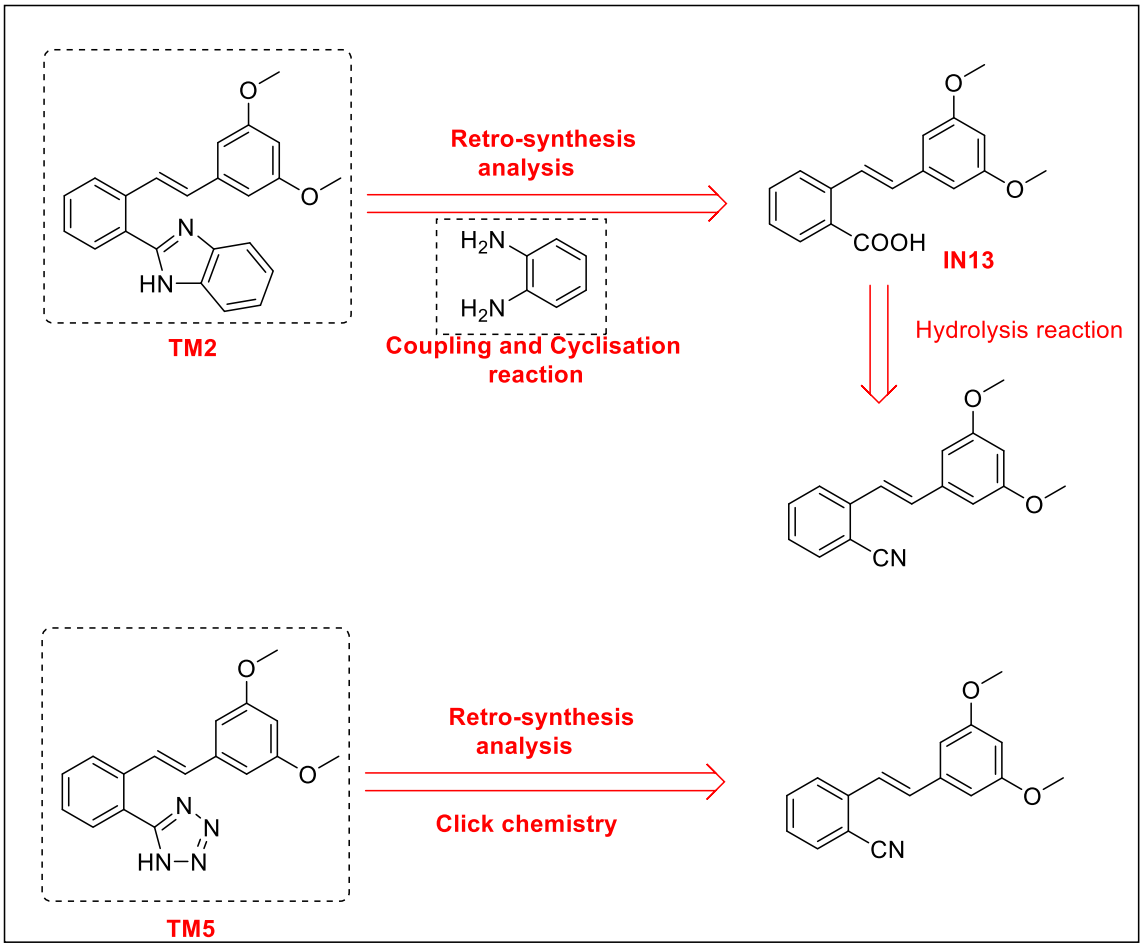

Figure 1-20: Retrosynthetic analysis of 2′-substituted heterocyclic resveratrol derivatives.

1.10. Project Aims:

Overall aims of this project were to:

i) Develop an improved synthetic route towards resveratrol derivatives or resveralogues.

ii) Design and synthesise a range of novel resveralogues that involves
   a) 4′-hydroxy substituted resveratrol derivatives in order to understand steric and electronic effects of substituents.
   b) 4′-amino substituted resveratrol derivatives.
   c) Non-planar resveratrol derivatives including 2′-substituted heterocyclic derivatives and other amino derivatives.

iii) Evaluate the effect of synthesised compounds on primary human cells; including their toxicity, propensity to induce cellular senescence, effects on SIRT1 activity and pro-inflammatory cytokine release (IL6).

iv) Develop a multidimensional predictive model of the key structural features of resveratrol derivatives.

Chapter 2. Chemistry methods

2.1. Materials:

All the solvents and starting reagents were obtained commercially and used directly without purification. The NMR spectra of compounds were recorded on Brüker FT-^{1}H NMR at 400 MHz and ^{13}C NMR at 100 MHz spectrometer in $CDCl_3$ and DMSO-d_6 using Tetramethylsilane (TMS) as an internal standard. The δ values represent chemical shifts reported in parts per million (ppm) and coupling constant (*J*) value in (Hz). ESI-HRMS were recorded on Brüker MicroTOF. Melting points were recorded at University of Brighton, Brighton and they were all uncorrected. Flash chromatography was conducted on Silica (100-200 mesh). Thin layer chromatography was performed on TLC Silica Gel 60 F254 (Merck).

The successful synthesis schemes described in this chapter are summarised in following schemes. A total of 43 compounds were synthesised and characterised, 20 of which are entirely novel and others had no prior data relating to their biological activities.

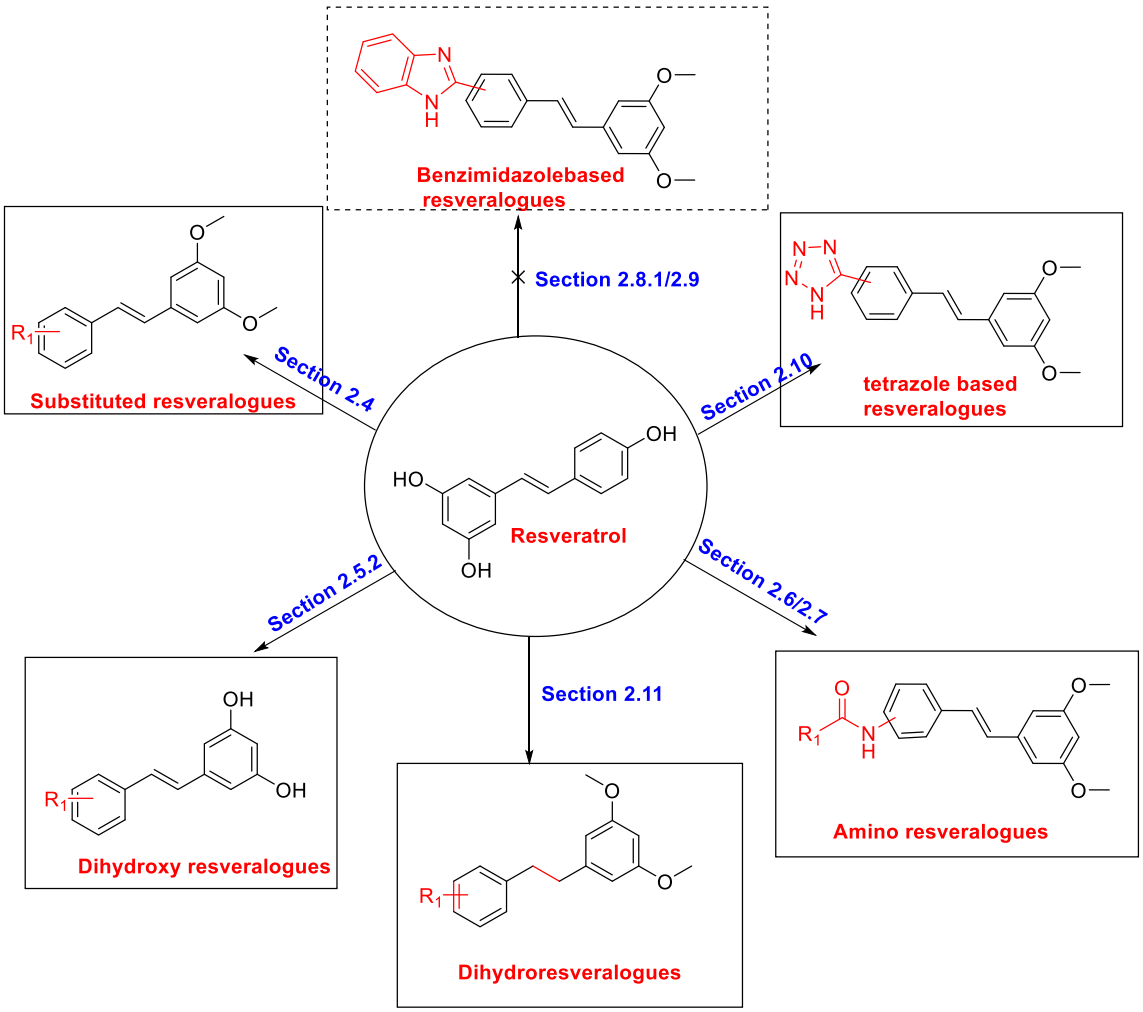

Scheme 2-1 Overall summary of novel modifications in resveratrol.

2.2. Synthesis of 'resveralogues':

2.2.1. Attempted synthesis using organozinc reagent methods:

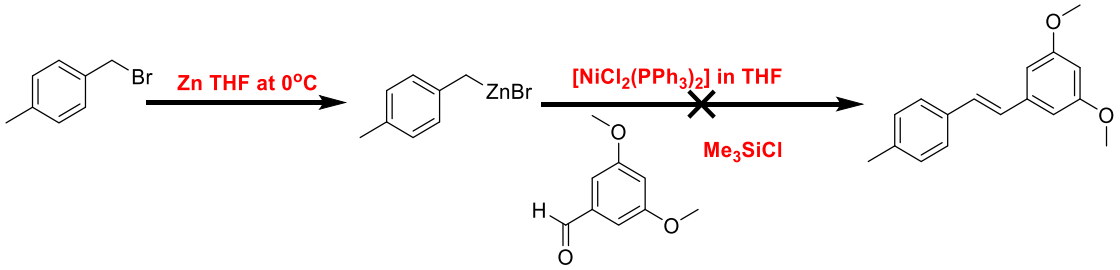

Zinc dust (0.53 g, 8.10 mmol) in dry THF (1.5 ml) was added to a three-necked flask equipped with an argon inlet, a thermometer, and an addition funnel. A solution of the benzylic bromide (0.5 g, 2.7 mmol) in dry THF (5.5 mL) and DMSO (1.5 mL) was added dropwise at room temperature. The reaction mixture was stirred at room temperature for 22-24 hrs. Benzylzinc halides were prepared following Knochels procedure from above step. [19] $[NiCl_2(PPh3)_2]$ (0.2 g, 0.3 mmol) in THF (2 mL) was added to a solution of benzylzinc halides in THF at 0 °C. After stirring the mixture for 2 min, the reaction was allowed to reach room temperature. A solution of benzaldehyde (1.06 g, 10 mmol) and Me_3SiCl (2.18 g, 20 mmol) in THF (10 mL) was then added dropwise. The reaction mixture was stirred at room temperature for 8 h.

2.3. Method development for One-pot synthesis:

2.3.1. Stoichiometric use of $P(OEt)_3$:

The synthesis of intermediate phosphonate is synthesised from Michaelis–Arbuzov reaction in which the triphenylphosphine was heated with benzyl bromide. A simple and convenient one-pot method is developed using sequential Michaelis-Arbuzov rearrangement and HWE chemistry. The overall scheme of One-pot synthesis is illustrated **Scheme 2-2.**

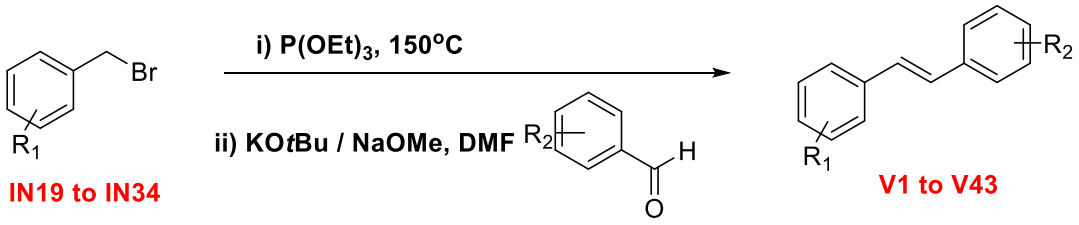

Scheme 2-2 Synthetic scheme of One-Pot synthesis.

We selected the Michaelis-Arbuzov rearrangement as the most versatile method available for the preparation of phosphonate esters [156, 157]. The overall mechanism for this reaction is shown in **Scheme 2-3**. In this step, we reacted our substituted benzyl bromide with a single molar equivalent of triethyl phosphite in the absence of solvent with heating to 150ºC. The developed protocol abrogates the need for the large excesses of triethyl phosphite utilised in earlier reports and also avoids potential by-product formed as a consequence of the reaction of ethyl bromide with the excess triethyl phosphite. The use of just one equivalent of triethyl phosphite in this part of the one pot synthesis does require an increased reaction time. The time to completion (as monitored by TLC) was increased by an insignificant margin (20-30 minutes) in the case of benzyl bromides bearing electron withdrawing groups in the 2- or 4- position, but more was more noticeable (4-5 hours) with the less reactive halides (see **Table 2-1**)

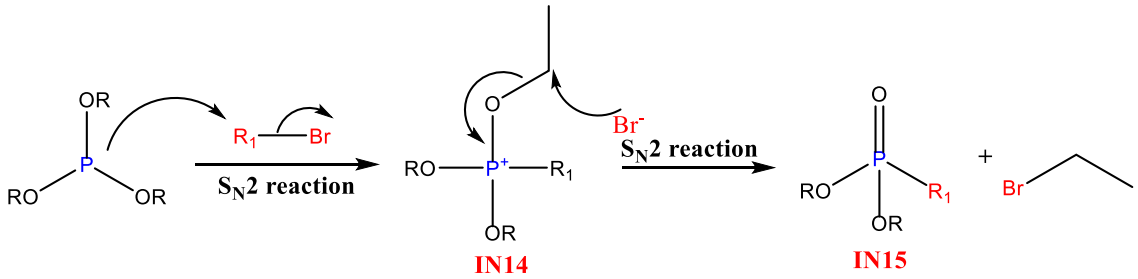

Where; R= CH_2CH_3 and R_1= substituted -CH_2Ph

Scheme 2-3 Overall mechanism of Michaelis-Arbuzov rearrangement. It involves the nucleophilic attack (S_N2 reaction) of phosphorous to the electrophilic carbon of aryl halide to give phosphonium intermediate (IN14). This intermediate again undergoes nucleophilic substitution reaction by attack of bromide to convert into corresponding phosphonate intermediate (IN15).

Table 2-1 : Effect of varying equivalents on triethyl phosphite on reaction time.

Substituent	Position of substituent	Time to completion in hours	
		2 equivalent of $P(OEt)_2$	1 equivalent of $P(OEt)_2$
$-NO_2$	2	4	4.2
-F	2	4.5	5.2
$-NO_2$	4	4	4.5
-CN	2	4.5	5
-Cl	3	5	11
-Me	4	5.5	10.2
-COOMe	4	5	6.2
-OMe	4	6	11
$-CF_3$	3	6.5	12

It is usual to isolate and then purify the diethyl phosphonate intermediate via column chromatography or distillation [158]. In our protocol, however, we continued directly to the HWE reaction, cooling to room temperature to add base and solvent and then introducing the required aldehyde after a short period stirring at room temperature. In most cases the conversion to *trans*-stilbene was complete after a further 12 h of heating to reflux, and the product could be crystallised directly from the reaction mixture by simple addition of ice and a small quantity of methanol. Where necessary, further purification was achieved by recrystallization from ethanol. The overall mechanism of Horner-Wadsworth-Emmons reaction is shown in **Scheme 2-4**.

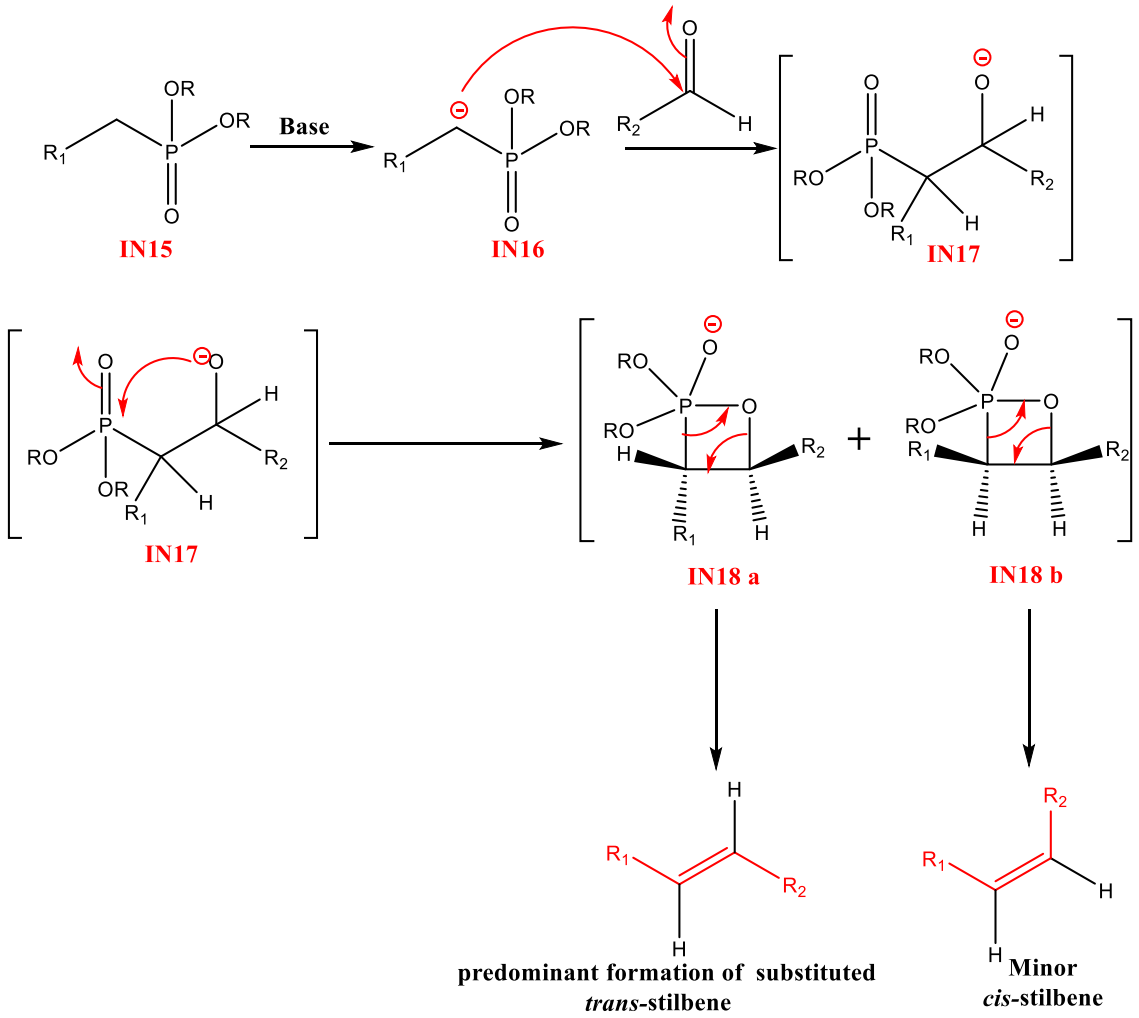

*** Where; R= CH_2CH_3; R_1= substituted phenyl group; R_2= substituted phenyl group;**

Scheme 2-4 Overall mechanism of Horner-Wadsworth-Emmons reaction and predominant formation of *trans*-stilbene. It involves the nucleophilic addition reaction of phosphonate (IN16, generated by deprotonation of IN15 using base) with aryl aldehyde to give intermediate (IN17). Intermediate (IN17) further undergoes intra-molecular nucleophilic addition reaction to the electrophlic phosphorous to give cyclic intermediate (IN18 a and IN18 b). Intermediates (IN18 a and IN18 undergo final elimination reaction to give predominantly *trans* isomer over *cis* isomer. (due to stablity of cyclic intermediate IN18 a over IN18 b).

2.3.2. Effect of Base:

The choice of the base was important to the success of the HWE reaction when conducted using one-pot synthesis. Initial reactions focused on the reaction of 2- and 4-substituted phosphonates (bearing electron withdrawing groups such as NO_2, F etc.) to give the relevant stilbenes and these proceeded readily to completion with the use of 1.2 equivalents of potassium *t*-butoxide as a base. However, when deactivating *meta* (e.g. V4, V7, V8, V17, V20 and V43) and/or electron donating substituents were present potassium *t*-butoxide was unsuccessful and a stronger base had to be used. We found that 1.1 equivalents of sodium methoxide were sufficient to ensure the reaction proceeded successfully when such groups were present, although in some cases the yield was a little reduced. (See **Table 2-2** for overall details and yields).

Table 2-2: Effect of base in one pot synthesis

Resveralogues	Substituent on benzyl bromide	Position of substituent	Base used	Isolated yield (%)
V1	-NO_2	4′-	KO*t*-Bu	90
V2	-F	2′-	KO*t*-Bu	74
V3	-OMe	4′-	NaOMe	60
V4	-Me	3′ & 5′-	NaOMe	81
V5	-F	2′ & 6′-	KO*t*-Bu	78
V6	-F	2′ & 4′-	KO*t*-Bu	74
V7	-Cl	3′-	NaOMe	77
V8	-CF_3	3′-	NaOMe	74
V9	-COOMe	4′-	NaOMe	59
V10	-CN	2′-	KO*t*-Bu	71
V14	-Me	4′-	NaOMe	84

V16	-NO_2	4′-	KO*t*-Bu	79
V17	-Cl	3′-	NaOMe	79
V18	-NO_2	2′-	KO*t*-Bu	79
V19	-CN	2′-	KO*t*-Bu	75
V20	-Cl	3′-	NaOMe	73
V21	-Cl	2′-, 6′-	NaOMe	79
V22	-NO_2	2′-	KO*t*-Bu	80
V25	-CN	2′-	KO*t*-Bu	85
V27	-NO_2	3′-	KO*t*-Bu	80
V28	-NO_2	4′-	KO*t*-Bu	80
V29	-no substituent	4′-	KO*t*-Bu	90
V33	-CN	4′-	KO*t*-Bu	80
V42	-no substituent	4′-	KO*t*-Bu	72
V43	-Cl	3′-	NaOMe	68

2.4. Synthesis of resveralogues using one-pot synthesis:

2.4.1. Synthesis of (*E*)-1,3-dimethoxy-5-(4-nitrostyryl)benzene (V1)

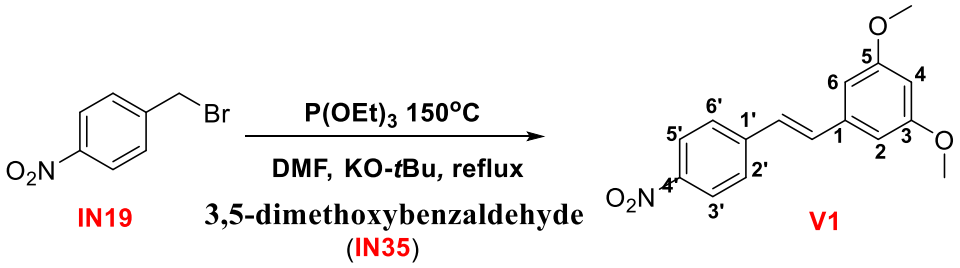

In a two-necked oven dried round-bottomed flask, the 1-(bromomethyl)-4-nitrobenzene (500 mg, 2.31 mmoles, IN19) and triethyl phosphite (0.4 mL, 2.31 mmol) were added

with N_2 purging. This reaction mixture was heated to 150 ^oC for 4-5 hours. The reaction was monitored by thin layer chromatography (eluent 10:90:: ethyl acetate: petroleum ether). After completion, the reaction mixture was cooled to room temperature and then diluted with *N, N* dimethylformamide (5 mL). KO*t*Bu (398 mg, 3.47 mmol) was added and stirred at the same temperature for 10 min. 3,5-dimethoxybenzaldehyde (300 mg, 1.85 mmol) was added to the reaction mixture which was then stirred at room temperature for one hour and then heated to reflux for 12 hours. The reaction was cooled to room temperature and quenched by adding ice and a small amount of methanol. The resulting yellow precipitate was then filtered and dried to give the crude stilbene as title product. The crude product was recrystallized from ethanol to give the fine and pure yellow crystals. (594 mg, 90% yield).

M.p. = 137-138 °C (literature m.p. = 135-137 °C [23]), Rf (10:90::ethyl acetate: petroleum ether) = 0.48, IR ν (cm^{-1}) = 3051, 2839, 1636, 1592, 1503, 1329, 1295, 1205, 1106, 948, 824, ^1H NMR (400 MHz, $CDCl_3$) δ (ppm) = 3.86 (6H, s, OMe), 6.47 (1H, t, *J*2.4 Hz, H4), 6.71 (2H, d, *J*2.4 Hz, H2, H6), 7.11 (1H, d, *J*18.0 Hz, -C=C-H), 7.20 (1H, d, *J*18.0 Hz, -C=C-H), 7.63 (2H, d, *J*9.7 Hz, H2', H6'), 8.22 (2H, d, *J*9.7 Hz, H3', H5'), ^{13}C NMR(100 MHz, $CDCl_3$) δ(ppm) = 55.4 (OMe), 101.0 (C4), 105.12 (C2, C6), 124.1 (C3', C5'), 126.8 (C=C), 126.9 (C2',C6'), 133.3 (C=C), 138.1 (C1'), 143.7 (C1), 146.8 (C4'), 161.1 (C3, C5). HRMS 308.08817 $[(M+Na)]^+$. **[See Appendix B page 225-227 for all spectra]**

2.4.2. Synthesis of (*E*)-1-(2-fluorostyryl)-3,5-dimethoxybenzene (V2)

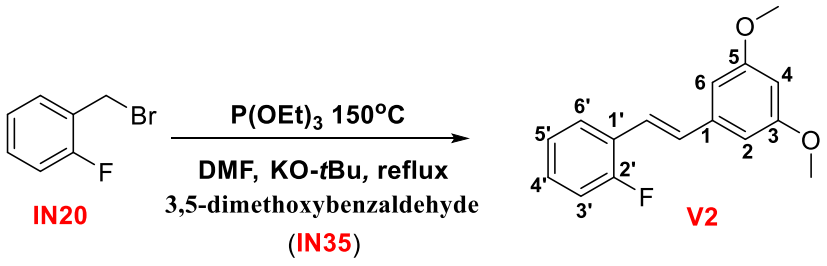

In a two-necked oven dried round-bottomed flask, the 1-(bromomethyl)-2-fluorobenzene (500 mg, 2.64 mmoles, IN20) and triethyl phosphite (0.46 mL, 2.64 mmoles) were added with N_2 purging. This reaction mixture was heated at 150 ^oC for 4-5 hours. The reaction was monitored by thin layer chromatography eluent (10:90:: ethyl acetate: petroleum ether). After completion, the reaction mixture was cooled to room temperature and then diluted with *N, N* dimethylformamide (5 mL). KO*t*Bu (450 mg, 3.96 mmoles) was added

and stirred at the same temperature for 10 min. 3,5-dimethoxybenzaldehyde (351 mg, 2.11 mmoles) was added to the reaction mixture which was then stirred at room temperature for one hour. Then it heated to reflux for 12 hours. The reaction was cooled to room temperature and quenched by adding ice and a small amount of methanol. The resulting yellow precipitate was then filtered and dried to give the crude stilbene as title product. The crude product was recrystallized from ethyl acetate to give the fine and pure white crystals. (505 mg, 74%)

M.p. = 62 °C, Rf (10:90::ethyl acetate: petroleum ether) = 0.64, IR ν (cm^{-1}) = 3001, 2997, 2954, 1590, 1488, 1357, 1152, 1053, 966, 825, 677, ^{1}H NMR (400 MHz, $CDCl_3$) δ (ppm) = 3.83 (6H, s, -OMe), 6.41 (1H, t, *J*2.2 Hz, H4), 6.69 (d, *J*2.2 Hz, H2, H6), 7.06 (1H, dd, *J*1.2/7.8 Hz, H3'), 7.09 (1H, dd, *J*1.2/8.4 Hz, H6'), 7.10 (1H, d, *J*16.4 Hz, -C=C-H), 7.24 (1H, d, *J*16.4 Hz, -C=C-H), 7.19-7.22 (1H, m, H5'), 7.59 (1H, td, *J*=7.7,1.6 Hz, H4'), ^{13}C NMR (100 MHz, $CDCl_3$) δ (ppm) = 55.4 (-OMe), 100.4 (C4), 104.8 (C2, C6), 115.8 (C3', J_{C-F} 21.9 Hz), 121.5 (C=C, J_{C-F} 3.1 Hz), 124.2 (C6', J_{C-F} 3.1 Hz), 125.1 (C1', J_{C-F} 11.7 Hz), 127.2 (C4', J_{C-F} 3.5 Hz), 128.9 (C5', J_{C-F} 8.5 Hz), 131.0 (C=C, J_{C-F} 4.7 Hz), 139.3 (C1), 161.0 (C3, C5), 160.5 (C2', J_{C-F} 247.9 Hz). HRMS 281.07161 $[(M+Na)]^{+}$. **[see Appendix B 228-230 for all spectra]**

2.4.3. Synthesis of Synthesis of (E)-1,3-dimethoxy-5-(4 methoxystyryl)benzene (V3)

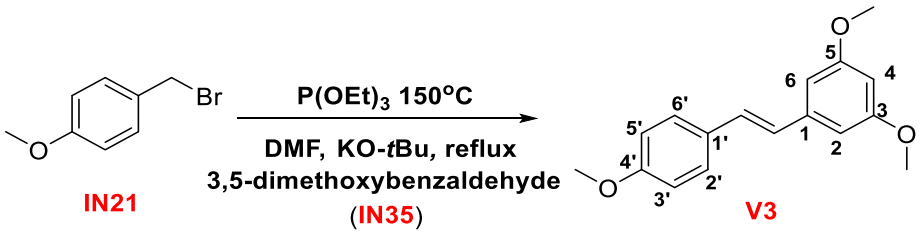

In a two-necked oven dried round-bottomed flask, the 1-(bromomethyl)-2-fluorobenzene (500 mg, 2.48 mmol, IN21) and triethyl phosphite (0.46 mL, 2.64 mmol) were added with N_2 purging. This reaction mixture was heated to 150 °C for 4-5 hours. The reaction was monitored by thin layer chromatography eluent (10:90:: ethyl acetate: petroleum ether). After completion, the reaction mixture was cooled to room temperature and then diluted with *N, N* dimethylformamide (5 mL). KO*t*Bu (450 mg, 3.96 mmol) was added and stirred at the same temperature for 10 min. 3,5-dimethoxybenzaldehyde (351 mg, 2.11 mmol) was added to the reaction mixture which was then stirred at room temperature for one hour. Then it was heated to reflux for 12 hours. The reaction was cooled to room

temperature and quenched by adding ice and a small amount of methanol. The resulting yellow precipitate was then filtered and dried to give the crude stilbene as title product. The crude product was recrystallized from ethyl acetate to give the fine and pure white crystals. (403 mg, 60%)

M.p. = 59-61 °C (literature m.p. = 55-58 °C, [21]), Rf (10:90::ethyl acetate: petroleum ether) = 0.48, IR ν (cm^{-1}) = 2960, 2912, 2837, 1605, 1517, 1442, 1239, 965, 824, ^{1}H NMR (400 MHz, $CDCl_3$) δ (ppm) = 3.83 (9H, s, -OMe), 6.38 (1H, t, *J*2.0 Hz, H4), 6.65 (2H, d, *J*2.0 Hz, H2, H6), 6.89 (2H, d, *J*8.8 Hz, H2', H6'), 6.90 (1H, d, *J*16.2 Hz, -C=C-H), 7.04 (1H, d, *J*16.2 Hz, -C=C-H), 7.44 (d, *J*8.8 Hz, H3', H5'), ^{13}C NMR (100 MHz, $CDCl_3$) δ(ppm) = 55.3 (OMe), 55.4 (2xOMe), 99.7 (C4), 104.4 (C2, C6), 114.2 (C2', C6'), 126.6 (C=C), 127.8 (C3',C5'), 128.8 (C=C), 130.0 (C1'), 139.7 (C1), 159.4 (C4'), 161.0 (C3, C5). HRMS 293.09290 $[(M + Na)]^{+}$. **[See Appendix B 231-233 for all spectra].**

2.4.4. Synthesis of (*E*)-1-(3,5-dimethoxystyryl)-3,5-dimethylbenzene (V4)

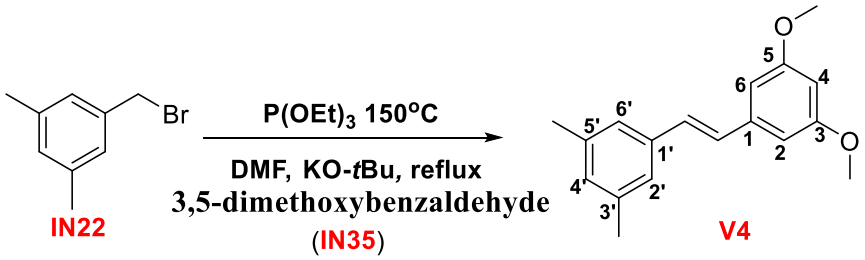

In a two-necked oven dried round-bottomed flask, the 1-(bromomethyl)-3,5-dimethylbenzene (500 mg, 2.51 mmol, IN22) and triethyl phosphite (0.43 mL, 2.51 mmol) were added with N_2 purging. This reaction mixture was heated to 150 ºC for 4-5 hours. The reaction was monitored by thin layer chromatography eluent (10:90:: ethyl acetate: petroleum ether). After completion, the reaction mixture was cooled to room temperature and then diluted with *N*, *N* dimethylformamide (5 mL). NaOMe (200 mg, 3.76 mmol) was added and stirred at the same temperature for 10 min. 3,5-dimethoxybenzaldehyde (331 mg, 2.00 mmol) was added to the reaction mixture which was then stirred at room temperature for one hour. Then it was heated to reflux for 12 hours. The reaction was cooled to room temperature and quenched by adding ice and a small amount of methanol. The resulting yellow precipitate was then filtered and dried to give the crude stilbene as title product. The crude product was recrystallized from ethyl acetate to give the fine and pure white crystals. (545 mg, 81%)

M.p. = 66-68 °C, Rf (10:90::ethyl acetate: petroleum ether) = 0.47, IR ν (cm^{-1}) = 3256, 3009, 2923, 1598, 1463, 1326, 1164, 1071, 962, 839, 690, ^{1}H NMR (400 MHz, d_6-DMSO) δ (ppm) = 2.29 (6H, s, CH_3), 3.78 (6H, s, OMe), 6.40 (1H, t, *J*2.4 Hz, H4), 6.75 (2H, d, *J*2.4 Hz, H2, H6), 6.91 (broad s, H4'), 7.11 (1H, d, *J*16.4 Hz, C=C-H), 7.18 (1H, d, *J*16.4 Hz, C=C-H), 7.25 (broad s, H2', H6'), ^{13}C NMR (100 MHz, d_6-DMSO) δ (ppm) = 20.9 (Me), 55.1 (OMe), 99.8 (C4), 104.3 (C2, C6), 124.3 (C2', C6'), 128.0 (C=C), 129.0 (C=C), 129.2 (C4'), 136.7 (C1'), 137.5 (C3', C5'), 139.1 (C1), 160.6 (C3, C5). HRMS 291.13523 $[(M+Na)]^+$. **[See Appendix B page 234-236 for all spectra]**

2.4.5. Synthesis of (*E*)-2-(3,5-dimethoxystyryl)-1,3-difluorobenzene (V5)

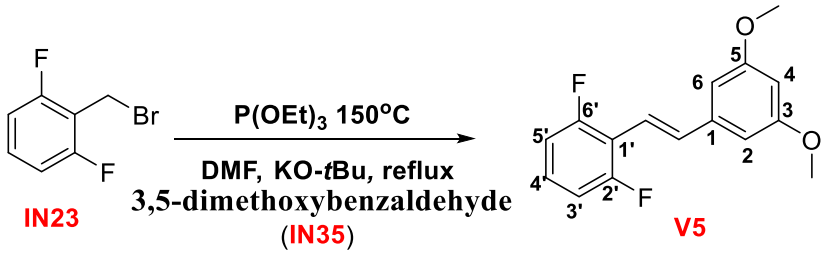

In a two-necked oven dried round-bottomed flask, the 2-(bromomethyl)-1,3-difluorobenzene (500 mg, 2.41 mmol, IN23) and triethyl phosphite (0.41 mL, 2.41 mmol) were added with N_2 purging. This reaction mixture was heated to 150 °C for 4-5 hours. The reaction was monitored by thin layer chromatography eluent (10:90:: ethyl acetate: petroleum ether). After completion, the reaction mixture was cooled to room temperature and then diluted with *N, N* dimethylformamide (5 mL). KO*t*Bu (406 mg, 3.62 mmol) was added and stirred at the same temperature for 10 min. 3,5-dimethoxybenzaldehyde (321 mg, 1.93 mmol) was added to the reaction mixture which was then stirred at room temperature for one hour. Then it was heated to reflux for 12 hours. The reaction was quenched cooled to room temperature by adding ice and a small amount of methanol. The resulting yellow precipitate was then filtered and dried to give the crude stilbene as title product. The crude product was recrystallized from ethyl acetate to give the fine and pure white crystals. (520 mg, 78%)

M.p. 85-86 °C, Rf (10:90::ethyl acetate: petroleum ether) = 0.64, IR ν (cm^{-1}) = 3009, 2973, 2844, 1589, 1463, 1306, 1200, 1152, 979, 788, 682, ^{1}H NMR (400 MHz, $CDCl_3$) δ (ppm) = 3.83 (6H, s, OMe), 6.43 (1H, t, *J*2.2 Hz, H4), 6.69 (2H, d, *J*2.2 Hz, H2, H6), 6.92 (2H, t, *J*8.4 Hz, H3', H5'), 7.10 (d, *J*16.8 Hz, -C=C-H) 7.15 (1H, tt, *J*8.4, 8.4 Hz, H4'), 7.37 (1H, d, *J* 16.4Hz, -C=C-H), ^{13}C NMR (100 MHz, $CDCl_3$) δ (ppm) = 55.4 (OMe),

100.6 (C4), 104.7 (C2, C6), 111.7 (C3', C5', J_{C-F}6.47 Hz), 114.7 (C1', J_{C-F}15.1 Hz), 115.7 (C=C), 128.0 (C4', J_{C-F}10.7 Hz), 135.1 (C=C, J_{C-F}8.35 Hz), 139.6 (C1), 160.9 (C2', C6', J_{C-F}250, 7.7 Hz), 161.0 (C3, C5). HRMS 299.10582 $[(M+Na)]^+$. **[see the Appendix A page 237-239 for all spectra]**

2.4.6. Synthesis of (*E*)-1-(3,5-dimethoxystyryl)-2,4-difluorobenzene (V6)

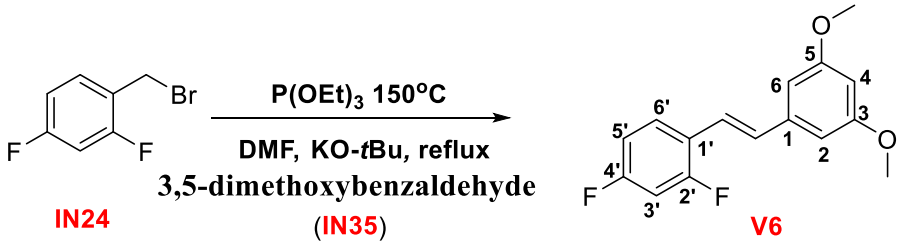

In a two-necked oven dried round-bottomed flask, the 1-(bromomethyl)-2,4-difluorobenzene (500 mg, 2.41 mmol, IN24) and triethyl phosphite (0.42 mL, 2.41 mmol) were added with N_2 purging. This reaction mixture was heated to 150 °C for 4-5 hours. The reaction was monitored by thin layer chromatography eluent (10:90:: ethyl acetate: petroleum ether). After completion, the reaction mixture was cooled to room temperature and then diluted with *N, N* dimethylformamide (5 mL). KO*t*Bu (406 mg, 3.62mmol) was added and stirred at the same temperature for 10 min. 3,5-dimethoxybenzaldehyde (320 mg, 1.93 mmol) was added to the reaction mixture which was then stirred at room temperature for one hour. Then it was heated to reflux for 12 hours. The reaction was quenched cooled to room temperature by adding ice and a small amount of methanol. The resulting yellow precipitate was then filtered and dried to give the crude stilbene as title product. The crude product was recrystallized from ethyl acetate to give the fine white crystals. (494 mg, 74%)

M.p. 85-86 °C, Rf (10:90::ethyl acetate: petroleum ether) = 0.64, IR ν (cm^{-1}) = 3009, 2973, 2844, 1589, 1463, 1306, 1200, 1152, 979, 788, 682, ^{1}H NMR (400 MHz, $CDCl_3$) δ (ppm) = 3.83 (6H, s, OMe), 6.43 (1H, t, *J*2.2 Hz, H4), 6.69 (2H, d, *J*2.2 Hz, H2, H6), 6.92 (2H, t, *J*8.4 Hz, H3', H5'), 7.10 (d, *J*16.8 Hz, -C=C-H) 7.15 (1H, tt, *J*8.4, 8.4 Hz, H4'), 7.37 (1H, d, *J*16.4 Hz, -C=C-H), ^{13}C NMR (100 MHz, $CDCl_3$) δ (ppm) = 55.4 (OMe), 100.6 (C4), 104.7 (C2, C6), 111.7 (C3', C5', J_{C-F}6.47 Hz), 114.7 (C1', J_{C-F}15.1 Hz), 115.7 (C=C), 128.0 (C4', J_{C-F}10.7 Hz), 135.1 (C=C, J_{C-F}8.35 Hz), 139.6 (C1), 160.9 (C2', C6', J_{C-F}250, 7.7 Hz), 161.0 (C3, C5). HRMS 299.10582 $[(M+Na)]^+$. **[see the Appendix A page 240-242 for all spectra]**

2.4.7. Synthesis of (*E*)-1-chloro-3-(4-methoxystyryl)benzene (V7)

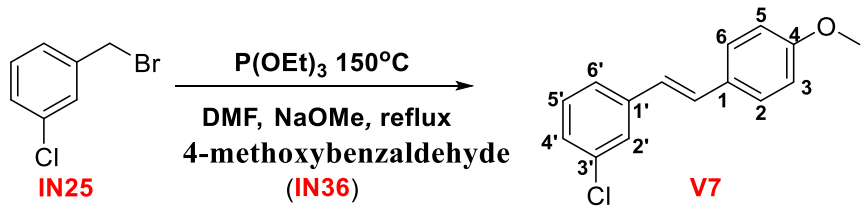

In a two-necked oven dried round-bottomed flask, the 1-(bromomethyl)-3-chlorobenzene (500 mg, 2.43 mmol, IN25) and triethyl phosphite (0.42 mL, 2.43 mmol) were added with N_2 purging. This reaction mixture was heated to 150 °C for 4-5 hours. The reaction was monitored by thin layer chromatography eluent (10:90:: ethyl acetate: petroleum ether). After completion, the reaction mixture was cooled to room temperature and then diluted with *N, N* dimethylformamide (5 mL). NaOMe (197 mg, 3.64 mmol) was added and stirred at the same temperature for 10 min. 4-methoxybenzaldehyde (323 mg, 1.94 mmol) was added to the reaction mixture which was then stirred at room temperature for one hour. Then it was heated to reflux for 12 hours. The reaction was quenched cooled to room temperature by adding ice and a small amount of methanol. The resulting yellow precipitate was then filtered and dried to give the crude stilbene as title product. The crude product was recrystallized from ethyl acetate to give the brown crystals (506 mg, 85%).

M.p. =91-93 °C (literature m.p. = 96 °C [159]), Rf (10:90::ethyl acetate: petroleum ether) =0.4, IR ν (cm^{-1}) = 3016, 2933, 2836, 1588, 1560, 1258, 1034, 966, 825, 680. ^{1}H NMR (400 MHz, $CDCl_3$) δ (ppm) = 3.83 (3H, s, OMe), 6.92-6.87 (3H, m, H2, H6 and -C=C-H), 7.05 (1H, d, *J*16.4 Hz, -C=C-H), 7.19 (1H, dq, *J*1.2 and 7.6 Hz, H4'), 7.26 (1H, t, *J*7.6 Hz, H2'), 7.34 (1H, dt, *J*1.6 and 8 Hz, H5'), 7.48-7.43 (1H, m, H2', H3 and H5), ^{13}C NMR (100 MHz, $CDCl_3$) δ (ppm) = 55.3 (OMe), 55.3 (OMe), 114.2(C2, C6), 124.5(C5'), 125.1(-C=C-H), 126.(C2'), 127.1(C4'), 127.1(C4'), 127.9(C2,C5), 129.7(-C=C-H), 129.8(C1), 134.6(C1'), 139.6(C3'), 159.7(C4). HRMS no expected peak was found. **[see the Appendix B page 243-245 for all spectra.]**

2.4.8. Synthesis of (*E*)-N,N-dimethyl-4-(3-(trifluoromethyl)styryl)aniline (V8)

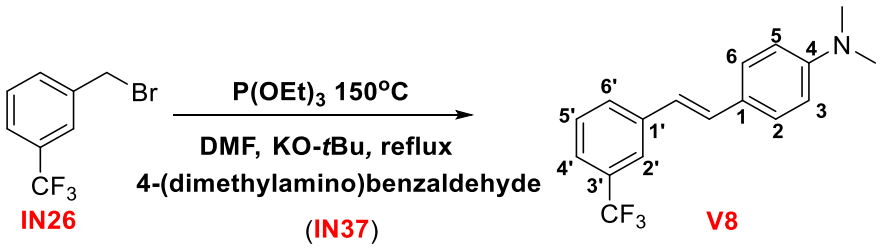

In a two-necked oven dried round-bottomed flask, the 1-(bromomethyl)-3-(trifluoromethyl)benzene (500 mg, 2.09 mmoles, IN26) and triethyl phosphite (0.41 mL, 2.09 mmoles) were added with N_2 purging. This reaction mixture was heated at 150 ^oC for 4-5 hours. The reaction was monitored by thin layer chromatography eluent (10:90:: ethyl acetate: petroleum ether). After completion, the reaction mixture was cooled to room temperature and then diluted with *N, N* Dimethylformamide (5 mL). NaOMe (169 mg, 3.13 mmol) was added and stirred at the same temperature for 10 min. 4-(dimethylamino)benzaldehyde (249 mg, 1.67 mmol) was added to the reaction mixture which was then stirred at room temperature for one hour. Then it was heated to reflux for 12 hours. The reaction was cooled to room temperature and quenched by adding ice and a small amount of methanol. The resulting yellow precipitate was then filtered and dried to give the crude stilbene as title product. The crude product was recrystallized from ethyl acetate to give the fine and pure white crystals. (450 mg, 74%)

M.p. = 146 °C, Rf (10:90::ethyl acetate: petroleum ether) = 0.56, IR ν (cm^{-1}) = 3026, 2810, 1601, 1521, 1327, 1115, 1071, 965, ^1H NMR (400 MHz, $CDCl_3$) δ (ppm) = 2.99 (6H, s, -$N(CH_3)_2$), 6.72 (2H, dd, *J*7.2, 2.0 Hz, H2, H6), 6.91 (1H, d, *J*16.0 Hz, -C=C-H), 7.10 (1H, d, *J*16.0 Hz, -C=C-H), 7.40-7.44 (4H, m, H4', H6', H3, H5), 7.62 (1H, distorted t, H5'), 7.70 (1H, s, H2'), ^{13}C NMR (100 MHz, $CDCl_3$) δ (ppm) = 40.4 ($N(CH_3)_2$), 112.4 (C2, C6), 122.5 (C2', $J_{C\text{-}F}$ 3 Hz), 122.7 (C=C), 123.0 (C4', $J_{C\text{-}F}$ 3 Hz), 124.3 (CF_3, $J_{C\text{-}F}$ 272 Hz), 125.3 (C1'), 127.9 (C3, C5), 129.0 (C6'), 130.8 (C=C), 131.0 (C3', $J_{C\text{-}F}$ 32 Hz), 139.1 (C1), 150.5 (C4). HRMS 292.13062 $[(M+H)]^+$. [**see Appendix B page 246-248 for all spectra.**]

2.4.9. Synthesis of methyl (*E*)-4-(3,5-dimethoxystyryl)benzoate (V9)

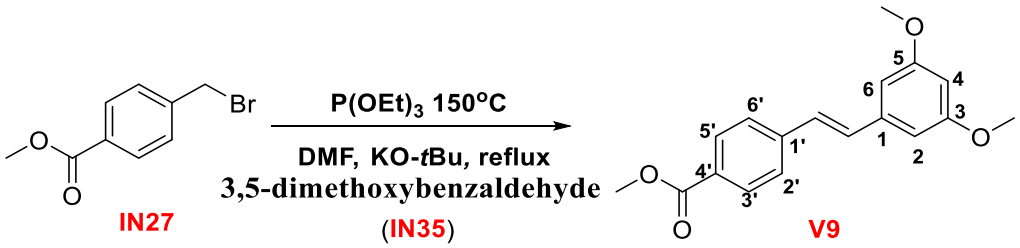

In a two-necked oven dried round-bottomed flask, the methyl 4-(bromomethyl)benzoate (500 mg, 2.18 mmoles, IN27) and triethyl phosphite (0.37 mL, 2.18 mmoles) were added with N_2 purging. This reaction mixture was heated to 150 ºC for 4-5 hours. The reaction was monitored by thin layer chromatography eluent (10:90:: ethyl acetate: petroleum ether). After completion, the reaction mixture was cooled to room temperature and then diluted with *N, N* dimethylformamide (5 mL). KO*t*Bu (367 mg, 3.27 mmoles) was added and stirred at the same temperature for 10 min. 3,5-dimethoxybenzaldehyde (289 mg, 2.18 mmoles) was added to the reaction mixture which was then stirred at room temperature for one hour. Then it was heated to reflux for 12 hours. The reaction was cooled to room temperature and quenched by adding ice and a small amount of methanol. The resulting yellow precipitate was then filtered and dried to give the crude stilbene as title product. The crude product was recrystallized from ethyl acetate to give white crystals. (384 mg, 59%)

M.p.=121-122 ºC (literature m.p.=117-121 ºC,[160]), Rf (10:90::ethyl acetate:petroleum ether) = 0.51, IR ν (cm^{-1}) = 3080, 2999, 2945, 1708, 1587, 1433, 1273, 1152, 966, 697, ^{1}H NMR (400 MHz, $CDCl_3$) δ (ppm) = 3.83 (6H, s, OMe), 3.92 (3H, s, COOMe), 6.43 (1H, t, *J*2.2 Hz, H4), 6.69 (2H, d, *J*2.2 Hz, H2, H6), 7.08 (1H, d, *J*16.4 Hz, -C=C-H), 7.14 (1H, d, *J*16.4 Hz, -C=C-H), 7.55 (2H, d, *J*8.3Hz, H2', H6'), 8.02 (d, *J*8.2 Hz, H3', H5'), ^{13}C NMR (100 MHz, $CDCl_3$) δ (ppm) = 52.1 (COOMe), 55.4 (OMe), 100.6 (C4), 104.9 (C2, C6), 126.4 (C2', C6'), 128.1 (C=C), 129.0 (C1'), 130.03 (C3',C5'), 131.2 (C=C), 138.8 (C1), 141.65 (C4'), 161.1 (C3, C5), 166.8 (COOMe). HRMS 321.10598 [(M + Na)]$^+$ and 619.22537 [(2M + Na)]$^+$. **[see the Appendix B page 249-251 for all spectra.]**

2.4.10. Synthesis of (*E*)-2-(3,5-dimethoxystyryl)benzonitrile (V10)

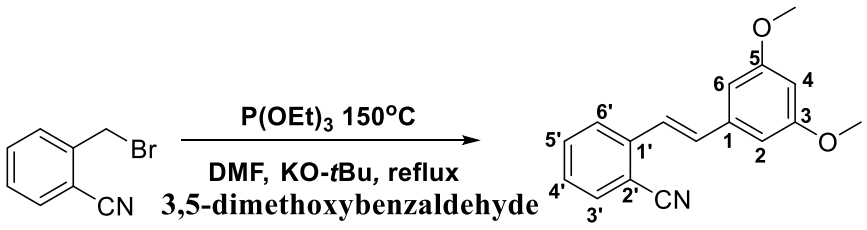

In a two-necked oven dried round-bottomed flask, the 2-(bromomethyl)benzonitrile (500 mg, 2.55 mmol, IN28) and triethyl phosphite (0.44 mL, 2.55 mmol) were added with N_2 purging. This reaction mixture was heated to 150 °C for 4-5 hours. The reaction was monitored by thin layer chromatography eluent (10:90:: ethyl acetate: petroleum Ether). After completion, the reaction mixture was cooled to room temperature and then diluted with *N, N* dimethylformamide (5 mL). KO*t*Bu (429 mg, 3.82 mmol) was added and stirred at the same temperature for 10 min. 3,5-dimethoxybenzaldehyde (338 mg, 2.04 mmol) was added to the reaction mixture which was then stirred at room temperature for one hour. After this time it was heated to reflux for 12 hours. The reaction was cooled to room temperature and quenched by adding ice and a small amount of methanol. The resulting yellow precipitate was then filtered and dried to give the crude stilbene as title product. The crude product was recrystallized from ethyl acetate to give the fine and pure white crystals. (478 mg, 71%)

M.p. = 72-73 °C, Rf (10:90::ethyl acetate: petroleum ether) = 0.27, IR ν (cm^{-1}) = 3068, 2948, 2838, 2219, 1588, 1425, 1352, 1152, 1056, 958, 755, ^{1}H NMR (400 MHz, $CDCl_3$) δ (ppm) = 3.84 (6H, s, -OMe), 6.45 (1H, t, *J*2 Hz, H4), 6.72 (2H, d, *J*2Hz, H2, H6), 7.19 (1H, d, *J*16 Hz, -C=C-H), 7.33 (1H, td, *J*7.6,1.1 Hz, H4'), 7.41 (1H, d, *J*16 Hz, -C=C-H), 7.57 (1H, td, *J*7.6, 1 Hz, H5'), 7.65 (1H, dd, *J*8.0, 1.0 Hz, H6'), 7.78 (1H, d, *J*8.0 Hz, H3'). ^{13}C NMR (100 MHz, $CDCl_3$) δ (ppm) = 55.4 (OMe), 101.2 (C4), 105.2 (C2, C6), 111.3 (C2'), 117.4 (CN), 124.6 (C=C), 125.4 (C3'), 127.6 (C4'), 132.7 (C5'), 133.2 (C6'), 133.5 (C=C), 138.2 (C1'), 140.4 (C1), 161.1 (C3, C5). HRMS 288.09945 $[(M+Na)]^+$ and 553.20737 $[2M+Na]^+$. **[see Appendix A page 252-254 for all spectra.]**

2.4.11. Synthesis of (*E*)-1,3-dimethoxy-5-(4-methylstyryl)benzene (V14)

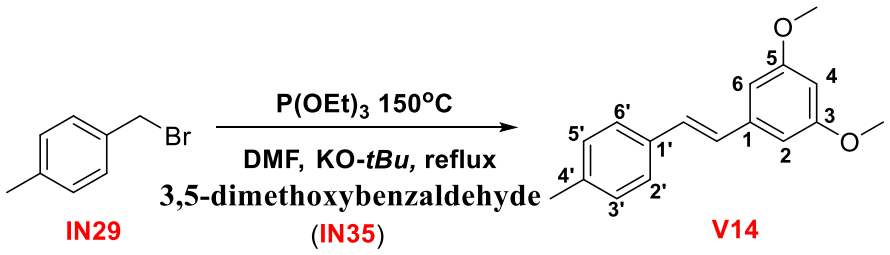

In a two-necked oven dried round-bottomed flask, the 2-(bromomethyl)-1,3-difluorobenzene (500 mg, 2.7 mmol, IN29) and triethyl phosphite (0.47 mL, 2.7 mmol) were added with N_2 purging. This reaction mixture was heated to 150 ^oC for 4-5 hours. The reaction was monitored by thin layer chromatography eluent (10:90:: ethyl acetate: petroleum ether). After completion, the reaction mixture was cooled to room temperature and then diluted with *N, N* dimethylformamide (5 mL). NaOMe (218 mg, 4.05 mmol) was added and stirred at the same temperature for 10 min. 3,5-dimethoxybenzaldehyde (358 mg, 2.16 mmol) was added to the reaction mixture which was then stirred at room temperature for one hour. Then it was heated to reflux for 12 hours. The reaction was cooled to room temperature and quenched by adding ice and a small amount of methanol. The resulting yellow precipitate was then filtered and dried to give the crude stilbene as title product. The crude product was recrystallized from ethyl acetate to give the fine and pure white crystals. (577 mg, 84 %)

M.p. = 56-57 °C (literature m.p. = 50-52 °C, [19]), Rf (10:90::ethyl acetate: petroleum ether) = 0.54, IR ν (cm^{-1}) = 3029, 2961, 2937, 1585, 1450, 1290, 1148, 955, 831, 754, ^1H NMR (400 MHz, CDCl3) δ (ppm) = 2.36 (3H, s, Me), 3.83 (6H, s, OMe), 6.39 (1H, t, *J*2.2 Hz, H4), 6.66 (2H, d, *J*2.2 Hz, H2, H6), 7.02 (1H, d, *J*16.2 Hz, C=C-H), 7.06 (1H, d, *J*16.2 Hz, C=C-H), 7.16 (2H, d, *J*7.9 Hz, H2', H6'), 7.40 (2H, d, *J*8.0 Hz, H3', H5'), ^{13}C NMR (100 MHz, $CDCl_3$) δ (ppm) = 21.2 (Me), 55.4 (OMe), 99.9 (C4), 104.5 (C2, C6), 126.5 (C3', C5'), 127.7 (C=C), 129.9 (C=C), 129.4 (C2', C6'), 134.4 (C1'), 137.7 (C4'), 139.6 (C1), 161.01 (C3, C5). HRMS 277.12461 $[(M+Na)]^+$. **[see the Appendix B page 264-266 for all spectra.]**

2.4.12. Synthesis of (*E*)-2,2'-(ethene-1,2-diyl)dibenzonitrile (V16)

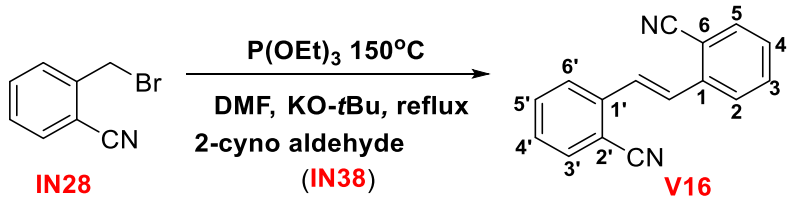

In a two-necked oven dried round-bottomed flask, the 2-(bromomethyl)benzonitrile (500 mg, 2.55 mmol, IN28) and triethyl phosphite (0.44 mL, 2.55 mmol) were added with N_2 purging. This reaction mixture was heated to 150 °C for 4-5 hours. The reaction was monitored by thin layer chromatography eluent (10:90:: ethyl acetate: petroleum ether). After completion, the reaction mixture was cooled to room temperature and then diluted with *N, N* dimethylformamide (5 mL). KO*t*Bu (429 mg, 3.82 mmol) was added and stirred at the same temperature for 10 min. 2-formylbenzonitrile (267 mg, 2.04 mmol) was added to the reaction mixture which was then stirred at room temperature for one hour. Then it was heated to reflux for 12 hours. The reaction was cooled to room temperature and quenched by adding ice and a small amount of methanol. The resulting yellow precipitate was then filtered and dried to give the crude stilbene as title product. The crude product was recrystallized from ethyl acetate to give the fine and pure white crystals. (463 mg, 79%)

M.p. = 200 °C Rf (10:90:: ethyl acetate: petroleum ether) =0.34, IR ν (cm^{-1}) 3069, 3050, 2958, 2224, 1486, 1263, 961, 726. ^{1}H NMR (400 MHz, $CDCl_3$) δ (ppm) = 7.42 (2H, td, *J*7.6/1 Hz, H4, H4'), 7.62 (2H, s, -C=C-H), 7.63 (2H, d, *J*7.6/1.2 Hz, H3, H3'), 7.69 (2H, dd, *J*7.6/1.2 Hz, H5, H5'), 7.91 (2H, d, *J*7.6 Hz, H2, H2'). ^{13}C NMR (100 MHz, $CDCl_3$) δ (ppm) = 112.0 (-CN), 117.6 (C6, C6'), 125.8 (C2, C2'), 128.6 (C=C), 128.7 (C4, C4'), 133.1 (C3, C3'), 133.1 (C5, C5'), 139.2 (C1, C1'). HRMS 253.06737 $[(M+Na)]^+$. **[see the Appendix B page 270-272 for all spectra]**

2.4.13. Synthesis of (*E*)-4-(3-chlorostyryl)-N,N-dimethylaniline (V17)

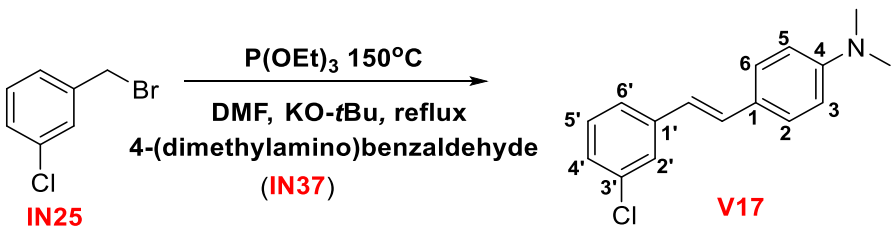

In a two-necked oven dried round-bottomed flask, the 1-(bromomethyl)-3-chlorobenzene (500 mg, 2.43 mmol, IN25) and triethyl phosphite (0.42 mL, 2.43 mmol) were added with N_2 purging. This reaction mixture was heated to 150 °C for 4-5 hours. The reaction was monitored by thin layer chromatography eluent (10:90:: ethyl acetate: petroleum ether). After completion, the reaction mixture was cooled to room temperature and then diluted with *N, N* dimethylformamide (5 mL). NaOMe (197 mg, 3.64 mmoles) was added and stirred at the same temperature for 10 min. 4-(dimethylamino)benzaldehyde (290 mg, 1.94 mmol) was added to the reaction mixture which was then stirred at room temperature for one hour. Then it was heated to reflux for 12 hours. The reaction was cooled to room temperature and quenched by adding ice and a small amount of methanol. The resulting yellow precipitate was then filtered and dried to give the crude stilbene as title product. The crude product was recrystallized from ethyl acetate to give the fine and pure white crystals. (495 mg, 79%)

M.p. = 138-139 °C. Rf (10:90::ethyl acetate: petroleum ether) = 0.56, IR ν (cm^{-1}) = 3031, 2893, 1608, 1582, 1065, 965, 808, 730, ^{1}H NMR (400 MHz, $CDCl_3$) δ (ppm) = 2.98 (6H, s, -N(CH_3)$_2$), 6.71 (distorted d, *J*8.8 Hz, H3, H5), 6.83 (1H, d, *J*16.4 Hz, -C=C-H), 7.02 (1H, d, *J*16.4 Hz, -C=C-H), 7.15 (1H, ddd, *J*8.0, 2.0,1.2 Hz, H6'), 7.24 (1H, t, *J*8 Hz, H5'), 7.32 (1H, distorted d, *J*7.6 Hz, H4'), 7.40 (2H, distorted d, *J*8.8 Hz, H2, H6), 7.45 (1H, t, *J*3.5 Hz, H2'), ^{13}C NMR (100 MHz, $CDCl_3$) δ (ppm) = 40.4 (N(CH_3)$_2$), 112.4 (C3,C5), 122.8 (C=C), 124.2 (C4'), 125.4 (C1), 125.8 (C2'), 126.5 (C6'), 127.8 (C2, C6), 129.7 (C5'), 130.3 (C=C), 134.5 (C1'), 140.2 (C3'), 150.4 (C4). HRMS 258.09288 $[(M+H)]^+$. **[See the Appendix B page 273-275 for all spectra.]**

2.4.14. Synthesis of (*E*)-1-(4-methoxystyryl)-2-nitrobenzene (V18)

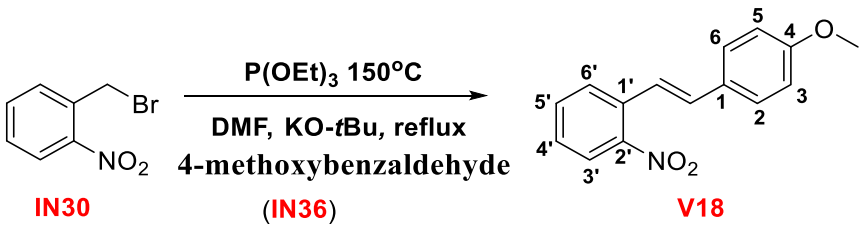

IN30 (IN36) V18

In a two-necked oven dried round-bottomed flask, the 1-(bromomethyl)-2-nitrobenzene (500 mg, 2.31 mmol, IN30) and triethyl phosphite (0.4 mL, 2.31 mmol) were added with N_2 purging. This reaction mixture was heated to 150 °C for 4-5 hours. The reaction was monitored by thin layer chromatography eluent (10:90 ethyl acetate: petroleum ether). After completion, the reaction mixture was cooled to room temperature and then diluted

with *N*, *N* dimethylformamide (5 mL). KO*t*Bu (389 mg, 3.47 mmol) was added and stirred at the same temperature for 10 min. 4-methoxybenzaldehyde (315 mg, 1.85 mmol) was added to the reaction mixture which was then stirred at room temperature for one hour. Then it was heated to reflux for 12 hours. The reaction was cooled to room temperature and quenched by adding ice and a small amount of methanol. The resulting yellow precipitate was then filtered and dried to give the crude stilbene as title product. The crude product was recrystallized from ethyl acetate to give yellow crystals (520 mg, 88%).

M.p. = 138-139 °C. Rf (10:90::ethyl acetate: petroleum ether) = 0.56, IR ν (cm^{-1}) = 3081, 2977, 2938, 1600, 1505, 1422, 1337, 1250, 1054, 968, 822, 768. ^{1}H NMR (400 MHz, $CDCl_3$) δ (ppm) = 3.84 (3H, s, -OMe), 6.91 (dd, *J*6.4/2 Hz, H3, H5), 7.05 (1H, d, *J*16 Hz, -C=C-H), 7.36 (1H, td, *J*8.4/1.2 Hz, H4'), 7.46 (1H, d, J16 Hz, -C=C-H), 7.48 (2H, dd, *J*6.8, 2 Hz, H2, H6), 7.55-7.59 (1H, m, *J*7.6 Hz, H5'), 7.75 (1H, dd, *J*8, 2 Hz, H2'), 7.93 (1H, dd, *J*8, 1.2 Hz, H3'), ^{13}C NMR (100 MHz, $CDCl_3$) δ (ppm) = 55.4 (-OMe), 114.3 (C3,C5), 121.1 (C=C-H), 124.8 (C3'), 127.5 (C4'), 127.9 (C2'), 128.5 (C2, C6), 129.4 (C1), 132.9 (C5'), 133.3 (C1'), 133.5 (-C=C), 147.9 (C2'), 160.1 (C4). HRMS 278.06168 $[(M+H)]^+$. **[See the Appendix B page 276-278 for all spectra]**

2.4.15. Synthesis of (*E*)-2-(4-methoxystyryl)benzonitrile (V19)

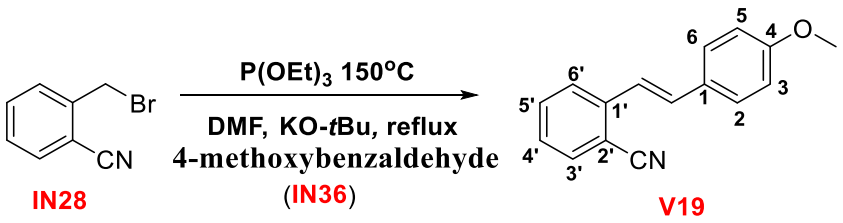

In a two-necked oven dried round-bottomed flask, the 2-(bromomethyl)-1,3-difluorobenzene (500 mg, 2.55 mmol, IN28) and triethyl phosphite (0.44 mL, 2.55 mmol) were added with N_2 purging. This reaction mixture was heated to 150 °C for 4-5 hours. The reaction was monitored by thin layer chromatography eluent (10:90:: ethyl acetate: petroleum ether). After completion, the reaction mixture was cooled to room temperature and then diluted with *N*, *N* dimethylformamide (5 mL). KO*t*Bu (429 mg, 3.82 mmol) was added and stirred at the same temperature for 10 min. 4-methoxybenzaldehyde (347 mg, 2.04 mmol) was added to the reaction mixture which was then stirred at room temperature for one hour. Then it was heated to reflux for 12 hours. The reaction was cooled to room temperature and quenched by adding ice and a small amount of methanol. The resulting

yellow precipitate was then filtered and dried to give the crude stilbene as title product. The crude product was recrystallized from ethyl acetate to give the fine and pure white crystals (474 mg, 79%).

M.p. = 142 °C. Rf (10:90:: ethyl acetate:petroleum ether) = 0.26, IR ν (cm^{-1}) = 3031, 2846, 2219, 1593, 1515, 1253, 1029, 961, 821, 762. ^{1}H NMR (400 MHz, $CDCl_3$) δ (ppm) = 3.85 (3H, s, -OMe), 6.93 (2H, dd, *J*8.8, 2 Hz, H3, H5), 7.20-7.34 (3H, m, (-C=C-H)$_2$, H5'), 7.50-7.57 (3H, m, H2, H6, H4'), 7.63 (1H, dd, *J*8, 1.2 Hz, H3'), 7.77 (1H, d, *J*8 Hz, H6'). ^{13}C NMR (100 MHz, $CDCl_3$) δ (ppm) = 55.4 (-OMe), 110.9 (-CN), 114.3 (C3, C5), 118.1 (C1'), 121.9 (C=C-H), 125.0 (C6'), 127.1 (C5'), 128.5 (C2, C6), 129.0 (C1), 132.7 (C4'), 133.0 (C3'), 133.1 (C=C-H), 141.0 (C1'), 160 (C4). HRMS 258.07709 $[(M+H)]^+$ and 493.16539 $[(2M+Na)]^+$. **[See the Appendix B page 279-281 for all spectra]**

2.4.16. Synthesis of (*E*)-1-(4-methoxystyryl)-3-nitrobenzene (V20)

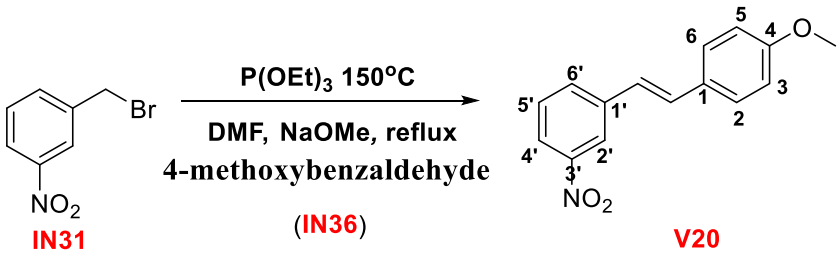

In a two-necked oven dried round-bottomed flask, the 1-(bromomethyl)-3-chlorobenzene (500 mg, 2.43 mmol, IN31) and triethyl phosphite (0.42 mL, 2.43 mmol) were added with N_2 purging. This reaction mixture was heated to 150 °C for 4-5 hours. The reaction was monitored by thin layer chromatography eluent (10:90:: ethyl acetate: petroleum ether). After completion, the reaction mixture was cooled to room temperature and then diluted with *N, N* dimethylformamide (5 mL). NaOMe (197 mg, 3.64 mmol) was added and stirred at the same temperature for 10 min. 4-nitrobenzaldehyde (265 mg, 1.94 mmol) was added to the reaction mixture which was then stirred at room temperature for one hour. Then it was heated to reflux for 12 hours. The reaction was cooled to room temperature and quenched by adding ice and a small amount of methanol. The resulting yellow precipitate was then filtered and dried to give the crude stilbene as title product. The crude product was recrystallized from ethyl acetate to give the fine and pure white crystals (476 mg, 73%).

M.p. = 152 °C. Rf (10:90::ethyl acetate: petroleum ether) = 0.48, IR ν (cm^{-1}) = ^{1}H NMR (400 MHz, $CDCl_3$) δ (ppm) = 6.92 (2H, dd, *J*6.8, 2 Hz, H2, H6), 7.22 (2H, d, *J*16 Hz,

(=C-H)$_2$), 7.37 (1H, td, *J*8, 2 Hz, H6'), 7.45-7.50 (3H, m, H3, H5,-C=C-H), 7.58 (1H, d, *J*6.8, 2 Hz, H4'), 7.75 (1H, dd, *J*8, 2 Hz, H2'), 7.94 (1H, dd, *J*8, 2 Hz, H5'). ^{13}C NMR (100 MHz, $CDCl_3$) δ (ppm) = 55.4 (-OMe), 114.3 (C2, C6), 121.2 (-C=C-), 124.8 (C5'), 127.5 (C6'), 127.9 (C2'), 128.5 (C3, C5), 129.4 (C1), 132.9 (C4'), 133.3(-C=C-), 133.5 (C1'), 147.9 (C3'), 160 (C4). HRMS 278.08092 $[(M+H)]^+$. **[see the Appendix B page 272-274 for all spectra for all spectra]**

2.4.17. Synthesis of (*E*)-1,3-dichloro-2-(3,5-dimethoxystyryl)benzene (V21)

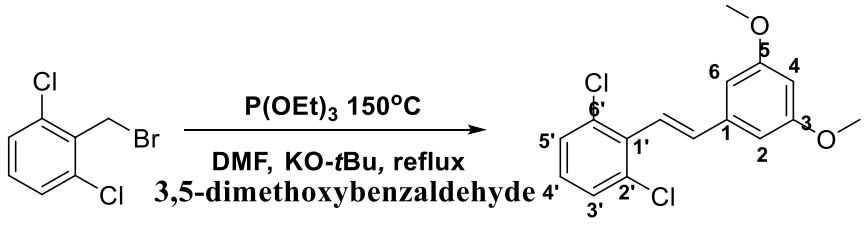

IN32 (**IN35**) **V21**

In a two-necked oven dried round-bottomed flask, the 2-(bromomethyl)-1,3-dichlorobenzene (500 mg, 2.08 mmol, IN32) and triethyl phosphite (0.36 mL, 2.08 mmol) were added with N_2 purging. This reaction mixture was heated at 150 °C for 4-5 hours. The reaction was monitored by thin layer chromatography eluent (10:90:: ethyl acetate: petroleum ether). After completion, the reaction mixture was cooled to room temperature and then diluted with *N, N* dimethylformamide (5 mL). KO*t*Bu (233 mg, 3.12 mmol) was added and stirred at the same temperature for 10 min. 3,5-dimethoxybenzaldehyde (276 mg, 1.66 mmol) was added to the reaction mixture which was then stirred at room temperature for one hour. Then it was heated to reflux for 12 hours. The reaction was cooled to room temperature and quenched by adding ice and a small amount of methanol. The resulting yellow precipitate was then filtered and dried to give the crude stilbene as title product. The crude product was recrystallized from ethyl acetate to give the fine and pure white crystals. (508 mg, 79%)

M.p. 66-67 °C, Rf (10:90::ethyl acetate: petroleum ether) = 0.64, IR ν (cm^{-1}) = 2959, 2897, 2833, 1598, 1424, 1348, 1206, 1152, 1054, 965, 819, 763, 676, ^{1}H NMR (400 MHz, *d*$_6$-DMSO) δ (ppm) = 3.78 (6H, s, OMe), 6.48 (1H, t, *J*2.0 Hz, H4), 6.78 (2H, d, *J*2.0 Hz, H2, H6), 6.99 (1H, d, *J*16.4 Hz, -C=C-H), 7.15 (1H, d, *J*16.4 Hz, -C=C-H), 7.32 (1H, t, *J*8.0 Hz, H4'), 7.52 (2H, d, *J*8.0 Hz, H3', H5'), ^{13}C NMR (100 MHz, d6-DMSO) δ (ppm) = 55.3 (OMe), 100.9 (C4), 104.7 (C2, C6), 122.7 (C=C), 128.8 (C3', C5'), 129.3 (C4'), 133.6 (C2', C6'), 134.1 (C1'), 136.8 (C=C), 138.1 (C1), 160.7 (C3, C5). HRMS

331.04468 $[(M+Na)]^+$ and 641.09081 $[(2M+Na)]^+$. **[see the Appendix B page 285-287 for all spectra.]**

2.4.18. Synthesis of (*E*)-1,3-dimethoxy-5-(2-nitrostyryl)benzene (V22)

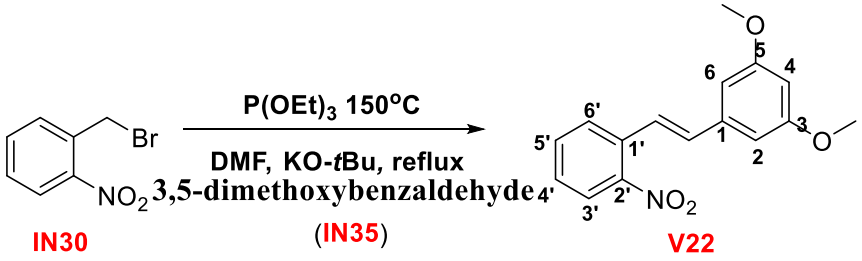

In a two-necked oven dried round-bottomed flask, the 1-(bromomethyl)-2-nitrobenzene (500 mg, 2.31 mmol, IN30) and triethyl phosphite (0.4 mL, 2.31 mmol) were added with N_2 purging. This reaction mixture was heated at 150 ºC for 4-5 hours. The reaction was monitored by thin layer chromatography eluent (10:90 ethyl acetate: petroleum ether). After completion, the reaction mixture was cooled to room temperature and then diluted with *N, N* dimethylformamide (5 mL). KO*t*Bu (389 mg, 3.47 mmol) was added and stirred at the same temperature for 10 min. 3,5-dimethoxybenzaldehyde (307 mg, 1.85 mmol) was added to the reaction mixture which was then stirred at room temperature for one hour. Then it was heated to reflux for 12 hours. The reaction was cooled to room temperature and quenched by adding ice and a small amount of methanol. The resulting yellow precipitate was then filtered and dried to give the crude stilbene as title product. The crude product was recrystallized from ethyl acetate to give the fine and pure white crystals. (528 mg, 80%)

M.p. = 72-73 °C, Rf (10:90::ethyl acetate: petroleum ether)=0.27, IR ν (cm^{-1}) = 3004, 2940, 2838, 1599, 1516, 1342, 1205, 1154, 1054, 951, 819, 744, 670, ^{1}H NMR (400 MHz, $CDCl_3$) δ (ppm) = 3.83 (6H, s, -OMe), 6.44 (1H, t, *J*2.4 Hz, H4), 6.68 (2H, d, *J*2.4 Hz, H2, H6), 7.00 (1H, d, *J*16.4 Hz, H-C=C-), 7.40 (1H, td, *J*8.4,1.3 Hz, H4'), 7.59 (1H, d, *J*16 Hz, H-C=C-), 7.59 (1H, t, *J*7.4 Hz, H5'), 7.74 (d, *J*7.6 Hz, H6'), 7.96 (1H, dd, *J*8.1,1.1 Hz, H3'). ^{13}C NMR (100 MHz, $CDCl_3$) δ (ppm) = 55.4 (OMe), 100.9 (C4), 105.2 (C2, C6), 124.0 (C=C), 124.8 (C3'), 128.0 (C4'), 128.2 (C6'), 132.9 (C5'), 133.1 (C=C), 133.9 (C1'), 138.5 (C1), 148.1 (C2'), 161.1 (C3, C5). HRMS 308.10436 $[(M+Na)]^+$. **[see the Appendix B page 288-290 for all spectra.]**

2.4.19. Synthesis of (*E*)-2-(2-nitrostyryl)benzonitrile (V25)

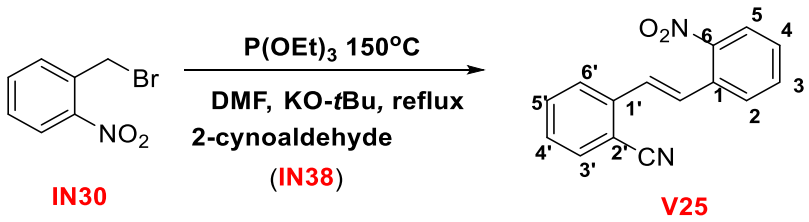

In a two-necked oven dried round-bottomed flask, the 1-(bromomethyl)-2-nitrobenzene (500 mg, 2.31 mmol, IN30) and triethyl phosphite (0.41 mL, 2.31 mmol) were added with N_2 purging. This reaction mixture was heated at 150 ºC for 4-5 hours. The reaction was monitored by thin layer chromatography eluent (10:90:: ethyl acetate: petroleum ether). After completion, the reaction mixture was cooled to room temperature and then diluted with *N*, *N* dimethylformamide (5 mL). KO*t*Bu (389 mg, 3.47 mmol) was added and stirred at the same temperature for 10 min. 2-formylbenzonitrile (303 mg, 1.85 mmol) was added to the reaction mixture which was then stirred at room temperature for one hour. Then it was heated to reflux for 12 hours. The reaction was cooled to room temperature and quenched by adding ice and a small amount of methanol. The resulting yellow precipitate was then filtered and dried to give the crude stilbene as title product. The crude product was recrystallized from ethyl acetate to give the fine and pure brown crystals. (542 mg, 85%)

M.p. = 149-150 °C (literature m.p. = 152 °C,), Rf (10:90::ethyl acetate: petroleum ether) =0.39 IR ν (cm^{-1})= 3055, 3026, 2224, 1520, 1350, 1267, 966, 753. ^{1}H NMR (400 MHz, $CDCl_3$) δ (ppm) = 7.38-7.43 (2H, m, C=C-H, H3), 7.49 (1H, td, *J*8.4, 1.6 Hz, H4), 7.61-7.70 (3H, m, *J*7.6/1.2 Hz, H2', H3', H4'), 7.78 (H, d, *J*16 Hz, C=C-H), 7.84 (2H, t, *J*8.8 Hz, H5', H6'), 8.04 (1H, dd, *J*8, 2 Hz, H2). ^{13}C NMR (100 MHz, $CDCl_3$) δ (ppm) = 111.9 (-CN), 117.7 (C2'), 125.0 (C2), 125.9 (C5'), 128.5 (C=C-H), 128.6 (C3), 128.8 (C4), 129.0 (C5), 129.1(C=C-), 132.1(C1), 133.0 (C4'), 133.1 (C3'), 133.5 (C6'), 139.7 (C1'), 148.1 (C6'). HRMS 273.06043 $[(M+Na)]^+$. **[See Appendix B page 297-299 for all spectra]**

2.4.20. Synthesis of (*E*)-1,3-dimethoxy-5-(3-nitrostyryl)benzene (V27)

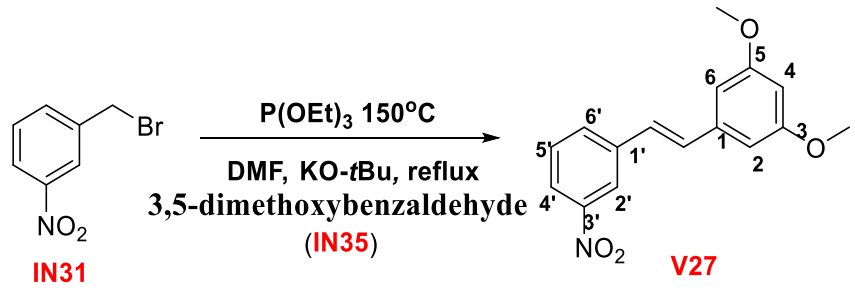

In a two-necked oven dried round-bottomed flask, the 1-(bromomethyl)-3-nitrobenzene (500 mg, 2.31 mmol, IN31) and triethyl phosphite (0.4 mL, 2.31 mmol) were added with N_2 purging. This reaction mixture was heated to 150 ºC for 4-5 hours. The reaction was monitored by thin layer chromatography eluent (10:90:: ethyl acetate: petroleum ether). After completion, the reaction mixture was cooled to room temperature and then diluted with *N, N* dimethylformamide (5 mL). KO*t*Bu (389 mg, 3.47 mmol) was added and stirred at the same temperature for 10 min. 3,5-dimethoxybenzaldehyde (307 mg, 1.85 mmol) was added to the reaction mixture which was then stirred at room temperature for one hour. Then it was heated to reflux for 12 hours. The reaction was cooled to room temperature and quenched by adding ice and a small amount of methanol. The resulting yellow precipitate was then filtered and dried to give the crude stilbene as title product. The crude product was recrystallized from ethyl acetate to give the fine yellow crystals. (508 mg, 78%)

M.p. = 72-73 °C, Rf (10:90::ethyl acetate:petroleum ether)=0.27, IR ν (cm-1) = 3074, 3006, 2841, 1588, 1501, 1335, 1243, 1117, 1025, 957, 811, 719. ^{1}H NMR (400 MHz, $CDCl_3$) δ (ppm) = 3.82 (3H, s, -OMe), 3.89 (3H, s, -OMe), 6.85 (2H, d, *J*1.6 Hz, H2, H6), 7.15 (1H, t, *J*1.6 Hz, H4), 7.39 (1H, d, *J*15.2 Hz, H-C=C-), 7.45 (1H, td, *J*8.4,1.3 Hz, H4'), 7.59 (1H, d, *J*16 Hz, H-C=C-), 7.59 (1H, t, *J*7.4 Hz, H5'), 7.74 (s, H2'), 7.58-7.61 (2H, m, C=C-H, H5'), 7.80 (1H, dd, *J*=8, 1.2 Hz, H6'), 7.94 (1H, dd, *J*=8.4, 1.2 Hz, H4'), ^{13}C NMR (100 MHz, $CDCl_3$) δ (ppm) = 55.8 (-OMe), 56.2 (-OMe), 112.2 (C6), 112.4 (C2), 115.1 (C6), 124.0 (C=C), 124.7 (C4'), 126.3 (C1'), 127.7 (C6'), 128.3 (C2'), 128.7 (C=C), 133.0 (C5'), 133.5 (C1'), 148.1 (C3'), 151.8 (C5), 153.8 (C3). HRMS 308.08810 $[(M+Na)]^+$. **[See Appendix B page 303-305 for all spectra for all spectra.]**

2.4.21. Synthesis of (*E*)-2,4-dimethoxy-1-(4-nitrostyryl)benzene (V28)

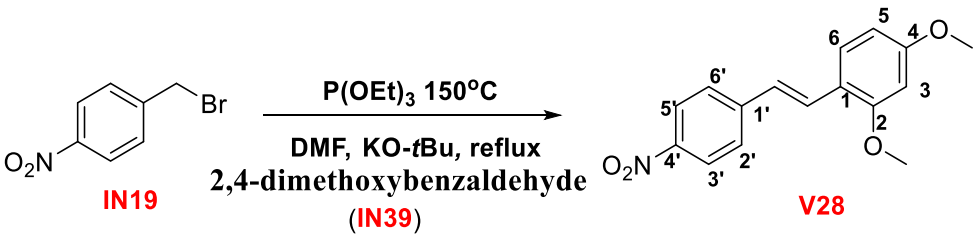

In a two-necked oven dried round-bottomed flask, the 1-(bromomethyl)-3-nitrobenzene (500 mg, 2.31 mmol, IN19) and triethylphosphite (0.4 mL, 2.31 mmol) were added with N_2 purging. This reaction mixture was heated to 150 °C for 4-5 hours. The reaction was monitored by thin layer chromatography eluent (10:90:: ethyl acetate: petroleum ether). After completion, the reaction mixture was cooled to room temperature and then diluted with *N, N* dimethylformamide (5 mL). KO*t*Bu (389 mg, 3.47 mmol) was added and stirred at the same temperature for 10 min. 2,4-dimethoxybenzaldehyde (307 mg, 1.85 mmol) was added to the reaction mixture which was then stirred at room temperature for one hour. Then it was heated to reflux for 12 hours. The reaction was cooled to room temperature and quenched by adding ice and a small amount of methanol. The resulting yellow precipitate was then filtered and dried to give the crude stilbene as title product. The crude product was recrystallized from ethyl acetate to give the fine yellow crystals. (528 mg, 80%)

M.p. =72-73 °C, Rf (10:90:: ethyl acetate: petroleum ether)=0.27, IR ν (cm-1) = 2929, 2841, 1598, 1505, 1316, 1107, 952, 840, 689. ^{1}H NMR (400 MHz, $CDCl_3$) δ (ppm) = 3.83 (3H, s, -OMe), 3.87 (3H, s, -OMe), 6.87 (2H, d, *J*2 Hz, H5, H6), 7.14 (1H, d, *J*16.8 Hz, C=C-H), 7.15 (1H, t, *J*2 Hz, H3), 7.60-7.66 (3H, m, H3', H5', -C=C-H), 8.20 (2H, dd, *J*7.6, 1.2 Hz, H2', H6'), ^{13}C NMR (100 MHz, $CDCl_3$) δ (ppm) = 55.9 (-OMe), 56.2 (-OMe), 112.1 (C=C), 112.4 (C5), 115.2 (C6), 124.1 (C3', C5'), 126 (C1'), 126.9 (C2', C6'), 128.1 (C=C-), 144.4 (C4'), 146.7 (C1'), 151.9 (C4'), 153.8 (C2), HRMS 308.08232 $[(M+Na)]^+$. **[See Appendix B page 306-308 for all spectra]**

2.4.22. Synthesis of (*E*)-1,2-diphenylethene (V29)

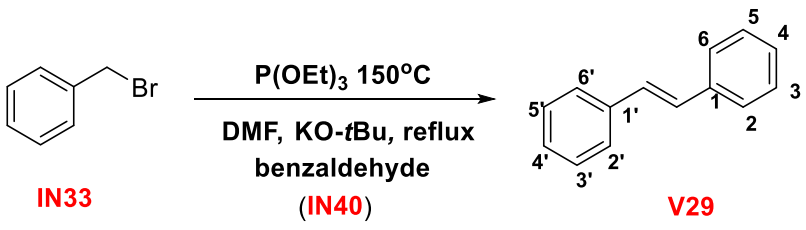

In a two-necked oven dried round-bottomed flask, the (bromomethyl)benzene (500 mg, 2.92 mmol, IN33) and triethyl phosphite (0.5 mL, 2.92 mmol) were added with N_2 purging. This reaction mixture was heated to150 ºC for 4-5 hours. The reaction was monitored by thin layer chromatography eluent (10:90:: ethyl acetate: petroleum ether). After completion, the reaction mixture was cooled to room temperature and then diluted with *N, N* dimethylformamide (5 mL). KO*t*Bu (492 mg, 4.38 mmol) was added and stirred at the same temperature for 10 min. benzaldehyde (248 mg, 2.33 mmol) was added to the reaction mixture which was then stirred at room temperature for one hour. Then it was heated to reflux for 12 hours. The reaction was cooled to room temperature and quenched by adding ice and a small amount of methanol. The resulting yellow precipitate was then filtered and dried to give the crude stilbene as title product. The crude product was recrystallized from ethyl acetate to give the fine white crystals. (474 mg, 90%)

M.p. = 121 °C (literature m.p. 123-124 ºC [161]), Rf (10:90::ethyl acetate: petroleum ether)=0.24, IR ν (cm^{-1}) = 3069, 3065, 3021, 1603, 1496, 1457, 961, 767, 694. ^{1}H NMR (400 MHz, $CDCl_3$) δ (ppm) = 7.1 (2H, s, C=C-H), 7.23 (2H, t, *J*8.4 Hz, H4, H4'), 7.34 (4H, t, *J*8 Hz, H3, H5, H3', H5'), 7.50 (4H, d, *J*8 Hz, H2, H6, H2', H6'), ^{13}C NMR (100 MHz, $CDCl_3$) δ (ppm) = 126.6 (C2, C6, C2', C6'), 127.7 (C4, C4'), 128.7 ((C=C)$_2$), 128.8 (C3, C5, C3', C5'), 137.4 (C1, C1'), HRMS no expected mass peak was found. **[see the Appendix B page 309-311 for all spectra]**

2.4.23. Synthesis of (*E*)-4-(3,5-dimethoxystyryl)benzonitrile (V33)

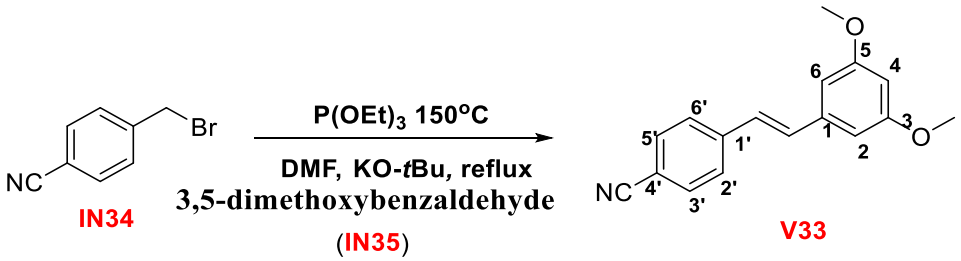

In a two-necked oven dried round-bottomed flask, the 4-(bromomethyl)benzonitrile (500 mg, 2.55 mmol, IN34) and triethyl phosphite (0.46 mL, 2.55 mmol) were added with N_2 purging. This reaction mixture was heated to 150 ºC for 4-5 hours. The reaction was monitored by thin layer chromatography eluent (10:90:: ethyl acetate: petroleum Ether). After completion, the reaction mixture was cooled to room temperature and then diluted with *N, N* dimethylformamide (5 mL). KO*t*Bu (429 mg, 3.82 mmol) was added and stirred at the same temperature for 10 min. 3,5-dimethoxybenzaldehyde (338 mg, 2.04

mmol) was added to the reaction mixture which was then stirred at room temperature for one hour. Then it was heated to reflux for 12 hours. The reaction was cooled to room temperature and quenched by adding ice and a small amount of methanol. The resulting yellow precipitate was then filtered and dried to give the crude stilbene as title product. The crude product was recrystallized from ethyl acetate to give the fine and pure white crystals. (541 mg, 80%)

M.p.=105-107 °C (literature m.p.= 106-107 °C[162]), Rf (10:90::ethyl acetate:petroleum ether) = 0.54, IR ν (cm^{-1}) = 2959, 2937, 2841, 2220, 1587, 1340, 1208, 1169, 1066, 948, 833, 679, ^{1}H NMR (400 MHz, $CDCl_3$) δ (ppm) = 3.84 (6H, s, OMe), 6.45 (1H, t, *J*2.2 Hz, H4), 6.68 (2H, d, *J*2.2 Hz, H2, H6), 7.05 (1H, d, *J*16.2 Hz, -C=C-H), 7.13 (1H, d, *J*16.2 Hz, -C=C-H), 7.59 (2H, d, *J*8.3 Hz, H2', H6'), 7.64 (2H, d, *J*8.3Hz, H3', H5'), ^{13}C NMR (100 MHz, $CDCl_3$) δ (ppm) = 55.4 (OMe), 100.9 (C4), 105.1 (C2, C6), 110.7 (C4'), 119.0 (CN), 126.9 (C2', C6'), 127.2 (C=C), 132.4 (C=C), 132.6 (C3', C5'), 138.3 (C1'), 141.7 (C1), 161.1 (C3, C5). HRMS 288.12135 $[(M+Na)]^{+}$. **[See the Appendix B page 321-323 for all spectra]**

2.4.24. Synthesis of (*E*)-1,3-dimethoxy-5-styrylbenzene (V42)

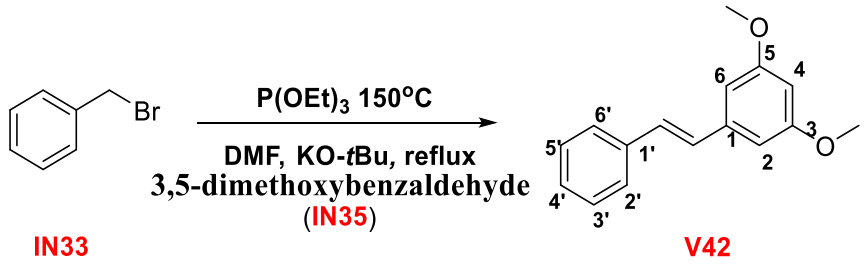

IN33 V42

In a two-necked oven dried round-bottomed flask, the (bromomethyl)benzene (500 mg, 2.33 mmol, IN33) and triethyl phosphite (0.5 mL, 2.33 mmol) were added with N_2 purging. This reaction mixture was heated at 150 °C for 4-5 hours. The reaction was monitored by thin layer chromatography eluent (10:90:: ethyl acetate: petroleum Ether). After completion, the reaction mixture was cooled to room temperature and then diluted with *N, N* dimethylformamide (5 mL). NaOMe (406 mg, 4.38 mmol) was added and stirred at the same temperature for 10 min. 3,5-dimethoxybenzaldehyde (388 mg, 2.33 mmol) was added to the reaction mixture which was then stirred at room temperature for one hour. Then it was heated to reflux for 12 hours. The reaction was cooled to room temperature and quenched by adding ice and a small amount of methanol. The resulting yellow precipitate was then filtered and dried to give the crude stilbene as title product.

The crude product was recrystallised from ethyl acetate to give the fine and pure white crystals. (505 mg, 72%)

M.p. = 51-54 °C (literature m.p. = 59 °C[163]), Rf (10:90::ethyl acetate:petroleum ether) =0.38, IR ν (cm^{-1}) = 3016, 2963, 2841, 1598, 1423, 1161, 1054, 971, 830, 694. ^{1}H NMR (400 MHz, $CDCl_3$) δ (ppm) = 3.84 (6H, s, OMe), 6.40 (1H, t, *J*2.2 Hz, H4), 6.67 (2H, d, *J*2.2 Hz, H2, H6), 7.03 (1H, d, *J*16 Hz, -C=C-H), 7.09 (1H, d, *J*16Hz, -C=C-H), 7.24-7.28 (1H, m, H4'), 7.35 (2H, t, *J*7.2 Hz, H2', H6'), 7.50 (2H, dd, J=8.4, 1.2, H3', H5'), ^{13}C NMR (100 MHz, $CDCl_3$) δ (ppm) = 55.6 (OMe), 100.0 (C4), 104.6 (C2, C6), 126.6 (C3', C5'), 127.7 (C4'), 128.7 (C2', C6'), 129.2 ($(C=C)_2$), 137.2 (C1), 139.4 (C1'), 161.0 (C3, C5). HRMS 503.18844 $[(2M+Na)]^+$. **[See the Appendix B page 345-347 for all spectra]**

2.4.25. Synthesis of (*E*)-1-(3-chlorostyryl)-3,5-dimethoxybenzene (V43)

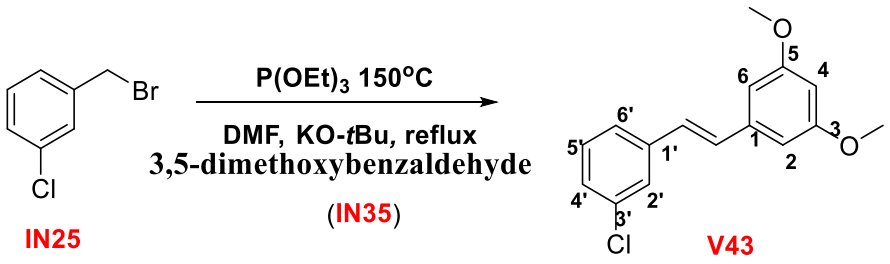

In a two-necked oven dried round-bottomed flask, the 1-(bromomethyl)-3-chlorobenzene (500 mg, 2.43 mmol, IN25) and triethyl phosphite (0.41 mL, 2.43 mmol) were added with N_2 purging. This reaction mixture was heated to 150 °C for 6 hours. The reaction was monitored by thin layer chromatography eluent (10:90:: ethyl acetate: petroleum ether). After completion, the reaction mixture was cooled to room temperature and then diluted with *N, N* dimethylformamide (5 mL). NaOMe (197 mg, 3.64 mmol) was added and stirred at the same temperature for 10 min. 3,5-dimethoxybenzaldehyde (323 mg, 1.93 mmol) was added to the reaction mixture which was then stirred at room temperature for one hour. Then it was heated to reflux for 12 hours. The reaction was cooled to room temperature and quenched by adding ice and a small amount of methanol. The resulting yellow precipitate was then filtered and dried to give the crude stilbene as title product. The crude product was purified with column chromatography to give the colourless liquid. (454 mg, 68%)

B.p. >300 °C, Rf (10:90::ethyl acetate: petroleum ether) = 0.47, IR ν (cm^{-1}) = 3030, 2995, 2898, 1603, 1542, 1357, 1205, 1053, 968, 825, 677, 1 H NMR (400 MHz, $CDCl_3$) δ (ppm) = 3.83 (6H, s, OMe), 6.41 (1H, t, *J*2.2 Hz, H4), 6.66 (2H, d, *J*2.2 Hz, H2, H6), 6.98

(1H, distorted d, *J*16.2 Hz, -C = C-H), 7.03 (1H, distorted d, *J*16.2 Hz, -C = C-H), 7.22 (1H, dt, *J*8.4,1.2 Hz H6′), 7.26 (1H, dd, *J*8.8, 7.6 Hz, H5′), 7.35 (dt, *J*7.5, 1.2 Hz, H4′), 7.49 (1H, t, *J*1.6 Hz, H2′), ^{13}C NMR (100 MHz, $CDCl_3$) δ (ppm) = 55.4 (OMe), 100.4 (C4), 104.8 (C2, C6), 124.8 (C4′), 126.4 (C2′), 127.6 (C6′), 127.7 (C = C), 129.9 (C5′), 130.2 (C = C), 134.7 (C1′), 138.84 (C3′), 139.08 (C1), 161.06 (C3, C5). HRMS 297.06374 $[(M + Na)]^+$ and 571.13963 $[(2M + Na)]^+$. **[See Appendix B page 348-350 for all spectra.]**

2.5. Demethylation: Synthesis of dihydroxy derivatives of Resveralogues:

The demethylation of resveralogues was tried using pyridine hydrochloride and boron tribromide reaction. The details of both reaction conditions are described in section **2.5.1** and **2.5.2.**

2.5.1. Attempted demethylation using pyridine hydrochloride:

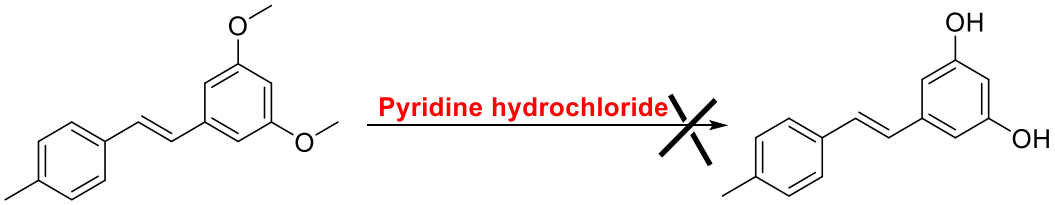

V14 V13

A homogeneous mixture of (*E*)-1,3-dimethoxy-5-(4-methylstyryl)benzene (**V14**) (200 mg, 0.7 mmol, 1 equivalent), and of pyridine hydrochloride (500 mg, 3.5 mmol, 5 equivalents) is heated at about 165 °C. for 3 hours. The cooled, oily reaction mass was then introduced into 5 mL of 2N hydrochloric acid and the crude product is isolated by extraction with diethyl ether.

2.5.2. Demethylation using BBr_3 in dichloromethane:

The demethylation reaction not successful using pyridine hydrochloride reagent. BBr_3 dichloromethane was then used to convert the methoxy resveralogues into dihydroxy resveralogues. This conversion was successful and the overall mechanism of demethylation of resveralogues is summarised in **Scheme 2-5**.

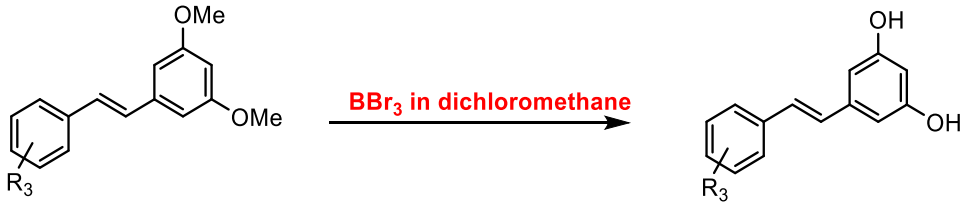

Where; R_3=4-Me (V14), 2-CN (V10), 3, 5-DiMe (V4), 4-NHCOMe (V11), 4-NHCObenzyl (V36), 2,4-DiF (V5) and 2-NHCObenzyl (V39)

Where; R_3=4-Me (V13), 2-CN (V23), 3, 5-DiMe (V26), 4-NHCOMe (V31), 4-NHCObenzyl (V37), 2,4-DiF (V40) and 2-NHCObenzyl (V41)

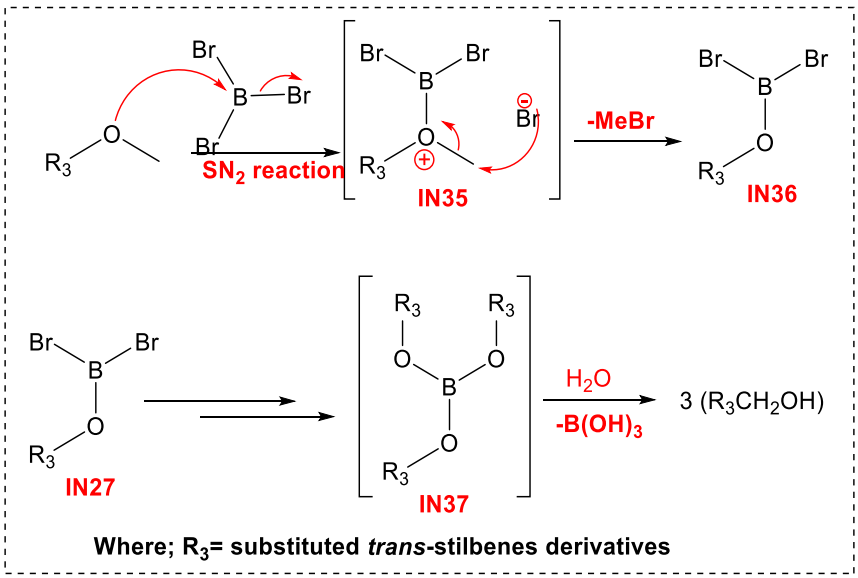

Scheme 2-5 Demethylation of resveralogues using BBr_3. This involves nucleophlic attack of lone pair of electron of oxygen to the electophilic vacant p-orbital of boron to give charged intermediate (IN35). IN35 undergoes second intra-molecular nucleophlic addition-elimination reaction to give intermediate (IN36). Similarly, this reaction continues till all of the bromine atoms of BBr_3 replaced to give corresponding boron ester intermediate IN37. IN37 then undergoes hydrolysis reaction to yield the corrosponding alcohol. In this demethylation reaction, a single molecule of BBr_3 deprotect three molecules of methyl ether derivatives.

2.5.3. Synthesis of (*E*)-5-(4-methylstyryl)benzene-1,3-diol (V13)

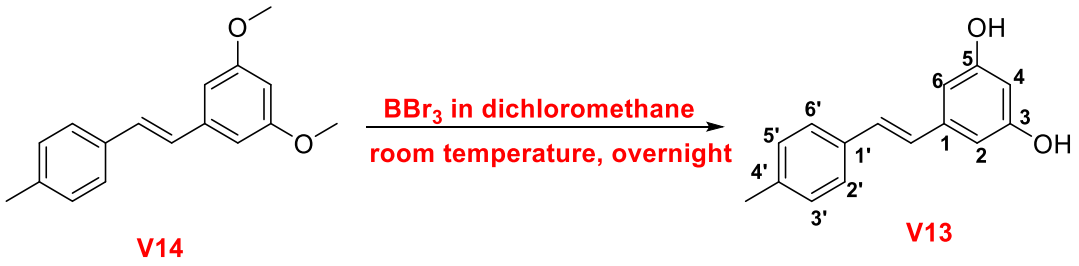

A solution of (*E*)-1,3-dimethoxy-5-(4-methylstyryl)benzene (**V14**) (200 mg, 0.7 mmol) and 1M BBr_3 in dichloromethane (1.17 mmol , 1.2 mL) in dry 1,2-dichloroethane (5 mL) was stirred at room temperature under nitrogen atmosphere for 1 days. The reaction was monitored by TLC and then it was concentrated under vacuum. The crude product was dissolved in ethyl acetate (10 mL) and washed with 2 M sodium bicarbonate solution (10 mL). The resulting organic layer was further washed with water (10 mL) and then with saturated brine solution (10 mL). The ethyl acetate layer was distilled off and the resulting crude was purified with column chromatography to give the (*E*)-5-(4-methylstyryl)benzene-1,3-diol (**V13**) as a white solid (60 mg, 30%).

M.p. =93-97 °C, Rf (20:80::ethyl acetate: chloroform) = 0.17, IR ν (cm^{-1}) = 3254, 3021, 2919, 1598, 1471, 1311, 1258, 1151, 995, 835,709. ^{1}H NMR (400 MHz, $CDCl_3$) δ (ppm) = 2.86 (3H, s,-Me), 6.15 (1H, t, J2 Hz, H4), 6.41 (2H, d, J2 Hz, H2, H6), 6.97 (2H, s, -C=C-H), 7.16 (1H, d, J8 Hz, H2' H6'), 7.45 (2H, d, J8 Hz, H3', H5'), 9.18 (2H, s, OH). ^{13}C NMR (100 MHz, $CDCl_3$) δ (ppm) = 20.8 (-Me), 102.2 (C4), 104.5 (C2, C5), 126.3 (C3', C5'), 127.7 (-C=C-), 127.9 (C=C), 129.2 (C2', C6'), 134.2 (C4'), 136.8 (C1), 138.8 (C1'), 158.5 (C3, C5). HRMS 249.09281 $[(M+Na)]^+$ and 475.19580 $[2M+Na]^+$. **[see the Appendix B page 261-263 for all spectra]**

2.5.4. Synthesis of (*E*)-2-(3,5-dihydroxystyryl)benzonitrile (V23)

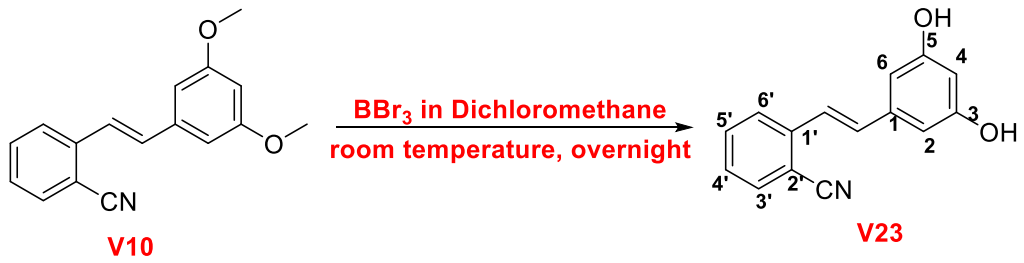

A solution of (*E*)-2-(3,5-dimethoxystyryl)benzonitrile (**V10**) (300 mg, 1.1mmol) and 1M BBr_3 in dichloromethane (1.7 mmol, 1.8 mL) in dry 1,2-dichloroethane (5 mL) was

stirred at room temperature under nitrogen atmosphere for 1 days. The reaction was monitored by TLC and then it was concentrated under vacuum. The crude product was dissolved in ethyl acetate (10 mL) and washed with 2 M sodium bicarbonate solution (10 mL). The resulting organic layer was further washed with water (10 mL) and then with saturated brine solution (10 mL). The ethyl acetate layer was distilled off and the resulting crude was purified with column chromatography to give the (*E*)-2-(3,5-dihydroxystyryl)benzonitrile (**V23**) as a brown coloured solid (108 mg, 40%).

M.p. = 112 °C, Rf (10:90::ethyl acetate:chloroform)=0.3, IR ν (cm^{-1}) = 3298, 3065, 2890, 2224, 1598, 1486, 1165, 1020, 961, 753, 675. ^{1}H NMR (400 MHz, $CDCl_3$) δ (ppm) = 6.22 (1H, t, *J*2.1 Hz, H4), 6.50 (2H, d, J2.1 Hz, H2, H5), 7.21 (1H, d, *J*16.2 Hz, H-C=C-), 7.35 (1H, d, *J*16.2 Hz, H-C=C-), 7.44 (1H, t, *J*7.6 Hz, H4'), 7.70 (1H, t, *J*7.6 Hz, H5'), 7.81 (d, *J*7.2 Hz, H6'), 8.00 (1H, d, *J*7.6 Hz, H3'). ^{13}C NMR (100 MHz, $CDCl_3$) δ (ppm) = 103.4 (C4), 105.0 (C2, C6), 110.0 (CN), 117.8 (C2'), 122.7 (-C=C-), 125.4 (C3'), 128.0 (C4'), 133.0 (C6'), 133.3 (C5'), 134.0 (C=C), 137.6 (C1), 139.8 (C1'), 158.7 (C3, C5). HRMS 260.05225 $[(M+Na)]^{+}$. **[See Appendix B page 291-293 for all spectra]**

2.5.5. Synthesis of (*E*)-5-(3,5-dimethylstyryl)benzene-1,3-diol (V26)

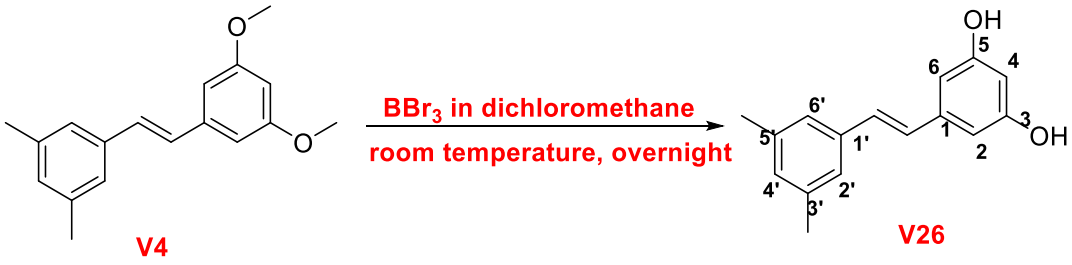

A solution of (*E*)-1-(3,5-dimethoxystyryl)-3,5-dimethylbenzene (**V4**) (200 mg, 0.07 mmol) and 1M BBr_3 in dichloromethane (1.1 mmol,1.3 mL) in dry 1,2-dichloroethane (5 mL) was stirred at room temperature under nitrogen atmosphere for 1 days. The reaction was monitored by TLC and then it was concentrated under vacuum. The crude product was dissolved in ethyl acetate (10 mL) and washed with 2 M sodium bicarbonate solution (10 mL). The resulting organic layer was further washed with water (10 mL) and then with saturated brine solution (10 mL). The ethyl acetate layer was distilled off and the resulting crude was purified with column chromatography to give the (*E*)-5-(3,5-dimethylstyryl)benzene-1,3-diol (**V26**) as a light brown coloured solid (80 mg, 45%).

M.p. =109 °C, Rf (10:90::ethyl acetate:chloroform)=0.32, IR ν (cm-1) = IR ν (cm^{-1})= 3249, 3035, 2924, 1560, 1481, 1345, 1156, 961, 840, 689. ^{1}H NMR (400 MHz, $CDCl_3$) δ (ppm) = 2.28 (6H, s, -Me), 6.15 (1H, t, *J*2 Hz, H4), 6.41 (2H, d, *J*2 Hz, H2, H6), 6.89 (1H, s, H4'), 6.96 (2H, d, *J*16.4 Hz, H-C=C-), 7.17 (2H, s, H2', H5'), 9.19 (2H, s, -OH). ^{13}C NMR (100 MHz, $CDCl_3$) δ (ppm) = 20.9 (Me), 104.6 (C4), 124.3 (C2, C6), 127.9 (C2', C6'), 128.5 (C=C), 128.7 (C4'), 136.8 (C1'), 137.5 (C3', C5'), 138.6 (C1'), 158.5 (C3, C5). HRMS 263.09747 $[(M+Na)]^+$, 503.20861 $[(2M+Na)]^+$ and 743.31312 $[(3M+Na)]^+$. **[See the Appendix B page 300-302 for all spectra]**

2.5.6. Synthesis of (*E*)-N-(4-(3,5-dihydroxystyryl)phenyl)acetamide (V31)

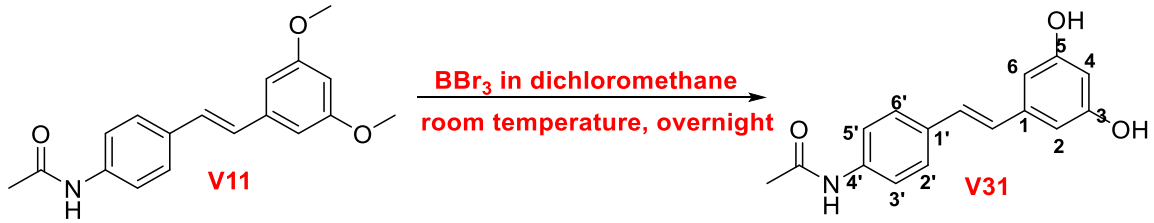

A solution of (*E*)-N-(4-(3,5-dimethoxystyryl)phenyl)acetamide (**V11**) (200 mg, 0.067 mmol) and 1 M BBr_3 in dichloromethane (1.0 mmol , 1 mL) in dry 1,2-dichloroethane (5 mL) was stirred at room temperature under nitrogen atmosphere for 1 days. The reaction was monitored by TLC and then it was concentrated under vacuum. The crude product was dissolved in ethyl acetate (10 mL) and washed with 2 M sodium bicarbonate solution (10 mL). The resulting organic layer was further washed with water (10 mL) and then with saturated brine solution (10 mL). The ethyl acetate layer was distilled off and the resulting crude was purified with column chromatography to give the (*E*)-N-(4-(3,5-dihydroxystyryl)phenyl)acetamide (**V31**) as a light brown coloured solid (82 mg, 45%).

M.p. = 112 °C, Rf (10:90::ethyl acetate:chloroform)=0.4, IR ν (cm-1) = 3327, 3050, 2890, 2671, 1593, 1510, 1170, 966, 840, 631. ^{1}H NMR (400MHz, $CDCl_3$) δ (ppm) = 2.05 (3H, s, -NMe), 6.14 (1H, t, *J*2 Hz, H4), 6.41 (2H, d, *J*2 Hz, H2, H6), 6.95 (2H, d, *J*16.8 Hz, C=C-H), 7.50 (2H, d, *J*8.8 Hz, H2', H6'), 7.57 (2H, d, *J*=8.8 Hz, H3', H5'), 9.22 (2H, s, -OH), 9.98 (1H, s, NH). ^{13}C NMR (100 MHz, $CDCl_3$) δ (ppm) = 24.0 (N-Me), 102.1 (C4), 104.5 (C2, C6), 119.0 (C3', C5'), 126.9 (C2', C6'), 127.4 ($(C=C-)_2$), 131.7 (C1), 138.7 (C1'), 138.9 (C4'), 158.5 (C3, C5), 168.2 (CO), HRMS 292.07937 $[(M+Na)]^+$ and 561.18057 $[(2M+Na)]^+$. **[See the Appendix B page 315-317 for all spectra]**

2.5.7. Synthesis of (*E*)-N-(4-(3,5-dihydroxystyryl)phenyl)benzamide (V37)

A solution of (*E*)-N-(4-(3,5-dimethoxystyryl)phenyl)benzamide (**V36**) (300 mg, 1.1 mmol) and 1 M BBr_3 in dichloromethane (1.7 mmol, 1.3 mL) in dry 1,2-dichloroethane (5 mL) was stirred at room temperature under nitrogen atmosphere for 1 days. The reaction was monitored by TLC and then it was concentrated under vacuum. The crude product was dissolved in ethyl acetate (10 mL) and washed with 2M sodium bicarbonate solution (10 mL). The resulting organic layer was further washed with water (10 mL) and then with saturated brine solution (10 mL). The ethyl acetate layer was distilled off and the resulting crude was purified with column chromatography to give the (*E*)-N-(4-(3,5-dihydroxystyryl)phenyl)acetamide (**V37**) as a light brown coloured solid (32 mg, 10%).

M.p. = 185 °C, Rf (10:90::ethyl acetate: chloroform)=0.24, IR ν (cm^{-1}) = 3424, 3254, 3055, 1607, 1510, 1146, 961, 845, 704, 685, ^{1}H NMR (400 MHz, $CDCl_3$) δ (ppm) = 6.15 (1H, t, *J*2 Hz, H4), 6.43 (2H, d, *J*2 Hz, H2, H6), 7.00 (2H, s, -C=C-H), 7.54-7.60 (5H, m, Aryl H), 7.71 (2H, d, *J*8.3 Hz, H2', H6'), 7.96 (2H, d, *J*8.3 Hz, H3', H5'), 9.24 (2H, s, OH), 10.30 (1H, s, NH), ^{13}C NMR (100 MHz, $CDCl_3$) δ (ppm) = 102.1 (C4), 104.5 (C2, C6), 120.3 (C2', C6'), 126.6 (C3', C5'), 126.8 (2C aryl), 127.4 (C=C), 127.7 (C=C), 128.4 (2C, aryl), 131.5 (1C Aryl), 132.4 (C1), 134.9 (C1'), 138.6 (1C, aryl), 138.9 (C4'), 158.6 (C3, C5), 165.4(CO), HRMS 354.08941 $[(M+Na)]^+$. **[See the Appendix B page 330-332 for all spectra]**

2.5.8. Synthesis of (*E*)-5-(2,4-difluorostyryl)benzene-1,3-diol (V40)

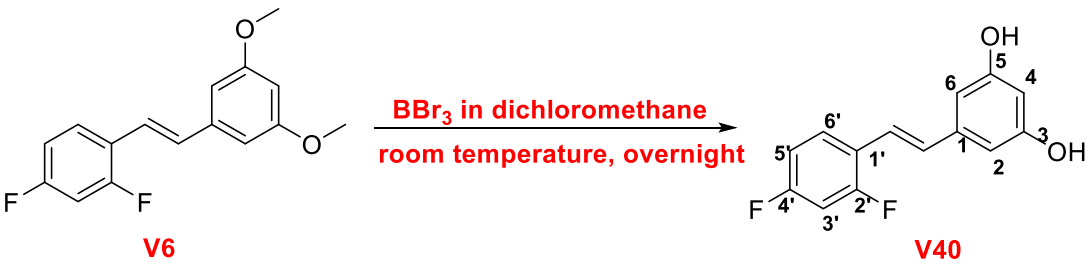

A solution of (*E*)-1-(3,5-dimethoxystyryl)-2,4-difluorobenzene (**V6**) (300 mg, 1.1 mmol) and 1 M BBr_3 in dichloromethane (1.7 mmol, 1.3 mL) in dry 1,2-dichloroethane (5 mL) was stirred at room temperature under nitrogen atmosphere for 1 days. The reaction was monitored by TLC and then it was concentrated under vacuum. The crude product was dissolved in ethyl acetate (10 mL) and washed with 2 M sodium bicarbonate solution (10 mL). The resulting organic layer was further washed with water (10 mL) and then with saturated brine solution (10 mL). The ethyl acetate layer was distilled off and the resulting crude was purified with column chromatography to give the (*E*)-5-(2,4-difluorostyryl)benzene-1,3-diol (**V40**) as a light brown coloured solid (109 mg, 40%).

m.p. = 73 °C, Rf (10:90::ethyl acetate:chloroform) =0.37, IR ν (cm^{-1}) = 3307, 2987, 2928, 2618, 2506, 1651, 1598, 1457, 1146, 961, 825, 762, 689. ^{1}H NMR (400 MHz, $CDCl_3$) δ (ppm) = 6.18 (1H, t, *J*2 Hz, H4), 6.44 (2H, d, *J*2 Hz, H2, H6), 7.03 (1H, d, *J*16.8 Hz, -C=C-H), 7.11 (1H, d, J=16.8 Hz, C=C-H), 7.12 (1H, td, *J*7.2/3.6 Hz, H6'), 7.27 (1H, td, J=7.2/2.8 Hz, H5'), 7.48-7.84 (1H, m, H3'), 9.29 (2H, s, -OH), ^{13}C NMR (100 MHz, $CDCl_3$) δ (ppm) = 102.8 (C4), 104.1 (C3', t, J_{C-F}25.9 Hz), 104.8 (C2, C6), 111.9 (C5', t, J_{C-F} 21.9 Hz), 118.6 (C=C-), 121.3 (C1', q, J_{C-F}14.8 Hz), 128.6 (C6', q, J_{C-F}5.2 Hz), 131.5 (C1'), 138.4 (C1), 158.6 (C3, C5), 159.2 (C2', d, J_{C-F}236.5 Hz), 161.7 (C4', d, J_{C-F}245.6 Hz), HRMS 382.12716 $[(M+Na)]^+$. **[See the Appendix B page 339-341 for all spectra]**

2.5.9. Synthesis of (*E*)-N-(2-(3,5-dihydroxystyryl)phenyl)benzamide (V41)

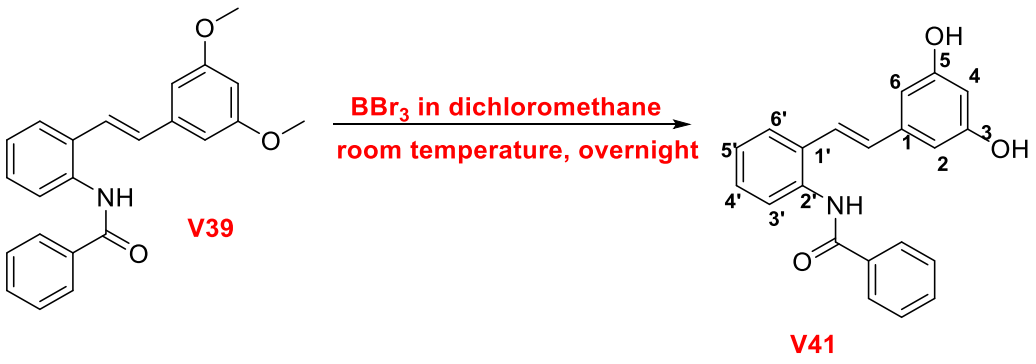

A solution of (*E*)-N-(2-(3,5-dimethoxystyryl)phenyl)benzamide (**V39**) (100 mg, 1.1 mmol) and 1 M BBr_3 in dichloromethane (1.7 mmol , 1.3 mL) in dry 1,2-dichloroethane (5 mL) was stirred at room temperature under nitrogen atmosphere for 1 days. The reaction was monitored by TLC and then it was concentrated under vacuum. The crude product was dissolved in ethyl acetate (10 mL) and washed with 2 M sodium bicarbonate solution (10 mL). The resulting organic layer was further washed with water (10 mL) and

then with saturated brine solution (10 mL). The ethyl acetate layer was distilled off and the resulting crude was purified with column chromatography to give the (*E*)-N-(2-(3,5-dihydroxystyryl)phenyl)benzamide (**V41**) as a light brown coloured solid (46 mg, 80%).

M.p. = 110 $^{\circ}$C, Rf (10:90::ethyl acetate: chloroform)=0.28, IR ν (cm^{-1}) = 3244, 2982, 2880, 1593, 1515, 1141, 966, 757, 699. ^{1}H NMR (400 MHz, $CDCl_3$) δ (ppm) = 6.04 (1H, t, *J*2 Hz, H4), 6.28 (2H, d, *J*2 Hz, H2, H6), 6.95 (1H, d, *J*16.4 Hz, -C=C-H), 7.05 (1H, d, *J*16.4 Hz, -C=C-H), 7.22-7.29 (3H, m, H3' H5' H6'), 7.44-7.55 (3H, m, aryl 3H), 7.73-7.75 (1H, m, H4'), 7.93 (2H, d, J6.8 Hz, aryl 2H), ^{13}C NMR (100 MHz, $CDCl_3$) δ (ppm) = 102.4 (C4), 104.7 (C2, C6), 123.5 (C=C), 125.4 (1C Aryl), 126.4 (C4'), 127.6 (C3', C5'), 128.0 (C6'), 128.5 (2C Aryl), 130.0 (C=C), 131.6 (1C aryl), 133.1 (1C aryl), 134.6 (C1), 135.4 (C1'), 136.4 (1C aryl), 138.8 (C2'), 158.5 (C3, C5), 165.8 (CO), HRMS 354.08292 $[(M+Na)]^{+}$. **[See the Appendix B page 342-344 for all spectra]**

2.6. Syntheses of 4′-amino substituted resveratrol derivatives:

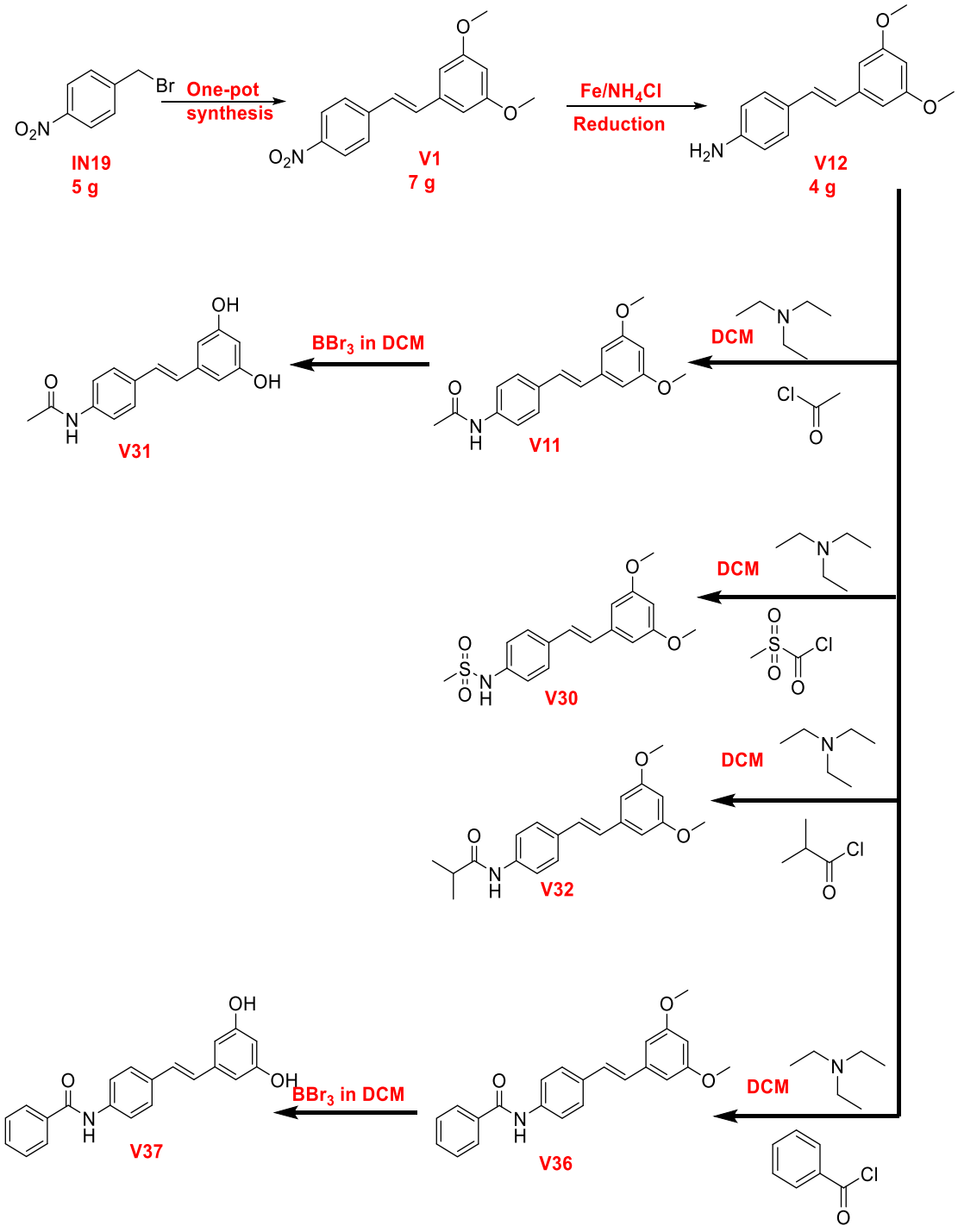

Scheme 2-6 Summary of synthesis of 4′-substituted novel amino resveralogues.

2.6.1. Attempted reduction reaction using $SnCl_2$/MeOH:

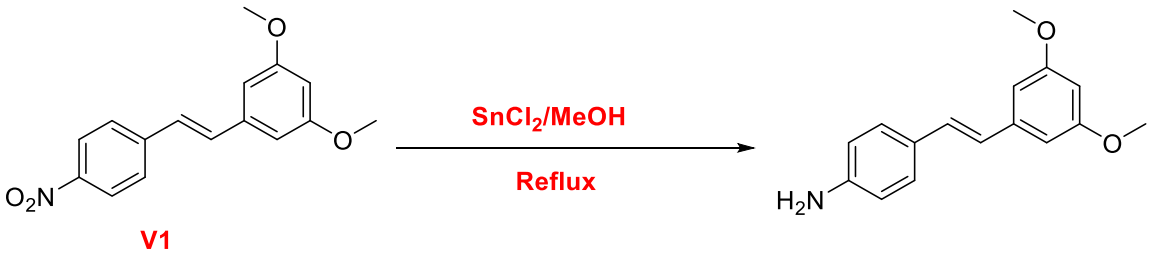

To a solution of (*E*)-1,3-dimethoxy-5-(4-nitrostyryl)benzene (**V1**) (500 mg, 1 equivalents, 1.75 mmol) in ethyl acetate, stannous chloride (1.66 g, 5 equivalents, 8.76 mmol) was added. After refluxing for 6 h, the mixture was cooled to room temperature, and saturated sodium bicarbonate solution was added until the solution was basic. Ethyl acetate was added, and the organic layer was separated. Solvent removal yielded the crude product, which was purified by silica gel column chromatography (EtOAc::petroleum ether::8:2 as the eluent) to provide the target product. (20 mg, yield 8%).

2.6.2. Change of solvent for reduction reaction:

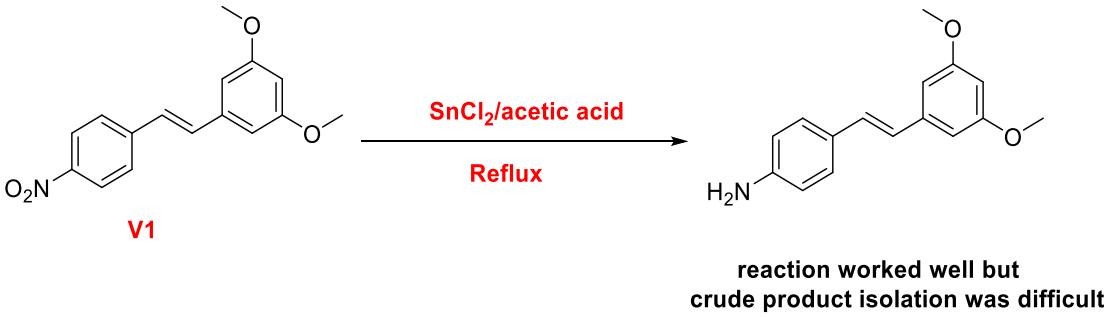

To a solution of (*E*)-1,3-dimethoxy-5-(4-nitrostyryl)benzene (**V1**) (0.5 g, 1 equivalents, 1.75 mmoles) in ethyl acetate, stannous chloride (1.66 g, 5 equivalents, 8.76 mmoles) was added. After refluxing for 6 h, the mixture was cooled to room temperature, and saturated sodium bicarbonate solution was added until the solution was basic. Ethyl acetate was added, and the organic layer was separated. Solvent removal yielded the crude product, which was purified by silica gel column chromatography (EtOAc::petroleum ether::8:2 as the eluent) to provide the target product.

2.6.3. Reduction reaction using zinc metal:

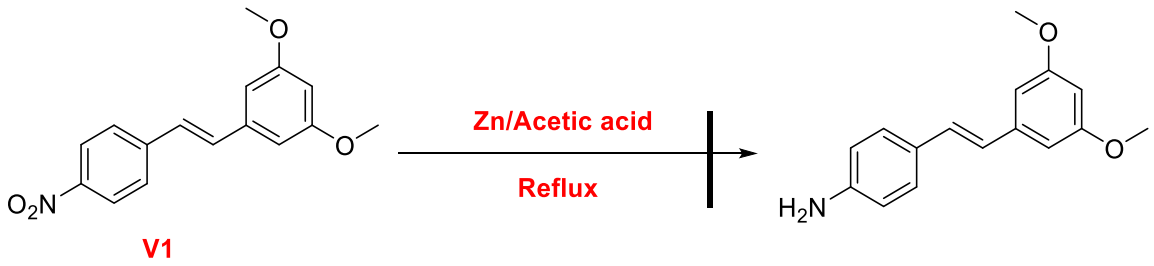

To a stirred solution of (*E*)-1,3-dimethoxy-5-(4-nitrostyryl)benzene (**V1**) (500 mg, 1 equivalents, 1.75 mmol) in acetic acid (10 mL) was added zinc dust (450 mg, 4 equivalents, 7 mmol). After 2 h, the solution was filtered under vacuum through silica gel and the filtrate was concentrated under vacuum. The product was separated by silica gel/celite to obtain compounds.

2.6.4. Synthesis of (*E*)-4-(3,5-dimethoxystyryl)aniline (V12):

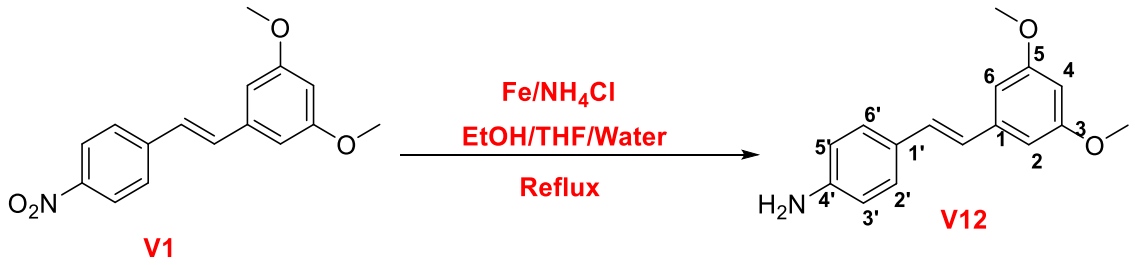

To a solution of (*E*)-1,3-dimethoxy-5-(4-nitrostyryl)benzene (V1) (10 g, 35 mmol, 1 equivalent) in mixture of EtOH/THF/Water (100 mL in ratio 10:5:2.5) were added ammonium chloride (9.37 g, 175.3 mmol, 5.0 equivalents) and iron powder (6.85 g, 122.6 mmol, 3.5 equiv) and the reaction mixture was refluxed at 80 ^{o}C for overnight period. After completion of the reaction (through TLC), the reaction mixture was filtered through celite before cooling. This solution was evaporated to dryness under reduced pressure. The resulting crude was dissolved in saturated 2 M sodium bicarbonate solution (250 mL) and it was further extracted with ethyl acetate (2X100 mL). The organic ethyl acetate layer was washed with water (1X100 mL) and then with saturated brine solution (1X100 mL). This was then dried with excess anhydrous sodium sulphate and filtered under normal gravity. The dried ethyl acetate layer was evaporated to dryness under reduced pressure. The crude product was purified by flash column chromatography (2:8 EtOAc::Petroleum ether) to afford the (*E*)-4-(3,5-dimethoxystyryl)aniline (V12) (5.98 g, 67%).

M.p. = 87-90 °C, (literature m.p. 90-91 °C [132]), Rf (30:90::ethyl acetate:petroleum ether) = 0.3, IR ν (cm^{-1})= 3409, 3307, 3001, 2831, 1593, 1515, 1204, 1151, 961, 825, 670. ^{1}H NMR (400 MHz, $CDCl_3$) δ (ppm) = 3.84 (3H, s, -OMe), 6.38 (1H, t, J2 Hz, H4), 6.65 (2H, d, J2.1 Hz, H2, H6), 6.69 (2H, dd, J6.8/2 Hz, H2',H6'), 6.87 (1H, d, J16.4 Hz, -C=C-H), 7.02 (1H, d, J16.4 Hz, -C=C-H), 7.34 (2H, dd, J6.8/2 Hz, H3', H5'). ^{13}C NMR (100 MHz, $CDCl_3$) δ (ppm) = 55.3 (OMe), 99.5 (C4), 104.3 (C2, C6), 115.2 (C2', C6'), 125.2 (C=C), 127.8 (C3', C5'), 127.9 (C1'), 129.3 (C=C), 140.1 (C1'), 146.3 (C4'), 161.0 (C3, C5), HRMS 256.13189 $[M+H]^+$ **.[see the Appendix B page 258-260 for all spectra]**

2.6.5. Synthesis of (*E*)-N-(4-(3,5-dimethoxystyryl)phenyl)acetamide (V11):

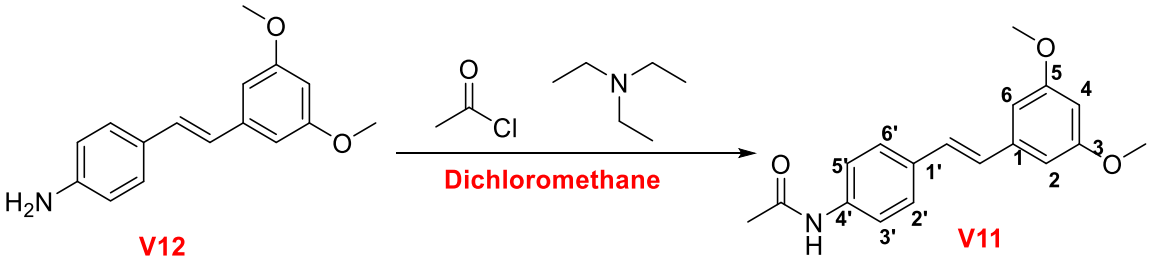

To a solution a of (*E*)-4-(3,5-dimethoxystyryl)aniline (V12) (1 g, 3.91 mmol, 1 equivalent) in dichloromethane (10 mL), triethylamine (3.1 g, 5.87 mmol, 1.5 equivalents) was added at room temperature and reaction mass cooled to 0 °C with stirring. After 30 min, acetyl chloride (0.399 g, 5.09 mmol, 1.3 equivalents) was slowly added to reaction mixture at 0 °C and stirred at RT for overnight period. The reaction mixture was poured into water (25 mL) and extracted with ethyl acetate (2 X 25 mL) organic layer washed with 1N hydrochloric acid (1X5 mL) and water (1 X 10 mL). The organic ethyl acetate layer was evaporated under vacuum to give crude product, which was purified with column chromatography with ((ethyl acetate: petroleum ether (2:8)) to obtain the (*E*)-N-(4-(3,5-dimethoxystyryl)phenyl)acetamide (**V11**) as a light brown solid. (2.45 g, 70%)

M.p. = 103 °C, Rf (10:90::ethyl acetate:petroleum ether) = 0.22, IR ν (cm^{-1}) = 3337, 3079, 2924, 1666, 1583, 1204, 1156, 961, 821, 685. ^{1}H NMR (400 MHz, $CDCl_3$) δ (ppm) = 2.18 (3H, s, -NMe), 3.77 (3H, s, -OMe), 6.31 (1H, t, *J*2.1 Hz, H4), 6.59 (2H, d, J2.1 Hz, H2, H6), 6.88 (1H, d, *J*16.4 Hz, -C=C-H), 6.97 (1H, d, *J*16.4 Hz, -C=C-H), 7.36 (2H, d, J8.8 Hz, H2' and H6'), 7.65 (2H, d, *J*8.8 Hz, H3', H5'), 9.12 (1H, s, -NH). ^{13}C NMR (100 MHz, CDCl3) δ (ppm) = 24.4 (-CO-Me), 55.3(OMe) 99.8 (C4), 104.5 (C2, C6), 120.0 (C3', C5'), 126.9 (C2', C6'), 127.3 (C=C), 128.7 (C=C), 132.4 (C1), 138.6 (C1'), 139.5

(C4'), 160.9 (C3, C5), 169.1 (CO). HRMS 320.11541 $[(M+Na)]^+$ and 617.24234 $[(2M+Na)]^+$. **[See the Appendix B page 255-257 for all spectra]**

2.6.6. Synthesis of (*E*)-N-(4-(3,5-dimethoxystyryl)phenyl)methanesulfonamide (V30)

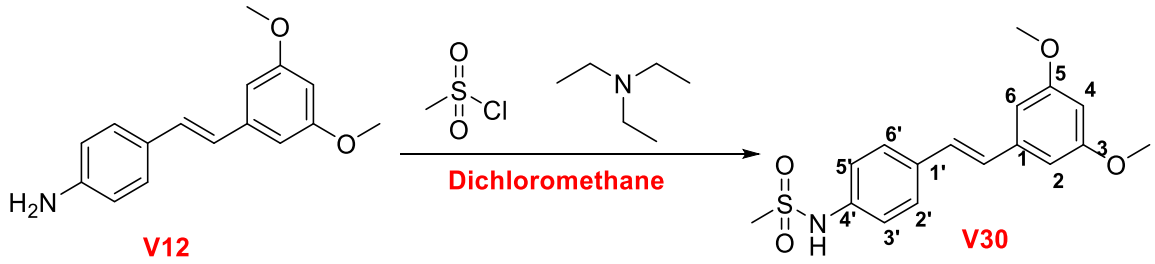

To a solution of (*E*)-4-(3,5-dimethoxystyryl)aniline (V12) (300 mg, 3.91mmol, 1 equivalent) in dichloromethane (10 mL), triethylamine (3.1 g, 5.87 mmol, 1.5 equivalents) was added at room temperature and reaction mass cooled to 0°C with stirring. After 30 min, methane sulphonyl chloride (399 mg, 5.09 mmol, 1.3 equivalents) was slowly added to reaction mass at 0 °C and stirred at RT for overnight period. Reaction mass was poured into water (1X25 mL) and extracted with ethyl acetate (2X 25 mL) organic layer washed with 1N hydrochloric acid (1X5 mL) and water (1X10 mL). The organic ethyl acetate layer evaporated in vacuum to give crude product, which was purified with column chromatography with (ethyl acetate: petroleum ether (2:8)) to obtain the (*E*)-N-(4-(3,5-dimethoxystyryl)phenyl)acetamide (**V30**) as yellow solid. (351 mg, 90%).

M.p. = °C, Rf (10:90: ethyl acetate: petroleum ether) = 0.32 IR ν (cm^{-1}) = 3031, 2943, 2831, 1588, 1360, 1161, 1063, 966, 898, 757, 685. ^{1}H NMR (400 MHz, $CDCl_3$) δ (ppm) = 2.21 (3H, s, -NMe), 3.84 (3H, s, -OMe), 6.42 (1H, t, *J*2.1 Hz, H4), 6.67 (2H, d, *J*2.1 Hz, H2, H6), 7.07 (2H, s, -C=C-H), 7.34 (2H, dd, *J*8.4/2 Hz, H2', H6'), 7.59 (2H, dd, *J*8.4/2 Hz, H3' and H5'). ^{13}C NMR (100 MHz, $CDCl_3$) δ (ppm) = 42.7 (-SOOMe), 55.4 (OMe), 100.5 (C4), 104.9 (C2, C6), 127.4 (C=C), 127.6 (C3', C5'), 130.9 (C2', C6'), 131.2 (C=C), 132.2 (C1'), 138.6 (C1), 139.6 (C4'), 160.0 (C3, C5), HRMS 355.06069 $[(M+Na)]^+$. **[See the Appendix B page 312-314 for all spectra]**

2.6.7. Synthesis of (*E*)-N-(4-(3,5-dimethoxystyryl)phenyl)isobutyramide (V32)

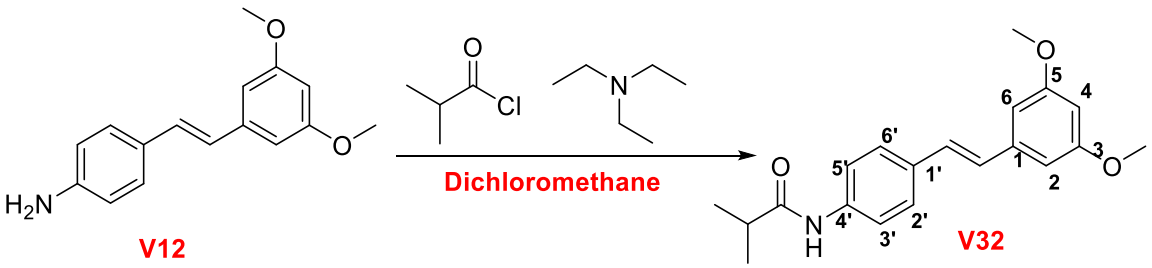

To a solution of (*E*)-4-(3,5-dimethoxystyryl)aniline (V12) (200 mg, 0.783 mmol, 1 equivalent) in dichloromethane (10 mL), triethylamine (3.1 g, 1.17 mmol, 1.5 equivalents) was added at room temperature and reaction mass cooled to 0°C with stirring. After 30 minutes, isobutyryl chloride (399 g, 1.01 mmol, 1.3 equivalents) was slowly added to reaction mass at 0 °C and stirred at RT for overnight period. Reaction mass was poured into water (25 mL) and extracted with ethyl acetate (2X 25mL ethyl acetate) organic layer washed with 1 N hydrochloric acid (5 mL) and water (10 mL). The organic ethyl acetate layer was evaporated under vacuum to give the crude product, which was purified with column chromatography with (ethyl acetate: Petroleum ether (2:8)) to obtain the (*E*)-N-(4-(3,5-dimethoxystyryl)phenyl)acetamide (**V32**) as brown solid. (332 mg, 87%).

M.p. = 89 °C, Rf (10:90::ethyl acetate:petroleum ether)=0.4, IR ν (cm^{-1}) = 3283, 2982, 2953, 2608, 2496, 1661, 1593, 1476, 1161, 1039, 966, 830. ^{1}H NMR (400 MHz, $CDCl_3$) δ (ppm) = 1.24 (6H, d, J6.8 Hz, -$(CH_3)_2$), 2.67 (1H, m, CH$(CH3)_2$), 3.83 (6H, s, -OMe), 6.38 (1H, t, J2 Hz, H4), 6.65 (2H, d, J2 Hz, H2, H6), 6.99 (2H, d, J16 Hz, C=C-H), 7.44 (2H, d, J8.2 Hz, H2', H6'), 7.66 (2H, d, J=8.2 Hz, H3', H5'), 8.16 (1H, s, NH). ^{13}C NMR (100 MHz, CDCl3) δ (ppm) = 8.6 (CH3), 36.4 (-C$(CH_3)_2$), 55.4 (OMe), 99.9 (C4), 104.4 (C2, C6), 119.9 (C3', C5'), 127.0 (C2', C6'), 127.5 (C=C-), 128.7 (C=C-), 132.7 (C1), 138.2 (C1'), 139.5 (C4'), 161.0 (C3, C5), 175.7 (CO), HRMS 348.14857 $[(M+Na)]^+$ and $[(M-CONH(iPropyl))]^+$ 239.20871. **[See the Appendix B page 318-320 for all spectra]**

2.6.8. Synthesis of (*E*)-N-(4-(3,5-dimethoxystyryl)phenyl)benzamide (V36):

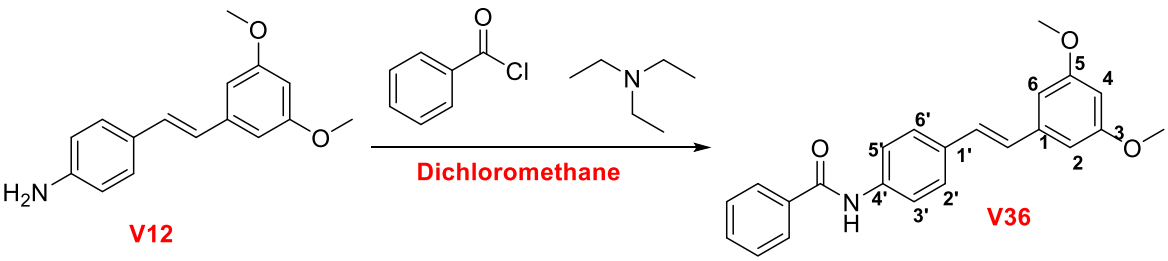

To a solution of (*E*)-4-(3,5-dimethoxystyryl)aniline (V12) (200 mg, 0.55 mmol, 1 equivalent) in dichloromethane (10 mL), triethylamine (3.1 g, 0.85 mmol, 1.5 equivalents) was added at room temperature and reaction mass cooled to 0°C with stirring. After 30 min, isobutyryl chloride (399 mg, 5.09 mmol, 1.3 equivalents) was slowly added to reaction mass at 0 °C and stirred at RT for overnight period. Reaction mass was poured into water (25 mL) and extracted with ethyl acetate (2X 25 mL) organic layer washed with 1N hydrochloric acid (5 mL) and water (10 mL). The organic ethyl acetate layer evaporated in vacuum to give crude product, which was purified with column chromatography with ((ethyl acetate: Petroleum ether (2:8)) to obtain the (*E*)-N-(4-(3,5-dimethoxystyryl)phenyl)acetamide (**V36**) as solid. (592 mg, 80%)

M.p. =167 °C Rf (10:90: ethyl acetate: petroleum ether) =0.29, IR ν (cm^{-1}) = 3283, 2977, 2938, 2618, 2496, 1656, 1593, 1520, 1326, 1165, 957, 689. ^{1}H NMR (400 MHz, $CDCl_3$) δ (ppm) = 3.83 (6H, s, OMe), 6.39 (1H, t, J2 Hz, H4), 6.67 (2H, d, J2 Hz, H2, H6), 7.02 (2H, d, J16.4 Hz, -C=C-H), 7.30-7.55 (5H, m, Aryl H), 7.78 (2H, d, J8.8 Hz, H2', H6'), 7.97 (2H, d, J8.8 Hz, H3', H5'), 8.64 (1H, s, NH), ^{13}C NMR (100 MHz, $CDCl_3$) δ (ppm) = 55.4 (OMe), 99.9 (C4), 104.5 (C2, C6), 120.6 (C2', C6'), 127.1 (2C Aryl), 127.4 (C3', C5'), 127.8 (C=C), 128.6 (C=C), 128.7 (2C Aryl), 131.8 (1C aryl), 133.2 (C1), 134.8 (C1'), 137.9 (1C aryl), 139.4 (C4'), 161.1 (C3, C5), 165.9(CO). HRMS 382.10940 $[(M+Na)]^{+}$. [**See the Appendix B page 327-329 for all spectra**]

2.7. Syntheses of 2′-amino substituted resveratrol derivatives:

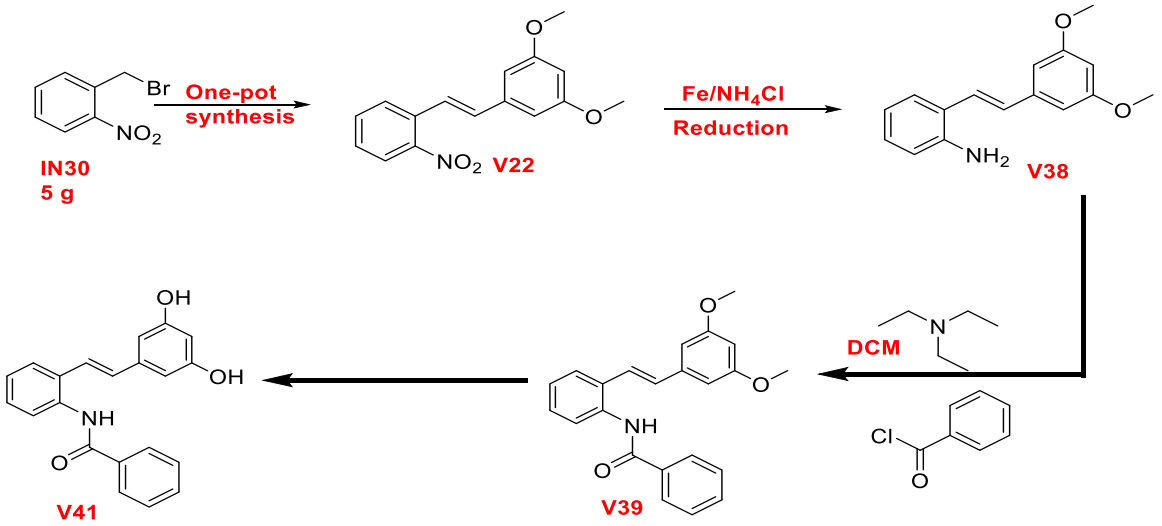

Scheme 2-7 Synthetic scheme for 2′-amino resveralogues.

2.7.1. Synthesis of (*E*)-2-(3,5-dimethoxystyryl)aniline (V39)

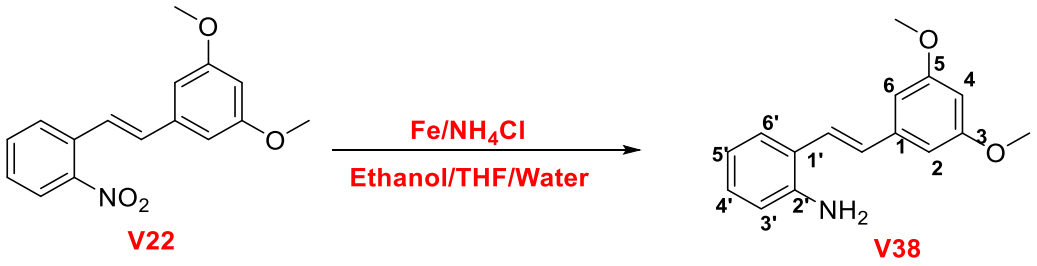

To a solution of (*E*)-1,3-dimethoxy-5-(4 nitrostyryl) benzene (V22) (5 g, 17.6 mmol, 1 equivalent) in EtOH/THF/Water (ratio 10:5:2.5) were added ammonium chloride (4.65 g, 87.5 mmol, 5.0 equivalents) and iron powder (3.43 g, 61.3 mmol, 3.5 equiv) and the reaction mixture was refluxed at 80 ^{o}C for overnight period. After completion of the reaction, the reaction mixture was filtered through celite when it was hot. This solution was then distilled off to remove the solvent. The resulting crude was dissolved in 250 mL 2M sodium bicarbonate solution and it was further extracted with twice with 100 mL ethyl acetate. The organic ethyl acetate layer was wash with 100 mL of water and then with saturated brine solution. This was then dried with sodium sulphate (2 g) and then filtered through normal gravity filtered. This dried ethyl acetate layer was then distilled of to give crude. The crude product was purified by flash column chromatography (2:8 EtOAc/ petroleum ether) to afford the title compound. (2.8 g, 67%).

M.p. =78 $^{\circ}$C, Rf (10:90::ethyl acetate:petroleum ether) = 0.54, IR ν (cm^{-1}) = 3375, 3215, 3001, 2938, 2841, 1593, 1452, 1204, 971, 743, 680. ^{1}H NMR (400 MHz, $CDCl_3$) δ (ppm) = 3.83 (6H, s, OMe), 6.39 (1H, t, *J*2 Hz, H4), 6.66 (2H, d, *J*2 Hz, H2, H6), 6.71 (1H, dd, *J*8, 1.2 Hz, H6'), 6.80 (1H, td, *J*8, 1.2 Hz, H4'), 6.91 (1H, d, *J*16 Hz, C=C-H), 7.10 (1H, td, *J*8, 1.2 Hz, H5'), 7.15 (1H, d, J16 Hz, C=C-H), 7.39 (1H, dd, J8., 1.2 Hz, H3'), ^{13}C NMR (100 MHz, $CDCl_3$) δ (ppm) = 55.4 (OMe), 99.9 (C4), 104.6 (C2, C6), 116.3 (C6'), 119.2 (C4'), 123.7 (C1), 124.8 (C=C), 127.3 (C3'), 128.9 (C5'), 130.3 (C=C-), 139.7 (C1'), 144.0 (C2'), 161.0 (C3, C5). HRMS 256.12666 [(M+Na)]$^{+}$. **[See the Appendix B page 333-335 for all spectra]**

2.7.2. Synthesis of (*E*)-N-(2-(3,5-dimethoxystyryl)phenyl)benzamide (V39):

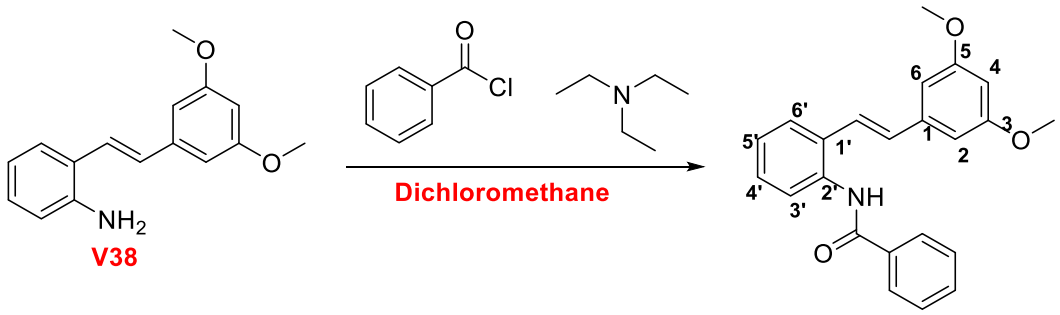

V39

To a solution of (*E*)-4-(3,5-dimethoxystyryl)aniline (V38) (1 g, 3.91 mmol, 1 equivalent) in dichloromethane (10 mL), Triethylamine (3.1 g, 5.87 mmol, 1.5 equivalents) was added at room temperature and reaction mass cooled to 0°C with stirring. After 30 min, isobutyryl chloride (399 mg, 5.09 mmol, 1.3 eq,) was slowly added to reaction mass at 0° C and stirred at RT for overnight period. Reaction mass was poured into water (25 mL) and extracted with ethyl acetate (2X 25 mL ethyl acetate) organic layer washed with 1 N hydrochloric acid (5 mL) and water (10 mL). The organic ethyl acetate layer was evaporated under vacuum to give crude product, which was purified with column chromatography with ethyl acetate: petroleum ether (2:8) to obtain the (*E*)-N-(2-(3,5-dimethoxystyryl)phenyl)benzamide (**V39**) as a solid. (382 mg, 85%)

M.p. =103 °C, Rf (10:90::ethyl acetate:petroleum ether) =0.37, IR ν (cm^{-1}) = 3307, 2987, 2928, 2618, 2506, 1651, 1598, 1457, 1146, 961, 825, 762, 689. ^{1}H NMR (400 MHz, $CDCl_3$) δ (ppm) = 3.80 (6H, s, OMe), 6.42 (1H, t, *J*2.4 Hz, H4), 6.64 (2H, d, *J*2 Hz, H2, H6), 6.98 (1H, d, *J*16.4 Hz, -C=C-H), 7.21 (1H, d, J=16.4 Hz, C=C-H, H6'), 7.24 (1H, td, *J*7.8/2 Hz, H4'), 7.35 (1H, td, J=8/1.2 Hz, H5'), 7.48-7.59 (4H, m, 3H aryl ring, H3'), 7.91-7.98 (3H, m, H6', 2H aryl ring), ^{13}C NMR (100 MHz, $CDCl_3$) δ (ppm) = 55.4 (OMe), 100.4 (C4), 104.8 (C2, C6), 124.1 (C=C), 124.3 (C6'), 125.7 (C4'), 127.1 (2C aryl), 127.2 (C3'), 128.5 (C5'), 128.9 (2C aryl), 130.6 (C1'), 131.9 (1C aryl), 132.9 (C=C), 134.7 (1C aryl), 134.9 (C2'), 139.0 (C1), 161.1(C3, C5), 165.8 (CO), HRMS 382.12716 $[(M+Na)]^+$. **[See the Appendix B page 336-338 for all spectra]**

2.8. Synthesis of heterocyclic based Resveralogues:

The target molecule **TM4** was designed to investigate the effect of heterocyclic substituted resveratrol derivative on SIRT1 activation and their toxicity to MRC-5 cells.

The planned synthetic methods are shown in **Scheme 2-8**. The designed plan was based on Horner-Wittig reaction of intermediate **IN10** and corresponding aldehyde. The intermediate **IN10** was 4′-substituted benzimidazole phosphonate ester whose preparation was planned from 4′-substituted carboxylic acid phosphonate ester (**IN11**) through acid-amine coupling reaction followed by acid cyclisation [164]. However, the intermediate synthesis was not achieved by using this method.

2.8.1. Attempted synthesis of target molecule TM4:

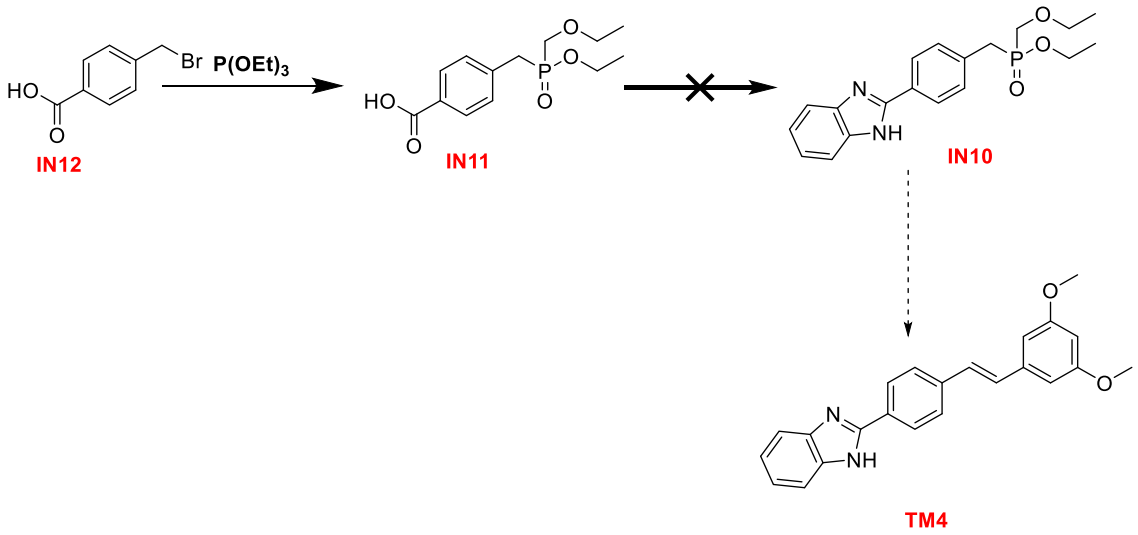

Scheme 2-8 Synthetic scheme for the synthesis of target molecule TM4, a 4′-substituted benzimidazole heterocyclic analogues of resveratrol.

2.8.2. Synthesis of Intermediate IN11:

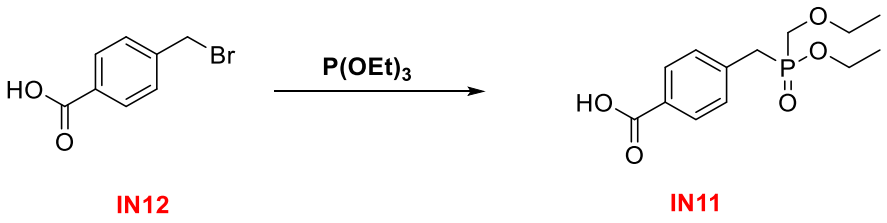

A suspension of 4- (bromomethyl)benzoic acid (4.3 g, 20 mmol) in triethyl phosphite (3.77 mL, 22 mmol) was heated to reflux temperature for the overnight period. The reaction was allowed to slowly cool to room temperature. The precipitate was collected by gravity filtration, washed intensively with n-hexane (100 mL), and dried in vacuo to give the 4-(diethylphosphono-methyl)benzoic acid as a tan solid. (5.34 g, 98%)

2.8.3. Synthesis of intermediate IN10 using oxalyl chloride:

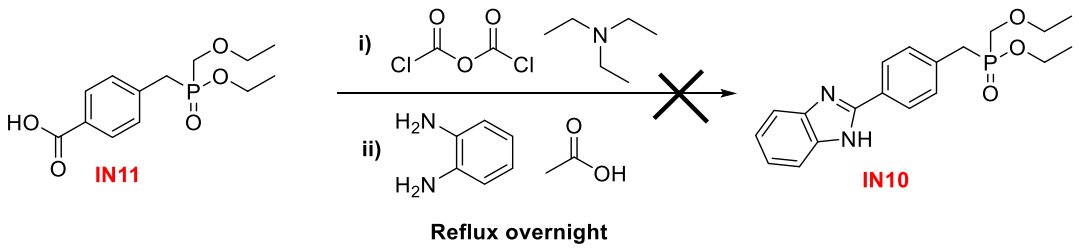

To a stirred solution of Intermediate IN11 (1 g, 3.67 mmol, 1 equivalents) and triethyl amine (747 mg, 7.34 mmol, 2 equivalents) in dicholoromethane (15 mL) (one or two drops of DMF was added) oxalyl chloride (699 mg, 5.55 mmol, 1.5 equivalents) was added dropwise at 0 ^{o}C. The reaction was then stirred at room temperature overnight period. After completion of reaction (by monitoring TLC), reaction mixture solvent was evaporated to dryness on a vacuum pump. This crude reaction mixture was then dissolved in acetic acid (10 mL) and benzene-1,2-diamine (396 mg, 3.67 mmol, 1 equivalents) was added. Reaction mixture was then heated at reflux temperature for the overnight period.

2.8.4. Synthesis of intermediate IN10 using thionyl chloride:

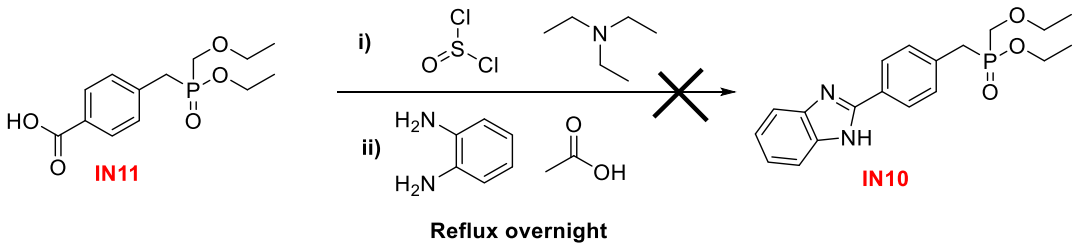

To a stirred solution of Intermediate IN11 (1 g, 3.67 mmol, 1 equivalents) and triethyl amine (747 mg, 7.34 mmol, 2 equivalents) in dicholoromethane (15 mL) (one or two drops of DMF was added) thionyl chloride (655 mg, 5.55 mmol, 1.5 equivalents) was added dropwise at 0 ^{o}C. The reaction was then stirred at room temperature for the overnight period. After completion of reaction (by monitoring TLC), reaction mixture solvent was evaporated to dryness on the vacuum pump. This crude reaction mixture was then dissolved in acetic acid (10 mL) and benzene-1,2-diamine (396 mg, 3.67 mmoles, 1 equivalents) was added.

2.9. Attempted synthesis of 2′-substituted benzimidazole (TM2) derivative of resveratrol:

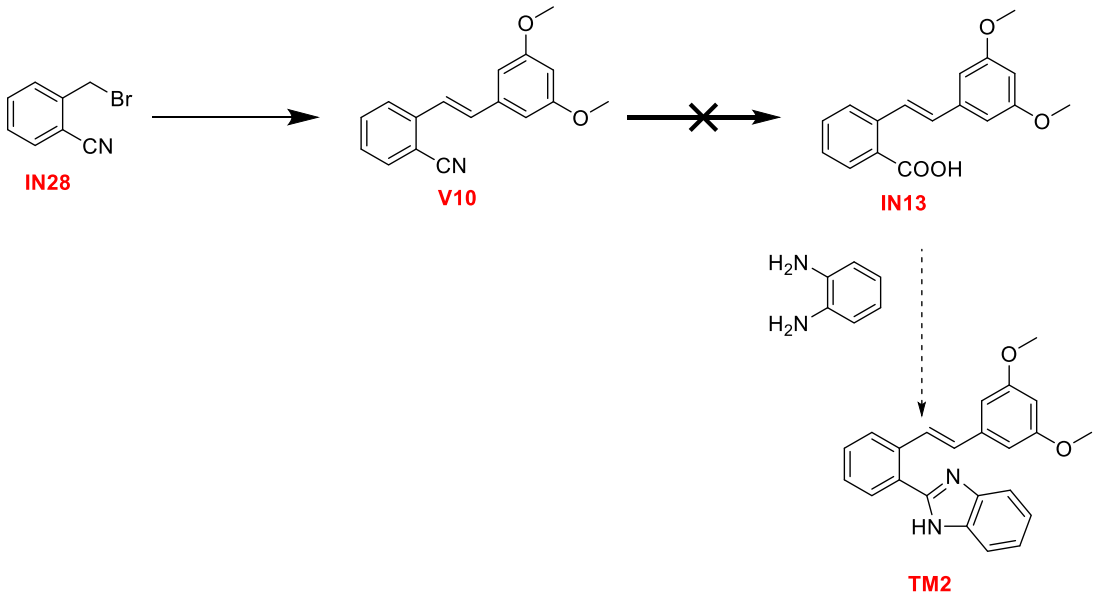

Scheme 2-9 Synthesis of 2′-substituted benzimidazole resveratrol (TM2) derivatives.

2.9.1. Attempted synthesis of intermediate IN13 using lithium hydroxide:

To a stirred solution of (*E*)-2-(3,5-dimethoxystyryl)benzonitrile (**V10**) (200 mg, 0.7 mmol, 1 equivalents) in methanol (10 mL) 2 M LiOH solution (3.75 mL, 3.76 mmol, 5 equivalents) was added. The reaction mixture was stirred at room temperature for the overnight period.

2.9.2. Attempted intermediate IN13 using sodium hydroxide:

To a stirred solution of (*E*)-2-(3,5-dimethoxystyryl)benzonitrile (**V10**) (200 mg, 0.7 mmol, 1 equivalents) in methanol (10 mL) 2 M NaOH solution (3.8 mL, 3.76 mmol, 5 equivalents) was added. The reaction mixture was stirred at room temperature for the overnight period.

2.10. Modified molecules: Synthesis of tetrazole based resveratrol molecules:

The designed benzimidazole target molecule synthesis was not achieved successfully. The aim behind the design was to understand the role of 2′ and 4′-substituted five-member heterocyclic rings on resveratrol and its SIRT1 activation. Further, 4′ and 2′ substituted tetrazole substituted derivatives were synthesised using following methods.

2.10.1. Synthesis of (*E*)-5-(4-(3,5-dimethoxystyryl)phenyl)-2H-tetrazole (V24):

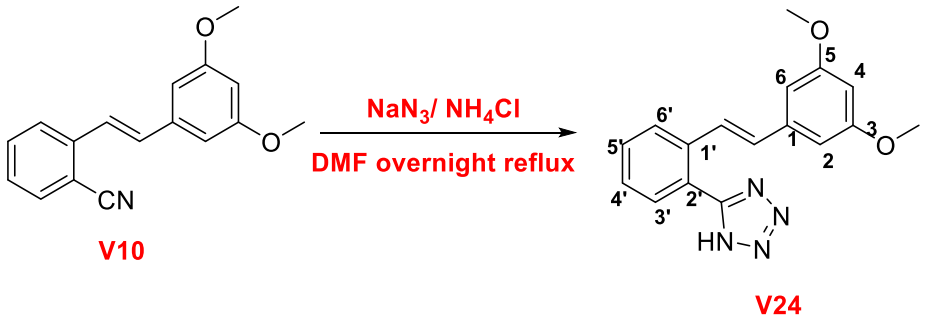

A solution of (*E*)-2-(3,5-dimethoxystyryl)benzonitrile (V10) (1 g, 581.9 mmol, 1.00 eq.) in anhydrous DMF (600 mL) was placed in a flask that had been purged and maintained with an inert atmosphere of nitrogen. Ammonium chloride (302 mg, 5.65 mmol, 1.5 equivalents) was added, followed by the addition of sodium azide (367 mg, 5.65 mmol, 1.5 equivalents). The resulting solution was stirred overnight while maintaining the temperature at 100 °C then allowed to cool to room temperature. The resulting precipitate was filtered off and washed with EtOAc (20 mL). The crude material were purified with column chromatography under gravity (10:90::MeOH:Chloroform) to give the (*E*)-5-(4-(3,5-dimethoxystyryl)phenyl)-2H-tetrazoleas a brown solid. (190 mg, 16.4%)

Mp =214.01°C Rf (10:90:: chloroform: MeOH) = 0.19. IR ν (cm^{-1}) = 2997, 2841, 2763, 1598, 1423, 1301, 1214, 1156, 1059, 961, 835, 753, 680. ^{1}H NMR (400 MHz, $CDCl_3$) δ (ppm) = 3.77 (6H, s, -OMe), 6.47 (1H, t, J2 Hz, H4), 6.70 (2H, d, J2 Hz, H2 and H6), 7.22 (1H, d, J16.2 Hz, -C=C-H), 7.50 (1H, td, J7.6, 1.2 Hz, H5'), 7.61 (1H, td, J1.2, 7.6 Hz, H4'), 7.64 (1H, d, J16.2 Hz, -C=C-H), 7.75 (1H, dd, J1.2, 7.6 Hz, H6'), 7.97 (1H, d, J8 Hz, H3'). ^{13}C-NMR (400 MHz, CDCl3) δ (ppm) = 55.4 (OMe), 99.8 (C4), 104.9 (C2, C6), 123.1 (C=N), 126.4 (-C=C-H, C3'), 128.0 (C5'), 129.9 (C6'), 130.9 (C4'), 131.3 (-C=C-), 136.2 (C1), 139.0 (C1'), 160.7 (C3,C5). HRMS 331.11873 $[M + Na]^+$ and 281.13286 $[M-N_2]^+$. [**See the Appendix B page 294-296 for all spectra**]

2.10.2. Synthesis of Synthesis of (*E*)-5-(4-(3,5-dimethoxystyryl)phenyl)-2H-tetrazole (V34):

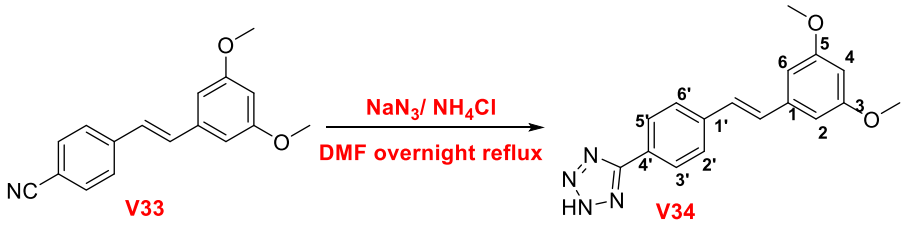

A solution of (*E*)-4-(3,5-dimethoxystyryl)benzonitrile (V33) (1 g, 581.9 mmol, 1.00 equiv) in anhydrous DMF (6 mL) was placed in a flask that had been purged and maintained with an inert atmosphere of nitrogen. Ammonium chloride (302 mg, 5.65 mmol, 1.5 equivalents) was added, followed by the addition of sodium azide (367 mg, 5.65 mmol, 1.5 equivalents). The resulting solution was stirred overnight, while maintaining the temperature at 100 °C then allowed to cool to room temperature. The resulting precipitate was filtered off and washed with EtOAc. The crude material were purified with column chromatography under gravity (10:90::MeOH:Chloroform) to give (*E*)-5-(4-(3,5-dimethoxystyryl)phenyl)-2H-tetrazole (V34) as a white solid. (420 mg, 37.1%).

M.p. 213.95 ºC. Isolated Rf (10:90:: chloroform:meoh)=0.17; IR ν (cm^{-1}) = 3016, 2836, 2710, 1583, 1457, 1316, 1156, 1059, 971, 840, 680. ^{1}H NMR (400 MHz, $CDCl_3$) δ (ppm)= 3.75 (6H, s, -OMe), 6.43 (1H, t, *J*2 Hz, H4), 6.69 (2H, d, *J*2 Hz, H2 and H6), 7.13 (1H, d, *J*16.2 Hz, -C=C-H), 7.64 (2H, d, *J*8.4 Hz, H2'and H6'), 8.10 (2H, d, *J*8.4 Hz, H3'and H5'), ^{13}C-NMR (400 MHz, CDCl3) δ (ppm)= 55.4 (OMe), 100.4 (C4), 104.8 (C2, C6), 127.0 (C2',C6'), 127.6 (C3',C5'), 127.4 (C4'), 128.0 (-C=C-), 130.5 (-C=C-), 138.8 (-C=N), 138.8 (C1), 139.7 (C1'), 161.0 (C3,C5), HRMS 639.23572 $[2M+Na]^{+}$. **[See the Appendix B page 314-316 for all spectra]**

2.11. Synthesis of dihydroresveratrol derivatives:

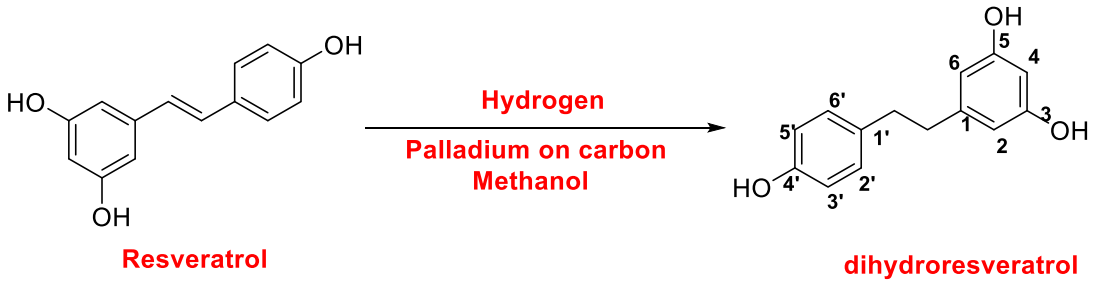

trans-resveratrol (500 mg, 0.66 mmol) was stirred with 10% Pd/C catalyst in methanol (10 mL) at room temperature under supply of hydrogen gas (with balloon). The reaction mixture was stirred overnight period. The catalyst was removed by filtration through celite and the filtrate evaporated to give a solid residue which was purified over silica gel (7:3, hexane:ethyl acetate) to obtain a brown sticky powder (497 mg, 84%). This was recrystallised from ethyl acetate/hexane to give a white solid.

MP= 138-140 ^{o}C, Yield (497 mg, 84%). IR ν (cm^{-1}) = 3001, 2929, 2841, 1598, 1457, 1355, 1209, 1151, 1059, 821, 689. ^{1}H NMR (400 MHz, $CDCl_3$) δ (ppm) = 2.64-2.76 (m, 4H, CH_2-CH_2), 6.18 (t, *J*2.4 Hz, H4), 6.19 (2H, d, *J*2.4 Hz, H2, H6), 6.69 (2H, d, J8.4 Hz, H2', H6'), 6.96 (2H, d, J8.4 Hz, H3', H5'), 7.97 (2H, s, OH), 8.04(1H, s, OH) ^{13}C NMR (100 MHz, $CDCl_3$) δ (ppm) = 36.6 (-CH_2), 38.19 (-CH_2), 100.7 (C4), 107.2 (C2, C6), 115.3 (C2', C6'), 129.2 (C3', C5'), 132.9 (C1'), 144.3 (C1'), 154.9 (C4'), 157.9 (C3, C5). HRMS 253.06737 $[(M+Na)]^{+}$ **[see the Appendix B page 350-352 for all spectra]**

2.11.1. Synthesis of 1,3-dimethoxy-5-(4-methylphenethyl)benzene (V15):

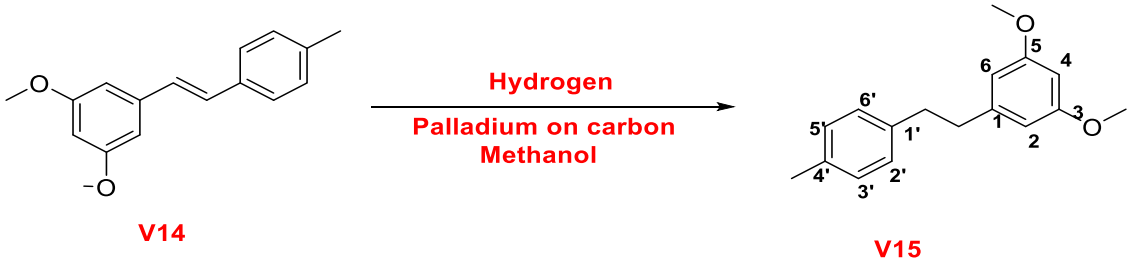

V14 V15

(*E*)-1,3-dimethoxy-5-(4-methylstyryl)benzene (V14) (500 mg, 0.66 mmol)was stirred with 10% Pd/C catalyst in methanol (10 mL) at room temperature in supply of hydrogen gas with balloon. The reaction mixture was stirred overnight period. The catalyst was removed by filtration through celite and the filtrate evaporated to give a solid residue which was purified over silica gel (7:3, hexane:ethyl acetate) to obtain a brown sticky powder. (497 mg, 84%)

M.p.= 165 ^{o}C, IR ν (cm^{-1}) = 3001, 2929, 2841, 1598, 1457, 1355, 1209, 1151, 1059, 821, 689. ^{1}H NMR (400 MHz, $CDCl_3$) δ (ppm) = 2.93 (s, CH_3), 2.83-2.92 (m, 4H, CH_2-CH_2), 6.33(t, *J*2.4 Hz, H4), 6.37 (2H, d, *J*2.4/1 Hz, H2, H6), 7.11 (4H, s, H2', H3', H5', H6'). ^{13}C NMR (100 MHz, $CDCl_3$) δ (ppm) = 37.2 (-CH_2), 38.4 (-CH_2), 55.3(-CH_3), 98.0 (C4), 106.5 (C2, C6), 128.3 (C2', C6'), 129.0 (C3', C5'), 135.4 (C4'), 138.7 (C1'), 144.3 (C1),

160.7 (C3, C5'). HRMS 279.13863 $[(M+Na)]^+$. **[See the Appendix B page 267-269 for all spectra]**

Chapter 3. Biological material and methods:

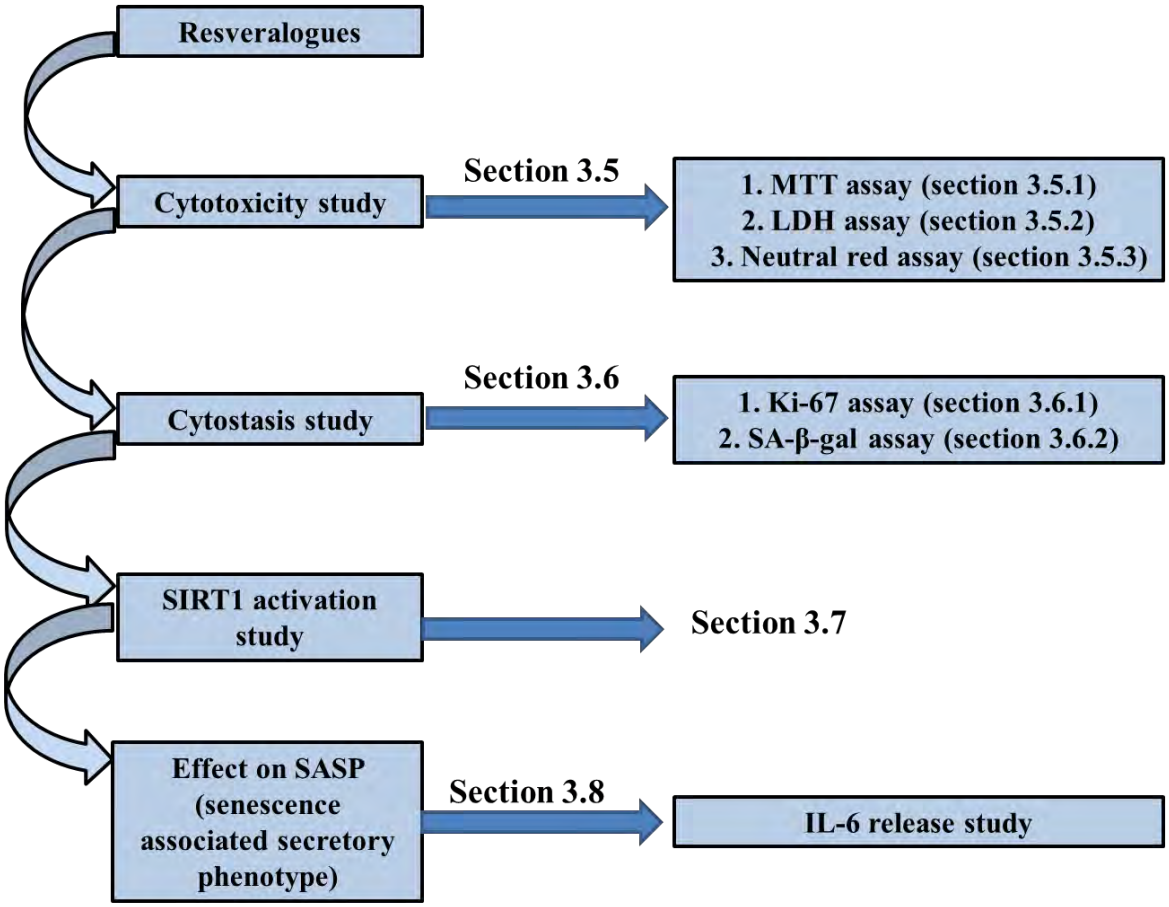

Figure 3-1 Overall summery of biological screening study for resveralogues.

3.1. Materials, Chemicals and glassware:

All reagents were of biological grade and purchased from Sigma (UK) or BD life sciences (UK). They were stored as per manufacturer directions. Tissue culture flasks were 25 and 75cm^2 were from Greiner and 6, 12 and 24 well plates were from Falcon. Plastics were from Fischer scientific.

3.2. Instruments:

Microscope: Axiovert 25 inverted light microscope from Carl Zeiss was used and Fluorescence microscopy was done by Leica TCS SP5 confocal microscope.

Plate reader: Lab systems ascent plate reader was used.

Fluorescence plate reader: Synergy HT multimode was used for fluorescence determination study.

Incubators and tissue culture hoods: HERA cells incubators and ESCO Airstream tissue culture hoods were used.

3.3. Preparation of standard buffers and assay kits:

All of the standard buffers were prepared in deionised water at room temperature.

Tissue culture medium: The culture medium (CM) for MRC-5 human diploid fibroblasts was modified Eagles medium (MEM) with 2 mM sodium glutamate (500 mL), 15% FBS (fetal bovine serum, 75 mL), and 1% non-essential amino acids (5 mL). (all of them purchased from GE lifesciences, UK)

Freezing medium: Freezing media (10 mL) (**FM**) were prepared from 60% culture media (6 mL), 30% FBS (fetal bovine serum, 3 mL) and 10% dimethyl sulphoxide (1 mL).

PBS/FBS solution (PBS/FBC): PBS/FBS solution was prepared from 1X PBS and FBS (9:1 ratio).

Mouse monoclonal ki67 antibody was purchased from Genentech, UK and used at a final dilution of 1/20 in PBS/FBS solution. (80 µL of ki67 antibody in PBS/FBS solution which includes 4 µL of ki67 antibody and 76 µL of PBS/FBS (9 mL of PBS/1 mL of FBS)

Goat anti-rabbit FITC conjugated secondary antibody was purchased from Dako chemicals, UK and used at final dilution of 1/30 in PBS/FBS solution. (80 µL goat anti-rabbit of antibody in PBS/FBS solution which includes 4 µL of goat anti-rabbit antibody and 76 µL of PBS/FBS (9 mL of PBS/1 mL of FBS)

Phosphate buffer solution (1XPBS): PBS tablets were obtained from Gibco chemicals, UK and for 1X PBS solution one tablet was dissolved in 100 mL deionised water and sterilised by standard autoclave technique.

3-(4,5-dimethylthiazol-2-yl)-2,5-diphenyl tetrazolium bromide (**MTT dye solution**)**:** MTT dye (catalogue no. M5655-100MG, Sigma, UK) was prepared in PBS solution with concentration of 0.5 mg/mL.

Preparation of resveralogues stock: All 'resveralogue' stock solutions (2 mM , 10 mM and 20 mM) were prepared in cell culture grade dimethylsulphoxide. 5 µL of each stock solution was added to cell medium to get final concentration of 10 µM, 50 µM and 100 µM. The final concentration of DMSO was maintained between 0.5% and 0.2%. Compounds were denoted as V1-V41.

Cytotoxicity assay kits: Lactate dehydrogenase assay kit was purchased from Pierce (LDH Cytotoxicity Assay Kit Catalog number: 88953, UK) and used as per the manufacturers protocol.

Neutral red assay was purchased from Sigma-Aldrich Company, UK (catalogue no TOX4-1KT) and used as per the manufacturers protocol.

Senescence-associated β galactosidase assay (SA-β-gal assay) was purchased from cell signalling, UK (catalogue no # 9860S).

SIRT1 activity kit:

Three kits were used; Enzo-life sciences, USA (catalogue no **BML-AK555-0001)**; Sigma-Aldrich company **(**catalogue no **CS1040-1KT)** and Cayman chemicals, UK (catalogue no 10010401). Final kit used was Cayman chemicals.

IL-6 assay kit: Human IL-6 ELISA Kit II (BD life sciences, UK catalogue no 550799) was used to determine the IL-6 release, as per manufactures protocol.

3.4. Cell strain and standard maintenance:

Human diploid foetal lung fibroblasts (MRC5) are widely used in ageing research. Cells were obtained from the Coriell Institute for Medical Research (AG05965B). The cells were maintained of a density of 1.3×10^4 cells/cm^2. Cells were sub-cultured every 5–10 days by standard trypsin dispersion. Viable cell counts were determined by live or dead exclusion using trypan blue. The population doubling (PD) was determined at every passage using the standard equation.

Population doubling = 3.32 X [$\log_{10}N_H$ - $\log_{10}N_s$]

Where,

N_H = total no of cells harvested cells.

N_s = total number of cells seeded.

3.4.1. Cell passage:

Cells were passaged at 80-95% confluency using standard trypsin dispersion method. In brief, the medium was aspirated off and the cells washed 1XPBS. Cells were recovered into a suspension by treatment with trypsin: EDTA (0.25%) neutralised by the addition of culture medium (8 mL) where the FCS neutralises the action of trypsin. Cell suspension centrifuged at 400g for 4min. The supernatant was aspirated and the pellet re-suspended in fresh culture medium and counted using a Bright line haemocytometer. Cells were then seeded at a density of 1.3×10^4 cells/cm^2.

3.4.2. Cryopreservation:

Cells were harvested as shown in **Section 3.4.1** and then cells were re-suspended at $1x10^6$ cells/mL in freezing medium (**FM**). The cryovials were placed into a Nalgene freezing container for overnight at -70 ^{0}C before being transferred to liquid nitrogen for long-term storage.

3.5. Cytotoxicity assay:

To evaluate the cytotoxicity of synthesised novel resveralogues on cells three principle assays were used and included MTT, Neutral red and LDH toxicity assay.

3.5.1. MTT:

3.5.1.1. Introduction:

3-(4,5-di**m**ethyl**t**hiazol-2-yl)-2,5-diphenyl **t**etrazolium bromide (**MTT**) assay is a colorimetric method used to quantify cell viability and proliferation [165]. The MTT dye enters into the cells and passes to the mitochondria of live cells. Mitochondrial dehydrogenase enzymes, present only in mitochondria of living cells, reduce MTT to produce formazan (an insoluble purple crystal product). The amount of formazan (quantify using absorbance value 570 nm) is directly link to the cell viability. A typical reduction reaction that takes place in mitochondria of live cells shown in **Figure 3-2**:

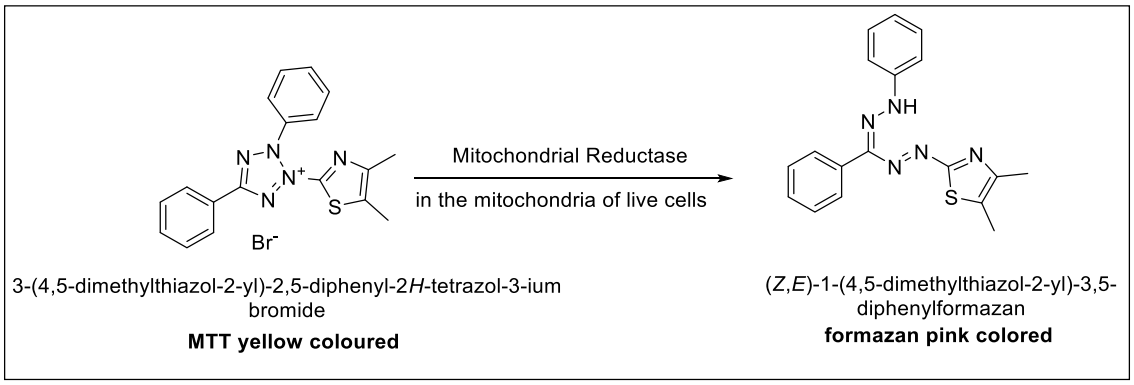

Figure 3-2: Formation of formazan reaction.

3.5.1.2. Protocol:

MRC-5 cells were seeded in 24 well plates at seeding density a 1.3X 10^4 cells /cm^2 and incubated at 37 ^oC (5% CO_2 and 95% air) for 24hrs. After 24 hours of incubation time compounds (final concentration 10, 50 and 100 μM) were added and further incubated for next 24 hours before washed in PBS. Samples were incubated with 0.2 mL MTT solution (0.5 g/mL) and incubated for 1 h period. After 1hr time, the formazan crystals formed were dissolved in 200 μL of DMSO and the absorbance was determined at 540 nm. The percentage cell viability was analysed using the following equations;

$$= \left[\frac{\text{Optical density of sample treated cells – optical density of DMSO as a blank}}{\text{[Optical density of control untreated cells- optical density of DMSO as a blank]}}\right] \text{ X 100}$$

Where, blank represent the optical density shown by DMSO only.

3.5.2. LDH:

3.5.2.1. Introduction:

LDH toxicity assay is a colorimetric assay that has been used to measure and quantify the LDH activity in cells [166]. Lactate dehydrogenase is a cytosolic enzyme that is present in all cells. When cells are damaged, thereafter it releases Lactate dehydrogenase into the medium. This released Lactate dehydrogenase can then be converted to a red coloured formazan dye using two consecutive enzymatic reactions. In the first step, the NAD^+ reduced to its counterpart NADH using LDH that released from damaged cells. Further in second enzymatic reaction, the reduced NADH then catalyses the conversion of a tetrazolium salt into pink coloured formazan. A typical reaction is shown in **Figure 3-3**;

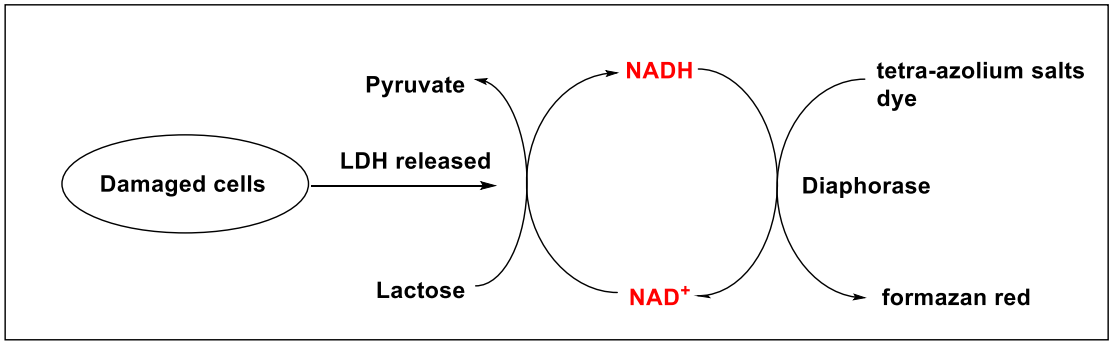

Figure 3-3: LDH assay principle modified from Pierce LDH assay protocol.

3.5.2.2. Protocol:

The toxicity studies were performed by using Pierce LDH Cytotoxicity assay kit protocol. MRC5 cells were seeded in 24 well plates with 1.3 $X10^4$ cells/cm^2 for 24 hours at 37 ^oC humid incubator (5% CO_2 and 95% air) in culture medium. After 24 hours of incubation time compounds (final concentration 10, 50 and 100 µM) was added and further incubated for next 24 hours. Then, assay protocol was followed as per the manufactures directions. The percentage LDH release was analysed from the following equation;

$$\% \text{ LDH release} = \frac{\text{Compound-treated LDH activity} - \text{Spontaneous LDH activity}}{\text{Maximum LDH activity} - \text{Spontaneous LDH activity}} \times 100$$

Where,

Spontaneous LDH activity is water treated cells to determine the LDH activity in media as a background.

Maximum LDH activity is Triton X treated cells as a positive control for LDH release.

3.5.3. Neutral red:

3.5.3.1. Introduction:

Neutral red assay is based on ability of incorporation and binding of neutral red (3-amino-7-dimethylamino-2-methylphenazine hydrochloride) dye into lysosomes of live cells [167]. This dye is then extracted from cells using an acidified solution whose absorbance gives the quantification of the viability of cells.

3.5.3.2. Protocol:

MRC5 cells were seeded in 24 well plates with 1.3 $X10^4$ cells/cm^2 for 24 hours at 37ºC humid incubator (5% CO_2 and 95% ir) in media. After 24 hours of incubation time compounds (at a final concentration 10, 50 and 100 μM) was added and further incubated for next 24 hours. Then, assay protocol was followed as per the manufactures protocol. The percentage cells viability was analysed by the following equation;

$$\text{Cell viability} = \left[\frac{\text{Optical density of sample treated cells – optical density of DMSO as a blank}}{\text{Optical density of control untreated cells- optical density of DMSO as a blank}}\right] \times 100$$

3.6. Cell cytostasis study:

To study the effect of resveralogues on MRC5 cells cytostasis, proliferation marker ki-67 assay and Senescence-associated β-galactosidase assay (SA-β-gal assay) were used.

3.6.1. Ki-67 immunofluorescence assay:

3.6.1.1. Introduction:

Ki-67 is a nuclear antigen expressed predominantly in proliferating cells during all parts of the cell cycle S, G1 and G2 (except G0 phase). This assay determines the number of proliferating cells using immunofluorescence in which the primary antibody of ki-67 reacts with an epitope on a nuclear antigen ki-67. The detailed protocol for assay is described in **Section 3.6.1.2**

3.6.1.2. Protocol:

MRC-5 cells were seeded onto sterile 13mm coverslips with seeding density $1.3X10^4$ cells/cm^2 and incubated at 37° C (5% CO_2 and 95% air) for 24 h. The MRC-5 cells were treated with specific resveralogues for a further 24 h before being washed once in 1XPBS and fixed in 1 mL mixture of methanol and acetone (1:1) for 5–10 min at room temperature. Fixed cells were washed in PBS and incubated with mouse monoclonal anti-ki-67 antibody was added (at final dilution 1/20 in PBS/FCS) and incubated in humid chambers at 4 °C for the overnight period. Cells then washed with PBS and incubated with goat anti-rabbit FITC conjugated (1/30 in PBS/FCS) for 1 h at room temperature. Finally, the cells were washed with PBS and mounted using DAPI mountant, before being viewed using fluorescence microscope. To calculate the percentage of proliferating cells, either total 1000 cells or 200 positive cells were calculated.

Percentage of proliferating nuclei = Number of positive nuclei (green FITC stain) x 100

Number of normal nuclei (blue DAPI stain).

3.6.2. Senescence associated-β-galactosidase assay (SA-β-gal assay):

3.6.2.1. Introduction:

An *in-vitro* biomarker of senescent cells was first described by Dimri and co-workers [19]. This method is based on an increased level of lysosomal β-galactosidase activity in senescent cells which was detected using a cytochemical assay at pH 6. This is called as Senescence associated-β-galactosidase activity (SA-β-gal activity). However, most of (presenescent, quiescent or immortal cells) can produce SA-β-gal activity only at pH 4 and not at pH6.

3.6.2.2. Protocol:

MRC-5 cells were seeded onto sterile 13mm coverslips with seeding density $1.3X10^4$ cells/cm^2 and incubated at 37 °C (5% CO_2 and 95% Air) for 24 hrs. The MRC-5 cells were treated with specific compounds for a further 24 hrs. Then, the assay was performed as per manufactures protocol and the percentage of Senescence associated-β-galactosidase positive cells (SA-β-gal activity) were analysed by using following equation;

Percentage of SA-β-gal positive cells = $\frac{\text{Number of positive nuclei (green stain)}}{\text{Number of normal nuclei.}}$ **x 100**

3.7. SIRT1 assay:

3.7.1. Introduction:

SIRT1 activity was determined by an *in-vitro* enzymatic assay. The assay principle is based on two step enzymatic reaction. In the first step, human SIRT1 recombinant protein deacetylates the acetylated SIRT1 substrate (**1**) in the presence of cofactor NAD^+, See **Figure 3-4**. This deacetylates substrate (**2**) further incubated with developer II which was then releases fluorescence substrate (**3**). The fluorescence substrate then analysed using an excitation wavelength 360 nm and an emission wavelength of 460 nm.

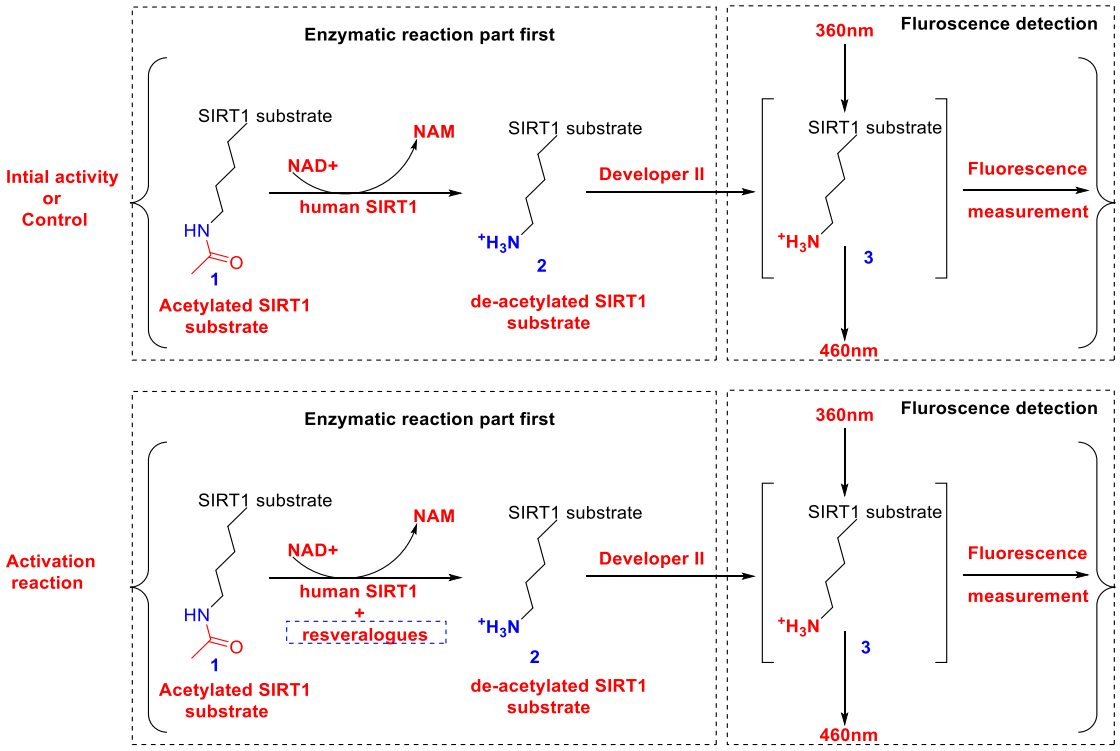

Figure 3-4: Enzymatic SIRT1 Fluorescent activation assay.

3.7.2. Protocol and optimisation of assay kits:

Three assay kits were tested for suitability for determination of SIRT1 activity. These kits included Sigma, Enzo-lifes sciences and Cayman chemicals. However, the first two kits did not work properly even though changing the assay conditions and reagents concentrations. The controls for the assay failed to work effectively and therefore not

used. For a summary of the running conditions see **Appendix A**. The kit from Cayman chemicals was the only one worked effectively. Therefore, all SIRT1 activity was determined using this kit following the protocol provided by the manufacturer.

SIRT Assay procedure:

The enzyme activation studies were performed as per the instructions given in the kit (SIRT1 Fluorometric drug discovery kit, Cayman catalogue no 10010401). As per the supplier protocol all the reactions were carried in a reaction buffer that consisted of 50 mM Tris/HCl, pH 8.0, 137 mM NaCl, 2.7 mM KCl, 1 mM $MgCl_2$, 1 mg/cl BSA in the presence of 2% DMSO. Initially 5 µL compounds from the stock made in DMSO (250 µM for 25 µM final concentration and 1 mM for 100 µM final concentration) were diluted in the 25 microliter reaction buffer and were followed by the addition of 5 µL of diluted SIRT1 enzyme (catalogue no 10010994 and diluted using kit protocol) provided by supplier kit. The reaction was initiated by addition of 15 µM of substrate solution. (The substrate solution for the deacetylase reaction was prepared by kit protocol in which final concentration of peptide was 125 µM and 3 mM for NAD+ in deacetylase reaction.) Then, the plate was covered with plated cover and incubates on a shaker for 45 minutes at room temperature. After 45 minutes reaction time, the reaction was stopped by 50 microliter of stop solution which was prepared as per assay kit instruction and plate was further incubated for 30 minutes at room temperature. Fluorescence reading was measured using Synergy HT multimode Plate Reader with excitation set at 360/40 nm and emission measured at 460/40 nm.

% SIRT1 Activation

$$= \frac{\text{[Fluorescence of sample – Fluorescence of SIRT1 enzyme only activity]}}{\text{Fluorescence of SIRT1 enzyme only activity}} \times 100$$

Where,

An SIRT1 enzyme only activity represents as control SIRT1 enzyme activation reaction carried out in the presence of 0.5% DMSO without any resveralouge.

3.8. Effect on Senescence-associated secretory phenotype (SASP):

3.8.1. Introduction:

When cells became senescent it altered the cells environment through producing pro-inflammatory molecules, growth promoting and remodelling factors. (e.g. TNF-α, IL6, IL-8). To evaluate the effect of synthesised resveralogues on SASP, IL-6 release was studied using Sandwich enzyme-linked immunosorbent assay (ELISA).

3.8.2. IL-6 assay protocol:

The release of IL-6 by MRC-5 cells cultures was determined by ELISA assay (BD Biosciences Catalogue No.550799) according to the manufacturer's recommendations. MRC5 cells were seeded in 24 well plates with $1.3X10^4$ cells/cm^2 for 24 hours at 37ºC humid incubator (5% CO2 and 95% Air) in media. After 24 hours of incubation time compounds (at a final concentration of 10, 50 and 100 μM) were added and incubated further 24 hours. After the incubation time, media was collected from each sample and stored at -20^{O}C until required. The assay was run as per the manufacture's protocol.

3.9. Data and statistical analysis:

All data was analysed using Graphpad Prism 5 software. MTT, Neutral red and LDH, Ki-67, SA-β-gal and IL-6 assay data values from three different biological replicates were transformed into percentage control and mean ± standard deviation was calculated for error bars. Statistical analyses were carried out using Dunnett's multiple comparison test. Significance was detected at p-value of <0.05 (*), <0.01(**) and <0.001(***).

Chapter 4. Biological results:

4.1. Effect of DMSO on cells viability:

Resveralogue stock solutions were prepared in DMSO with a final concentration of DMSO maintained up to 0.5%. Cell viability assay was carried out in order to investigate the effect of DMSO on cell viability. DMSO at 0.5% and 0.2% on cell viability was analysed in comparison to untreated cells. Significance change in cell viability was seen with treatment of 0.5% and 0.2% DMSO, See **Figure 4-1**.

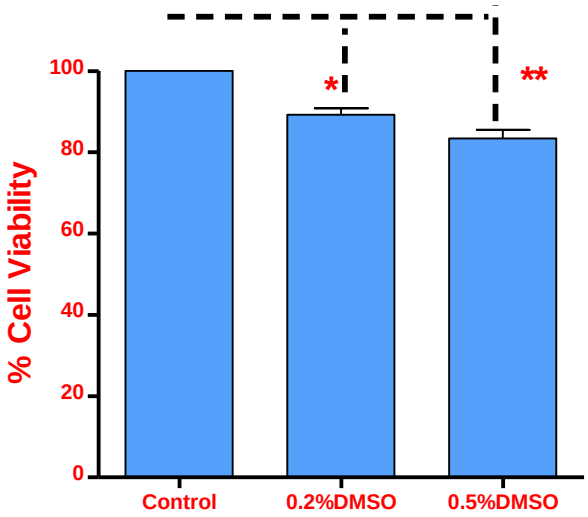

Figure 4-1: Effect of DMSO on MRC5 cells viability after 48 hours incubation time. The y-axis shows the percentage of cell viability when MRC5 cells were treated with 0.2% and 0.5% DMSO for n = 3 different biological replicate cultures (± standard deviation). Dotted black line represent the statistical comparison between control cells with 0.2% and 0.5% of DMSO treated cells. Statistical significance was analysed using one-way ANOVA followed by Dunnett's multiple comparison test: (*) $p < 0.05$, (**) $p < 0.01$, (***) $p < 0.001$, versus control which represents untreated cells.

4.2. Morphological changes in MRC5 cells:

Resveralogues (V1-V41) were prepared in DMSO at a final concentration less than 0.5%. Resveralogue precipitations were noted in media at 50 µM and 100 µM for V1, V7, V17, V22, V26, V27, V28, V30, V32, V33 and V38, see **Figure 4-2 to Figure 4-12 .** Typical morphological changes observed at 24 h post incubation time after treatment at 10 µM, 50 µM and 100 µM are shown in **Figure 4-2** to **Figure 4-12**. At 10 µM concentration there were no changes observed in cells morphology except in the cases of resveralogues V19, V17, V16, V15 and V11, see **Figure 4-5** to **Figure 4-7**. In general, a change in morphology was observed post-treatment with resveralogues (including resveratrol) at 50 µM and 100 µM (resveratrol, V1, V2, V5, V6, V8, V11, V12, V15, V16, V17, V18, V19, V20, V23, V26, V27, V30, V37, V42 and V40, see **Figure 4-2** to **Figure 4-10** and **Figure 4-12**). In case of resveralogues V11, V19, V23, V27 and V42 cell shrinkage was noted at 50 and 100 µM (see **Figure 4-5**, **Figure 4-7** to **Figure 4-9** and **Figure 4-12**). This suggested the apoptotic type of cell death when MRC5 cells were treated with these resveralogues. However, resveralogues V2, V5, V6, V10, V13, V18, V21, V22, V29 and resvedratrol treatment shown elongation or increase in cells morphology which was nearly double of control untreated cells (see **Figure 4-2** to **Figure 4-7** and **Figure 4-9**). This indicated the induction of senescence when MRC5 cells were treated with these compounds above 10 µM. At 100 µM concentration, all of the resveralogues was found to affect cell morphology (**Figure 4-2** to **Figure 4-12**). In case of V36, V39, V40 and V41 there was no cells was noted in culture flask at 100 µM of these compounds (see, **Figure 4-11** to **Figure 4-12**). No morphological changes were observed for DHRSV, V24, V31 and V34 resveralogues (**Figure 4-8** and **Figure 4-10**).

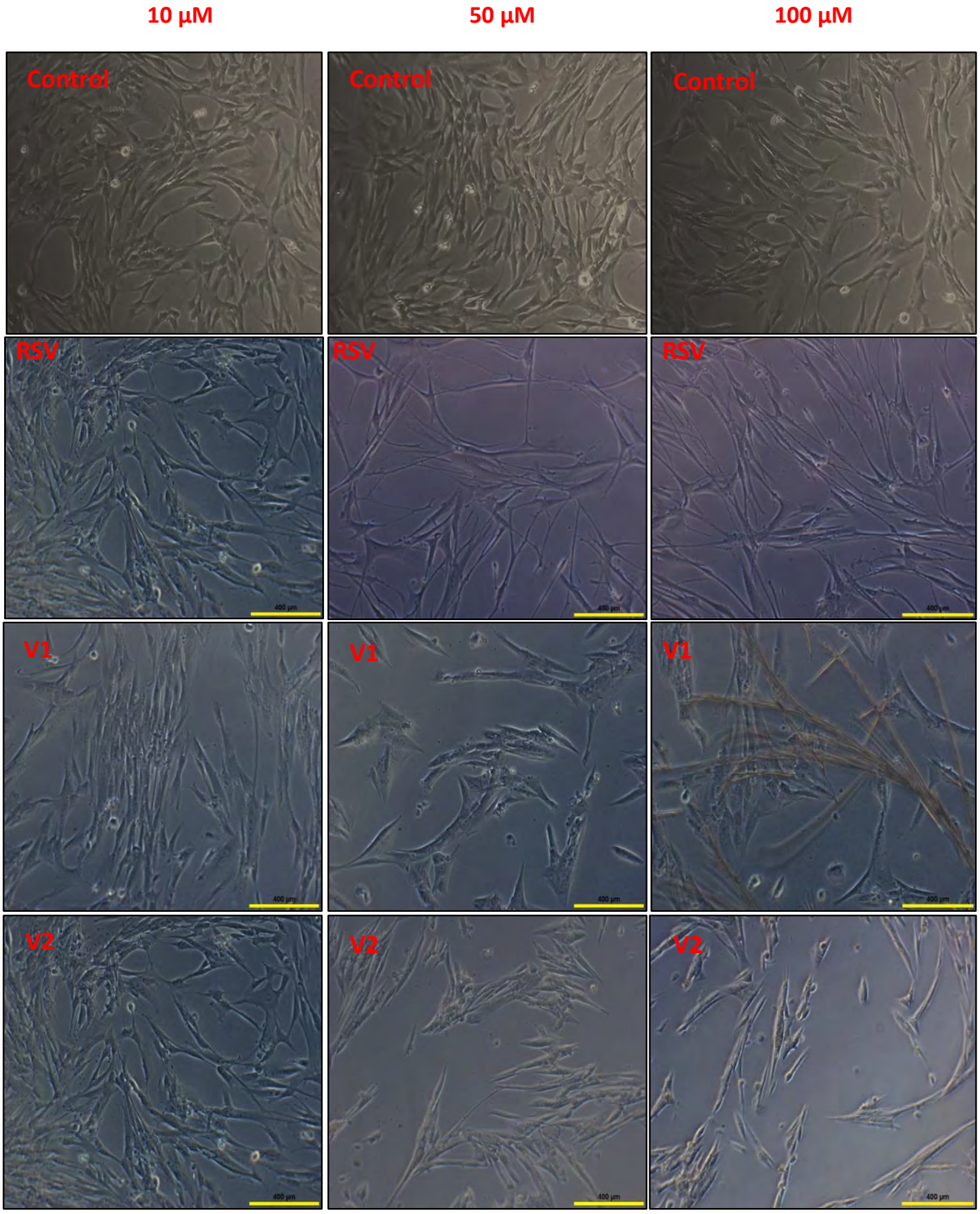

Figure 4-2 Morphological changes that were observed when cells were treated with resveralogues on primary human lung fibroblasts (MRC-5) at CPD 36-40. Cells were photographed under an inverted light microscope at ×20 magnifications where control represents cells without any treatment, RSV- Resveratrol, V1 and V2.

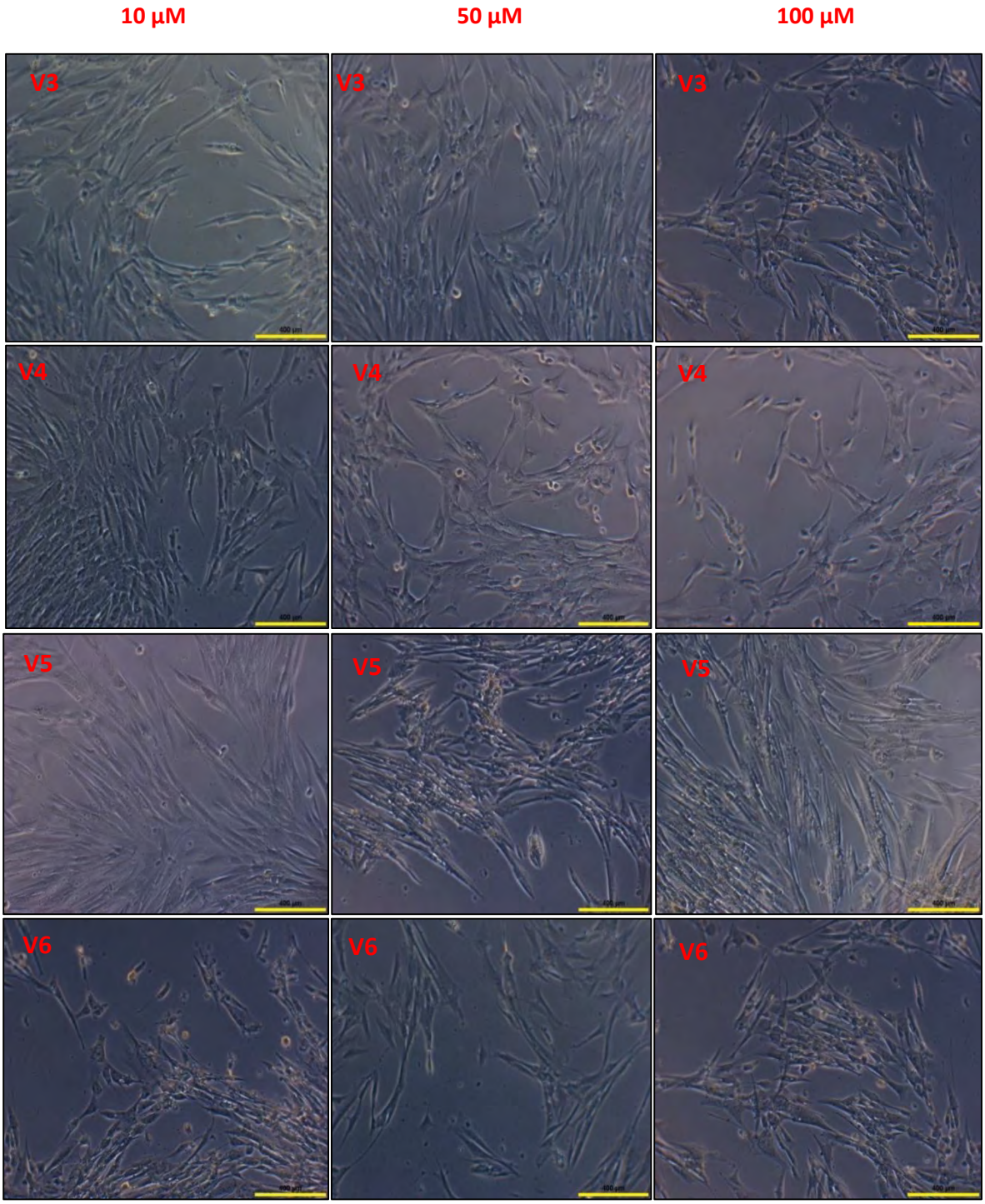

Figure 4-3 Morphological changes that were observed when cells were treated with resveralogues V3, V4, V5 and V6 on primary human lung fibroblasts (MRC-5) at CPD 36-40. Cells were photographed under an inverted light microscope at ×20 magnifications.

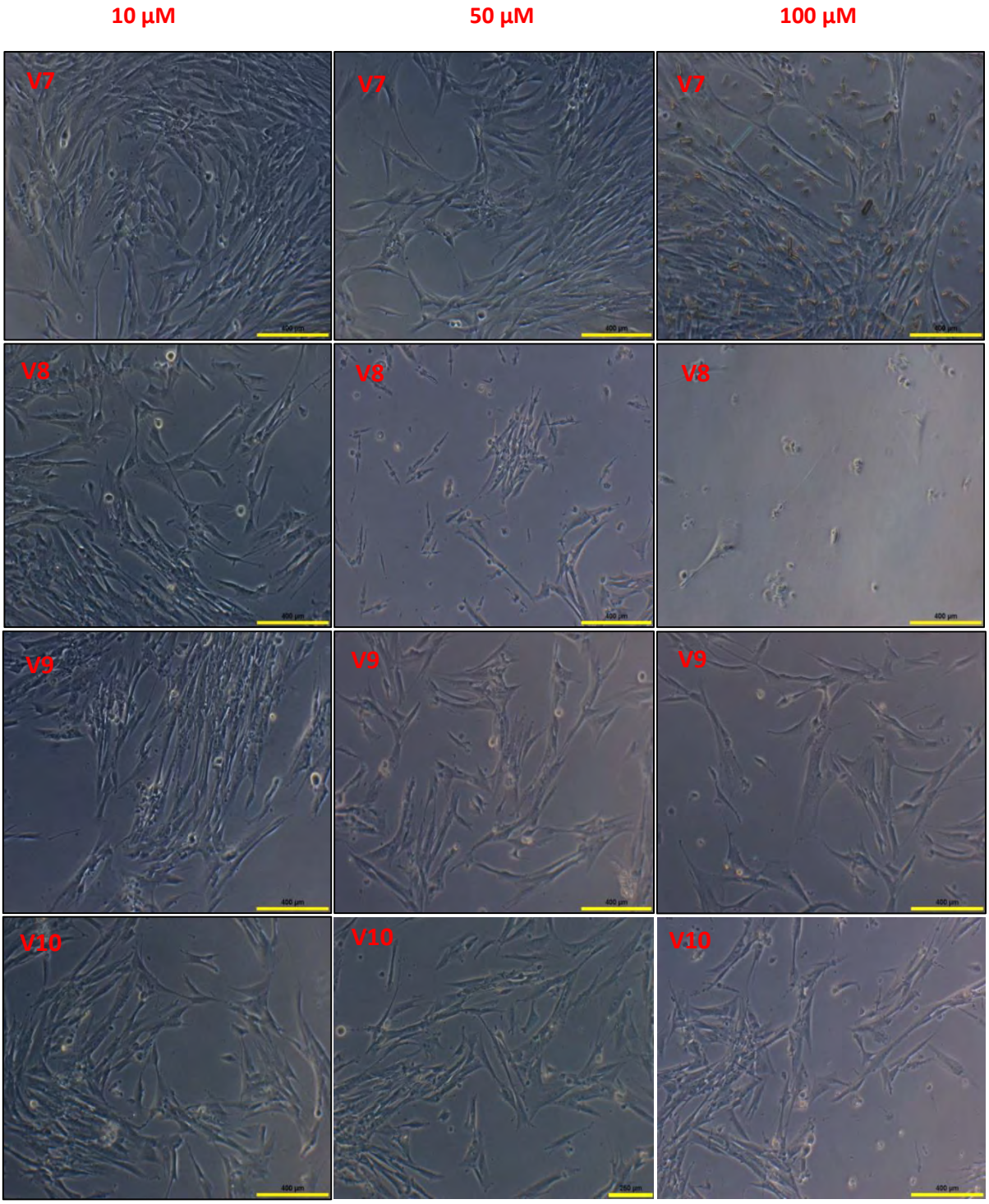

Figure 4-4 Morphological changes that were observed when cells were treated with resveralogues V7, V8, V9 and V10 on primary human lung fibroblasts (MRC-5) at CPD 36-40. Cells were photographed under an inverted light microscope at ×20 magnifications.

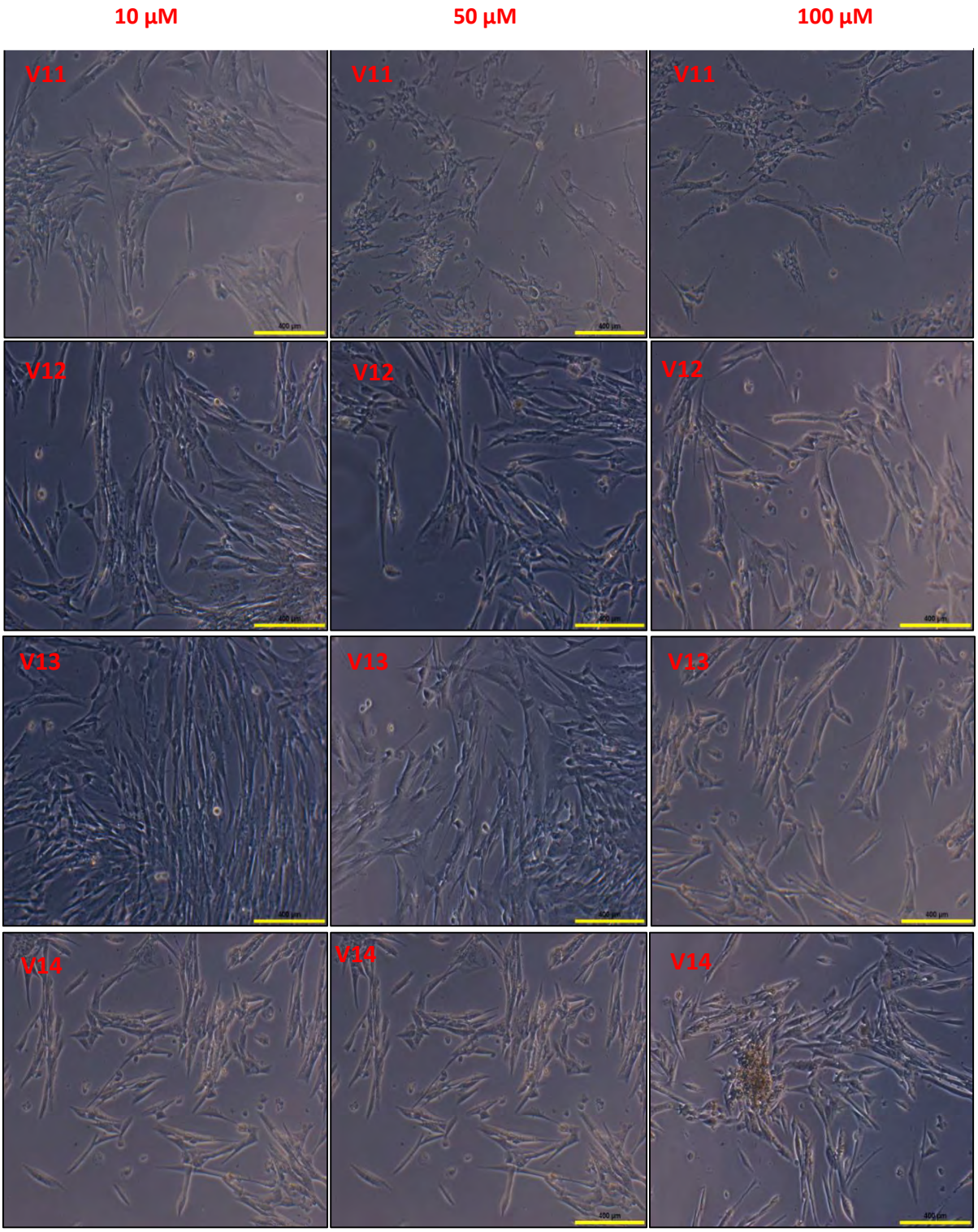

Figure 4-5 Morphological changes that were observed when cells were treated with resveralogues V11, V12, V13 and V14 on primary human lung fibroblasts (MRC-5) at CPD 36-40. Cells were ephotographed under an inverted light microscope at ×20 magnifications.

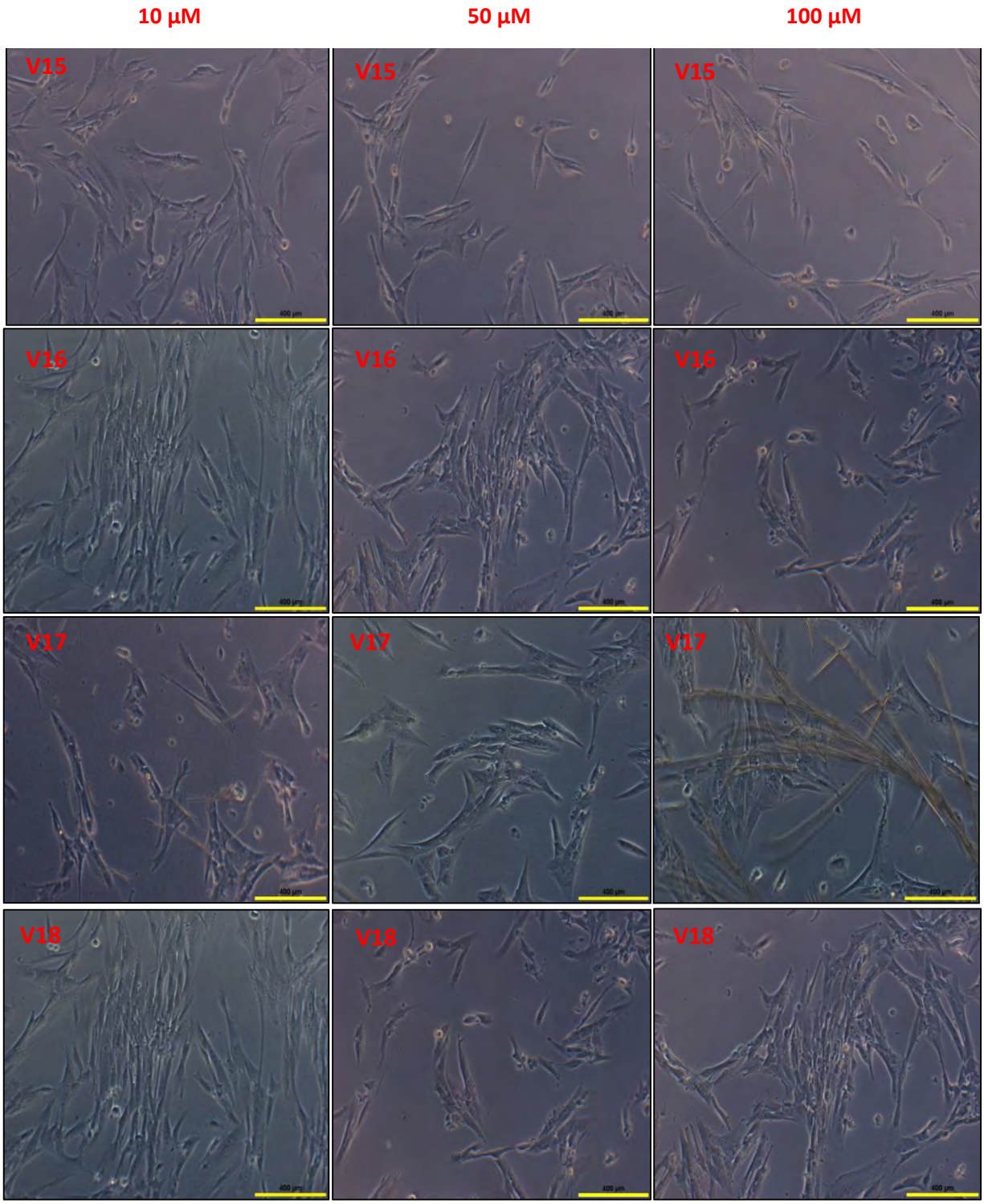

Figure 4-6 Morphological changes that were observed when cells treated with resveralogues V15, V16, V17 and V18 on primary human lung fibroblasts (MRC-5) at CPD 36-40. Cells were photographed under an inverted light microscope at ×20 magnifications.

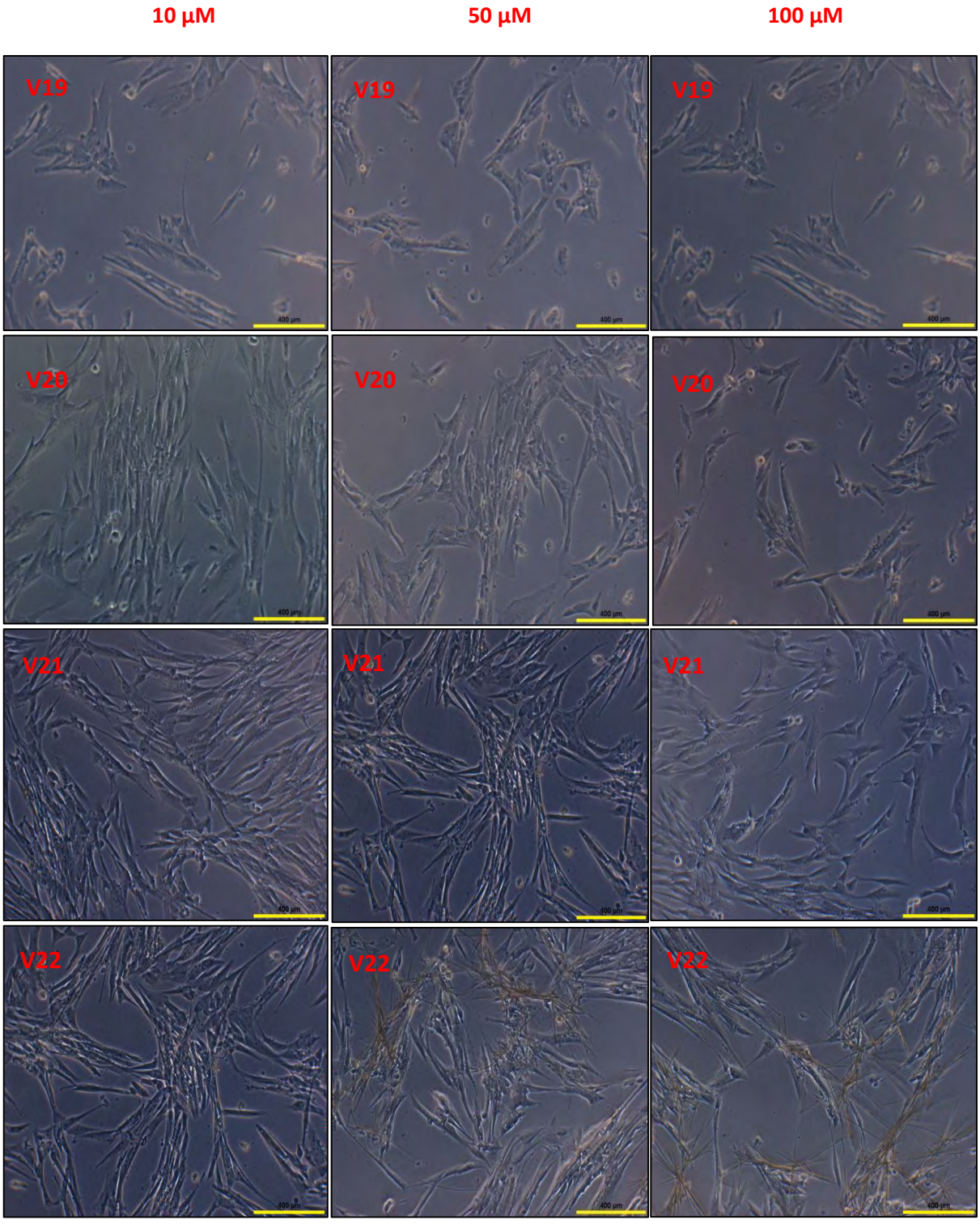

Figure 4-7 Morphological changes that were observed when cells were treated with resveralogues V19, V20, V21 and V22 on primary human lung fibroblasts (MRC-5) at CPD 36-40. Cells were photographed under an inverted light microscope at ×20 magnifications.

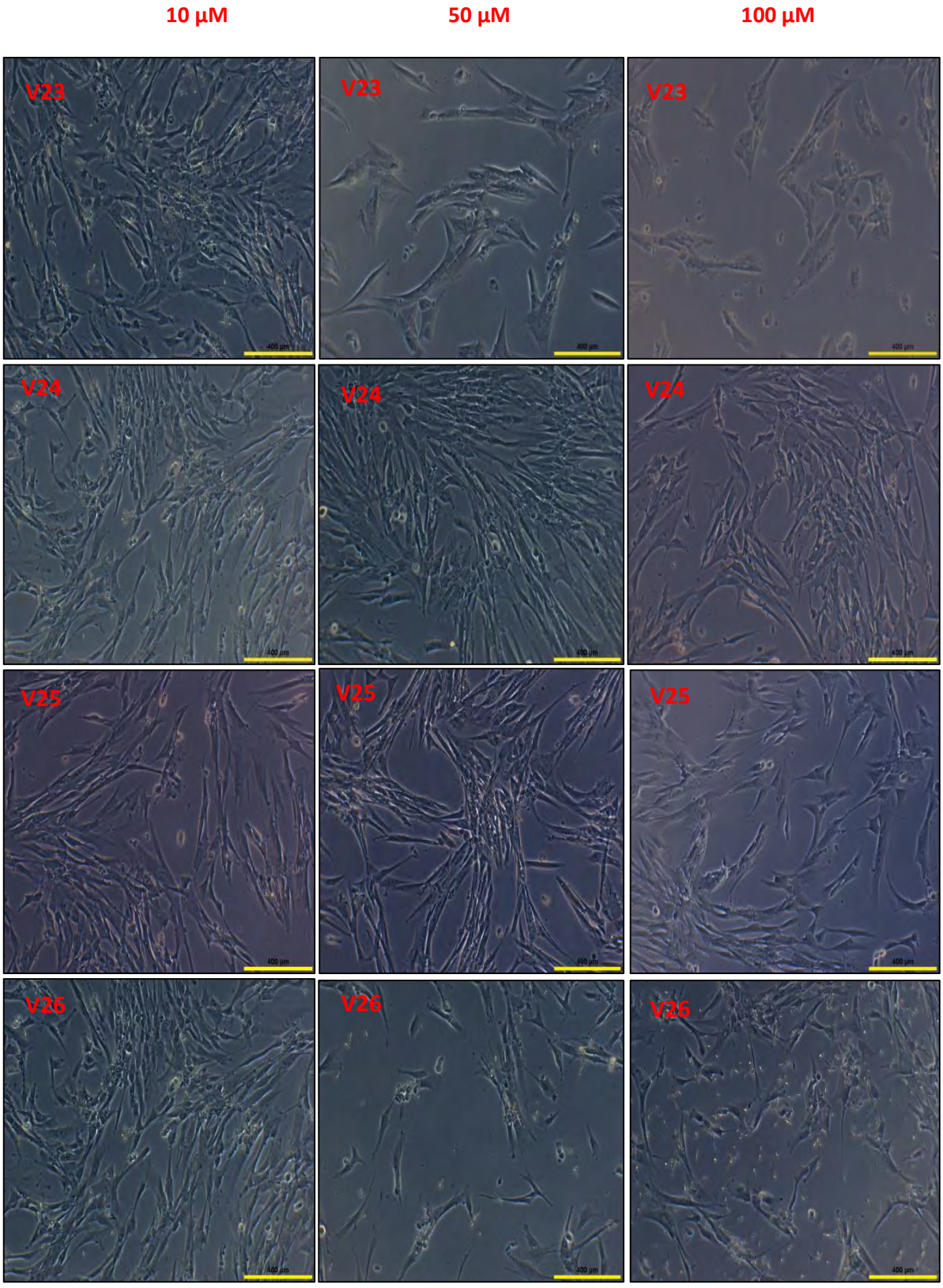

Figure 4-8 Morphological changes that were observed when cells were treated with resveralogues V23, V24, V25 and V26 on primary human lung fibroblasts (MRC-5) at CPD 36-40. Cells were photographed under an inverted light microscope at ×20 magnifications.

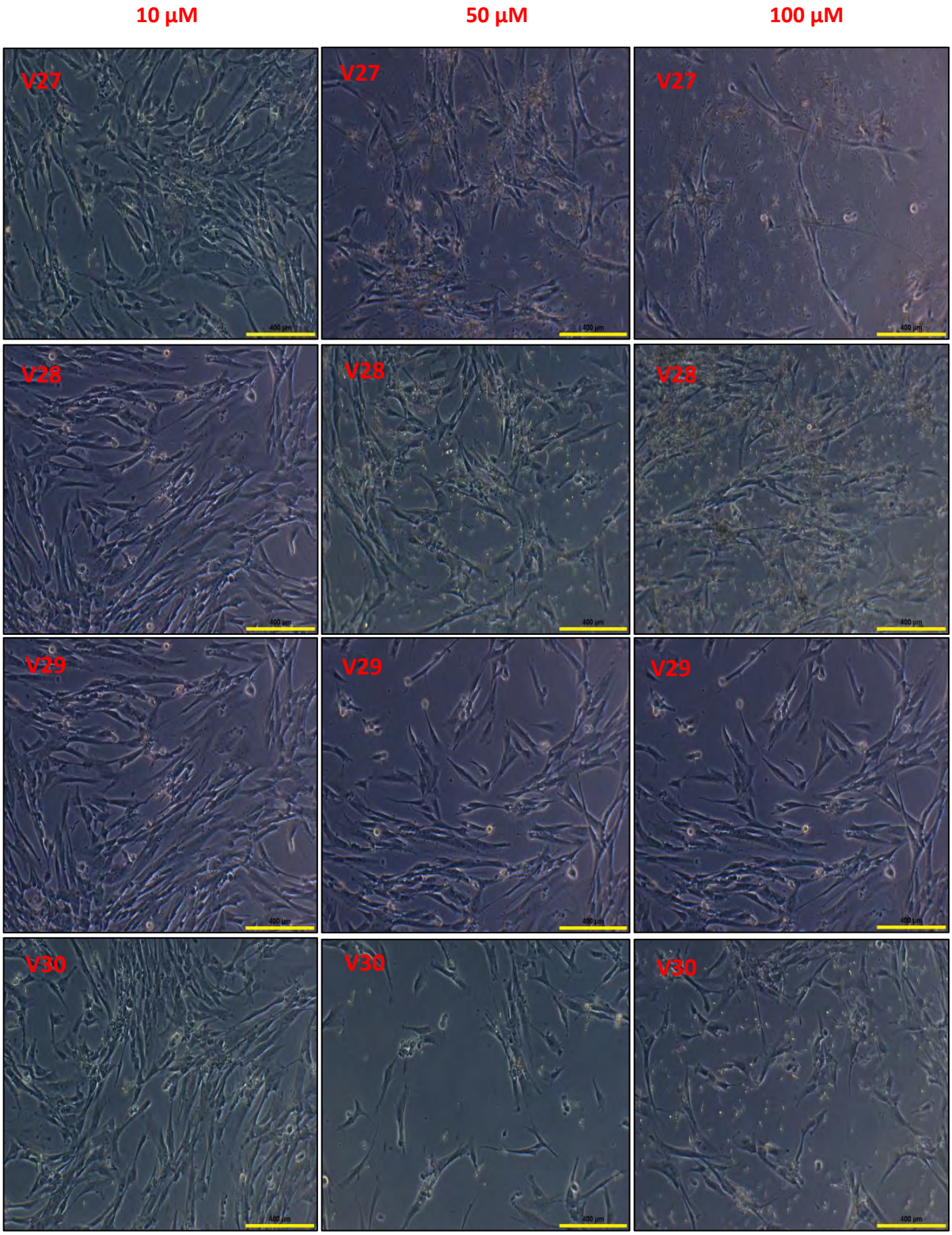

Figure 4-9 Morphological changes that were observed when cells were treated with resveralogues V27, V28, V29 and V30 on primary human lung fibroblasts (MRC-5) at CPD 36-40. Cells were photographed under an inverted light microscope at ×20 magnifications.

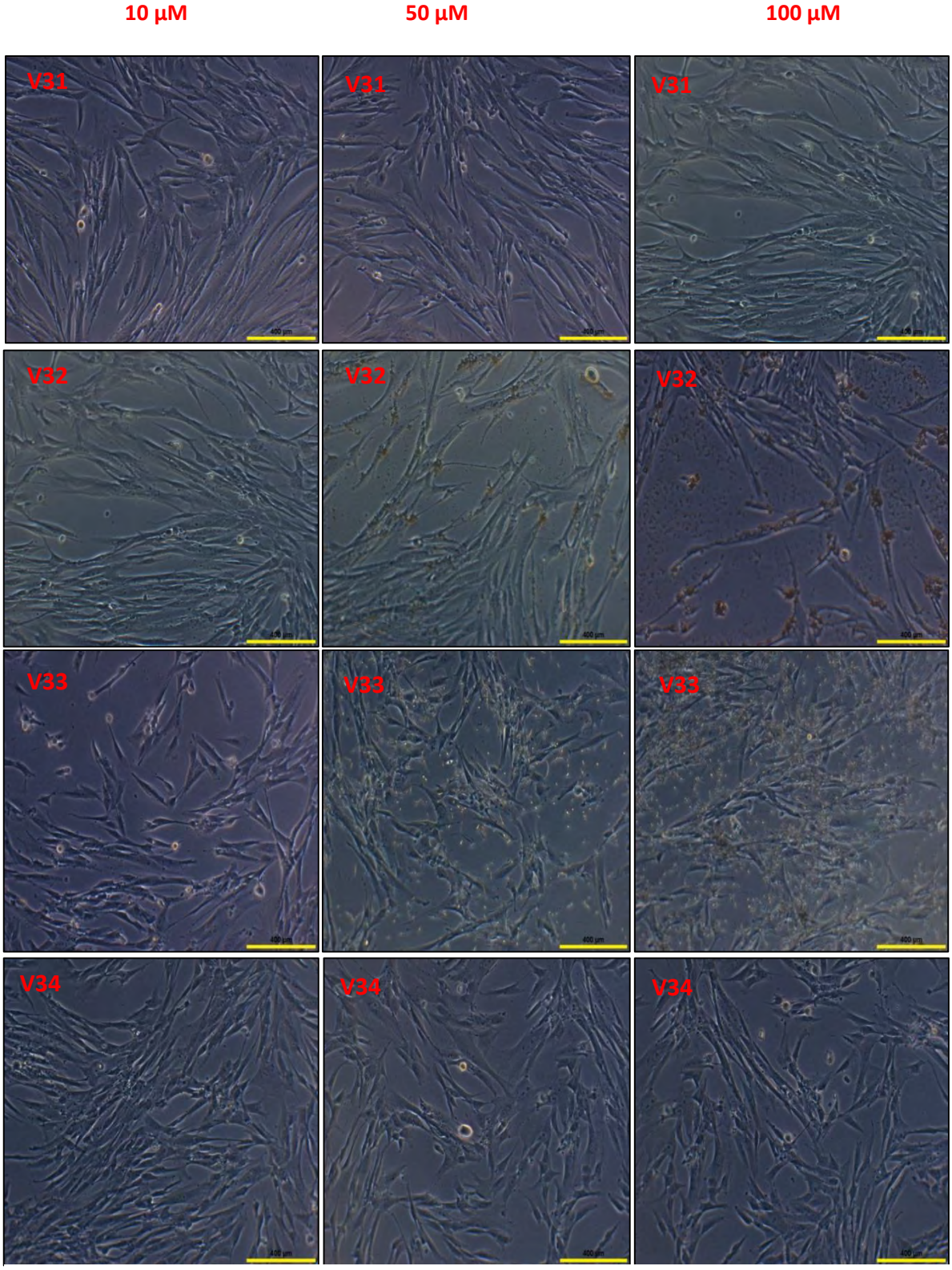

Figure 4-10 Morphological changes that were observed when cells were treated with resveralogues V31, V32, V33 and V34 on primary human lung fibroblasts (MRC-5) at CPD 36-40. Cells were photographed under an inverted light microscope at ×20 magnifications.

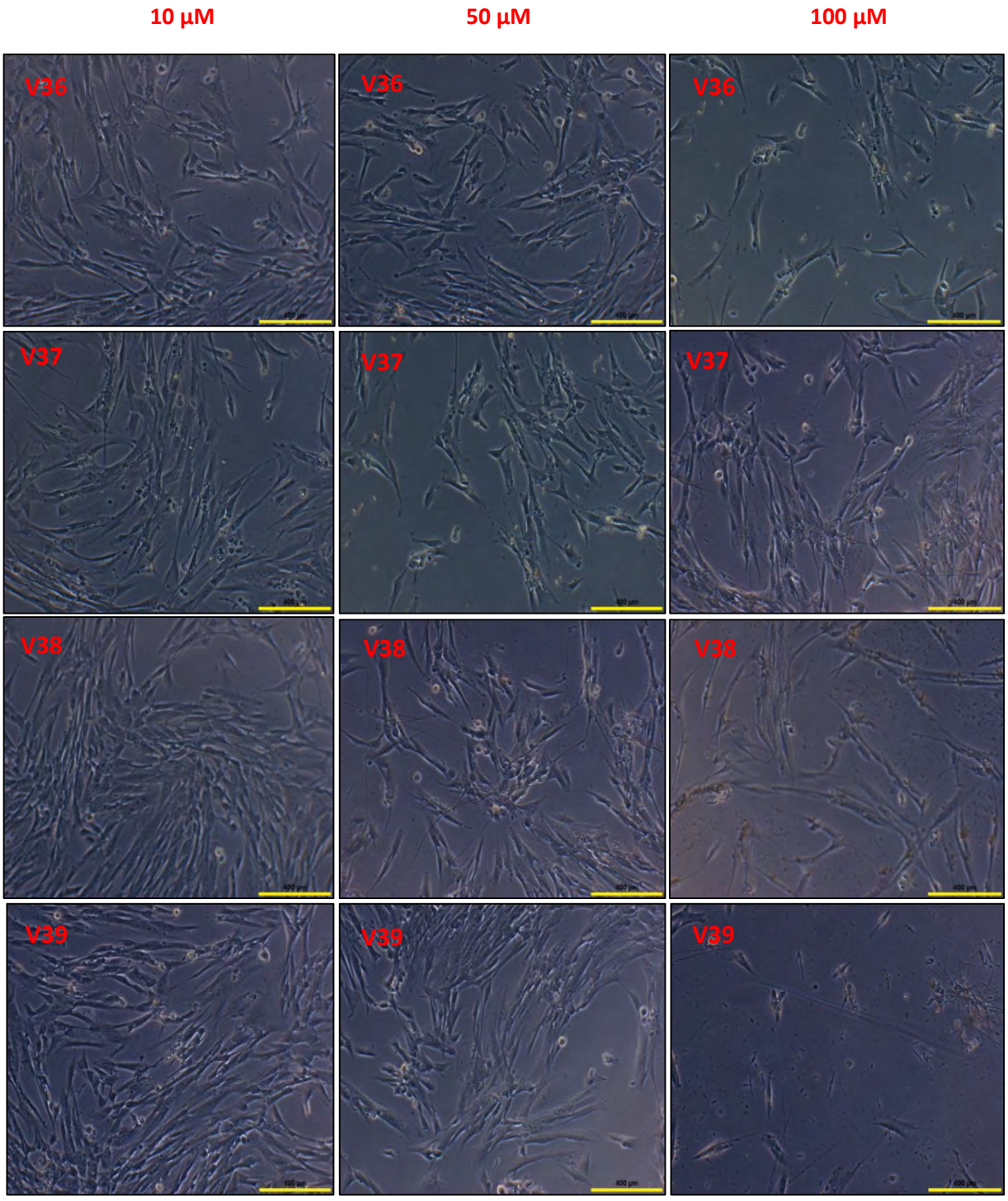

Figure 4-11 Morphological changes that were observed when cells were treated with resveralogues V36, V37, V38 and V39 on primary human lung fibroblasts (MRC-5) at CPD 36-40. Cells were photographed under an inverted light microscope at ×20 magnifications.

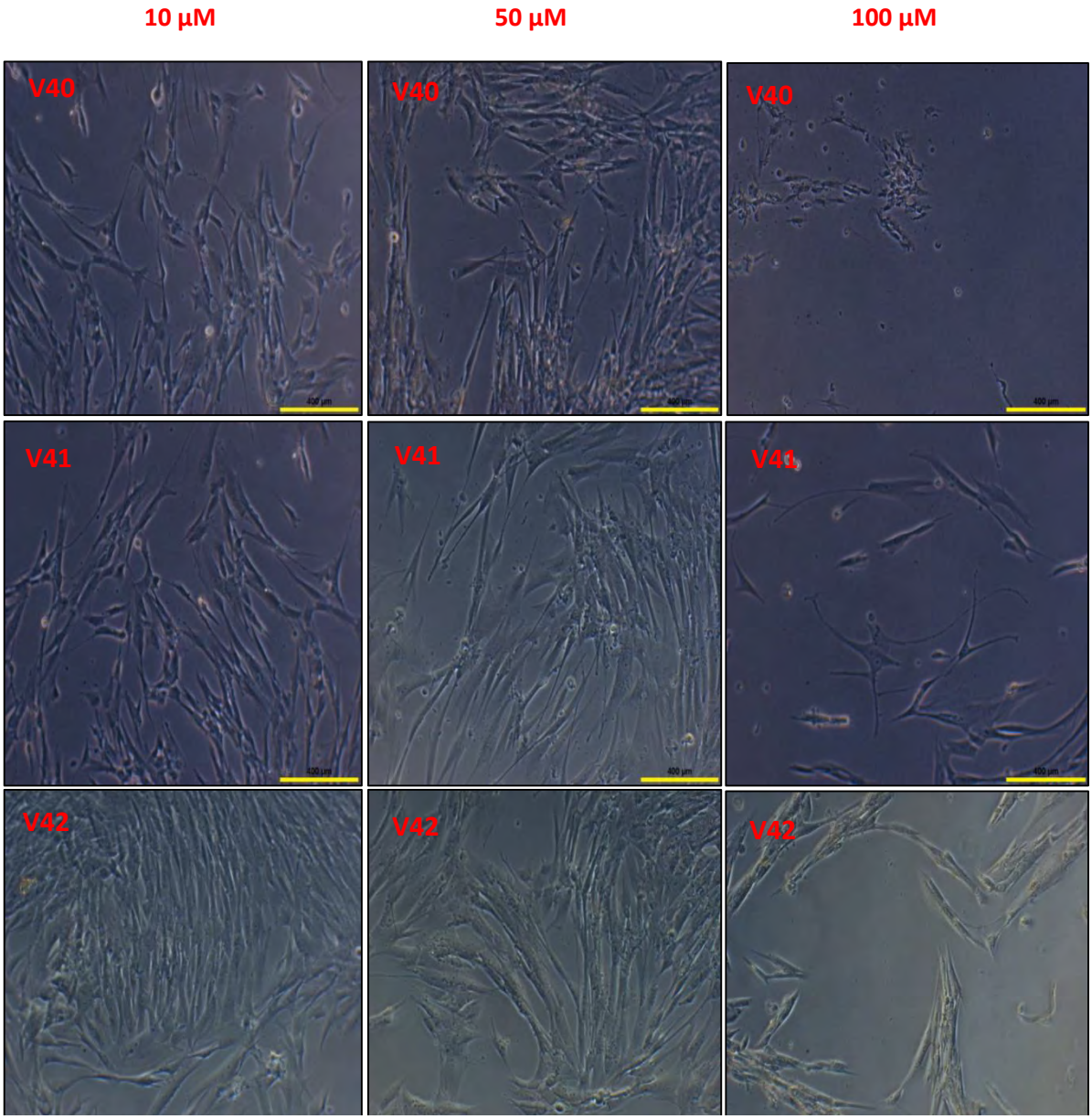

Figure 4-12 Morphological changes that were observed when cells were treated with resveralogues V40, V41, V42 on primary human lung fibroblasts (MRC-5) at CPD 36-40. Cells were photographed took under an inverted light microscope at ×20 magnifications.

4.3. Cytotoxicity of resveralogues:

4.3.1. MTT assay and Neutral red assay:

Cytotoxicity of resveralogues were analysed in normal human lung fibroblast cells (MRC-5) toxicity. Initially, toxicity of resveratrol and resveralogues V13, V23, V24, V34, V31, V36, V39, V41 and V42 was studied using an MTT assay. At 10 µM, 50 µM and 100 µM the MTT assay showed a dose dependent reduction in cell viability summarised in **Figure 4-13**. Interestingly, V24, V34, V31, V42 and dihydroresveratrol were found to be less toxic and significantly differ at 100 µM compare to resveratrol, **Figure 4-13**.

.

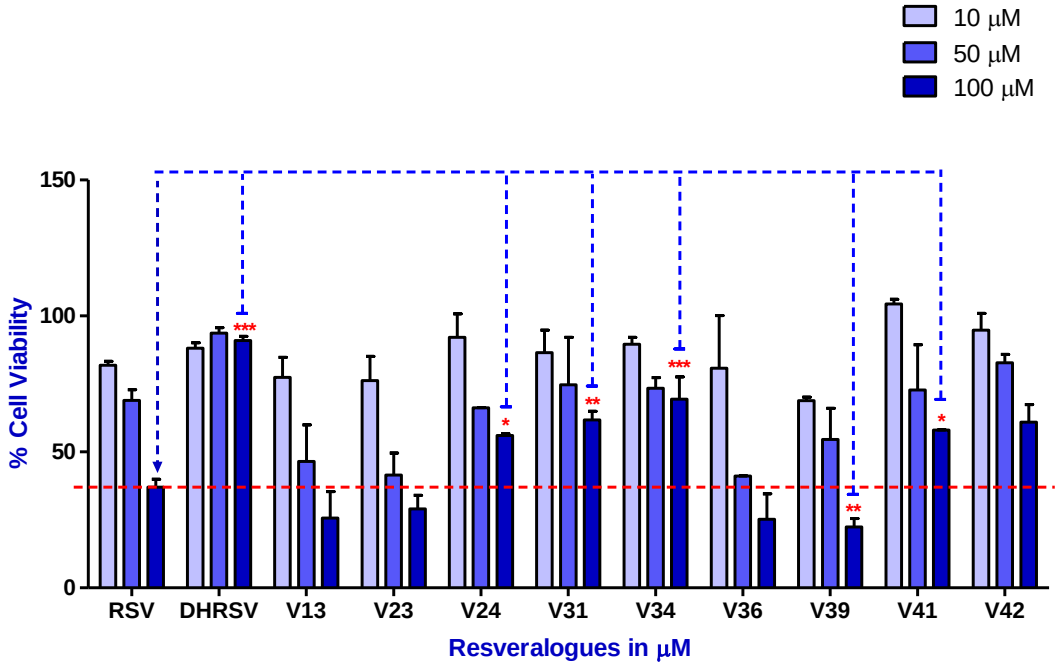

Figure 4-13 Effect of Resveralogue on percentage cell viability of primary human lung fibroblasts (MRC-5) at CPD 36-40 was determined by using MTT assay. The y-axis shows the percentage of cell viability at 10 µM, 50 µM and 100 µM of resveralogues for n = 3 different biological replicates (± standard deviation). Statistical significance was analysed using one way ANOVA followed by Dunnett's multiple comparison test : (∗) $p < 0.05$, (∗∗) $p < 0.01$, (∗∗∗) $p < 0.001$, versus control which represents vehicle only (DMSO treated cells). Blue coloured dotted line represent the statistical comparison between resveratrol and other resveralogues

while red dotted line represent the comparison between resveratrol (at 100 µM) with other resveralogues.

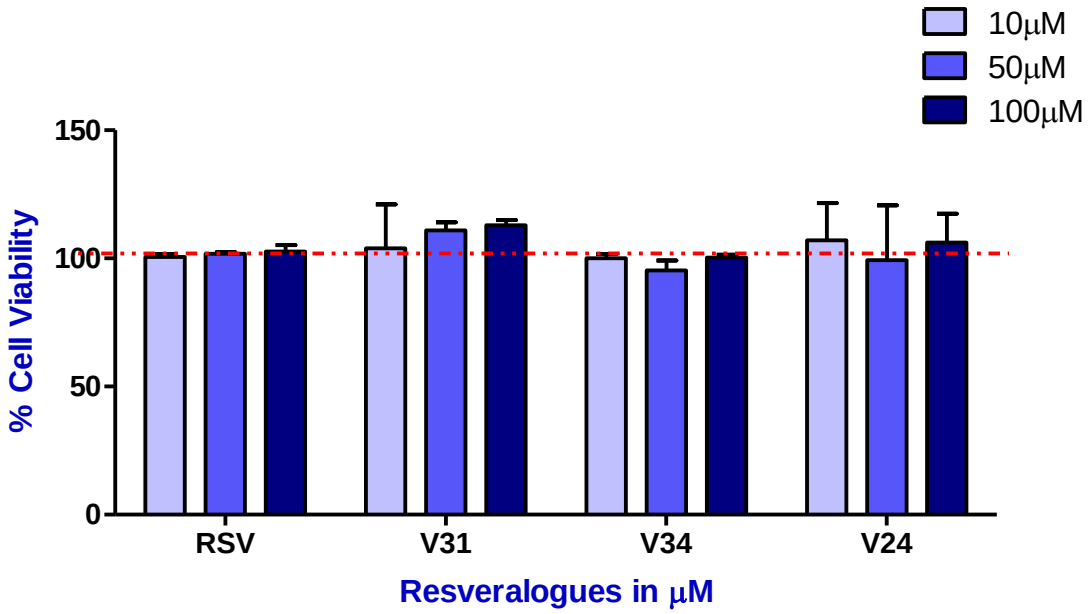

Figure 4-14 Effect of Resveralogue on cell viability of primary human lung fibroblasts (MRC-5) at CPD 36-40 was determined by using Neutral red uptake assay. The y-axis shows the percentage of cell viability at each concentration of resveralogues for n = 3 different biological replicate cultures (± standard deviation). Statistical significance was analysed using one way ANOVA followed by Dunnett's multiple comparison test : (∗) $p < 0.05$, (∗∗) $p < 0.01$, (∗∗∗) $p < 0.001$, versus control which represents untreated cells. Red coloured dotted line represent the comparison between resveratrol and other resveralogues.

Following from MTT analysis, Neutral red assay was performed. Resveratrol, V24, V34 and V31 toxicity was studied using neutral red assay. The neutral red assay is based on the initial protocol described by Borenfreund and Puerner [168]. This based on the uptake of the neutral red dye in the lysosomes of viable compared to dead or injured cells. **Figure 4-14** summarises that resveralogues were non-toxic and there was no significant difference between resveralogues including resveratrol. This was not consistant with previous findings with to the morphological dat

4.3.2. LDH assay:

LDH cytotoxicity assay was used in order to understand the toxicity mediated by the synthesised resveralogues. All of the resveralogues analysed using LDH assay were summarised in **Figure 4-15**. In general, no significant change of LDH release was observed at 10 μM and 50 μM compared to resveratrol. However, V26, V37 and V39 were found to significantly increase in LDH release at 100 μM compared to resveratrol. The structural analysis suggested that benzyl group substitution on ring increases the LDH release. e.g. V37 and V39.

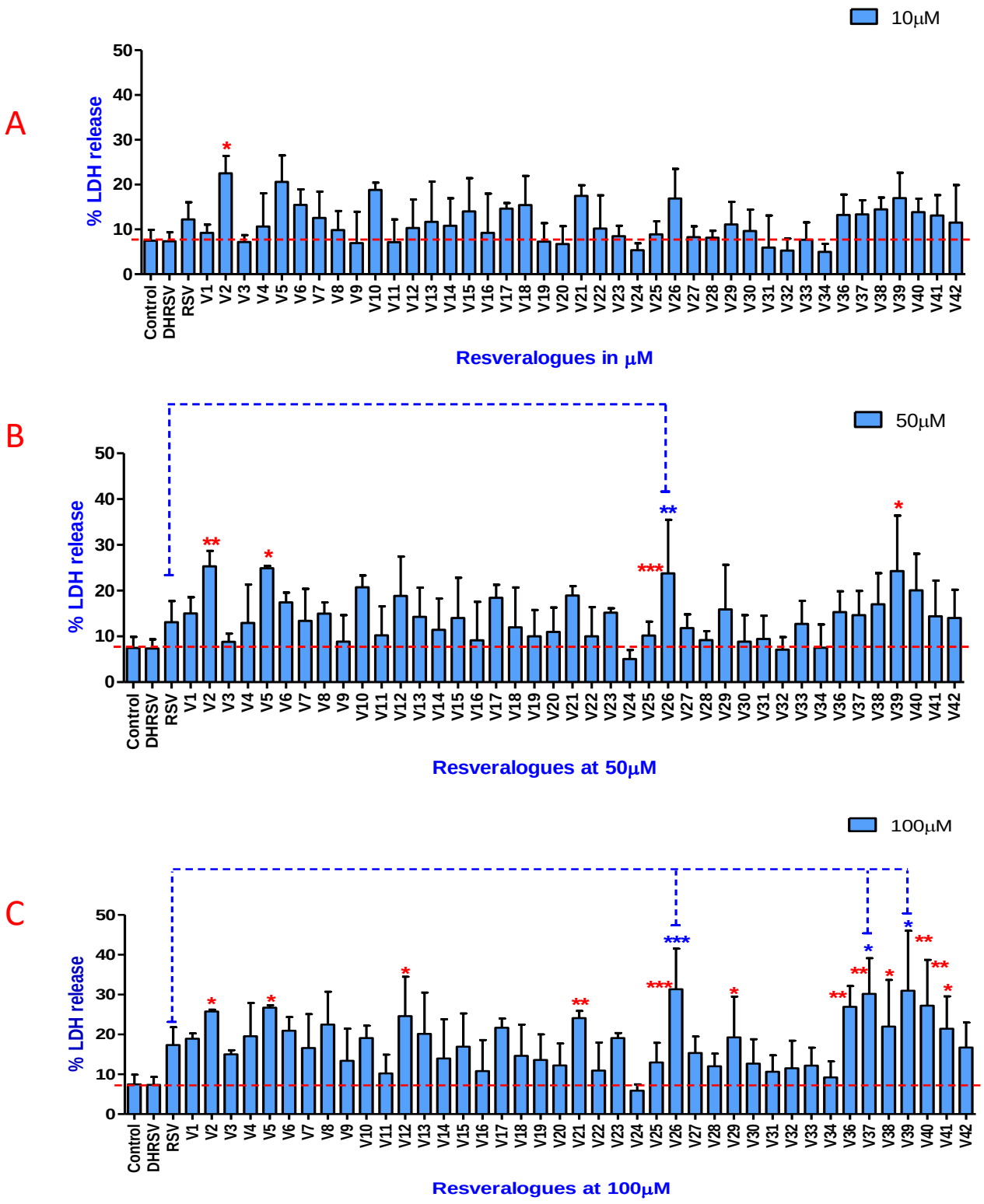

Figure 4-15 Effect of resveralogues V1-V42 on percentage LDH release of primary human lung fibroblasts (MRC-5) at CPD 36-40 was determined by using LDH assay. The y-axis shows the percentage of LDH at 10 µM (A), 50 µM (B) and 100 µM (C) concentration of resveralogues for n = 3 different biological cultures (±standard

deviation). Statistical significance was analysed using ANOVA followed by Dunnett's multiple comparison test: (∗) $p < 0.05$, (∗∗) $p < 0.01$, (∗∗∗) $p < 0.001$, versus control which represents vehicle only (DMSO treated cells). Blue coloured * represent statistical comparison between resveratrol and other resveralogues while red coloured * represent comparison between control and resveralogue.

4.4. Effect of resveralogues on cells cytostasis:

In order to investigate the effect resveralogues have on cytostasis, ki-67 (proliferation marker) and SA-β-gal, senescence marker were employed.

4.4.1. Effects on proliferation marker ki-67:

Resveralogue's effects on cell growth (proliferation) in MRC-5 cells, were investigated using immunocytochemistry, details of which are shown in **Figure 4-16**. This shows the staining of proliferating nuclei expressing ki-67 with FITC (green coloured) and cells nuclear staining with DAPI (blue coloured). The overlay of both was showing the proportion of proliferating nuclei (green coloured) in the population. MRC5 cells were treated with resveralogues V2, V5, V10, V11, V13, V15, V21, V23, V24, V30, V31, V32, V34, V36, V37, V39, V41, resveratrol and dihydroresveratrol at 10 μM, 25 μM, 50 μM and 100 μM. **Figure C-1 (Appendix C)** summarised that resveratrol showed a dose dependent decrease in the proliferating fraction of MRC-5 cells. Resveratrol produced an increase in proliferating fraction at 10 μM dose compared to control untreated cells [150]. This was also observed with resveralogues V2, V5, V10, V11, V15, V24, V30, and V34, **See Figure 4-17.** However, V23 and V13 demonstrated a significant decrease ($p < 0.001$) in proliferating fraction ki-67 compared to resveratrol, **Figure 4-17**.

Resveralogues such as V13, V21, V29, V31, V32, V36, V37, V39 and V41 were seen to have similar proliferating fraction ki-67 as the untreated cells, **Figure 4-17**. Additionally, V13, V23, V37 and V41 showed a significant decrease in proliferation compared to resveratrol, **See Figure 4-17**. At 25 μM, there was notable decrease in proliferating nuclei V10, V21, V23 and V37 compared to control as well as resveratrol, **Figure 4-18.** At 50 μM, a decrease in proliferation was observed in V2, V10, V21, V23 and V41 compared to resveratrol, **See Figure 4-19.** Finally, at 100 μM, V10, V23, V37, V39 and V41 were found to decrease the proliferation compared to resveratrol. However, at same concentration V15, V11, V24, V29, V30, V31, V32 and V34 were found to be less effect

on growth than resveratrol. Interestingly, V11, V15, DHRSV, V24, V30, V34 did not shown any change in proliferation and was parallel to that seen in untreated cells, **Figure 4-20.**

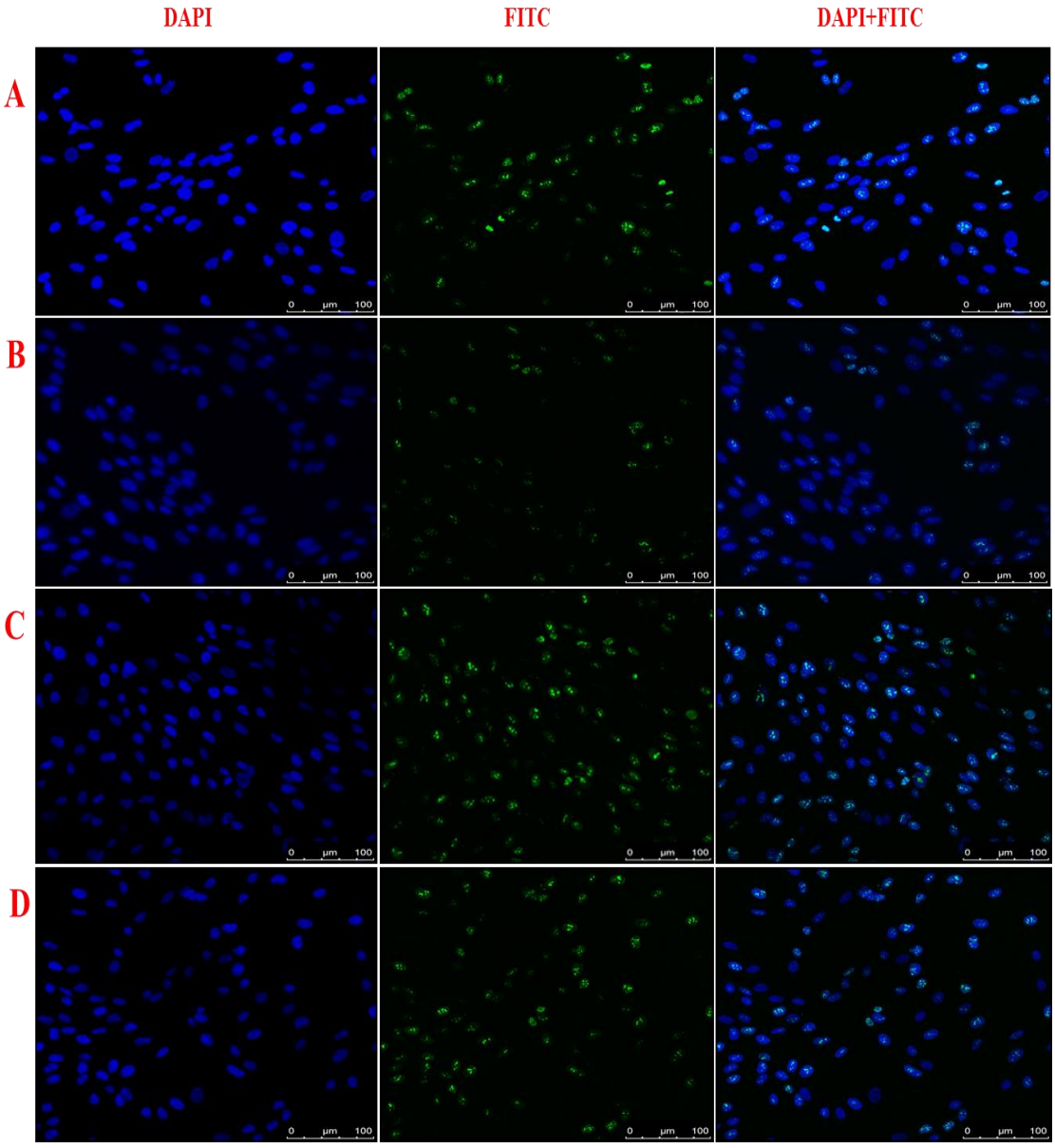

Figure 4-16 Representation images of ki-67 immuno-histochemistry in MRC5 cells when treated with A) control untreated cells B) resveratrol C) V24 and D) V34 at 100 µM. Cell nuclei were counterstained with DAPI (blue) and Ki67 nculei using FITC (green) at original magnification ×200.

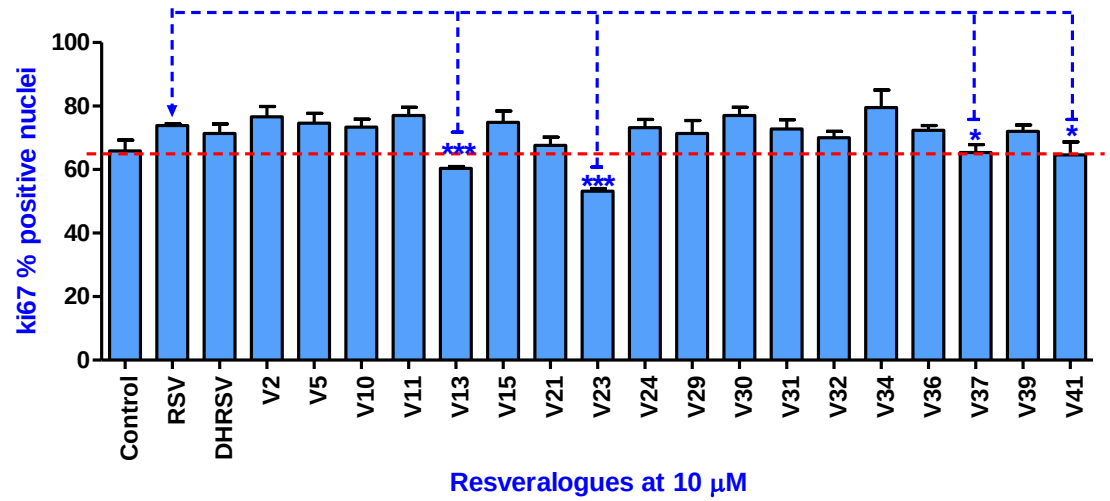

Figure 4-17 Effect of resveralogues (10 µM) on cell proliferation of primary human lung fibroblasts (MRC-5) at CPD 36-40 determined by using ki-67 immunocytochemistry. The y-axis shows the mean percentage of proliferation ki-67 nuclei at 10 µM of resveralogues for n = 3 different biological replicate cultures (± standard deviation). Statistical significance was analysed using one way ANOVA followed by Dunnett's multiple comparison test: (*) $p < 0.05$, (**) $p < 0.01$, (***) $p < 0.001$, versus control which represents vehicle only (DMSO treated cells). (blue coloured * represent statistical comparison between resveratrol and other resveralogues while red coloured * represent comparison between control and resveralogue.)

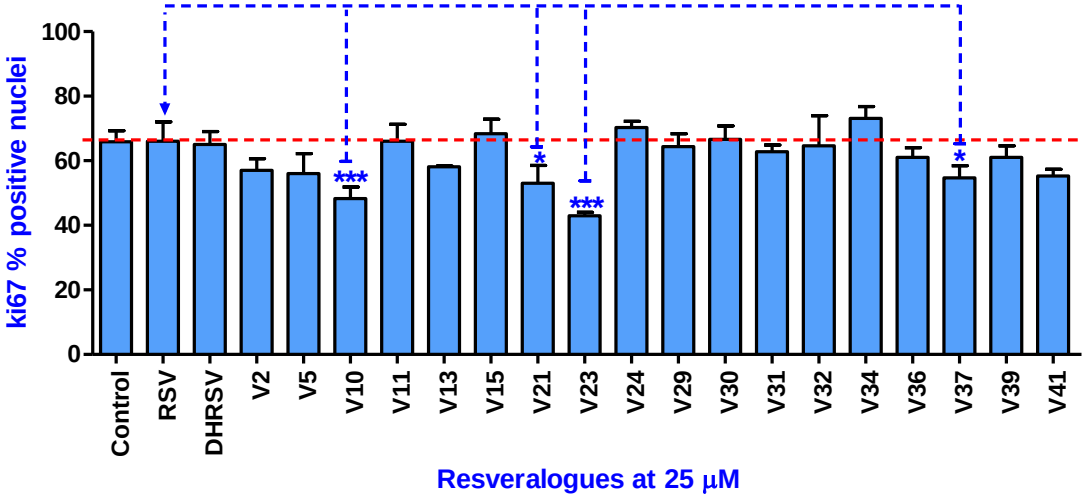

Figure 4-18 Effect of resveralogues (25 µM) on cell proliferation of primary human lung fibroblasts (MRC-5) at CPD 36-40 was determined by using ki-67 assay. The y-

axis shows the mean percentage of proliferation ki-67 nuclei at 25 µM of resveralogues for n = 3 different biological replicate cultures (±standard deviation). Statistical significance was analysed using one way ANOVA followed by Dunnett's multiple comparison test: (*) p < 0.05, (**) p < 0.01, (***) p < 0.001, versus control which represents vehicle only (DMSO treated cells). blue coloured * represent statistical comparison between resveratrol and other resveralogues while red coloured * represent comparison between control and resveralogue.

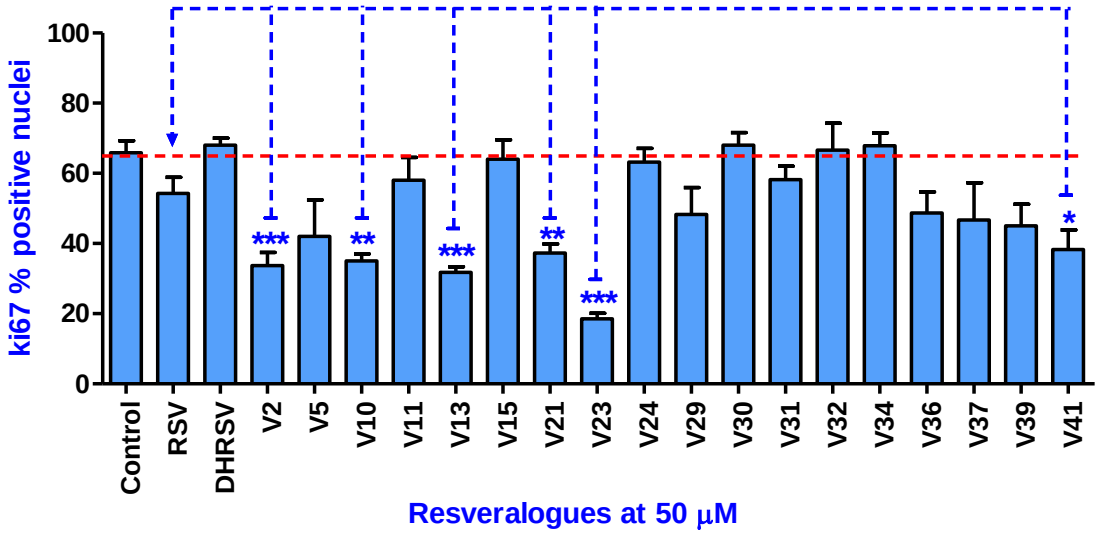

Figure 4-19 Effect of resveralogues (50 µM) on cell proliferation of primary human lung fibroblasts (MRC-5) at CPD 36-40 was determined by using ki-67 assay. The y-axis shows the mean percentage of proliferation ki-67 nuclei at 50 µM of resveralogues for n = 3 different biological replicate cultures (±standard deviation). Statistical significance was analysed using one way ANOVA followed by Dunnett's multiple comparison test: (*) p < 0.05, (**) p < 0.01, (***) p < 0.001, versus control which represents untreated cells. blue coloured * represent statistical comparison between resveratrol and other resveralogues while red coloured * represent comparison between control and resveralogue.

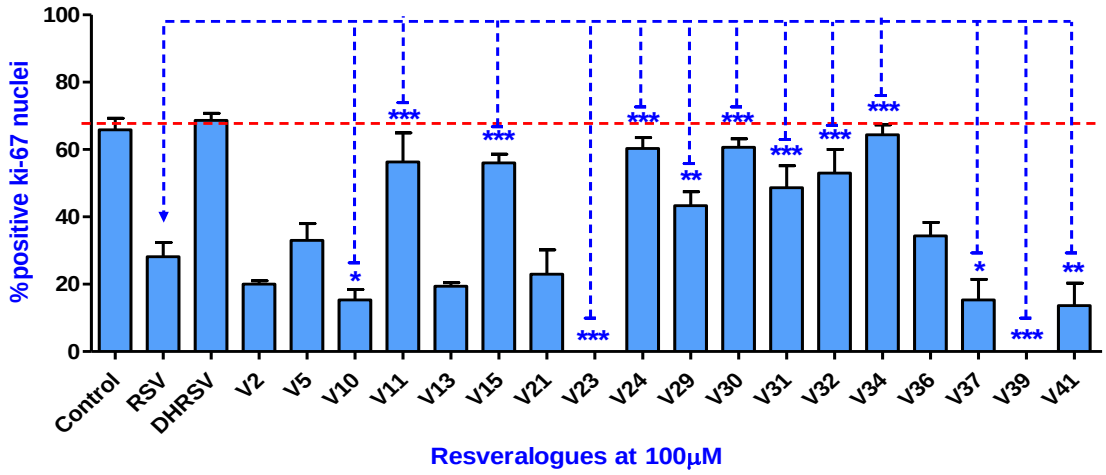

Figure 4-20 Effect of resveralogues on cell proliferation of primary human lung fibroblasts (MRC-5) at CPD 36-40 was determined by using ki-67 assay. The y-axis shows the mean percentage of proliferation ki-67 nuclei at 100 µM of resveralogues for n = 3 different biological replicate cultures (±standard deviation). Statistical significance was analysed using one way ANOVA followed by Dunnett's multiple comparison test: (∗) p < 0.05, (∗∗) p < 0.01, (∗∗∗) p < 0.001, versus control which represents untreated cells. (blue coloured * represent statistical comparison between resveratrol and other resveralogues while red coloured * represent comparison between control and resveralogue).

4.4.2. Effect on SA-β-gal activity:

Senescence associated beta galactose assay (**SA-β-gal**) was used to evaluate the presence of senescence cells in cell population and to test whether synthesised resveralogue induces premature senescence in MRC-5 cells. Earlier studies on resveratrol suggested that it induces senescence growth arrest at and above 25 µM concentration. Resveratrol and synthesised resveralogues were tested at 25 µM, 50 µM and 100 µM. Resveratrol was seen to increase the fraction of senescencent cells at and above 25 µM. It was seen that 80-85% of the culture was positive towards SA-β-gal activity at 100 µM dose of resveratrol compared to control cells**, Figure 4-23 and Figure C-1 in (Appendix C**). A similar trend was seen in V2, V5, V10, V11, V13, V21, V30, V32, V36, and V37, **Figure 4-21**, **Figure 4-22** and **Figure 4-23**. However, DHRSV, V24, V31 and V34 did not show an increase in positive SA-β-gal activity even at 100 µM, see **Figure 4-23**. This was further supported by using **Figure 4-24** which represent SA-β-Gal positive cells in MRC5

cells using catalytical immunocytochemistry technique at pH6 when treated with V24 and V34. There were very few SA-β-Gal positive cells (blue coloured nuclei represent SA-β-Gal positive cells in **Figure 4-24** observed in case of V24, V34 compared to resveratrol.

The results that were obtained from ki-67 assay and SA-β-gal assay suggested that decrease in proliferation ki-67 nuclei was associated with increase in senescent nuclei. Resveratrol and synthesised resveralogues V5, V11, V13, V21, V23, V36, V37, V39 and V41 all followed the same trend. However, in case of V30 and V32 no effect on ki-67 positive nuclei was seen, but a dose dependent increase in SA-β-gal senescence fraction was also noted at 25 μM, 50 μM and 100 μM concentration. (**Figure 4-21**, **Figure 4-22** and **Figure 4-23**)

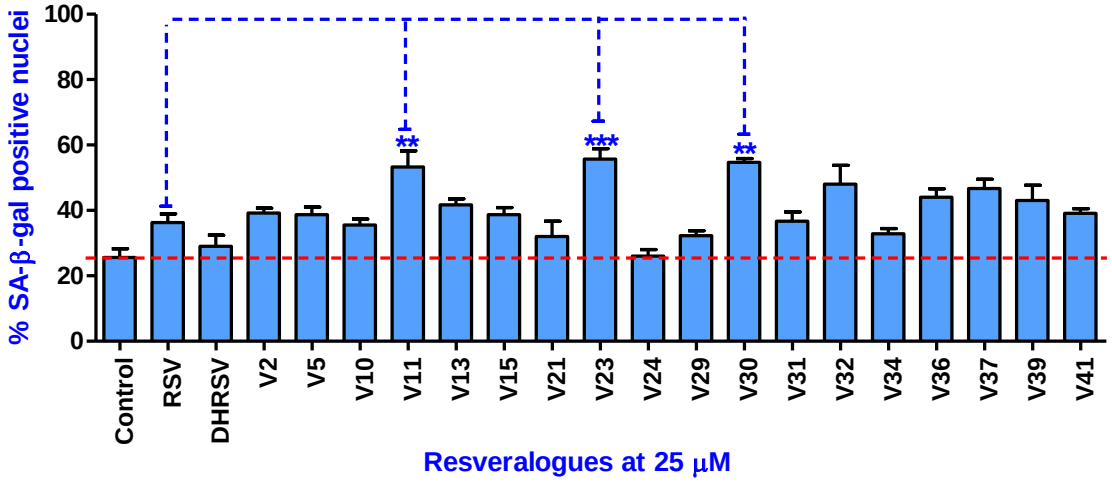

Figure 4-21 Effects of resveralogues on the fraction of SA-β-galactosidase positive cells in MRC5 fibroblasts cultures at a 36-40 CPD. The y-axis shows the percentage of SA-β-galactosidase positive nuclei at 25 μM of resveralogues for n = 3 different biological replicate cultures (±standard deviation). Statistical significance was analysed using one way ANOVA followed by Dunnett's multiple comparison test: (∗) $p < 0.05$, (∗∗) $p < 0.01$, (∗∗∗) $p < 0.001$, versus control which represents vehicle only (DMSO treated cells). (blue coloured * represent statistical comparison between resveratrol and other resveralogues while red coloured line represent comparison between control and resveralogue).

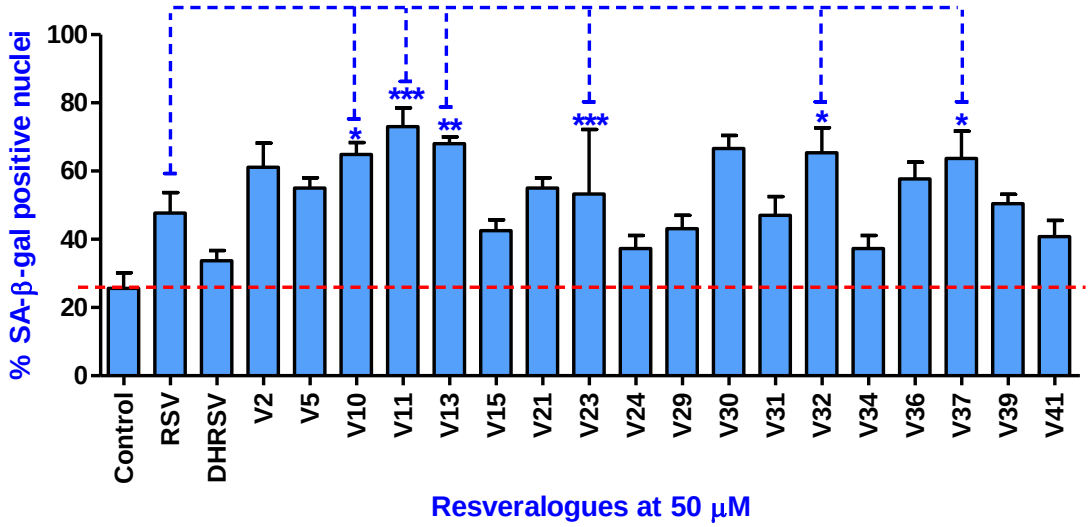

Figure 4-22 Effects of resveralogues on the fraction of SA-β-galactosidase positive cells in MRC5 fibroblasts cultures at a 36-40 CPD. The y-axis shows the percentage of SA-β-galactosidase positive nuclei at 50 μM of resveralogues for n = 3 different biological replicate cultures (±standard deviation). Statistical significance was analysed using one way ANOVA followed by Dunnett's multiple comparison test: (∗) $p < 0.05$, (∗∗) $p < 0.01$, (∗∗∗) $p < 0.001$, versus control which represents untreated cells. (blue coloured * represent statistical comparison between resveratrol and other resveralogues while red coloured line represent comparison between control and resveralogue).

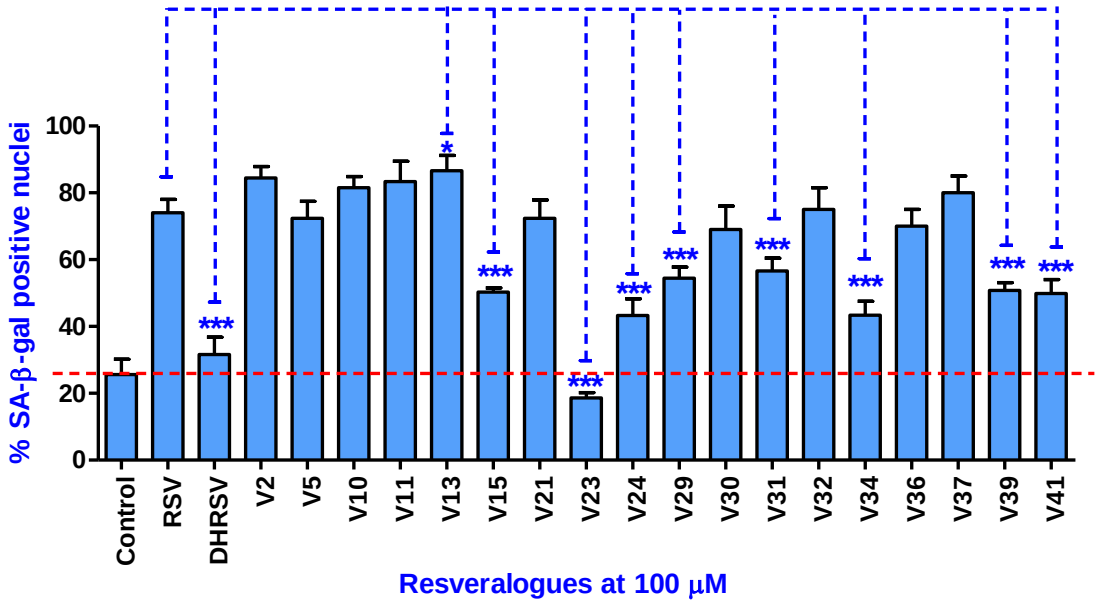

Figure 4-23 Effects of resveralogues on the fraction of SA-β-galactosidase positive cells in MRC5 fibroblasts cultures at a 36-40 CPD. The y-axis shows the percentage of SA-β-galactosidase positive nuclei at 100 μM of resveralogues for n = 3 different biological replicate cultures (±standard deviation). Statistical significance was analysed using one way ANOVA followed by Dunnett's multiple comparison test: (∗) $p < 0.05$, (∗∗) $p < 0.01$, (∗∗∗) $p < 0.001$, versus control which represents untreated cells. (blue coloured * represent statistical comparison between resveratrol and other resveralogues while red coloured line represent comparison between control and resveralogue).

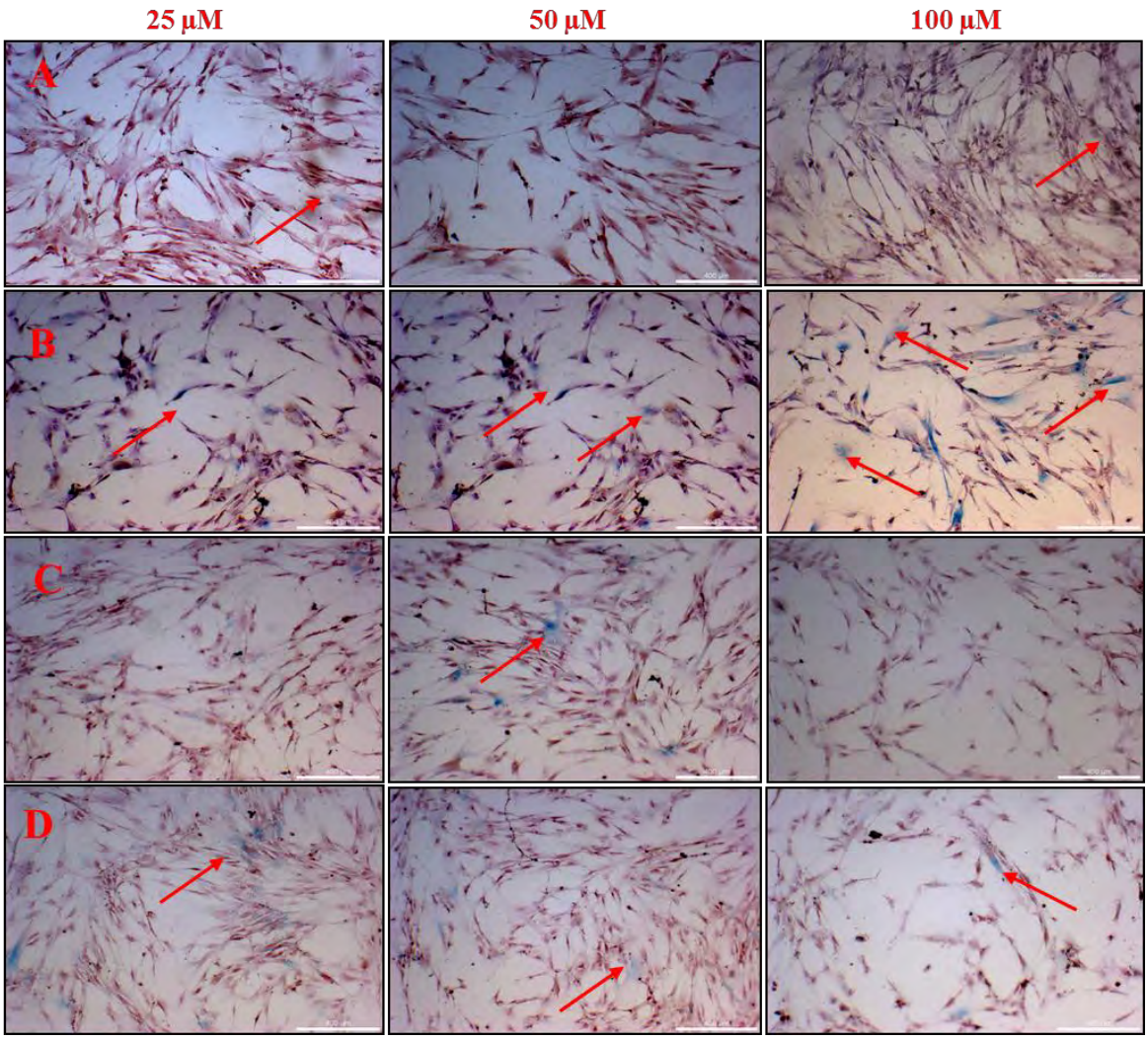

Figure 4-24 Typical images of senescence-associated β-galactosidase (SA-β-Gal) positive cells in MRC5 cells (200 magnification) using catalytic immuno-cytochemistry technique at pH6 when treated with A) control untreated cells, B) resveratrol, C) V24 and D) V34 at 25, 50 and 100 µM. (senescent postive cells shown blue coloured with red arrow)

4.5. SIRT1 activity of resveralogues:

To understand the effect of resveralogues on SIRT1 activation, a SIRT1 activation assay was performed using the Cayman Chemicals kit, **Section 3.7**. The data obtained using SIRT1 activity assay are shown in **Figures 4-26** and **Figure 4-27**. SIRT1 activation was studied at 25 µM and 100 µM resveralogues. During the SIRT1 activation assay resveratrol and sirtinol was used as positive and negative control for the assay. **Figure 4-25** summarises SIRT1 activity of resveratrol (as an activator of SIRT1), dihydroresveratrol, nicotamide and sirtinol (reported as inhibitors of resveratrol) and initial activity as SIRT1 activity without any treatment of sample. Resveratrol and dihydroresveratrol was observed to activate the SIRT1 enzyme while its activity was inhibited in presence of sirtinol. However, although NAM is reported as inhibitor of SIRT1, this was not the case in our hands, **Figure 4-25**.

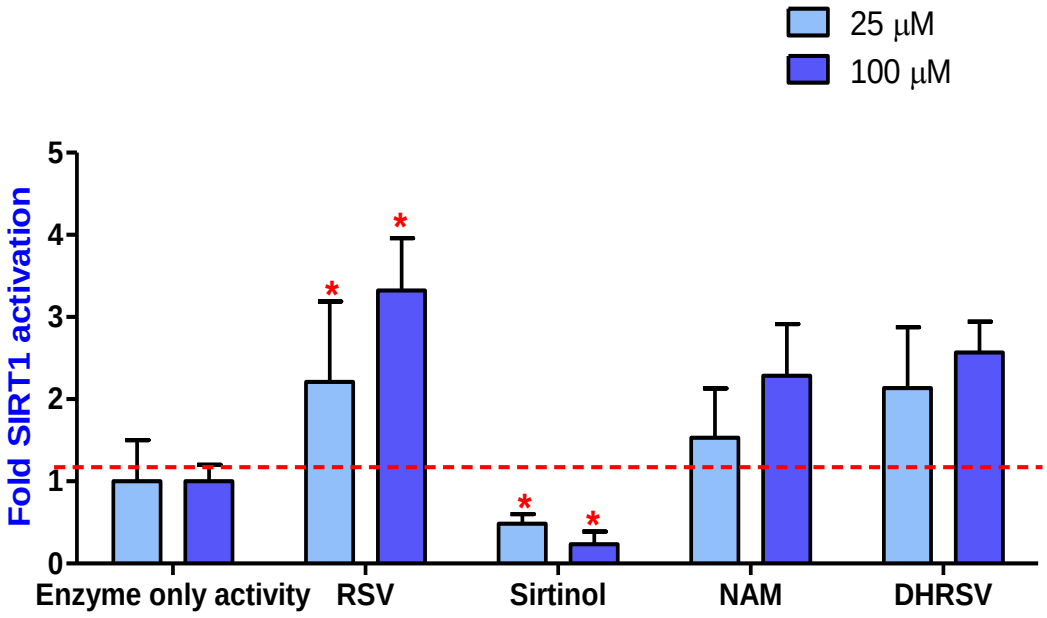

Figure 4-25 Activation of SIRT1 by resveratrol (RSV), sirtinol, NAM (nicotinamide) and DHRSV. Fold activations are calculated as the ratio of the deacetylation rate in SIRT1 reaction containing the resveralogues at 25 µM to that of initial SIRT1 activity reaction (where enzyme only activity represents the SIRT1 deacetylase reaction without any resveralogues). Mean data from n=3 different biological experiments (on same day) are shown ± standard deviation. Statistical significance was analysed using one way ANOVA followed by Dunnett's multiple comparison test: (∗) $p < 0.05$, (∗∗) $p < 0.01$, (∗∗∗) $p <$

0.001, versus control which represents untreated cells. (red coloured * represent statistical comparison between control and other compounds).

All resveralogues were analysed and seen to induce moderate SIRT1 activation compared with enzyme only SIRT1 activity at 25 μM and 100 μM. However, there was no significant increase in SIRT1 activity noted at 100 μM compared at 25 μM. Enzyme only activity represents SIRT1 enzyme activity in presence of 0.5% DMSO. Resveratrol was shown 2.2 fold increases in SIRT1 activity compared to enyme only activation reaction. Interestingly, dihydroresveratrol, a primary in-vivo metabolite of resveratrol also showed 2.2 fold increses in SIRT1 activation compared to initial SIRT1 activity reaction, **Figure 4-25**. Similar 2 to 3-fold activation was seen in case of resveralogues V1, V2, V3, V4, V5, V9, V13, V16, V17, V19, V20, V22 and V39, **Figures 4-26** and **Figure 4-27**. The other resveralogues showed SIRT1 activation similar to that of initial SIRT1 activity.

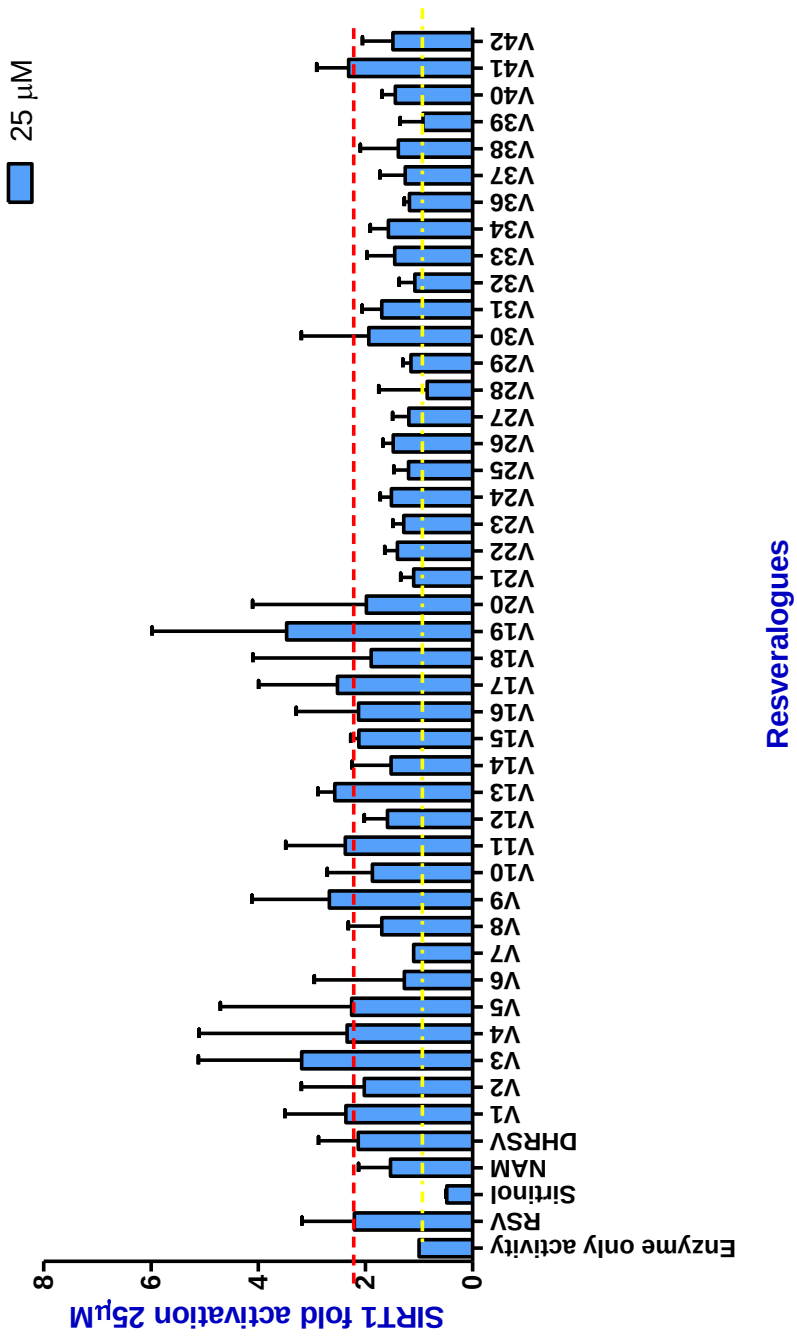

Figure 4-26 Activation of SIRT1 by resveratrol and synthesized resveralogues plus sirtinol and nicotinamide. Fold activations are calculated as the ratio of the deacetylation rate in SIRT1 reaction containing the resveralogues at 25 µM to that of enzyme only SIRT1 activity reaction (where enzyme only activity represents the SIRT1 deacetylase reaction with 0.5 % and without any resveralogues). Data from three independent biological experiments (on same day) are shown ± standard deviation. (red coloured line represent statistical comparison between resveratrol

and other resveralogues while yellow coloured line represent comparison between SIRT1 enzyme only activity and other resveralogue).

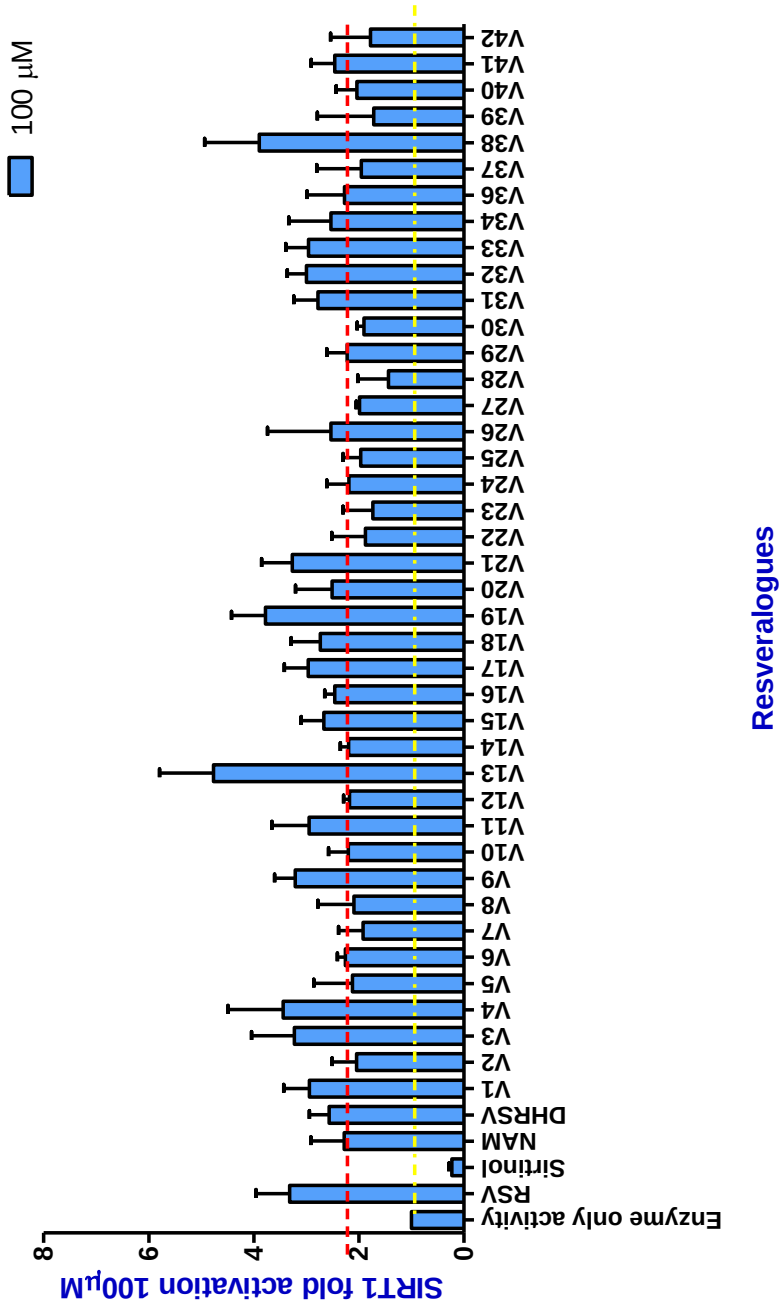

Figure 4-27 Fold activation of SIRT1 by resveratrol and synthesized resveralogues plus sirtinol and nicotinamide. Fold activations are calculated as the ratio of the deacetylation rate in SIRT1 reaction containing the resveralogues at 100 µM to that of enzyme only SIRT1 activity reaction (where enzyme only activity represents the

SIRT1 deacetylase reaction with 0.5% DMSO and without any resveralogues). Data from three independent biological experiments (on same day) are shown ± standard deviation. (red coloured line represent statistical comparison between resveratrol and other resveralogues while yellow coloured line represent comparison between SIRT1 enzyme only activity and other resveralogue).

4.6. Effect on Senescence associated secretory phenotype (SASP):

In order to understand the effect of resveralogues on SASP, IL-6 release from MRC-5 cells were studied. Human fibroblasts were treated with 10 µM, 50 µM and 100 µM of resveratrol and culture medium was collected after 24 hours to evaluate the IL-6 release on resveralogues treatment. This study was determined by commercially available ELISA kit from BD Biosciences Company. The data obtained from IL-6 ELISA assay shown variable results due to the presence of high background IL-6 in culture media, see Figure **C-1 to Figure C-31** (in **Appendix C**). However, a similar assay was run by collaborator (Prof. Lynne Cox, University of Oxford) using using a human specific IL6 antibody. The collaborator results are shown in **Figure 4-28.** The primary data suggests that the resveralogues reduces the IL-6 releases at a low dose (10 µM) compared to resveratrol. However, there was no dose dependent decrease in IL-6 release observed above 10 µM.

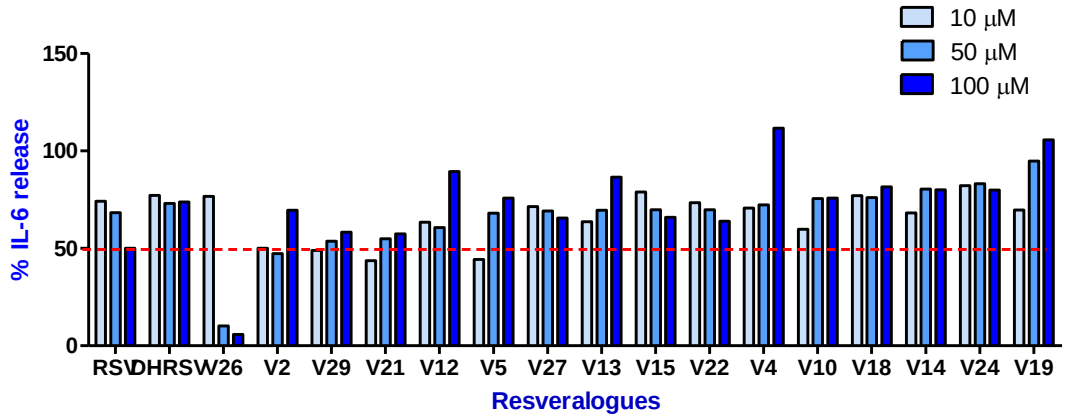

Figure 4-28 Effect of resveralogues on IL-6 release were analysed by a human specific IL6 antibody. This data presented using collaborator work. (This preliminary data was provided by collaborator Prof. Lynne Cox at University of

Oxford). Data represents n=1 experiments and red line represent the comparison between resveratrol and other resveralogues at 100 μM)

In addition, **Figure C-1 to Figure C-31** (in **Appendix C**) represents individual compounds effect on toxicity using LDH assay, the effect on ki-67 and β- galactosidase assay and IL-6 release. **Figure C-1 (resveratrol), Figure C-2 (dihydroresveratrol), Figure C-3 (V2), Figure C-4 (V5), Figure C-5 (V6), Figure C-6 (V8), Figure C-7 (V9), Figure C-8 (V10), Figure C-9 (V11), Figure C-10 (V13), Figure C-11 (V15), Figure C-12 (V17), Figure C-13 (V18), Figure C-14 (V19), Figure C-15 (V21), Figure C-16 (V22), Figure C-17 (V23), Figure C-18 (V24), Figure C-19 (V29), Figure C-20 (V30), Figure C-21 (V31), Figure C-22 (V32), Figure C-23 (V33), Figure C-24 (V34), Figure C-25 (V36), Figure C-26 (V37), Figure C-27 (V38), Figure C-28 (V39), Figure C-29 (V40), Figure C-30 (V41) and Figure C-31 (V42).**

Chapter 5. Chemistry discussion

5.1. One-pot synthesis of resveralogues:

Resveratrol and related molecules consist of a *trans*- stilbene or *trans*-1,2-diphenylethene core. The existing literature suggests various methods for preparation of these molecules [169]. To achieve the aims of the project, a catalytic method for preparation of *trans*-stilbene was selected using an organozinc reaction [170]. It required the conversion of a benzyl bromide into an organozinc intermediate using Knochels procedure and then the use of a nickel (II) catalyst [$NiCl_2$ $(PPh3)_2$]. However, TLC analysis showed there was no conversion of starting materials. The probable reason behind this was either no formation of benzyl zinc bromide or there were insufficiently inert conditions to maintain the reaction. This reaction was then carried out in argon gas atmosphere but gave the same result.

The Horner-Wadsworth-Emmons reaction was also considered as a suitable method for preparation of a carbon-carbon double bond formation by using stabilised phosphonates and corresponding carbonyl compounds [156]. This method was used successfully to accomplish the synthesis of resveratrol derivatives. This first involved the formation of a phosphonate from the corresponding benzyl bromide (IN19-IN34) and then isolation or purification to get the corresponding phosphonate (IN3). This phosphonate was then reacted with an aldehyde (IN35-IN40) or ketone to result in carbon-carbon double bond formation. (Overall synthetic scheme shown in **Scheme 5-1**) In order to develop a simplified synthesis of *trans*-stilbene molecules, this method was selected over other methods. Another method that has been modified into suitable one-pot syntheses includes Wittig-Heck [147, 148], Organo-zinc [170] and palladium catalysis reactions but none are as convenient as the presently developed method. The synthetic scheme for the one-pot synthesis is shown in **Scheme 5-1**;

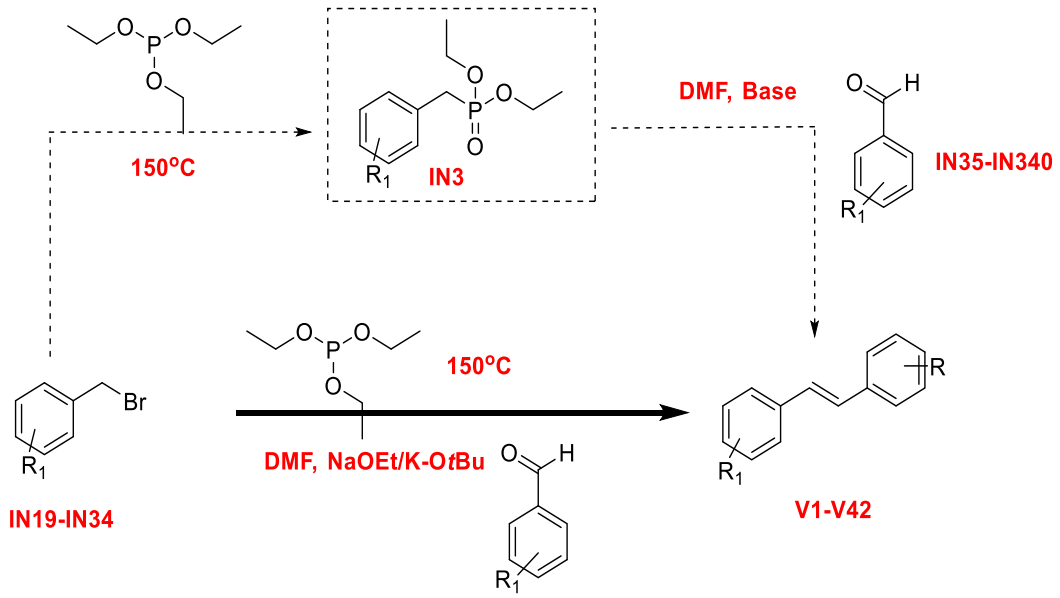

Scheme 5-1 Simplified one-pot synthesis of resveralogues using Horner-Wadsworth-Emmons reaction.

In order to achieve the simplified synthesis of resveratrol derivatives (termed resveralogues) significant method development was carried out as explained in the method **Section 2.3**. All the derivatives synthesised using newly developed one pot method are shown below in **Table 5-1.** A diverse range of resveratrol derivatives was synthesised in order to understand the role of substitution on *trans*-stilbene ring. Many substitutions focused on replacement of 4′-hydroxyl of resveratrol as it is considered to mediate detrimental activities at high concentrations [154]. Further, substituted *trans*-stilbene derivatives such as V7, V8, V16, V17, V25 and V29 were also synthesised in order to evaluate the role of steric and electronic effects on the *trans*-stilbene activity. All the resveralogues synthesised were formed in good yield and simple product isolation compared to existing protocols. The yield of all synthesised resveralogues derivatives was found to be 70-95% except V9 where a 59% yield was achieved. The probable reason was the 4′-COOMe group. In this case, the base may have hydrolysed the COOMe group and hence a lowered yield of the reaction was noted.

Table 5-1 Resveralogues synthesis using one-pot synthesis.

Resveralogue	Benzyl bromide (R)	Aldehyde (R_1)	Yield (%)
V1	4-NO_2	3,5-$(OMe)_2$	90
V2	2-F	3,5-$(OMe)_2$	74
V3	3-OMe	3,5-$(OMe)_2$	60
V4	3,5-dimethyl	3,5-$(OMe)_2$	81
V5	2,6-difluoro	3,5-$(OMe)_2$	78
V6	2,4-difluoro	3,5-$(OMe)_2$	74
V7	3-Cl	4-(OMe)	77
V8	3-CF_3	4-$N(Me)_2$	74
V9	4-COOMe	3,5-$(OMe)_2$	59
V10	2-CN	3,5-$(OMe)_2$	71
V14	4-Me	3,5-$(OMe)_2$	84
V16	2-CN	2-CN	79
V17	3-Cl	4-$N(Me)_2$	79
V18	2-NO_2	4-(OMe)	79
V19	2-CN	4-(OMe)	75
V20	3-NO_2	4-(OMe)	73
V21	2,6-dichloro	3,5-$(OMe)_2$	80
V22	2-NO_2	3,5-$(OMe)_2$	79

V25	2-CN	2-NO_2	85
V27	3-NO_2	3,5-$(OMe)_2$	80
V28	4-NO_2	2,4-$(OMe)_2$	80
V29	H	H	90
V42	H	3,5-$(OMe)_2$	72
V43	3-Cl	3,5-$(OMe)_2$	68

5.2. Proto-demethylation of resveralogues:

The synthesis of dihydroxy derivatives was attempted using pyridine hydrochloride as discussed in chemistry method **Section 2.5.1**. The reaction was not successful initially and even when it was carried out at a higher temperature such as 165 ^{o}C. The reaction showed consumption of starting material by TLC analysis. However, the product isolation was difficult as the reaction mixture turned into a black oily mass. Further, when it was introduced into 5 mL of 2 N hydrochloric acid and extracted with diethyl ether (twice), the ether layer did not show any compound by TLC analysis and there was no crude product noted once the ether layer had been distilled off. The reason might be the compound was not formed and the material formed was the result of degradation of starting material.

Then, the proto-demethylation of resveralogues was tried using BBr_3 in dichloromethane. The reaction worked well enough and the product was isolated using column chromatography. The proto-demethylation reaction resulted in a low yield of most of the resveralogues derivatives except V41 in which the product precipitated out of the solution and was then isolated using simple recrystallisation from ethanol. In all of the other resveralogues, the yield was found to be less than 45% yield. The potential reason was these resveralogues was strongly adsorbed onto the silica column. (There was a significant loss of compound noted when crude material was loaded onto the silica column). There might be strong interactions between silica and the hydroxyl group of resveralogues and hence they could not be eluted. This might be better eluted in future by

use of triethylamine as phenols are weak acidic in nature. The details of dihydroxy resveralogues are shown in **Table 5-2,**

Table 5-2: Synthesis of dihydroxy resveralogues using BBr_3 in dichloromethane.

Resveralogue	Methoxy resveralogue (R)	Yield (%)
V13	4-Me	30
V23	2-CN	40
V26	3,5-Dimethyl	45
V31	4-NHOAc	45
V37	4-NHCOPh	10
V40	2,4-difluoro	40
V41	2-NHOBenzyl	80

5.3. Synthesis of bioisostere amino-resveralogues of resveratrol:

The second aim of the project was to understand the effect of replacement of 4′- and 2′-hydroxyl with an amino group on SIRT1 activity. Further, 2′-substituted amino resveralogues were synthesised in order to understand the role of non-planar conformation in the regulation of SIRT1 activity. The synthesis was planned according to the design in **Figure 1-16** and synthetic procedure and scheme shown in method **Section 2-6** and **Section 2-7**. The amino resveralogue (V12) was synthesised from corresponding nitro resveralogues (V1) by reduction. The reduction was not successful using $SnCl_2$. The main problem was to isolate and purify the crude product from the reaction mass. Earlier literature also described the same problem while using stannous chloride complex [171]. Initially, the reduction was carried out in methanol solvent but no conversion occurred. Then, the reduction was carried out in acetic acid to understand the role of acidified solvent. The reaction worked well but the corresponding oily crude material could not be extracted with different organic solvents such as ethyl acetate, diethyl ether. The oily suspension was hard to get into a clear solution and hence this method was abandoned. Further, one of the reports used zinc in acetic acid to reduce the nitro compounds but this

reduction reaction was not successful. Then, following the method described in the literature reaction was carried out using iron ammonium chloride in a mixture of solvents which included ethanol/THF/water [172]. This reaction was successful and the 4′- and 2′-amino resveralogues were synthesised. Various amido resveralogues such as methyl, isopropyl, benzyl amide derivatives were then synthesised using corresponding acyl or sulphonyl chlorides. This reaction worked very well and resulted in good yields. The 4-substituted amido resveralogues include V11, V12, V30, V31, V36 and V37. Using a similar synthetic protocol 2′-substituted amido resveralogues were prepared including V38, V39 and V41. All details of nitrogen resveralogues are shown in **Table 5-3**; the yield of all the amido resveralogues was found to be good for all methylated variants (V11, V30, V32, V36, and V41) but gave a lower yield for the dihydroxy amino resveralogues such as V31, V37.

Table 5-3: 4′-substituted and 2′-substituted amino resveralogues:

Resveralogue	Amine	Acyl Chloride	Yield (%)
V11	4′-NH_2	MeCOCl	70
V12	4′-NH_2	-	61
V30	4′-NH_2	MeSOOCl	90
V31	4′-NH_2	MeCOCl	45
V32	4′-NH_2	$(CH_3)_2CHCOCl$	87
V36	4′-NH_2	PhCOCl	80
V37	4′-NH_2	PhCOCl	10
V38	2′-NH_2	-	55
V39	2′-NH_2	PhCOCl	85
V41	2′-NH_2	PhCOCl	80

5.4. Heterocyclic based resveralogues:

Details of heterocyclic based resveralogues are described here in method **Section 2-8, 2-9 and 2-10**. The 4′-substituted benzimidazole (**TM4**, **Figure 1-19**) was planned from intermediate phosphonate (**IN10**, **Figure 1-19**) and aldehyde. The synthesis of intermediate **IN1** was planned from intermediate (**IN11, Figure 1-19)** phosphonate that was obtained from the reaction of 4′-carboxy benzyl bromide (**IN12**, **Figure 1-19**) with triethyl phosphite in toluene under reflux condition. Then, the corresponding carboxyl phosphonate was subjected to cyclisation reaction with 1,2-diphenylamine via *in-situ* acyl chloride phosphonate formation (see **Section 2.8.3** and **2.8.4**). However, this was unsuccessful and due to the lack of formation *in-situ* intermediate acyl chloride phosphonate. The formation of this acyl chloride was tried using oxalyl chloride and then using thionyl chloride. The probable issue was that the acyl chloride formed was unstable and hence could not isolated. In the case of the second target molecule, 2′-substituted benzimidazole (**TM2**, **Figure 1-20**) formation of the key intermediate was synthesis of 2′-substituted acid (**IN13**, **Figure 1-20**). However, the formation of the acid from hydrolysis of corresponding 2′-cyano derivative (V10) failed. The hydrolysis reaction was tried using various bases including LiOH, NaOH, KOH. The details are mentioned in **Table 5-4**:

Table 5-4: Attempted hydrolysis of V10 and conditions used.

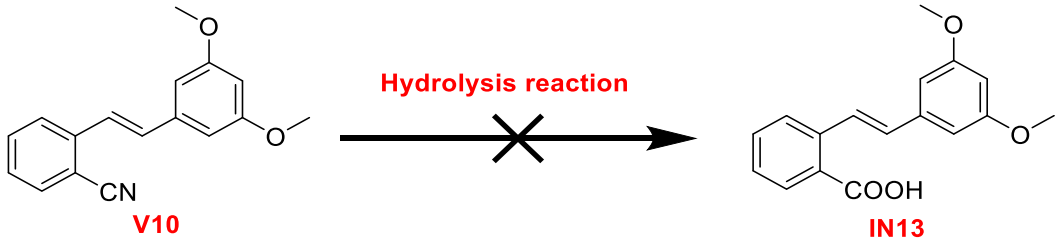

Base	Solvent	Temperature
2 M LiOH	DCM	Room temperature
2 M LiOH	THF	Reflux temperature
2 M LiOH	MeOH	Reflux temperature
2 M NaOH	MeOH	Room temperature
2 M NaOH	MeOH	Reflux temperature
Conc. NaOH	MeOH	Reflux temperature
Conc. NaOH	Water	Reflux temperature
2 M KOH	MeOH	Reflux temperature

Initial attempts at hydrolysis were tried with 2 M LiOH in DCM, THF and methanol at room temperature as well as reflux temperature. Various solvents were tried as the solvent polarity is likely to play a crucial role in hydrolysis. However, no reaction occurred even with LiOH in methanol. Sodium hydroxide was then tried to increase the basic condition of hydrolysis reaction but even at conc. NaOH in water reaction had no effect. Similar reaction conditions were used with KOH and also resulted in no hydrolysis reaction. TLC analysis from all of the reactions and their condition shown there was no consumption of a starting cyano (V10). The potential reason behind the failed hydrolysis reaction is due to the position of 2′-cyano group. Steric hindrance due to proximity to the double bond may cause the nucleophile to be unable to access the cyano group.

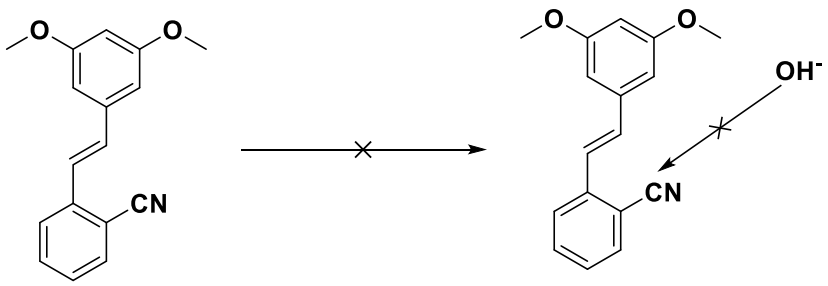

Scheme 5-2 Steric hindrance of 2′-cyano and double bond in the hydrolysis reaction of V10 and approach of nucleophile OH^-.

5.5. Alternative heterocyclic substitution:

To achieve the aim of the project and understand the role of five-membered substitutions on *trans*-stilbenes core the target molecule was changed. It is considered that five-membered heterocyclic ring such as imidazole, tetrazole ring are considered as biological isosteres of each other. Accordingly, the corresponding 4′-substituted and 2′-substituted tetrazole resveratrol derivatives were designed as new target molecules. The synthesis was achieved from corresponding cyano resveralogues using sodium azide click chemistry. The reaction worked very well although it was found that 4′-substituted tetrazole was formed in good yield compared to 2′-substituted tetrazole. However, the 2′-substituted reaction was low in yield probably due to steric hindrance. This reaction was kept for 2 days at reflux temperature and went to only 10% completion. This further suggested the impact of steric hindrance of cyano to reach the nucleophile (see **Scheme 5-3**). The product was isolated using column chromatography with chloroform and methanol as mobile phase in both 4′-and 2′-substituted analogues.

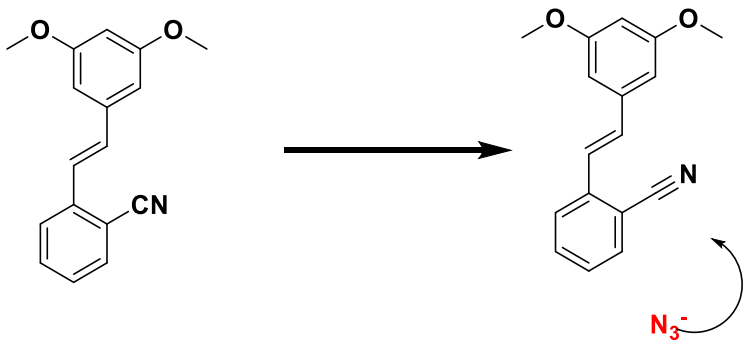

Scheme 5-3 Click chemistry reaction of 2′-cyano (V10) and sodium azide: approach of nucleophile.

5.6. Spectroscopic details of resveralogues:

All the synthesised resveralogues were characterised by ^{1}H and ^{13}C NMR, IR, HRMS and melting points. Each compound assignment was confirmed using COSY and HMQC NMR spectra. The detailed spectra and interpretation of results were included in **Appendix B**. The synthesised resveralogues are based on *trans*-stilbene core. Hence, the characteristic pattern of olefinic proton coupling constant (doublet with coupling constant more than 15 Hz in the case of *trans*-olefinic proton only) was clearly noted in NMR spectra of nearly all compounds. However, a few of them, such as V4, V13, V16,, V29, V30, and V37 showed a singlet in their ^{1}H NMR spectra. The reason behind the singlet might be the second order coupling effect between olefinic proton in which the $\Delta\nu$ /*J* value is very less. ($\Delta\nu$ represents the chemical shift differences between the protons and *J* is coupling constant). To attempt to resolve the singlet peak into doublet compounds spectra were also run in a small amount of DMSO. This further resulted into to resolve the singlet into doublets. (e.g. in compound V4 the NMR spectra in $CDCl_3$ was shown singlet for two olefinic protons at δ7.13 value and when it was run with small amount of *d6*-DMSO resulted into sharp doublet with coupling constant value (*J* equal to 16.4Hz, See **Figure 5-1**. A similar singlet olefinic proton noted in case V13, V30, V16, V29 and V37 but the singlet was not resolved into a doublet with the change of solvent.

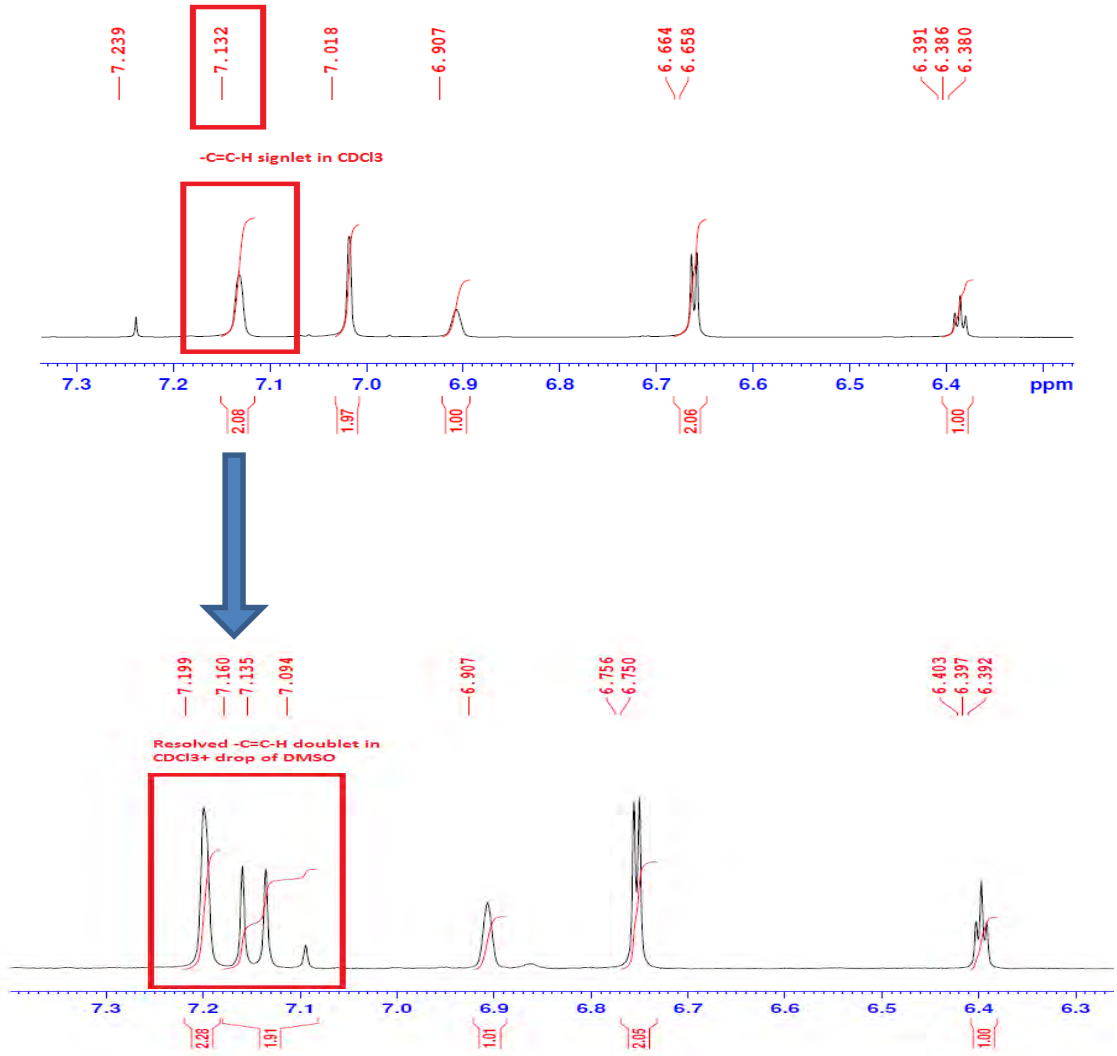

Figure 5-1 Effect of solvent polarity on olefinic proton peak separation in V4.

Instead, to confirm *trans*-olefinic double bond the IR spectrum was examined for each compound. The IR spectra of the synthesised compounds showed a characteristic band at 950-960cm^{-1} which represents the stretching frequency of *trans*-olefinic (C=C-H) double bond. Mass spectral analysis of compounds showed either [M+23] peak in all of the synthesised resveralogues. However, there was frequently also a dimer peak of [2M+23] noted with small intensity. In addition to this, some of the compounds were shown did not show actual or sodium adduct of mass number e.g. V29, V7. It was noted that some of the resveralogues were difficult to ionise for mass spectra and, therefore, it was difficult to get an exact mass peak or corresponding sodium adduct mass peak. All of the spectra are presented in Appendix section.

Chapter 6. Bioactivity discussion:

6.1. Cytotoxicity of resveralogues:

In drug discovery and development, any potentially new drug molecules are first evaluated through toxicity screening assays. This provides fundamental information such as LD50 (lethal dose) of the compound. Resveralogues were analysed for cytotoxicity assay using a range of methods. This study was performed on cells based assay and MRC-5 cells were used in order to the understand effect of resveralogue on normal cells. MRC-5 cells are human diploids lung fibroblast cells which widely used in ageing research as an in-vitro model [150]. All cytotoxicity studies were carried out on middle aged cells (i.e. CPD36-39). Earlier studies with resveratrol showed similar effects on growth arrest and toxicity, independent of cells population age [150]. Our secondary aim in conducting cytotoxicity assays was to overcome the earlier detrimental activities shown by resveratrol and find out the structural features that mediate these effects. In this project, three different toxicity screening assays namely MTT (based on mitochondrial activity), Neutral red (lysosomal activity) and LDH (membrane potential of live cells) was performed. The results from these assays suggested that LDH assay is a better method to assess the toxicity of these compounds. MTT assay gave anomalous results suggesting compounds were acting on the mitochondria without necessarily being toxic. (See **Figure 4-13** where dose dependent decreases in cells viability of resveralogues were noted using MTT assay). Additionally, neutral red assay was found to be inappropriate due to interference of these compounds at neutral red absorbance maxima. These results were consistent with other reports on *trans*-stilbene based compounds [173, 174]. In this study, we demonstrated that some of these compounds affect mitochondrial function. This suggested the role of 4′-hydroxy substitution on toxicity. The potential reason behind the apparent reduction in toxicity compared to resveratrol at 100 μM is the role of 4′-hydroxy group. It might cause mitochondrial damage through the formation of 4′-keto (quinone radical) which could potentially damage mitochondria. (See **Scheme 6-1**) All the tested analogues without a 4′-hydroxy group are non-toxic compounds (e.g. tetrazole, NHOAc, H group). However, when 4′-hydroxy was substituted with 2′-CN, 4′-Me, 4′-benzyl or 2′-benzyl exert same or more apparent toxicity than resveratrol. This suggests that these groups also increases mitochondrial dysfunction effect, increase stress and hence mediate apparent toxicity.

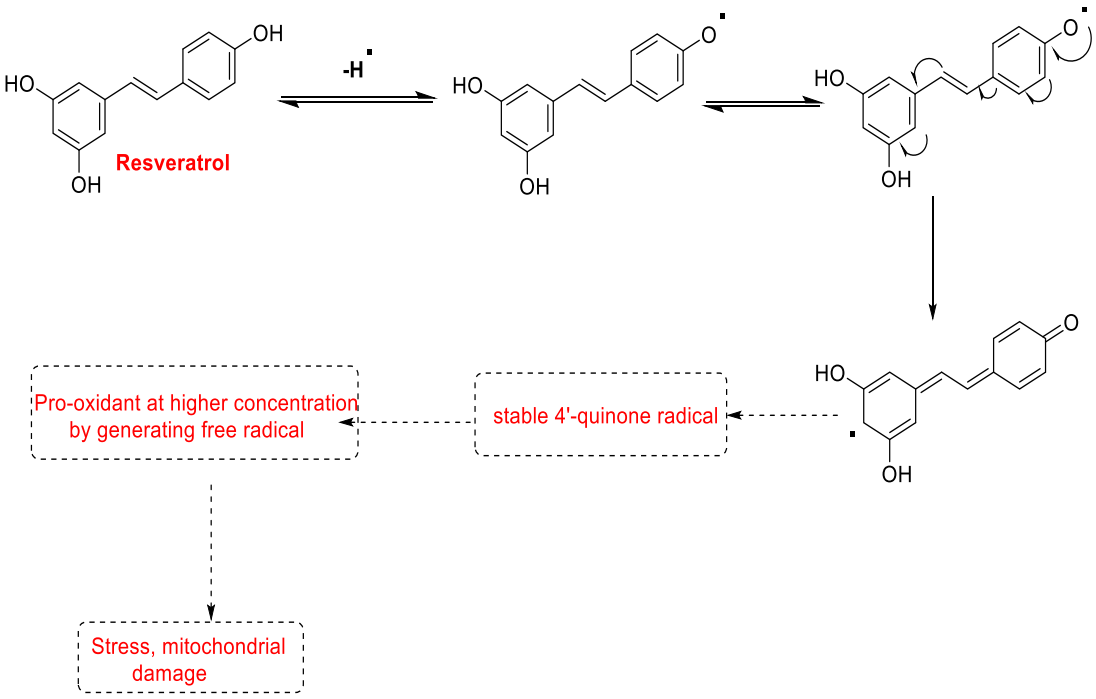

Scheme 6-1 Plausible mechanism behind resveratrol toxicity in MTT assay.

Toxicity data obtained from MTT and Neutral red suggested that these assays were not suitable to evaluate the actual cytotoxicity of resveralogues. LDH was found to be a much more appropriate method for determine the toxicity of synthesised resveralogues. The synthesised resveralogues were designed in such way that they have increased in lipophilicity but there was no structure-activity correlation between lipophilicity and toxicity by LDH assay **Figure 6-2**, indicating that these effects are not non-selective physical damage to the membrane. LDH assay is widely used to measure the cell death either through apoptosis or necrosis [175]. Here, resveralogues did not show any significant toxicity or LDH release at 100 µM. This suggested that these molecules were not cytotoxic and conflict with data produced by using the MTT assay. The increase in percentage cell death for synthesised resveralogues was shown in **Figure 6-1** and it suggested that these derivatives were not exerting a toxic effect through apoptosis or necrosis.

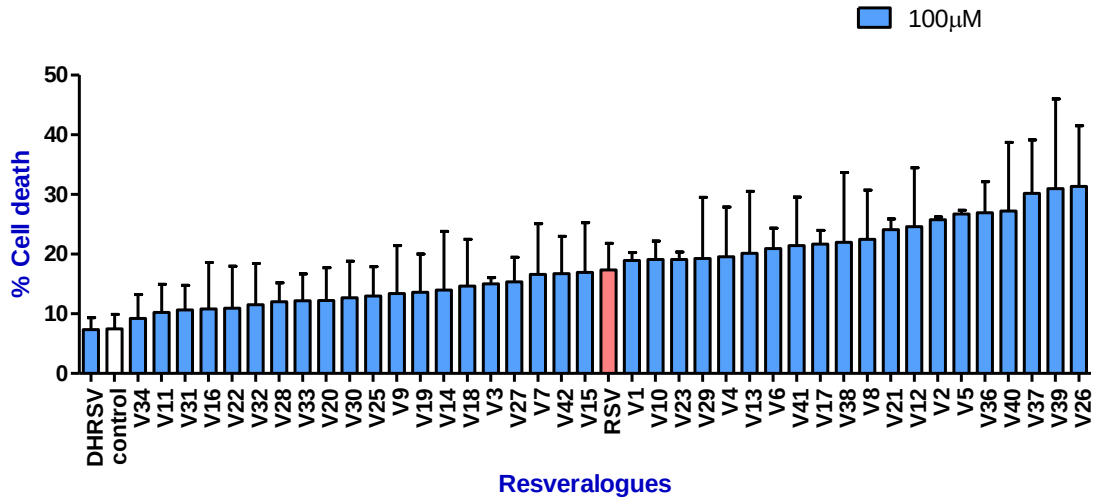

Figure 6-1 Effect of resveralogues V1-V42 on percentage LDH release (in increasing order) of primary human lung fibroblast (MRC-5) at CPD 36-40 was determined by using LDH assay. The y-axis shows the percentage of LDH at 100 µM concentration of resveralogues for n = 3 different biological replicate cultures (±standard deviation) vs control cells treated with vehicle only.

6.2. Cytotoxicity and lipophilicity:

Our results show that LDH assay is a good method to evaluate the toxicity of these molecules. Additionally, some of these molecules were found to mediate dysfunction in mitochondria [173]. Earlier reports on resveratrol toxicity were largely based on MTT assay. However, the present thesis work reveals for the first time that MTT overestimates cytotoxicity because it uses mitochondrial output. Hence, LDH assay is a more reliable method for evaluating resveralogue's toxicity. The calculated lipophilicity in the form of LogP was determined for each compound using Chemdraw software. Here, the small structural changes to substituents of resveratrol caused significant differences in Log P of the resveralogues. Correlation analysis between LogP and toxicity at each concentration showed a very weak positive linear relationship between lipophilicity and cellular toxicity. (Pearson coefficient r^2 was less than 0.4 see **Figure 6-2**).

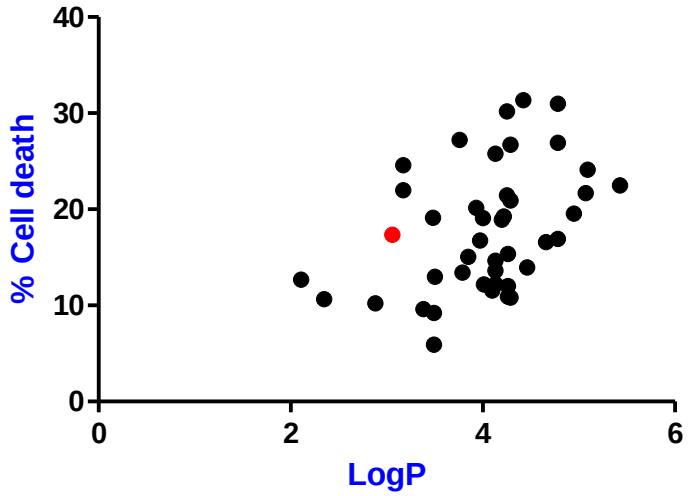

Figure 6-2 Correlation plot between Log P and percentage cell death using LDH assay for resveralogue at 100 µM concentration where Log P's were calculated using Chemdraw software. (Weak positive correlation Pearson coefficient $r^2 < 0.4$, p=0.0056)

6.3. Resveralogues effect on cytostasis:

Cytotoxicity evaluation of resveralogues from three different assays suggested that many of these molecules were not likely to exert the level of cytotoxicity that were reported earlier in literature. However, given that resveratrol induces senescence at higher doses, evaluation of cytostasis through ki-67 and SA-β-galactosidase were conducted [150]. Accordingly, we tested the least and more toxic resveralogues (including V2, V5, V10, V11, V13, V15, V21, V23, V24, V30, V31, V32, V34, V36, V37, V39 and V41). This allows us to understand the effect of position and the electronic distribution on the *trans*-stilbene double bond. Our results show that resveralogues that are (i.e. those exerting conjugative effects) substituted at the 2-position with F (V2), CN(V10), Cl(V21), CN(23), benzyl(V39) were found to affect Ki67 proliferation more than resveratrol. In fact, there were no signs of nuclei or cells in the case of V23, V39 at 100 µM. However, V11, V15, V24, V29, V30, V32, V31, V34 and dihydroresveratrol did not show any dose dependent decrease in proliferation marker ki-67 and in fact showed an increase at low doses. This increase in proliferation at low dose of resveralogues was significantly different from control untreated cells. Structural analysis shows that these molecules are either 4′-substituted with nitrogen group resveralogues or 2′-substituted nitrogen analogue

(V24). This was also the case with DHRSV and V15 neither of which bear a trans-stilbene double bond. Additionally, V29 (unsubstituted *trans*-stilbene) was also shown dose–dependent decrease of proliferating nuclei which suggested that trans-stilbene moiety is likely to be responsible for reduction in proliferation and senescence. This potentially implies that the *trans*-stilbene double bond is responsible for many of the negative effects observed.

In the case of resveratrol the decrease in ki-67 positive nuclei was associated with an increase in SA-β-galactosidase positive nuclei. This trend was continued in the case of V2, V5, V10, V13, V15, V21, V24, V29, V34, V37, V39, and V41. However, V11, V30, V32 was shown increase in SA-β-glactosidase with no effect on ki-67 proliferation index suggesting some other lysosomal effects.

6.4. Structural requirement of resveralogues for cell cytostasis activity

The overall result from ki-67 and SA-β-galactosidase assay suggested that high electron density around the trans-stilbenes core may be responsible for the cytostatic activity of resveratrol. This hypothesis was further supported by data from dihydroresveratrol and V15 where there was no sign of growth arrest observed. Overall data obtained from twenty structurally distinct resveralogues showed diverse effects on proliferation giving some indication of a structure activity relationship for this growth arrest. When the *trans*-stilbene core included an electron donating group (through a positive resonance effect) such OH (in case of resveratrol), F (V2 and V5), Cl (V21) senescence induction was greater than resveratrol, **Scheme No 6-1**. In the same way, electron withdrawing groups (through – resonance effect) such as CN, COBz (V23, V39, V41) gave a reduction in ki-67 fraction but without a propotionate increase in SA-β-galactosidase positive nuclei. This indicated that these molecules were cytostatic but might not induce senescence. However, V31, V24 and V34 were found to be exceptions to this rule. When this correlation was compared with MTT assay results it suggested that those molecules which were less toxic in the MTT assay also showed less cytostasis of MRC-5 cells. In other words resveralogues likely to increase the stress in mitochondria through increase in ROS was found to increase senescence growth arrest. Recently, it was also suggested that damage in mitochondria could be linked to various pathways that were involved in senescence [176].

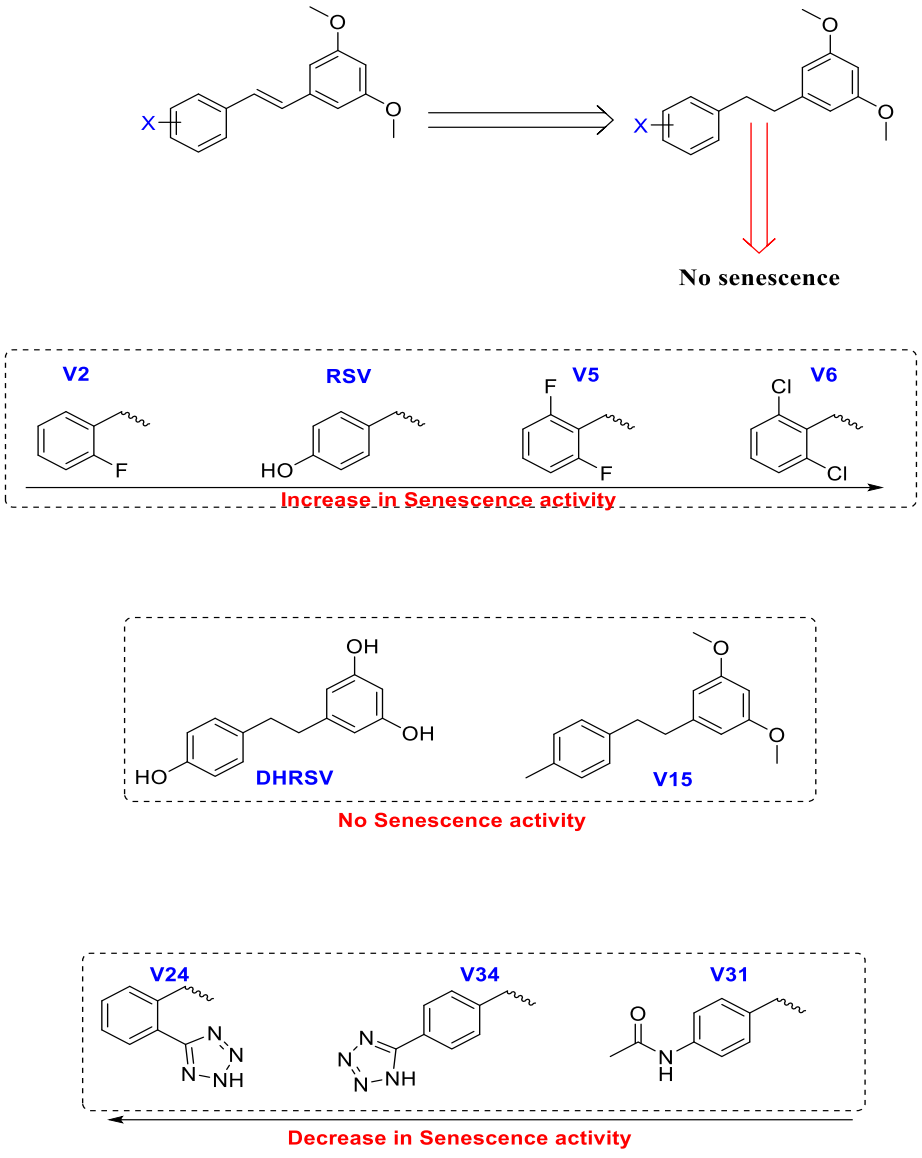

Scheme 6-2 Role of substitution on *trans*-stilbenes cells cytostasis activity.

Table 6-1: Role of 4-substitution on resveratrol on cell cytostasis.

Substituent (X)	Type of Resonance effect (R)	Effect on ki-67 marker	B-gal positive cells
4′-OH(RSV)	Electron donating +R	Dose dependent decrease	Dose dependent increase
2′-F (V2)	Electron donating +R	Dose dependent decrease	Dose dependent increase
2′,6′-F (V2)	Electron donating +R	Dose dependent decrease	Dose dependent increase
2′,6′-Cl (V21)	Electron donating +R	Dose dependent decrease	Dose dependent increase
2′-CN (V23)	Electron donating -R	Dose dependent decrease	No co-relation with decrease in ki-67 nuclei
2′-COBz (V41)	Electron donating -R	Dose dependent decrease	No co-relation with decrease in ki-67 nuclei
DHRSV	No trans-double bond	No effect	No effect
4′-Me	No trans-double bond	No effect	No effect

6.5. SIRT1 activation:

According to the literature, resveratrol is thought to mediate beneficial effects through SIRT1 activation, but there is no clear structure activity described in the literature. In addition, *trans*-stilbene molecules possess many other biological activities but their mechanisms of actions are still unknown. An aim of the project was to investigate whether the beneficial activities of *trans*-stilbenes that may be mediated through SIRT1 could be separated from the detrimental ones such as senescence. Here, we also investigated the *trans*-stilbene structural features responsible for SIRT1 activation. The results showed a small effect of substitution on SIRT1 activation but no significant increase in the SIRT1 activity compared to resveratrol. One of the hypotheses of the project was that modification of the 4′-hydroxy group could potentially increase the SIRT1 activity, whilst reducing toxicity. Equally, disturbing the planar confirmation may enhance its activity. The overall structural analysis of the synthesised molecules and its SIRT1 activity data suggested no obvious correlations and the structural features that

increase in SIRT1 activity by design modification are not clear. However, interestingly, DHRSV and V15 showed similar SIRT1 activity to that of resveratrol. This suggested that SIRT1 activity is independent of *trans*-stilbene double bond as both are dihydroderivatives. This helps us to answer the one of the project aims that SIRT1 activation is independent of *trans*-stilbene double bond and abrogates induction of cytostasis at 100 µM.

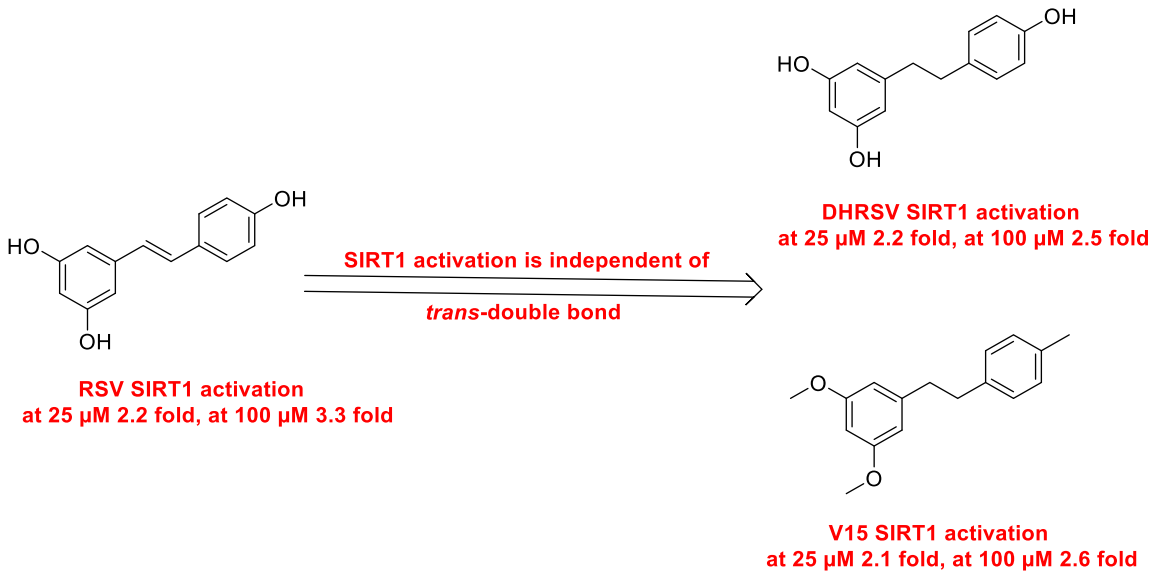

Scheme 6-3 Effect of *trans*-stilbene double bond on SIRT1 activation.

6.6. Relationship between SIRT1 activation, cytotoxicity (using LDH assay) and proliferation:

According to the literature, SIRT1 activation is a potential anti-ageing mechanism. This project is the first to examine the relationship between SIRT1 activation and a compounds effect on normal cells. There is no correlation observed between SIRT1 activity and MRC5 cell toxicity using LDH assay. However, a positive correlation was found between SIRT1 activation of resveralogue and proliferation marker ki-67. (Pearson coefficient r^2 =0.6378, $p < 0.005$).

A

Number of XY Pairs	43
Pearson r	-0.06389
95% confidence interval	-0.3574 to 0.2412
P value (two-tailed)	0.6840
P value summary	ns
Is the correlation significant? (alpha=0.05)	No
R square	0.004081

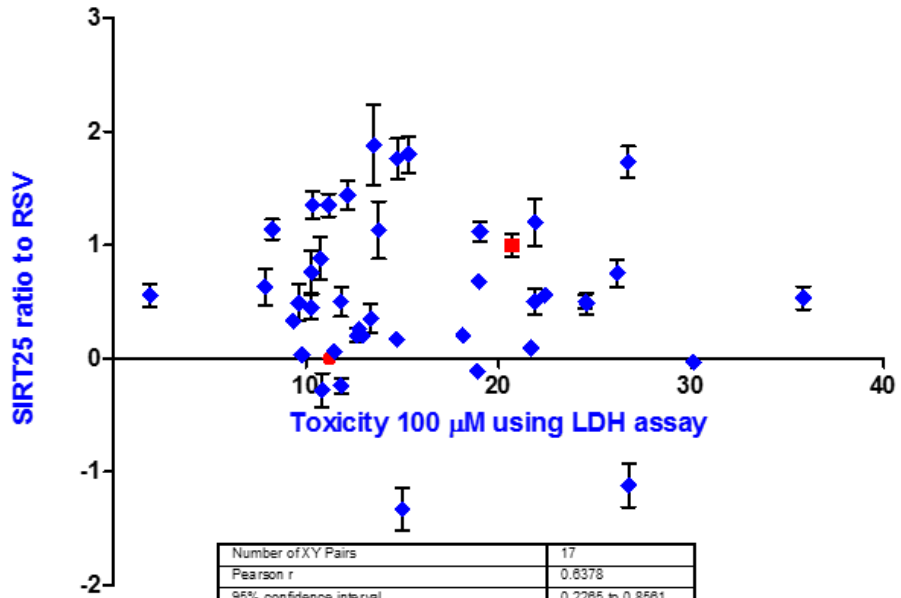

Number of XY Pairs	17
Pearson r	0.6378
95% confidence interval	0.2265 to 0.8561
P value (two-tailed)	0.0059
P value summary	**
Is the correlation significant? (alpha=0.05)	Yes
R square	0.4068

B

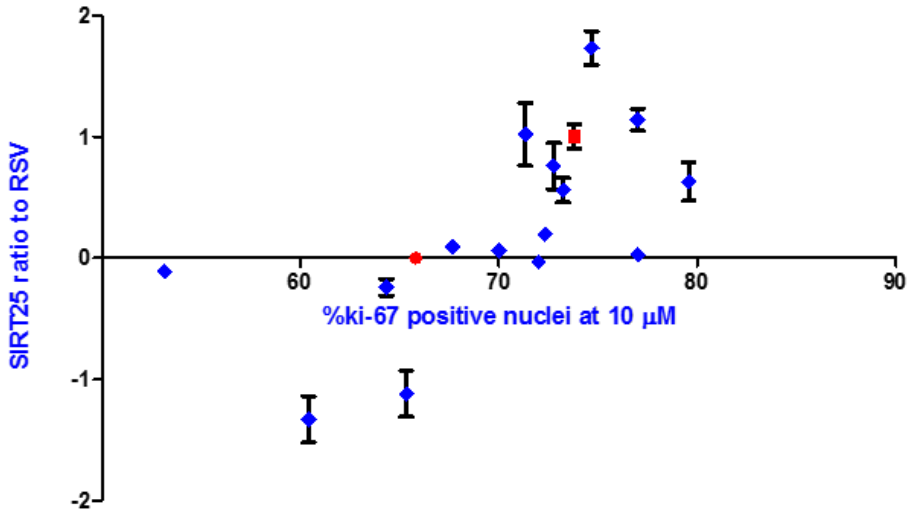

Figure 6-3 Correlation analysis of SIRT1 activation with A) toxicity (using LDH assay) no significant corelation was found A) with proliferation ki-67 marker where strong positive correlation was found r=0.6378, p <0.005 where red dot represent control and square represent resveratrol.

6.7. SIRT1 activation and IL-6 relation:

No structure activity relationship was found between resveralogues and IL-6 release. Here, we also investigated the link between SIRT1 and SASP component IL-6. There was no correlation found between SIRT1 activation and that of IL-6 release, **Figure 6-4**. This suggests that IL-6 release is mediated through means independent of SIRT1 activation. Recently, it has been reported that SASP is inversely mediated by SIRT1 protein. The SASP components such as IL-6 and IL-8 were shown to quickly accumulate in SIRT1 depleted cells. This study shows that the regulation of SASP is not entirely dependent on SIRT1 activation.

	SIRT 100 ratio
Number of XY Pairs	14
Pearson r	-0.3787
95% confidence interval	-0.7572 to 0.1902
P value (two-tailed)	0.1818
P value summary	ns
Is the correlation significant? (alpha=0.05)	No
R square	0.1434

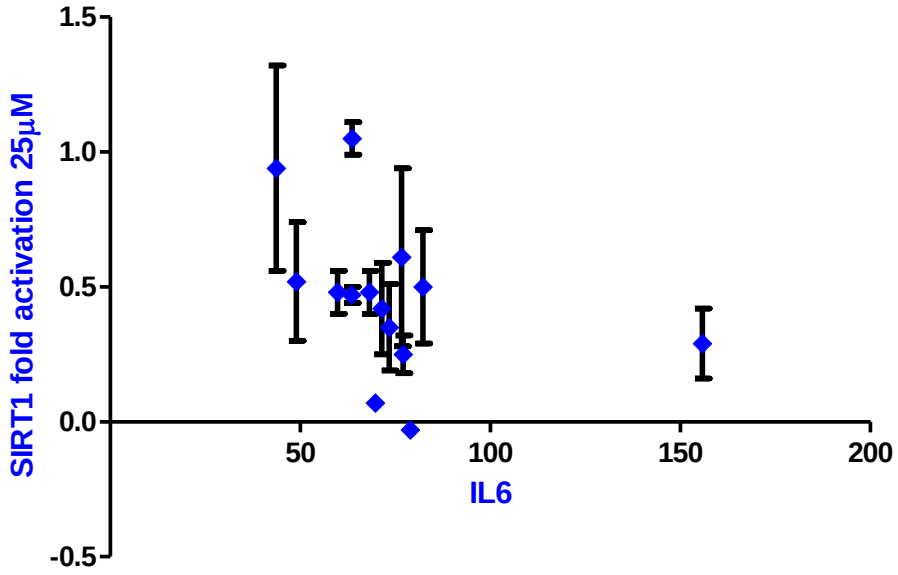

Figure 6-4 IL-6 release was independent of SIRT1 activation using collaborator data, Prof. Lynne Cox, University of Oxford.

6.8. Lead compound:

The overall conclusion and goal of this project was to discover the lead molecules with minimal detrimental activities that were associated with resveratrol. Our study, using a step by step biological screen discovered three lead resveralogues V24, V31 and V34. All of these are less toxic (MTT and LDH assay), have less effect on proliferation and senescence whilist retaining SIRT1 activity, see **Figure 6-5**. This demonstrates that the nitrogen resveralogues approach is an excellent foundation for drug discovery.

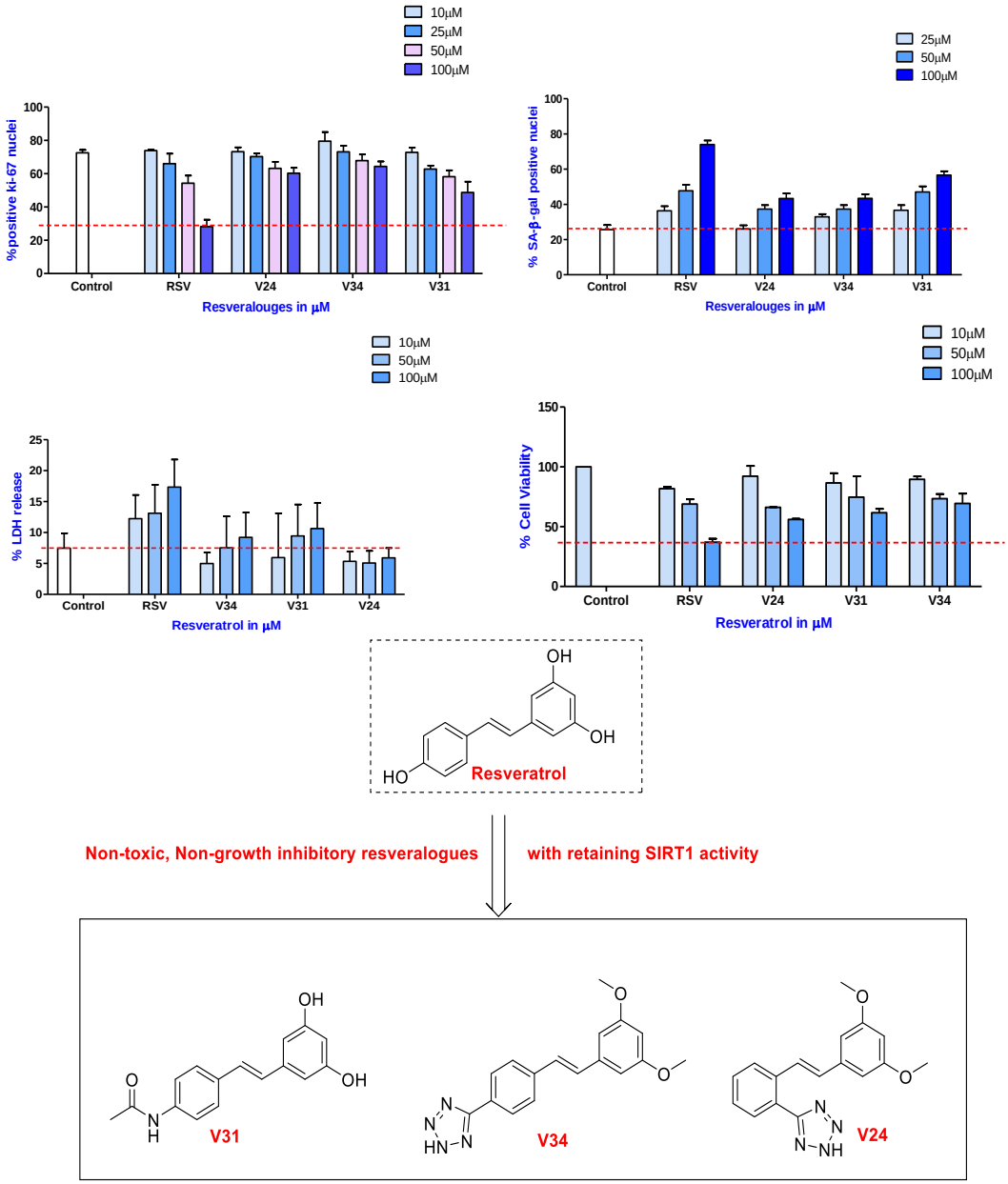

Figure 6-5 Development of non-toxic, non- growth inhibitory resveralogues with SIRT1 activity.

Chapter 7. Conclusion:

i) **Aim**: To develope an improved synthetic route for resveratrol derivatives.

Conclusion: This study developed a simplified one pot synthesis for resveralogues using Arbuzov and Horner-Wadsworth-Emmons reaction. This simplified synthesis allows us to synthesise resveralogues on a large scale. This one-pot protocol is very efficient and stereo-selective for the synthesis of a wide range of resveralogues. The utility and applicability of this method is enhanced by its simple work up procedure, rendering it also suitable for use in automated synthesis.

ii) **Aim**: Design and synthesise a range of novel resveralogues.

Conclusion: This study involved synthesis of more than 40 compounds, of which 20 are completely novel and a further 12 were previously totally uncharacterised with regard to their biological effects. The synthesised resveralogues involved

a) 4′-substituted methoxy analogues of resveratrol,

b) amido resveralogues (bio-isosteric replacement of hydroxyl) and

c) tetrazole based resveralogues.

All of the synthesised molecules were fully characterised using IR, ^{1}H and $^{13}CNMR$ and HRMS spectroscopy.

iii) **Aim**: Development of multidimensional predictive model of the key structural features of reveralogues.

Conclusion: This project investigated the effect of small structural modifications in resveratrol on its cytotoxicity, effect on proliferation fraction, senescence, SIRT1 activation and expression of SASP component IL-6.

a) Cell based toxicity assays showed that LDH was a good method to evaluate the cytotoxic effect of these molecules. Additionally, resveralogues were able to induce dysfunction in mitochondria giving unusual MTT assay results. Overall toxicity screening implied that most of these molecules were not cytotoxic to normal human lung fibroblast cells (MRC-5) and there was no correlation between small structural changes and toxicity.

b) Cell cytostasis studies revealed that the removal of the *trans*-stilbene bond prevented induction of senescence in MRC5 cells. Equally, this effect was abrogated in the case of dihydro resveralogues as well as compounds that contained bulky groups, including a loss of planarity.

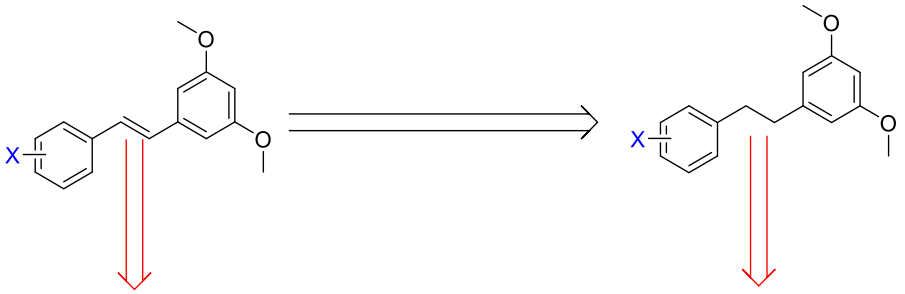

No senescence

c) SIRT1 activation studies showed that there was no significant increase in SIRT1 activation found in the case of synthesised substituted resveralogues, amino resveralogues and non-planar resveralogues when compared to resveratrol. However, this is the first time it has been shown that SIRT1 activation is independent of the *trans*-stilbene double bond and dihydro derivative of resveralogues were found to retain the SIRT1 activity.

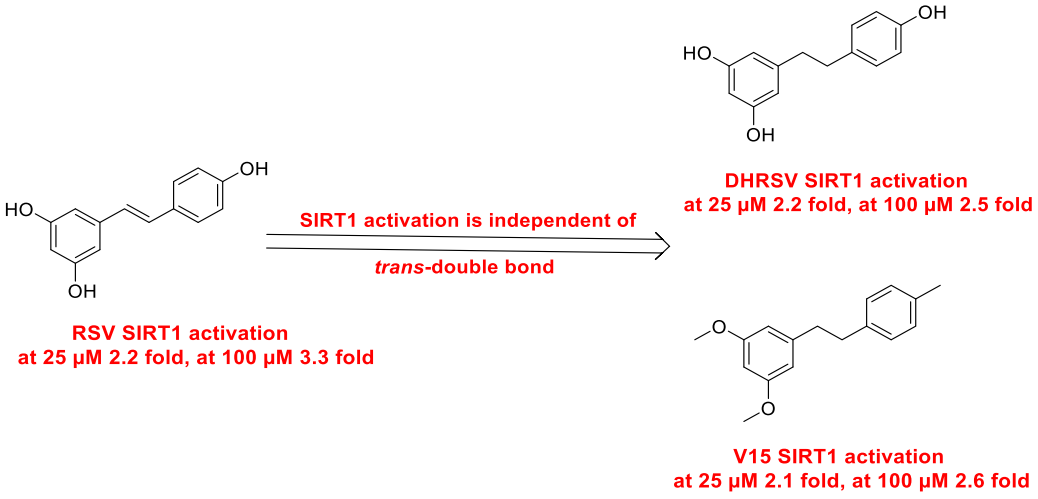

d) There was no correlation between SIRT1 activation, cytotoxicity and senescence growth of MRC-5 cells. However, SIRT1 activation and proliferation (ki-67 as proliferation marker) were found to be positively correlated (r^2=0.6378).

e) Additionally, SIRT1 activation and release of IL-6 exhibited no significant correlation and hence, it appears that inhibition of IL-6 is independent of SIRT1 activation.

iv) The overall goal of this project was to discover lead molecules with minimal detrimental activities and maximum positive ones associated with resveratrol. My work, using step by step biology screens discovered three lead resveralogues V24, V31 and V34. All of them were found to be less toxic (MTT and LDH assay), have less negative effects on proliferation and senescence whilst retaining SIRT1 activity.

The overall effect of modifications in resveratrol structure and its effect on toxicity (using LDH assay), growth fraction ki-67, senescence, SIRT1 activation and IL-6 release (using collaborator data) are summarised in **Figure 7-1**.

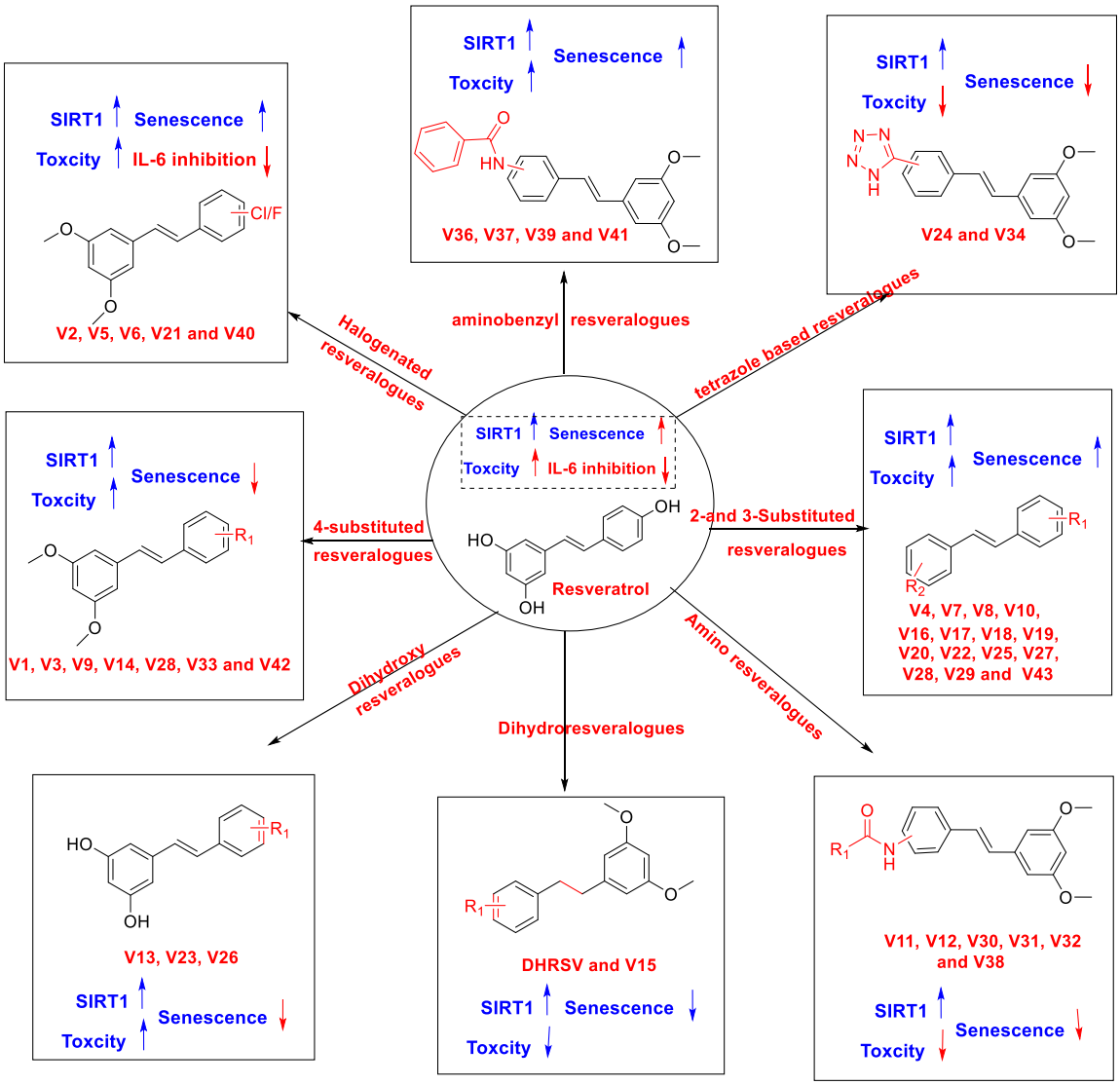

Figure 7-1 : Overall effect of structural modification in resveratrol on its bio-activitites such as toxicity (using LDH assay), senescence, SIRT1 activation and IL-6 inhibition (using collaborators data provided by Prof. Cox and co-worker).

Chapter 8. Future Work:

8.1. Application of One-pot Synthesis of Resveratrol metabolites:

The developed one-pot synthesis of *trans*-stilbene could be utilised to synthesise the resveratrol metabolites synthesis. The current literature lacks simple as well as practical synthesis of resveratrol 4′-sulphate and resveratrol 4′-glucuronide metabolites. The future strategy for synthesis of resveratrol metabolites is shown following **Scheme no 8-1**. This synthesis will help to provide ready access to resveratrol metabolites.

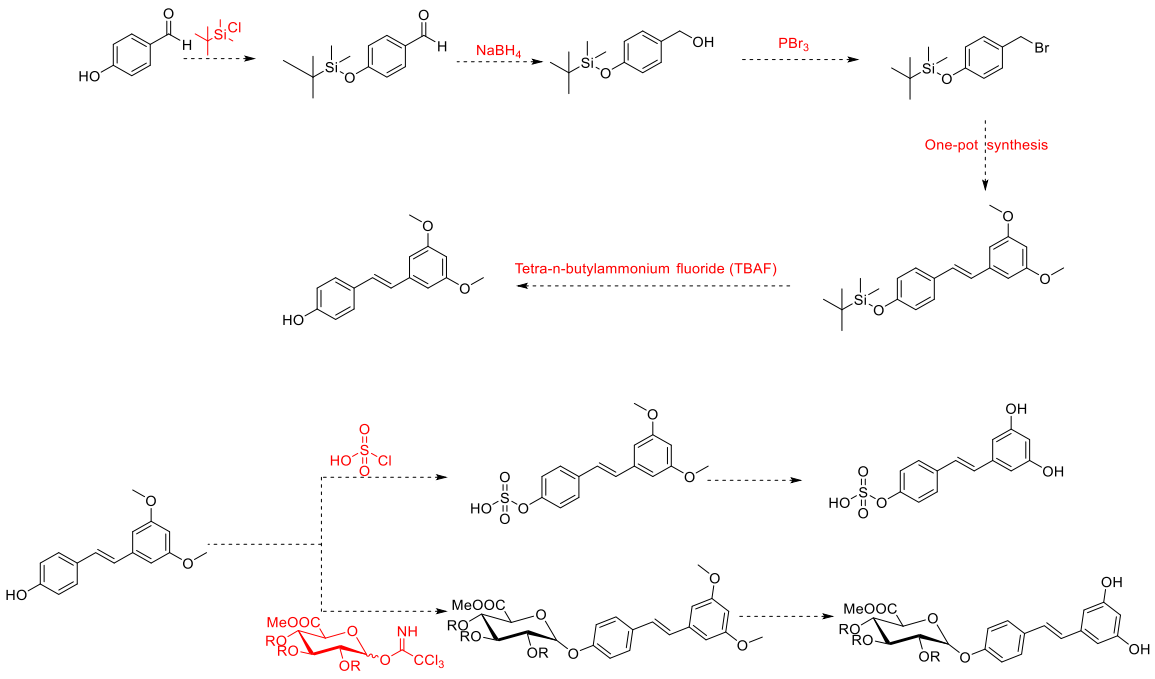

Scheme 8-1 Resveratrol metabolied synthesis strategies using one-pot synthesis.

8.2. Development of new Senolytes:

Senolytes are the new therapeutics targeting to kill senescent cells which in turn will help to reduce the age-related mortality and morbidity. This will then help to extending the health of model organisms and eventually humans. Resveratrol is considered as a potential anti-ageing molecule and hence the synthesised novel resveralogues based on resveratrol should be tested for their effects on old senescent cells. Along with the help of modern structure-based drug discovery techniques the strategy could potentially lead to develop novel senolytes to test in *in-vitro* models of senescent cells and then in longevity experiments in model organisms. The future screening strategies are in **Figure 8-1**;

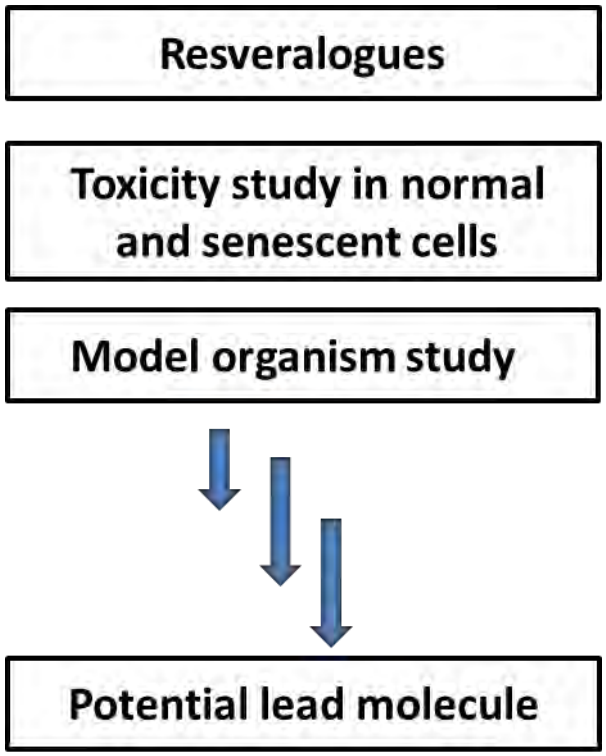

Figure 8-1 Development of resveratrol based senolytes.

Publication and patent:

"A facile, stereoselective, one-pot synthesis of resveratrol derivatives."

Vishal birar, Angela N Sheerin, Jana Milkovicova, Richard G A Faragher, Elizabeth L Ostler; ***Chemistry Central Journal. 2015; 9: 26.***

"Novel, non-toxic resveralogues and their effect on inhibiting senescence associated secretory phenotypes."

Vishal birar, Elizabeth Ostler.

Patent filling is in under progress.

Chapter 9. References:

1. Crews DE: **Artificial environments and an aging population: designing for age-related functional losses.** *Journal of physiological anthropology and applied human science* 2005, **24:**103-109.
2. Cutler RG, Mattson MP: **Introduction: The adversities of aging.** *Ageing Research Reviews* 2006, **5:**221-238.
3. Holliday R: **Understanding ageing.** *Philosophical Transactions of the Royal Society B: Biological Sciences* 1997, **352:**1793-1797.
4. Holliday R: **Understanding ageing.** *Philosophical Transactions of the Royal Society of London B: Biological Sciences* 1997, **352:**1793-1797.
5. Gavrilov LA, Gavrilova NS: **Evolutionary Theories of Aging and Longevity.** *TheScientificWorldJOURNAL* 2002, **2**.
6. Medawar PB: **An Unsolved Problem of Biology.** *HK Lewis & Co, London* 1952.
7. AES JPDM: *An Introduction to Gerontology.* Cambridge University press; March 2011.
8. Williams GC: **Pleiotropy, Natural Selection, and the Evolution of Senescence.** *Evolution* 1957, **11:**398-411.
9. López-Otín C, Blasco MA, Partridge L, Serrano M, Kroemer G: **The Hallmarks of Aging.** *Cell*, **153:**1194-1217.
10. Hayflick L: **The limited in vitro lifetime of human diploid cell strains.** *Experimental Cell Research* 1965, **37:**614-636.
11. Rodier F, Campisi J: **Four faces of cellular senescence.** *The Journal of cell biology* 2011, **192:**547-556.
12. d'Adda di Fagagna F, Reaper PM, Clay-Farrace L, Fiegler H, Carr P, Von Zglinicki T, Saretzki G, Carter NP, Jackson SP: **A DNA damage checkpoint response in telomere-initiated senescence.** *Nature* 2003, **426:**194-198.
13. Takai H, Smogorzewska A, de Lange T: **DNA Damage Foci at Dysfunctional Telomeres.** *Current Biology* 2003, **13:**1549-1556.
14. Ogryzko VV, Hirai TH, Russanova VR, Barbie DA, Howard BH: **Human fibroblast commitment to a senescence-like state in response to histone deacetylase inhibitors is cell cycle dependent.** *Molecular and cellular biology* 1996, **16:**5210-5218.
15. Lin AW, Barradas M, Stone JC, van Aelst L, Serrano M, Lowe SW: **Premature senescence involving p53 and p16 is activated in response to constitutive MEK/MAPK mitogenic signaling.** *Genes & development* 1998, **12:**3008-3019.
16. Parrinello S, Samper E, Krtolica A, Goldstein J, Melov S, Campisi J: **Oxygen sensitivity severely limits the replicative lifespan of murine fibroblasts.** *Nature cell biology* 2003, **5:**741-747.
17. McConnell BB, Starborg M, Brookes S, Peters G: **Inhibitors of cyclin-dependent kinases induce features of replicative senescence in early passage human diploid fibroblasts.** *Current biology : CB* 1998, **8:**351-354.
18. Goldstein S: **Replicative senescence: the human fibroblast comes of age.** *Science* 1990, **249:**1129-1133.

19. Dimri GP, Lee X, Basile G, Acosta M, Scott G, Roskelley C, Medrano EE, Linskens M, Rubelj I, Pereira-Smith O, et al.: **A biomarker that identifies senescent human cells in culture and in aging skin in vivo.** *Proceedings of the National Academy of Sciences of the United States of America* 1995, **92:**9363-9367.

20. Robbins E, Levine EM, Eagle H: **Morphologic changes accompanying senescence of cultured human diploid cells.** *The Journal of experimental medicine* 1970, **131:**1211-1222.

21. Brunk U, Ericsson JL, Ponten J, Westermark B: **Residual bodies and "aging" in cultured human glia cells. Effect of entrance into phase 3 and prolonged periods of confluence.** *Experimental eye research* 1973, **79:**1-14.

22. Rayess H, Wang MB, Srivatsan ES: **Cellular senescence and tumor suppressor gene p16.** *International Journal of Cancer* 2012, **130:**1715-1725.

23. Brenner AJ, Stampfer MR, Aldaz CM: **Increased p16 expression with first senescence arrest in human mammary epithelial cells and extended growth capacity with p16 inactivation.** *Oncogene* 1998, **17:**199-205.

24. Ramirez RD, Morales CP, Herbert BS, Rohde JM, Passons C, Shay JW, Wright WE: **Putative telomere-independent mechanisms of replicative aging reflect inadequate growth conditions.** *Genes & development* 2001, **15:**398-403.

25. Robles SJ, Adami GR: **Agents that cause DNA double strand breaks lead to p16INK4a enrichment and the premature senescence of normal fibroblasts.** *Oncogene* 1998, **16:**1113-1123.

26. Tchkonia T, Zhu Y, van Deursen J, Campisi J, Kirkland JL: **Cellular senescence and the senescent secretory phenotype: therapeutic opportunities.** *The Journal of clinical investigation* 2013, **123:**966-972.

27. Rodier F, Coppe JP, Patil CK, Hoeijmakers WA, Munoz DP, Raza SR, Freund A, Campeau E, Davalos AR, Campisi J: **Persistent DNA damage signalling triggers senescence-associated inflammatory cytokine secretion.** *Nature cell biology* 2009, **11:**973-979.

28. Baker DJ, Wijshake T, Tchkonia T, LeBrasseur NK, Childs BG, van de Sluis B, Kirkland JL, van Deursen JM: **Clearance of p16Ink4a-positive senescent cells delays ageing-associated disorders.** *Nature* 2011, **479:**232-236.

29. Campisi J: **Aging, Cellular Senescence, and Cancer.** *Annual Review of Physiology* 2013, **75:**685-705.

30. Parrinello S, Coppe J-P, Krtolica A, Campisi J: **Stromal-epithelial interactions in aging and cancer: senescent fibroblasts alter epithelial cell differentiation.** *Journal of Cell Science* 2005, **118:**485-496.

31. Tsai KKC, Chuang EY-Y, Little JB, Yuan Z-M: **Cellular Mechanisms for Low-Dose Ionizing Radiation–Induced Perturbation of the Breast Tissue Microenvironment.** *Cancer Research* 2005, **65:**6734-6744.

32. Bitto A, Sell C, Crowe E, Lorenzini A, Malaguti M, Hrelia S, Torres C: **Stress-induced senescence in human and rodent astrocytes.** *Experimental Cell Research* 2010, **316:**2961-2968.

33. Baker DJ, Wijshake T, Tchkonia T, LeBrasseur NK, Childs BG, van de Sluis B, Kirkland JL, van Deursen JM: **Clearance of p16Ink4a-positive senescent cells delays ageing-associated disorders.** *Nature* 2011, **479:**232-236.

34. Pan M-H, Lai C-S, Tsai M-L, Wu J-C, Ho C-T: **Molecular mechanisms for anti-aging by natural dietary compounds.** *Molecular Nutrition & Food Research* 2012, **56:**88-115.

35. BARSYTE D, LOVEJOY DA, LITHGOW GJ: **Longevity and heavy metal resistance in daf-2 and age-1 long-lived mutants of Caenorhabditis elegans.** *The FASEB Journal* 2001, **15:**627-634.

36. Masoro EJ: **Dietary restriction: current status.** *Aging* 2001, **13:**261-262.

37. Wang C, Maddick M, Miwa S, Jurk D, Czapiewski R, Saretzki G, Langie SA, Godschalk RW, Cameron K, von Zglinicki T: **Adult-onset, short-term dietary restriction reduces cell senescence in mice.** *Aging (Albany NY)* 2010, **2:**555-566.

38. Lamming DW, Ye L, Sabatini DM, Baur JA: **Rapalogs and mTOR inhibitors as anti-aging therapeutics.** *The Journal of clinical investigation* 2013, **123:**980-989.

39. Abraham RT, Wiederrecht GJ: **IMMUNOPHARMACOLOGY OF RAPAMYCIN1.** *Annual Review of Immunology* 1996, **14:**483-510.

40. Betz C, Hall MN: **Where is mTOR and what is it doing there?** *The Journal of cell biology* 2013, **203:**563-574.

41. Laplante M, Sabatini David M: **mTOR Signaling in Growth Control and Disease.** *Cell* 2012, **149:**274-293.

42. Vellai T, Takacs-Vellai K, Zhang Y, Kovacs AL, Orosz L, Muller F: **Genetics: Influence of TOR kinase on lifespan in C. elegans.** *Nature* 2003, **426:**620-620.

43. Kapahi P, Zid BM, Harper T, Koslover D, Sapin V, Benzer S: **Regulation of lifespan in Drosophila by modulation of genes in the TOR signaling pathway.** *Current biology : CB* 2004, **14:**885-890.

44. Kaeberlein M, Powers RW, Steffen KK, Westman EA, Hu D, Dang N, Kerr EO, Kirkland KT, Fields S, Kennedy BK: **Regulation of Yeast Replicative Life Span by TOR and Sch9 in Response to Nutrients.** *Science* 2005, **310:**1193-1196.

45. Harrison DE, Strong R, Sharp ZD, Nelson JF, Astle CM, Flurkey K, Nadon NL, Wilkinson JE, Frenkel K, Carter CS, et al: **Rapamycin fed late in life extends lifespan in genetically heterogeneous mice.** *Nature* 2009, **460:**392-395.

46. Selman C, Tullet JM, Wieser D, Irvine E, Lingard SJ, Choudhury AI, Claret M, Al-Qassab H, Carmignac D, Ramadani F, et al: **Ribosomal protein S6 kinase 1 signaling regulates mammalian life span.** *Science* 2009, **326:**140-144.

47. Lamming DW, Ye L, Katajisto P, Goncalves MD, Saitoh M, Stevens DM, Davis JG, Salmon AB, Richardson A, Ahima RS, et al: **Rapamycin-induced insulin resistance is mediated by mTORC2 loss and uncoupled from longevity.** *Science* 2012, **335:**1638-1643.

48. Hardie DG: **AMP-activated/SNF1 protein kinases: conserved guardians of cellular energy.** *Nature reviews Molecular cell biology* 2007, **8:**774-785.

49. Salminen A, Kaarniranta K: **AMP-activated protein kinase (AMPK) controls the aging process via an integrated signaling network.** *Ageing Res Rev* 2012, **11:**230-241.

50. Richter EA, Ruderman NB: **AMPK and the biochemistry of exercise: implications for human health and disease.** *The Biochemical journal* 2009, **418:**261-275.

51. Reznick RM, Zong H, Li J, Morino K, Moore IK, Yu HJ, Liu ZX, Dong J, Mustard KJ, Hawley SA, et al: **Aging-associated reductions in AMP-activated protein kinase activity and mitochondrial biogenesis.** *Cell metabolism* 2007, **5:**151-156.

52. Apfeld J, O'Connor G, McDonagh T, DiStefano PS, Curtis R: **The AMP-activated protein kinase AAK-2 links energy levels and insulin-like signals to lifespan in C. elegans.** *Genes & development* 2004, **18:**3004-3009.

53. Funakoshi M, Tsuda M, Muramatsu K, Hatsuda H, Morishita S, Aigaki T: **A gain-of-function screen identifies wdb and lkb1 as lifespan-extending genes in Drosophila.** *Biochemical and biophysical research communications* 2011, **405:**667-672.

54. Mihaylova MM, Shaw RJ: **The AMPK signalling pathway coordinates cell growth, autophagy and metabolism.** *Nature cell biology* 2011, **13:**1016-1023.

55. Camarda AJ, Butler WT, Finkelman RD, Nanci A: **Immunocytochemical localization of gamma-carboxyglutamic acid-containing proteins (osteocalcin) in rat bone and dentin.** *Calcified tissue international* 1987, **40:**349-355.

56. Li XN, Song J, Zhang L, LeMaire SA, Hou X, Zhang C, Coselli JS, Chen L, Wang XL, Zhang Y, Shen YH: **Activation of the AMPK-FOXO3 pathway reduces fatty acid-induced increase in intracellular reactive oxygen species by upregulating thioredoxin.** *Diabetes* 2009, **58:**2246-2257.

57. Salminen A, Hyttinen JM, Kaarniranta K: **AMP-activated protein kinase inhibits NF-kappaB signaling and inflammation: impact on healthspan and lifespan.** *Journal of molecular medicine* 2011, **89:**667-676.

58. Akbar DH: **Effect of metformin and sulfonylurea on C-reactive protein level in well-controlled type 2 diabetics with metabolic syndrome.** *Endocrine* 2003, **20:**215-218.

59. Howitz KT, Bitterman KJ, Cohen HY, Lamming DW, Lavu S, Wood JG, Zipkin RE, Chung P, Kisielewski A, Zhang LL, et al: **Small molecule activators of sirtuins extend Saccharomyces cerevisiae lifespan.** *Nature* 2003, **425:**191-196.

60. Tissenbaum HA, Guarente L: **Increased dosage of a sir-2 gene extends lifespan in Caenorhabditis elegans.** *Nature* 2001, **410:**227-230.

61. Satoh A, Brace Cynthia S, Rensing N, Cliften P, Wozniak David F, Herzog Erik D, Yamada Kelvin A, Imai S-i: **Sirt1 Extends Life Span and Delays Aging in Mice through the Regulation of Nk2 Homeobox 1 in the DMH and LH.** *Cell metabolism* 2013, **18:**416-430.

62. Partridge L, Mangel M: **Messages from mortality: the evolution of death rates in the old.** *Trends in Ecology & Evolution* 1999, **14:**438-442.

63. Faragher RG: **Should we treat aging as a disease? The consequences and dangers of miscategorisation.** *Front Genet* 2015, **6:**171.

64. Brody JA, Schneider EL: **Diseases and disorders of aging: an hypothesis.** *Journal of chronic diseases* 1986, **39:**871-876.

65. Burton DG: **Cellular senescence, ageing and disease.** *Age (Dordr)* 2009, **31:**1-9.

66. Le Maitre CL, Freemont AJ, Hoyland JA: **Accelerated cellular senescence in degenerate intervertebral discs: a possible role in the pathogenesis of intervertebral disc degeneration.** *Arthritis Res Ther* 2007, **9:**R45.

67. Rattan SIS: *Anti-ageing strategies: prevention or therapy?*; 2005.

68. Gems D: **What is an anti-aging treatment?** *Experimental Gerontology* 2014, **58:**14-18.

69. Warner HR, Ingram D, Miller RA, Nadon NL, Richardson AG: **Program for testing biological interventions to promote healthy aging.** *Mechanisms of Ageing and Development* 2000, **115:**199-207.

70. Michishita E, Park JY, Burneskis JM, Barrett JC, Horikawa I: **Evolutionarily conserved and nonconserved cellular localizations and functions of human SIRT proteins.** *Molecular biology of the cell* 2005, **16:**4623-4635.

71. Imai S, Armstrong CM, Kaeberlein M, Guarente L: **Transcriptional silencing and longevity protein Sir2 is an NAD-dependent histone deacetylase.** *Nature* 2000, **403:**795-800.

72. Sauve AA, Wolberger C, Schramm VL, Boeke JD: **The biochemistry of sirtuins.** *Annual review of biochemistry* 2006, **75:**435-465.

73. Guo X, Kesimer M, Tolun G, Zheng X, Xu Q, Lu J, Sheehan JK, Griffith JD, Li X: **The NAD+-dependent protein deacetylase activity of SIRT1 is regulated by its oligomeric status.** *Scientific Reports* 2012, **2:**640.

74. Howitz KT, Bitterman KJ, Cohen HY, Lamming DW, Lavu S, Wood JG, Zipkin RE, Chung P, Kisielewski A, Zhang L-L, et al: **Small molecule activators of sirtuins extend Saccharomyces cerevisiae lifespan.** *Nature* 2003, **425:**191-196.

75. Milne JC, Lambert PD, Schenk S, Carney DP, Smith JJ, Gagne DJ, Jin L, Boss O, Perni RB, Vu CB, et al: **Small molecule activators of SIRT1 as therapeutics for the treatment of type 2 diabetes.** *Nature* 2007, **450:**712-716.

76. Knutson MD, Leeuwenburgh C: **Resveratrol and novel potent activators of SIRT1: effects on aging and age-related diseases.** *Nutrition Reviews* 2008, **66:**591-596.

77. Vu CB, Bemis JE, Disch JS, Ng PY, Nunes JJ, Milne JC, Carney DP, Lynch AV, Smith JJ, Lavu S, et al: **Discovery of imidazo[1,2-b]thiazole derivatives as novel SIRT1 activators.** *Journal of medicinal chemistry* 2009, **52:**1275-1283.

78. Bemis JE, Vu CB, Xie R, Nunes JJ, Ng PY, Disch JS, Milne JC, Carney DP, Lynch AV, Jin L, et al: **Discovery of oxazolo[4,5-b]pyridines and related heterocyclic analogs as novel SIRT1 activators.** *Bioorganic & medicinal chemistry letters* 2009, **19:**2350-2353.

79. Hubbard BP, Sinclair DA: **Small molecule SIRT1 activators for the treatment of aging and age-related diseases.** *Trends in Pharmacological Sciences* 2014, **35:**146-154.

80. Borra MT, Smith BC, Denu JM: **Mechanism of human SIRT1 activation by resveratrol.** *The Journal of biological chemistry* 2005, **280:**17187-17195.

81. Pacholec M, Bleasdale JE, Chrunyk B, Cunningham D, Flynn D, Garofalo RS, Griffith D, Griffor M, Loulakis P, Pabst B, et al: **SRT1720, SRT2183, SRT1460, and Resveratrol Are Not Direct Activators of SIRT1.** *Journal of Biological Chemistry* 2010, **285:**8340-8351.

82. Mostoslavsky SKaR: **SIRT1 Activators: The Evidence STACks up.** *Imapact ageing* 2013, **5:**142-143.

83. Lakshminarasimhan M, Rauh D, Schutkowski M, Steegborn C: **Sirt1 activation by resveratrol is substrate sequence-selective.** *Aging (Albany NY)* 2013, **5:**151-154.

84. Hubbard BP, Gomes AP, Dai H, Li J, Case AW, Considine T, Riera TV, Lee JE, E SY, Lamming DW, et al: **Evidence for a Common Mechanism of SIRT1 Regulation by Allosteric Activators.** *Science* 2013, **339:**1216-1219.

85. Lin SJ, Defossez PA, Guarente L: **Requirement of NAD and SIR2 for life-span extension by calorie restriction in Saccharomyces cerevisiae.** *Science* 2000, **289:**2126-2128.

86. Haigis MC, Guarente LP: **Mammalian sirtuins—emerging roles in physiology, aging, and calorie restriction.** *Genes & development* 2006, **20:**2913-2921.

87. Baur JA, Sinclair DA: **Therapeutic potential of resveratrol: the in vivo evidence.** *Nature reviews Drug discovery* 2006, **5:**493-506.

88. Viswanathan M, Guarente L: **Regulation of Caenorhabditis elegans lifespan by sir-2.1 transgenes.** *Nature* 2011, **477:**E1-E2.

89. Rodgers JT, Lerin C, Haas W, Gygi SP, Spiegelman BM, Puigserver P: **Nutrient control of glucose homeostasis through a complex of PGC-1alpha and SIRT1.** *Nature* 2005, **434:**113-118.

90. Lagouge M, Argmann C, Gerhart-Hines Z, Meziane H, Lerin C, Daussin F, Messadeq N, Milne J, Lambert P, Elliott P, et al: **Resveratrol improves mitochondrial function and protects against metabolic disease by activating SIRT1 and PGC-1alpha.** *Cell* 2006, **127:**1109-1122.

91. Baur JA, Pearson KJ, Price NL, Jamieson HA, Lerin C, Kalra A, Prabhu VV, Allard JS, Lopez-Lluch G, Lewis K, et al: **Resveratrol improves health and survival of mice on a high-calorie diet.** *Nature* 2006, **444:**337-342.

92. Pearson KJ, Baur JA, Lewis KN, Peshkin L, Price NL, Labinskyy N, Swindell WR, Kamara D, Minor RK, Perez E, et al: **Resveratrol Delays Age-Related Deterioration and Mimics Transcriptional Aspects of Dietary Restriction without Extending Life Span.** *Cell metabolism* 2008, **8:**157-168.

93. Price Nathan L, Gomes Ana P, Ling Alvin JY, Duarte Filipe V, Martin-Montalvo A, North Brian J, Agarwal B, Ye L, Ramadori G, Teodoro Joao S, et al: **SIRT1 Is Required for AMPK Activation and the Beneficial Effects of Resveratrol on Mitochondrial Function.** *Cell metabolism* 2012, **15:**675-690.

94. Pearson KJ, Baur JA, Lewis KN, Peshkin L, Price NL, Labinskyy N, Swindell WR, Kamara D, Minor RK, Perez E, et al: **Resveratrol delays age-related deterioration and mimics transcriptional aspects of dietary restriction without extending life span.** *Cell metabolism* 2008, **8:**157-168.

95. Mitchell Sarah J, Martin-Montalvo A, Mercken Evi M, Palacios Hector H, Ward Theresa M, Abulwerdi G, Minor Robin K, Vlasuk George P, Ellis James L, Sinclair David A, et al: **The SIRT1 Activator SRT1720 Extends Lifespan and Improves Health of Mice Fed a Standard Diet.** *Cell Reports*, **6:**836-843.

96. Stein S, Matter CM: **Protective roles of SIRT1 in atherosclerosis.** *Cell cycle* 2011, **10:**640-647.

97. Linsel-Nitschke P, Tall AR: **HDL as a target in the treatment of atherosclerotic cardiovascular disease.** *Nature reviews Drug discovery* 2005, **4:**193-205.

98. Guarente L: **Sirtuins in aging and disease.** *Cold Spring Harbor symposia on quantitative biology* 2007, **72:**483-488.

99. Kim D, Nguyen MD, Dobbin MM, Fischer A, Sananbenesi F, Rodgers JT, Delalle I, Baur JA, Sui G, Armour SM, et al: **SIRT1 deacetylase protects against neurodegeneration in models for Alzheimer's disease and amyotrophic lateral sclerosis.** *The EMBO journal* 2007, **26:**3169-3179.

100. Parker JA, Arango M, Abderrahmane S, Lambert E, Tourette C, Catoire H, Neri C: **Resveratrol rescues mutant polyglutamine cytotoxicity in nematode and mammalian neurons.** *Nature genetics* 2005, **37:**349-350.

101. Hardy J, Selkoe DJ: **The amyloid hypothesis of Alzheimer's disease: progress and problems on the road to therapeutics.** *Science* 2002, **297:**353-356.

102. Donmez G, Wang D, Cohen DE, Guarente L: **SIRT1 suppresses beta-amyloid production by activating the alpha-secretase gene ADAM10.** *Cell* 2010, **142:**320-332.

103. Jiang M, Wang J, Fu J, Du L, Jeong H, West T, Xiang L, Peng Q, Hou Z, Cai H, et al: **Neuroprotective role of Sirt1 in mammalian models of Huntington's disease through activation of multiple Sirt1 targets.** *Nature medicine* 2012, **18:**153-158.

104. Jeong H, Cohen DE, Cui L, Supinski A, Savas JN, Mazzulli JR, Yates JR, 3rd, Bordone L, Guarente L, Krainc D: **Sirt1 mediates neuroprotection from mutant huntingtin by activation of the TORC1 and CREB transcriptional pathway.** *Nature medicine* 2012, **18:**159-165.

105. Donmez G, Arun A, Chung CY, McLean PJ, Lindquist S, Guarente L: **SIRT1 protects against alpha-synuclein aggregation by activating molecular chaperones.** *The Journal of neuroscience : the official journal of the Society for Neuroscience* 2012, **32:**124-132.

106. Lavu S, Boss O, Elliott PJ, Lambert PD: **Sirtuins--novel therapeutic targets to treat age-associated diseases.** *Nature reviews Drug discovery* 2008, **7:**841-853.

107. Zhang C, Cuervo AM: **Restoration of chaperone-mediated autophagy in aging liver improves cellular maintenance and hepatic function.** *Nature medicine* 2008, **14:**959-965.

108. MJ T: **Of the phenolic substances of white hellebore (Veratrum grandiflorum Loes. fil.).** *J Faculty Sci Hokkaido Imperial University* 1940, **3:**1-16.

109. Nonomura S, Kanagawa H, Makimoto A: **[Chemical Constituents of Polygonaceous Plants. I. Studies on the Components of Ko-J O-Kon. (Polygonum Cuspidatum Sieb. Et Zucc.)].** *Yakugaku zasshi : Journal of the Pharmaceutical Society of Japan* 1963, **83:**988-990.

110. Renaud S, de Lorgeril M: **Wine, alcohol, platelets, and the French paradox for coronary heart disease.** *Lancet* 1992, **339:**1523-1526.

111. Jang M, Cai L, Udeani GO, Slowing KV, Thomas CF, Beecher CW, Fong HH, Farnsworth NR, Kinghorn AD, Mehta RG, et al: **Cancer chemopreventive activity of resveratrol, a natural product derived from grapes.** *Science* 1997, **275:**218-220.

112. Bhullar KS, Hubbard BP: **Lifespan and healthspan extension by resveratrol.** *Biochimica et Biophysica Acta (BBA) - Molecular Basis of Disease* 2015, **1852:**1209-1218.

113. Timmers S, Auwerx J, Schrauwen P: **The journey of resveratrol from yeast to human.** *Aging (Albany NY)* 2012, **4:**146-158.

114. Bass TM, Weinkove D, Houthoofd K, Gems D, Partridge L: **Effects of resveratrol on lifespan in Drosophila melanogaster and Caenorhabditis elegans.** *Mechanisms of Ageing and Development* 2007, **128:**546-552.

115. Khanduja KL, Bhardwaj A, Kaushik G: **Resveratrol inhibits N-nitrosodiethylamine-induced ornithine decarboxylase and cyclooxygenase in mice.** *Journal of nutritional science and vitaminology* 2004, **50:**61-65.

116. Li ZG, Hong T, Shimada Y, Komoto I, Kawabe A, Ding Y, Kaganoi J, Hashimoto Y, Imamura M: **Suppression of N-nitrosomethylbenzylamine (NMBA)-induced esophageal tumorigenesis in F344 rats by resveratrol.** *Carcinogenesis* 2002, **23:**1531-1536.

117. Aziz MH, Afaq F, Ahmad N: **Prevention of ultraviolet-B radiation damage by resveratrol in mouse skin is mediated via modulation in survivin.** *Photochemistry and photobiology* 2005, **81:**25-31.

118. Garvin S, Ollinger K, Dabrosin C: **Resveratrol induces apoptosis and inhibits angiogenesis in human breast cancer xenografts in vivo.** *Cancer letters* 2006, **231:**113-122.

119. Igura K, Ohta T, Kuroda Y, Kaji K: **Resveratrol and quercetin inhibit angiogenesis in vitro.** *Cancer letters* 2001, **171:**11-16.

120. Bertelli AA, Giovannini L, Giannessi D, Migliori M, Bernini W, Fregoni M, Bertelli A: **Antiplatelet activity of synthetic and natural resveratrol in red wine.** *International journal of tissue reactions* 1995, **17:**1-3.

121. Wang Z, Huang Y, Zou J, Cao K, Xu Y, Wu JM: **Effects of red wine and wine polyphenol resveratrol on platelet aggregation in vivo and in vitro.** *International journal of molecular medicine* 2002, **9:**77-79.

122. Mercken EM, Crosby SD, Lamming DW, JeBailey L, Krzysik-Walker S, Villareal D, Capri M, Franceschi C, Zhang Y, Becker K, et al: **Calorie restriction in humans inhibits the PI3K/AKT pathway and induces a younger transcription profile.** *Aging Cell* 2013**:**n/a-n/a.

123. Jiang H, Shang X, Wu H, Gautam SC, Al-Holou S, Li C, Kuo J, Zhang L, Chopp M: **Resveratrol downregulates PI3K/Akt/mTOR signaling pathways in human U251 glioma cells.** *Journal of experimental therapeutics & oncology* 2009, **8:**25-33.

124. Brito PM, Devillard R, Negre-Salvayre A, Almeida LM, Dinis TC, Salvayre R, Auge N: **Resveratrol inhibits the mTOR mitogenic signaling evoked by oxidized LDL in smooth muscle cells.** *Atherosclerosis* 2009, **205:**126-134.

125. Afaq F, Adhami VM, Ahmad N: **Prevention of short-term ultraviolet B radiation-mediated damages by resveratrol in SKH-1 hairless mice.** *Toxicology and applied pharmacology* 2003, **186:**28-37.

126. Frankel EN, Waterhouse AL, Kinsella JE: **Inhibition of human LDL oxidation by resveratrol.** *Lancet* 1993, **341:**1103-1104.

127. Baur JA: **Resveratrol, sirtuins, and the promise of a DR mimetic.** *Mech Ageing Dev* 2010, **131:**261-269.

128. Jang M, Cai L, Udeani GO, Slowing KV, Thomas CF, Beecher CWW, Fong HHS, Farnsworth NR, Kinghorn AD, Mehta RG, et al: **Cancer Chemopreventive Activity of Resveratrol, a Natural Product Derived from Grapes.** *Science* 1997, **275:**218-220.

129. Carter LG, D'Orazio JA, Pearson KJ: **Resveratrol and cancer: focus on in vivo evidence.** *Endocrine-related cancer* 2014, **21:**R209-225.

130. Fulda S: **Resveratrol and derivatives for the prevention and treatment of cancer.** *Drug Discovery Today* 2010, **15:**757-765.

131. Kang SS, Cuendet M, Endringer DC, Croy VL, Pezzuto JM, Lipton MA: **Synthesis and biological evaluation of a library of resveratrol analogues as inhibitors of COX-1, COX-2 and NF-κB.** *Bioorganic & Medicinal Chemistry* 2009, **17:**1044-1054.

132. Sun B, Hoshino J, Jermihov K, Marler L, Pezzuto JM, Mesecar AD, Cushman M: **Design, synthesis, and biological evaluation of resveratrol analogues as aromatase and quinone reductase 2 inhibitors for chemoprevention of cancer.** *Bioorganic & Medicinal Chemistry* 2010, **18:**5352-5366.

133. Calamini B, Santarsiero BD, Boutin JA, Mesecar AD: **Kinetic, thermodynamic and X-ray structural insights into the interaction of melatonin and analogues with quinone reductase 2.** *The Biochemical journal* 2008, **413:**81-91.

134. Ito-Nagahata T, Kurihara C, Hasebe M, Ishii A, Yamashita K, Iwabuchi M, Sonoda M, Fukuhara K, Sawada R, Matsuoka A, Fujiwara Y: **Stilbene analogs of resveratrol improve insulin resistance through activation of AMPK.** *Bioscience, biotechnology, and biochemistry* 2013, **77:**1229-1235.

135. Kim JY, Lee JW, Kim YS, Lee Y, Ryu YB, Kim S, Ryu HW, Curtis-Long MJ, Lee KW, Lee WS, Park KH: **A Novel Competitive Class of α-Glucosidase Inhibitors: (E)-1-Phenyl-3-(4-Styrylphenyl)Urea Derivatives.** *ChemBioChem* 2010, **11:**2125-2131.

136. Hansen HC, Chiacchia FS, Patel R, Wong NC, Khlebnikov V, Jankowska R, Patel K, Reddy MM: **Stilbene analogs as inducers of apolipoprotein-I transcription.** *European journal of medicinal chemistry* 2010, **45:**2018-2023.

137. Kasiotis KM, Pratsinis H, Kletsas D, Haroutounian SA: **Resveratrol and related stilbenes: Their anti-aging and anti-angiogenic properties.** *Food and Chemical Toxicology* 2013, **61:**112-120.

138. Walle T, Hsieh F, DeLegge MH, Oatis JE, Walle UK: **HIGH ABSORPTION BUT VERY LOW BIOAVAILABILITY OF ORAL RESVERATROL IN HUMANS.** *Drug Metabolism and Disposition* 2004, **32:**1377-1382.

139. Leaver IH, Milligan B: **Fluorescent whitening agents—a survey (1974-82).** *Dyes and Pigments* 1984, **5:**109-144.

140. Flores-Rojas GG, Lijanova IV, Morales-Saavedra OG, Sanchez-Montes K, Martínez-García M: **Synthesis and NLO behavior of Oligo(phenylenevinylene)-Porphyrin Dendrimers.** *Dyes and Pigments* 2013, **96:**125-129.

141. Lijanova IV, Moggio I, Arias E, Klimova T, Martínez-García M: **Resorcinarene-dendrimers with stilbene moieties for optoelectronics.** *Tetrahedron* 2008, **64:**10258-10266.

142. Carbo N, Costelli P, Baccino FM, Lopez-Soriano FJ, Argiles JM: **Resveratrol, a natural product present in wine, decreases tumour growth in a rat tumour model.** *Biochemical and biophysical research communications* 1999, **254:**739-743.

143. Park JW, Choi YJ, Jang MA, Lee YS, Jun DY, Suh SI, Baek WK, Suh MH, Jin IN, Kwon TK: **Chemopreventive agent resveratrol, a natural product derived from grapes, reversibly inhibits progression through S and G2 phases of the cell cycle in U937 cells.** *Cancer letters* 2001, **163:**43-49.

144. Udenigwe CC, Ramprasath VR, Aluko RE, Jones PJ: **Potential of resveratrol in anticancer and anti-inflammatory therapy.** *Nutr Rev* 2008, **66:**445-454.

145. de la Lastra CA, Villegas I: **Resveratrol as an antioxidant and pro-oxidant agent: mechanisms and clinical implications.** *Biochemical Society transactions* 2007, **35:**1156-1160.

146. Wang J-X, Fu Y, Hu Y: **Carbon–Carbon Double-Bond Formation from the Reaction of Organozinc Reagents with Aldehydes Catalyzed by a Nickel(II) Complex.** *Angewandte Chemie International Edition* 2002, **41:**4170-4170.

147. Saiyed AS, Bedekar AV: **One-pot synthesis of stilbenes by dehydrohalogenation–Heck olefination and multicomponent Wittig–Heck reaction.** *Tetrahedron Letters* 2010, **51:**6227-6231.

148. Saiyed AS, Patel KN, Kamath BV, Bedekar AV: **Synthesis of stilbene analogues by one-pot oxidation-Wittig and oxidation-Wittig–Heck reaction.** *Tetrahedron Letters* 2012, **53:**4692-4696.

149. Jeffery T, Ferber Bt: **One-pot palladium-catalyzed highly chemo-, regio-, and stereoselective synthesis of trans-stilbene derivatives. A concise and convenient synthesis of resveratrol.** *Tetrahedron Letters* 2003, **44:**193-197.

150. Faragher RGA, Burton DGA, Majecha P, Fong NSY, Davis T, Sheerin A, Ostler EL: **Resveratrol, but not dihydroresveratrol, induces premature senescence in primary human fibroblasts.** *AGE* 2011, **33:**555-564.

151. Cardile V, Chillemi R, Lombardo L, Sciuto S, Spatafora C, Tringali C: **Antiproliferative activity of methylated analogues of E- and Z-resveratrol.** *Z Naturforsch C* 2007, **62:**189-195.

152. HORVATH Z, MARIHART-FAZEKAS S, SAIKO P, GRUSCH M, ÖZSÜY M, HARIK M, HANDLER N, ERKER T, JAEGER W, FRITZER-SZEKERES M, et al: **Novel Resveratrol Derivatives Induce Apoptosis and Cause Cell Cycle Arrest in Prostate Cancer Cell Lines.** *Anticancer Research* 2007, **27:**3459-3464.

153. Roberti M, Pizzirani D, Simoni D, Rondanin R, Baruchello R, Bonora C, Buscemi F, Grimaudo S, Tolomeo M: **Synthesis and Biological Evaluation of Resveratrol and Analogues as Apoptosis-Inducing Agents.** *Journal of medicinal chemistry* 2003, **46:**3546-3554.

154. Zheng L-F, Wei Q-Y, Cai Y-J, Fang J-G, Zhou B, Yang L, Liu Z-L: **DNA damage induced by resveratrol and its synthetic analogues in the presence of Cu (II) ions: Mechanism and structure-activity relationship.** *Free Radical Biology and Medicine* 2006, **41:**1807-1816.

155. Matsuoka A, Takeshita K, Furuta A, Ozaki M, Fukuhara K, Miyata N: **The 4'-hydroxy group is responsible for the in vitro cytogenetic activity of resveratrol.** *Mutation Research/Genetic Toxicology and Environmental Mutagenesis* 2002, **521:**29-35.

156. Michaelis A, Kaehne R: **Ueber das Verhalten der Jodalkyle gegen die sogen. Phosphorigsäureester oder O-Phosphine.** *Berichte der deutschen chemischen Gesellschaft* 1898, **31:**1048-1055.

157. Bhattacharya AK, Thyagarajan G: **Michaelis-Arbuzov rearrangement.** *Chemical Reviews* 1981, **81:**415-430.

158. Callahan JF, Lin G, Wan Z, Yan H: **Dual pharmacophores—PDE4-muscarinic antagonistics.** In *Book Dual pharmacophores—PDE4-muscarinic antagonistics* (Editor ed.^eds.). City: Google Patents; 2011.

159. Dubois JE, Ruasse MF: **Electrophilic bromination of aromatic conjugated olefins. II. Mechanism of the dual-path additions in stilbene bromination. Evidence from multiple substituent effects for carbonium ion intermediates.** *The Journal of Organic Chemistry* 1973, **38:**493-499.

160. Paul S, Mizuno CS, Lee HJ, Zheng X, Chajkowisk S, Rimoldi JM, Conney A, Suh N, Rimando AM: **In vitro and in vivo studies on stilbene analogs as potential treatment agents for colon cancer.** *European journal of medicinal chemistry* 2010, **45:**3702-3708.

161. Nasrollahzadeh M, Banaei A: **Hybrid Au/Pd nanoparticles as reusable catalysts for Heck coupling reactions in water under aerobic conditions.** *Tetrahedron Letters* 2015, **56:**500-503.

162. Sun B, Hoshino J, Jermihov K, Marler L, Pezzuto JM, Mesecar AD, Cushman M: **Design, synthesis, and biological evaluation of resveratrol analogues as aromatase and quinone reductase 2 inhibitors for chemoprevention of cancer.** *Bioorg Med Chem* 2010, **18:**5352-5366.

163. Söderman SC, Schwan AL: **1,2-Dibromotetrachloroethane: An Ozone-Friendly Reagent for the in Situ Ramberg–Bäcklund Rearrangement and Its Use in the Formal Synthesis of E-Resveratrol.** *The Journal of Organic Chemistry* 2012, **77:**10978-10984.

164. Kaul S, Kumar A, Sain B, Bhatnagar AK: **Simple and Convenient One-Pot Synthesis of Benzimidazoles and Benzoxazoles using N,N-Dimethylchlorosulfitemethaniminium Chloride as Condensing Agent.** *Synthetic Communications* 2007, **37:**2457-2460.

165. Mosmann T: **Rapid colorimetric assay for cellular growth and survival: Application to proliferation and cytotoxicity assays.** *Journal of Immunological Methods* 1983, **65:**55-63.

166. Sasaki T, Kawai K, Saijo-Kurita K, Ohno T: **Detergent cytotoxicity: simplified assay of cytolysis by measuring LDH activity.** *Toxicology in Vitro* 1992, **6:**451-457.

167. Repetto G, del Peso A, Zurita JL: **Neutral red uptake assay for the estimation of cell viability/cytotoxicity.** *Nat Protocols* 2008, **3:**1125-1131.

168. Fotakis G, Timbrell JA: **In vitro cytotoxicity assays: Comparison of LDH, neutral red, MTT and protein assay in hepatoma cell lines following exposure to cadmium chloride.** *Toxicology Letters* 2006, **160:**171-177.

169. Birar V, Sheerin A, Milkovicova J, Faragher R, Ostler E: **A facile, stereoselective, one-pot synthesis of resveratrol derivatives.** *Chemistry Central Journal* 2015, **9:**26.

170. Wang J-X, Fu Y, Hu Y: **Carbon–Carbon Double-Bond Formation from the Reaction of Organozinc Reagents with Aldehydes Catalyzed by a Nickel(II) Complex.** *Angewandte Chemie* 2002, **114:**2881-2884.

171. Ramadas K, Srinivasan N: **Iron-Ammonium Chloride - A Convenient and Inexpensive Reductant.** *Synthetic Communications* 1992, **22:**3189-3195.

172. Motiwala H, Kandre S, Birar V, Kadam KS, Rodge A, Jadhav RD, Mahesh Kumar Reddy M, Brahma MK, Deshmukh NJ, Dixit A, et al: **Exploration of pyridine containing heteroaryl analogs of biaryl ureas as DGAT1 inhibitors.** *Bioorganic & medicinal chemistry letters* 2011, **21:**5812-5817.

173. Sassi N, Mattarei A, Azzolini M, Szabo I, Paradisi C, Zoratti M, Biasutto L: **Cytotoxicity of mitochondria-targeted resveratrol derivatives: Interactions with respiratory chain complexes and ATP synthase.** *Biochimica et Biophysica Acta (BBA) - Bioenergetics* 2014, **1837:**1781-1789.

174. Biasutto L, Mattarei A, Marotta E, Bradaschia A, Sassi N, Garbisa S, Zoratti M, Paradisi C: **Development of mitochondria-targeted derivatives of resveratrol.** *Bioorganic & medicinal chemistry letters* 2008, **18:**5594-5597.

175. Chan FK, Moriwaki K, De Rosa MJ: **Detection of necrosis by release of lactate dehydrogenase activity.** *Methods Mol Biol* 2013, **979:**65-70.

176. Ziegler DV, Wiley CD, Velarde MC: **Mitochondrial effectors of cellular senescence: beyond the free radical theory of aging.** *Aging Cell* 2015, **14:**1-7.

Does SIRT1 or cytostasis underlie the anti-ageing activity of *trans*-stilbenes?

Vishal Chandrakumar Birar

Thesis Appendix

Appendix-A

Standardisation of Enzo-life science SIRT1 kit:

Assay reagent preparation and standard preparation:

Fluor de Lys deacetylated Standard (supplied in assay kit Enzo life sciences catalogue no BML-KI142) was used to prepare the standard curve to find out minimum and maximum range of deacetylase reaction fluorescence reading.

Preparation of standard curve for assay:

The deacetylase standard given in assay kit (10 mM stock catalogue no.BML-KI142-0030) was diluted to 100 µM solution using assay buffer provided in kit. The reaction was carried out using appropriate concentration of deacetylase standard in assay buffer with 50 µL of 0.2X diluted developer solution. The detail of reaction for standard curve experiment is shown in **Table A-1**: This was incubated for 15 minutes at 25 ºC and then fluorescence was recorded on Synergy multimode fluorescence plate reader. The outcome from above experiment was plotted fluorescence reading (y-axis) versus concentration of the Fluor de Lys deacetylase standard (x-axis) in **Figure A-1**

Table A-1 Experiment details for preparation of SIRT1 enzymatic reaction using Enzo-life sciences kit.

Required concentration of deacetylase substrate	Volume of 100 µM deacetylase substrate	Assay buffer	0.2 X developer
0 µM	0 µL	50 µL	50 µL
1 µM	0.5 µL	49.5 µL	50 µL
2 µM	1 µL	49 µL	50 µL
5 µM	2.5 µL	47.5 µL	50 µL
15 µM	5 µL	45 µL	50 µL
20 µM	10 µL	40 µL	50 µL
30 µM	20 µL	30 µL	50 µL
40 µM	30 µL	20 µL	50 µL
50 µM	40 µL	20 µL	50 µL

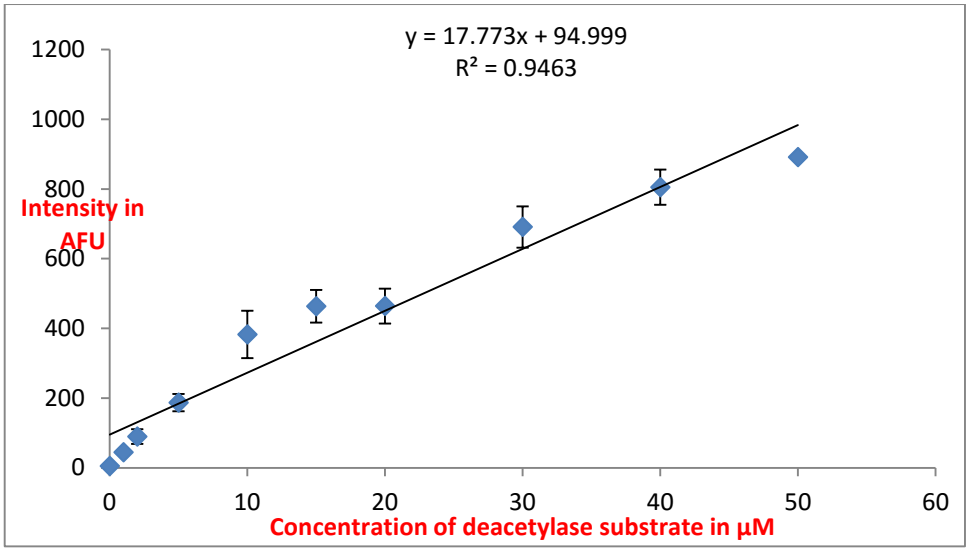

Figure A-1: Deacetylase standard curve. 50 µL of deacetylated Standard in assay buffer at the indicated concentrations, were mixed with 50 µL 0.2x Developer II and incubated 15 min., 25 °C. (Data represented from n=3 different biological replicate experiments with ± standard deviation). Fluorescence was then measured in the wells of the clear microplate with a fluorescence plate reader (Synergy multimode, Ex. 360 nm, Em. 460 nm, gain=35).

Assay protocol:

The SIRT1 enzymatic reaction was based on two step reactions; first step was deacetylation phase in which SIRT1 reaction was initiated by mixing 25 µL of a substrate solution with 25 µL containing the enzyme. Then it was incubated at room temperature for 45 minutes and then developer was added to it.

Determination of incubation time for reaction:

To investigate the incubation time for reaction initial SIRT1 reaction was carried out 25 µM substrate (prepared from 5 mM of Fluor de Lys SIRT1 deacetylase substrate) and 25 µM NAD^+ (prepared from 50 mM Sirtuin substrate, **Table A-2**). Then, diluted SIRT1 human recombinant protein (0.2 U/µL, prepared from 100 U/20µL) was added to start the reaction and it was incubated for 45 minutes. Then, 2 x developer solutions (prepared from 5X developer solution) were added to it. The results are shown in **Figure A-2**;

Table A-2 Composition of assay component for SIRT1 assay per well volume.

Time	Protein(0.2 U/µL)	83.5 µM Substrate	500 µM NAD^+	Developer
0	25 µL	15 µL	10 µL	50 µL
10	25 µL	15 µL	10 µL	50 µL
20	25 µL	15 µL	10 µL	50 µL
30	25 µL	15 µL	10 µL	50 µL
40	25 µL	15 µL	10 µL	50 µL
50	25 µL	15 µL	10 µL	50 µL
60	25 µL	15 µL	10 µL	50 µL
70	25 µL	15 µL	10 µL	50 µL
80	25 µL	15 µL	10 µL	50 µL

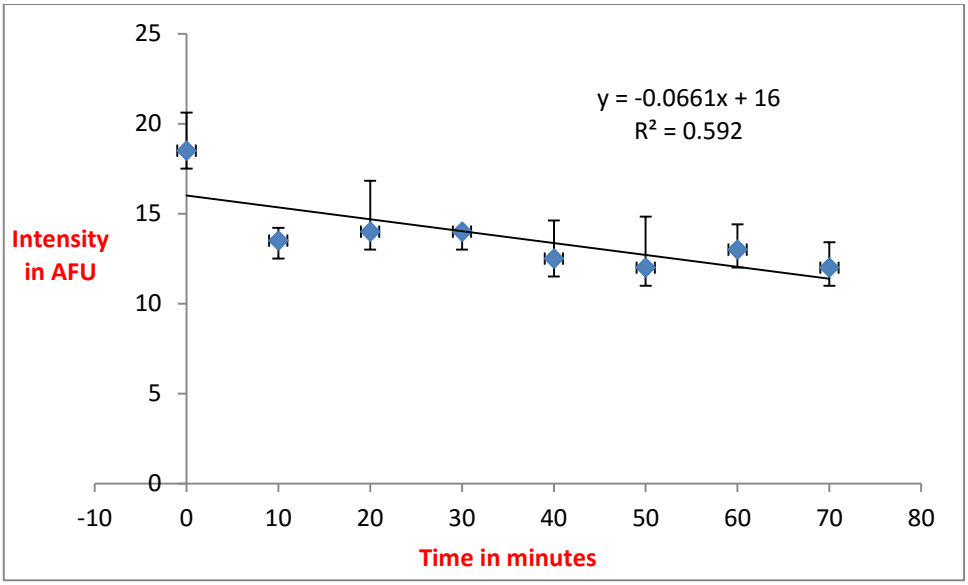

Figure A-2: Deacetylation reaction to determine incubation time for the SIRT1 assay. (Data represented from n=3 different biological experiments with ± standard deviation) 25 µL of SIRT1 protein in assay buffer were mixed with 15 µL of 83.5 µM of substrate and 10 µL of 500 µM and then reaction was stopped at 0, 10, 20, 30, 40, 50, 60, 70 and 80 time by adding 50 µL of developer. Fluorescence was then measured in the wells of the clear microplate with a fluorescence plate reader (Synergy multimode, Ex. 360 nm, Em. 460 nm, gain=35).

The similar SIRT1 deacetylase assay was carried out using increasing concentration of protein 2U (activity per unit).

Table A-3 Composition of assay component for SIRT1 assay per well volume.

Time	Protein (2 U/μL)	83.5 μM Substrate	500 μM NAD^+	Developer
0	25 μL	15 μL	10 μL	50 μL
10	25 μL	15 μL	10 μL	50 μL
20	25 μL	15 μL	10 μL	50 μL
30	25 μL	15 μL	10 μL	50 μL
40	25 μL	15 μL	10 μL	50 μL
50	25 μL	15 μL	10 μL	50 μL
60	25 μL	15 μL	10 μL	50 μL
70	25 μL	15 μL	10 μL	50 μL
80	25 μL	15 μL	10 μL	50 μL

The results are shown below and there was no straight line was recorded as per assay kit.

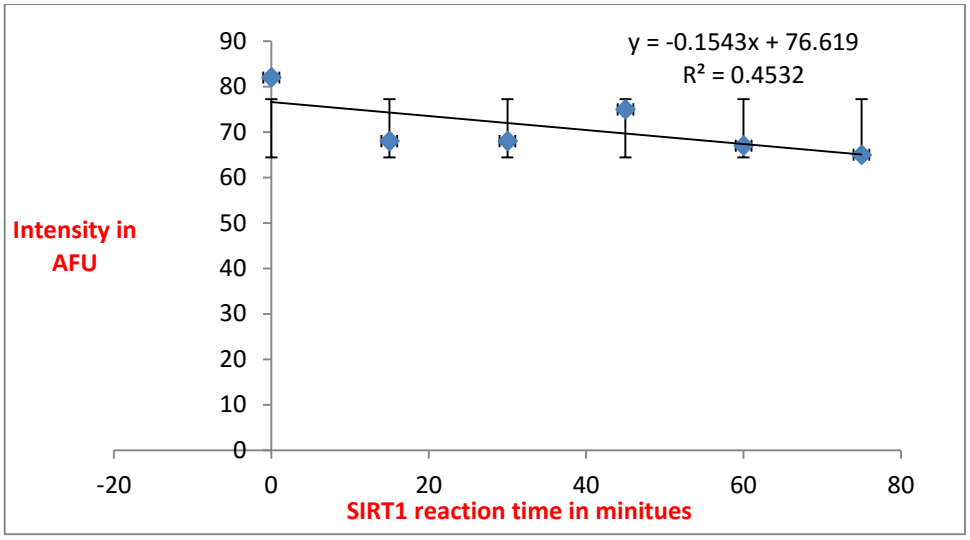

Figure A-3: Deacetylation reaction to determine incubation time for the SIRT1 assay. (Data represented from n=3 different biological experiments with ± standard deviation) 25 µL of SIRT1 protein (2 U/µL) in assay buffer were mixed with 15 µL of 83.5 µM of substrate and 10 µL of 500 µM and then reaction was stopped at 0, 10, 20, 30, 40, 50, 60, 70 and 80 time by adding 50 µL of developer. Fluorescence was then measured in the wells of the clear microplate with a fluorescence plate reader (Synergy multimode, Ex. 360 nm, Em. 460 nm, gain=35).

Then, SIRT1 deacetylase reaction was run using compounds including resveratrol (SIRT1 activator), Suramine (SIRT1 inhibitor). The concentration of peptide was chose such that 167 µM (SIRT1 substrate) and 500 µM NAD^+ protein concentration 2U/ well and then incubated for 45 minutes. The reaction was then stopped at 0, 10, 20, 30, 40, 50, 60 and 70-time interval. The reaction was stopped using developer by adding 25 µL of stopping solution or developer solution (380 µL AB + 100 µL developer + 20 µL NAM) fluorescence was then recorded over every 10 minutes time interval to get the maximum fluorescence intensity.

The results are shown below with SIRT1 deacetylase reaction was carried out in presence of compounds. In this experiment the control represents the normal SIRT1 reaction without any compounds or solvent. The other SIRT1 deacetylase reaction includes the resveratrol (5 µL), suramine (5 µL) and solvent (5 µL).

Table A-4 Composition of assay component for SIRT1 assay per well volume.

Time	Protein (2U)	83.5 µM Substrate	500 µM NAD^+	Developer
0	25 µL	15 µL	10 µL	50 µL
3	25 µL	15 µL	10 µL	50 µL
6	25 µL	15 µL	10 µL	50 µL
9	25 µL	15 µL	10 µL	50 µL
12	25 µL	15 µL	10 µL	50 µL
15	25 µL	15 µL	10 µL	50 µL
18	25 µL	15 µL	10 µL	50 µL
21	25 µL	15 µL	10 µL	50 µL
24	25 µL	15 µL	10 µL	50 µL

Table A-5 Composition of assay component for SIRT1 assay per well volume.

Compound	Protein (2U)	Assay buffer	167 µM Substrate	500µM NAD^+	Developer
blank	-	35 µL	9 µL	6 µL	50 µL
control	20 µL	15 µL	9 µL	6 µL	50 µL
Resveratrol (5 µL)	20 µL	10 µL	9 µL	6 µL	50 µL
Sur-amine (5 µL)	20 µL	10 µL	9 µL	6 µL	50 µL
Solvent (5 µL)	20 µL	10 µL	9 µL	6 µL	50 µL

The SIRT1 deacetylase reaction was then stopper every 3 minutes using developer solution. The reaction was then monitored using SIRT1 deacetylase developer which consists of NAM.The details are in **Table A-6**;

Table A-6 Composition of assay component for SIRT1 assay per well volume.

Time	Protein (2U)	Assay buffer	167 µM Substrate	500 µM NAD^+	Developer
0	25 µL	10 µL	9 µL	6 µL	50 µL
3	25 µL	10 µL	9 µL	6 µL	50 µL
6	25 µL	10 µL	9 µL	6 µL	50 µL
9	25 µL	10 µL	9 µL	6 µL	50 µL
12	25 µL	10 µL	9 µL	6 µL	50 µL
15	25 µL	10 µL	9 µL	6 µL	50 µL
18	25 µL	10 µL	9 µL	6 µL	50 µL
21	25 µL	10 µL	9 µL	6 µL	50 µL
24	25 µL	10 µL	9 µL	6 µL	50 µL

SIRT1 assay Sigma kit:

Standard curve for assay:

The standard curve for this assay was performed in two parts. The first part was intended to measure the fluorescence at different concentrations of the standard SIRT1 substrate (directly provided) and the second part was carried without developing solution.

The standard reaction was prepared in two sets of the standard curve in a 96 well plate according to **Table A-7**. Add 5µL of Developing Solution to each well in one set of the standard dilution series. 5 µL of assay buffer was added to other set of reaction instead of the developing solution to each well. This reaction was then mixed using a horizontal shaker. The 96 well plates were then incubated the plate at 37 °C for 10 minutes. The fluorescence was read in a plate reader. For calculation the net fluorescence signal of each standard sample was subtracted from the fluorescence signal of control sample (without Developing Solution). Then, the fluorescence signal (y-axis) versus concentration of the Standard (x-axis) was plotted and shown in **Figure A-4**

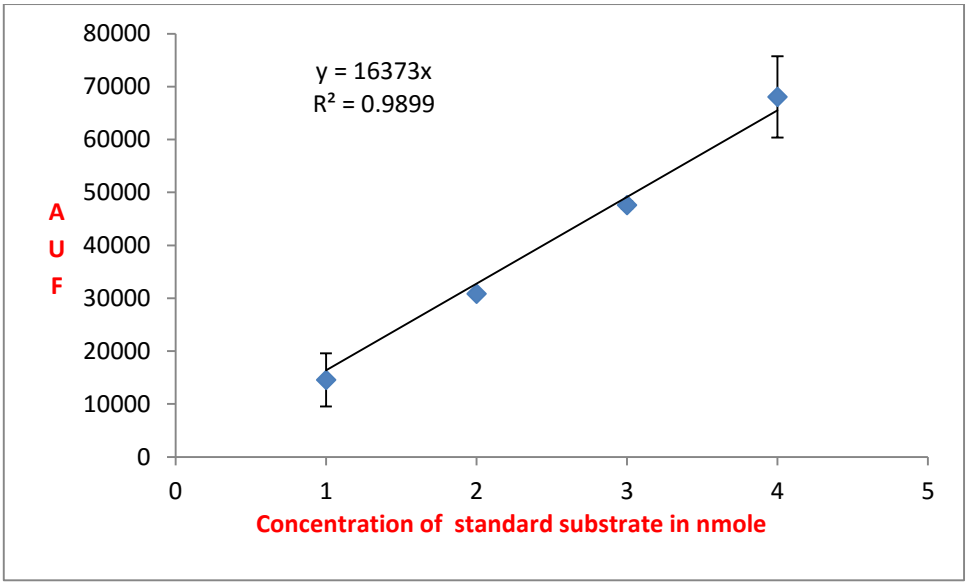

Figure A-4: Standard curve experiment for SIRT1 deacetylase reaction using sigma assay where Y-axis represent fluroscence signal and X-axis represent concentration of standard deacetylase substrate. (Data represented from n=3 different biological experiments with ± standard deviation)

Table A-7: Composition for preparing standard curve for Sigma assay

Well No.	Assay buffer	Standard solution (400 µM)	Standard amount/well	Standard final conc.
1, 2	47.5 µL	2.5 µL	1 nmole	20 µM
3, 4	45 µL	5 µL	2 nmole	40 µM
5, 6	42.5 µL	7.5 µL	3 nmole	60 µM
7, 8	40 µL	10 µL	4 nmole	80 µM

Table A-8: Assay reaction for SIRT1 activity (in presence of activator or inhibitor):

Well no	Assay reaction	Assay buffer	SIRT1 (~1.5 µg)	NAD^+ solution (µL)	Inhibitors solution (µL)	Activator solution (µL)
1, 2	SIRT1 purified enzyme	33 µL	2	5	-	-
3, 4	Inhibition reaction	28 µL	2	5	-	5
5, 6	Activation reaction	28 µL	2	5	5	-
7, 8	Blank	38 µL	2	-	-	-

Appendix B

^{1}H NMR of V1

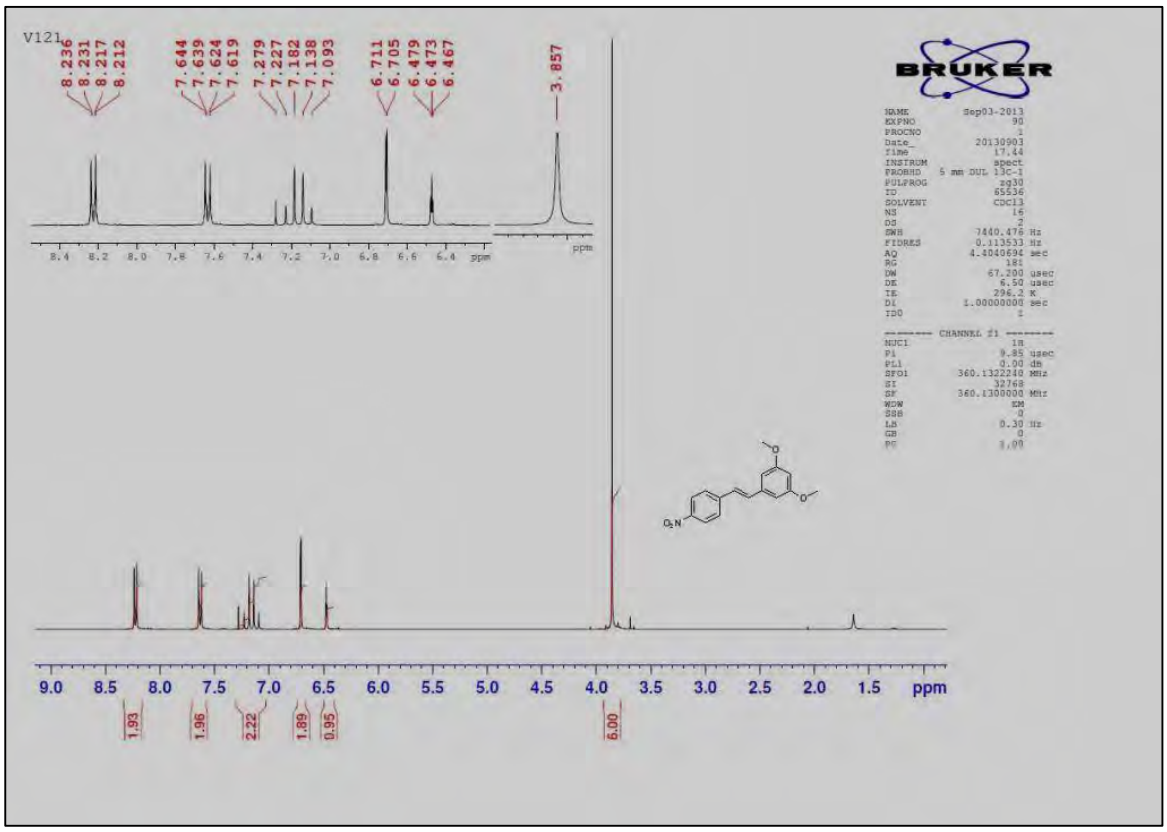

^{13}C NMR spectra of V1

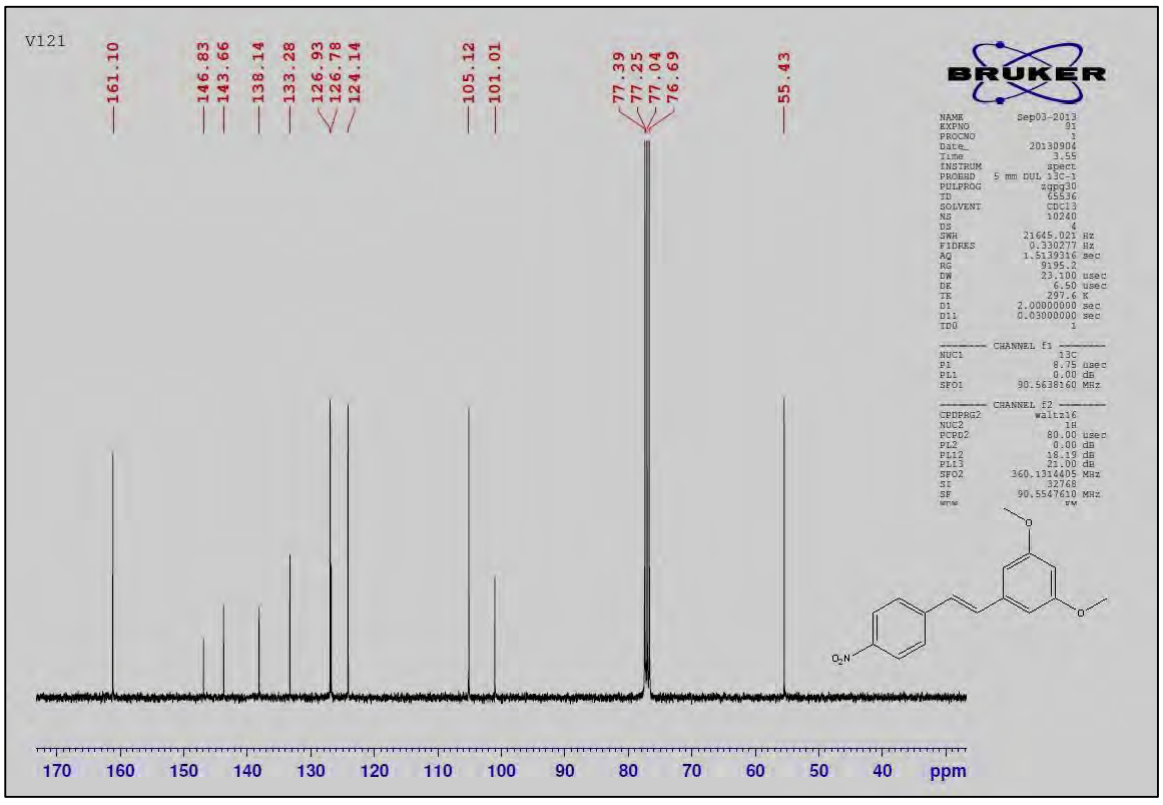

2D HSQC spectra of V1

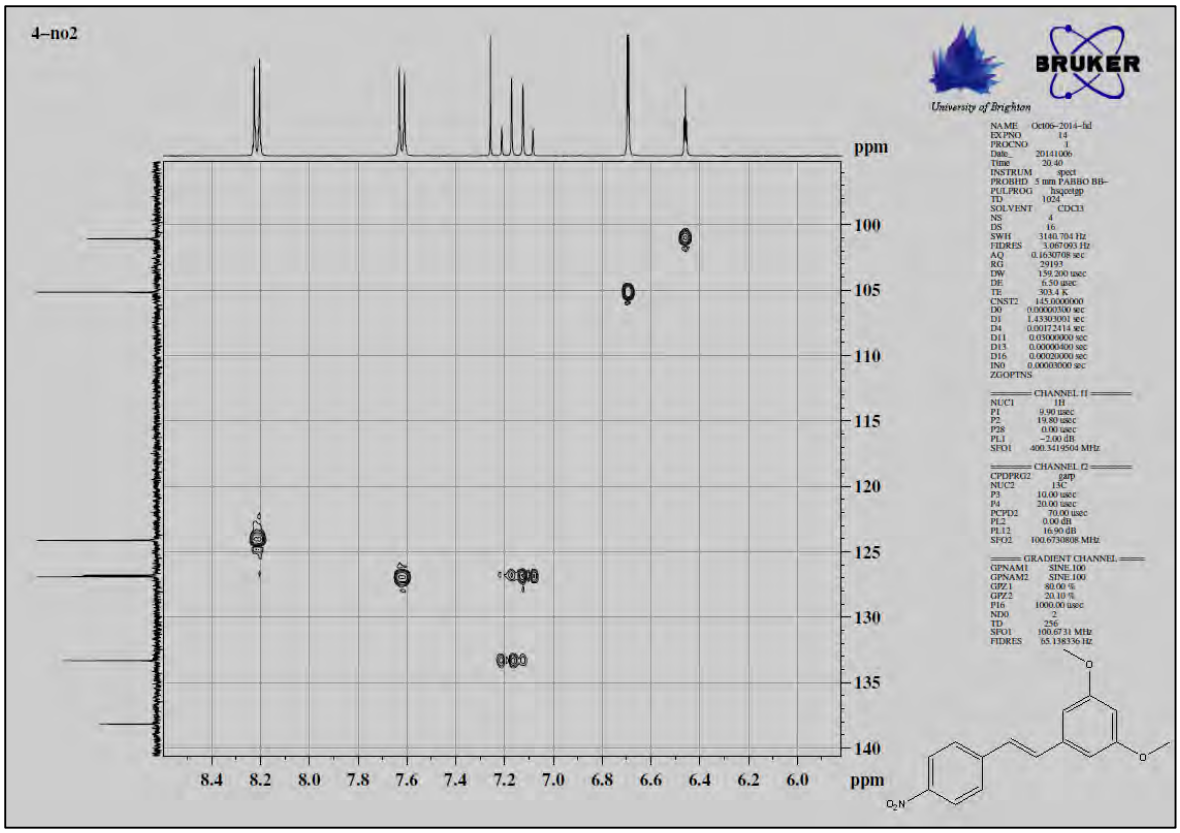

2D COSY spectra of V1

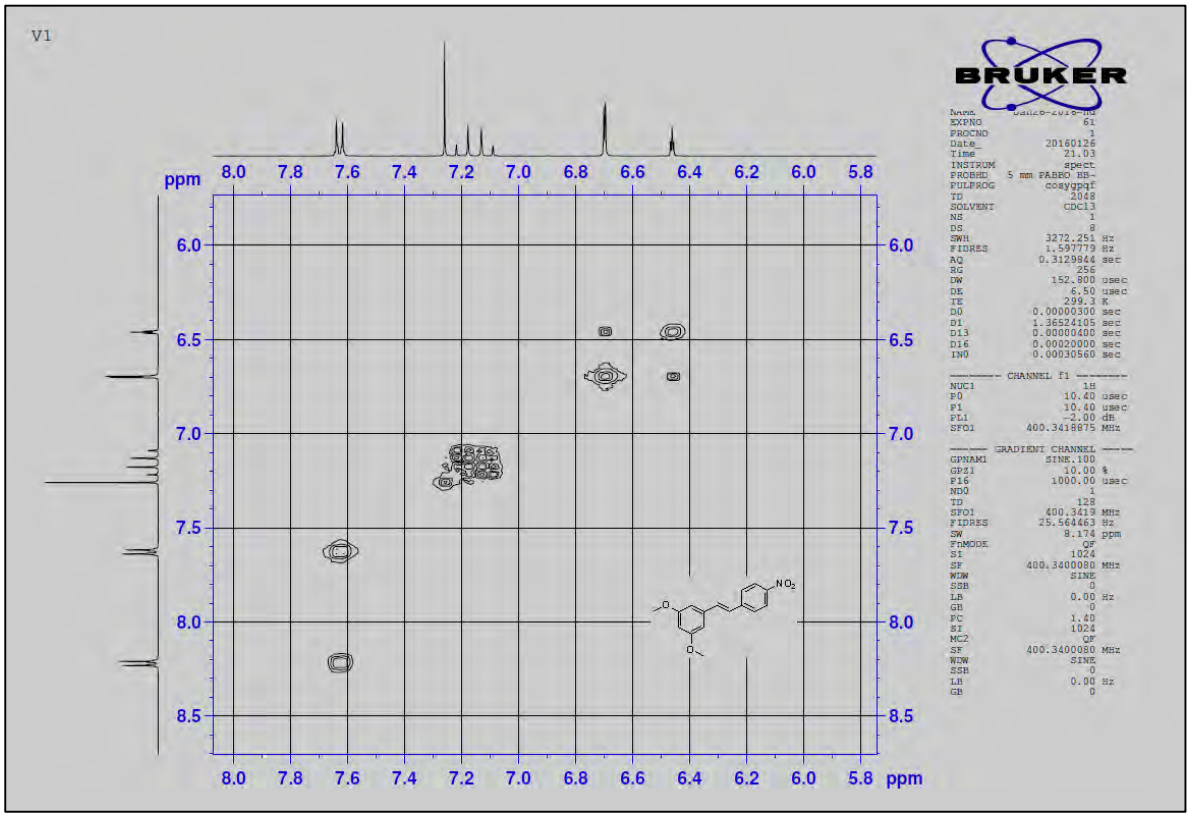

Mass spectra of V1:

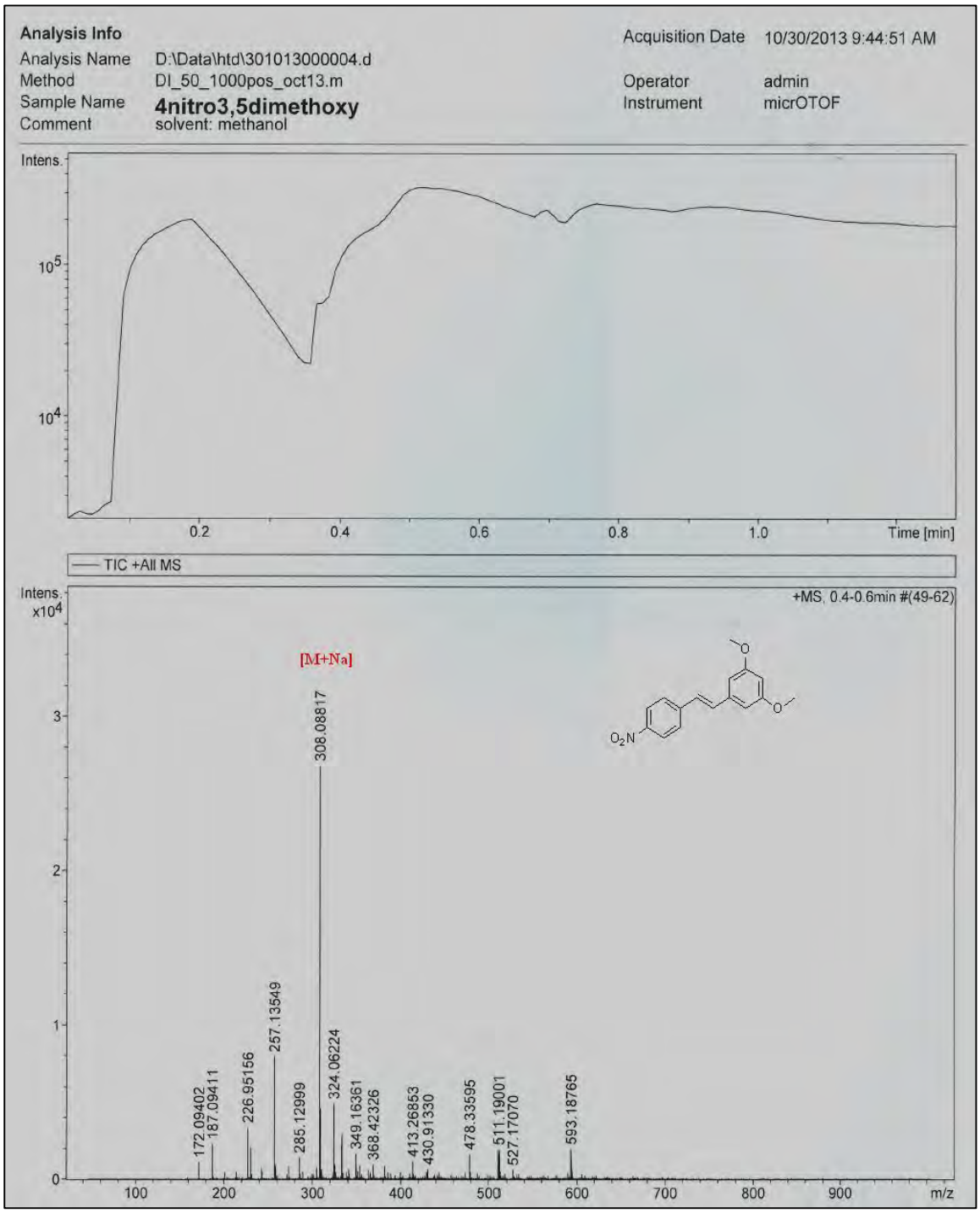

^{1}H NMR spectra of V2

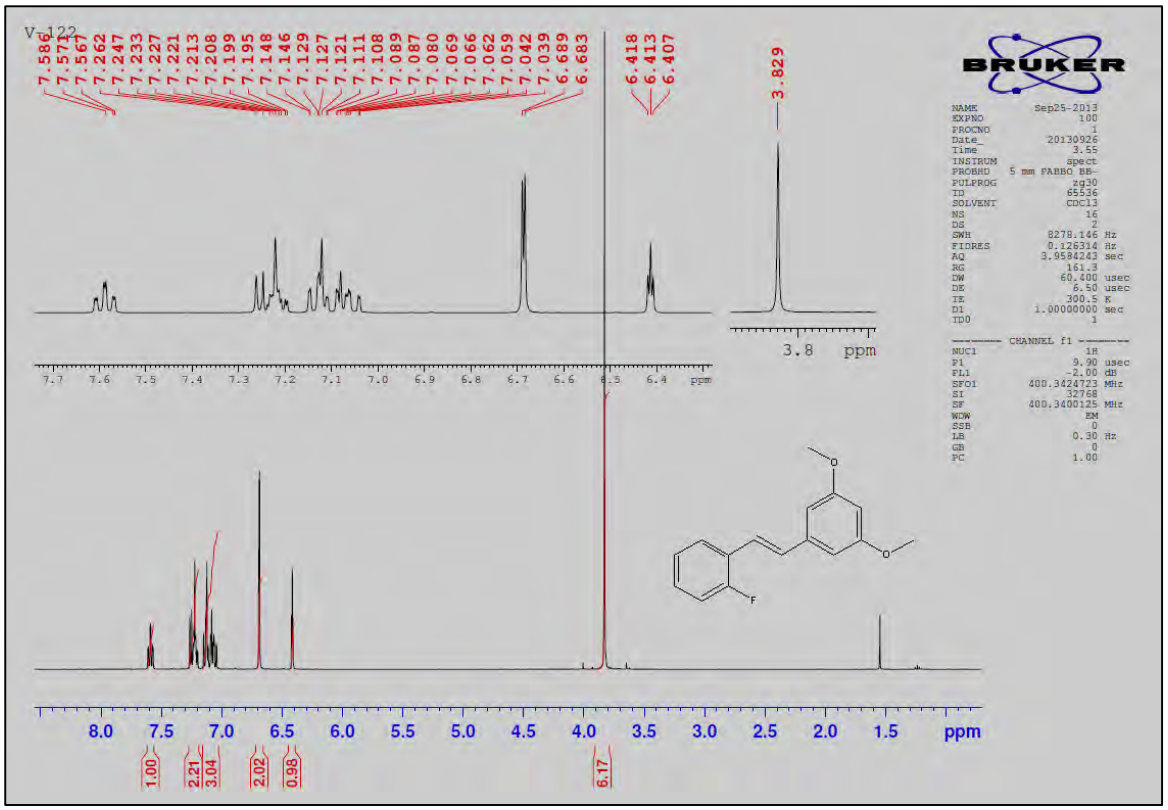

^{13}C NMR spectra of V2

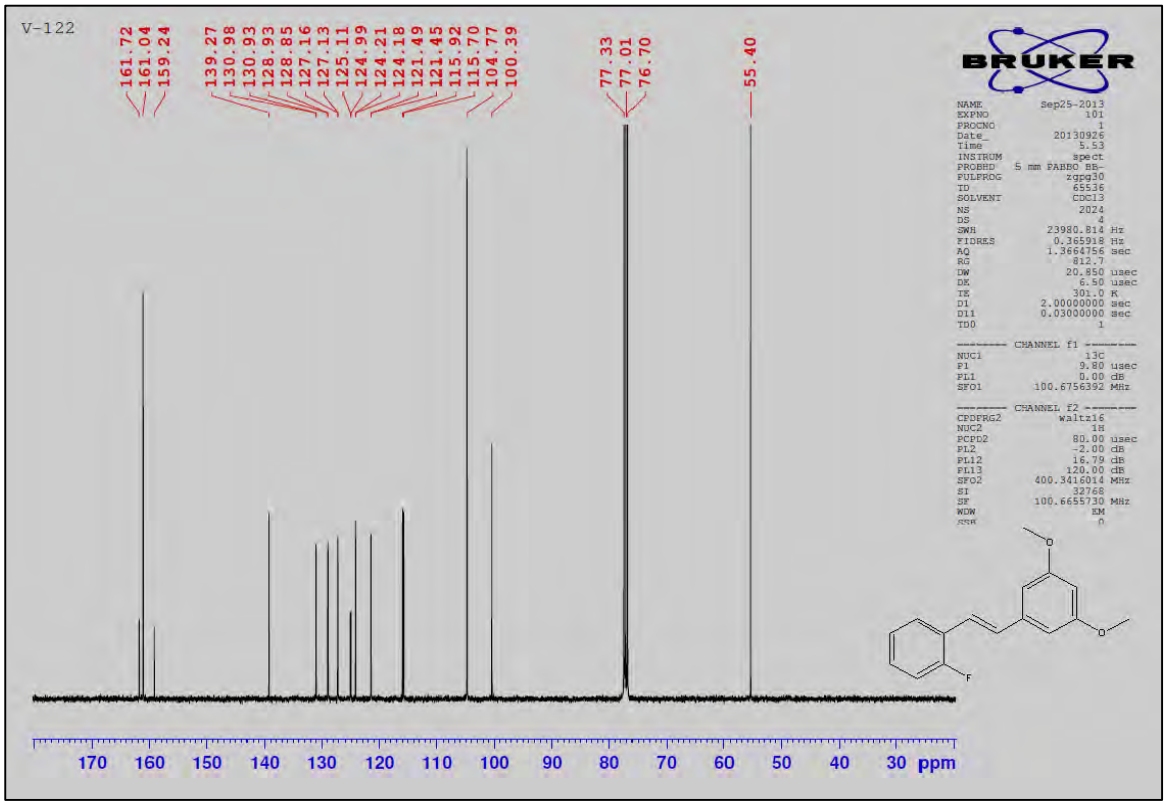

2D HSQC spectra of V2

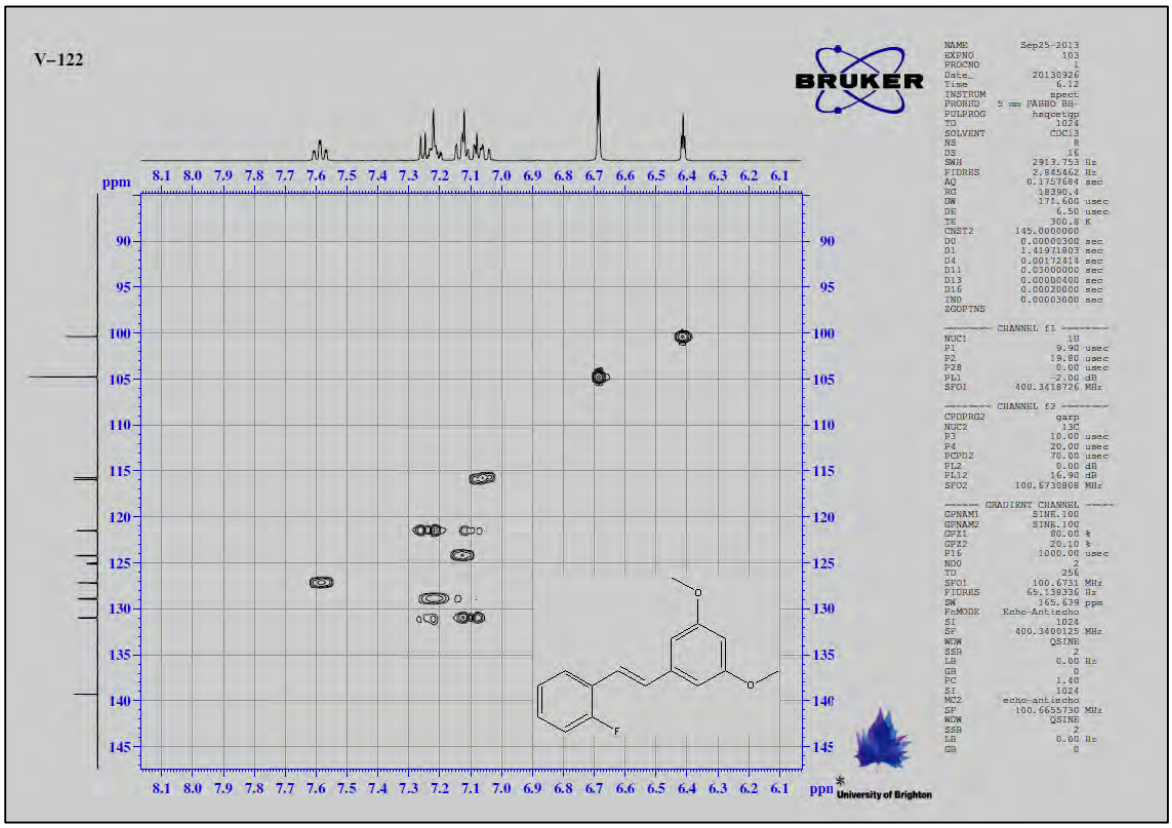

2D COSY spectra of V2

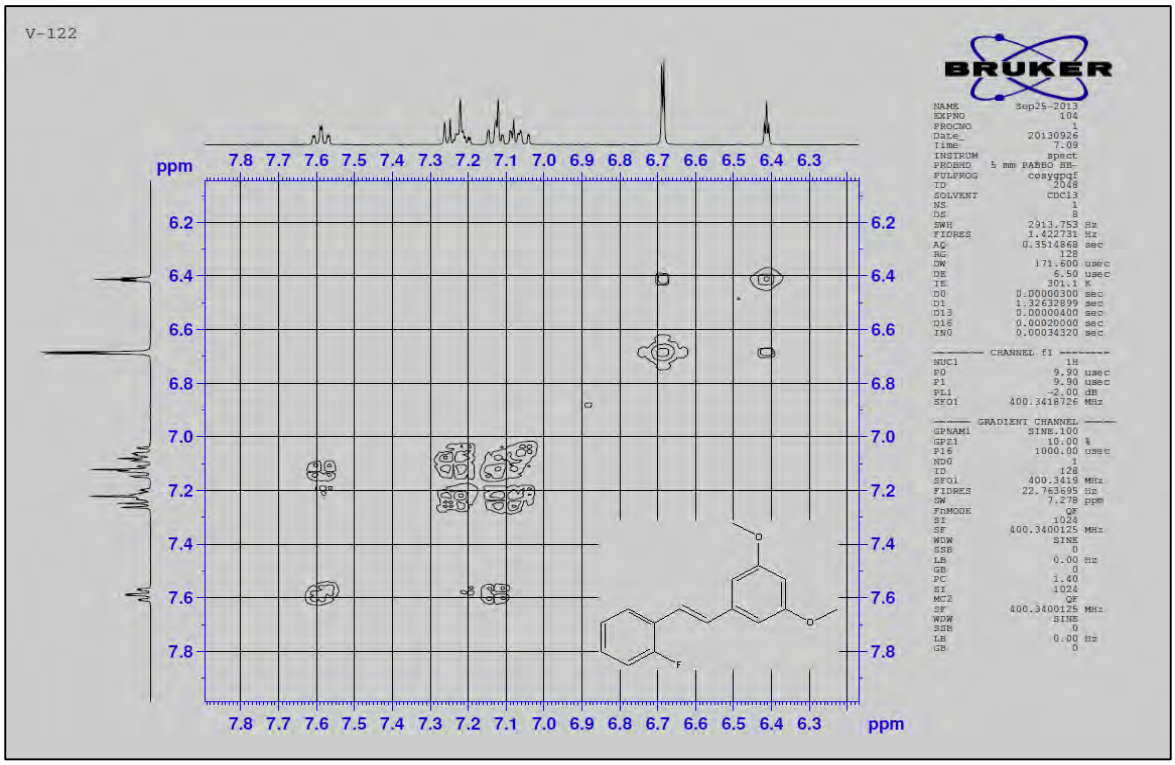

Mass spectra of V2

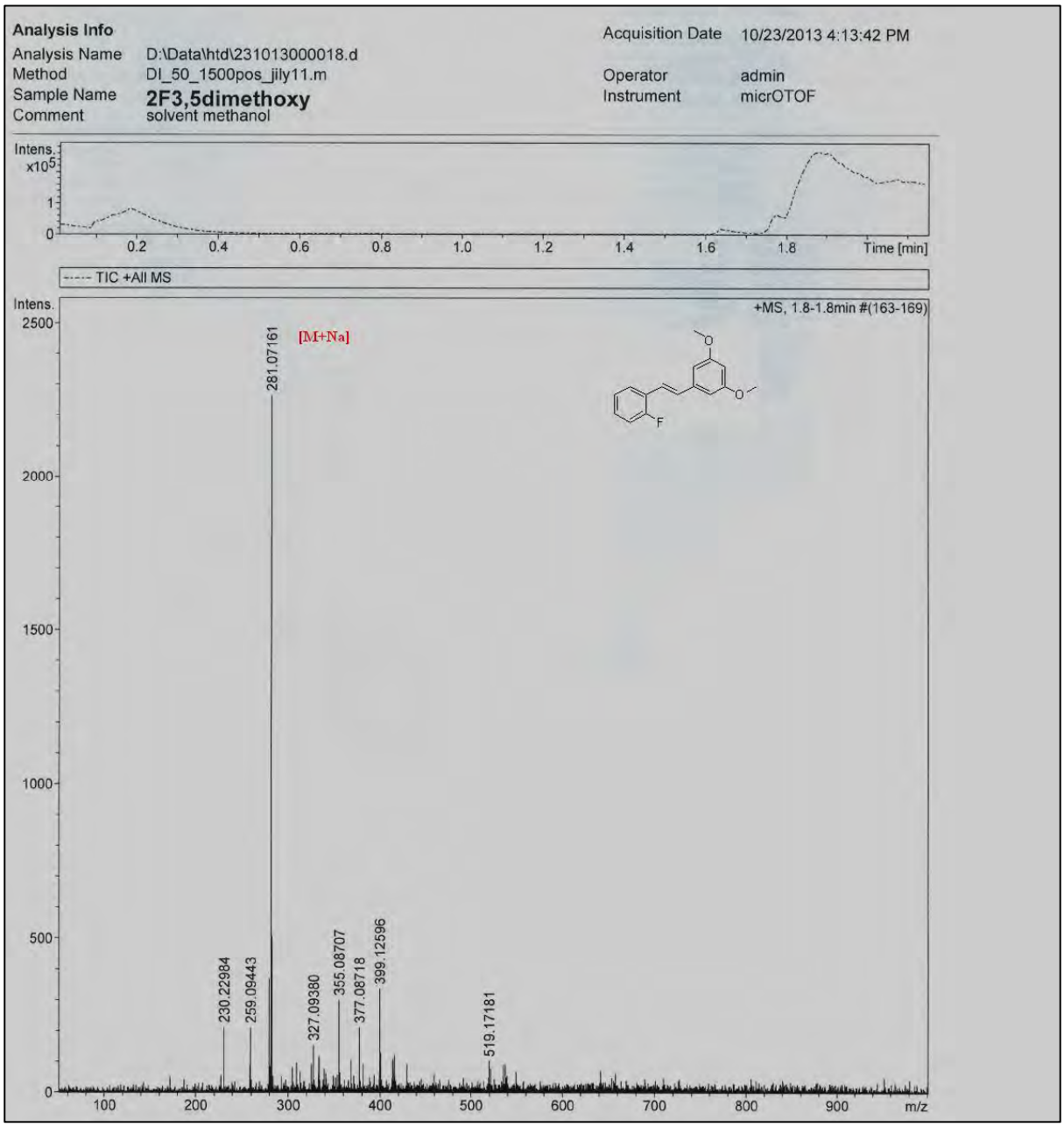

^{1}H NMR spectra of V3

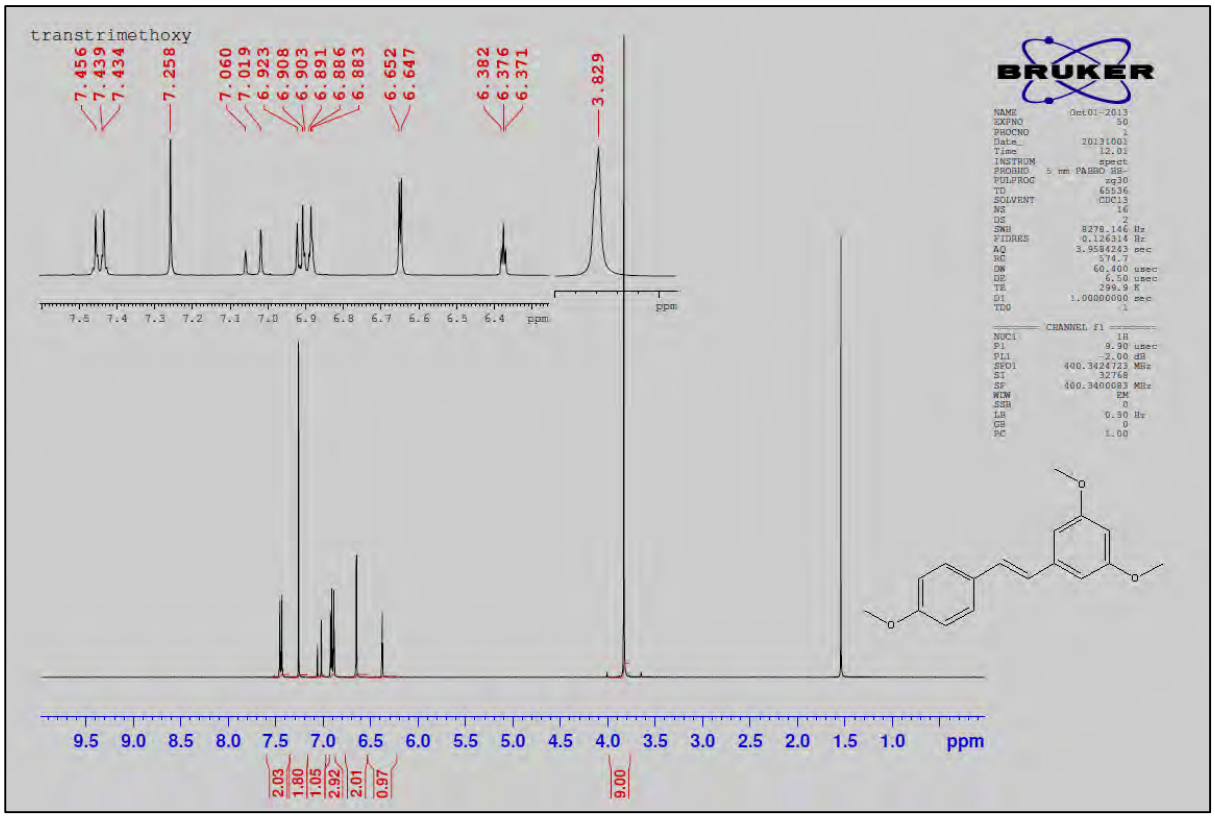

^{13}C Spectra of V3

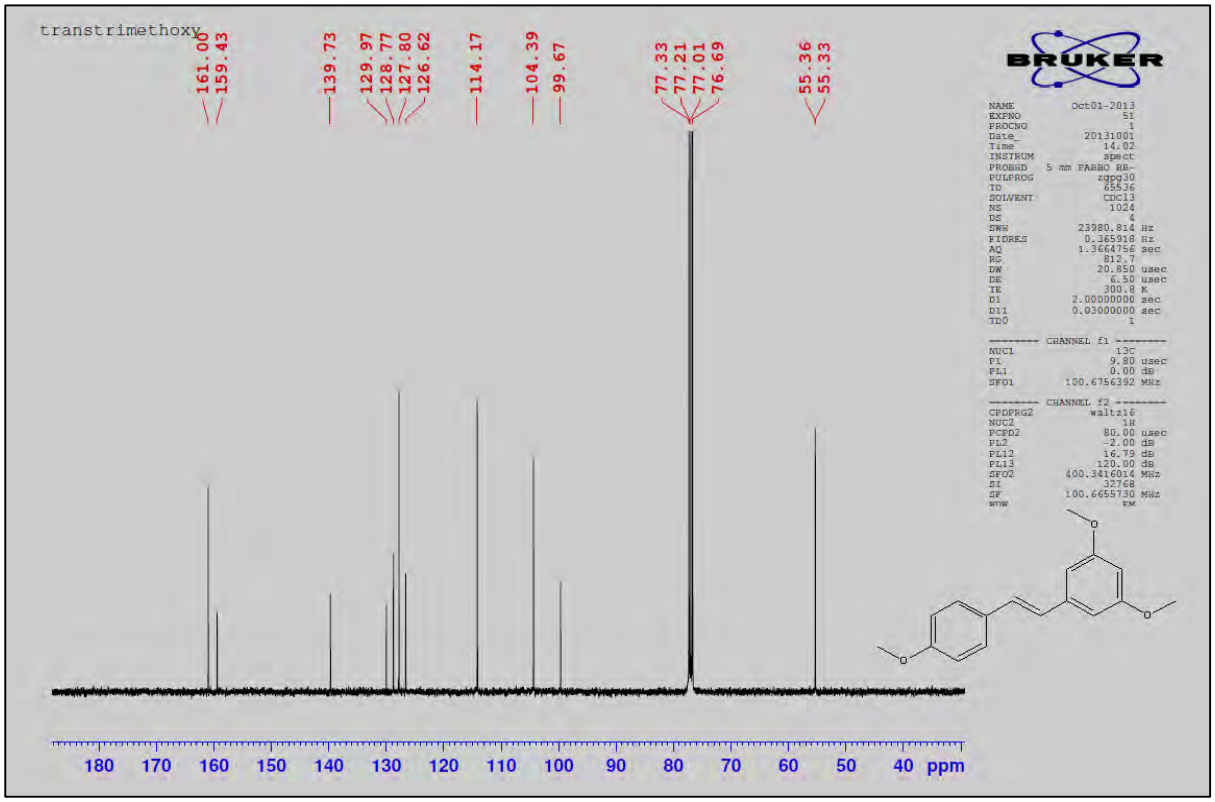

2D HSQC spectra of V3

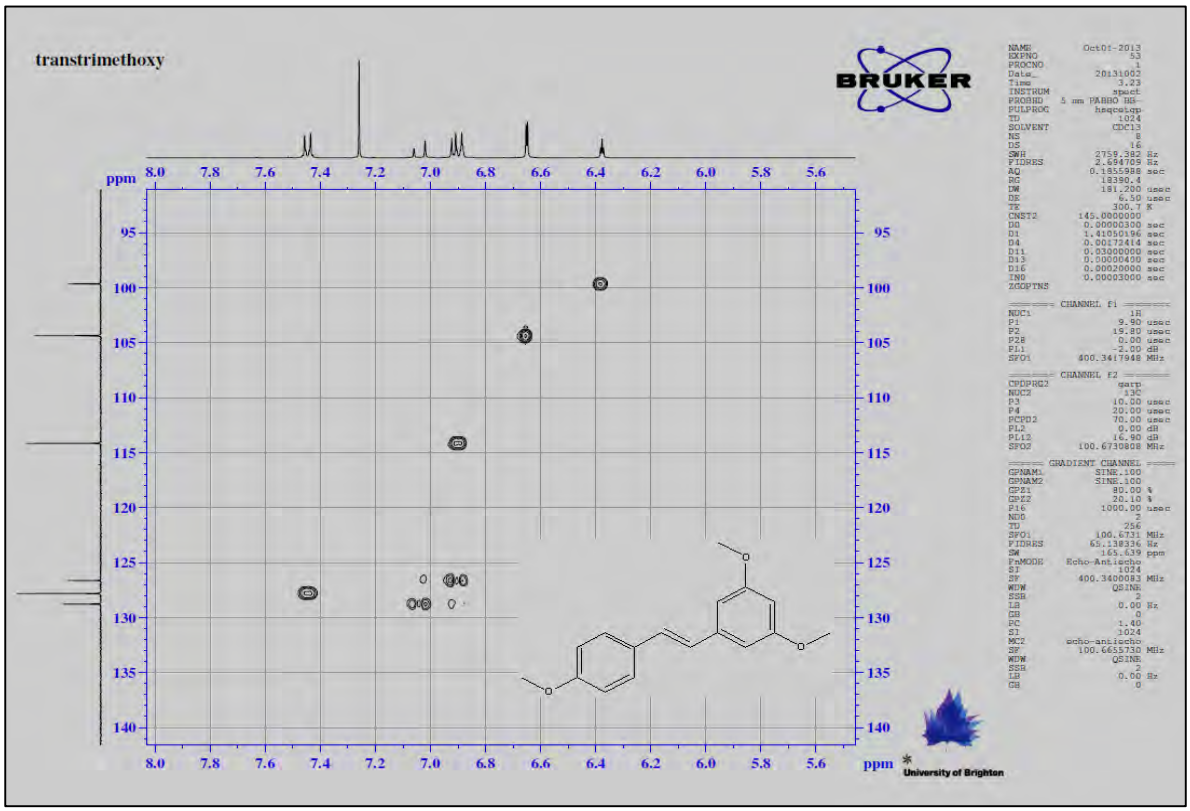

Mass spectra of V3

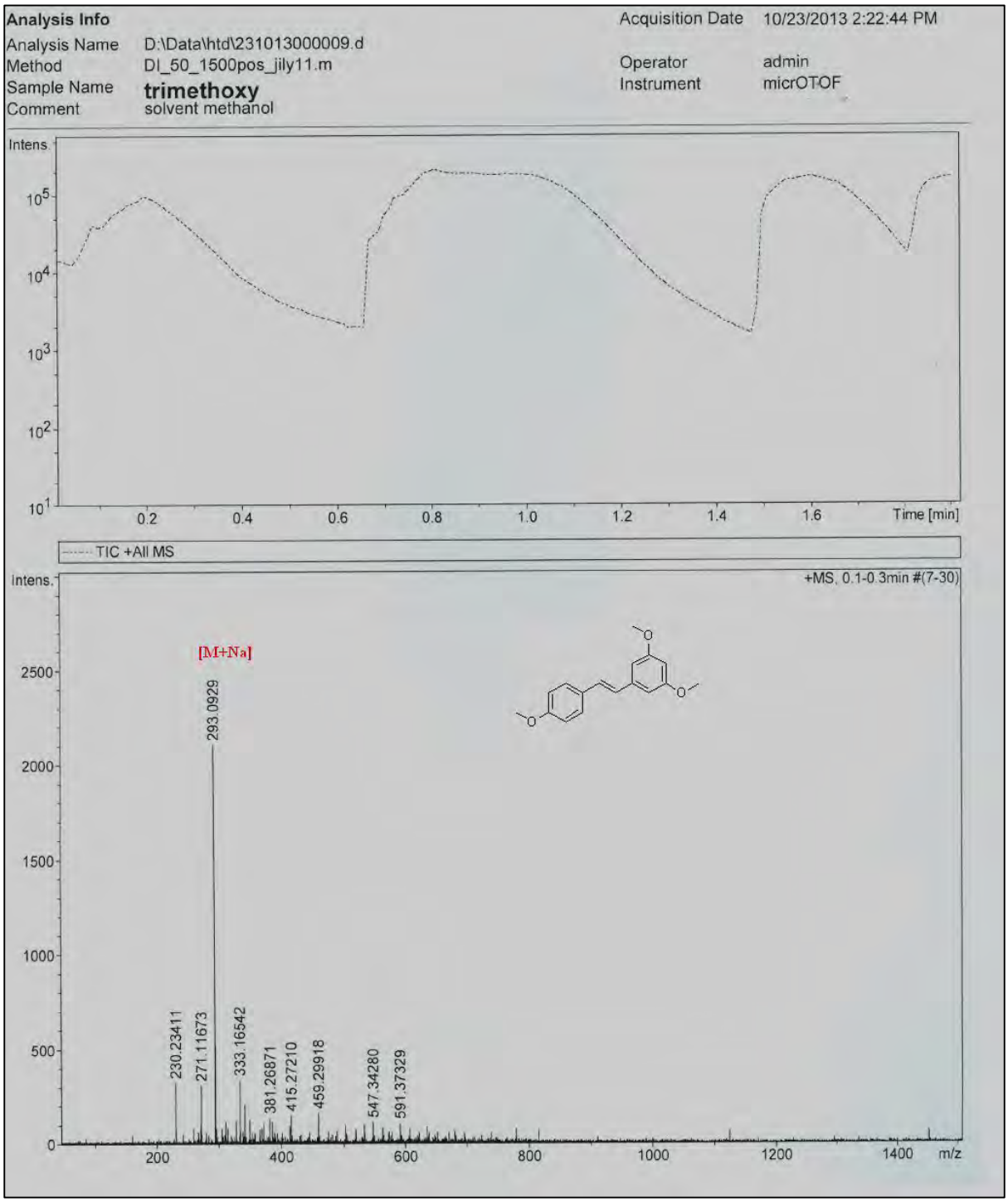

^{1}H NMR spectra of V4

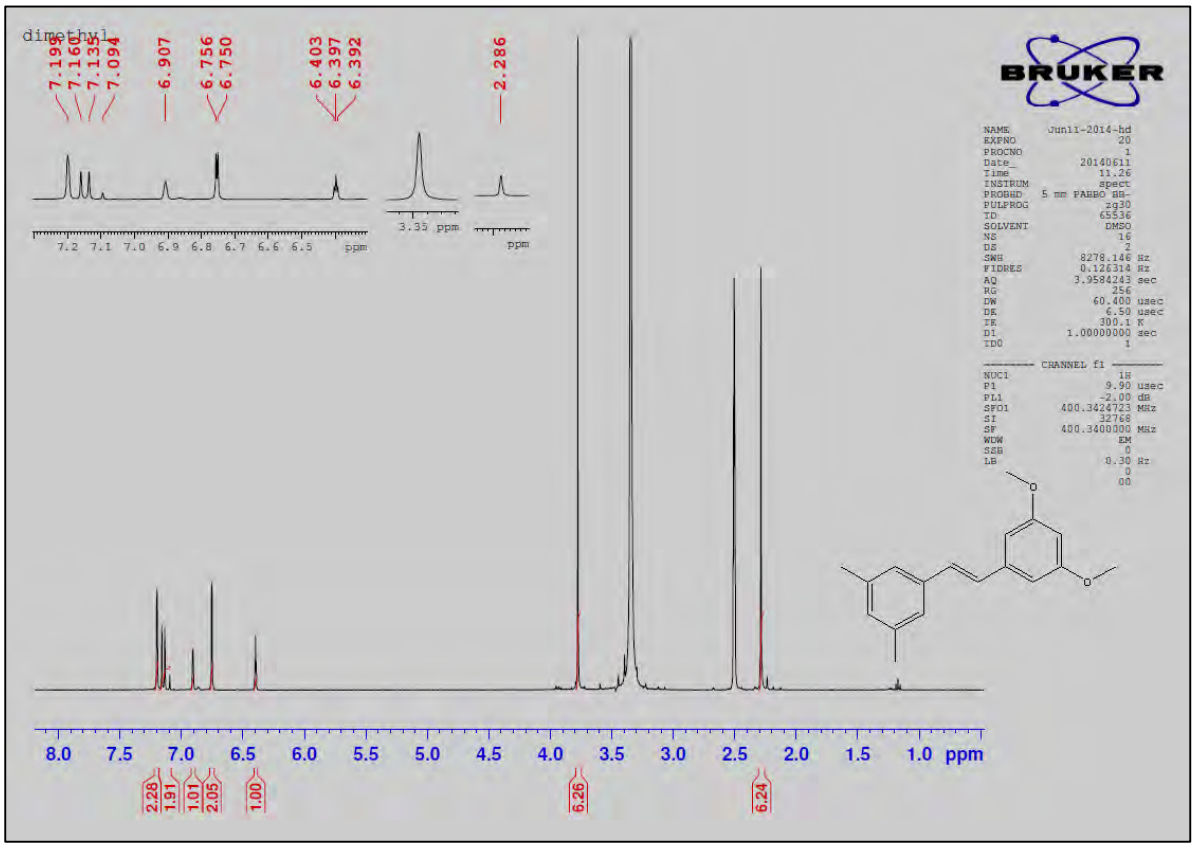

^{13}C NMR spectra of V4

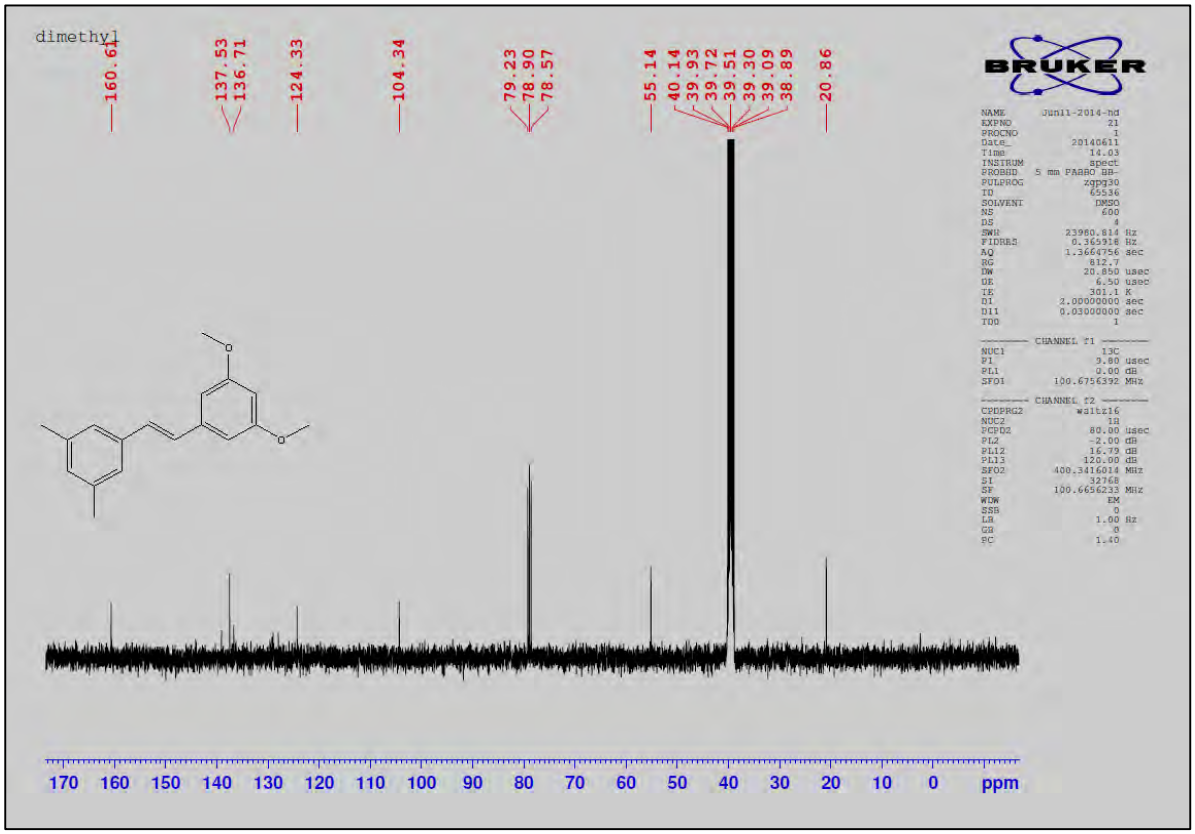

2D HSQC spectra of V4

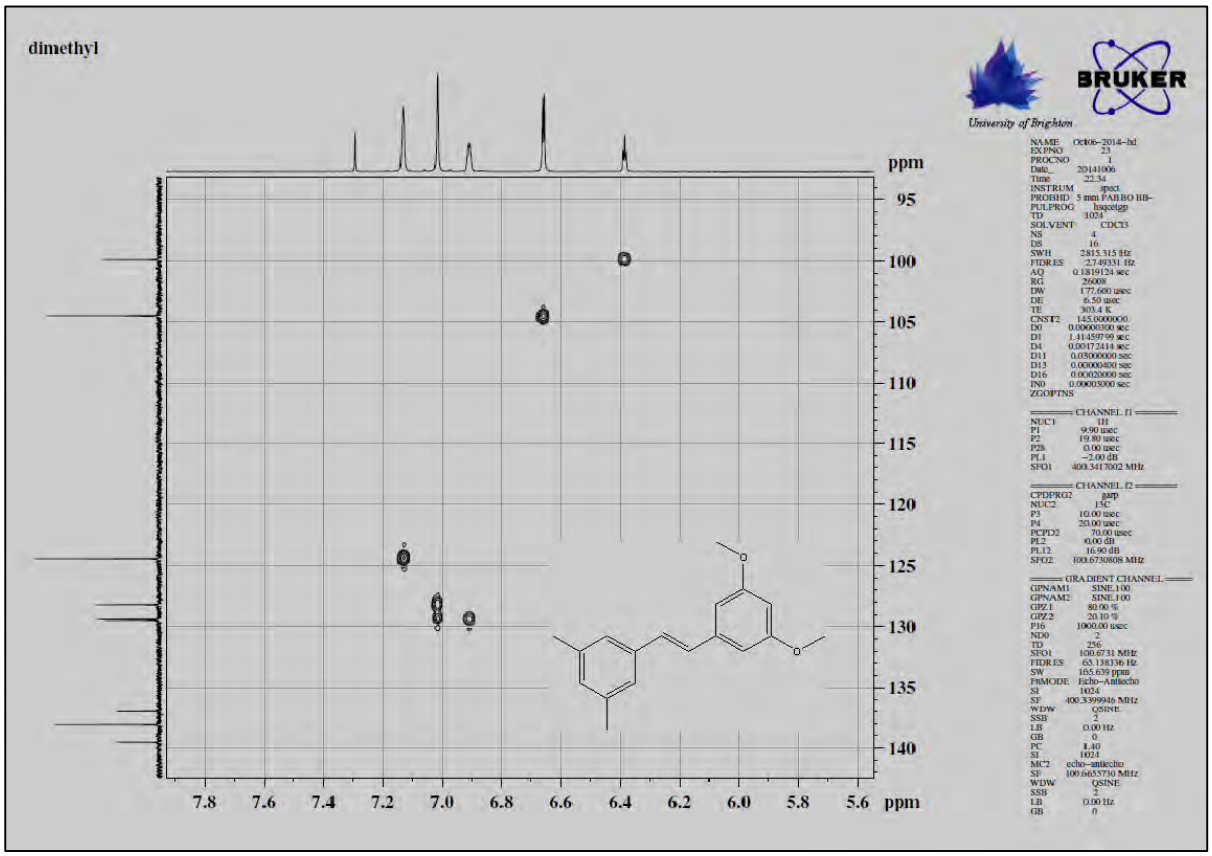

2D COSY spectra of V4

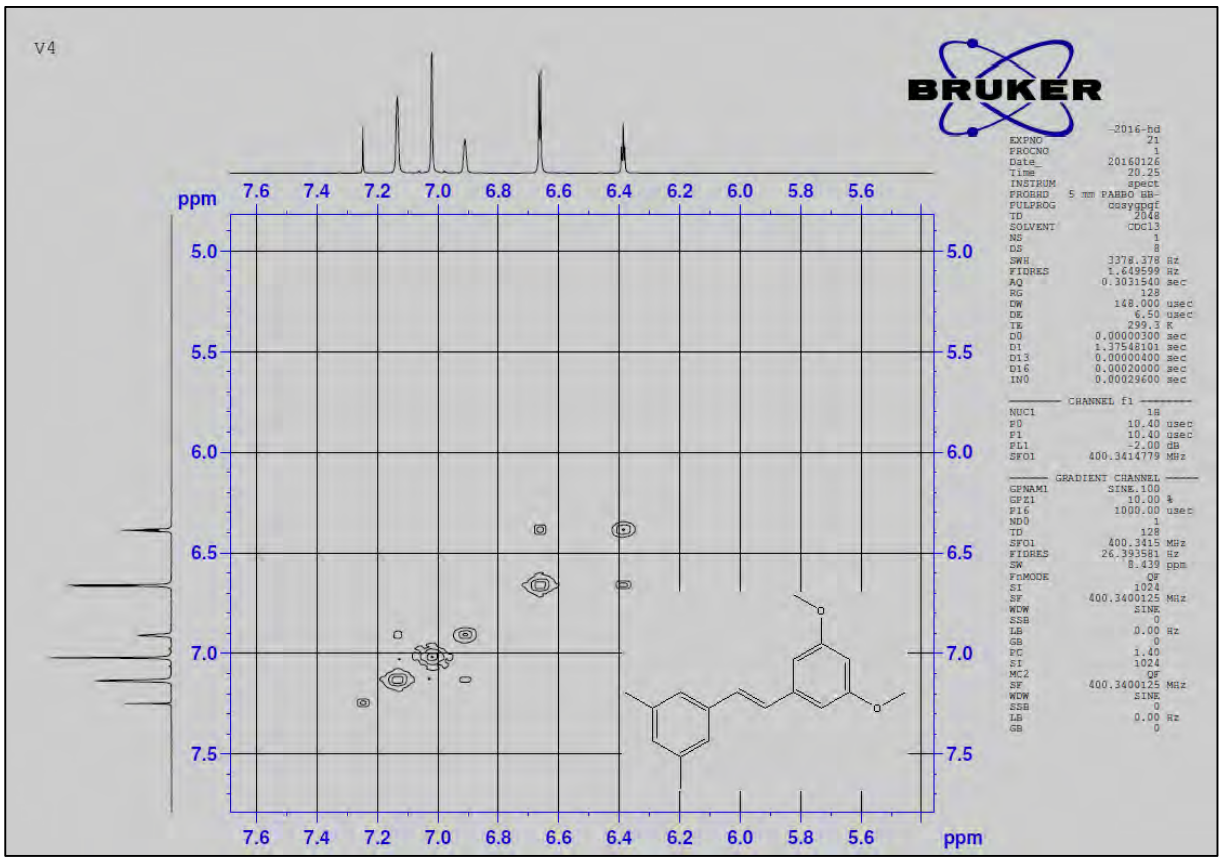

Mass spectra of V4

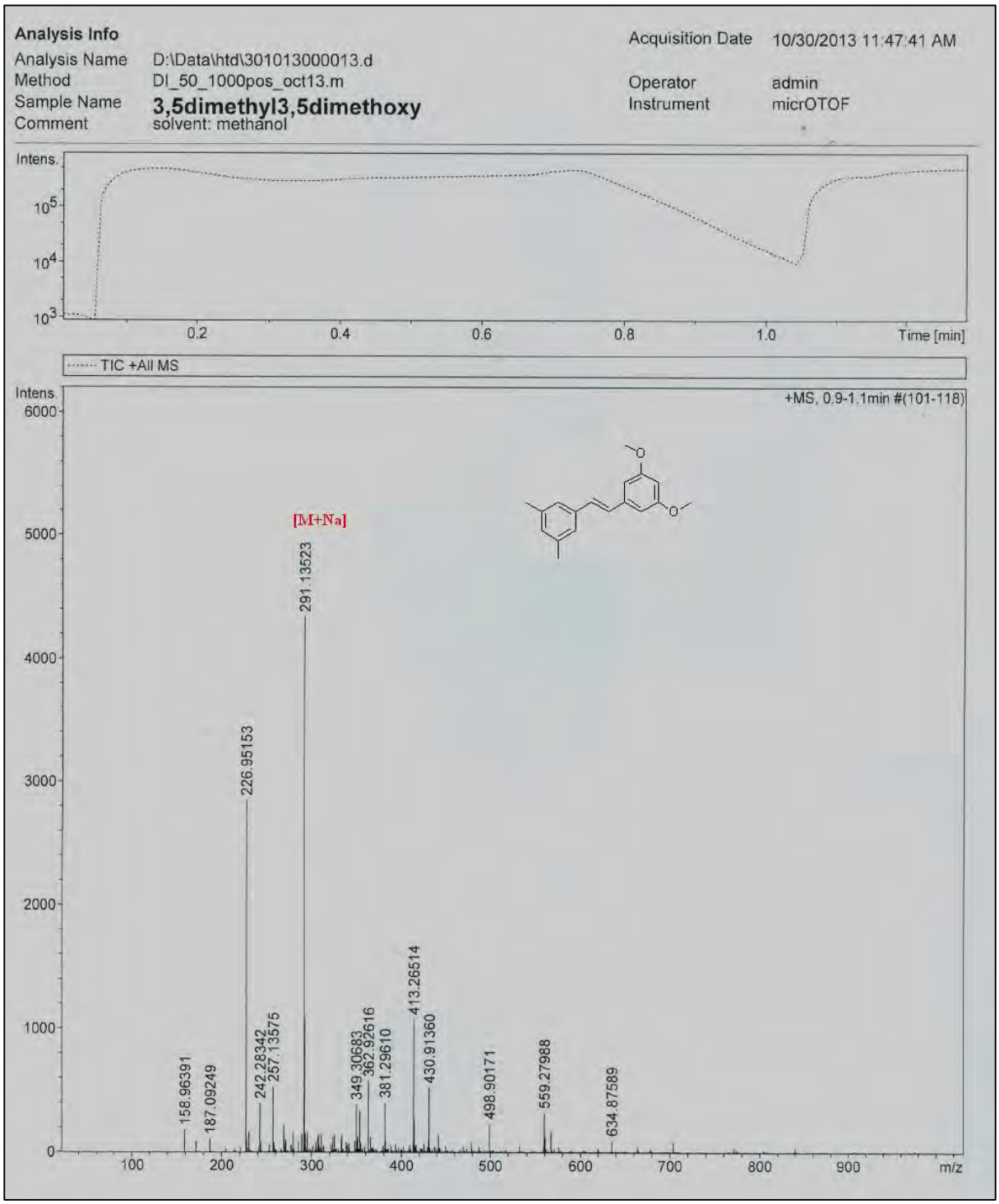

^{1}H NMR spectra of V5

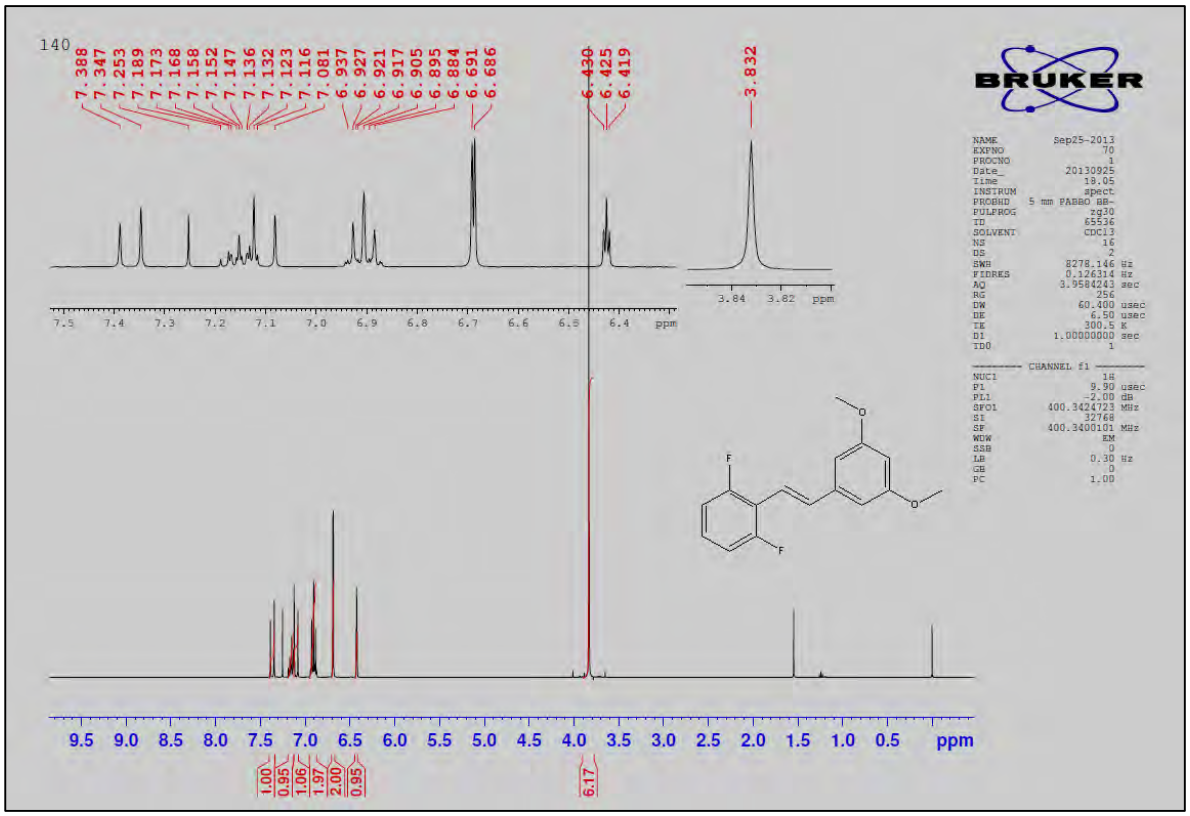

^{13}C NMR spectra of V5

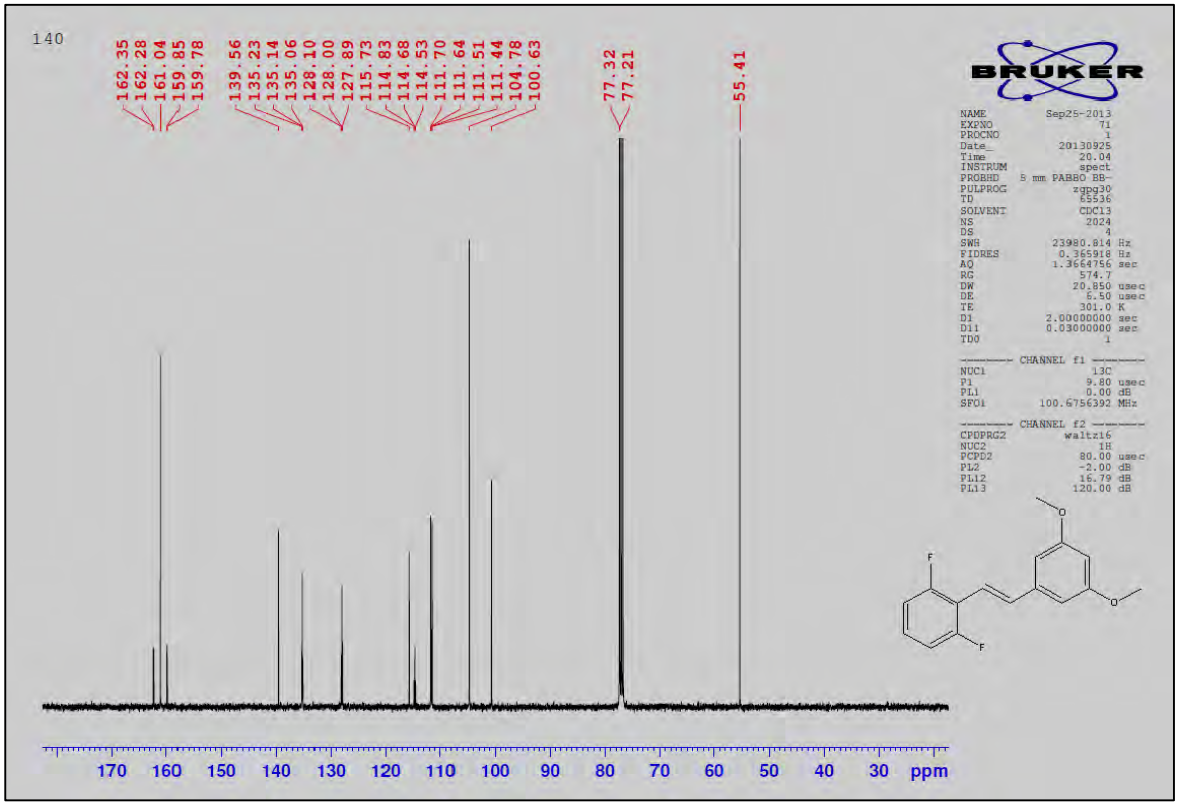

2D HSQC spectra of V5

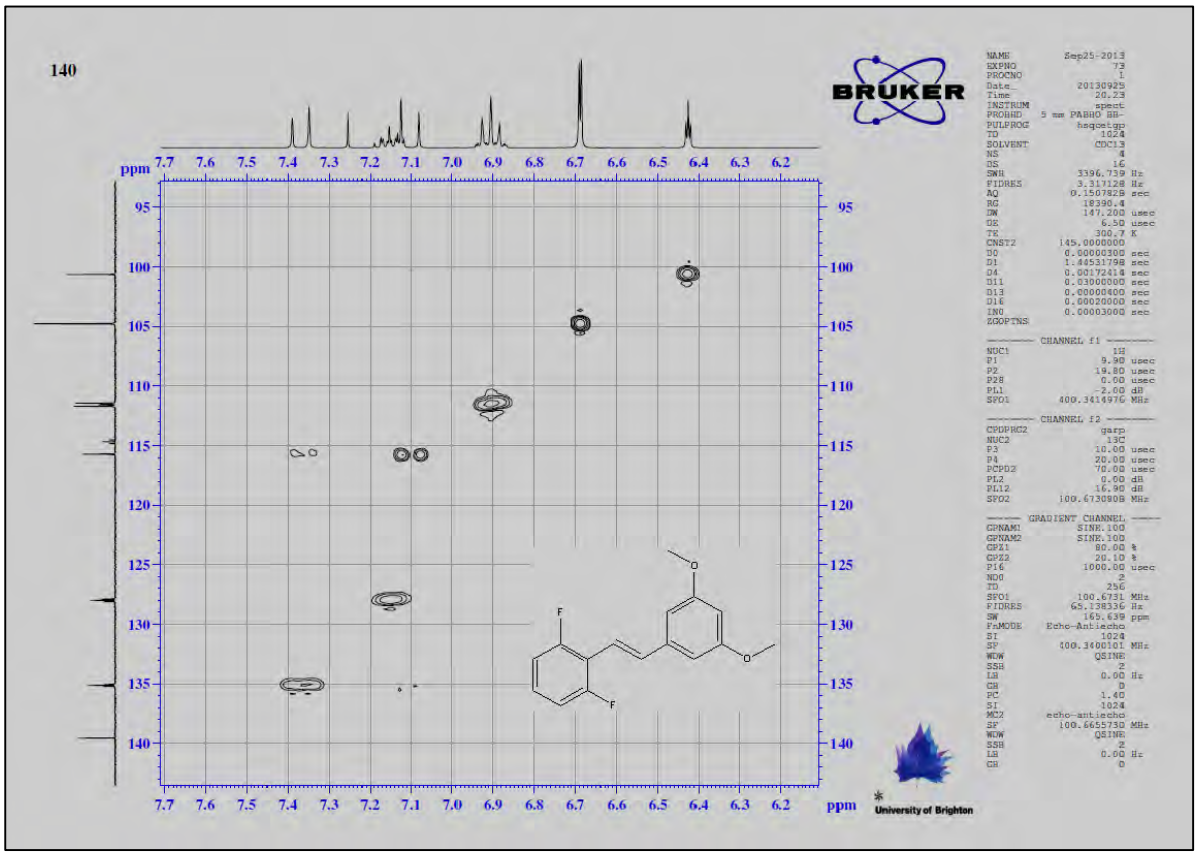

2D COSY spectra of V5

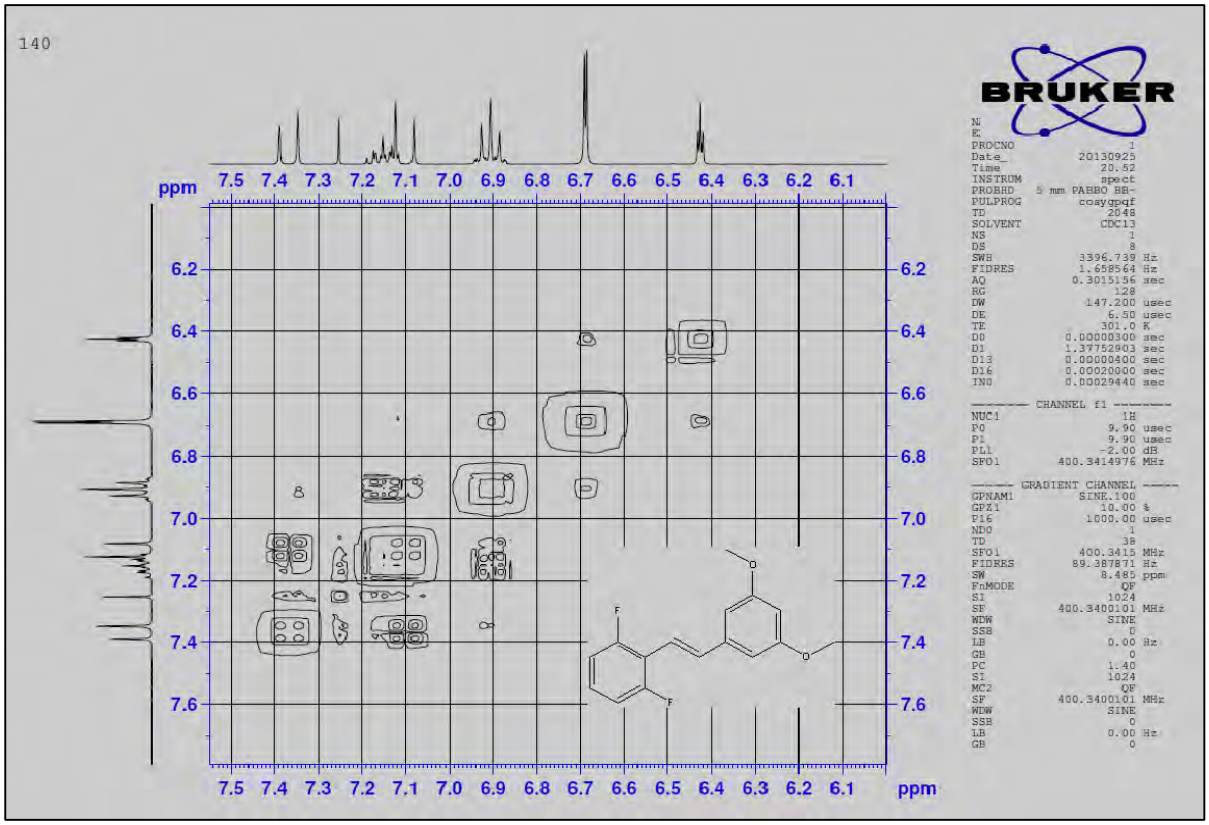

Mass spectra of V5

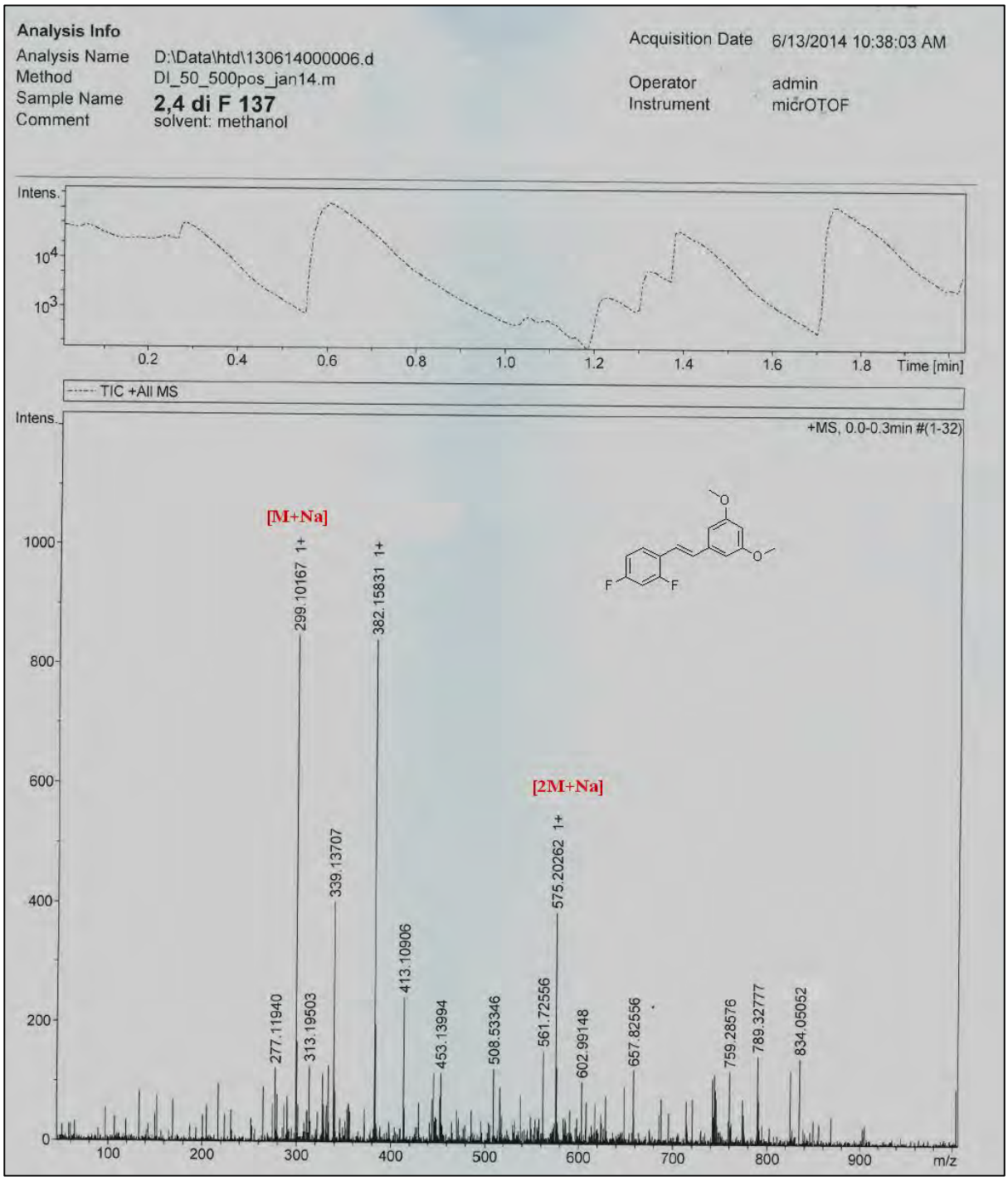

^{1}H NMR spectra of V6

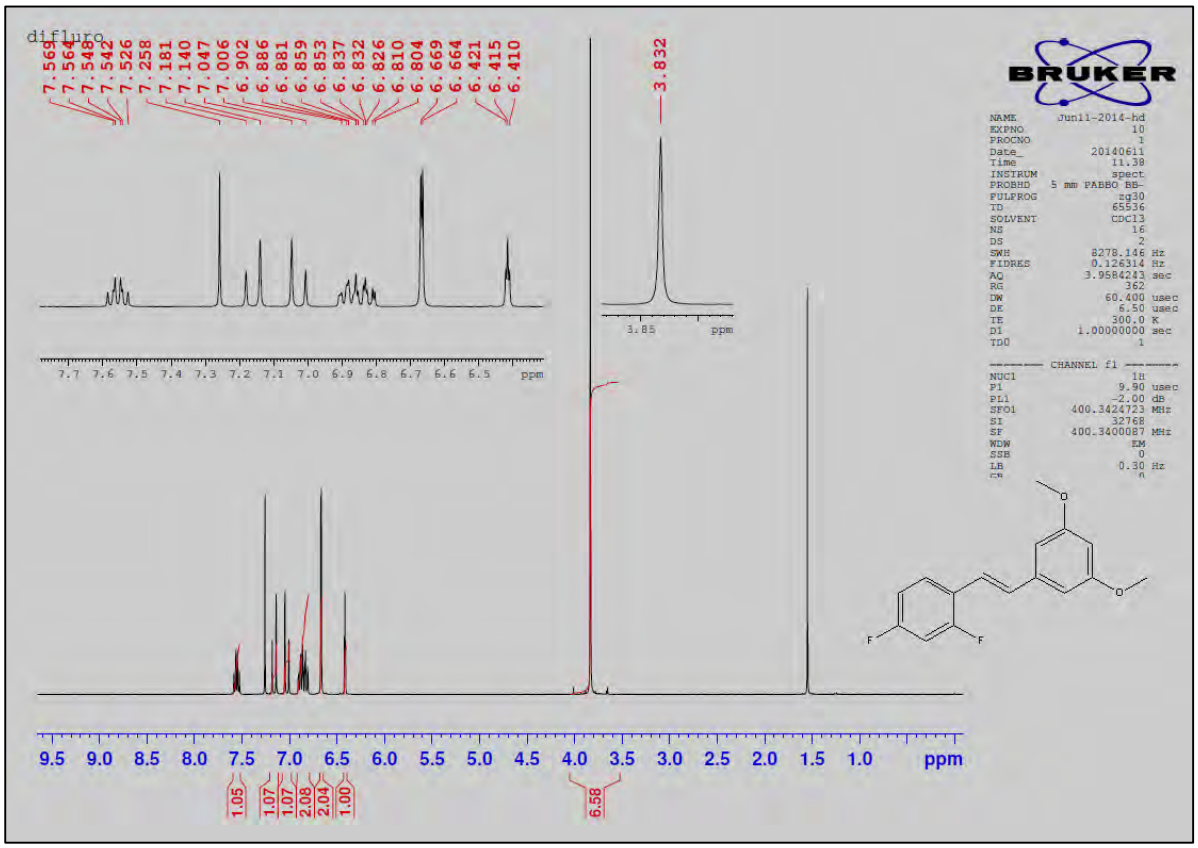

^{13}C NMR spectra of V6

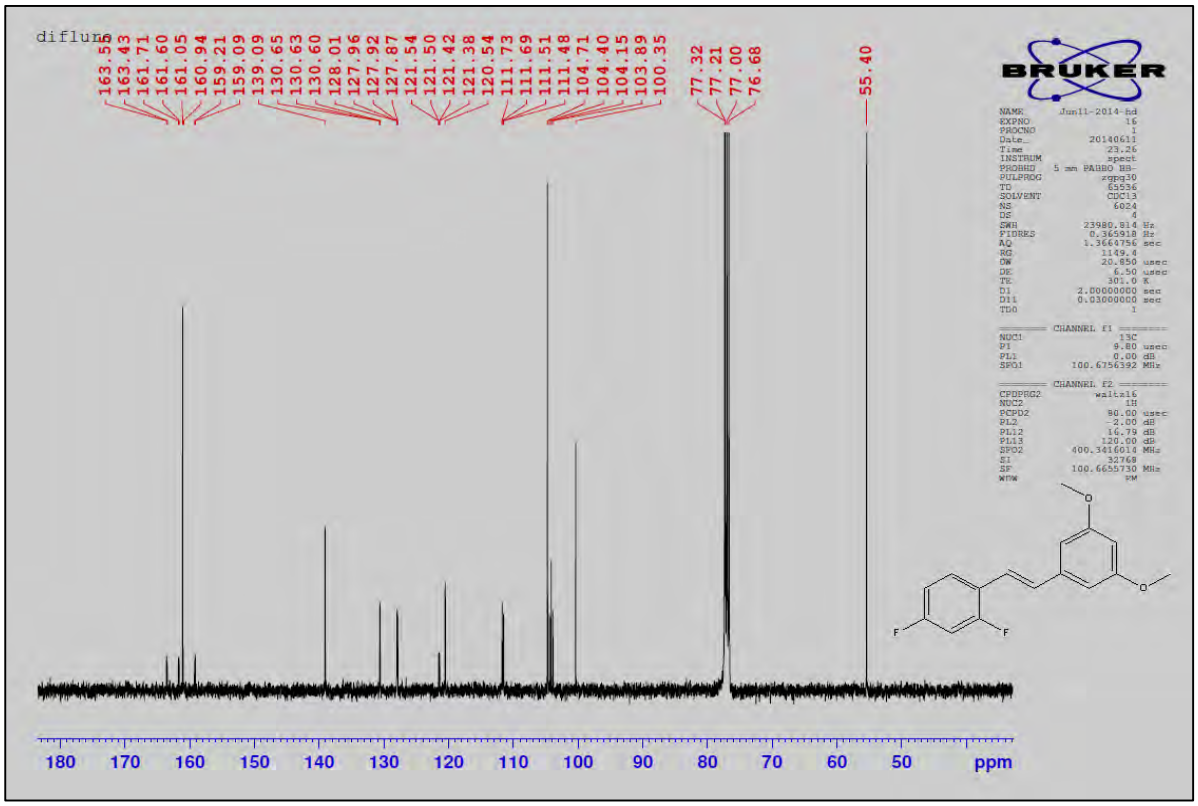

2D HSQC spectra of V6

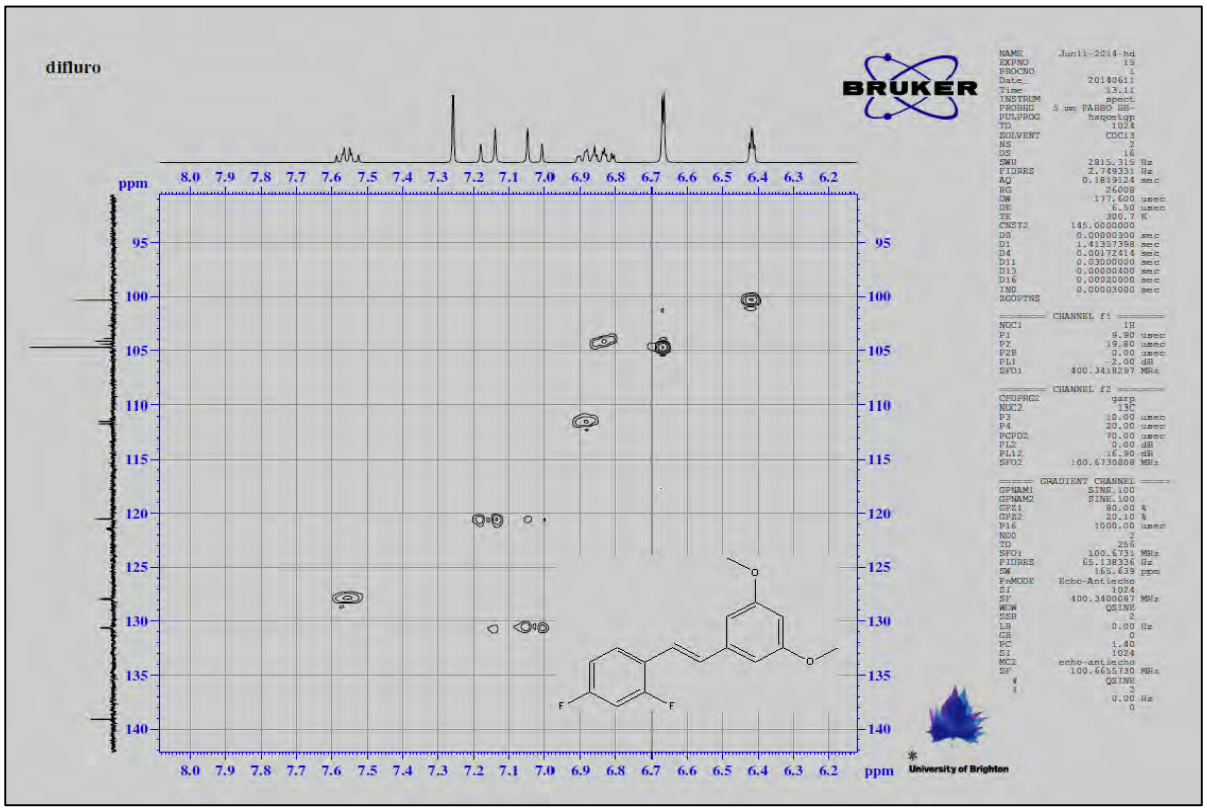

2D COSY spectra of V6

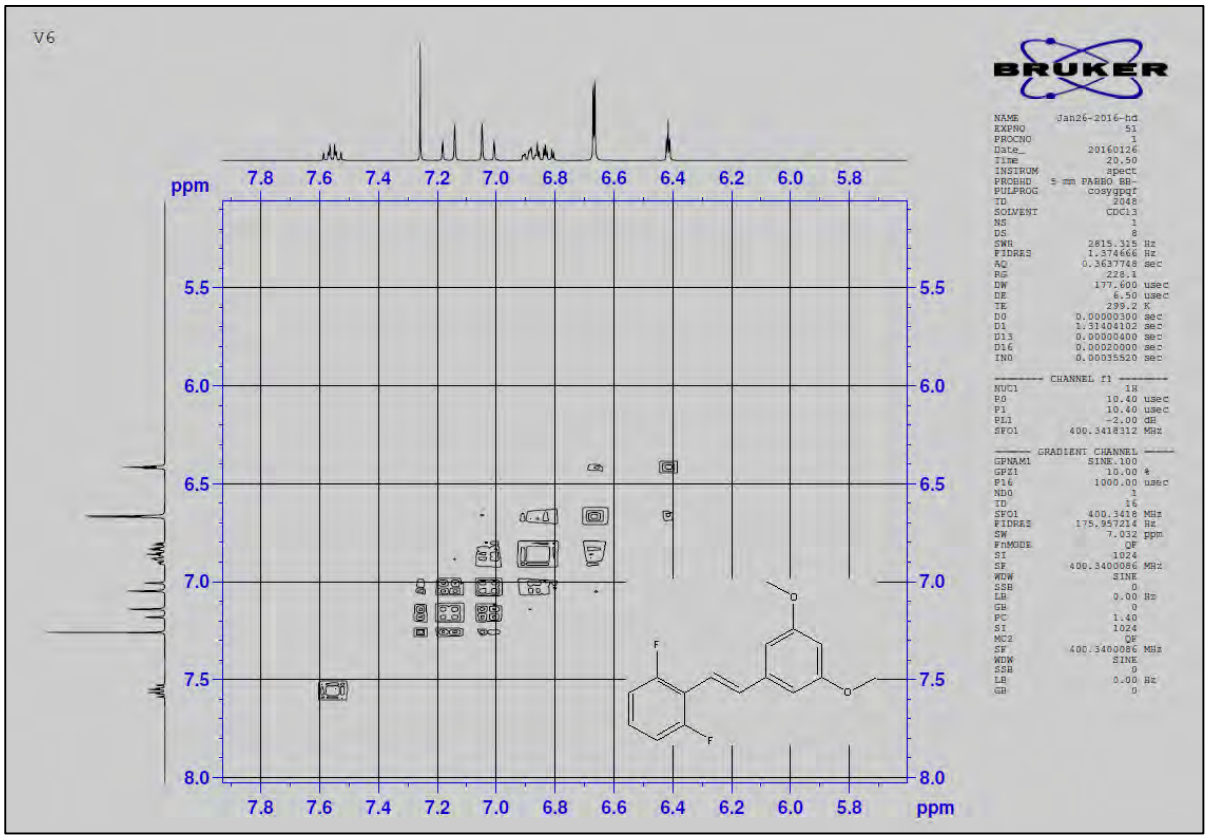

Mass spectra of V6

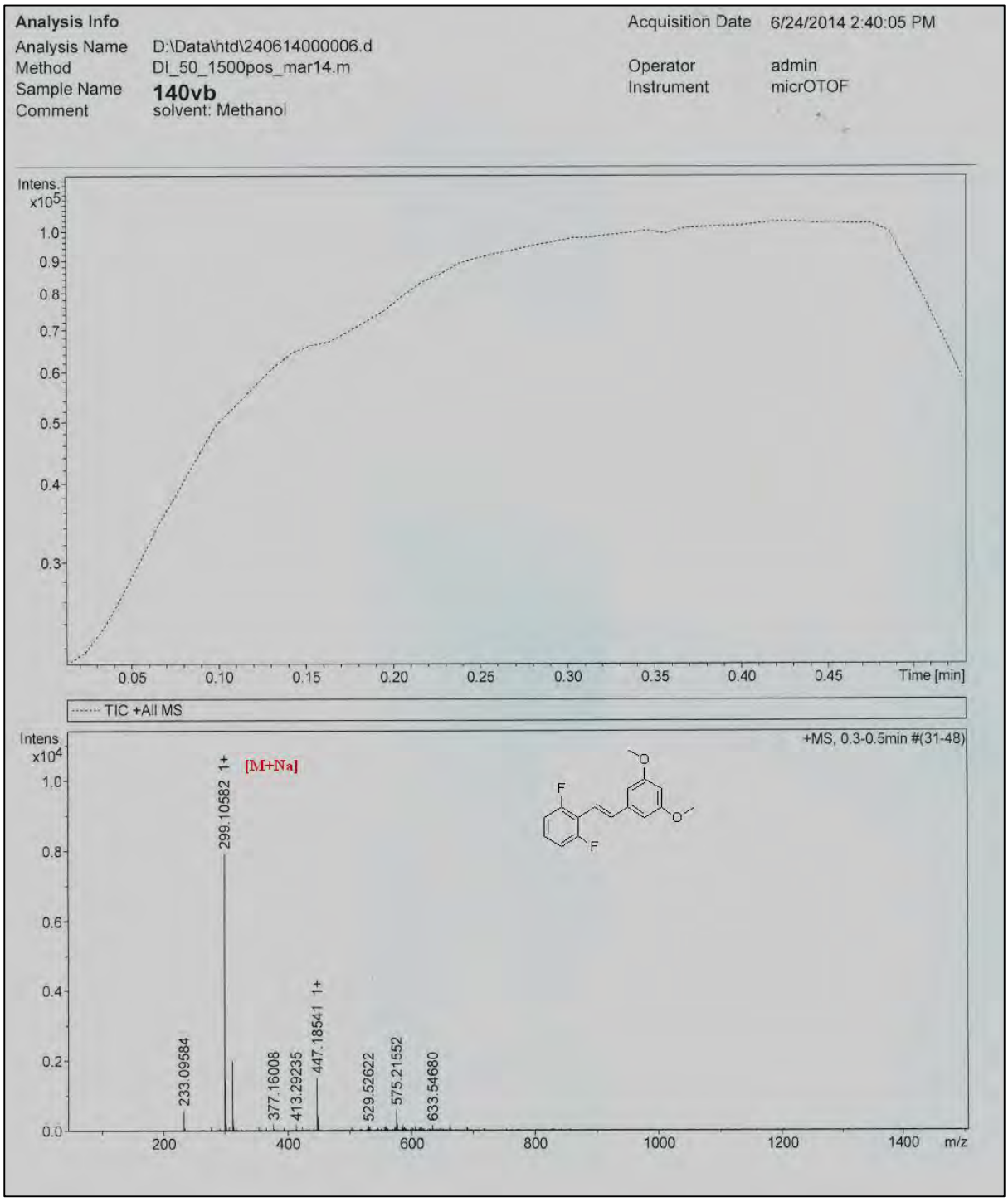

^{1}H NMR spectra of V7

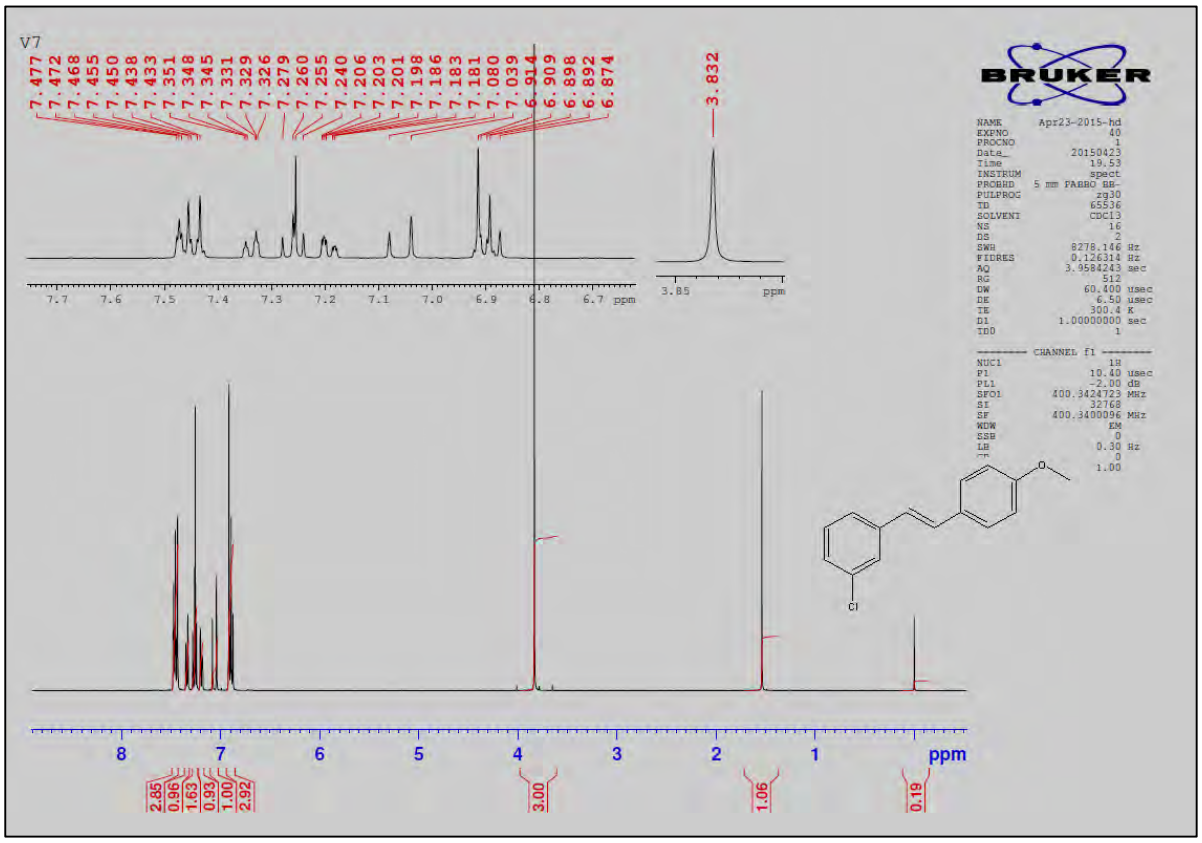

^{13}C NMR spectra of V7

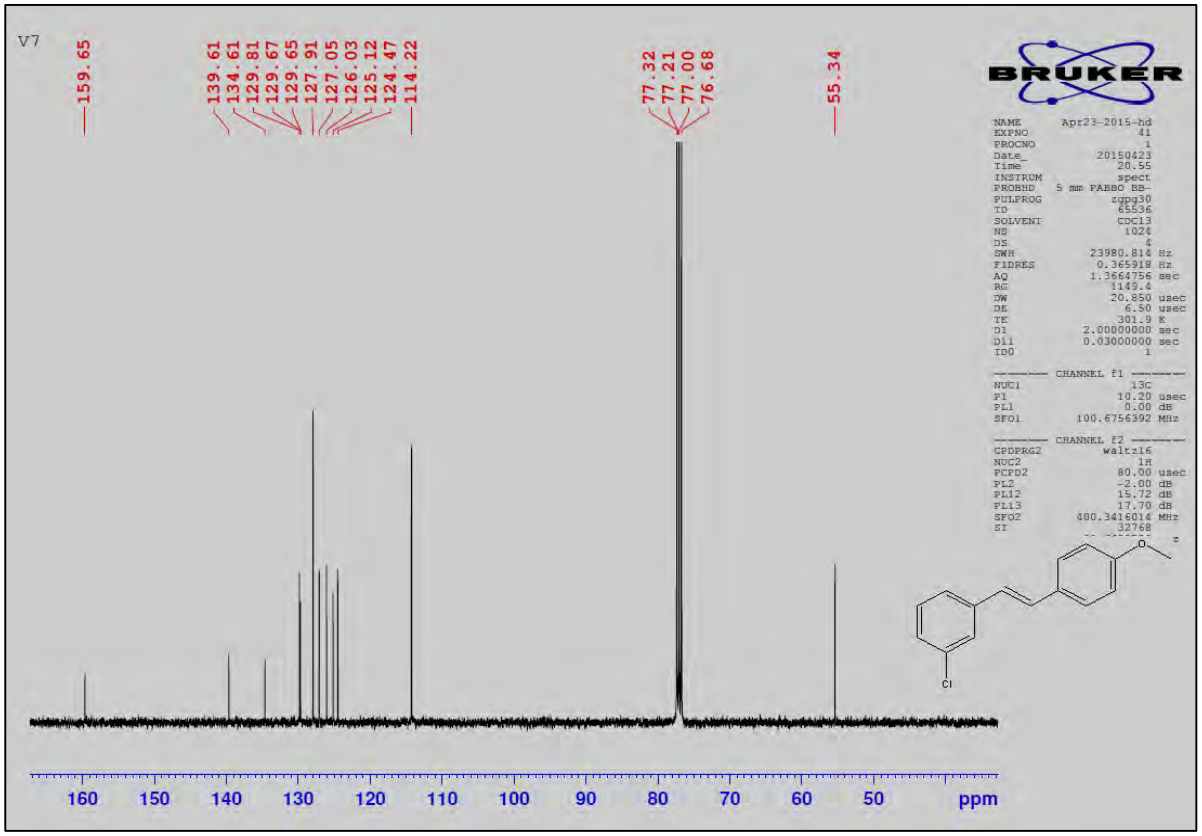

2D spectra of V7

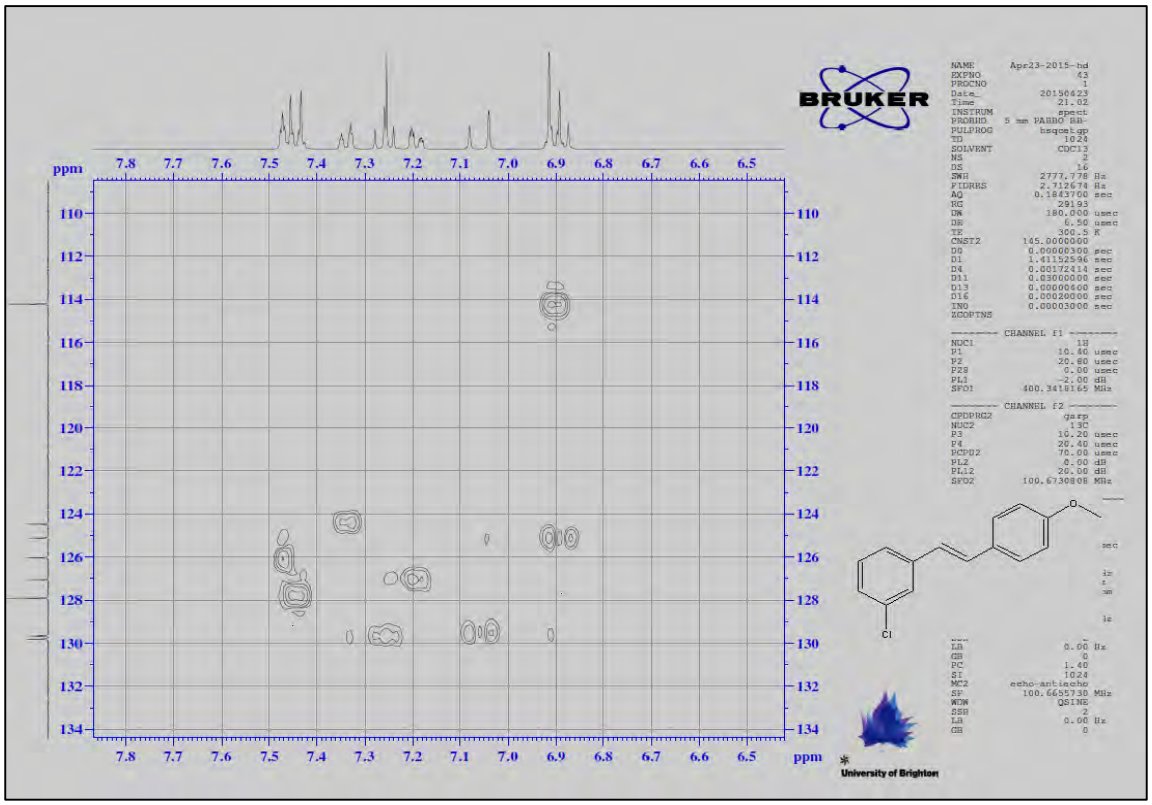

2D spectra of V7

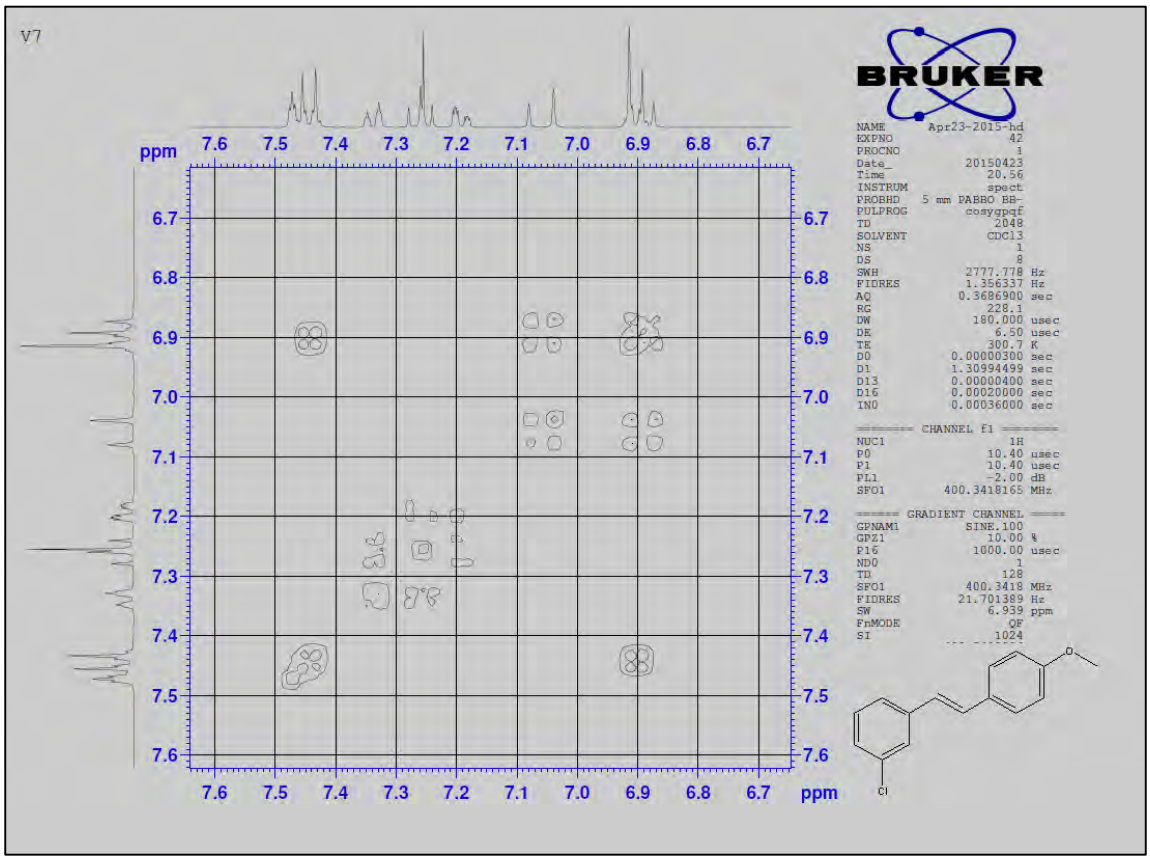

Mass spectra of V7

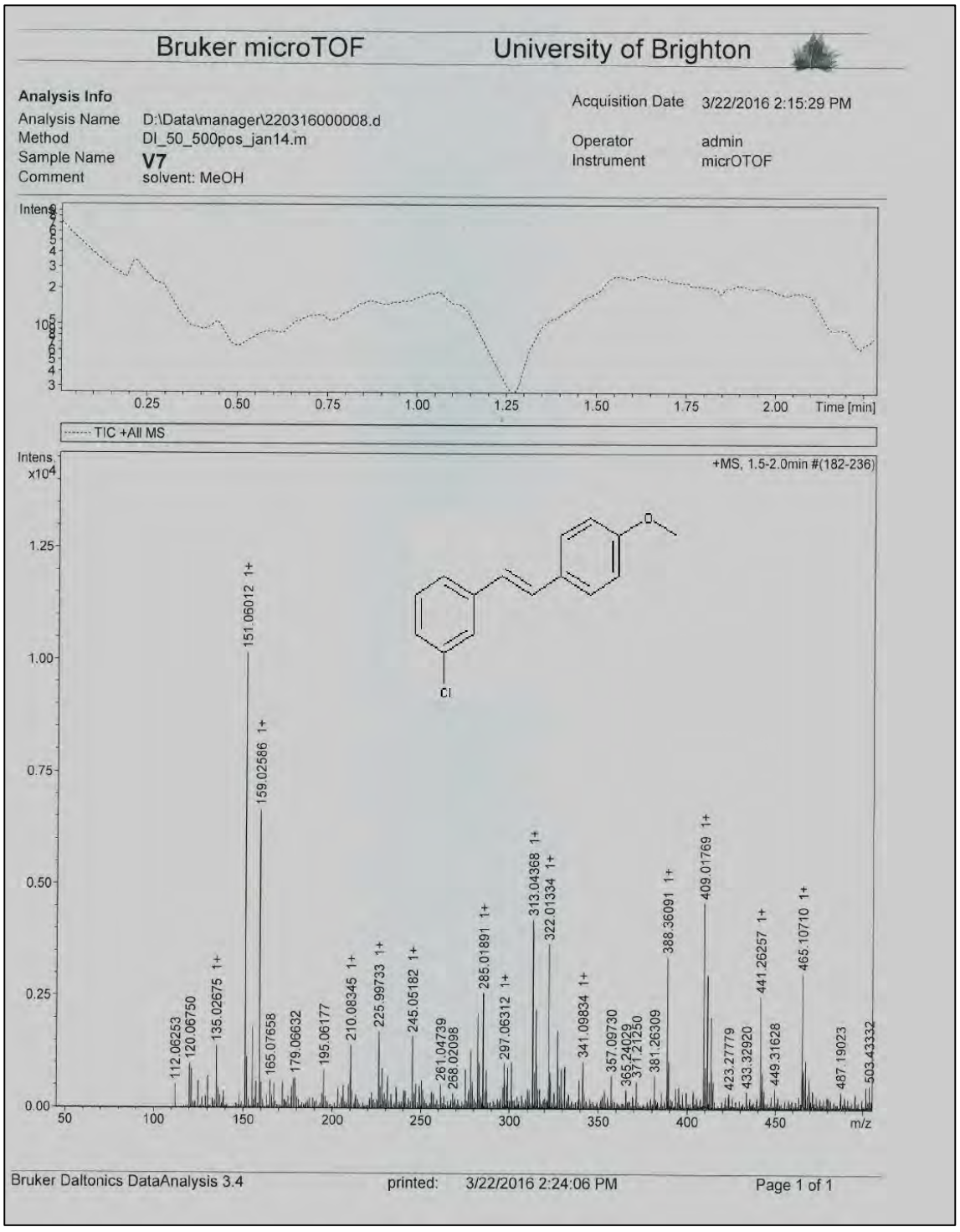

^{1}H NMR spectra of V8

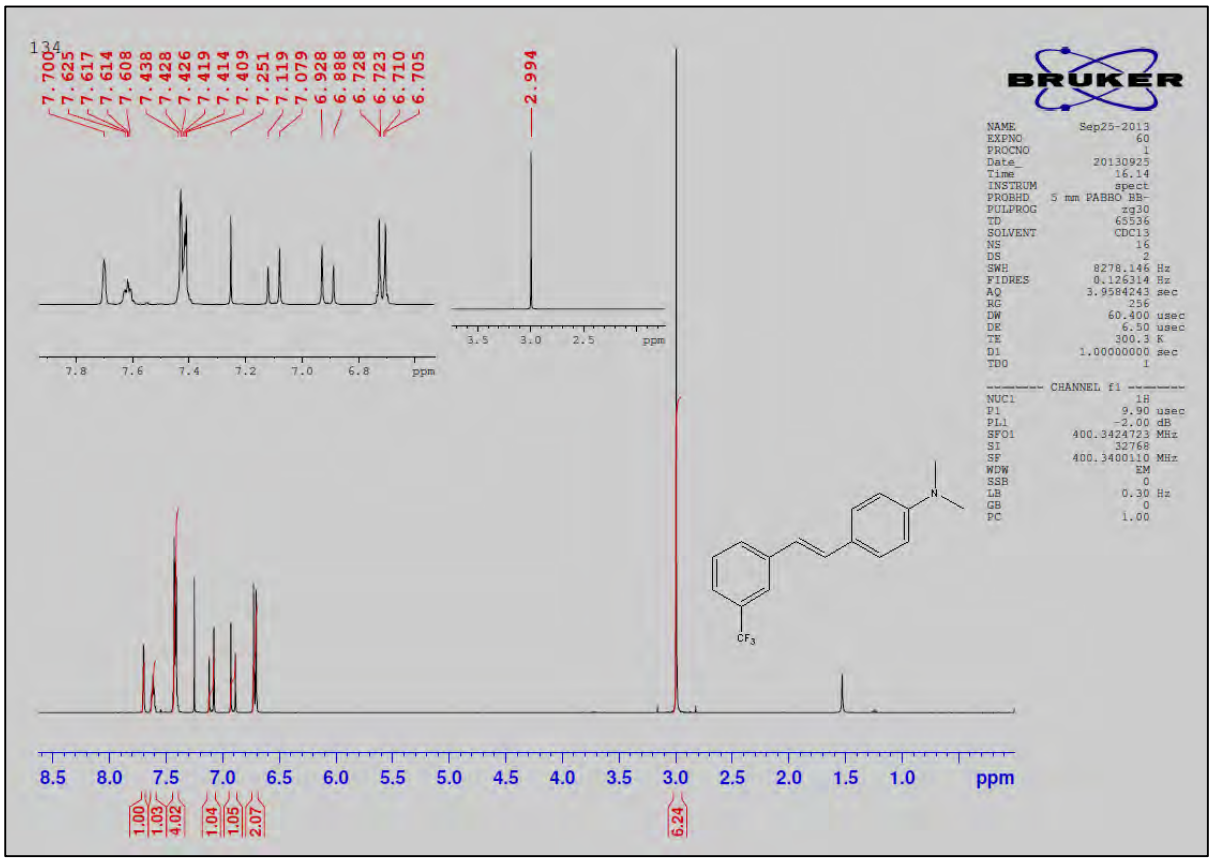

^{13}C NMR spectra of V8

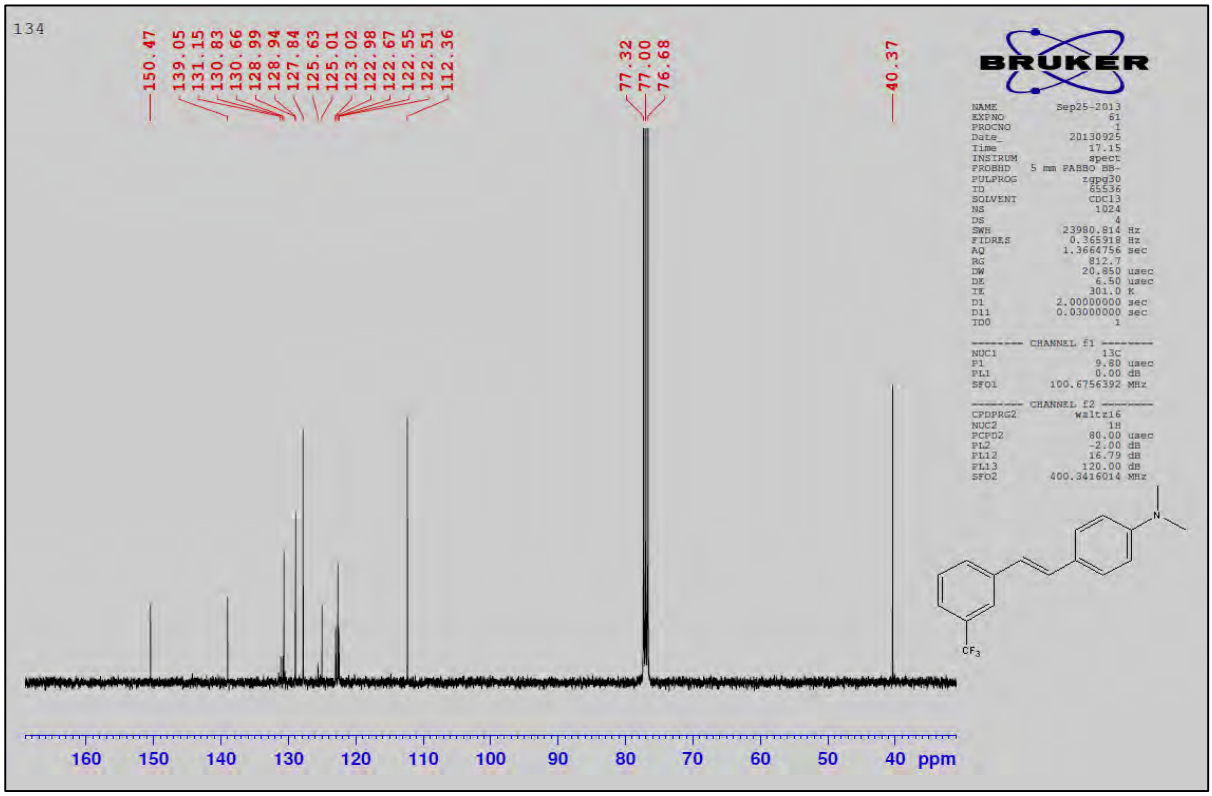

2D HSQC spectra of V8

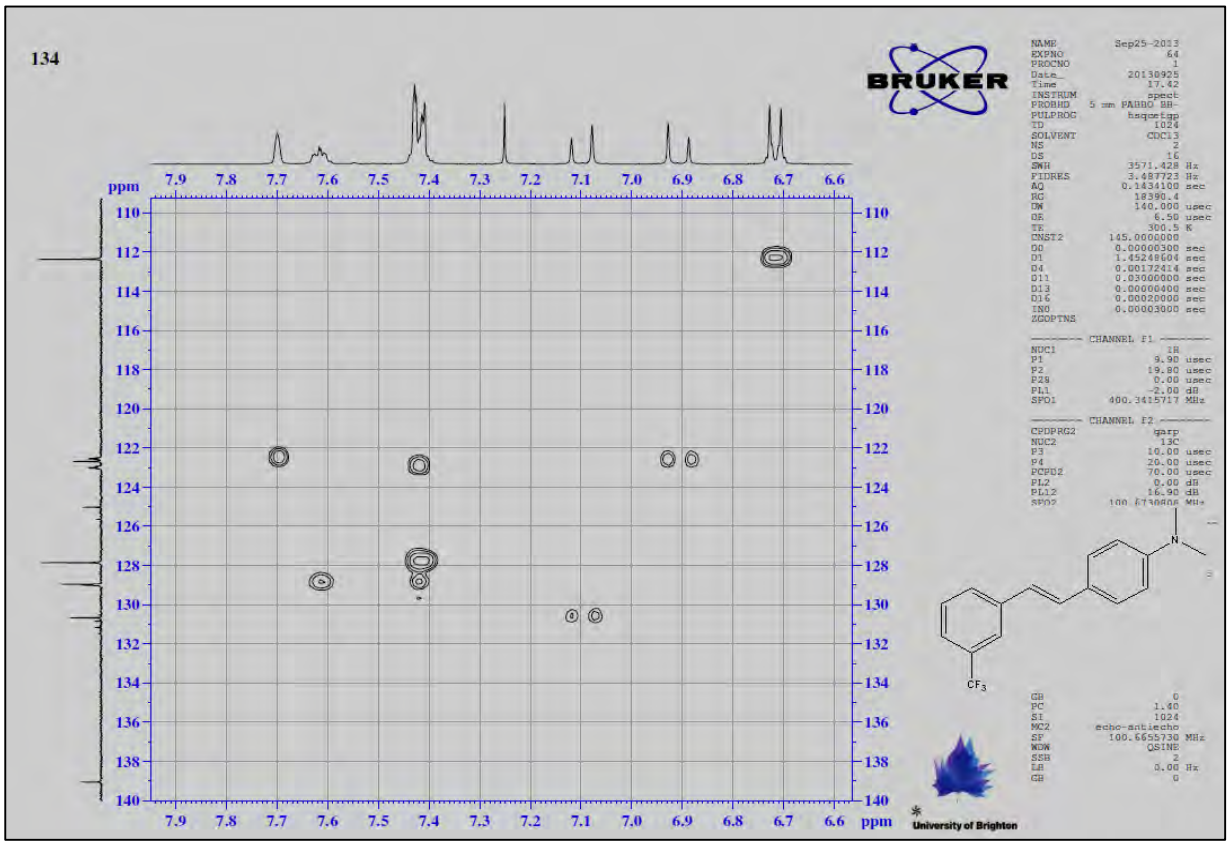

2D COSY spectra of V8

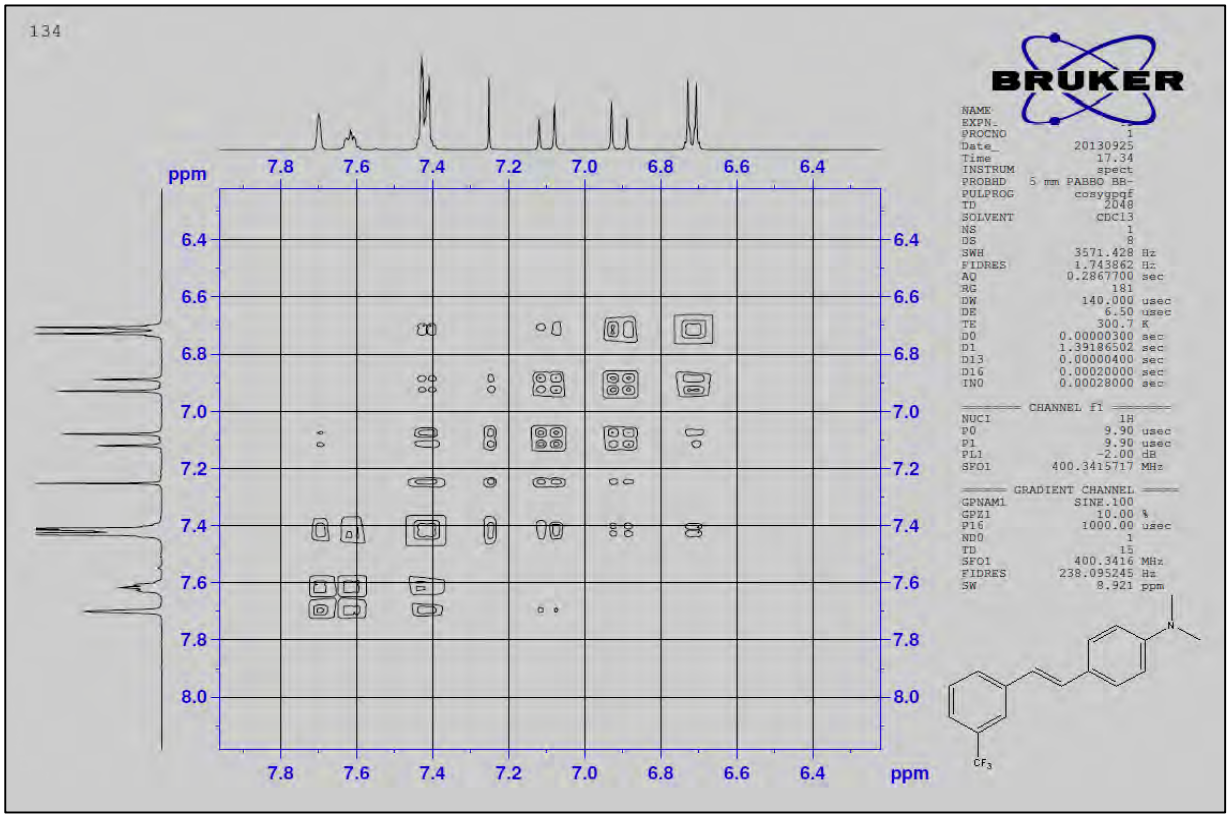

Mass spectra of V8

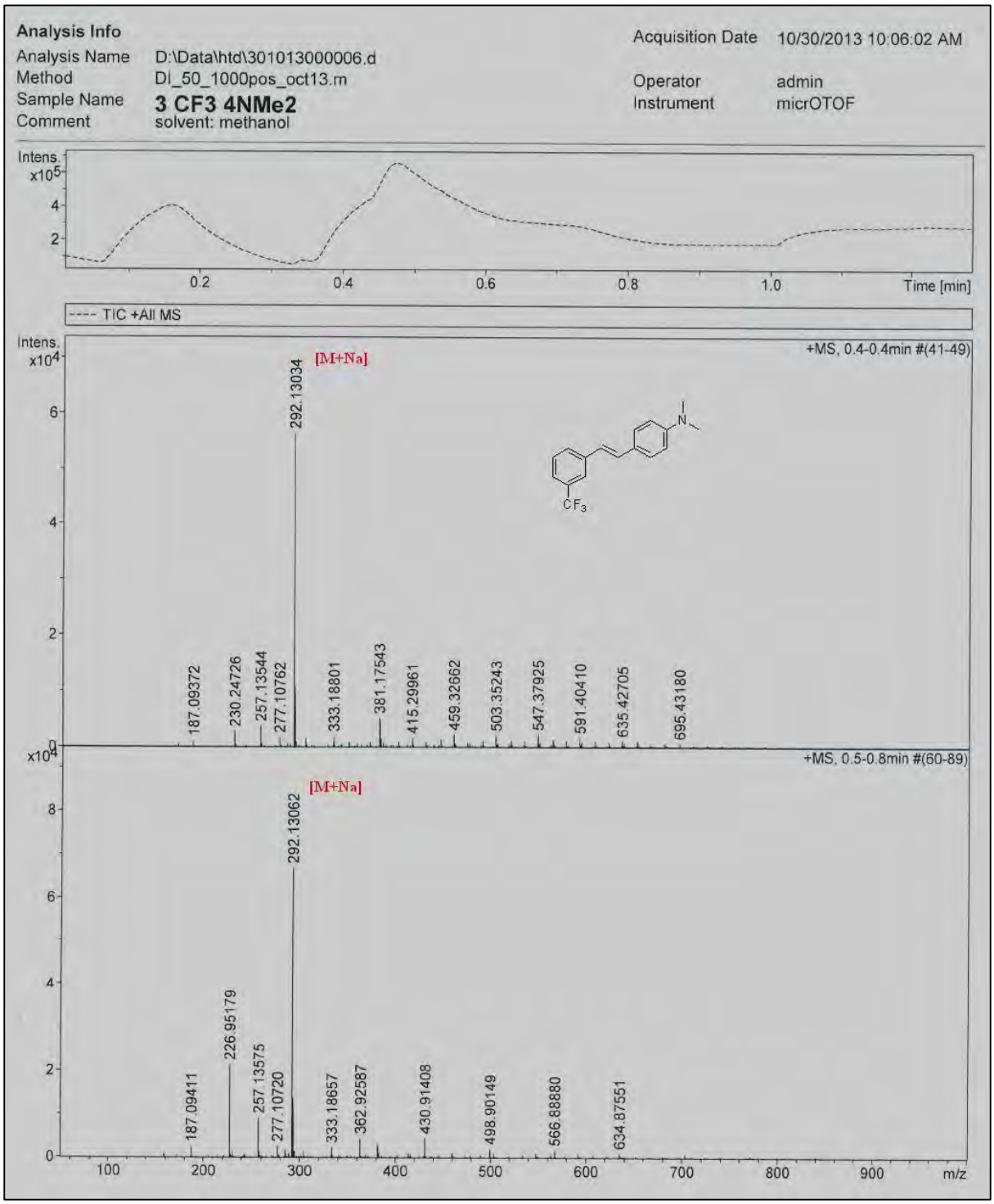

^{1}H NMR spectra of V9

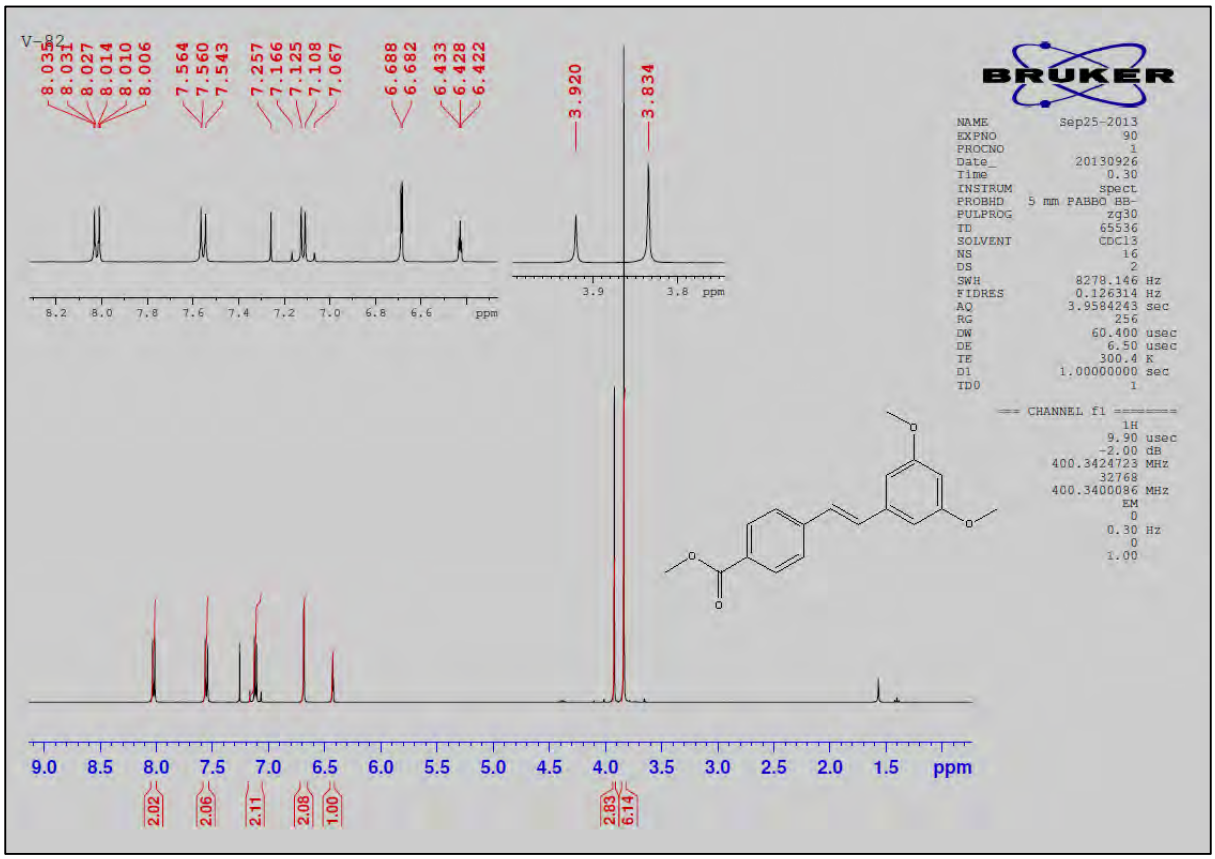

^{13}C NMR spectra of V9

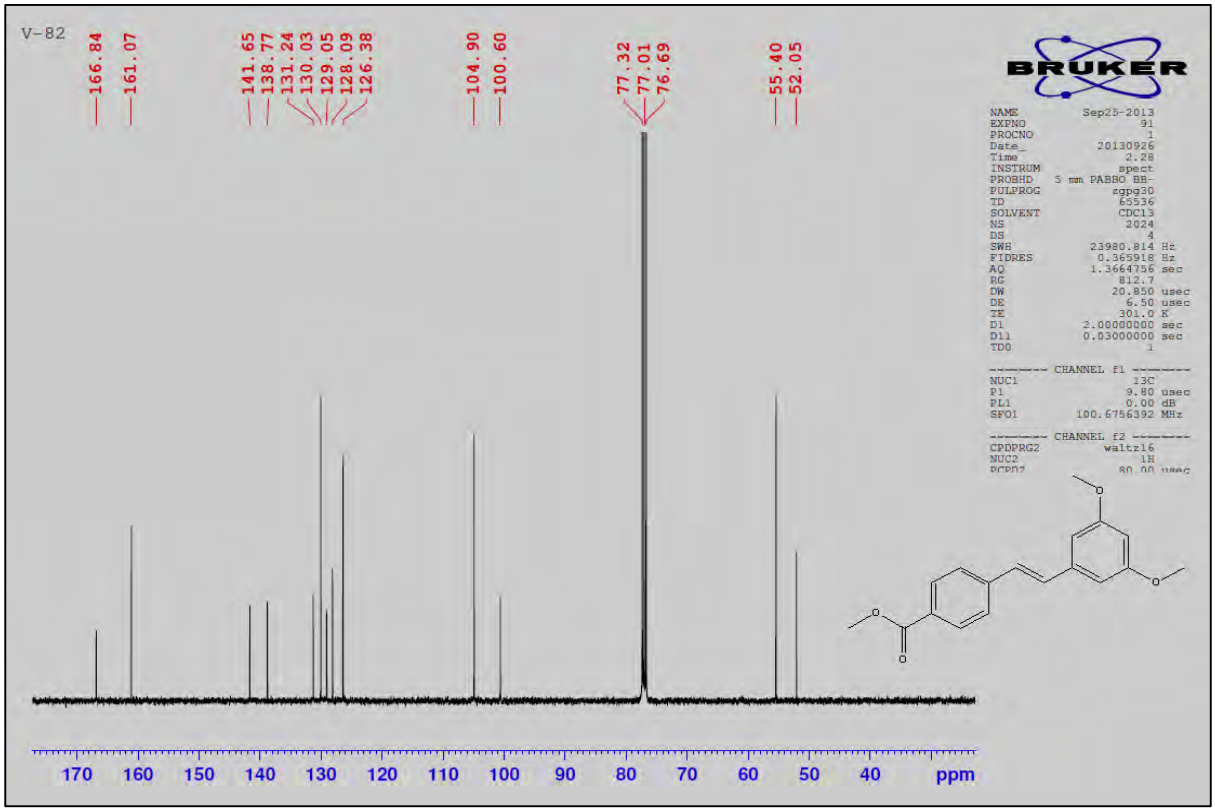

2D HSQC spectra of V9

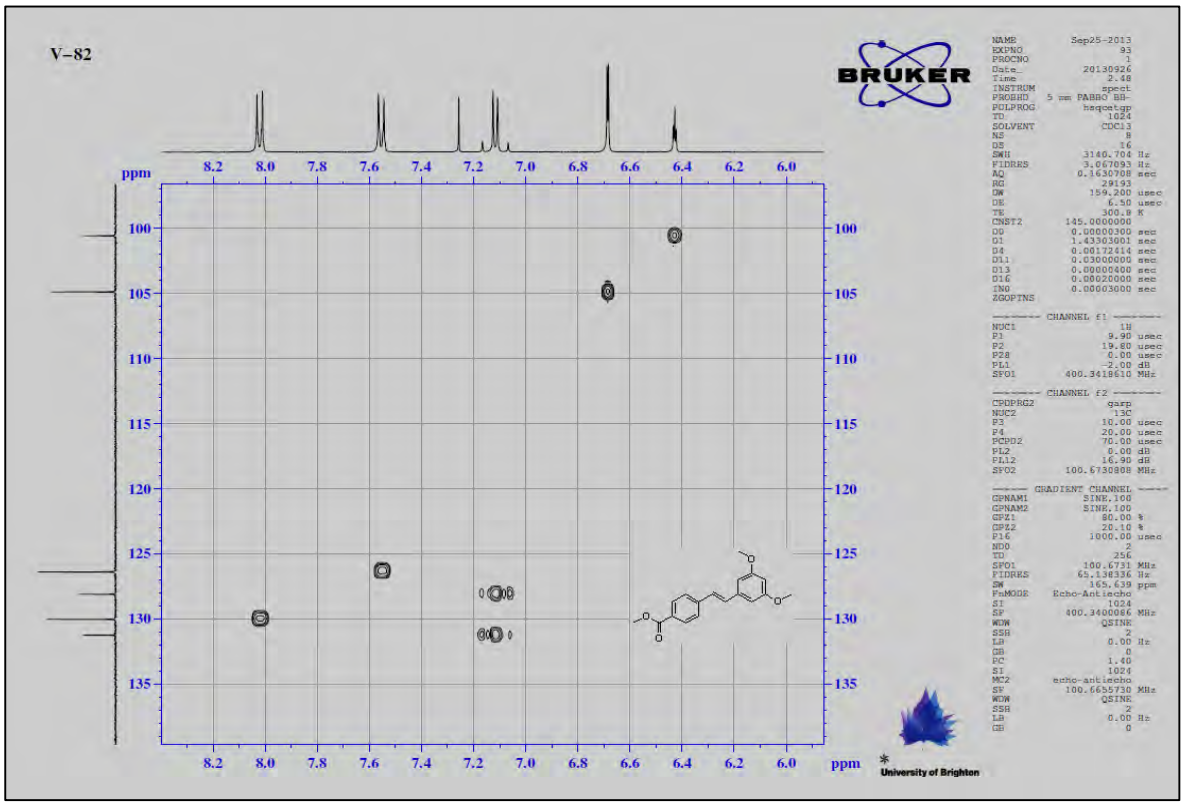

2D COSY spectra of V9

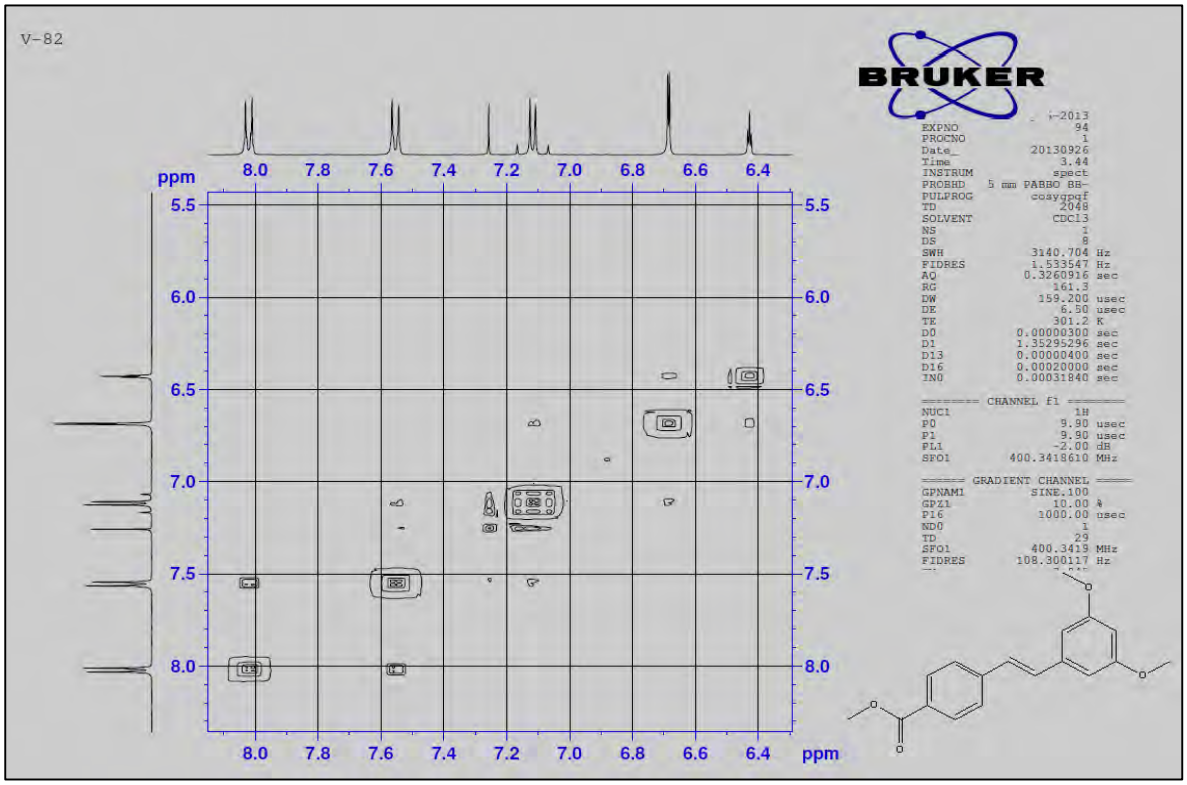

Mass spectra of V9

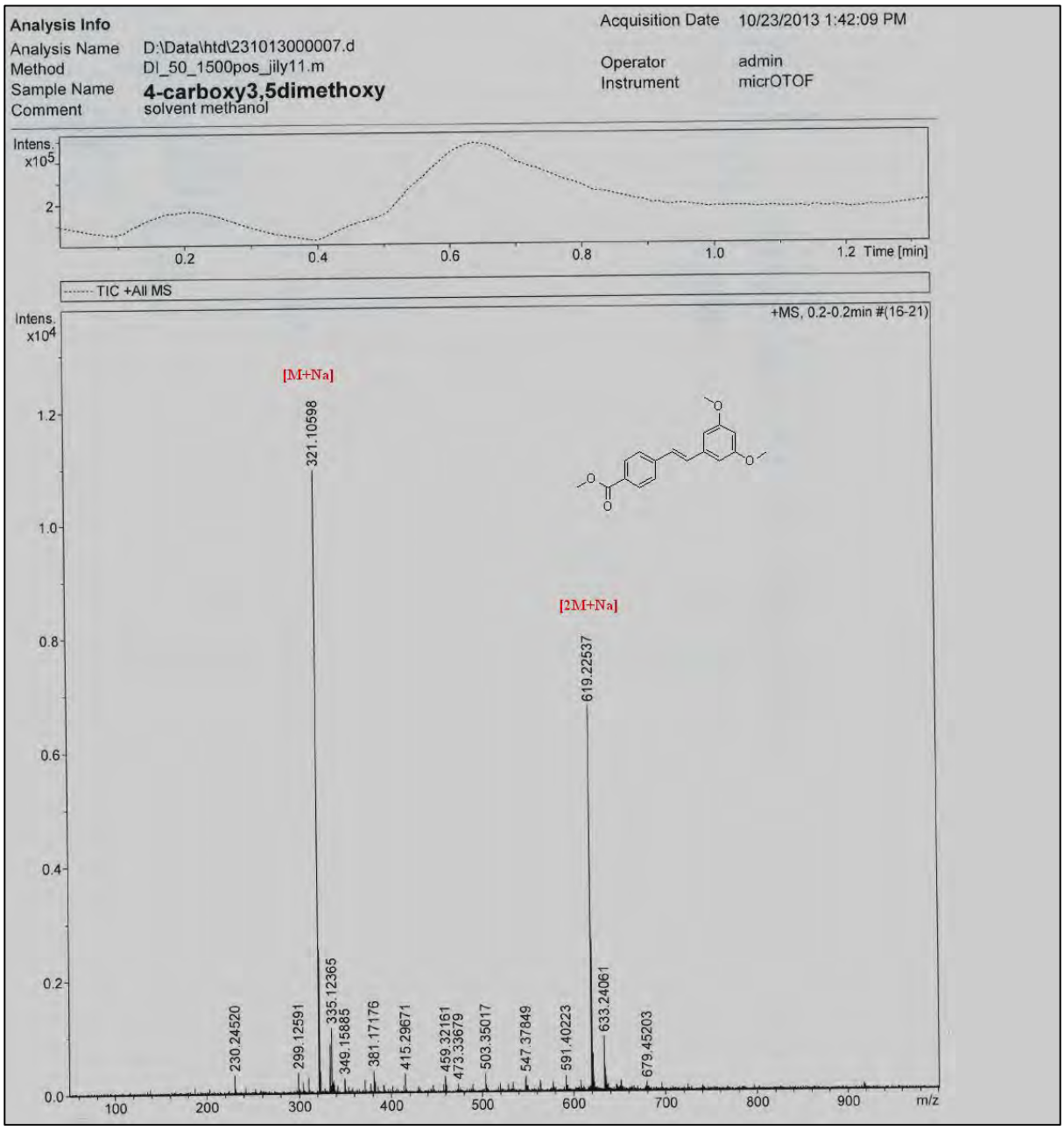

^{1}H NMR spectra of V10

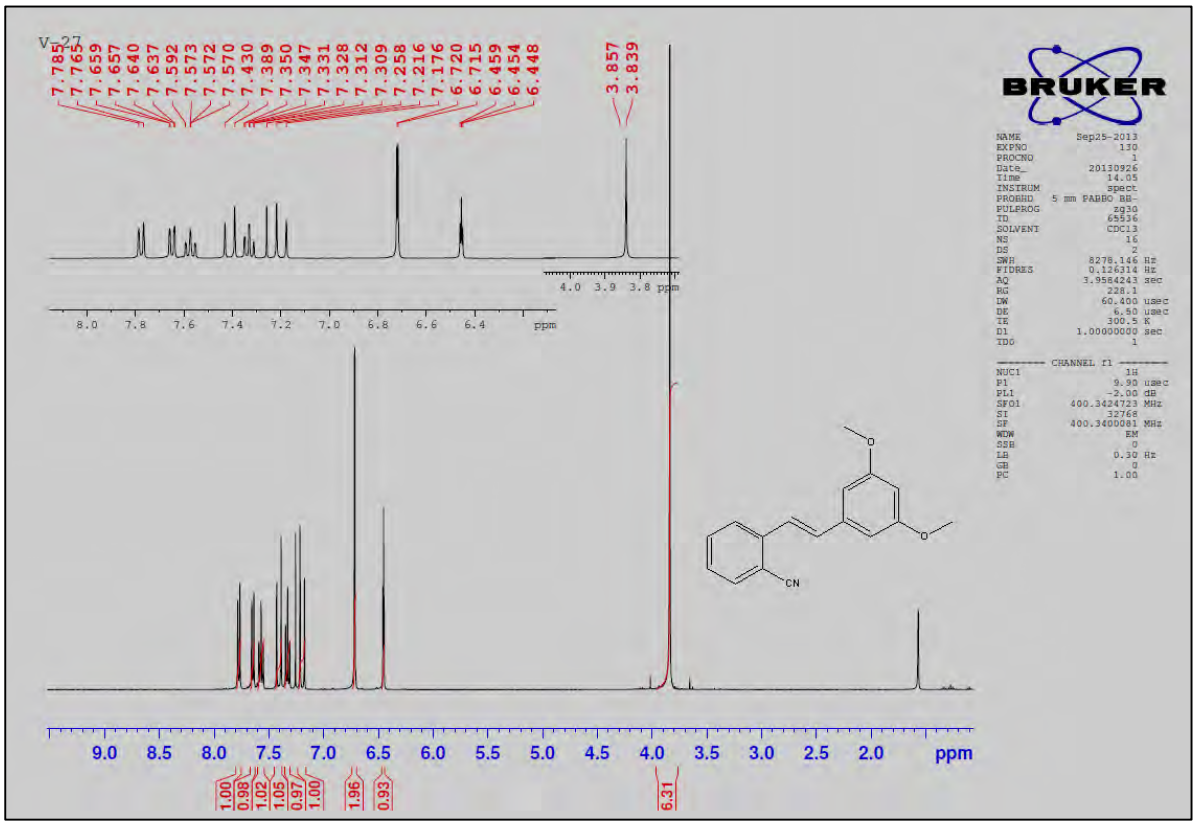

^{13}C NMR spectra of V10

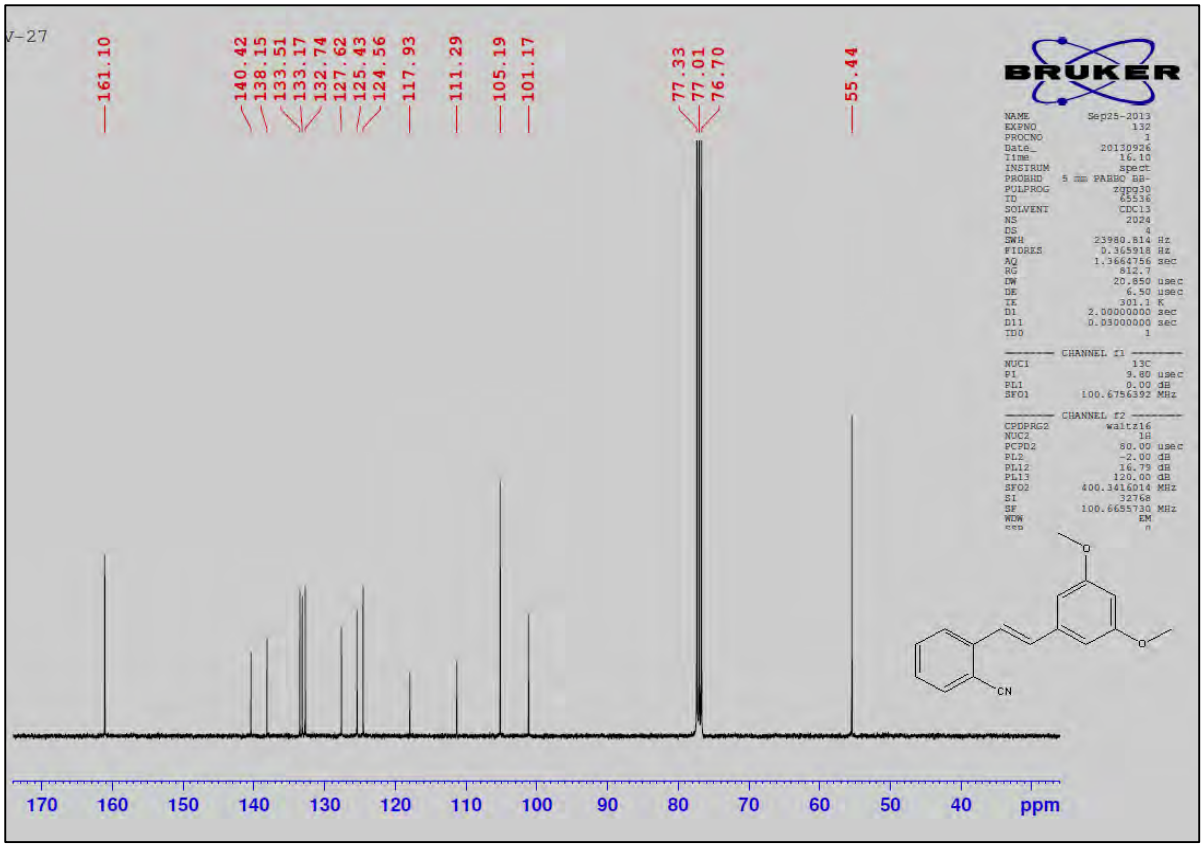

2D HSQC spectra of V10

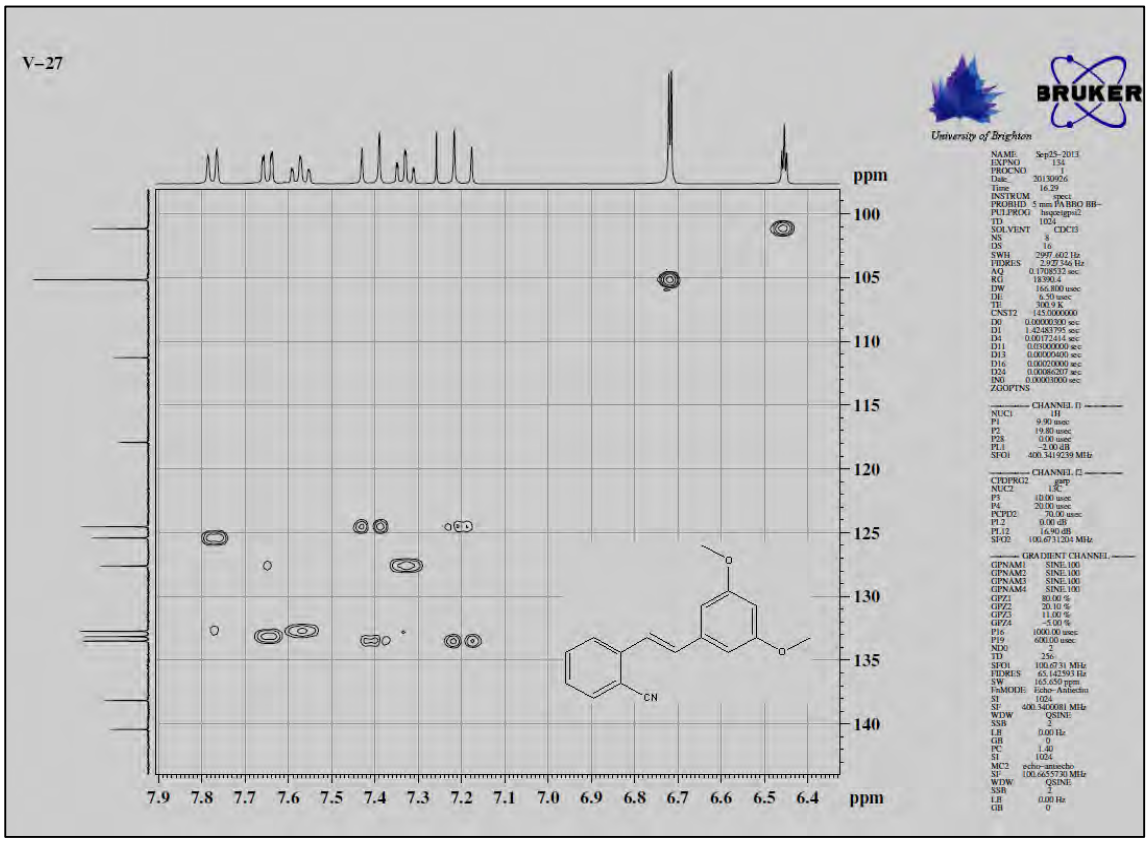

2D COSY spectra of V10

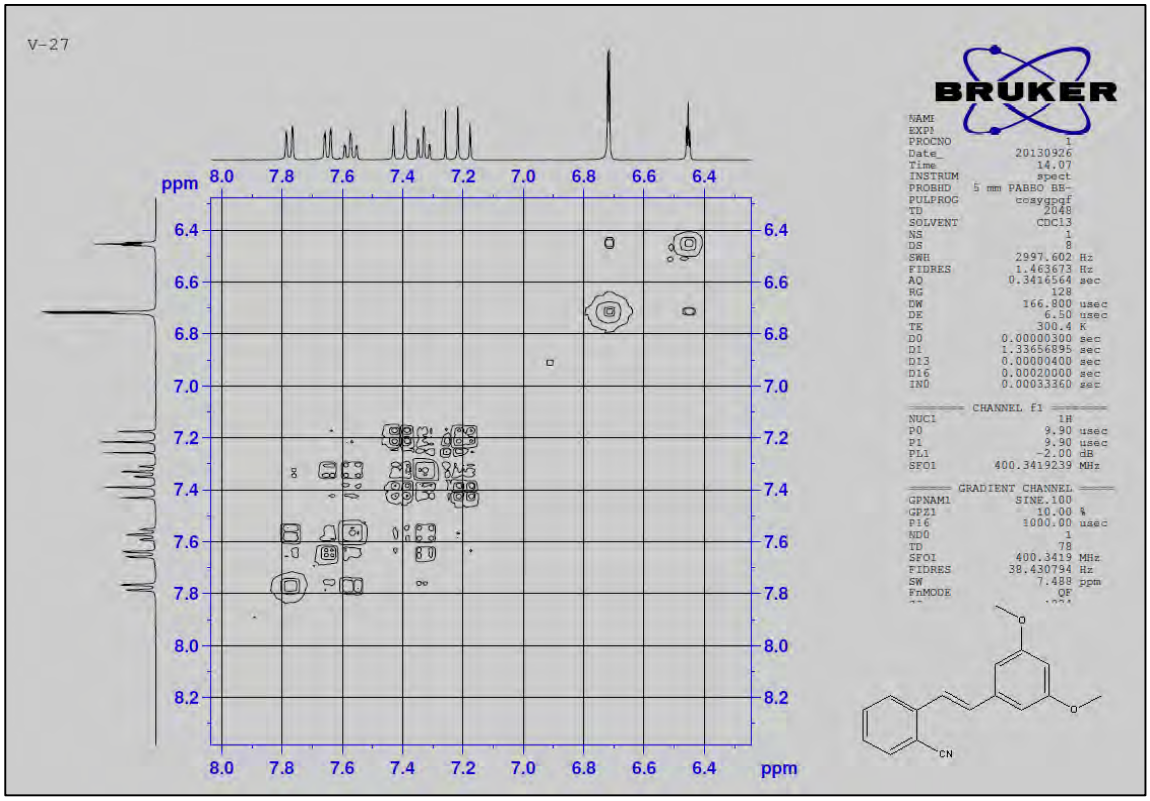

Mass spectra of V10

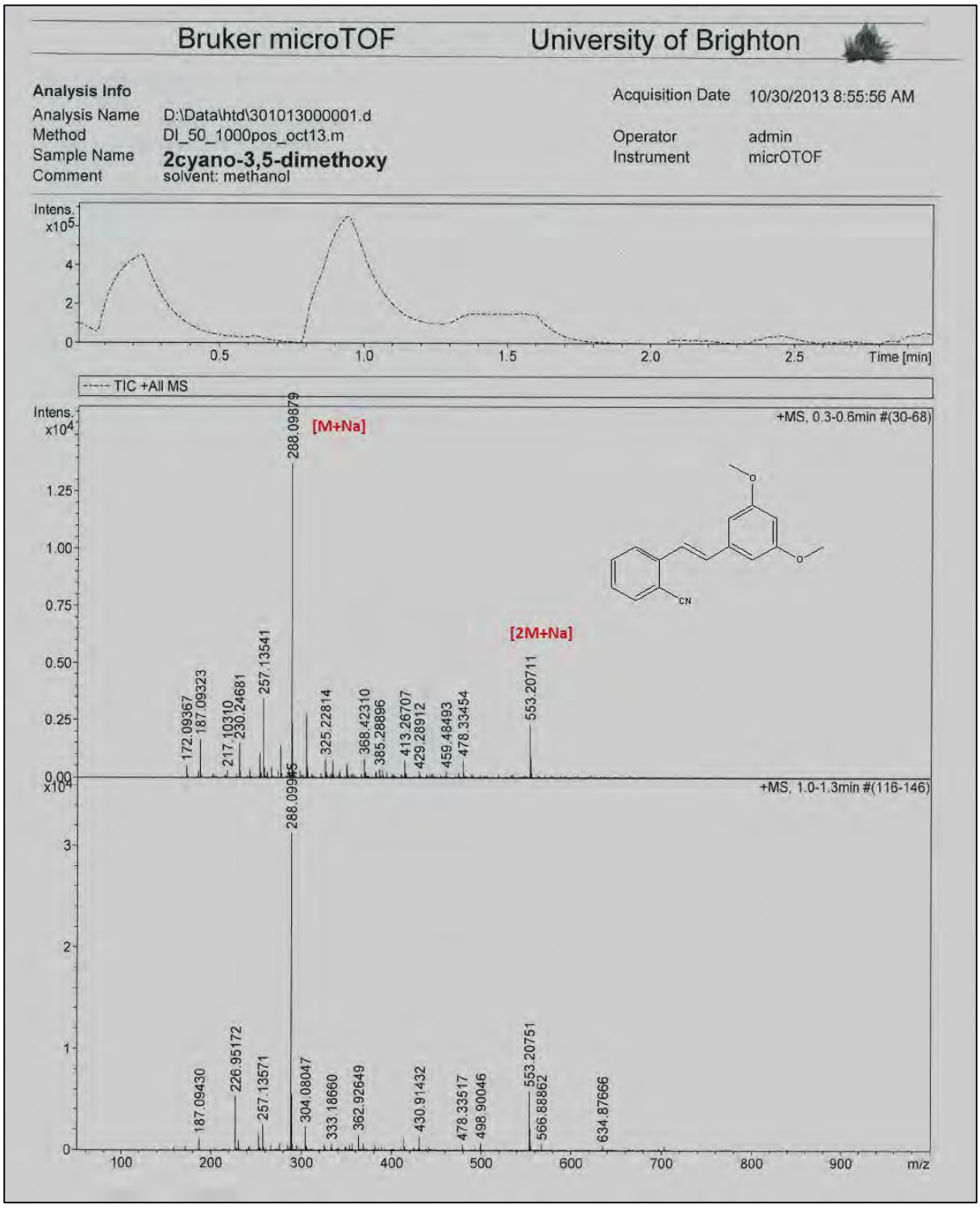

^{1}H NMR spectra of V11

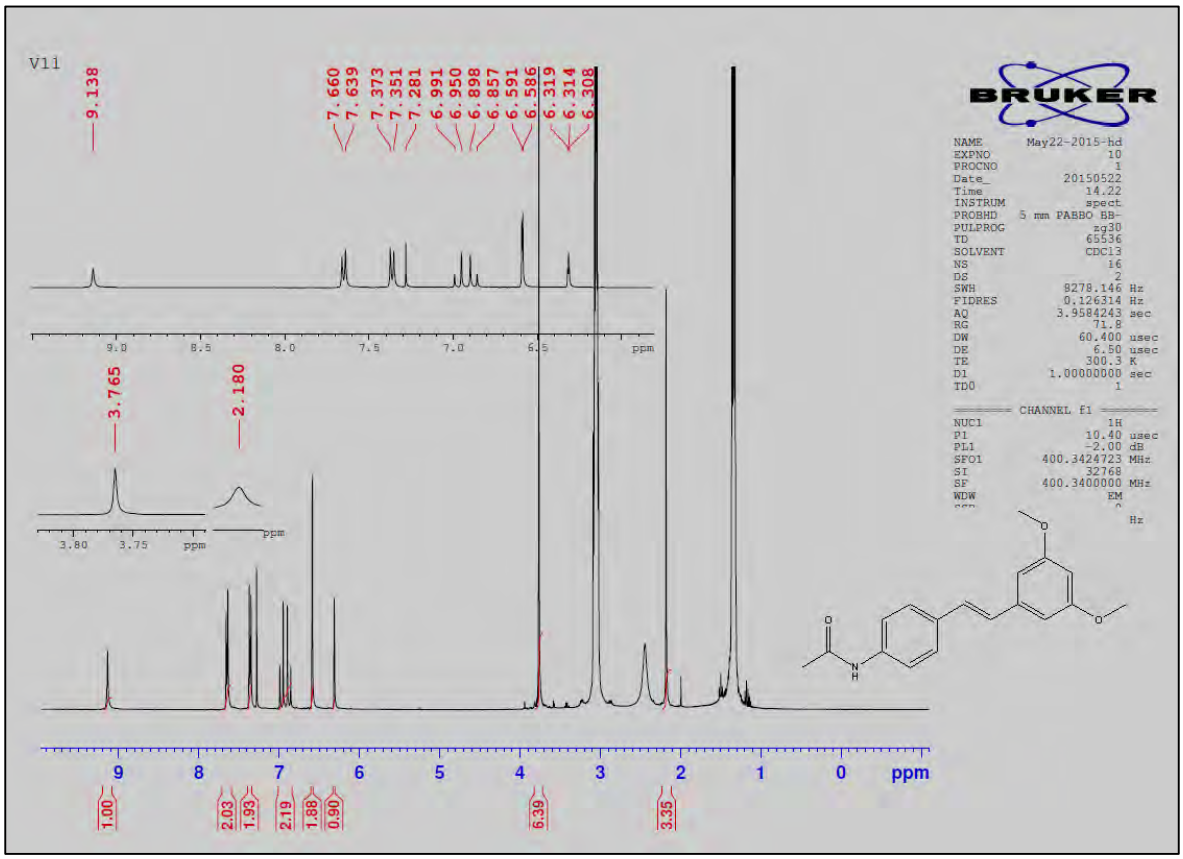

^{13}C NMR spectra of V11

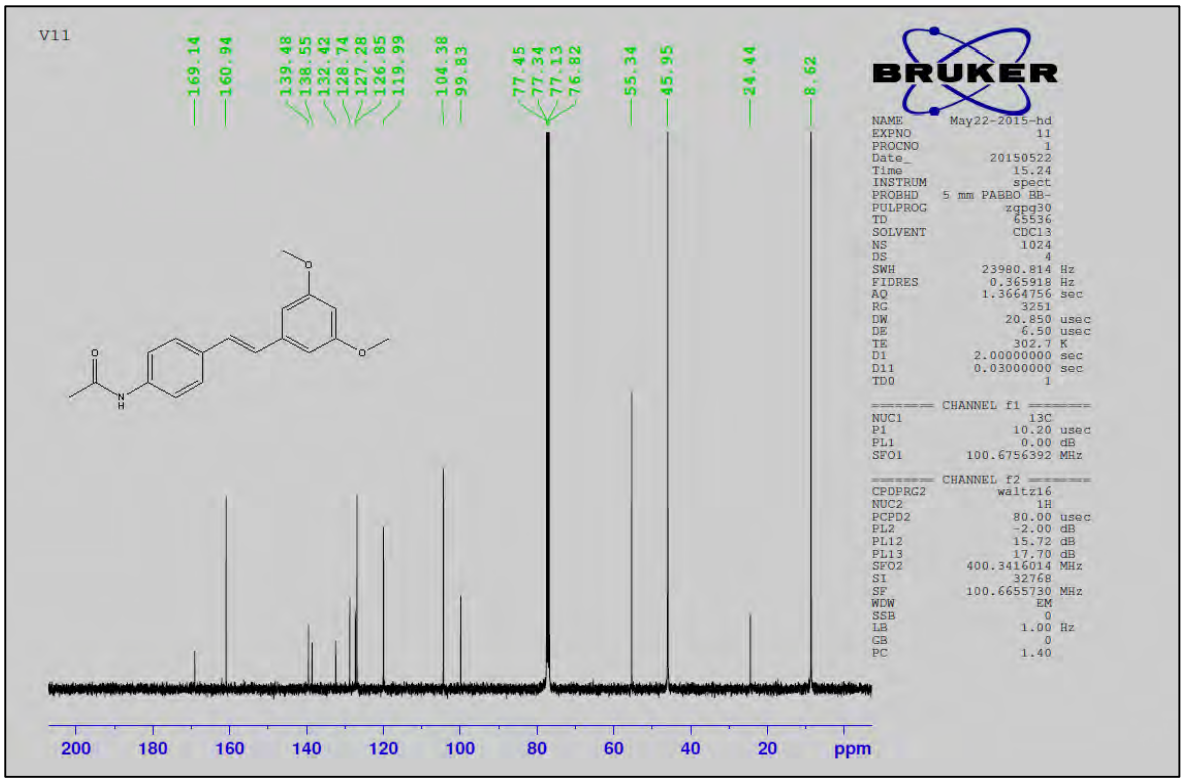

2D HSQC spectra of V11

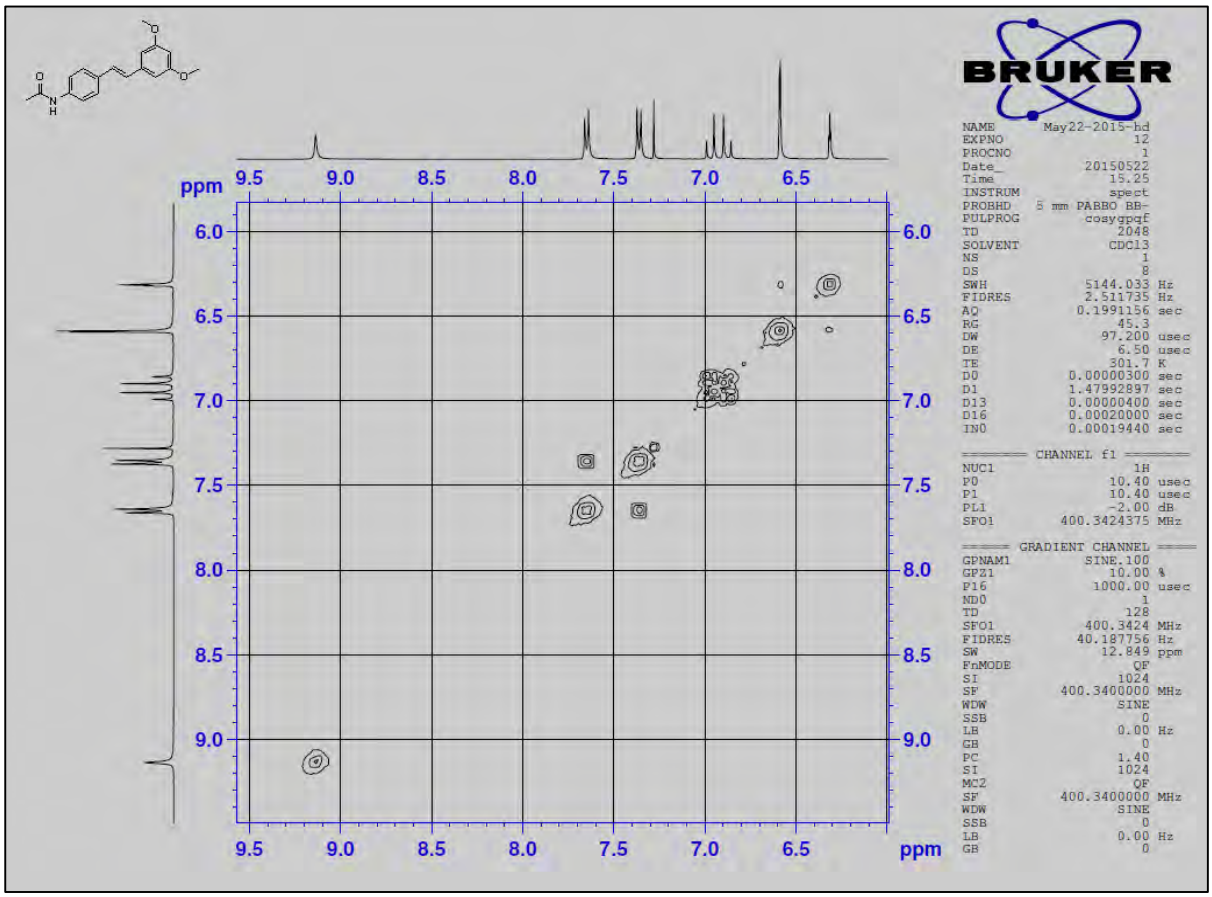

2D COSY spectra of V11

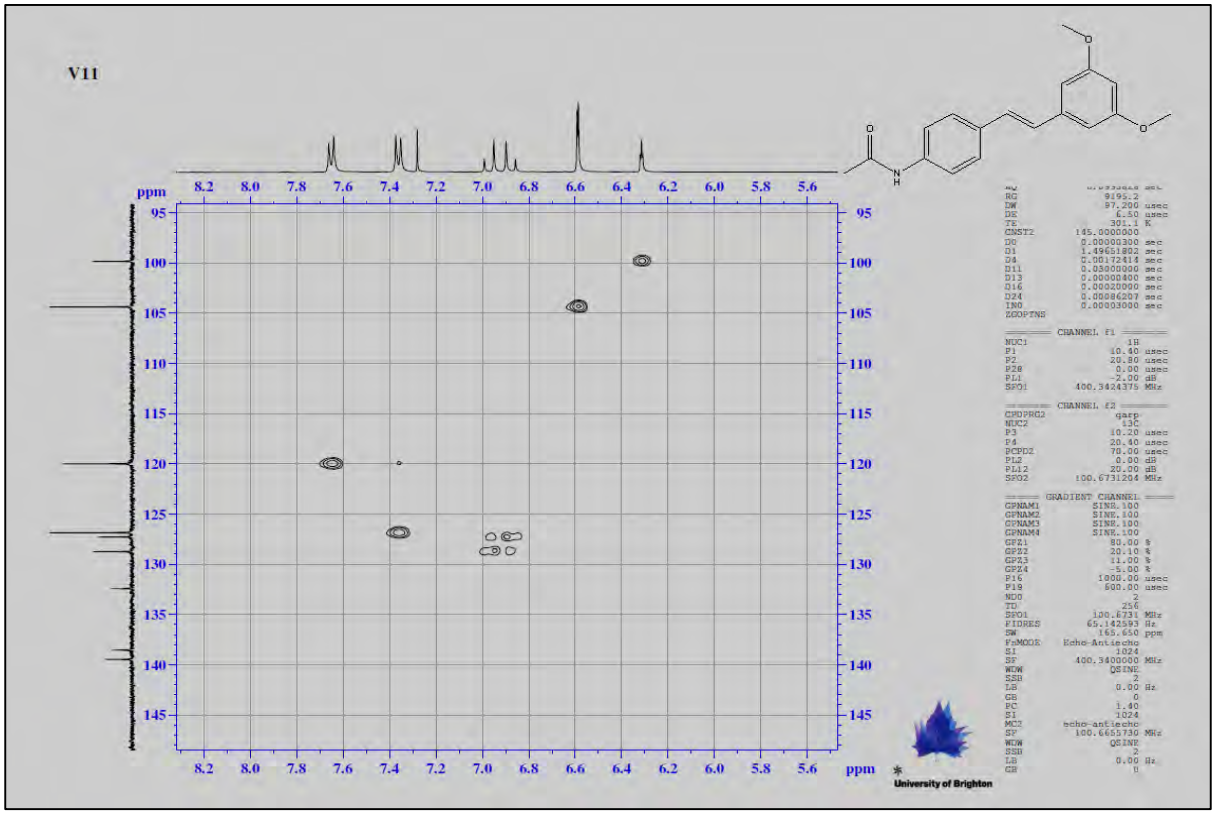

Mass spectra of V11

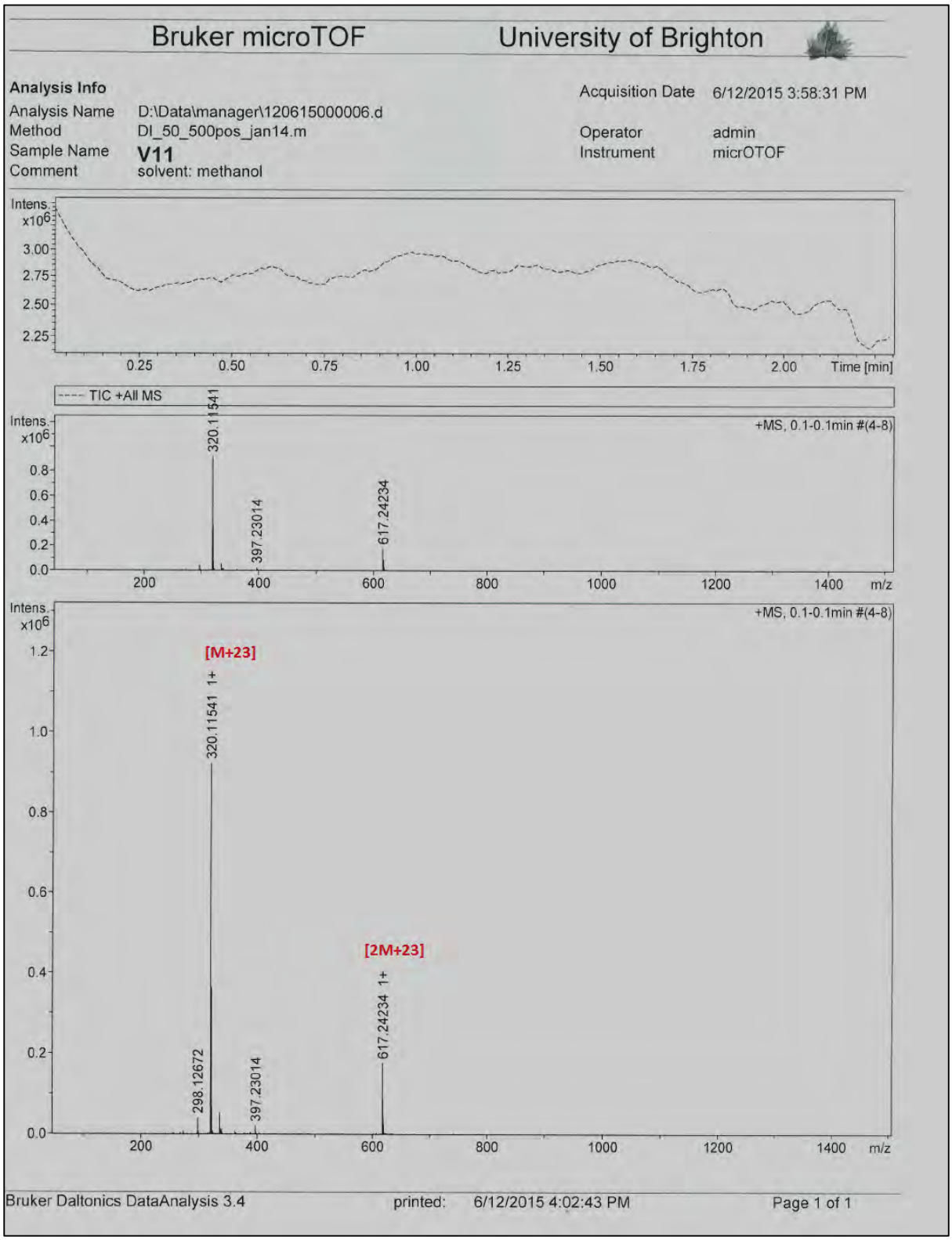

^{1}H NMR spectra of V12

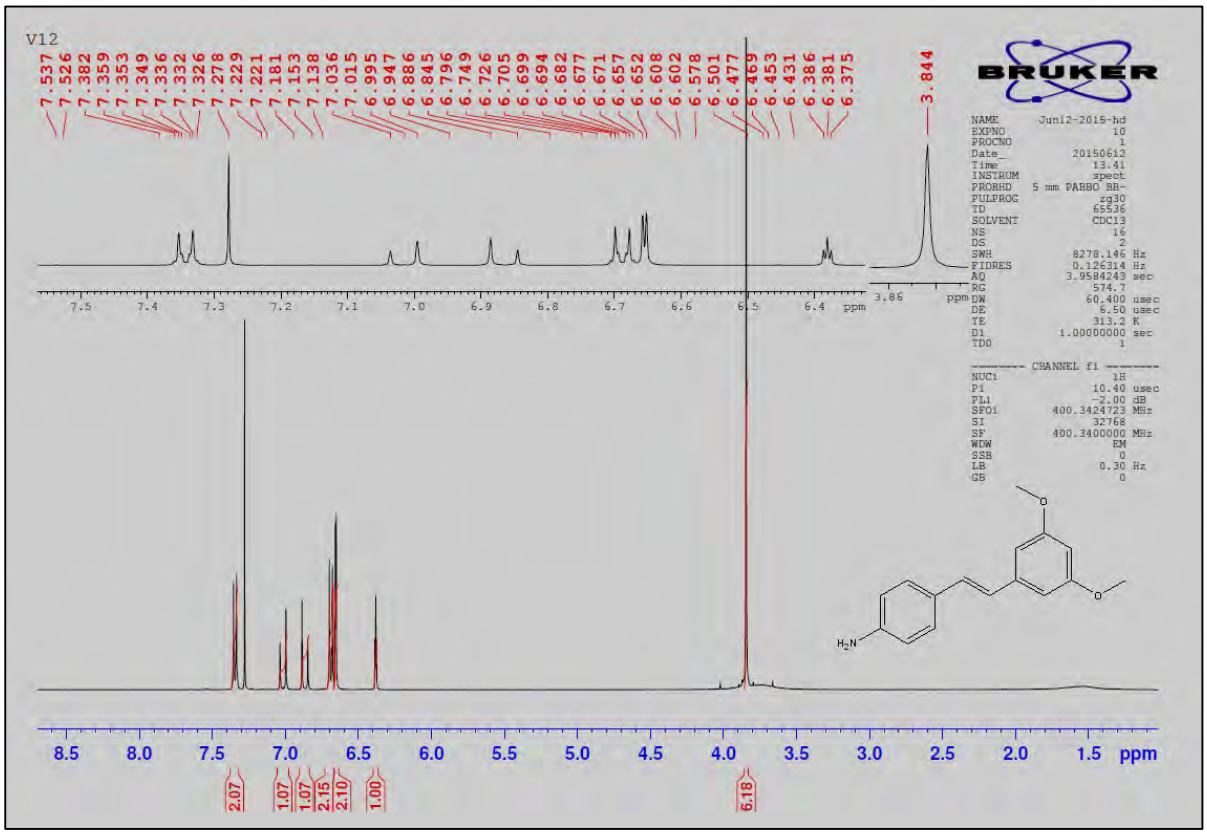

^{13}C NMR spectra of V12

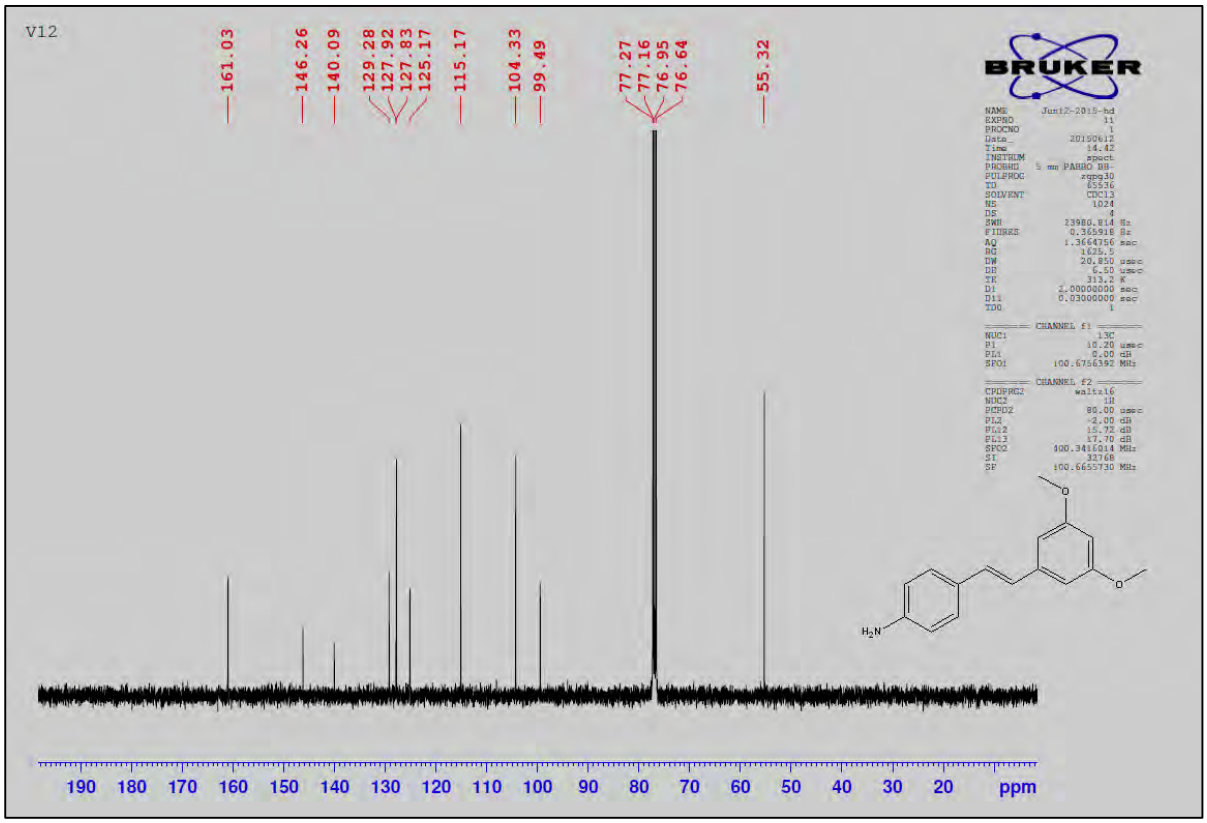

2D HSQC spectra of V12

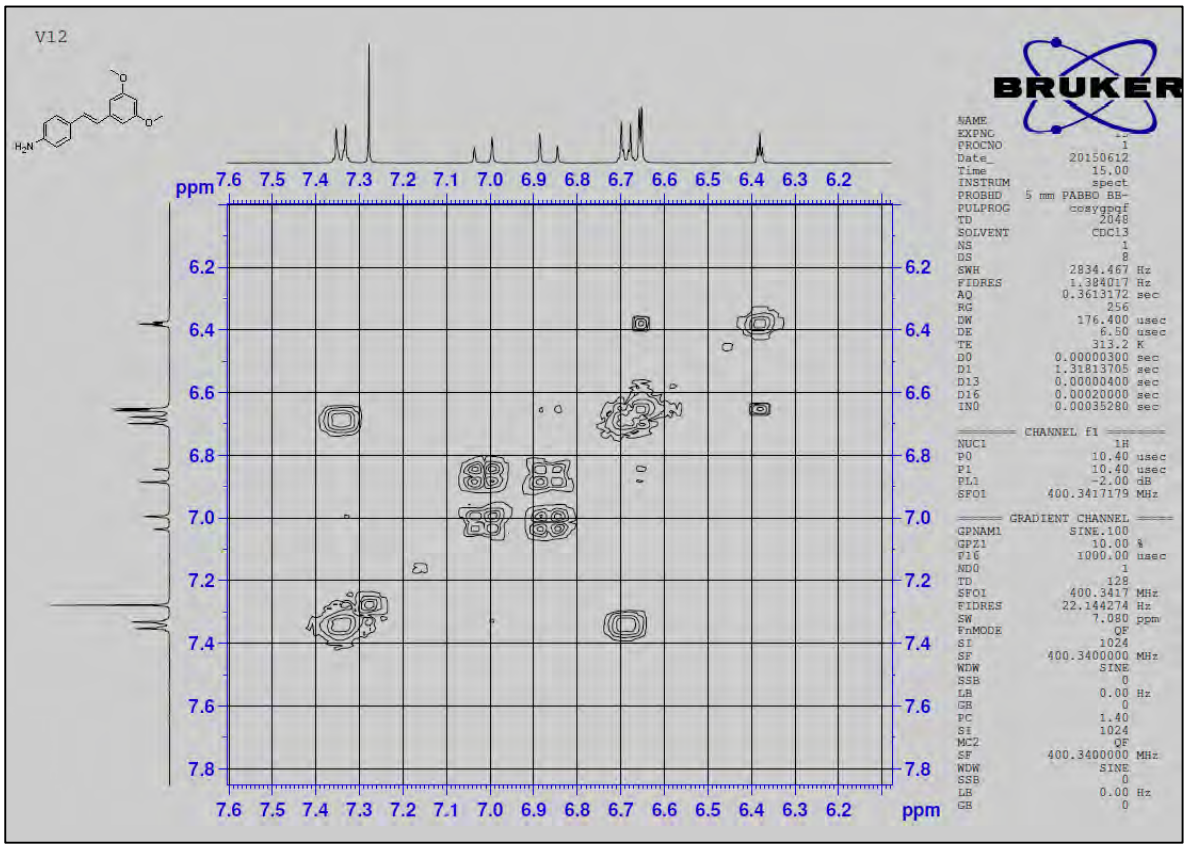

2D COSY spectra of V12

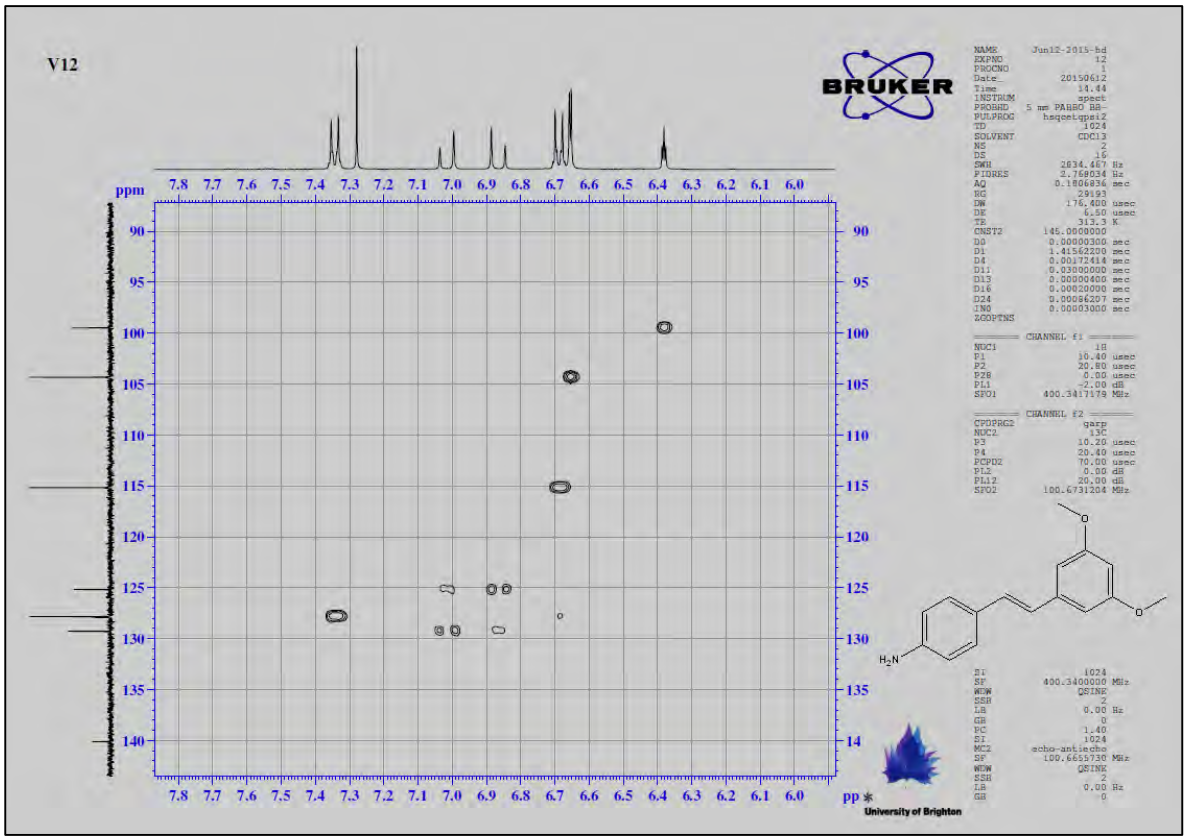

Mass spectra of V12

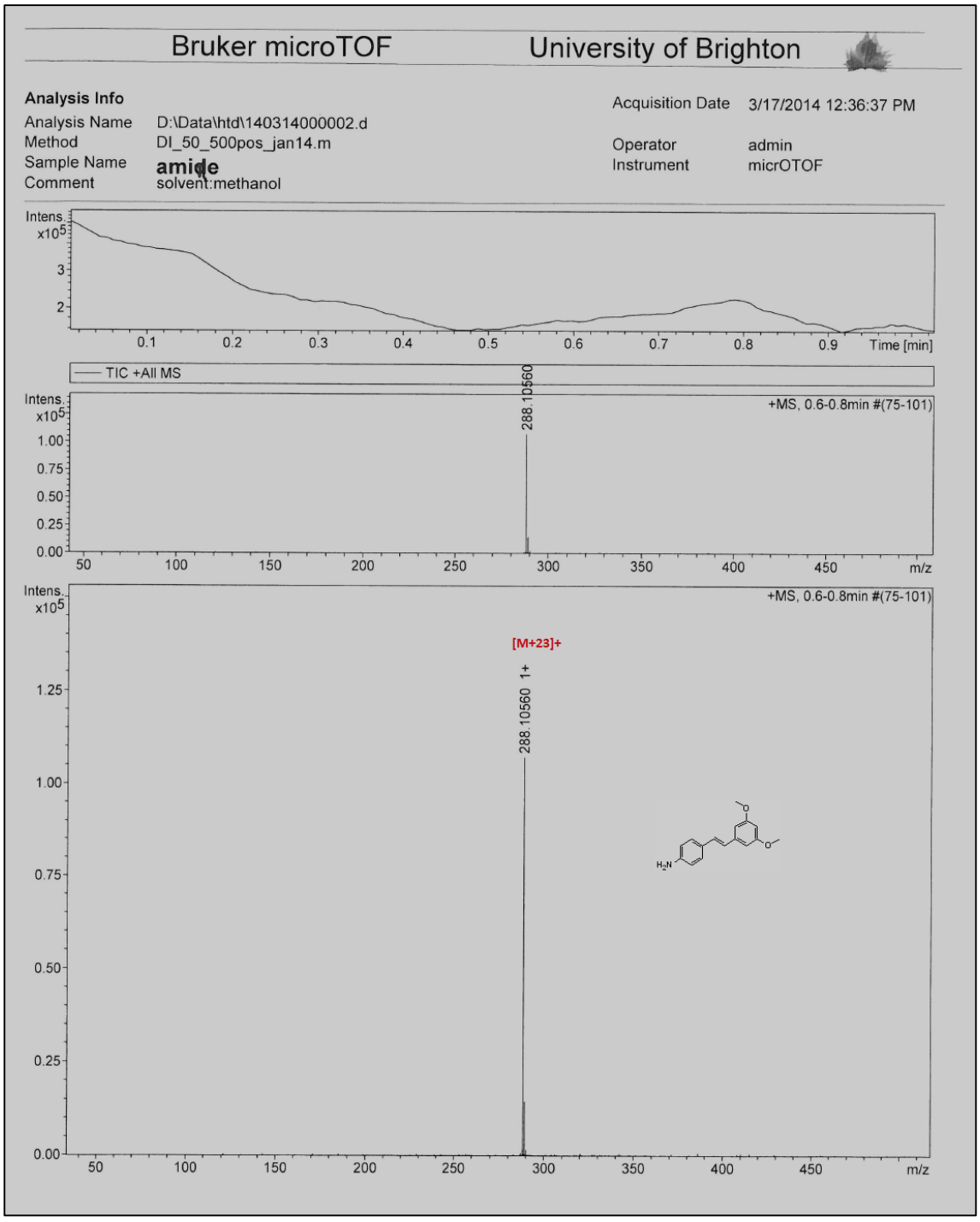

^{1}H NMR spectra of V13

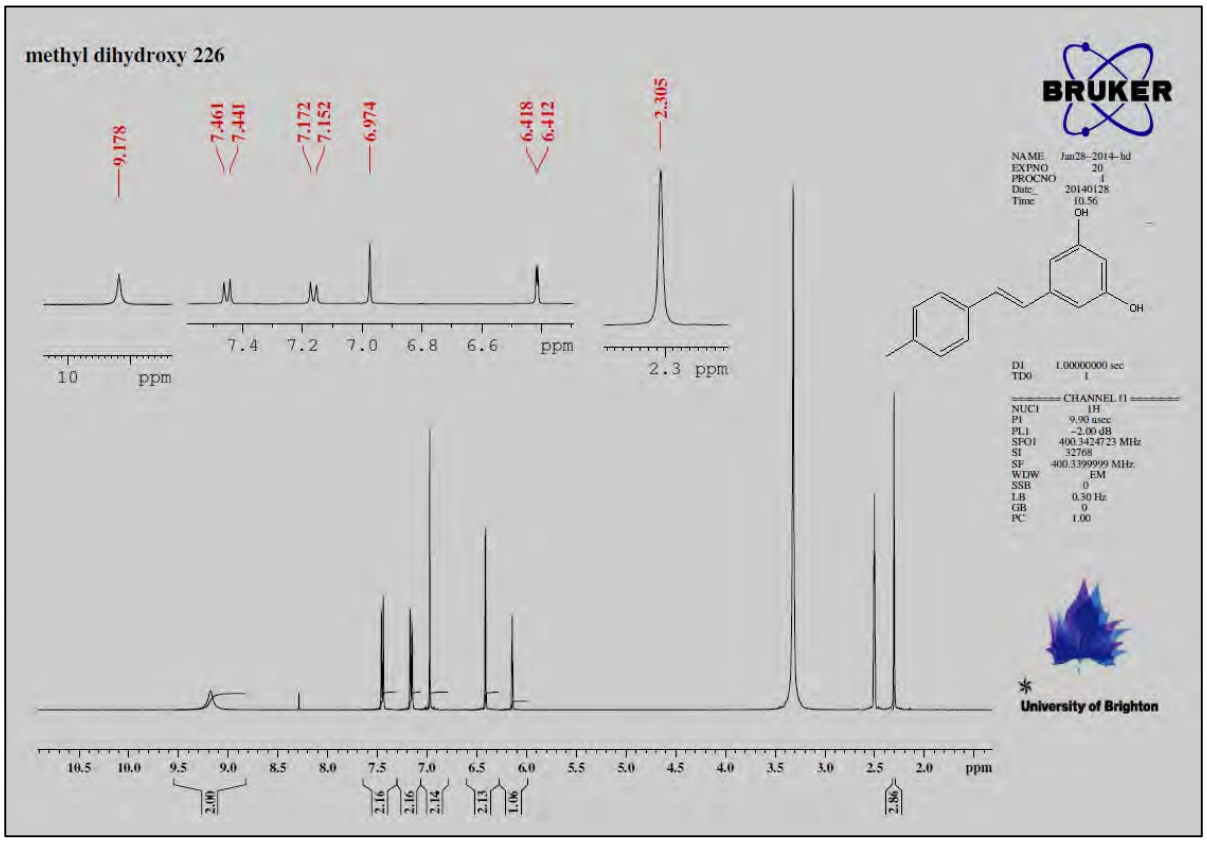

^{13}C NMR spectra of V13

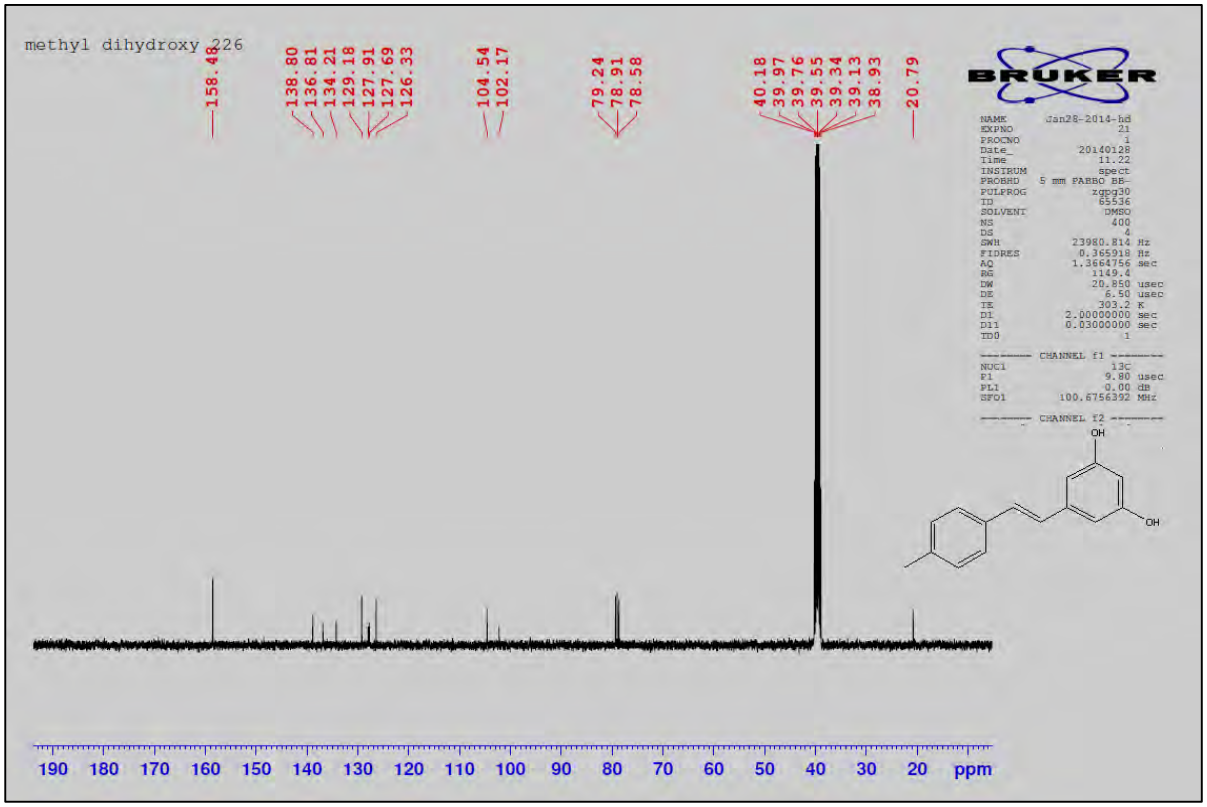

2D HSQC spectra of V13

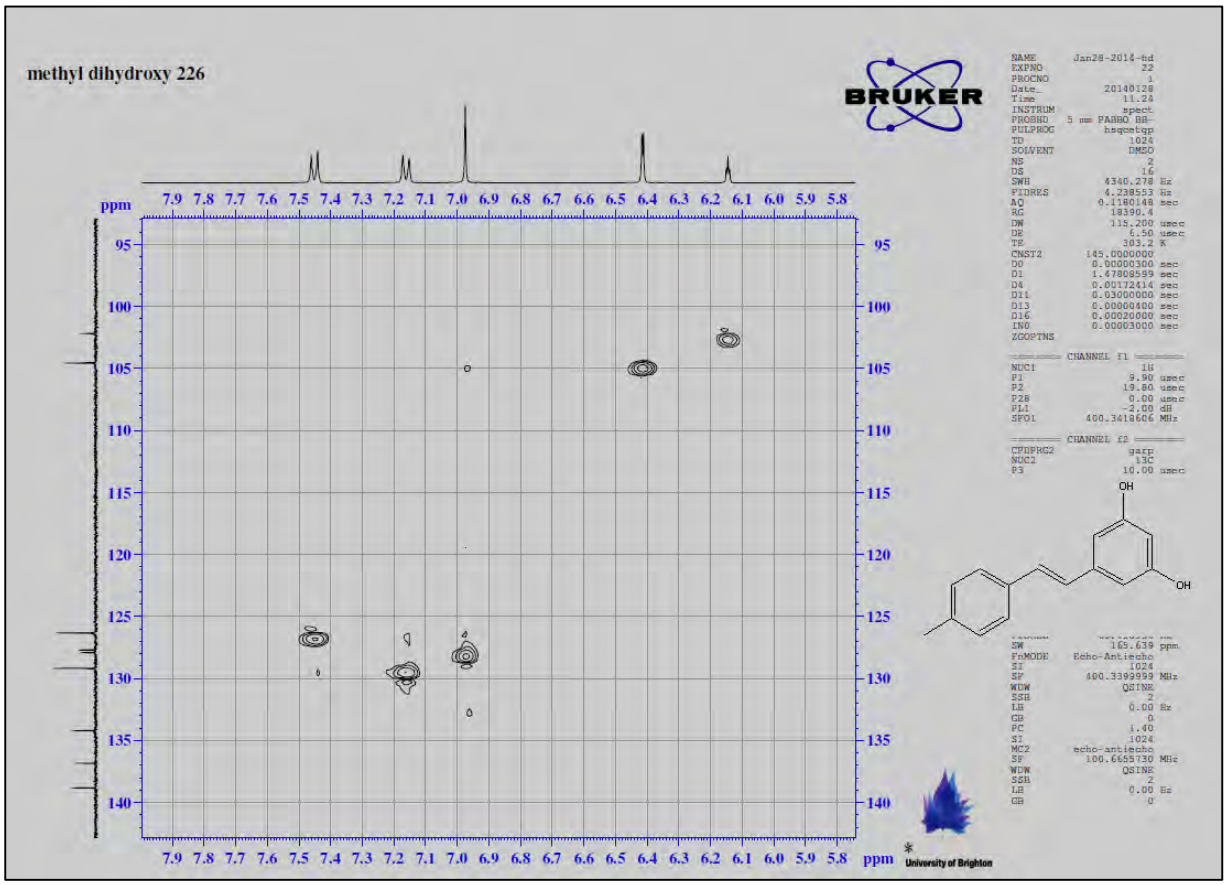

2D COSY spectra of V13

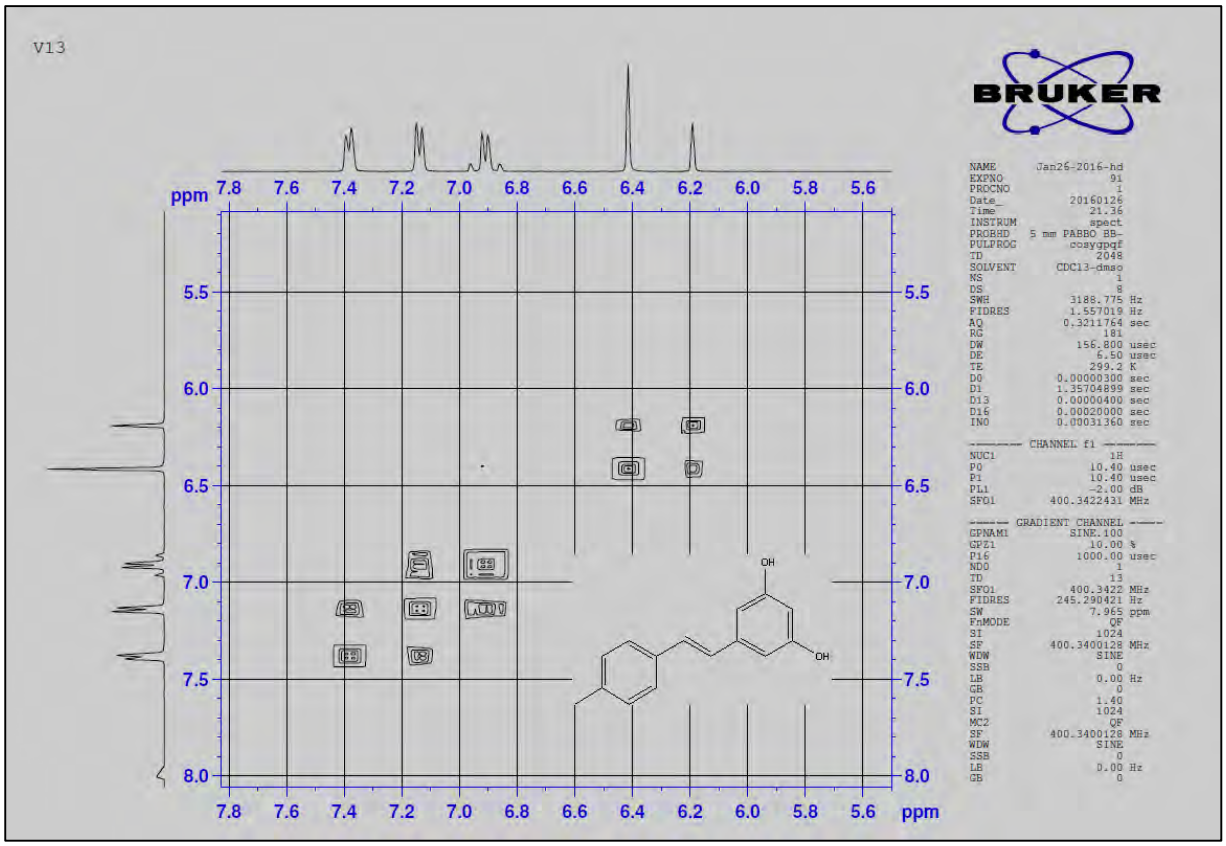

Mass spectra of V13

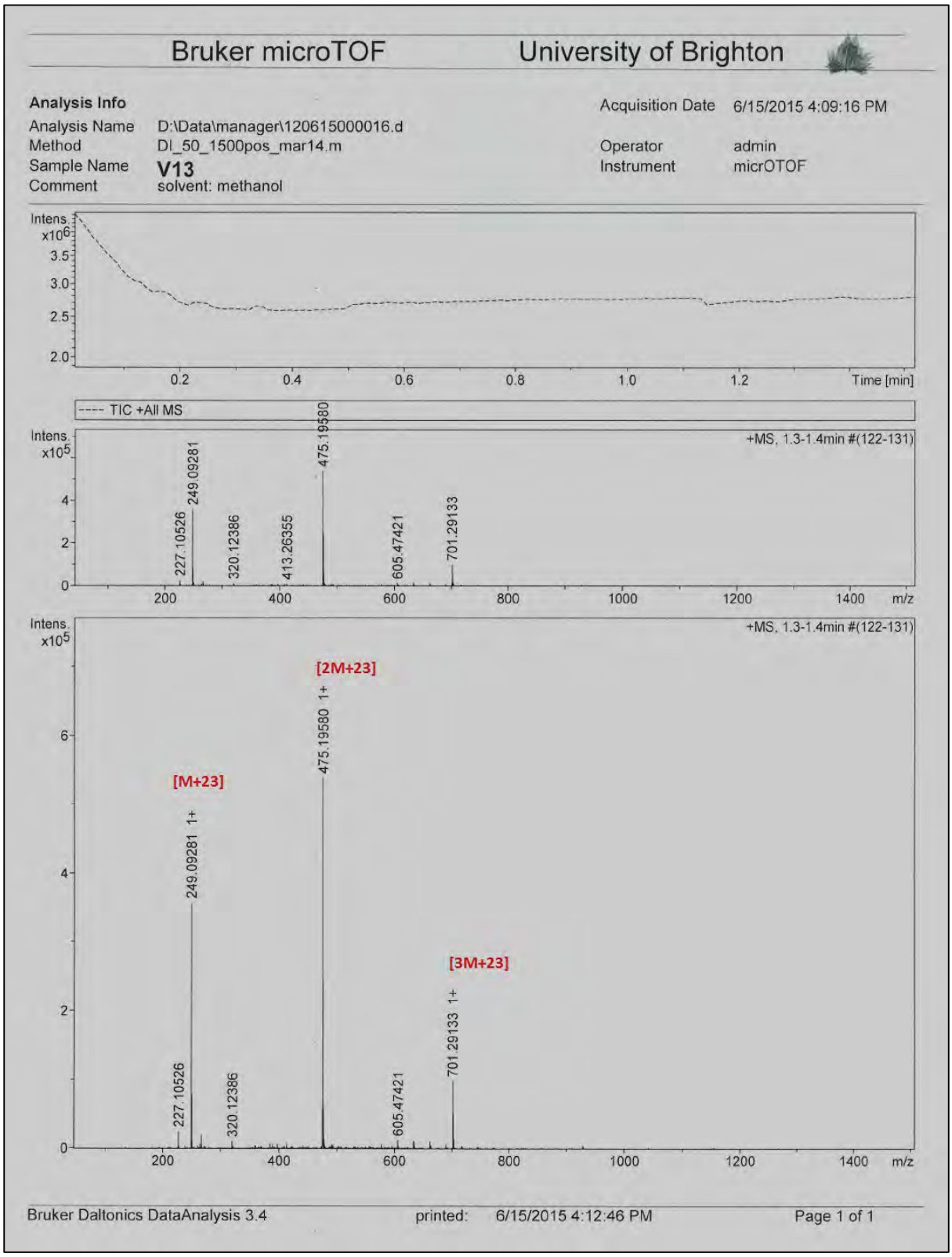

^{1}H NMR spectra of V14

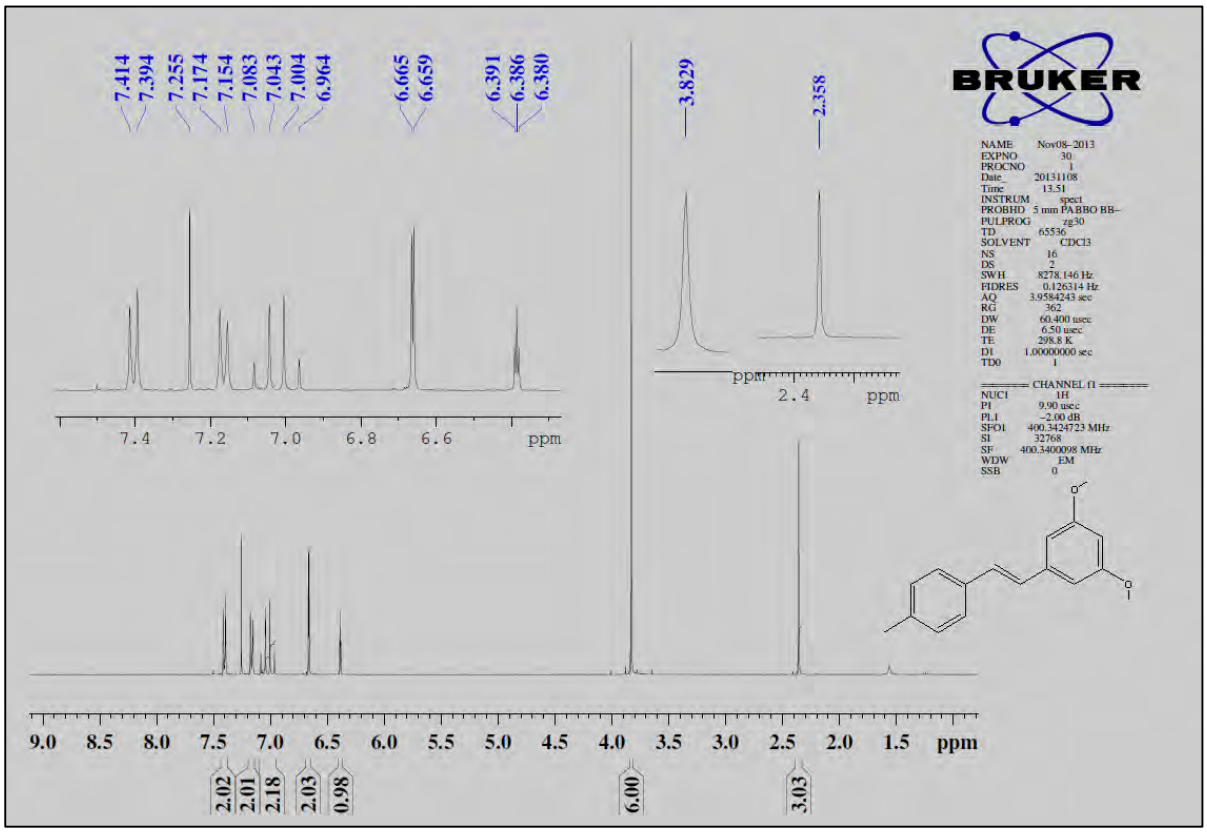

^{13}C NMR spectra of V14

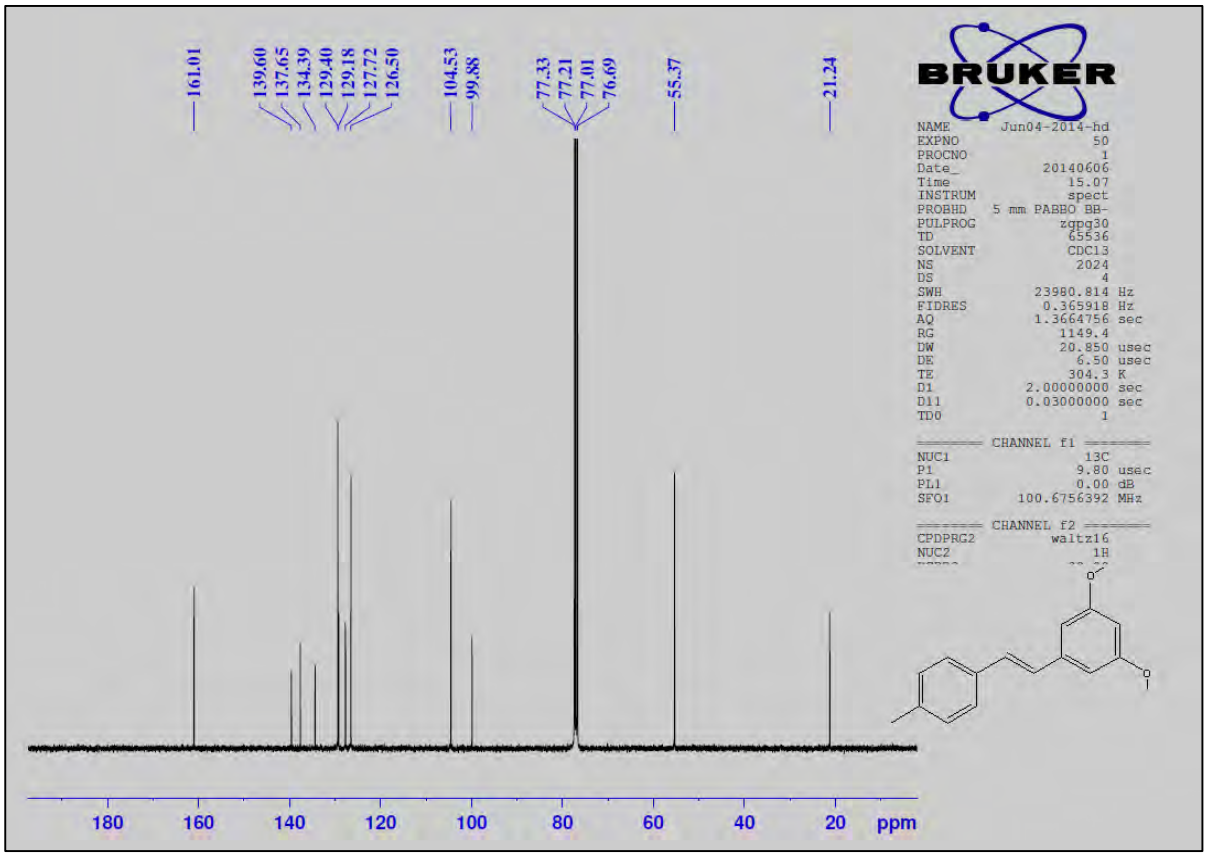

2D HSQC spectra of V14

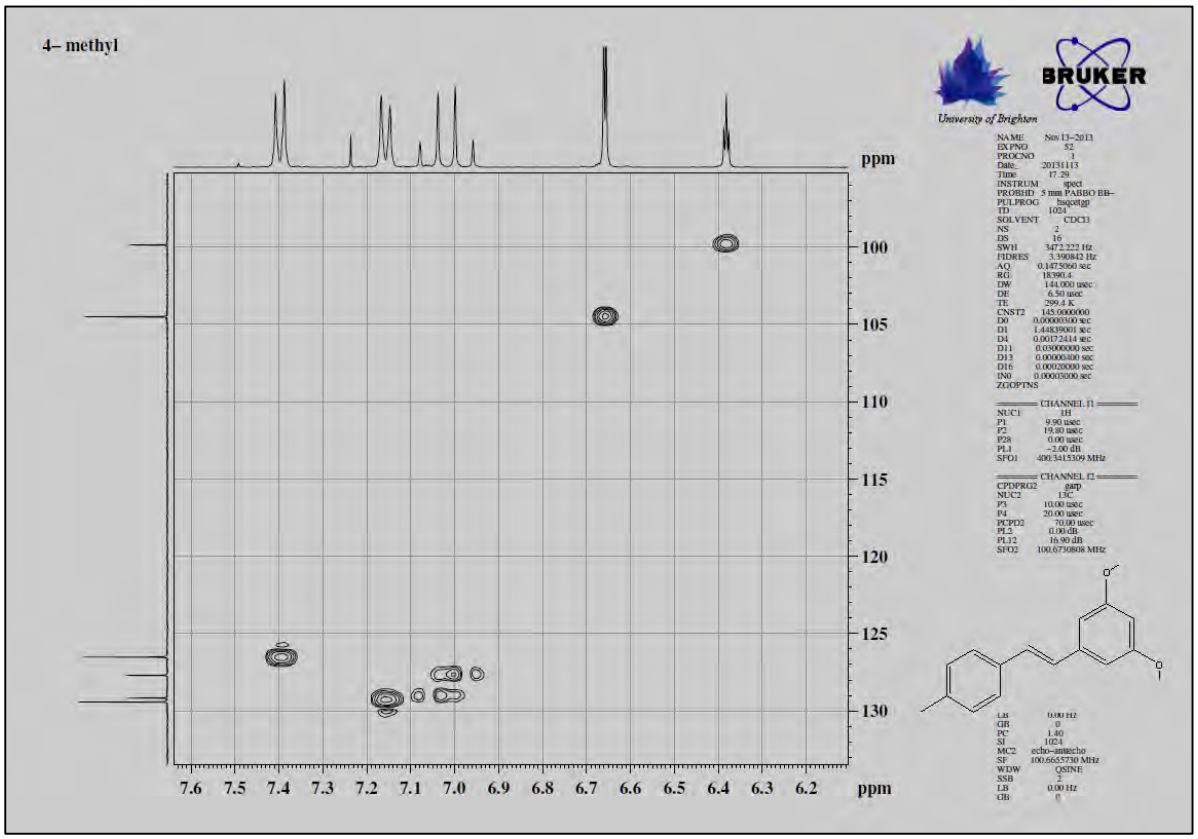

2D COSY spectra of V14

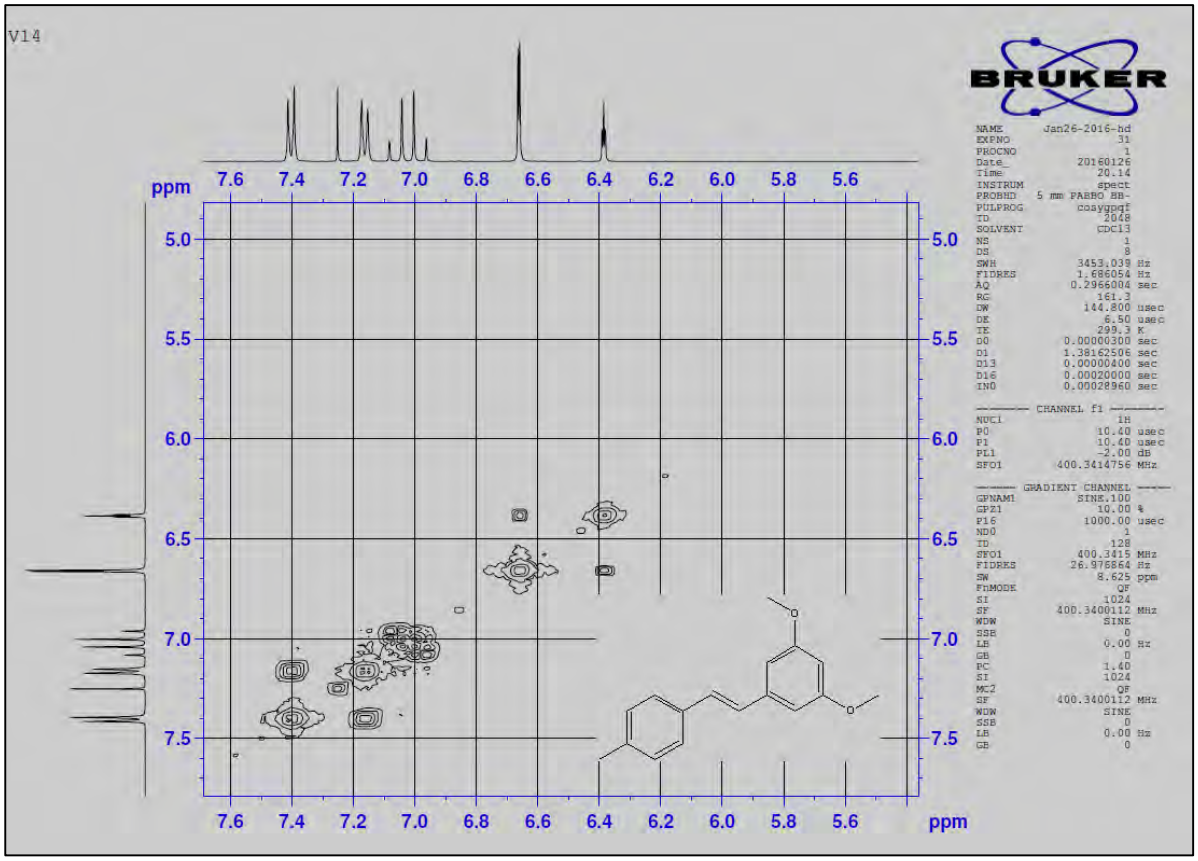

Mass spectra of V14

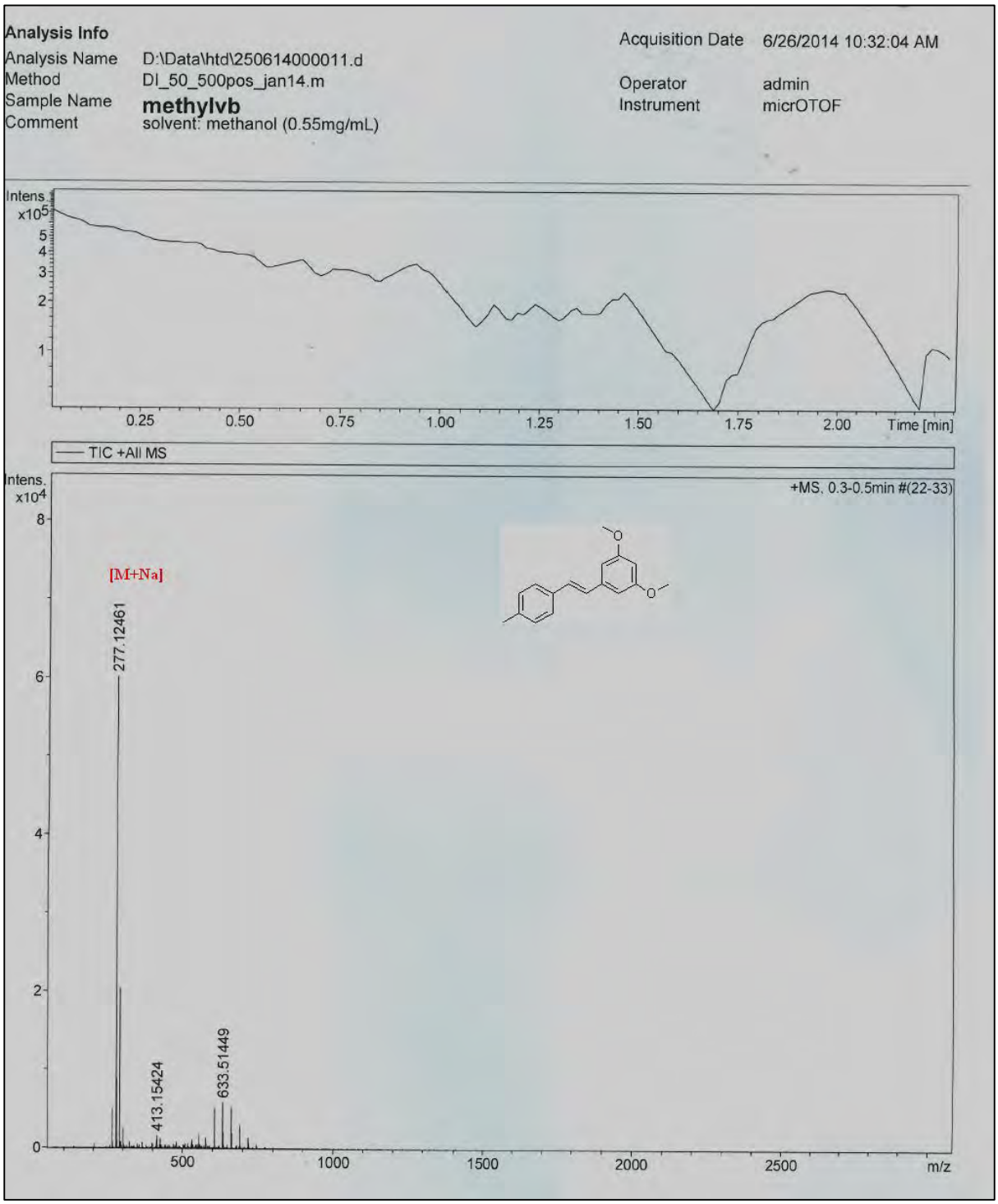

^{1}H NMR spectra of V15

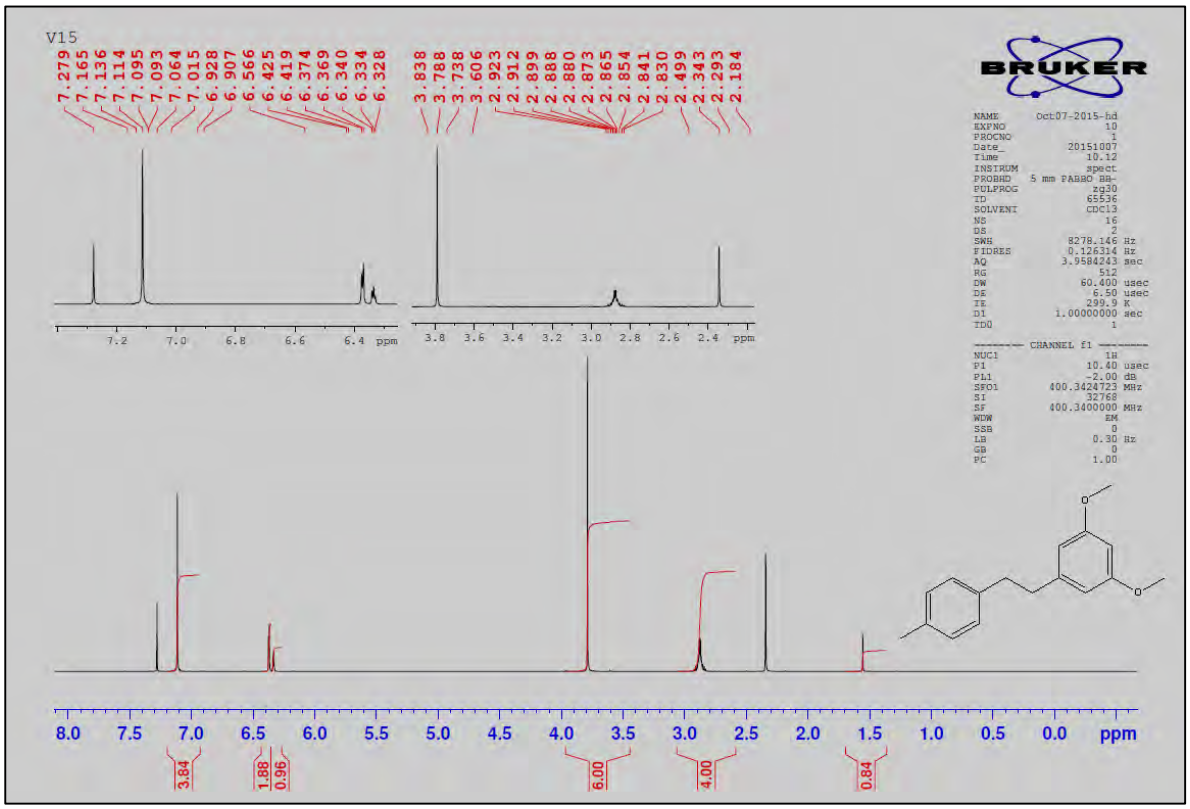

^{13}C NMR spectra of V15

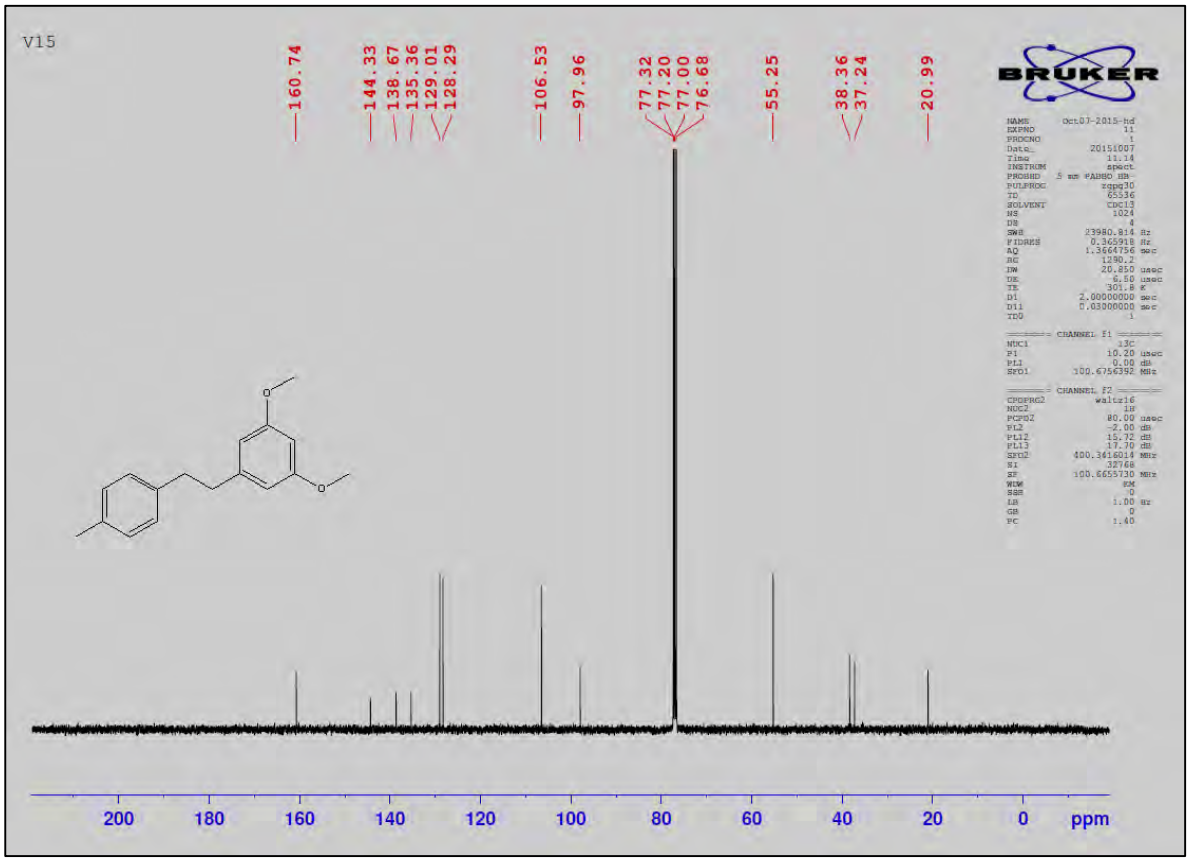

2D HSQC spectra of V15

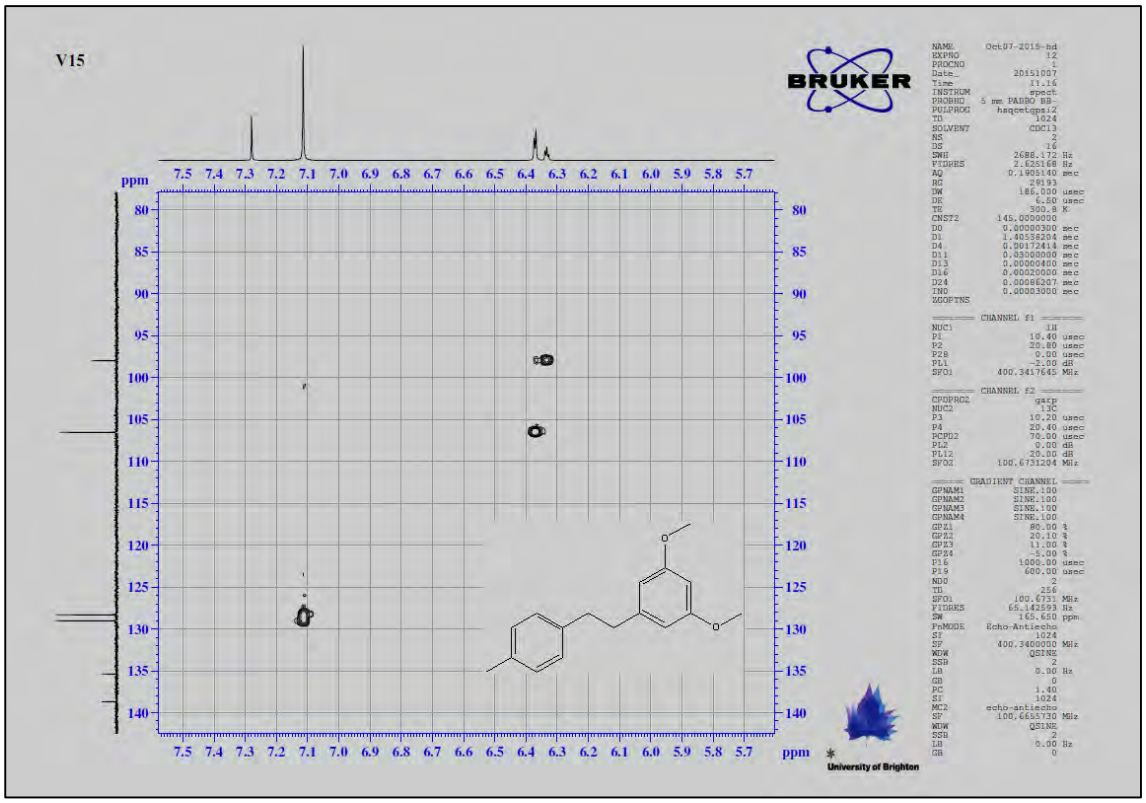

2D COSY spectra of V15

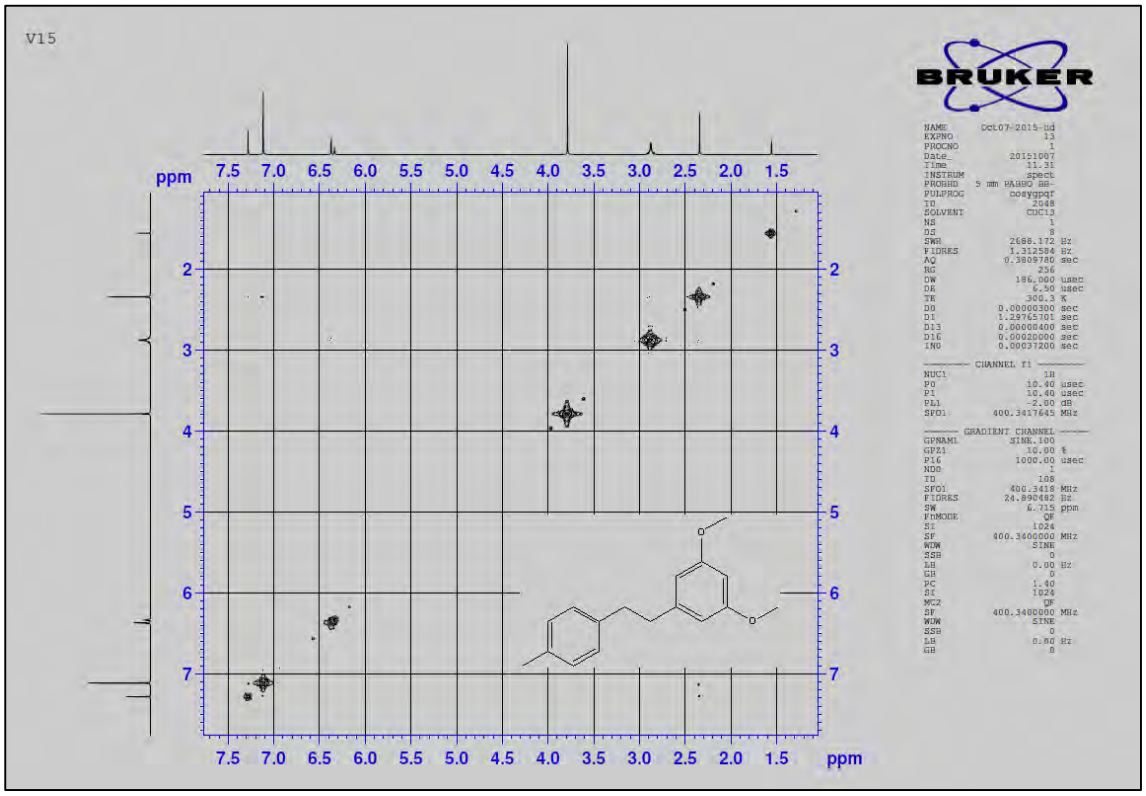

Mass spectra of V15

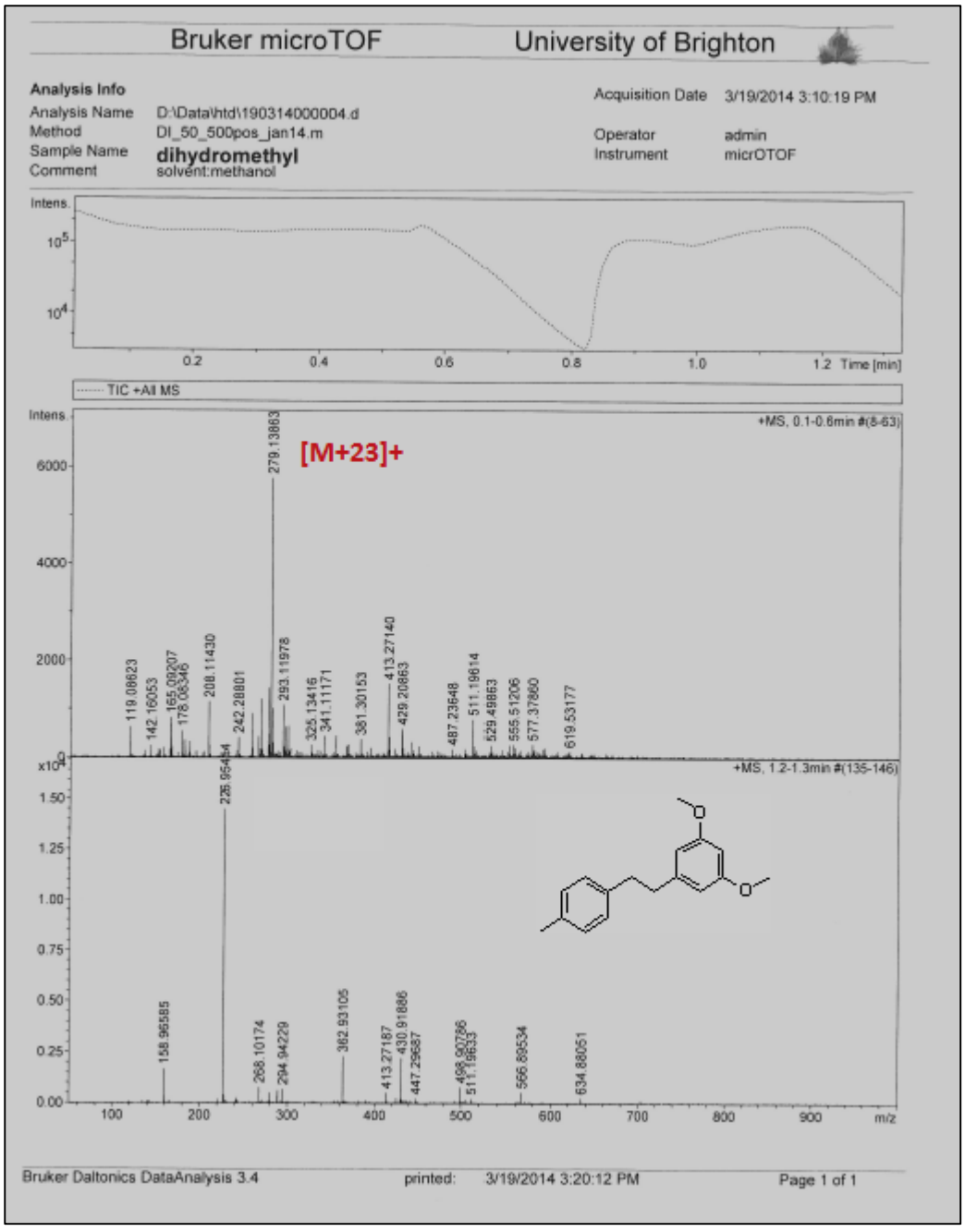

^{1}H NMR spectra of V16

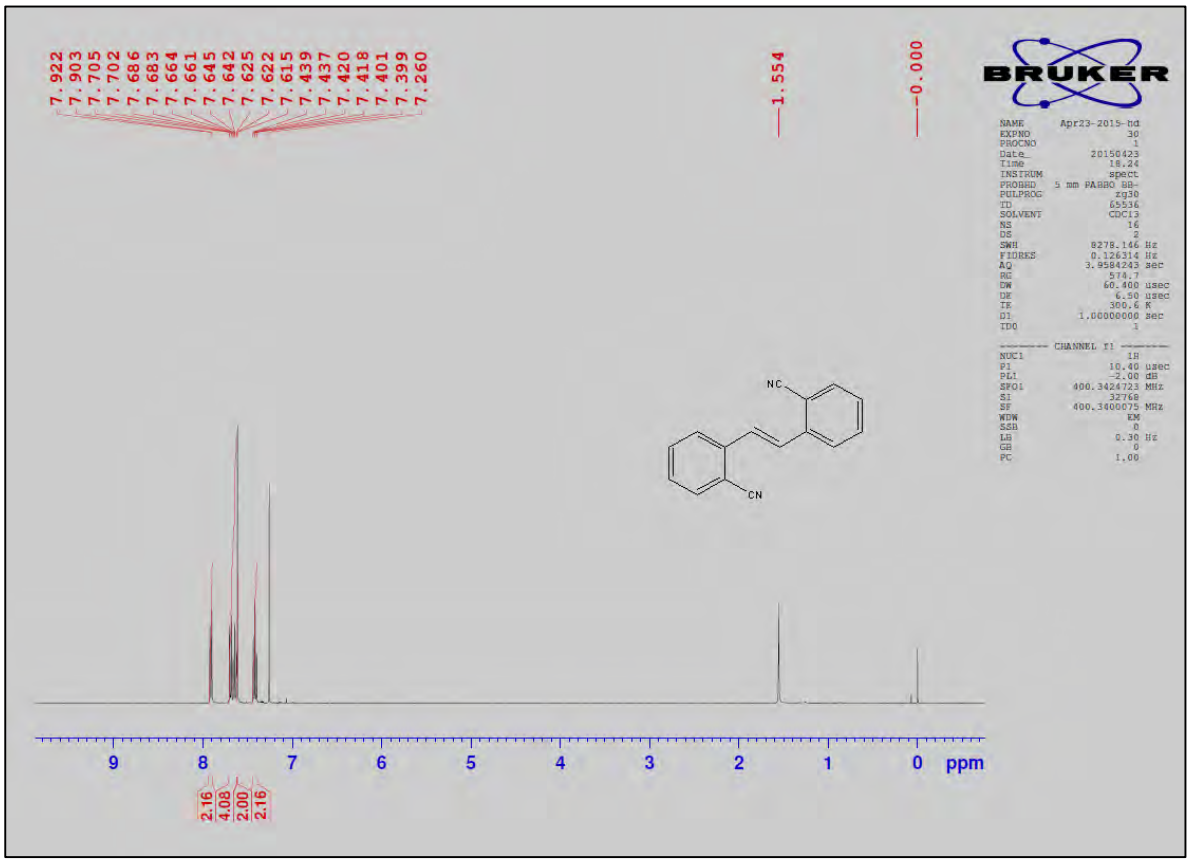

^{13}C NMR spectra of V16

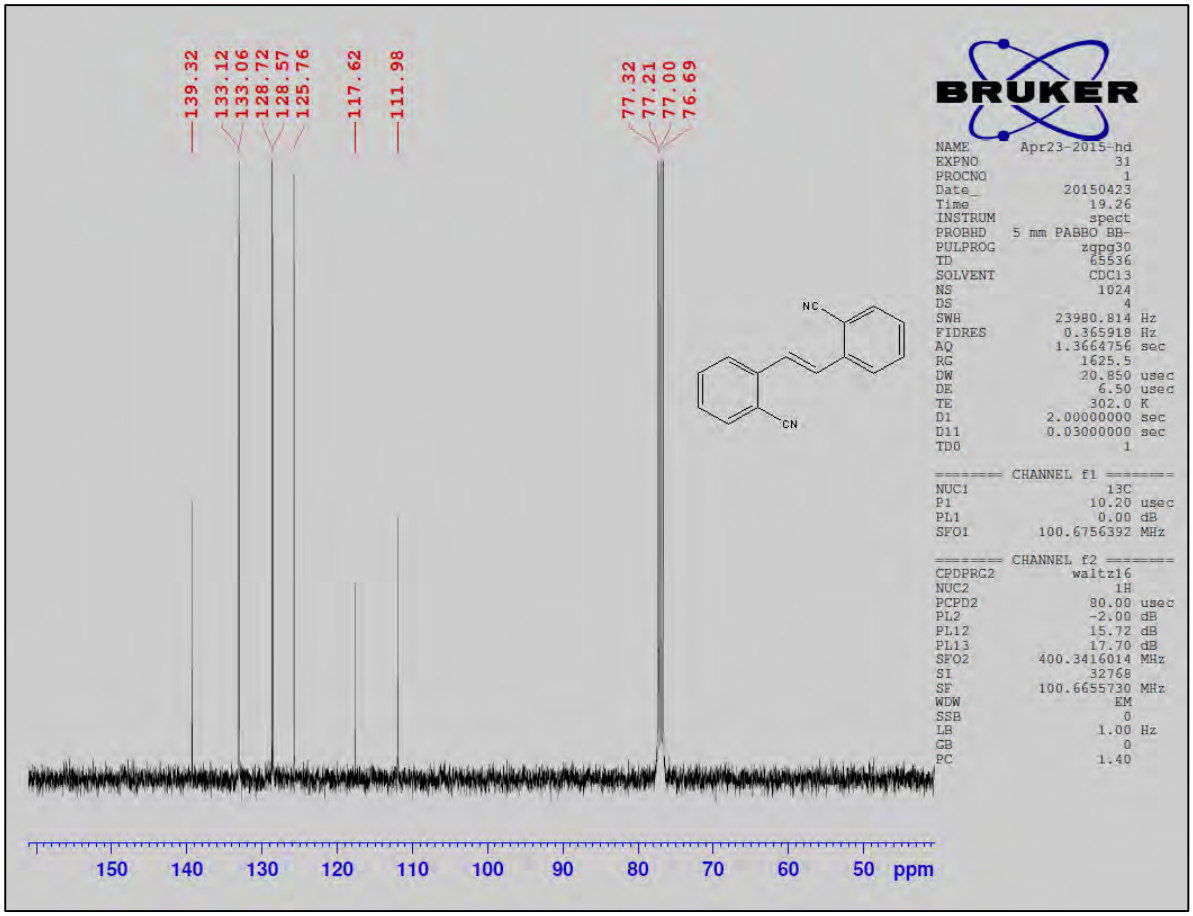

2D HSQC spectra of V16

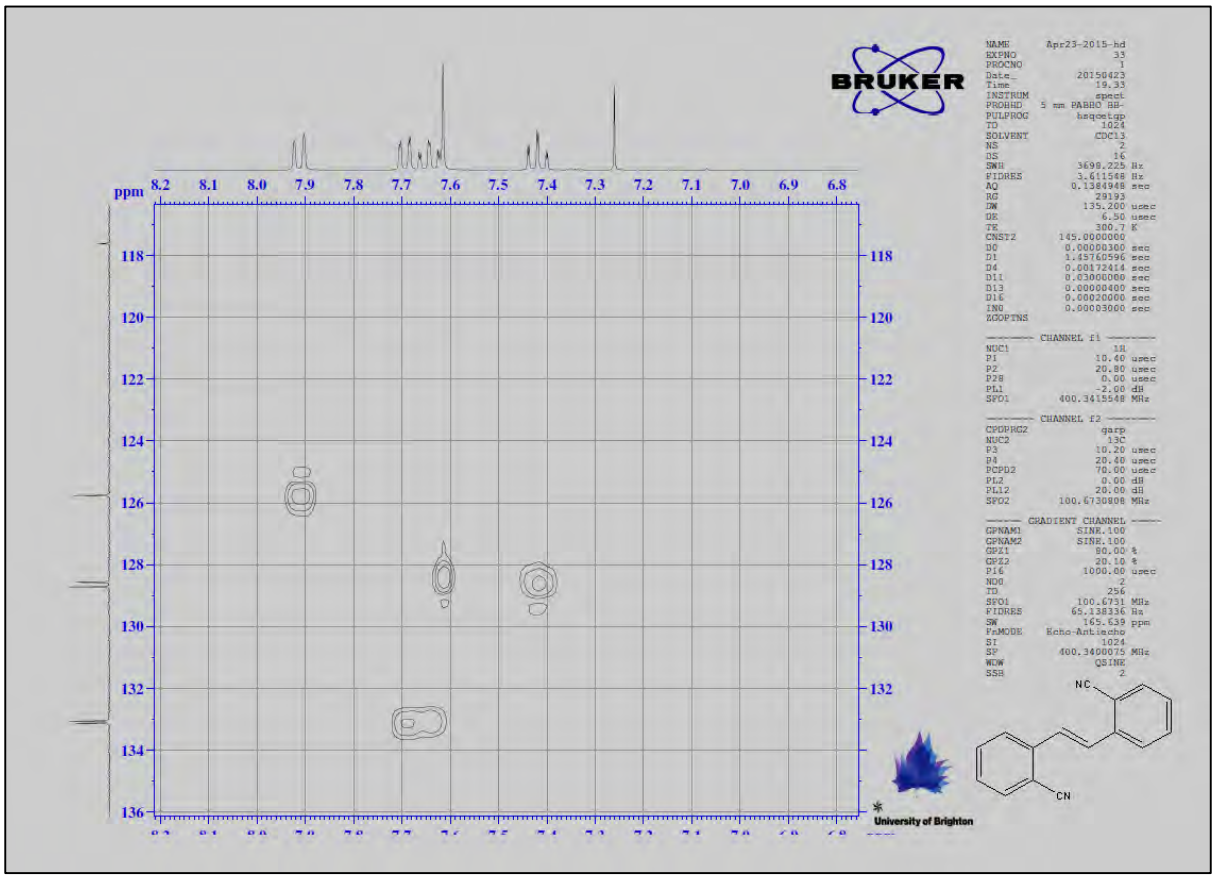

2D COSY spectra of V16

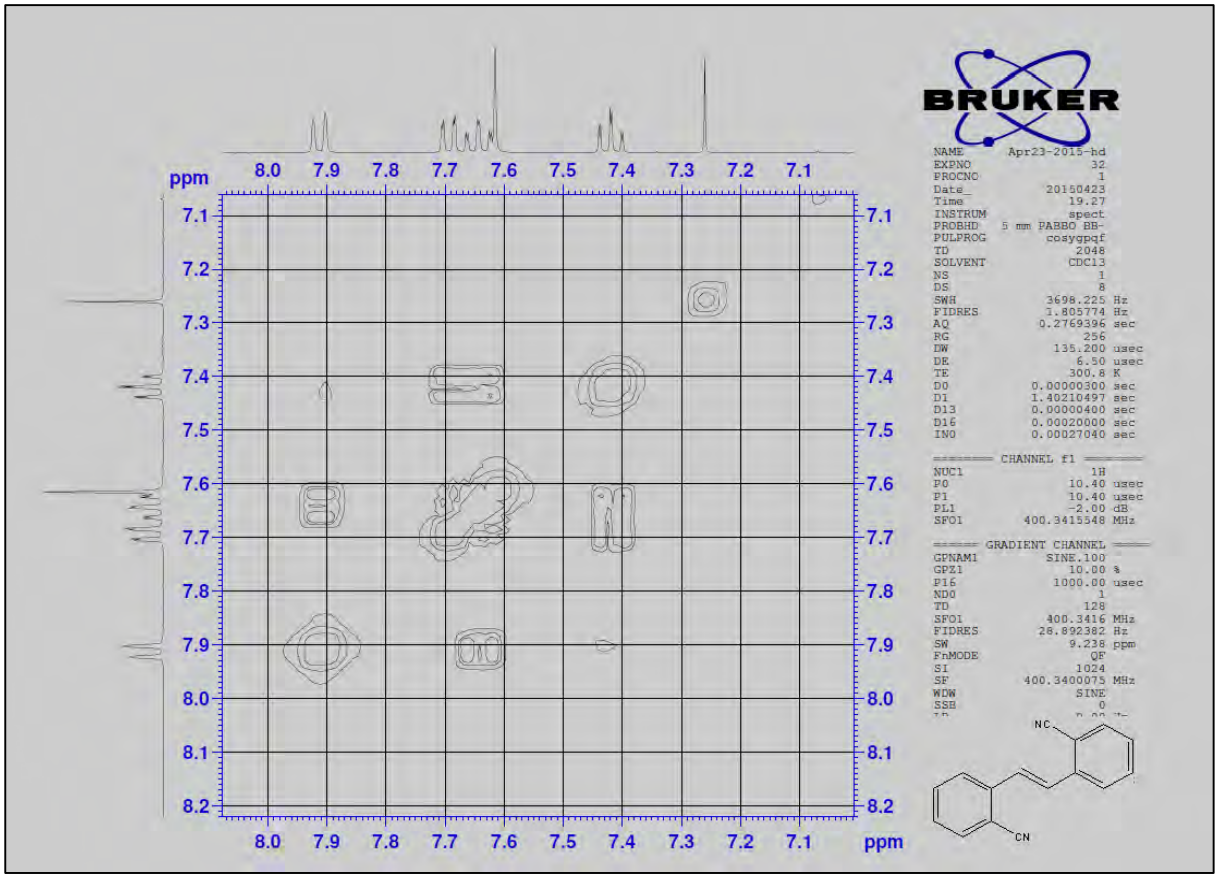

Mass spectra of V16

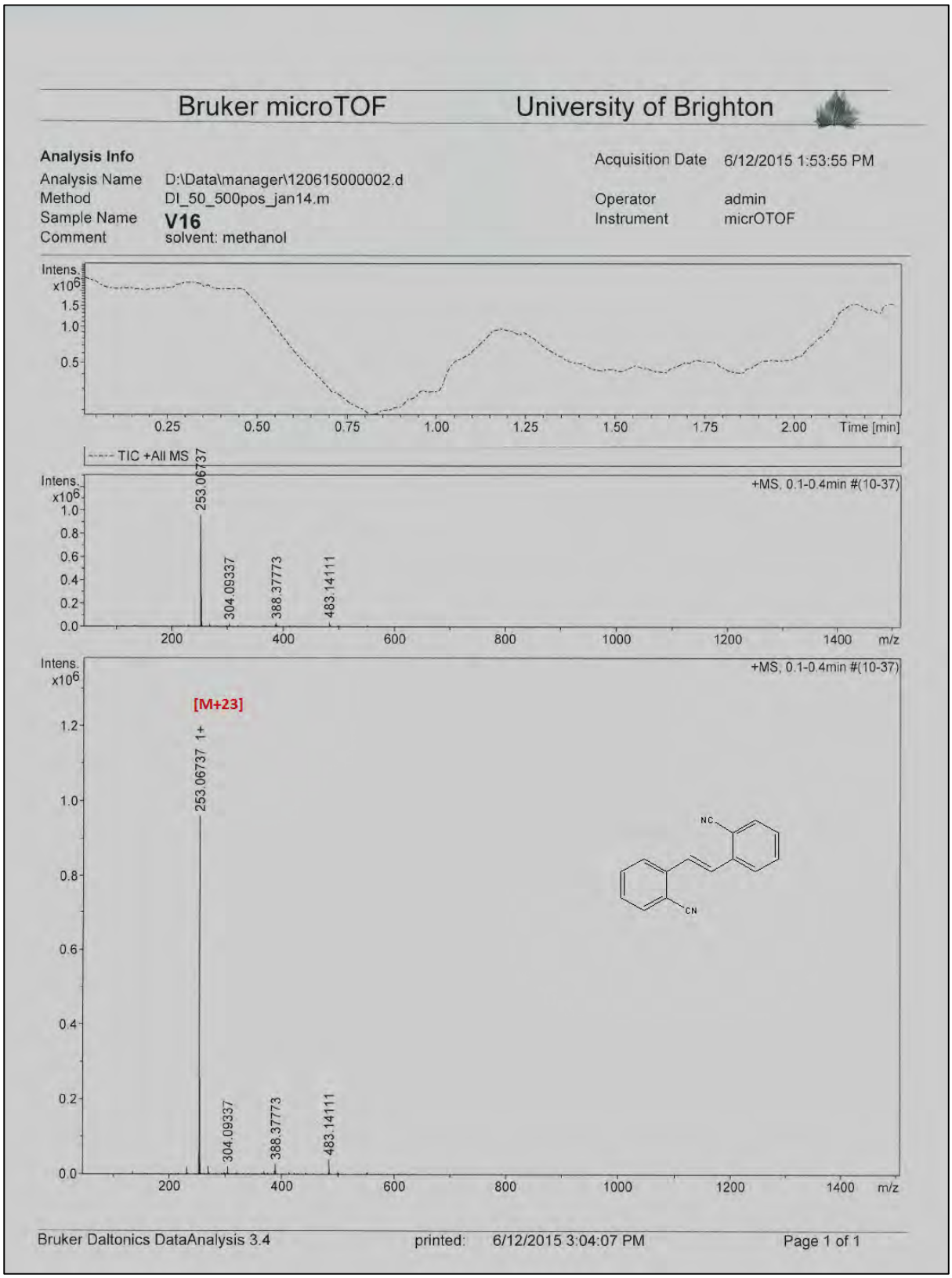

^{1}H NMR spectra of V17

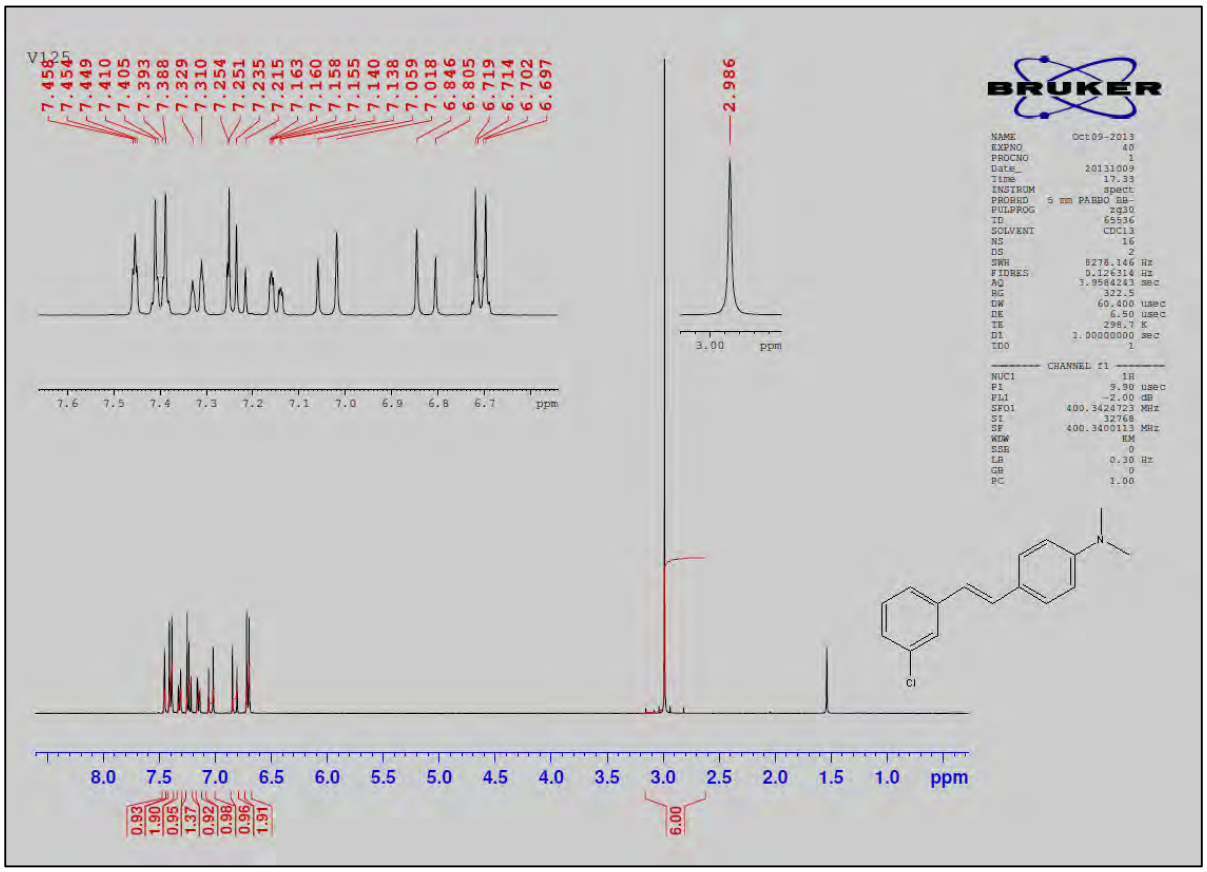

^{13}C NMR spectra of V17

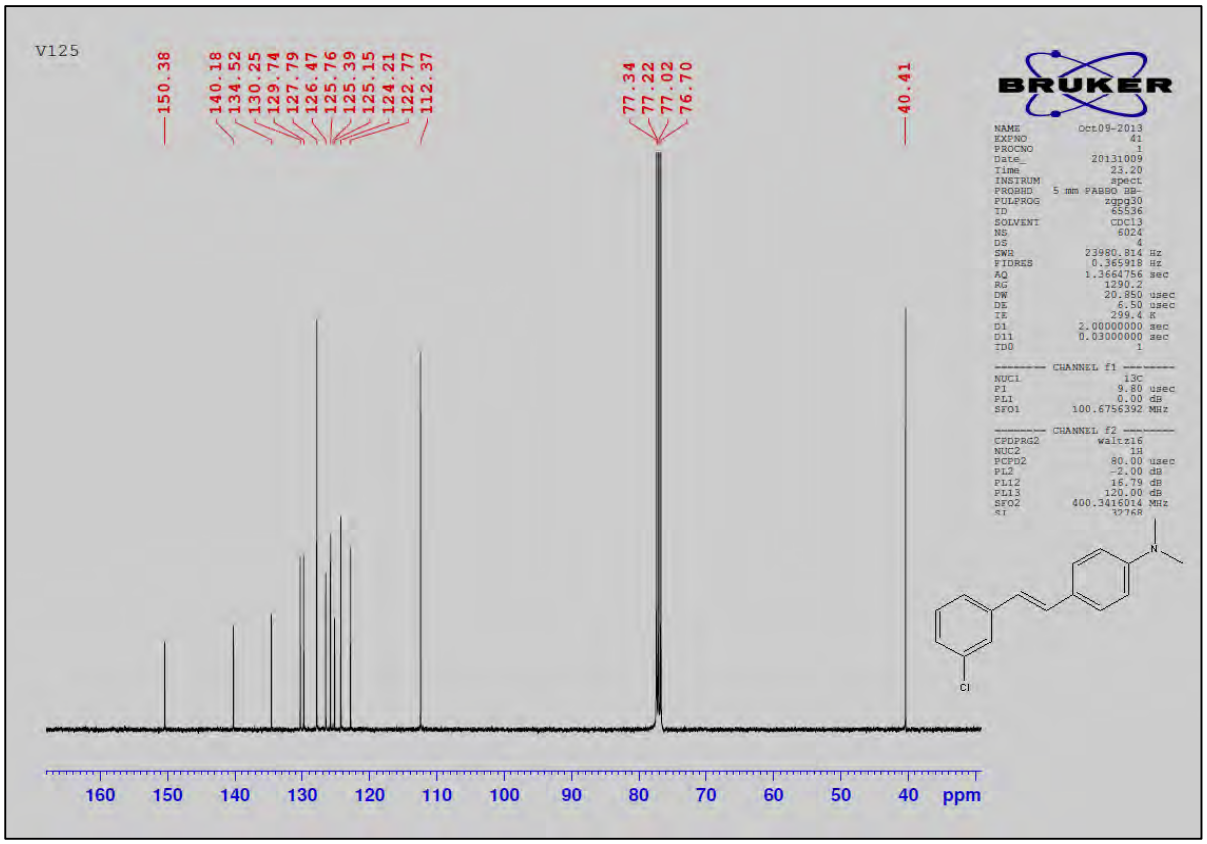

2D HSQC spectra of V17

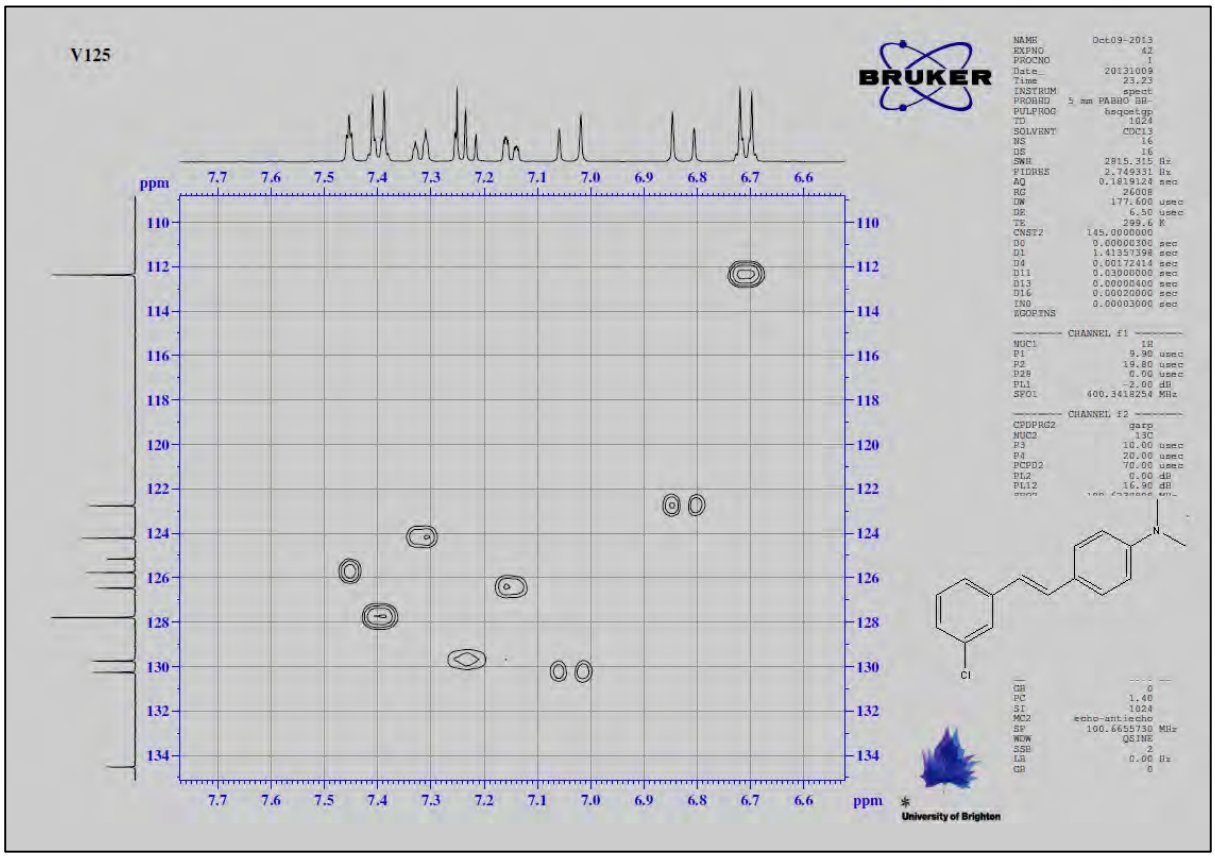

2D COSY spectra of V17

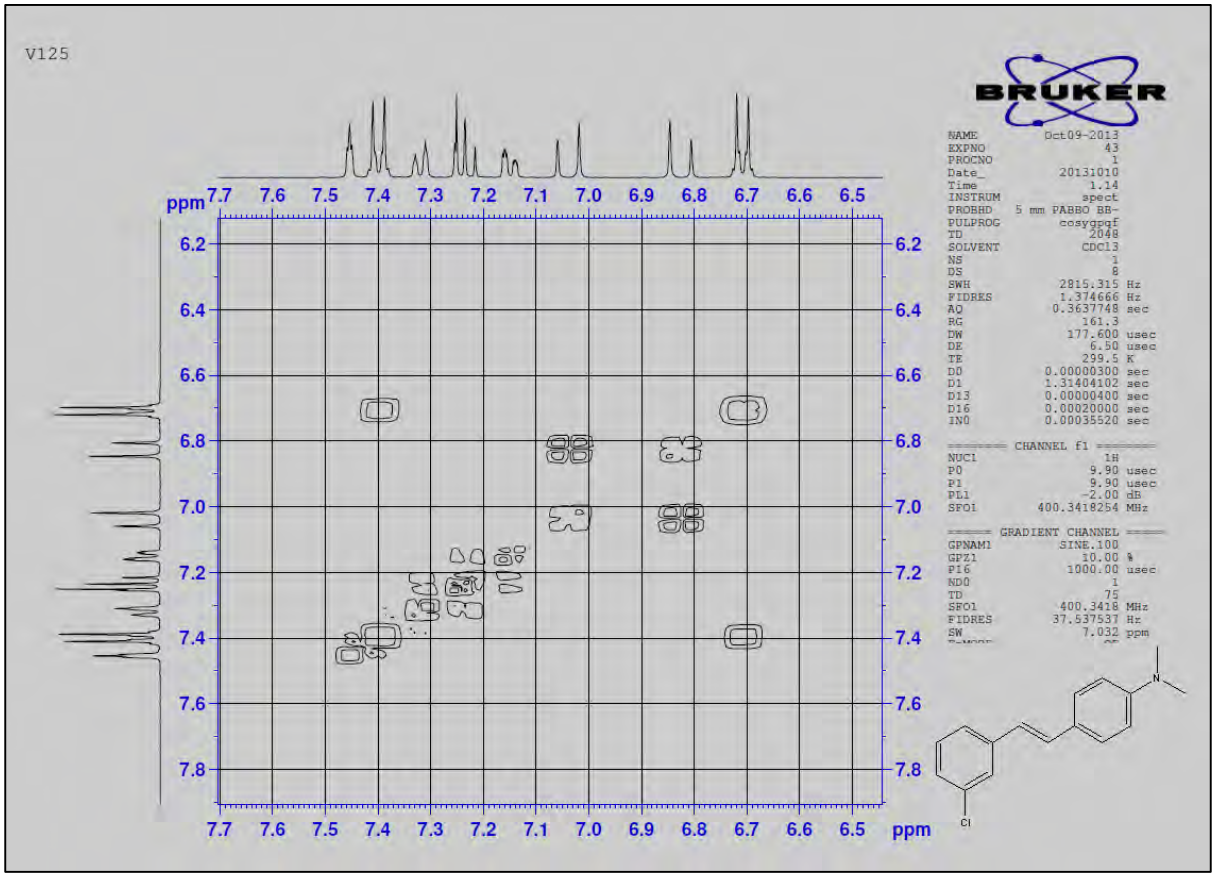

Mass spectra of V17

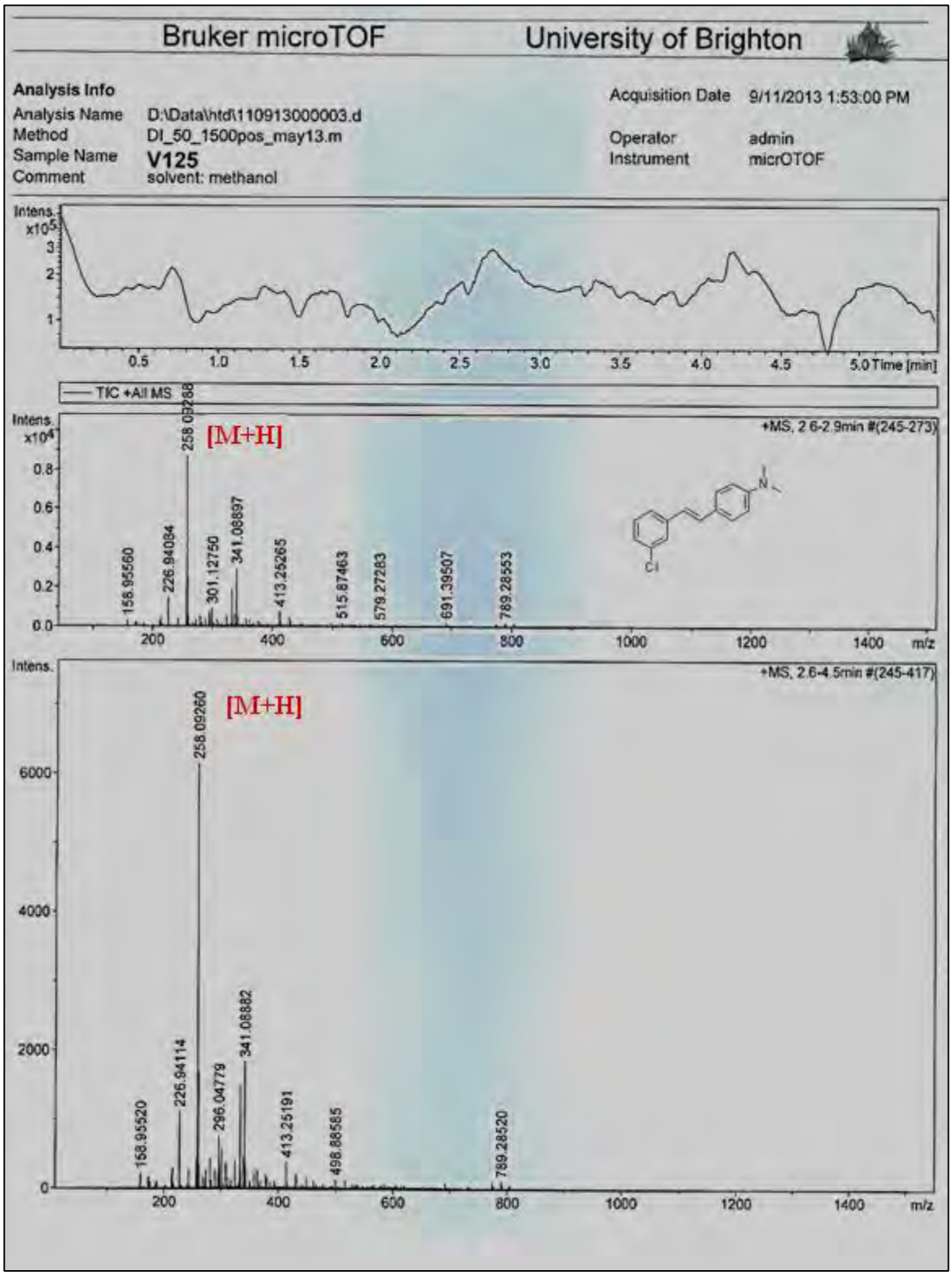

^{1}H NMR spectra of V18

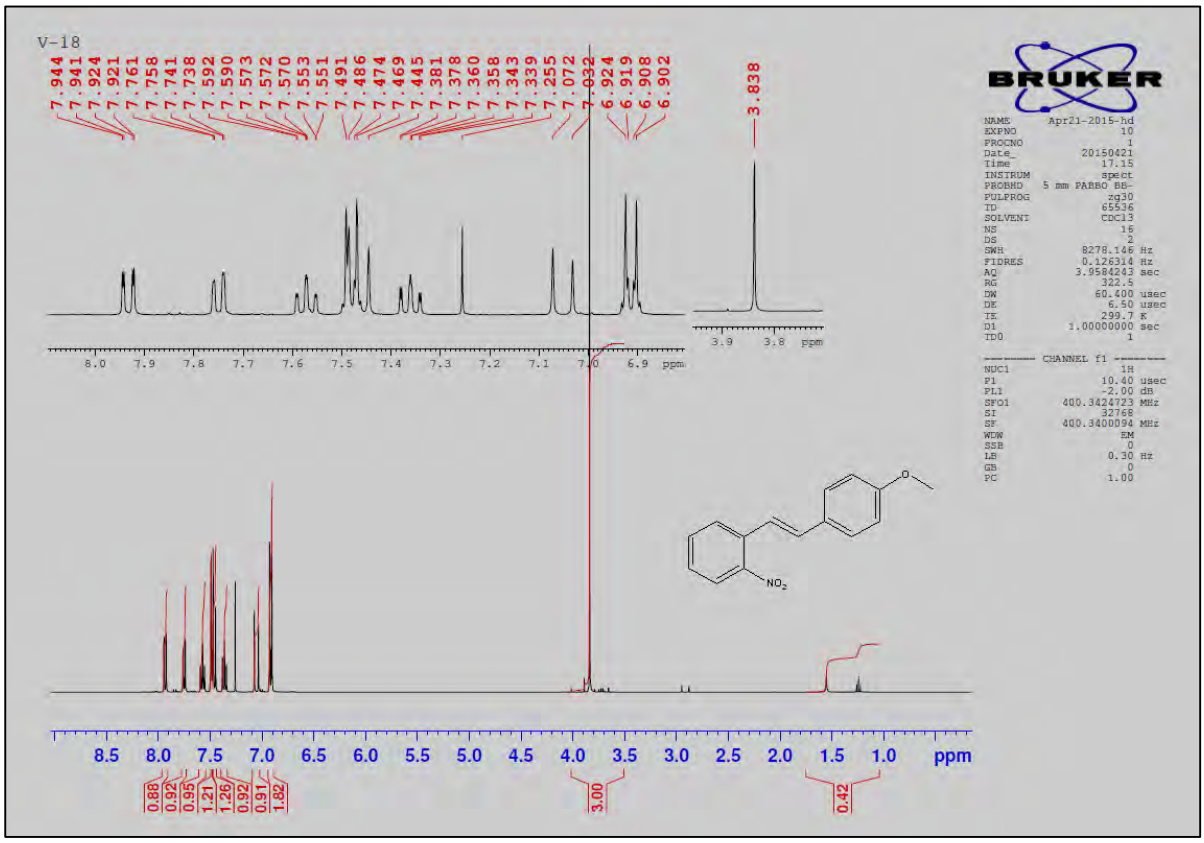

^{13}C NMR spectra of V18

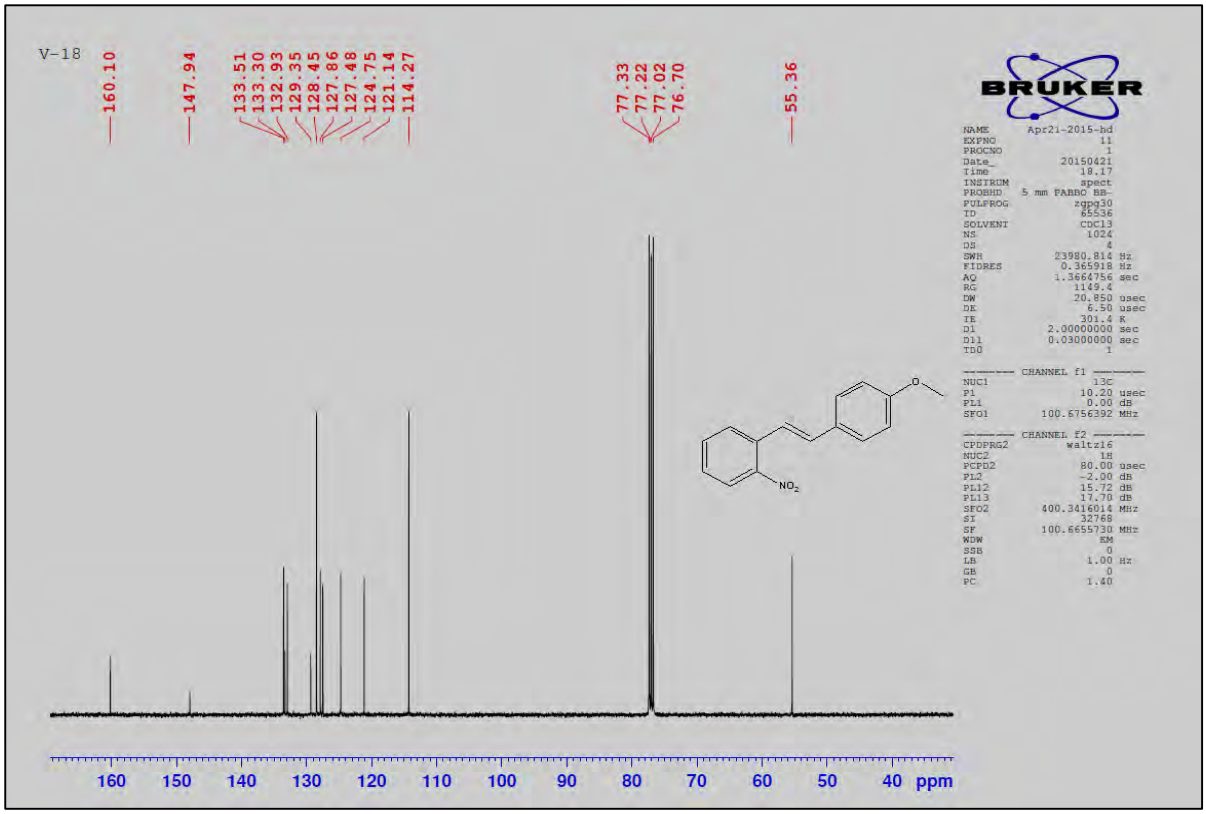

2D HSQC spectra of V18

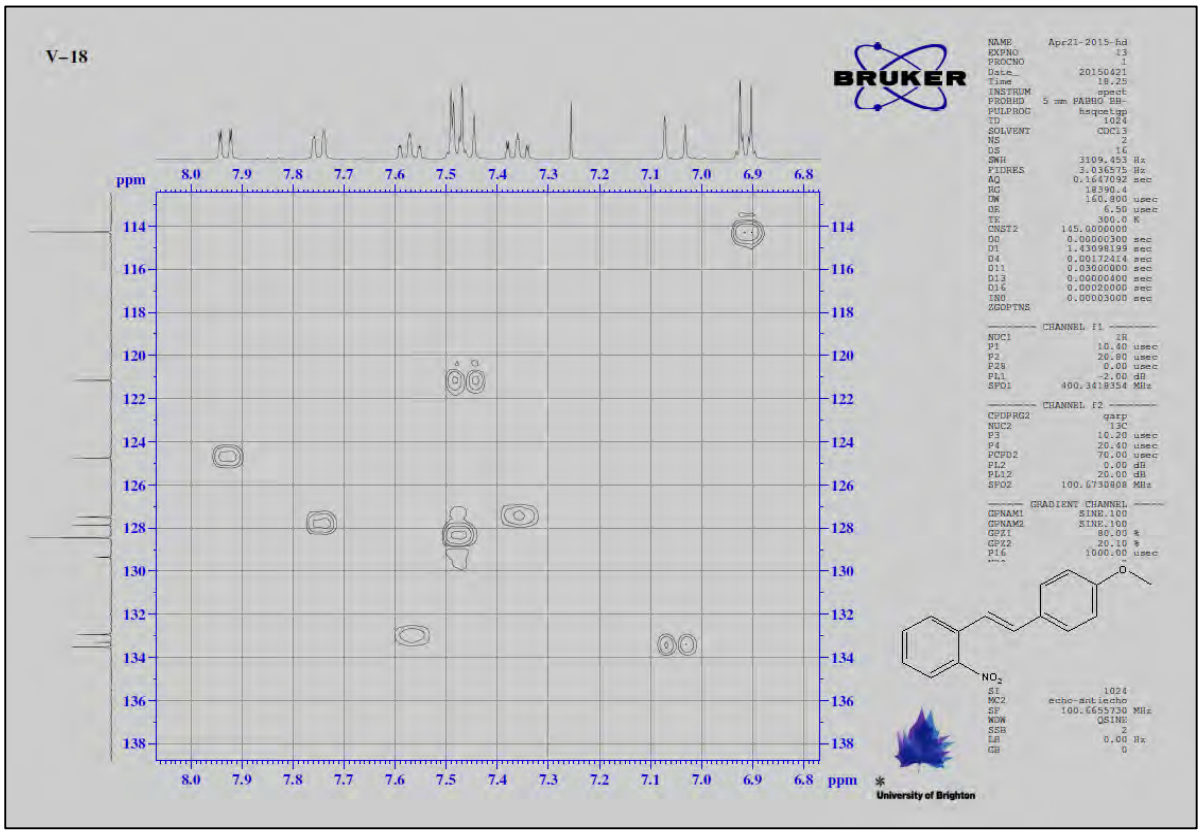

2D COSY spectra of V18

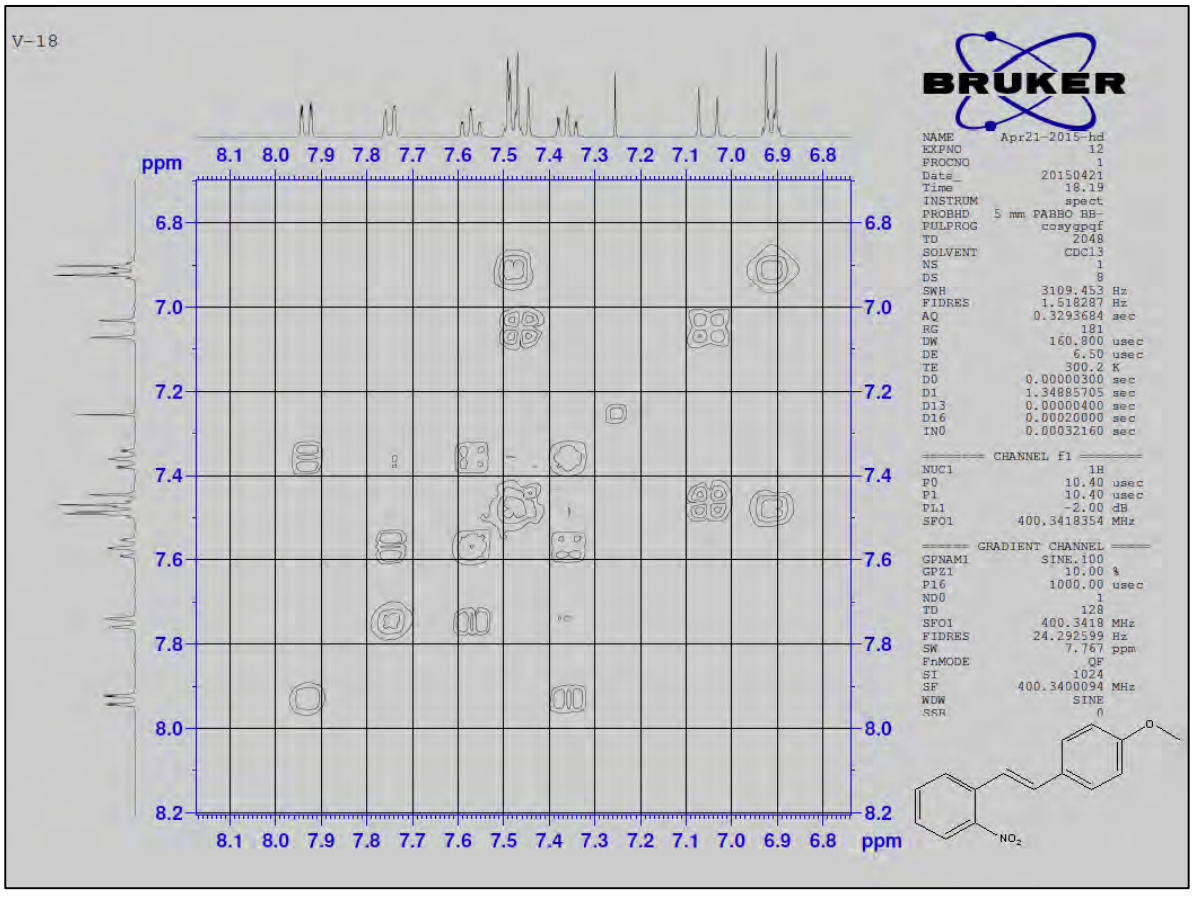

Mass spectra of V18

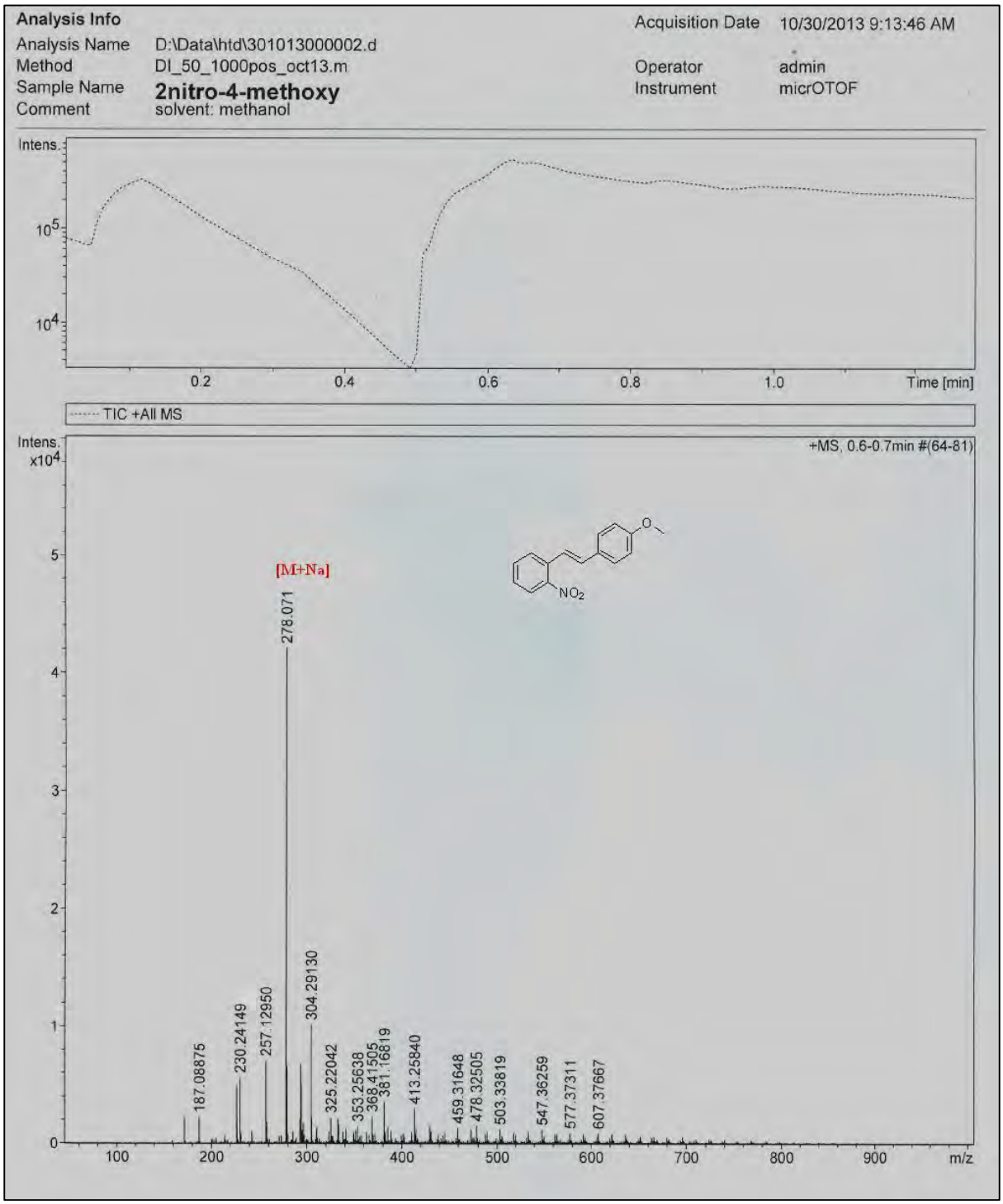

^{1}H NMR spectra of V19

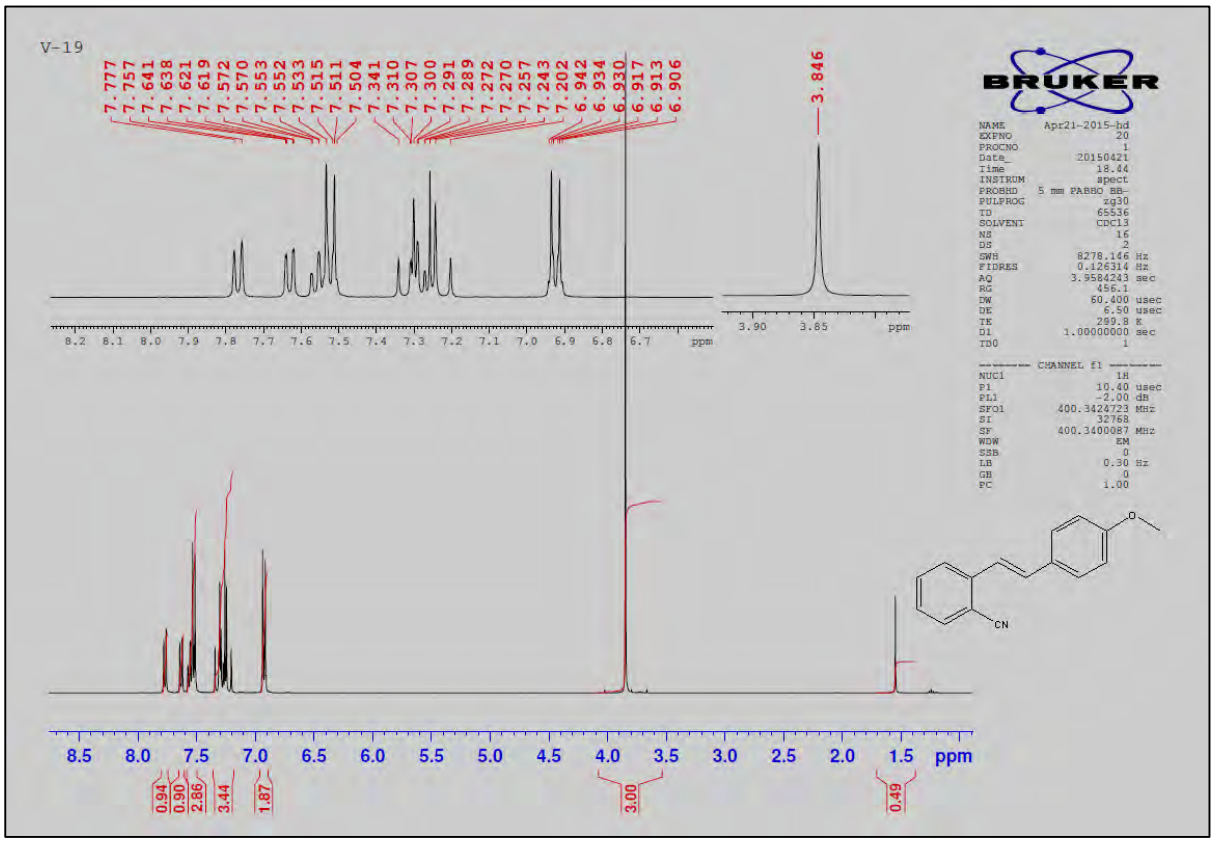

^{13}C NMR spectra of V19

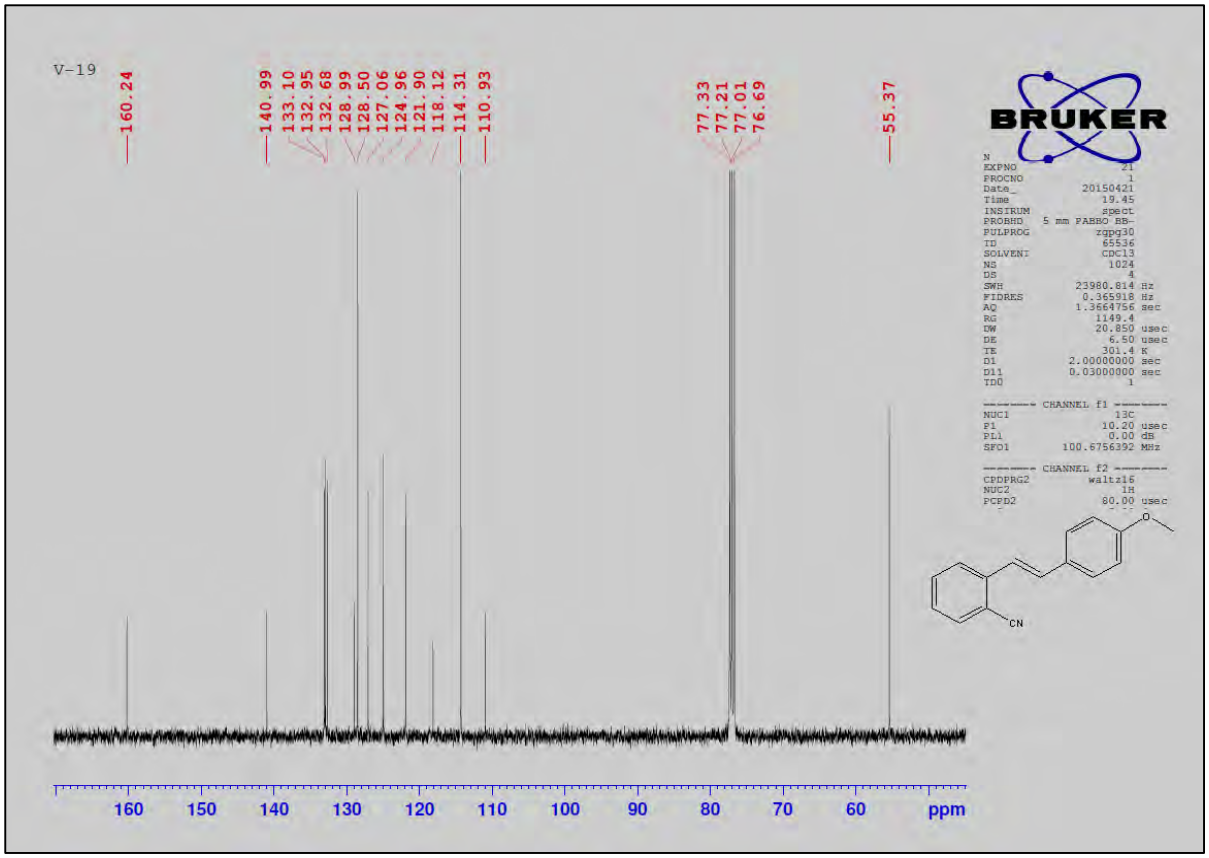

2D HSQC spectra of V19

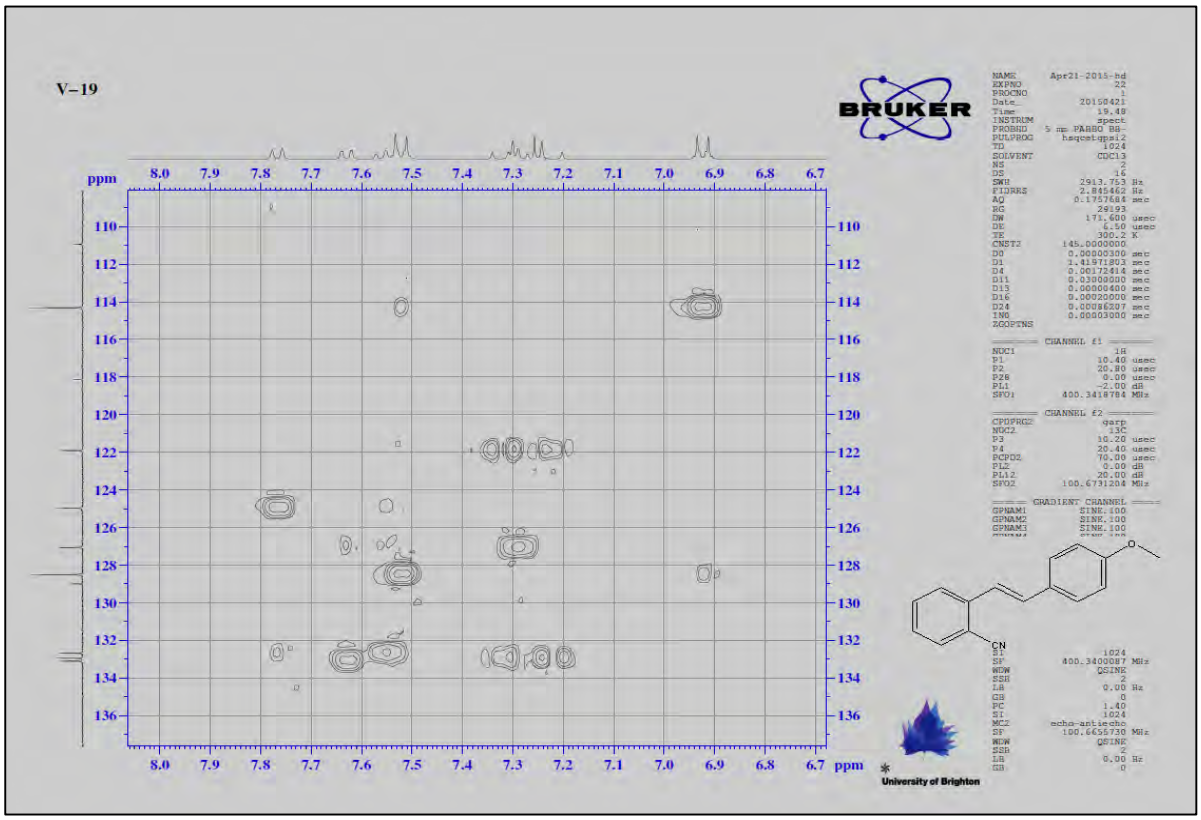

2D COSY spectra of V19

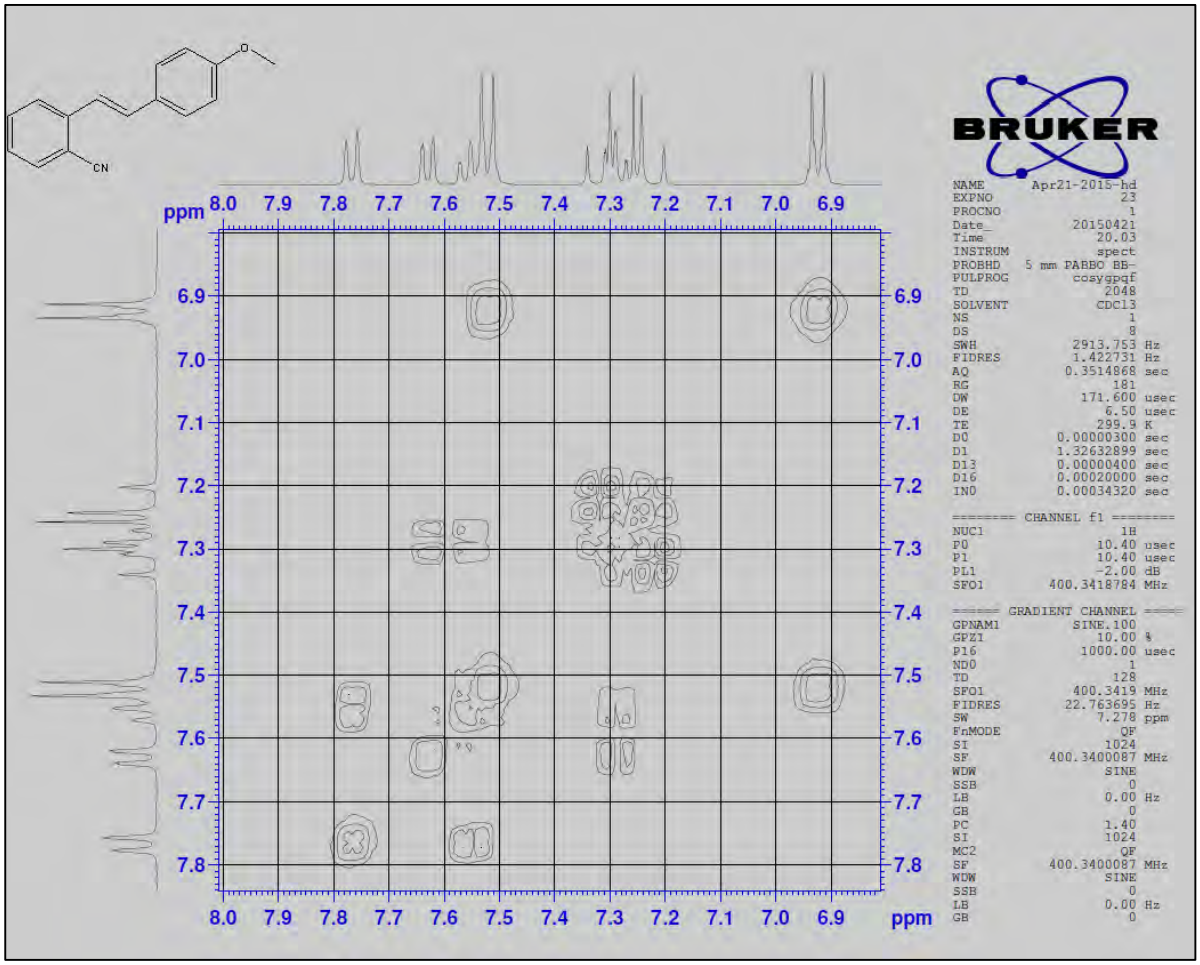

Mass spectra of V19

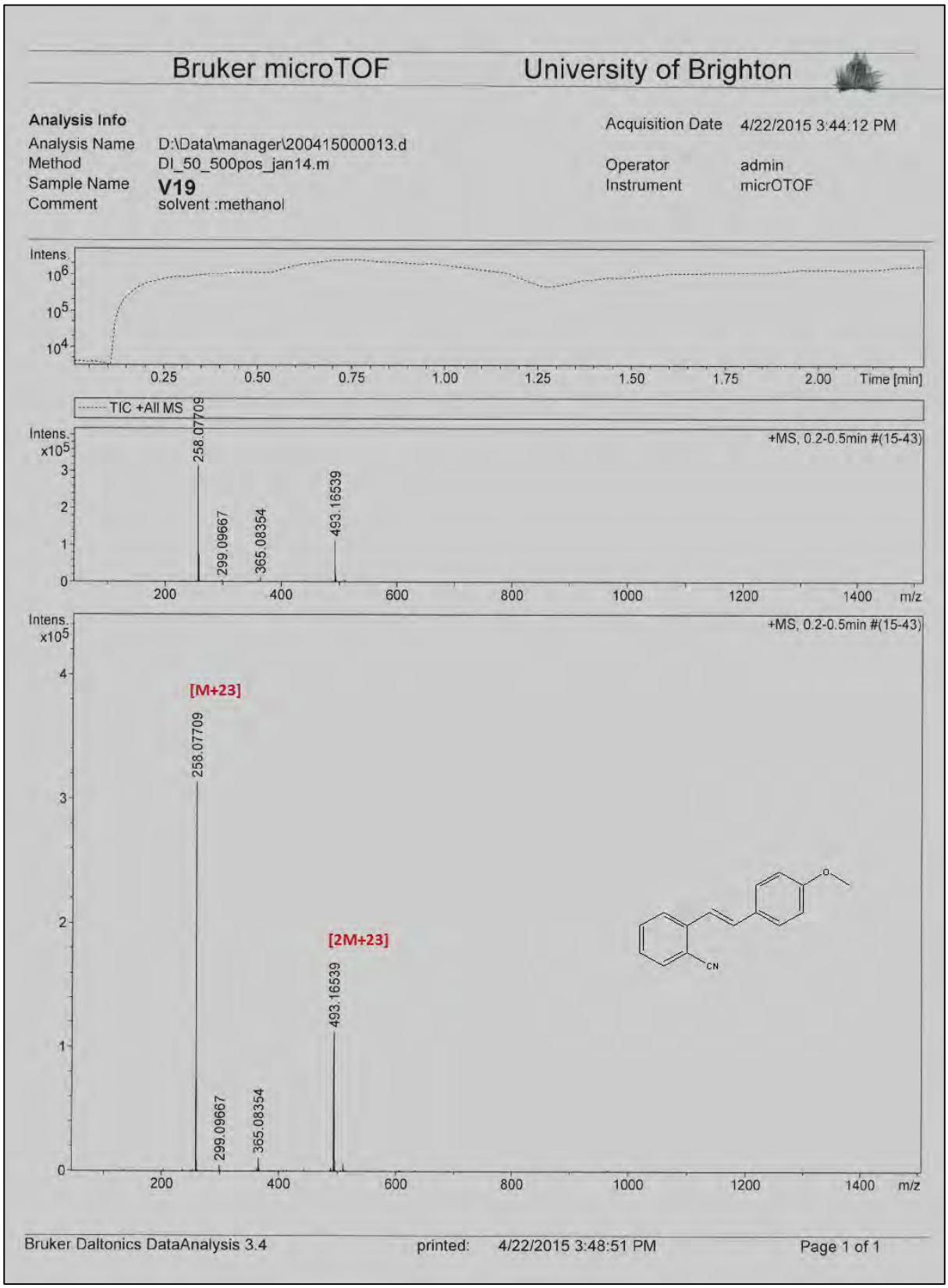

^{1}H NMR spectra of V20

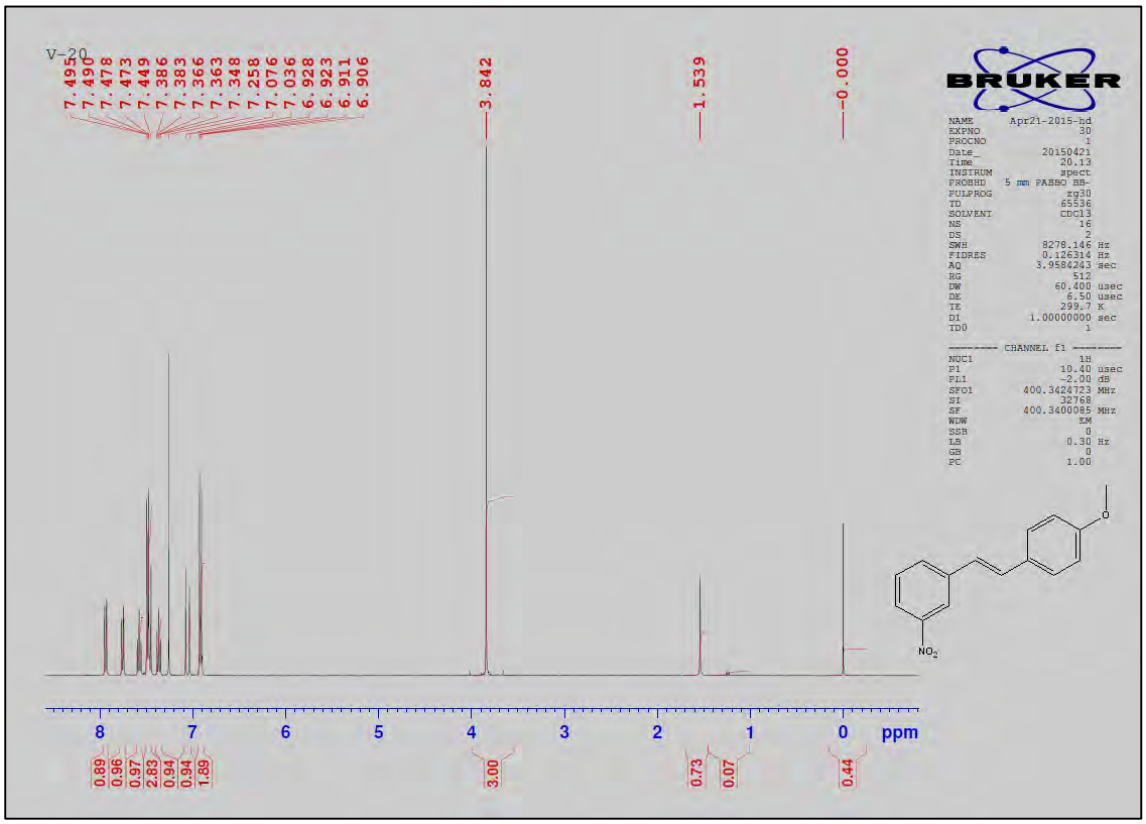

^{13}C NMR spectra of V20

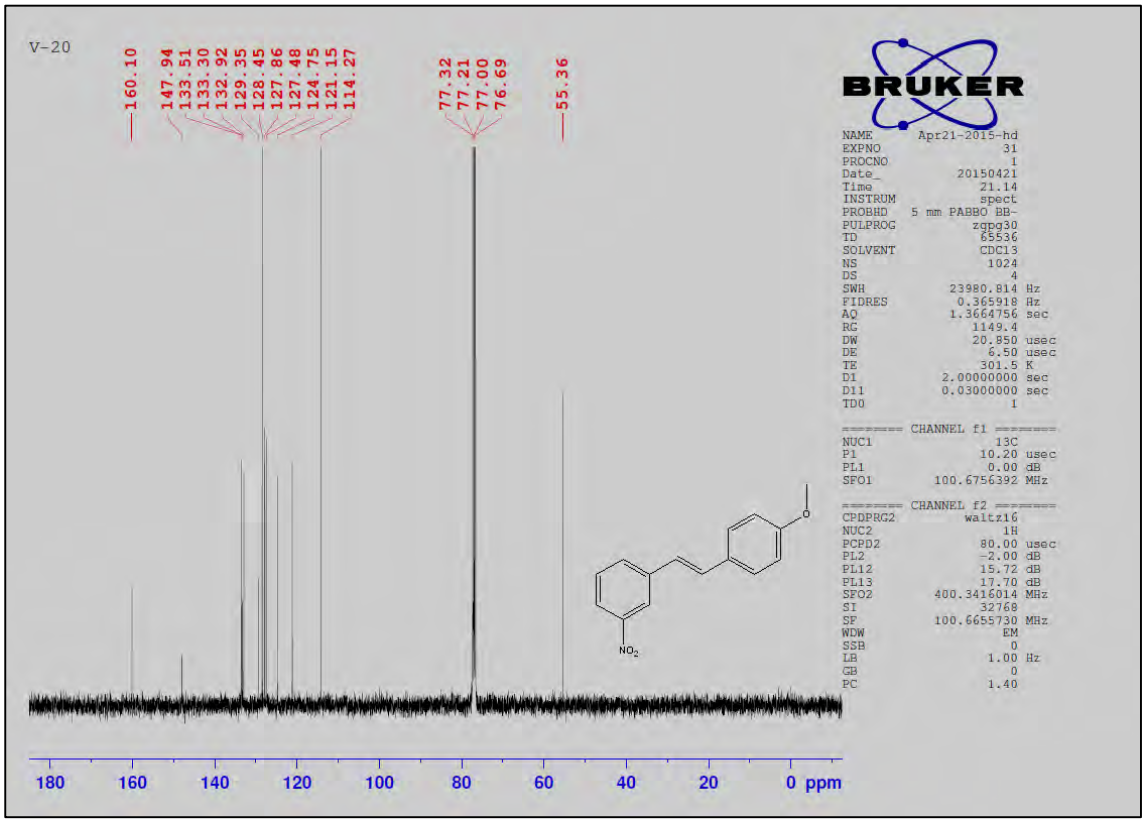

2D HSQC spectra of V20

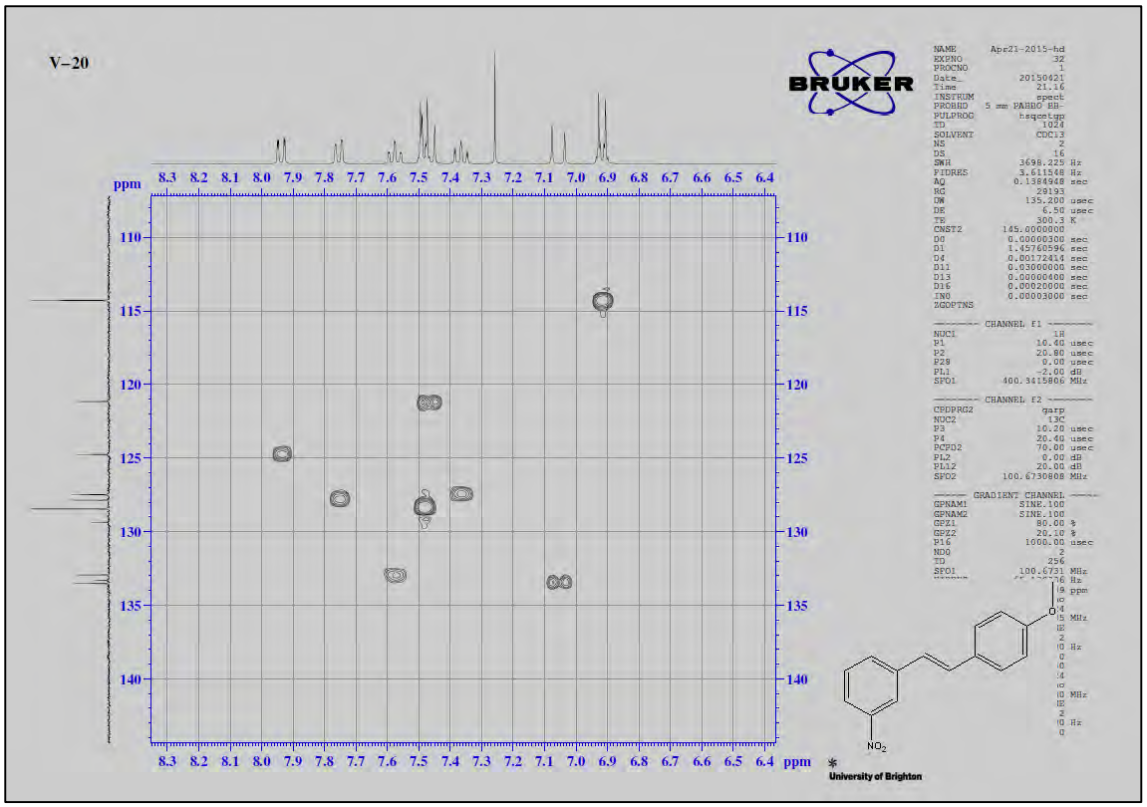

2D HSQC spectra of V20

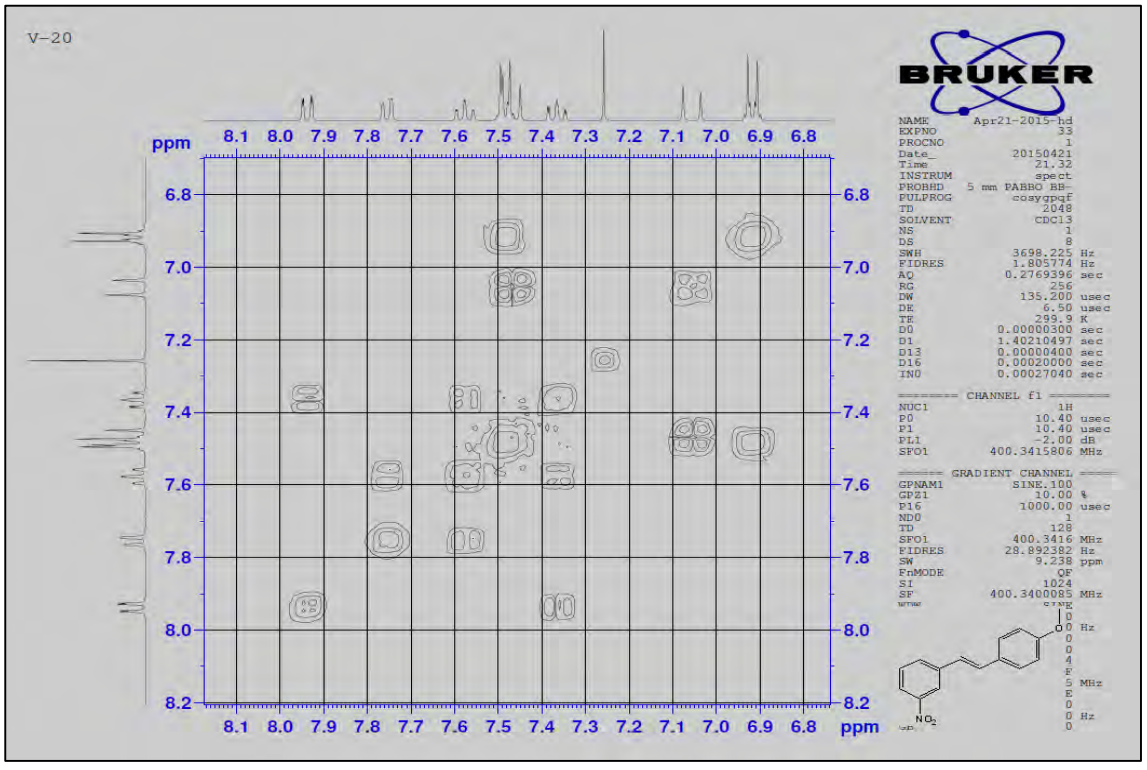

Mass spectra of V20

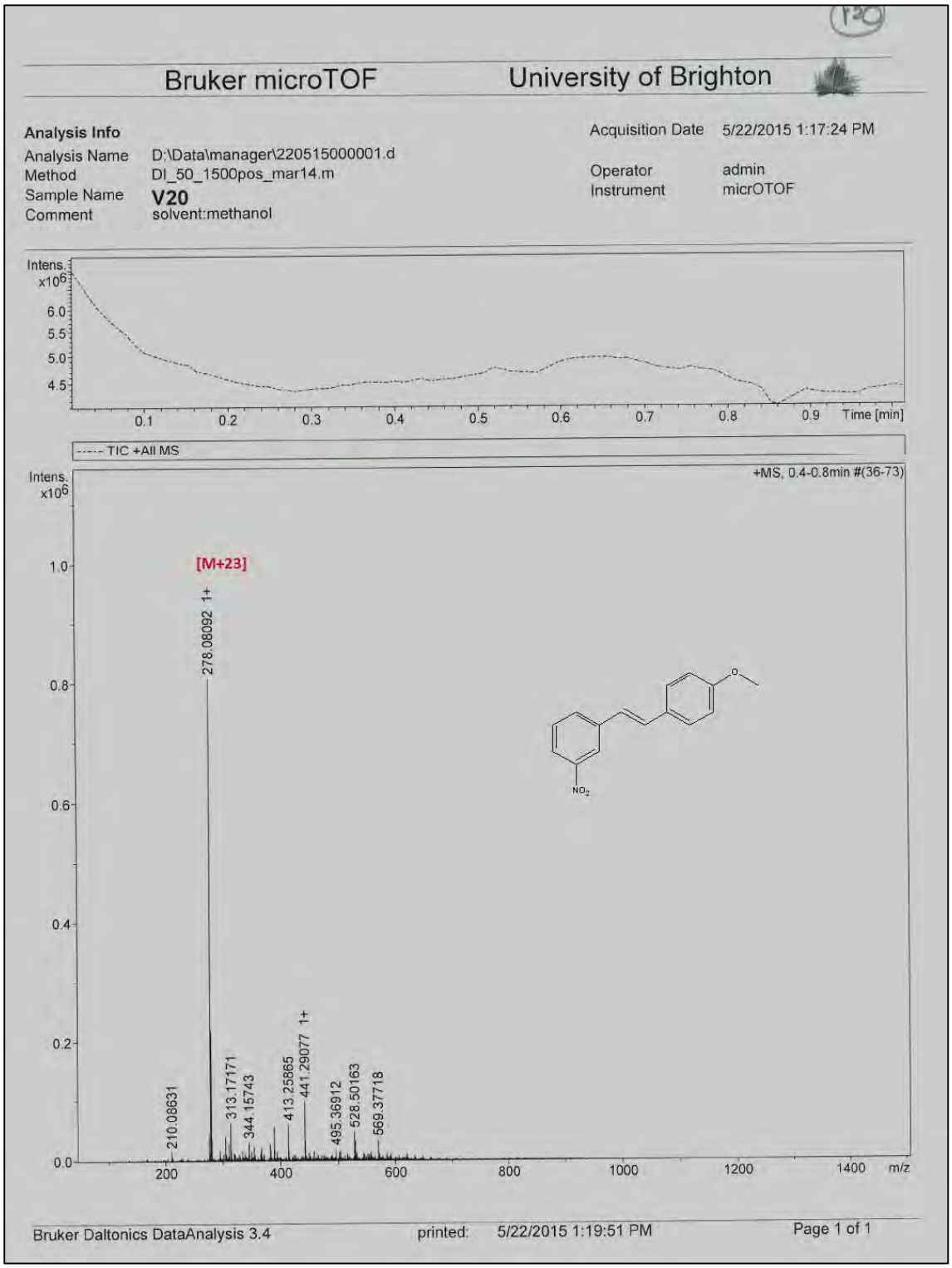

^{1}H NMR spectra of V21

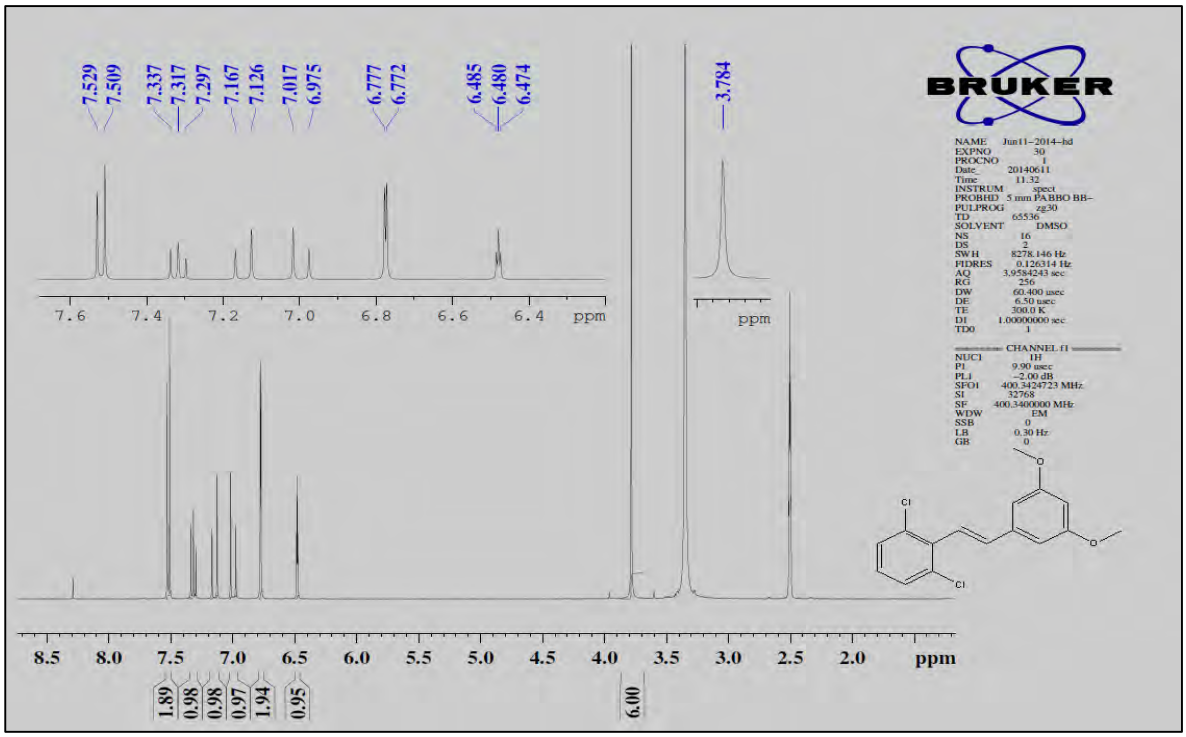

^{13}C NMR spectra of V21

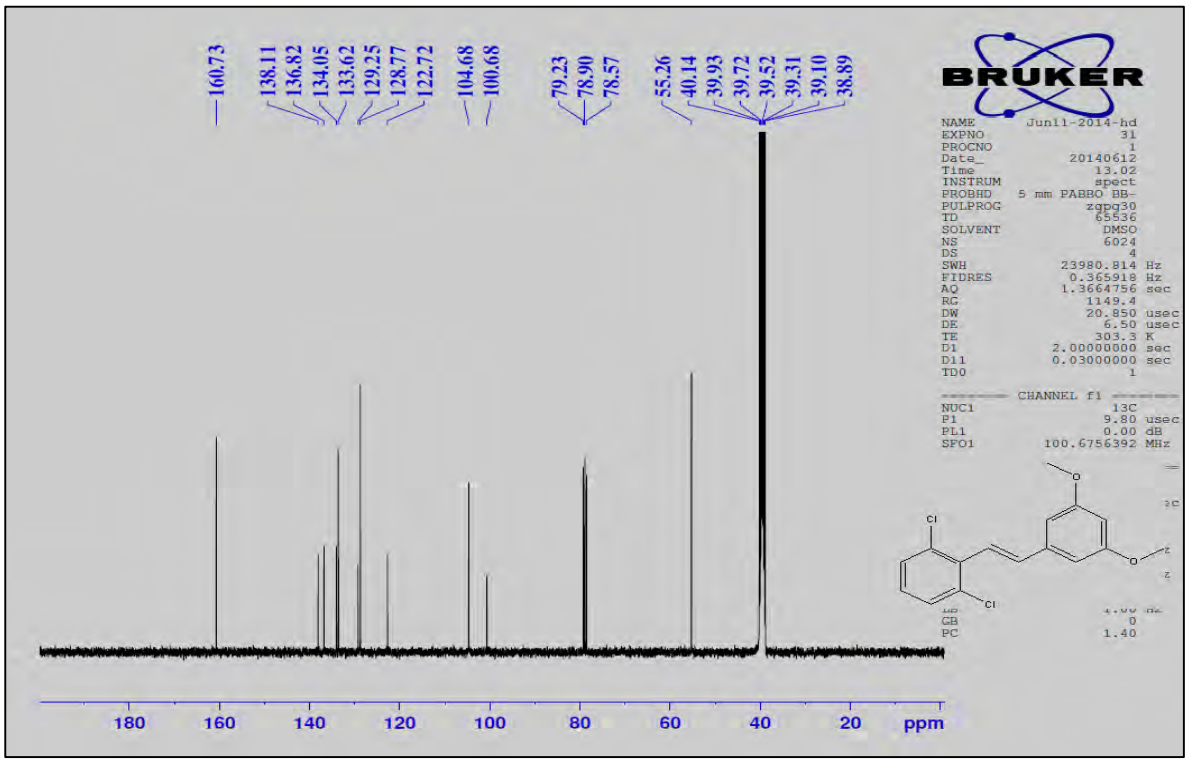

2D HSQC spectra of V21

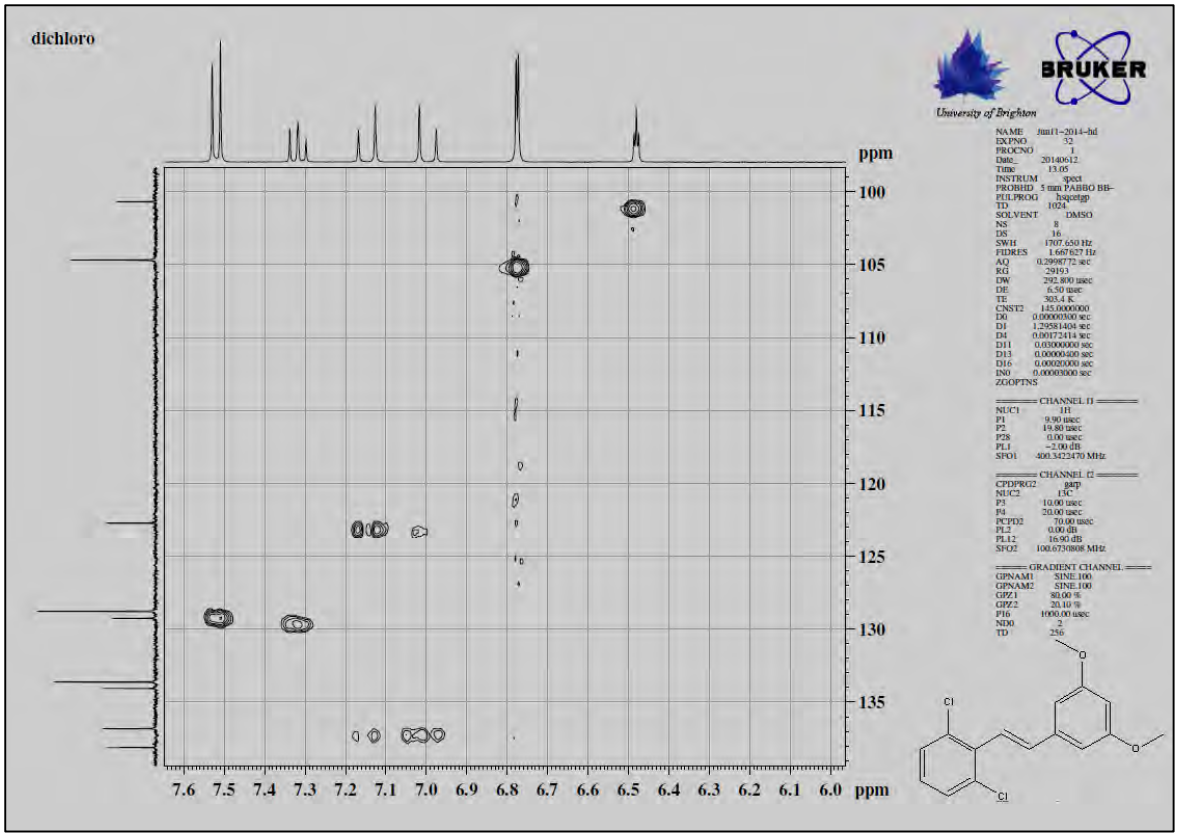

2D COSY spectra of V21

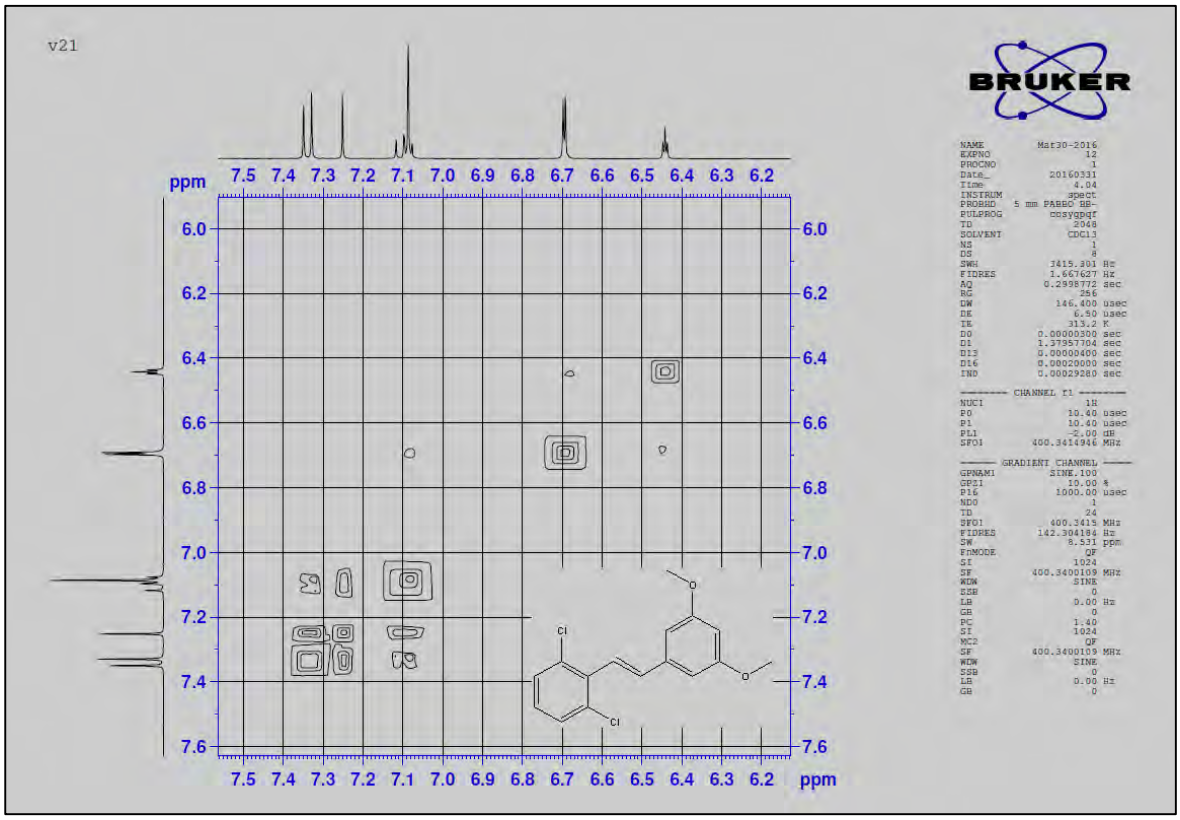

Mass spectra of V21

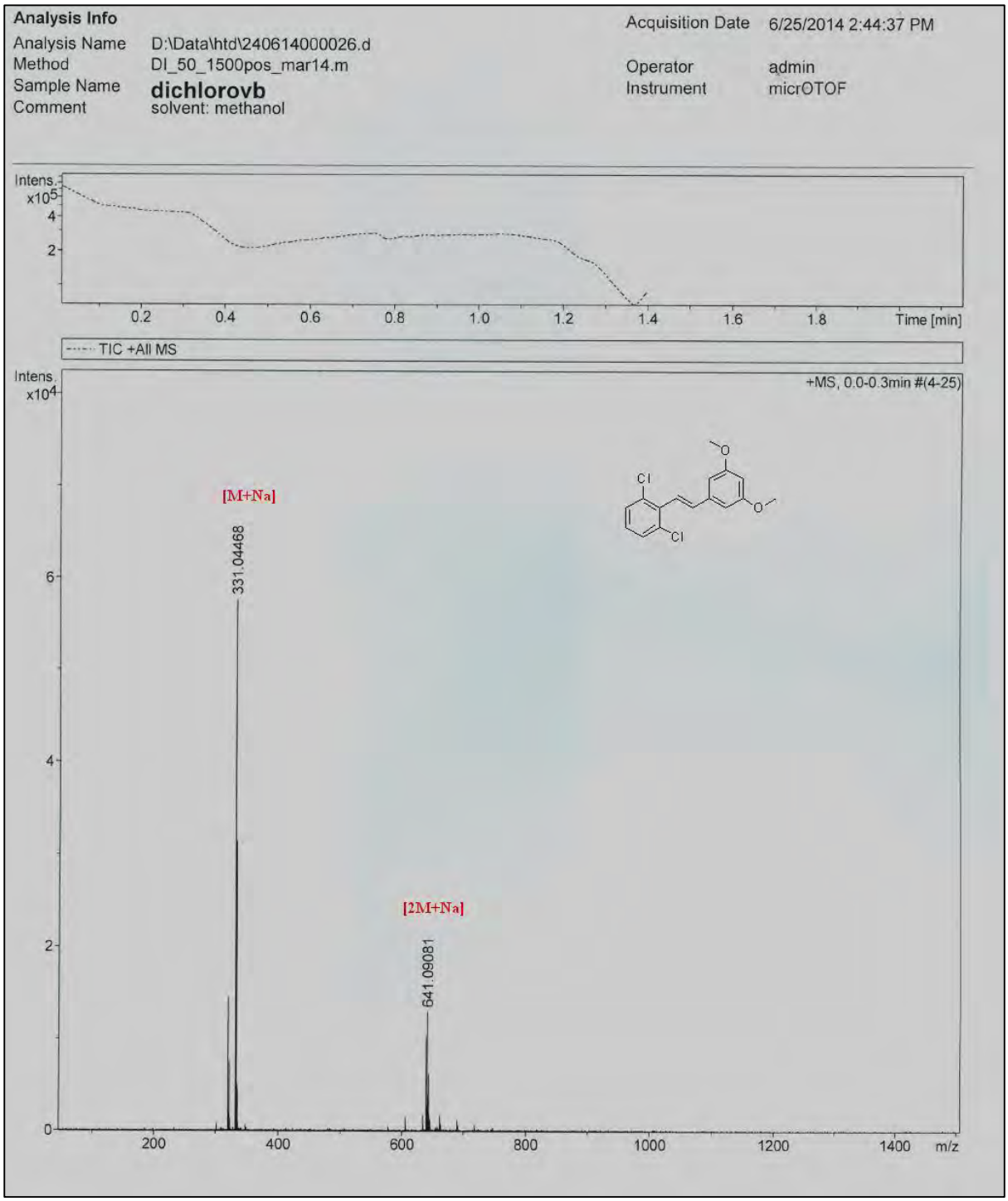

^{1}H NMR spectra of V22

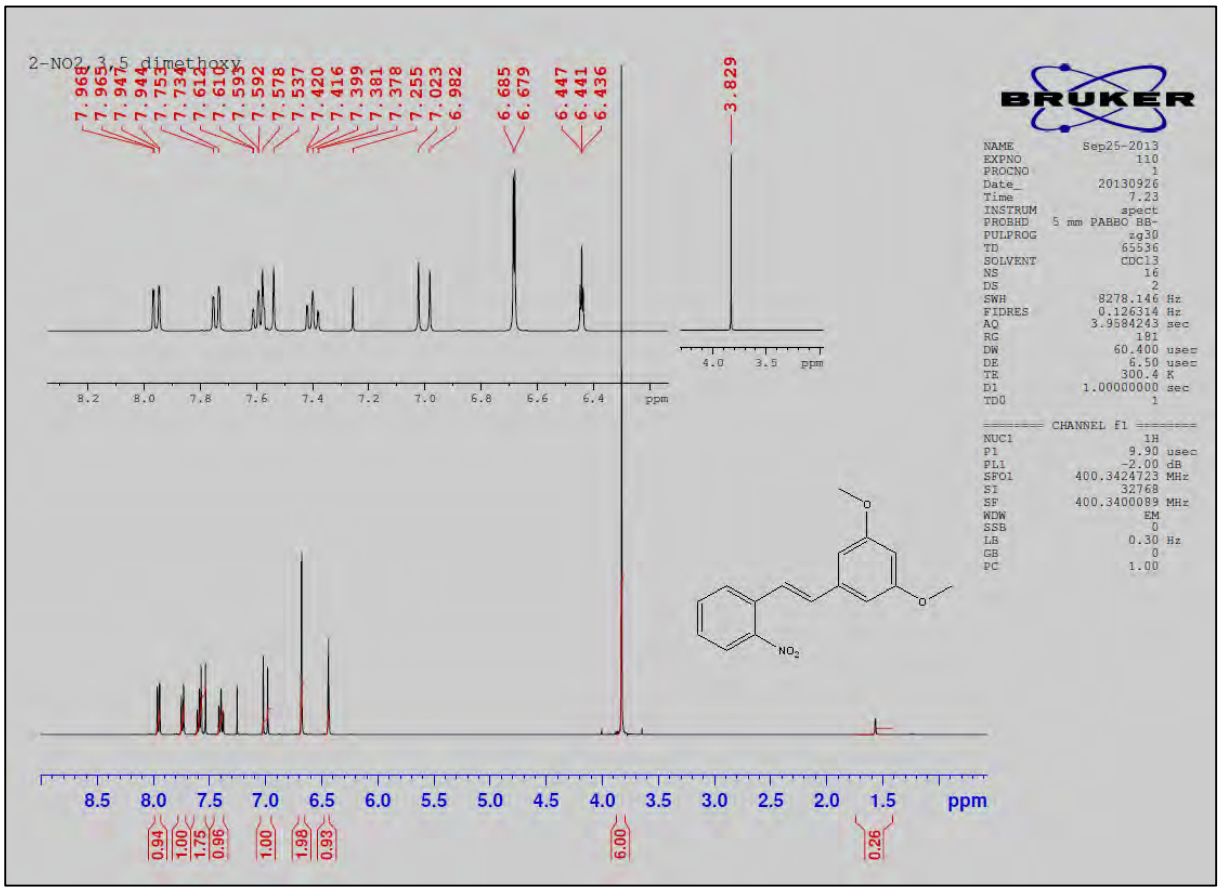

^{13}C NMR spectra of V22

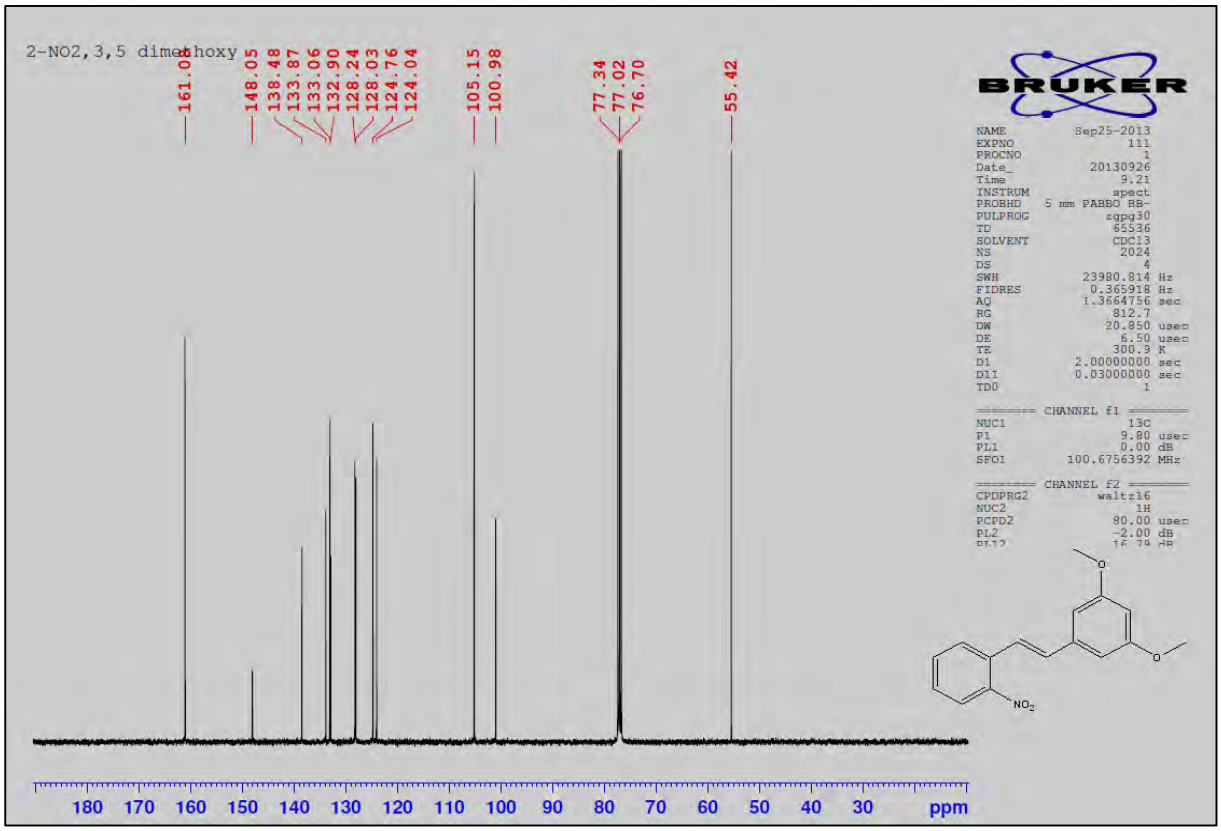

2D HSQC spectra of V22

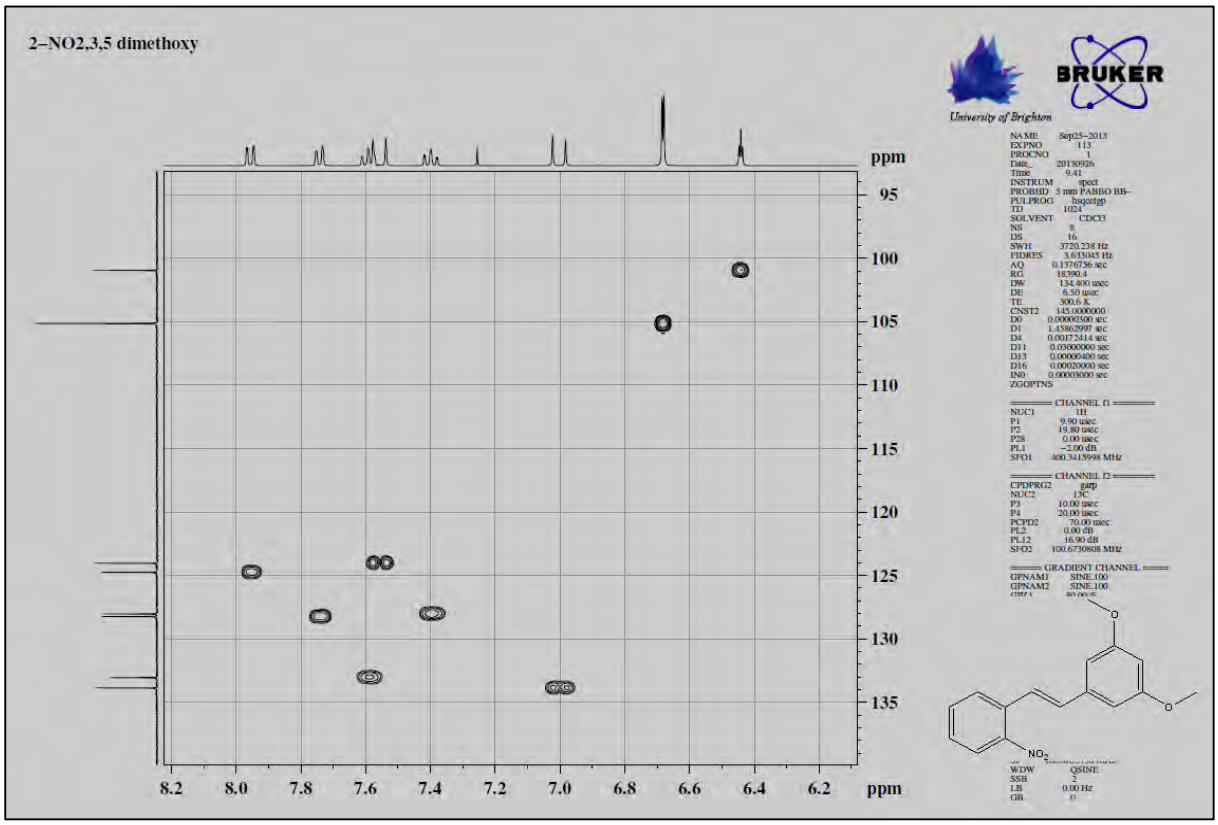

2D COSY spectra of V22

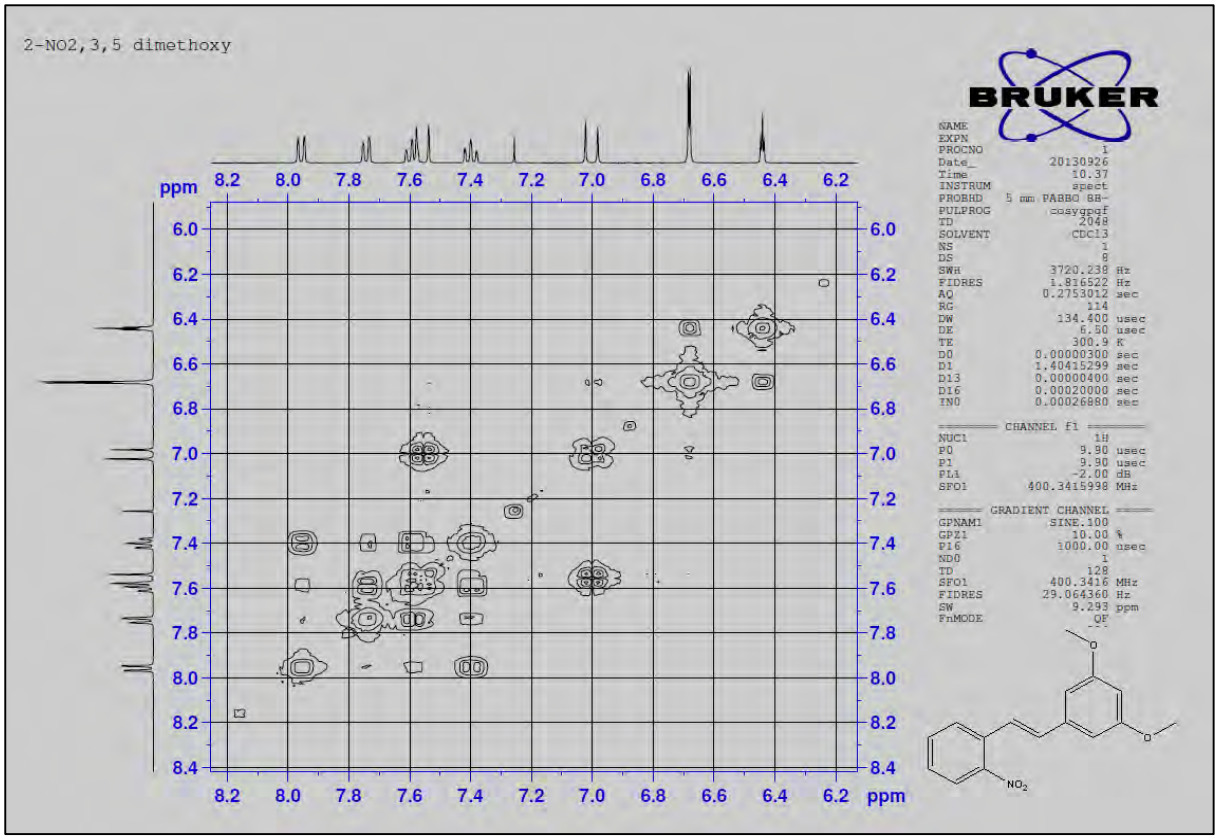

Mass spectra of V22

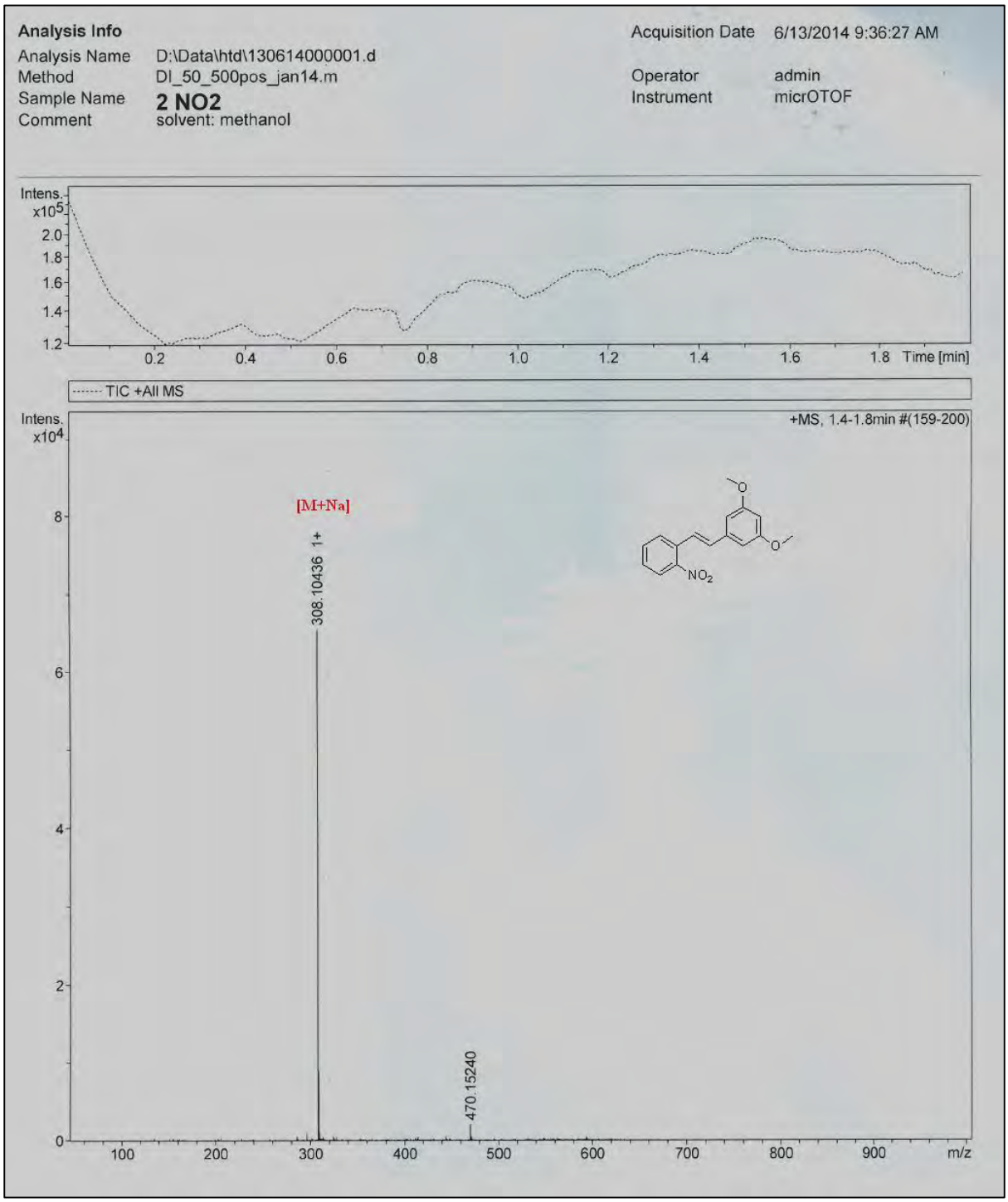

^{1}H NMR spectra of V23

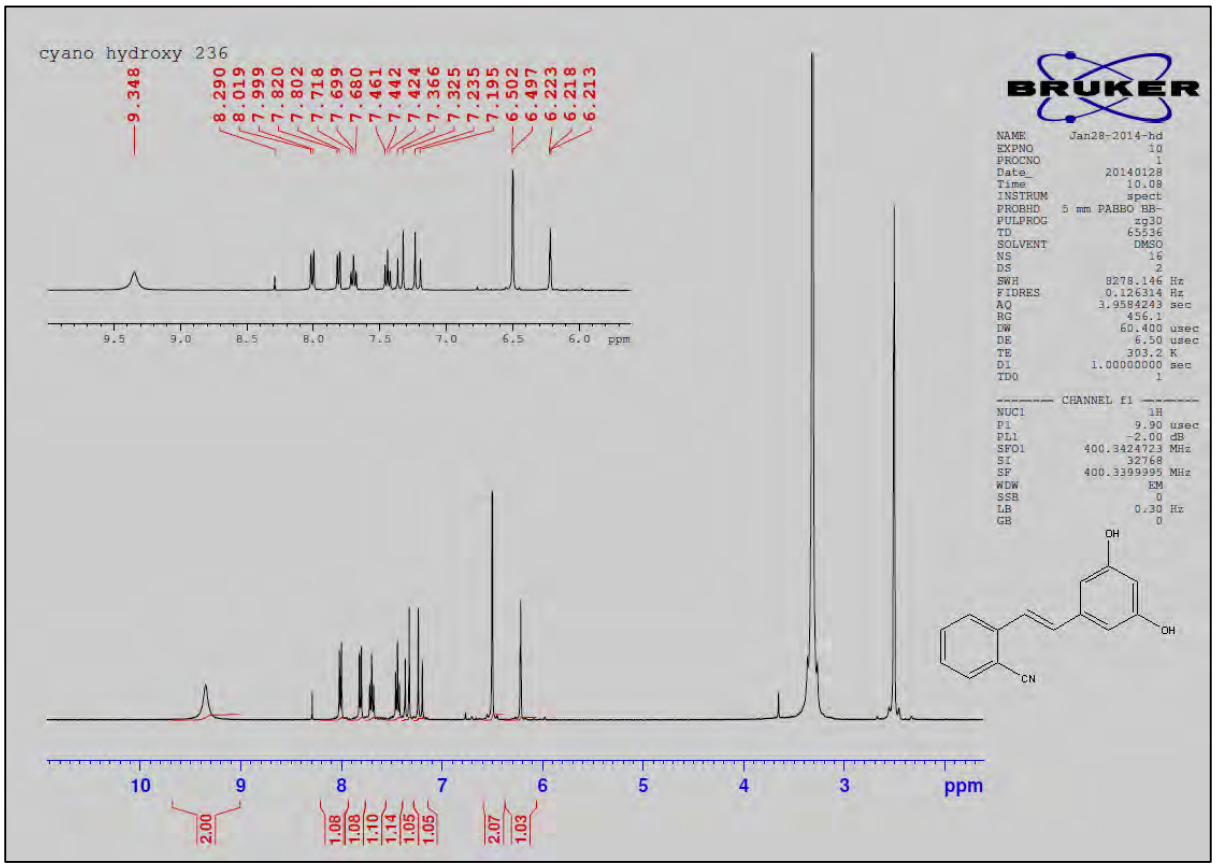

^{13}C NMR spectra of V23

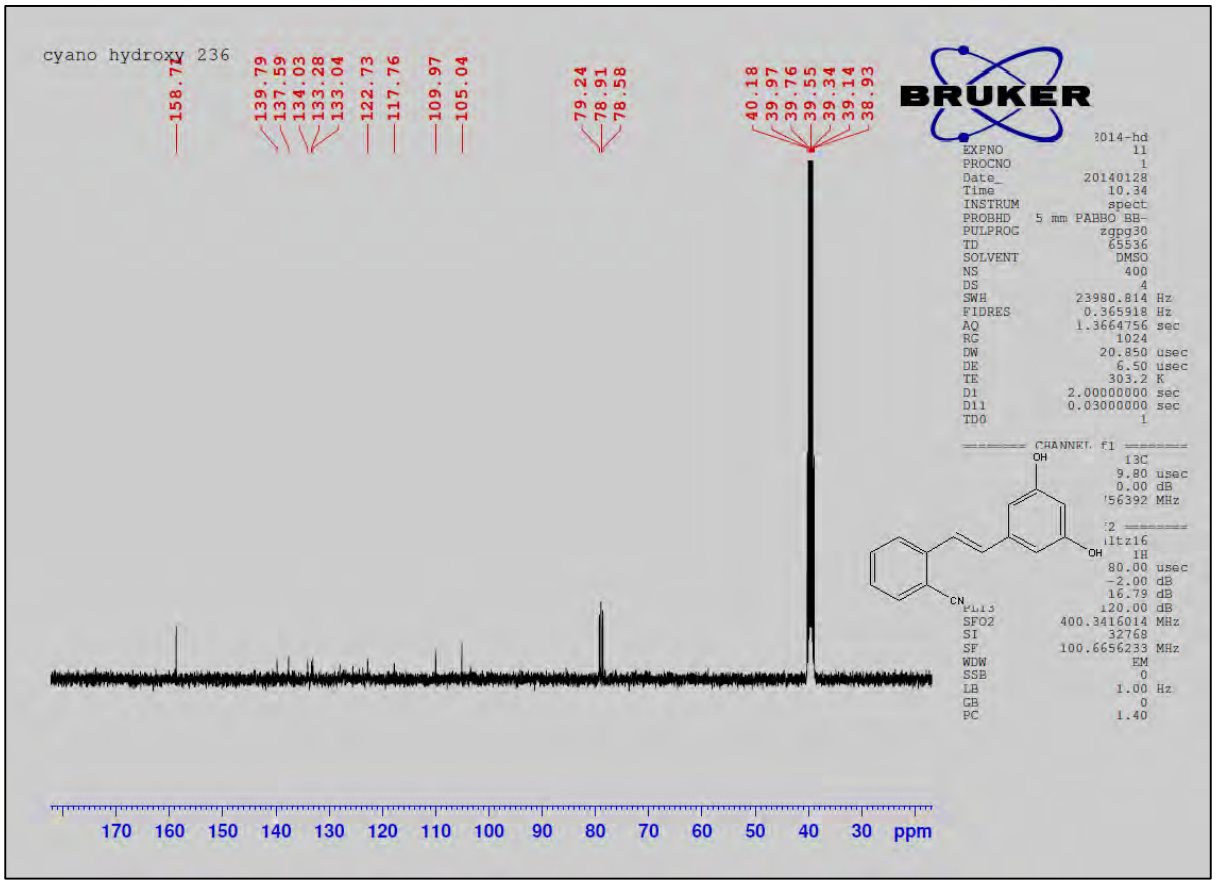

2D HSQC spectra of V23

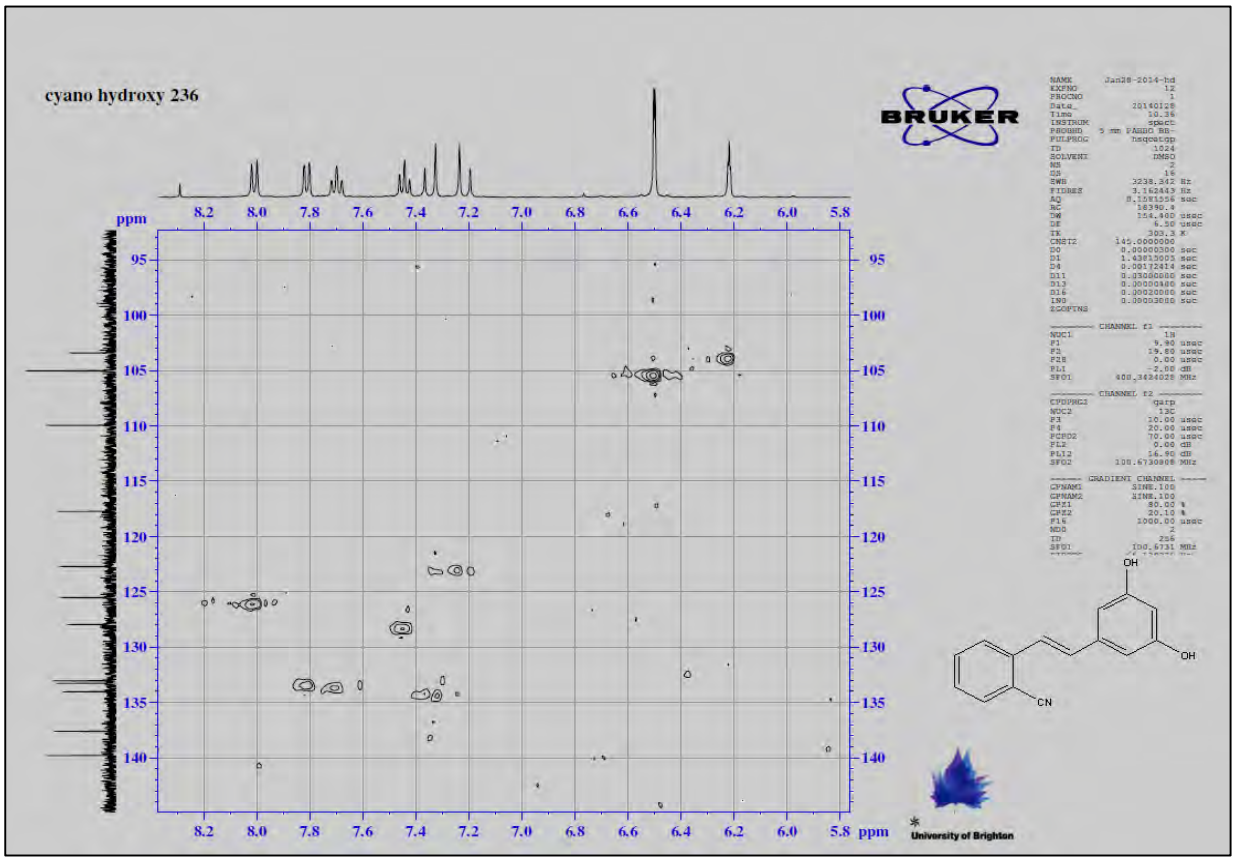

2D COSY spectra of V23

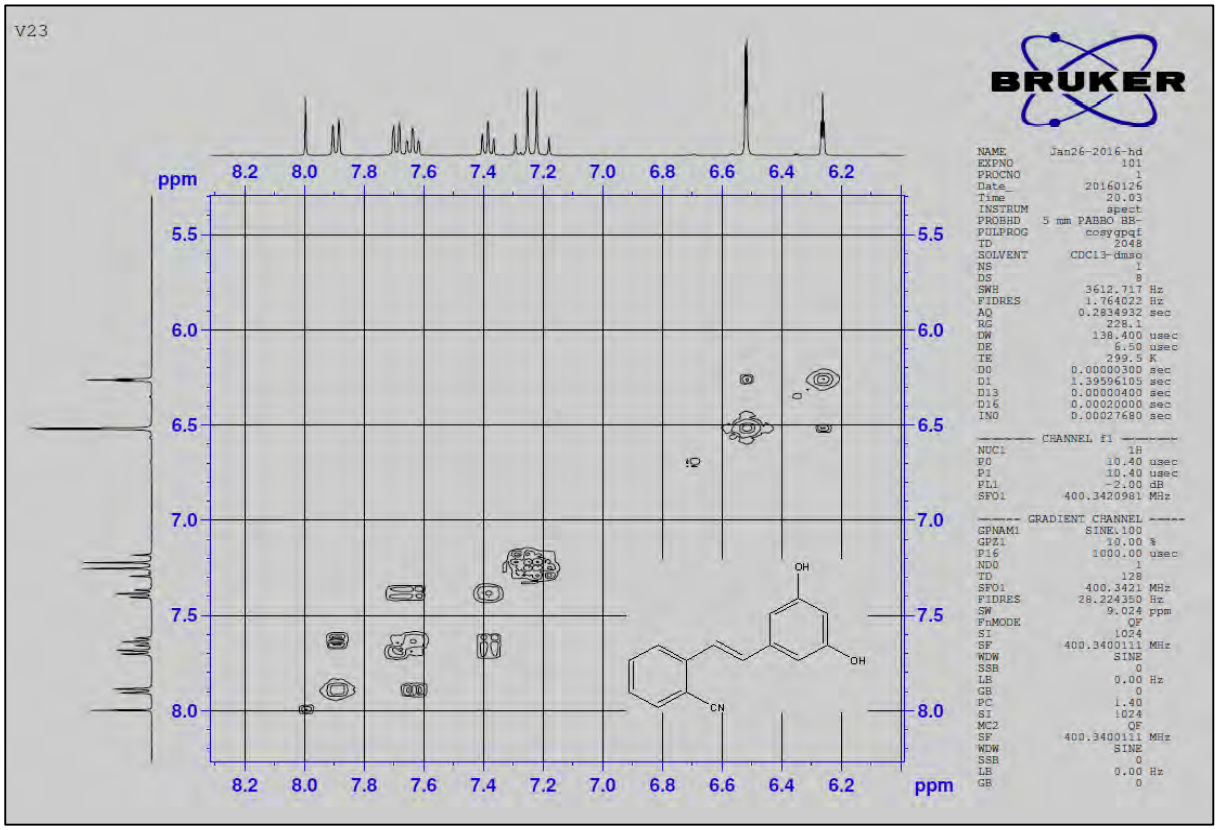

Mass spectra of V23

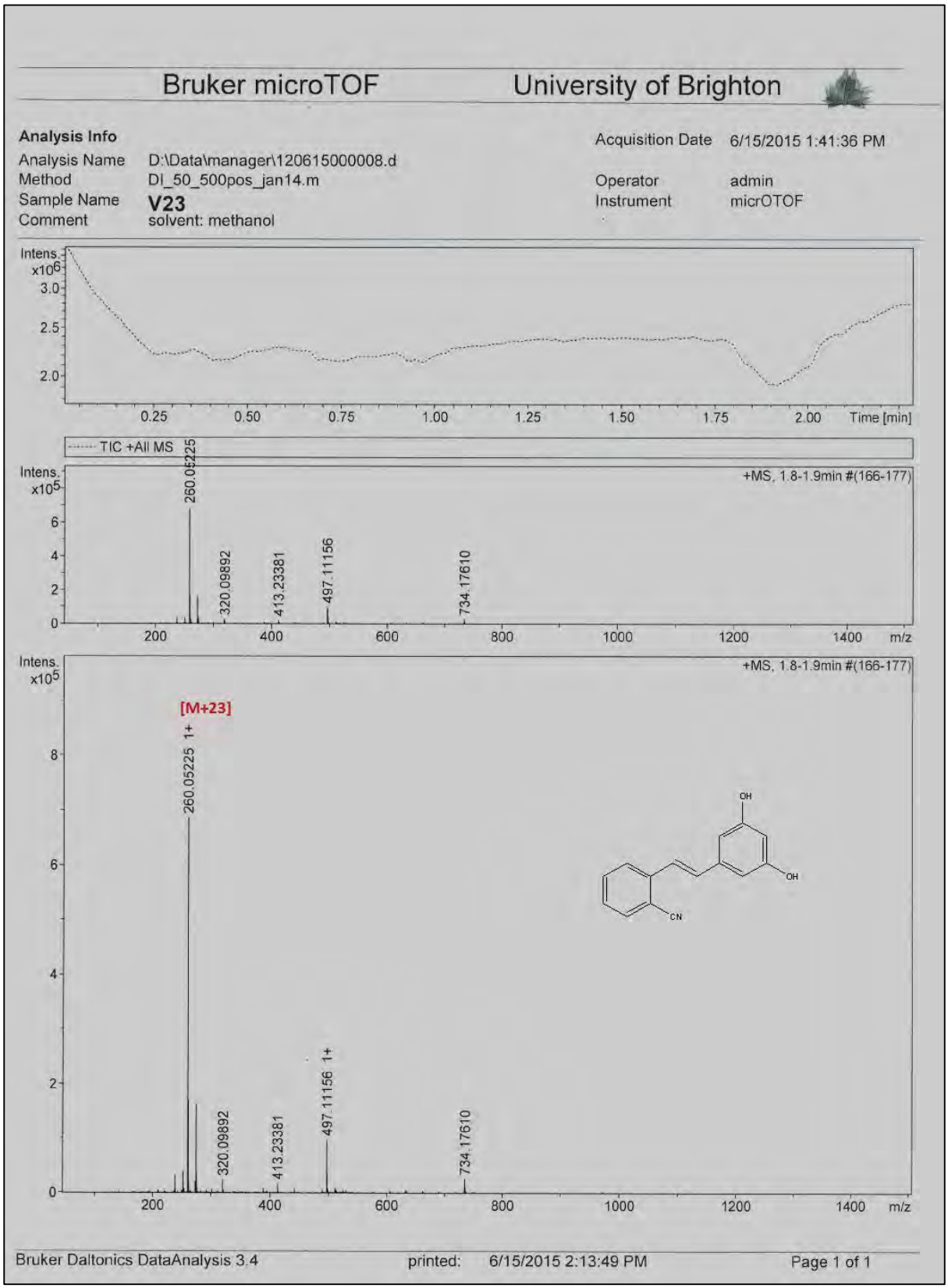

^{1}H NMR spectra of V24

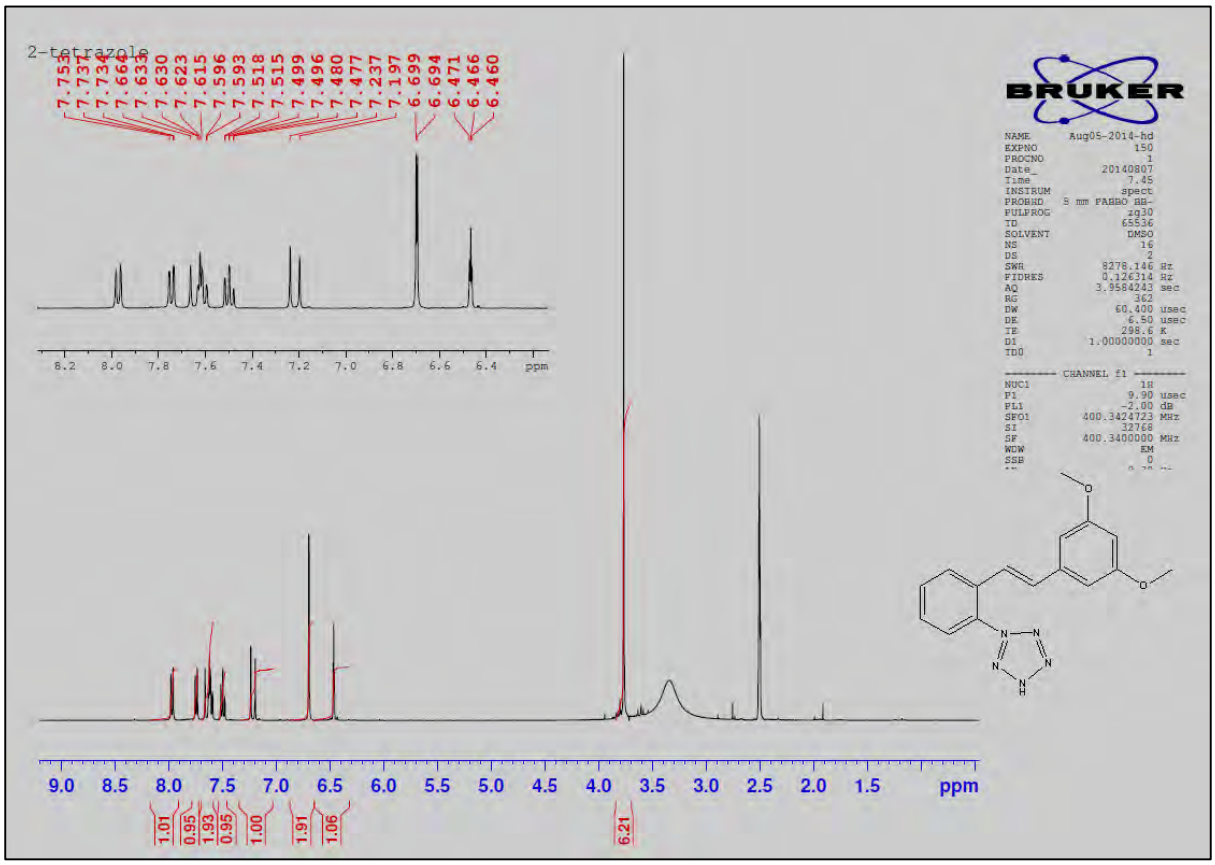

^{13}C NMR spectra of V24

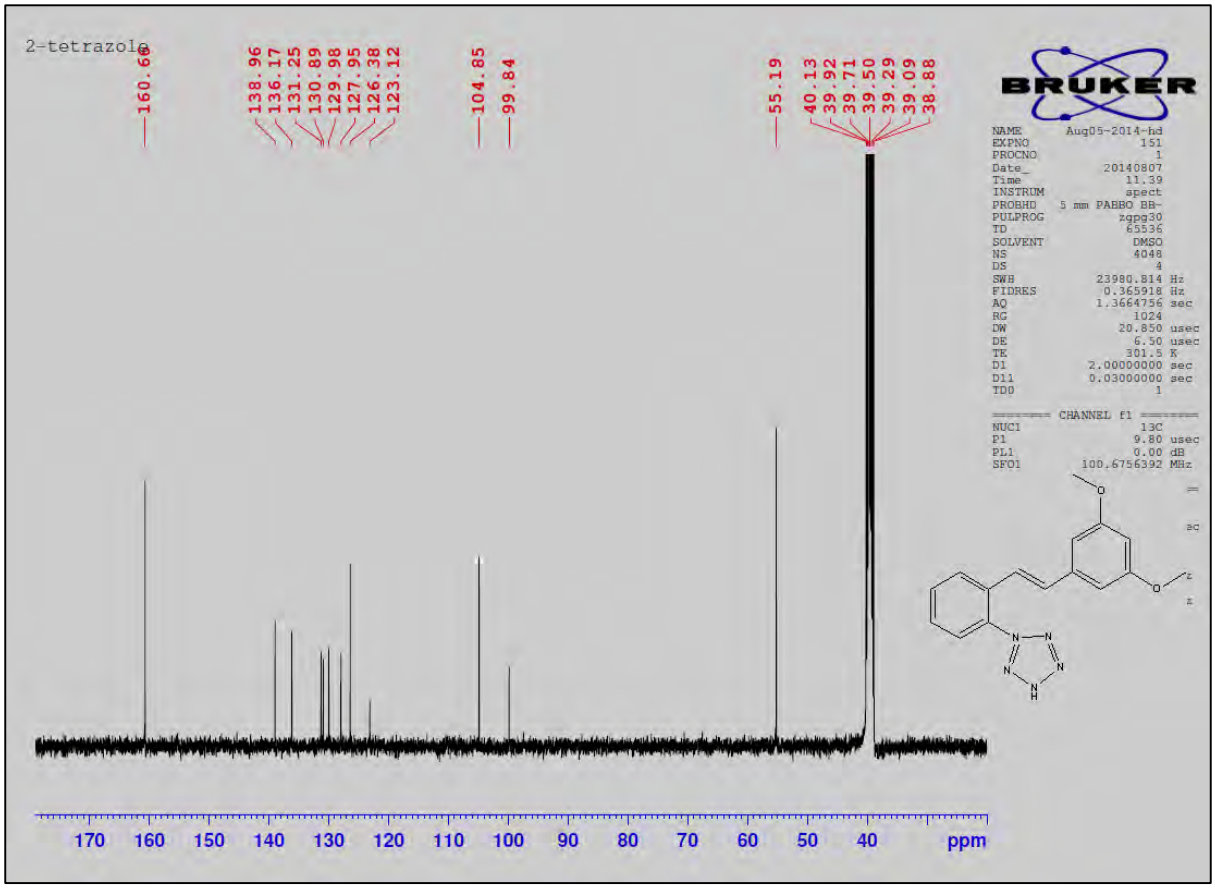

2D HSQC spectra of V24

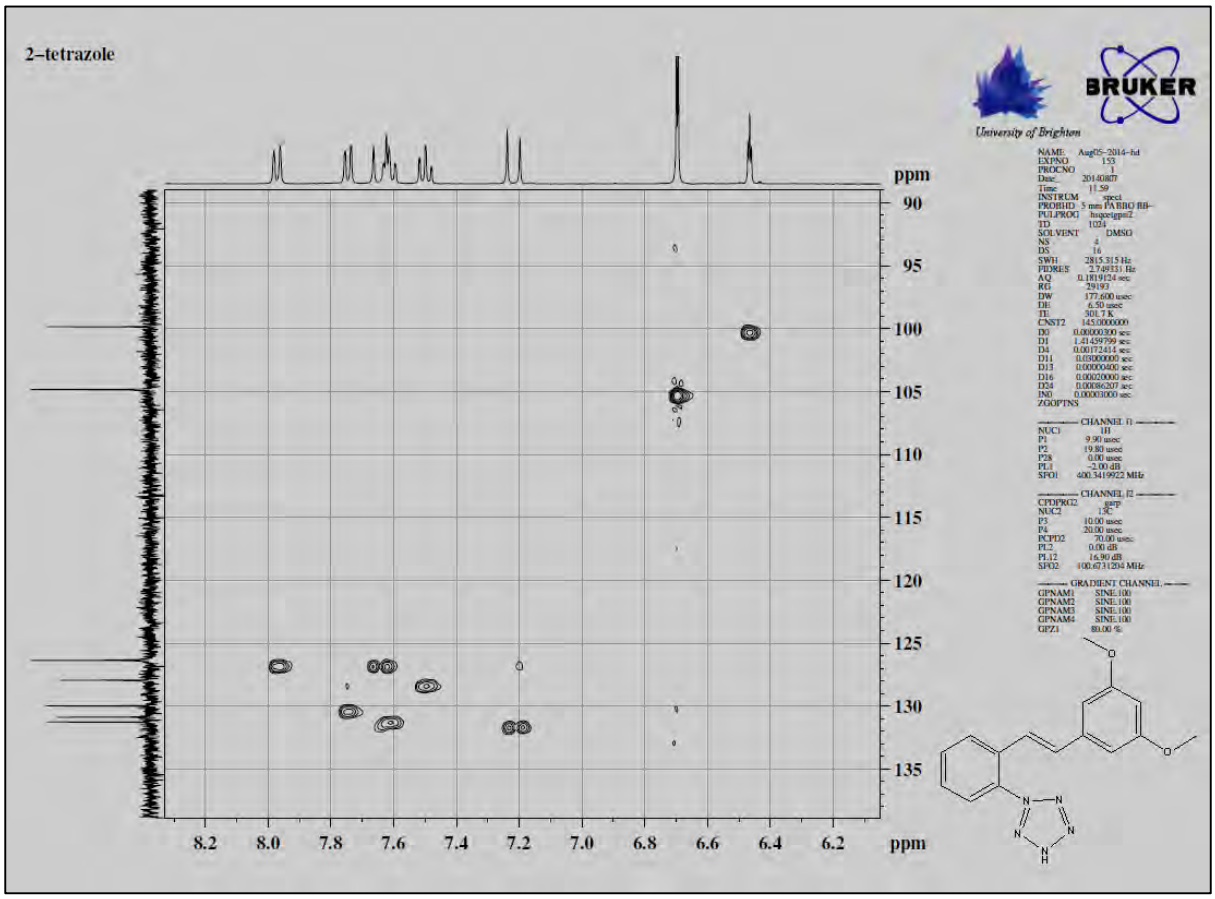

2D COSY spectra of V24

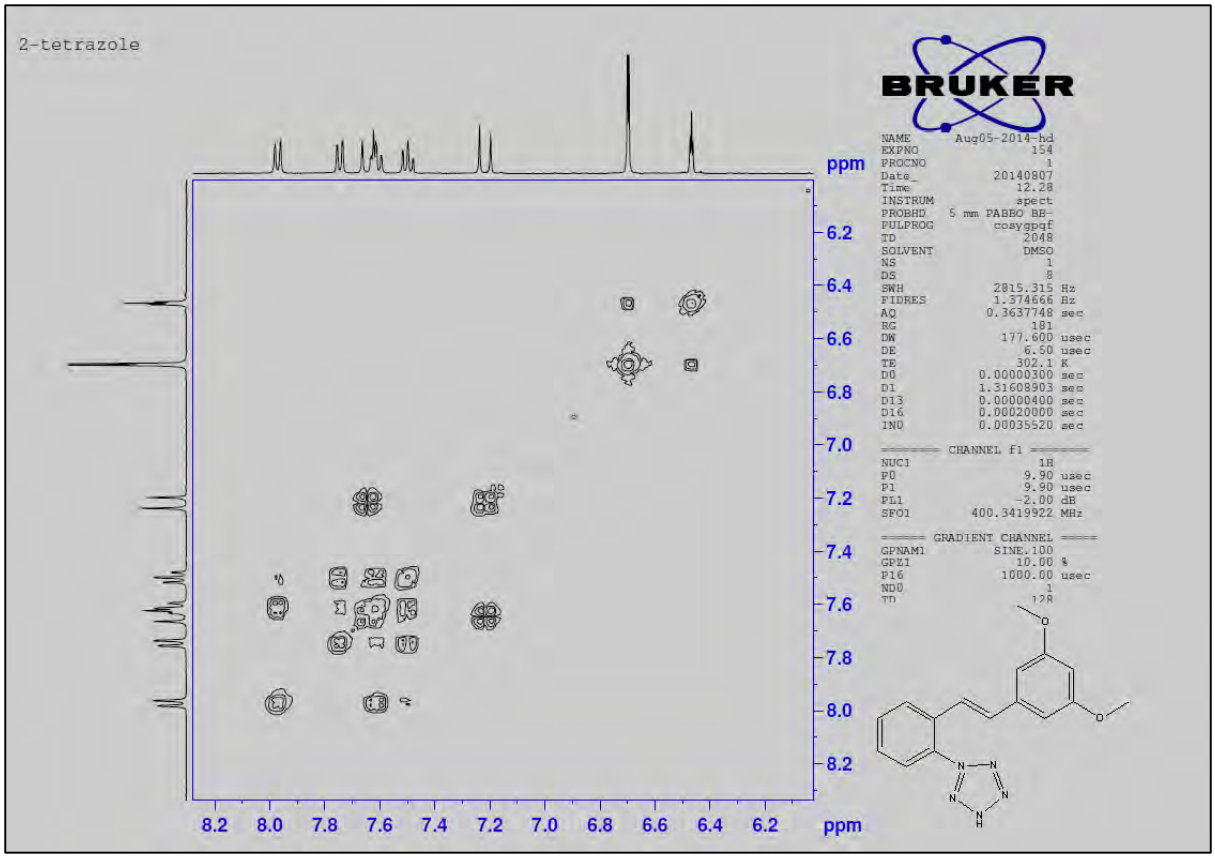

Mass spectra of V24

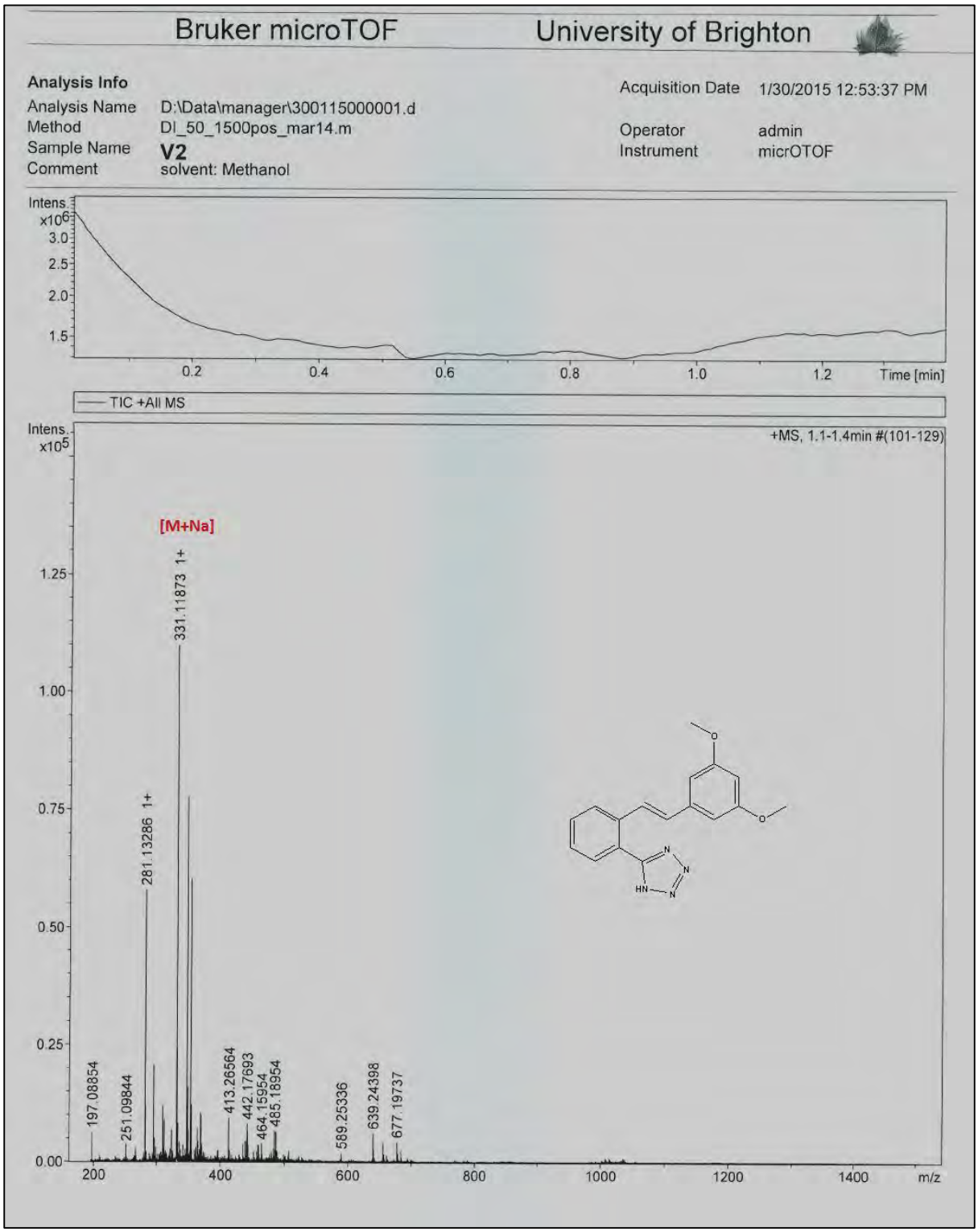

^{1}H NMR spectra of V25

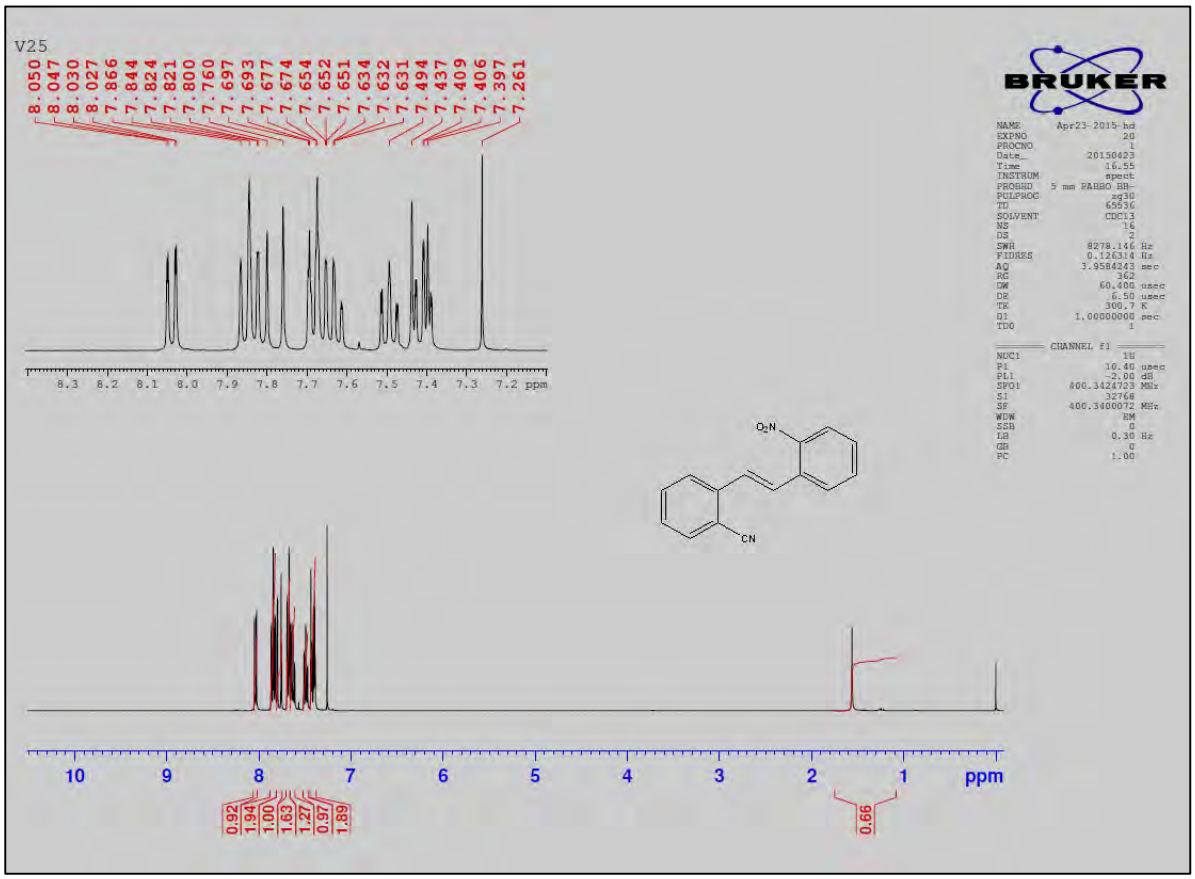

^{13}C NMR spectra of V25

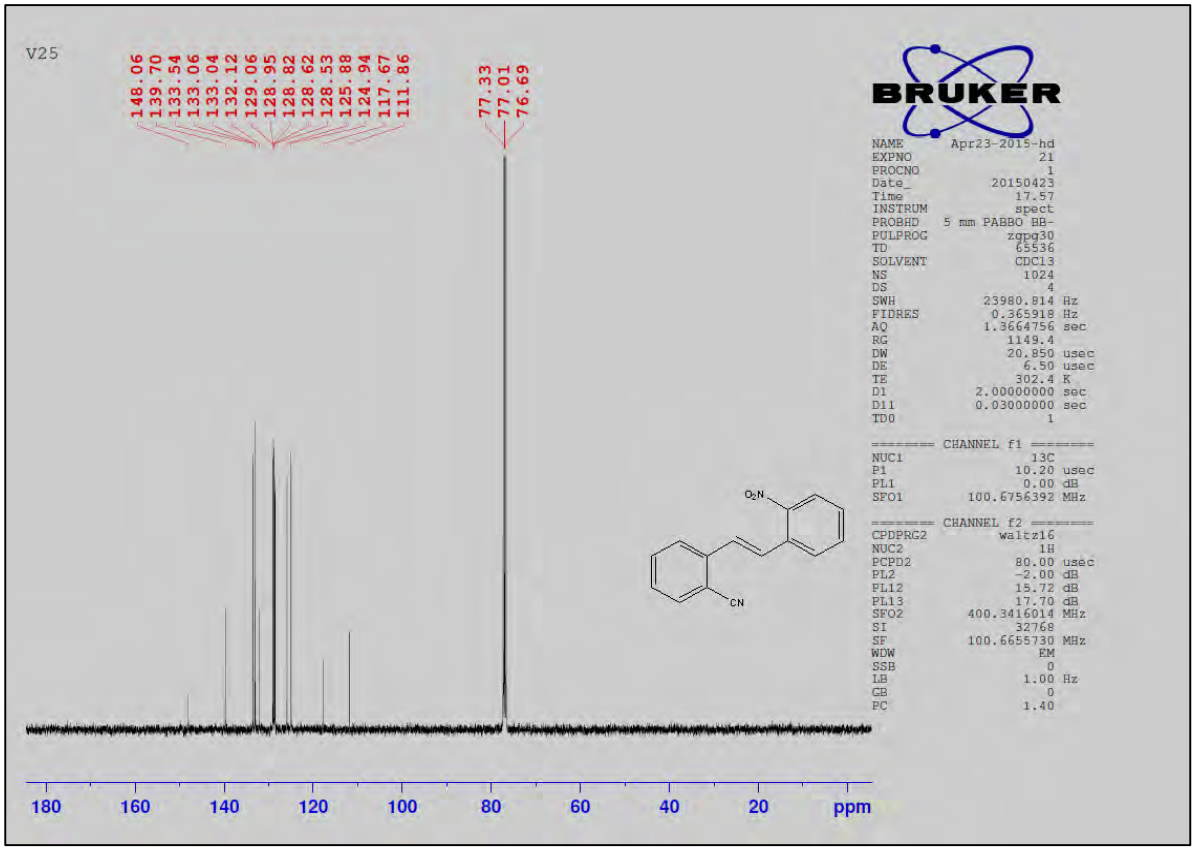

2D HSQC spectra of V25

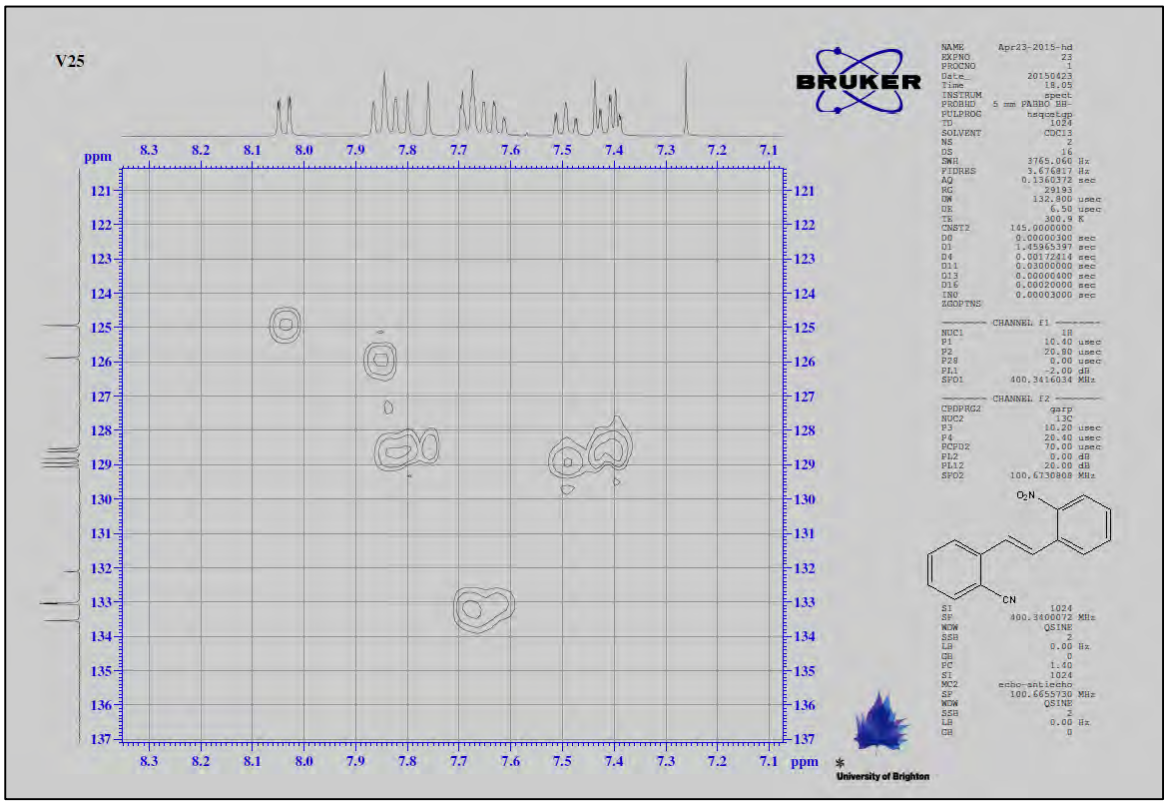

2D COSY spectra of V25

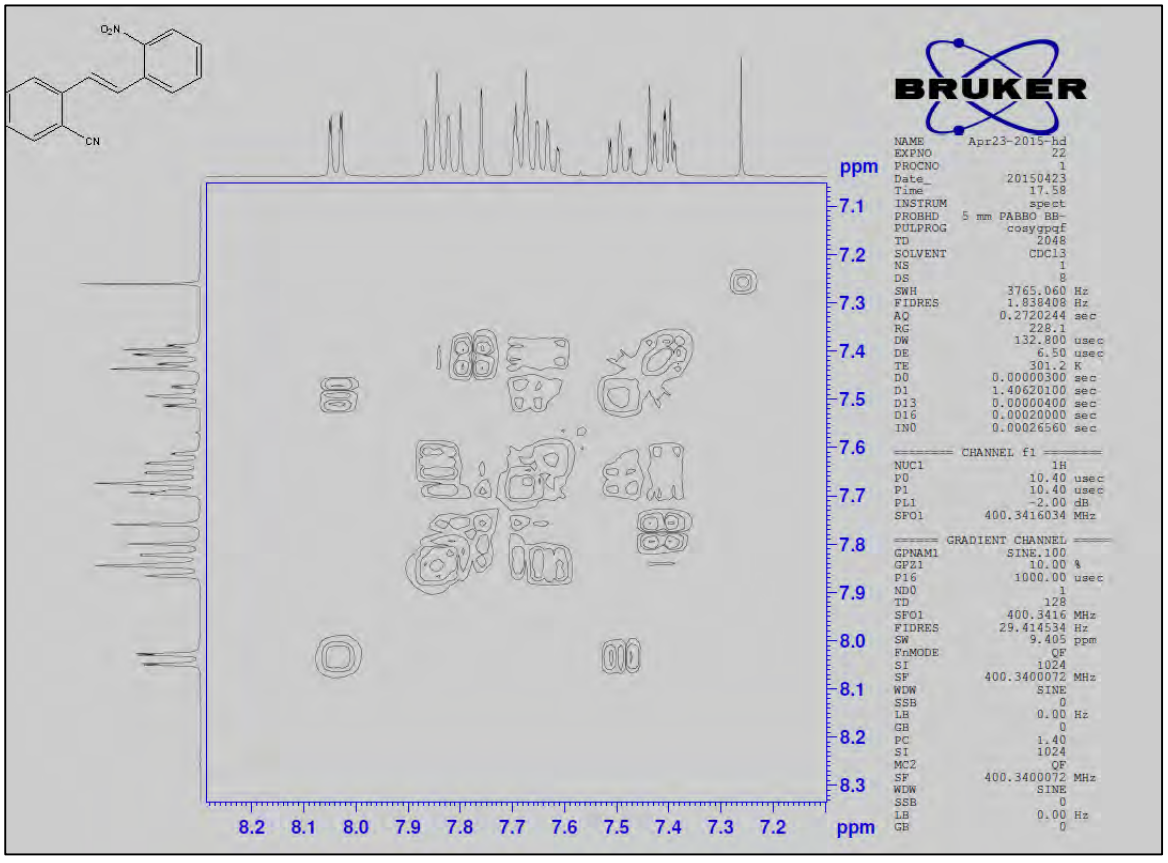

Mass spectra of V25

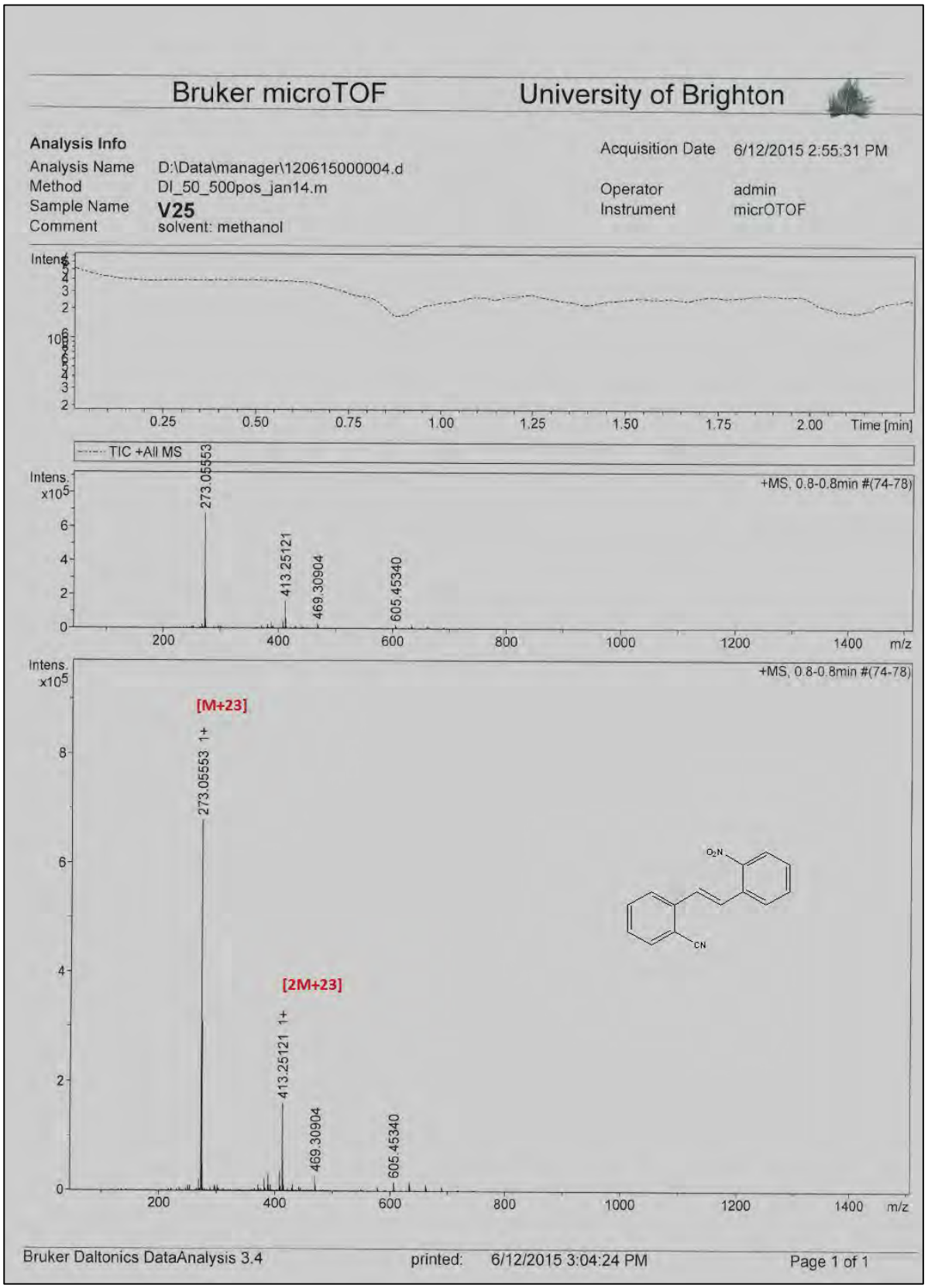

^{1}H NMR spectra of V26

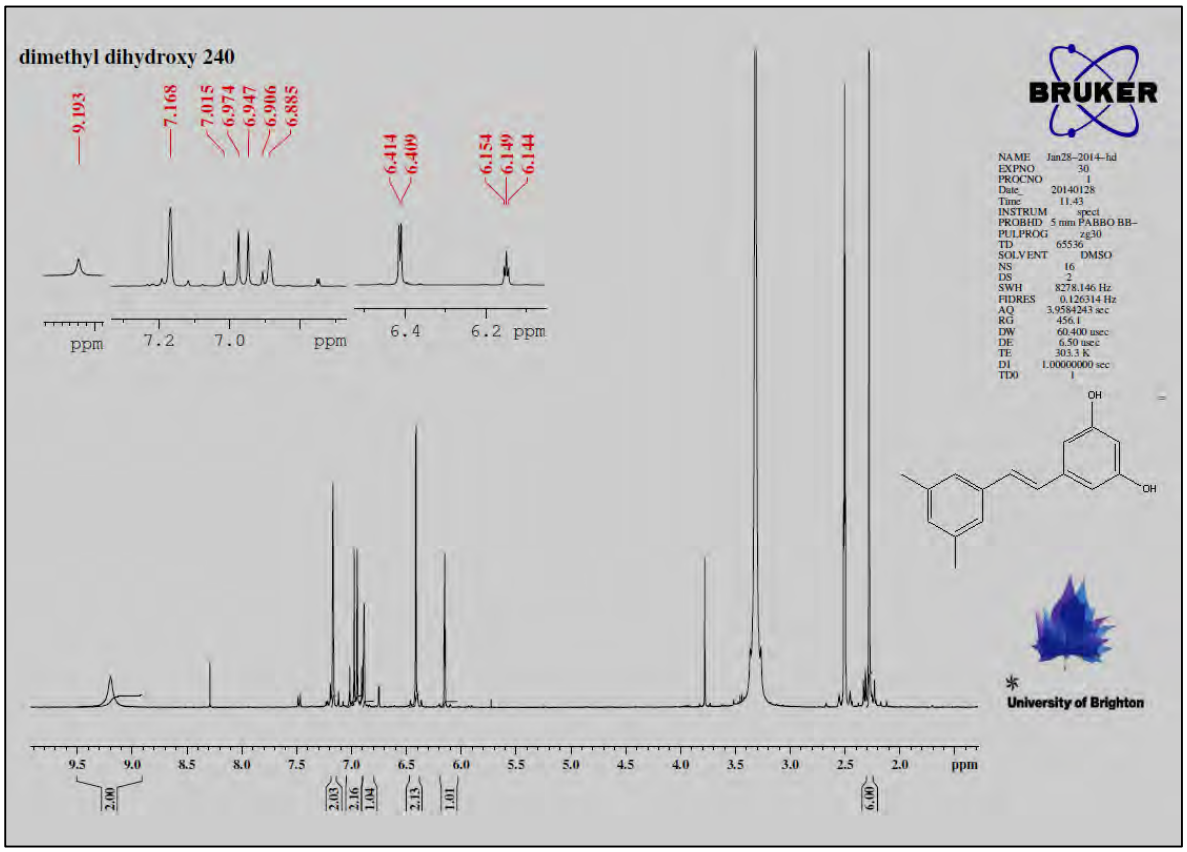

^{13}C NMR spectra of V26

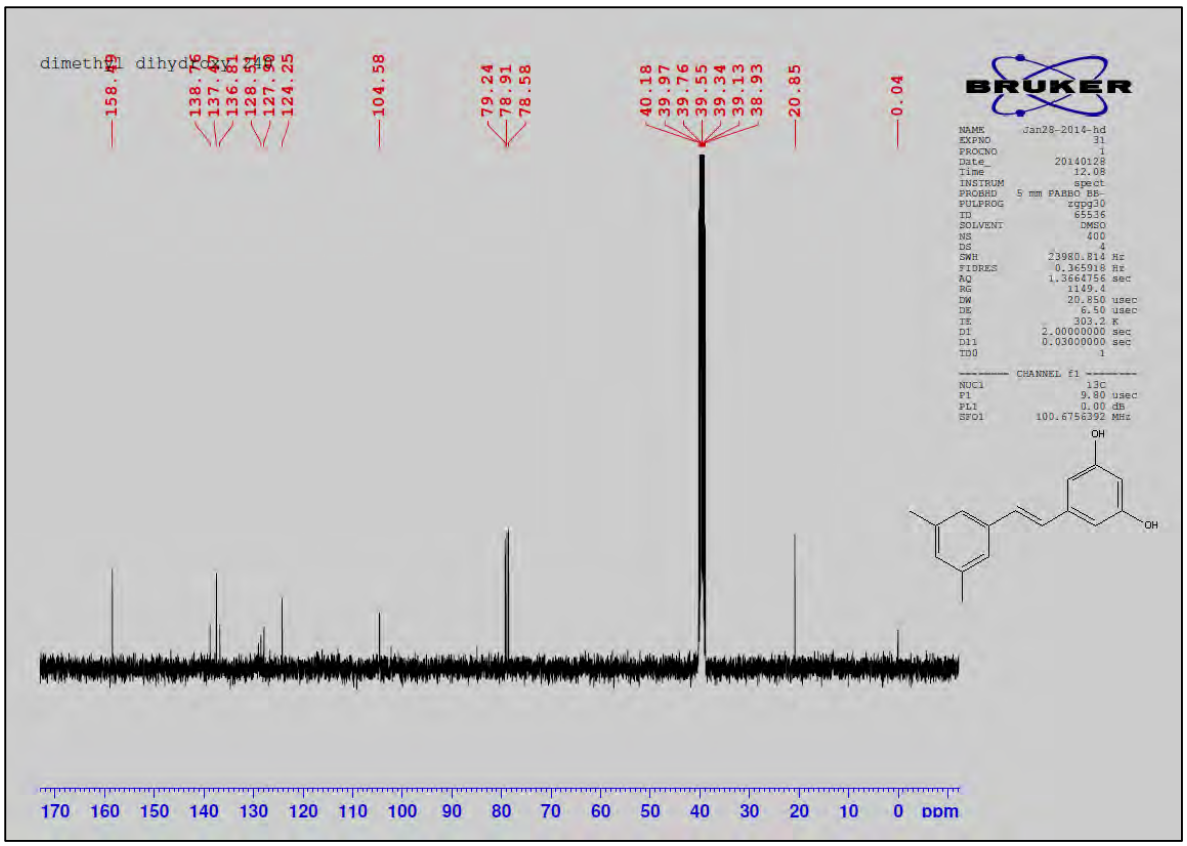

2D HSQC spectra of V26

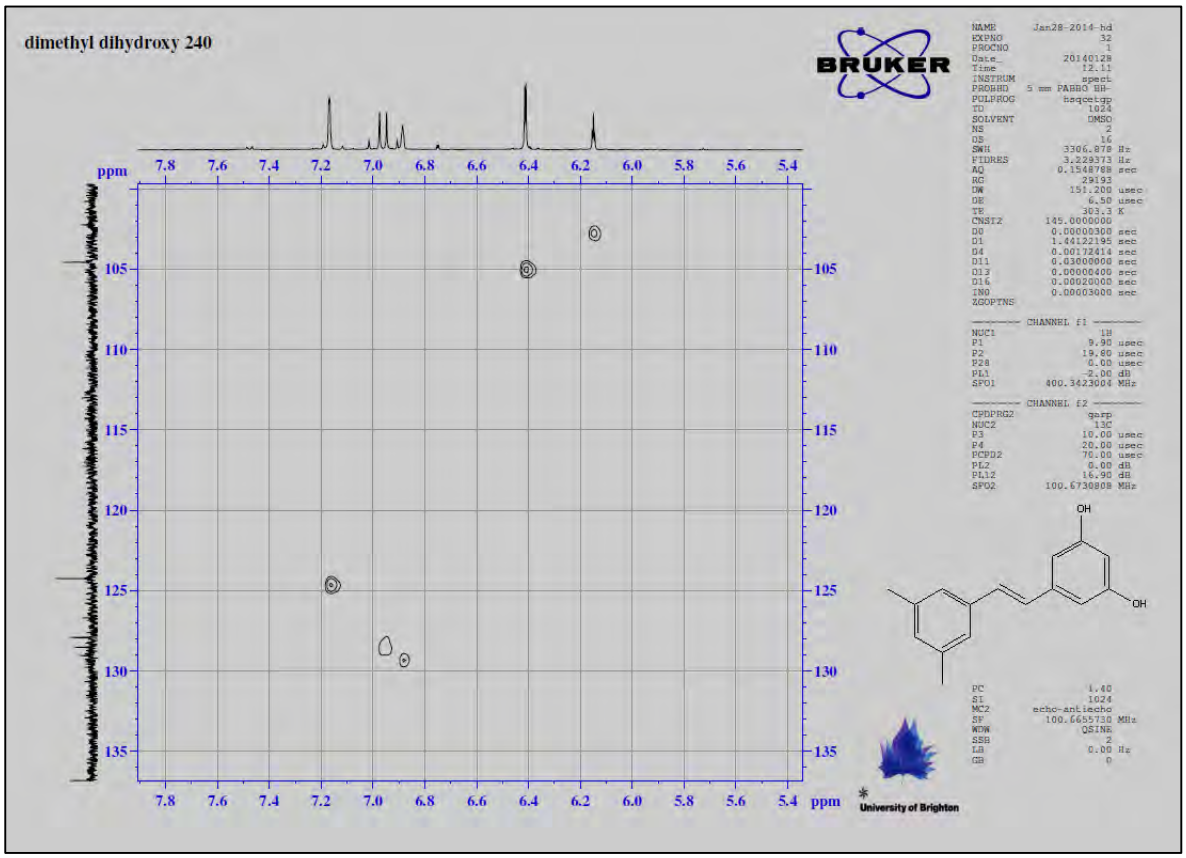

2D COSY spectra of V26

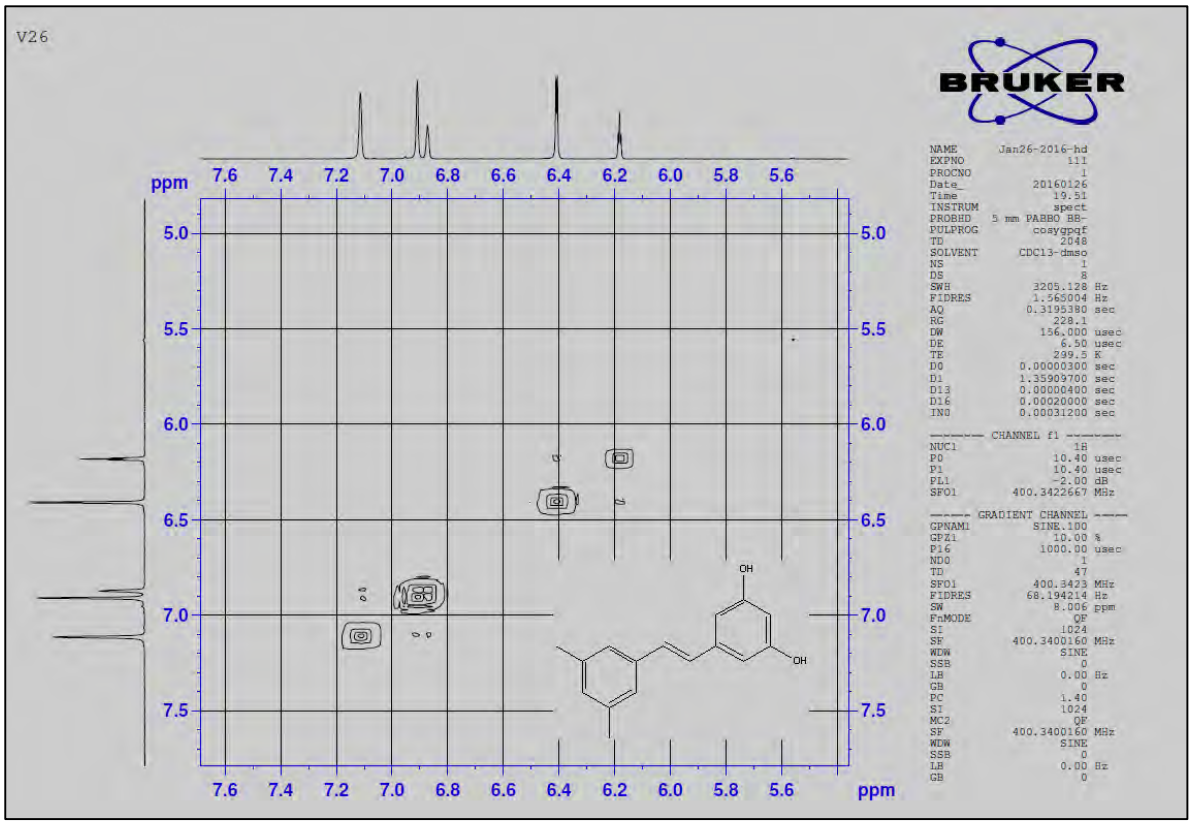

Mass spectra of V26

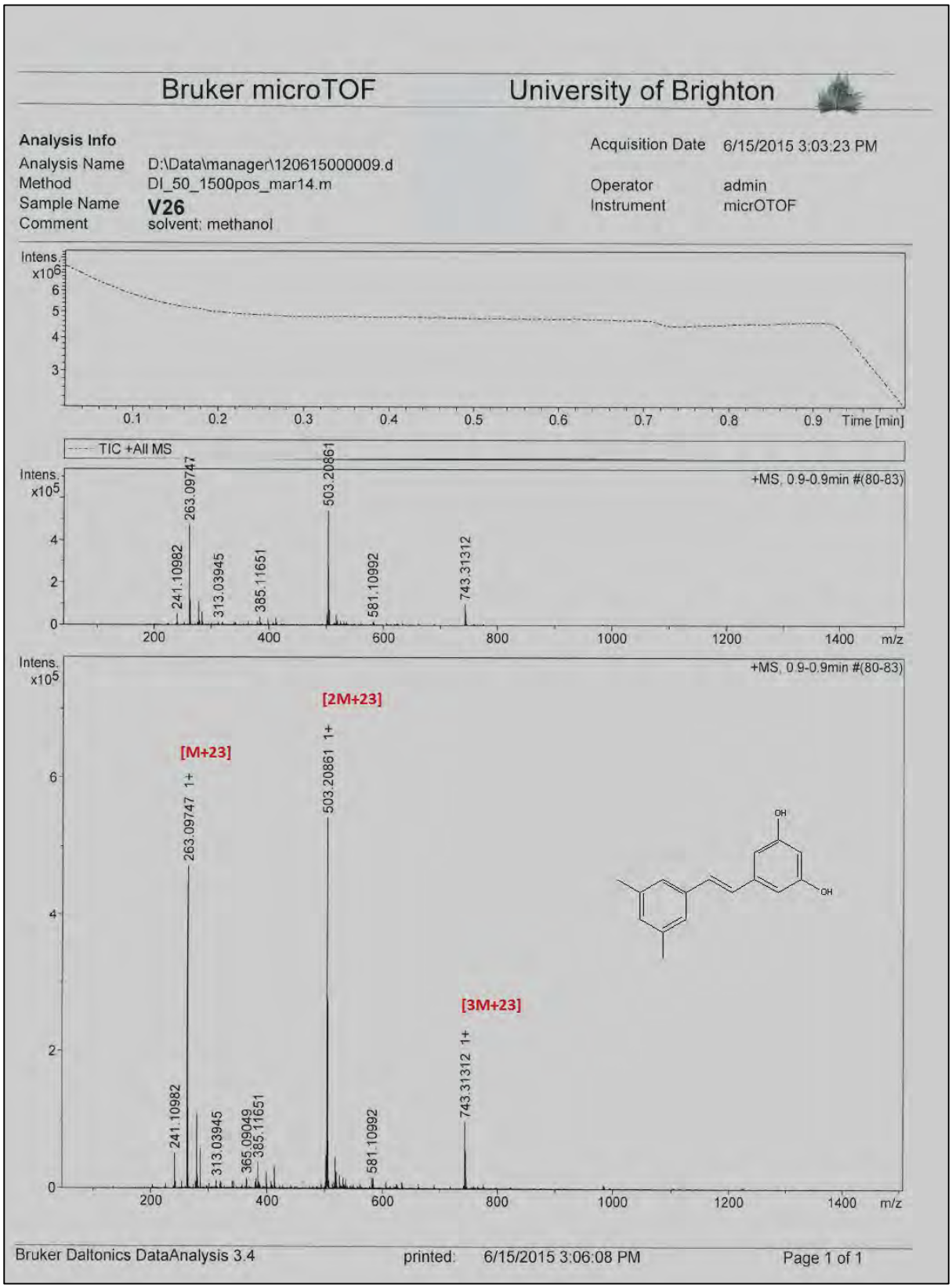

^{1}H NMR spectra of V27

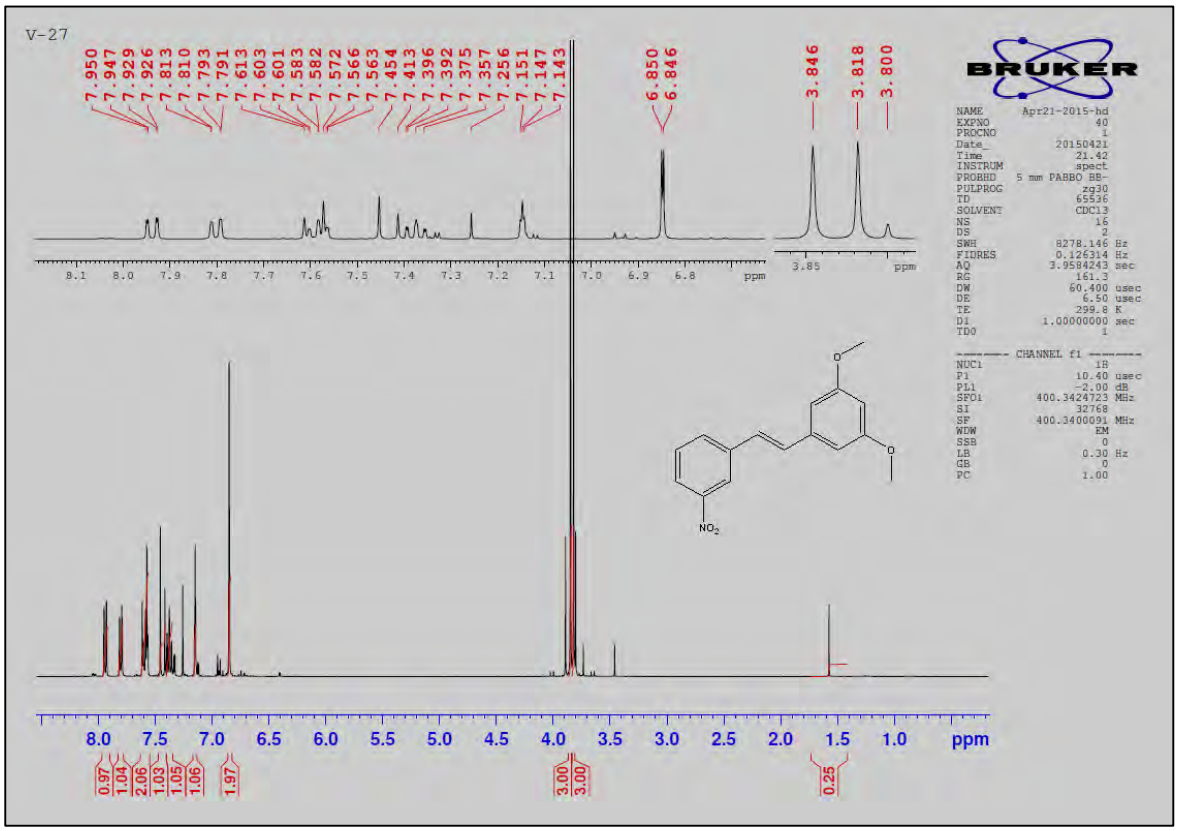

^{13}C NMR spectra of V27

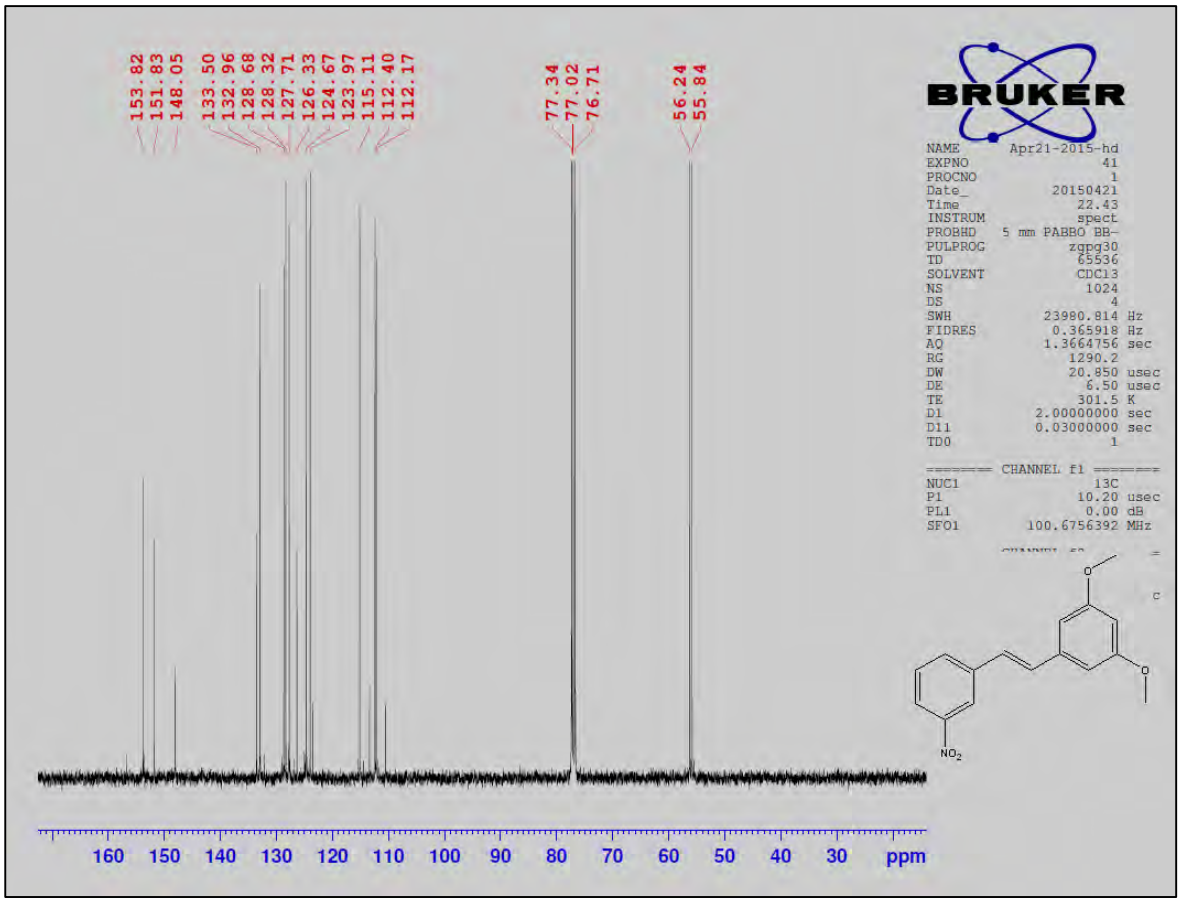

2D HSQC spectra of V27

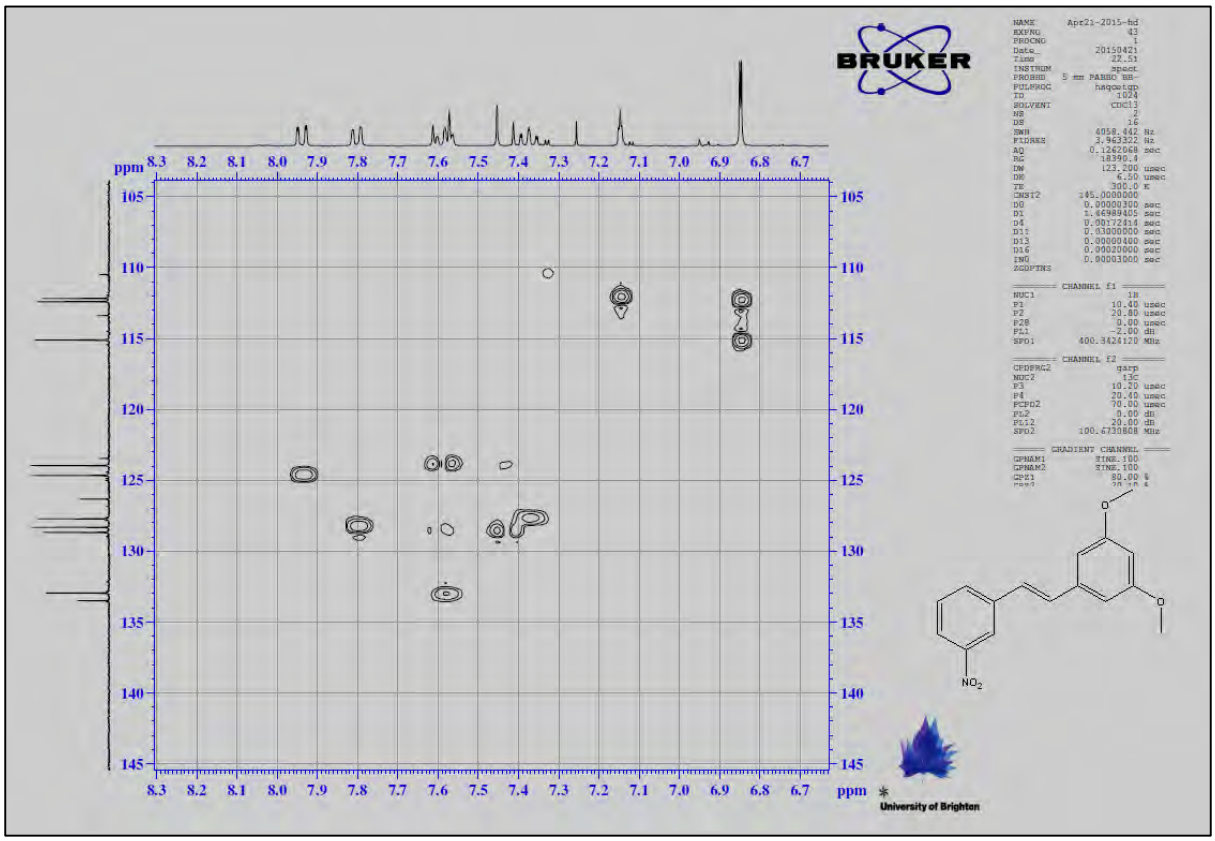

2D COSY spectra of V27

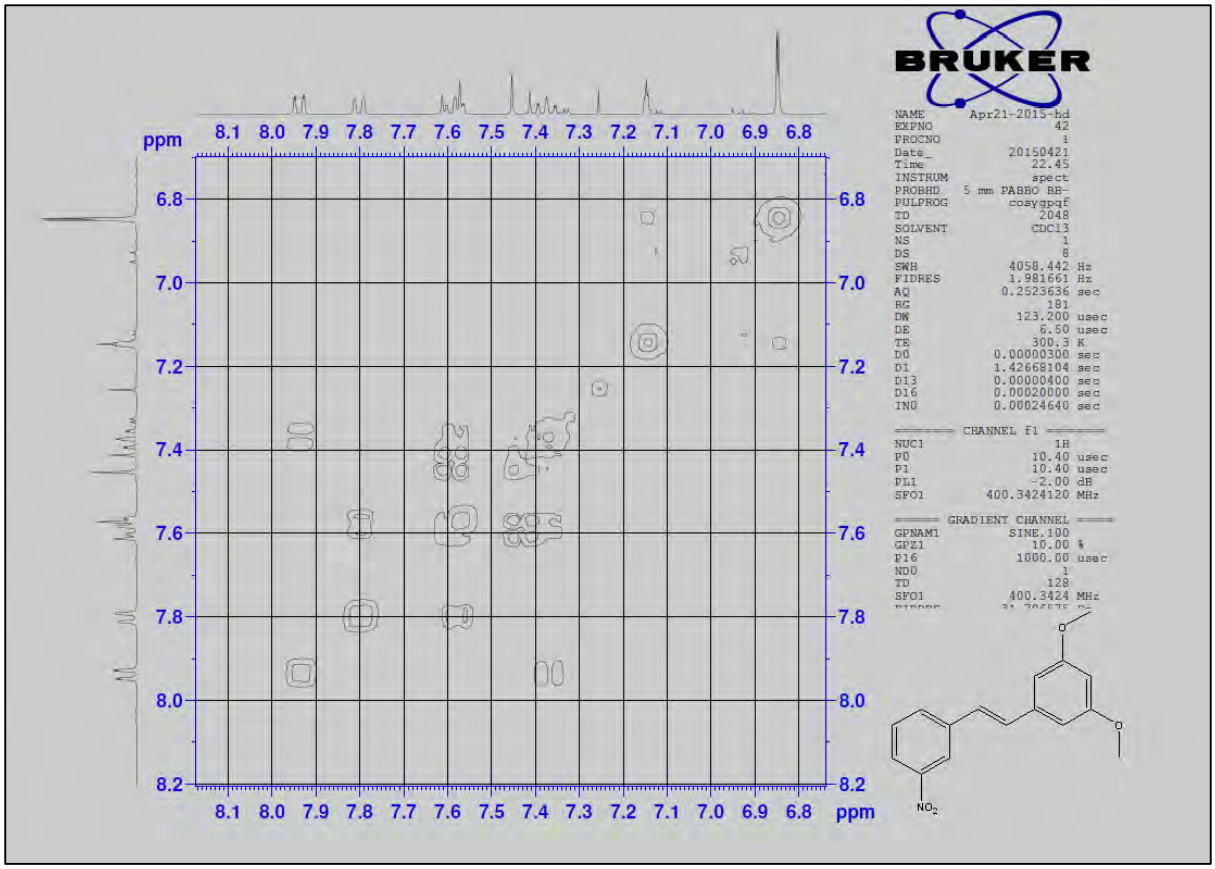

Mass spectra of V27

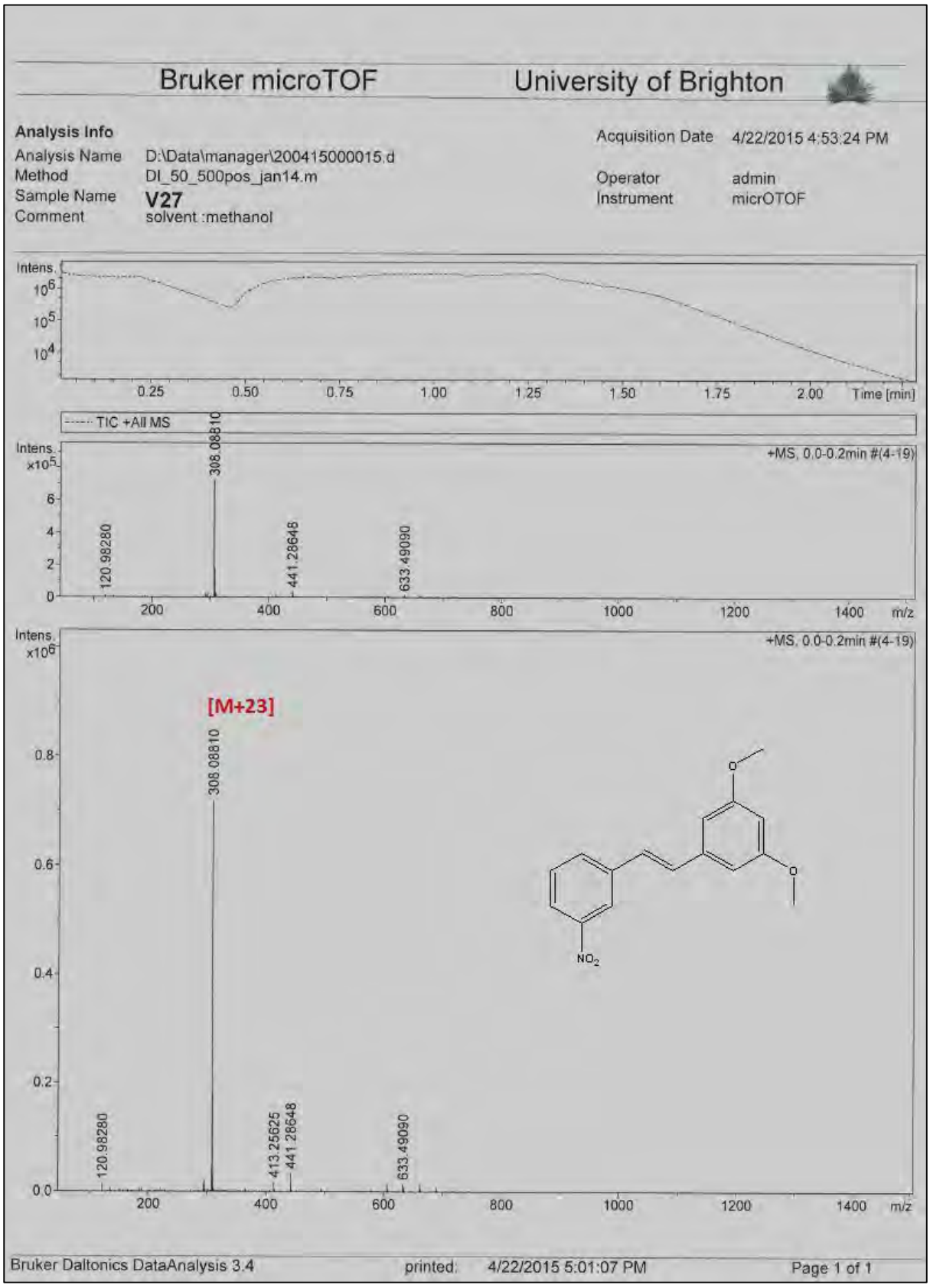

^{1}H NMR spectra of V28

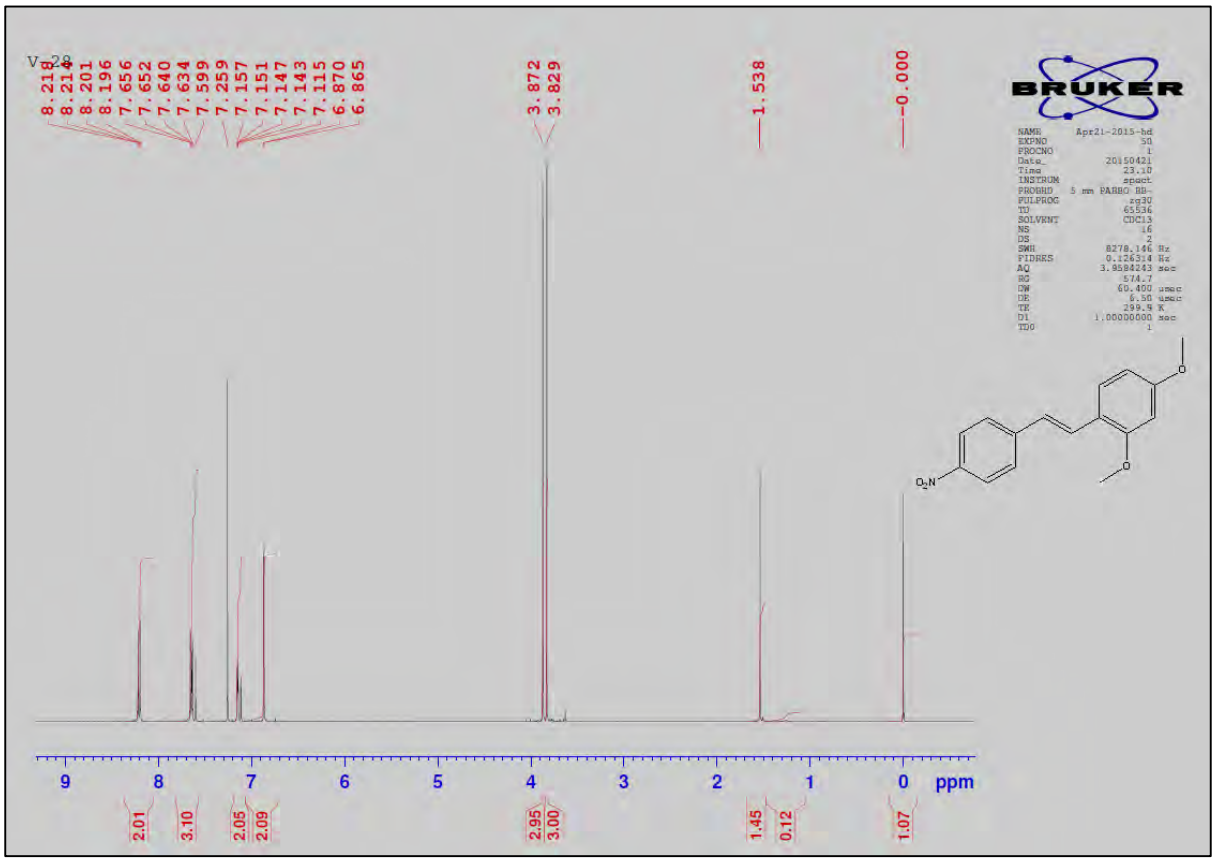

^{13}C NMR spectra of V28

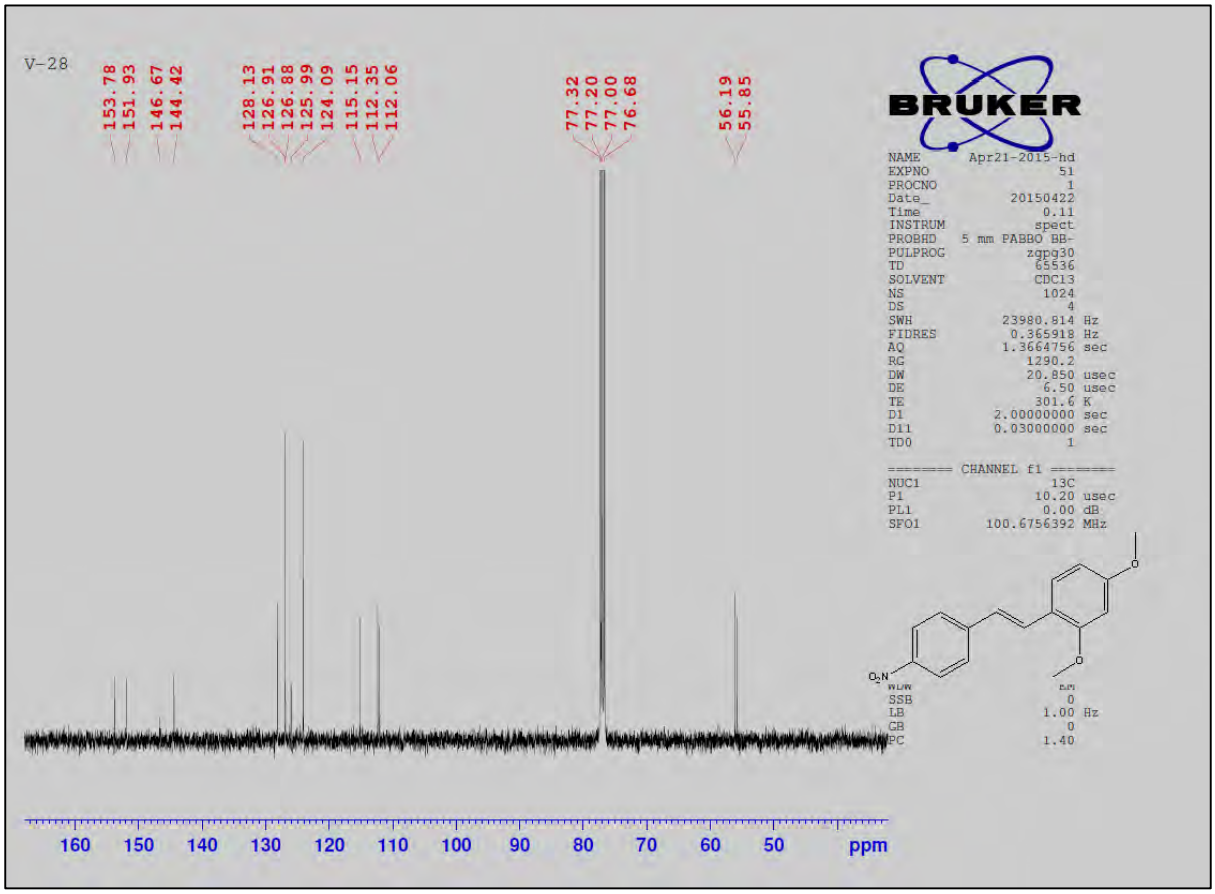

2D HSQC spectra of V28

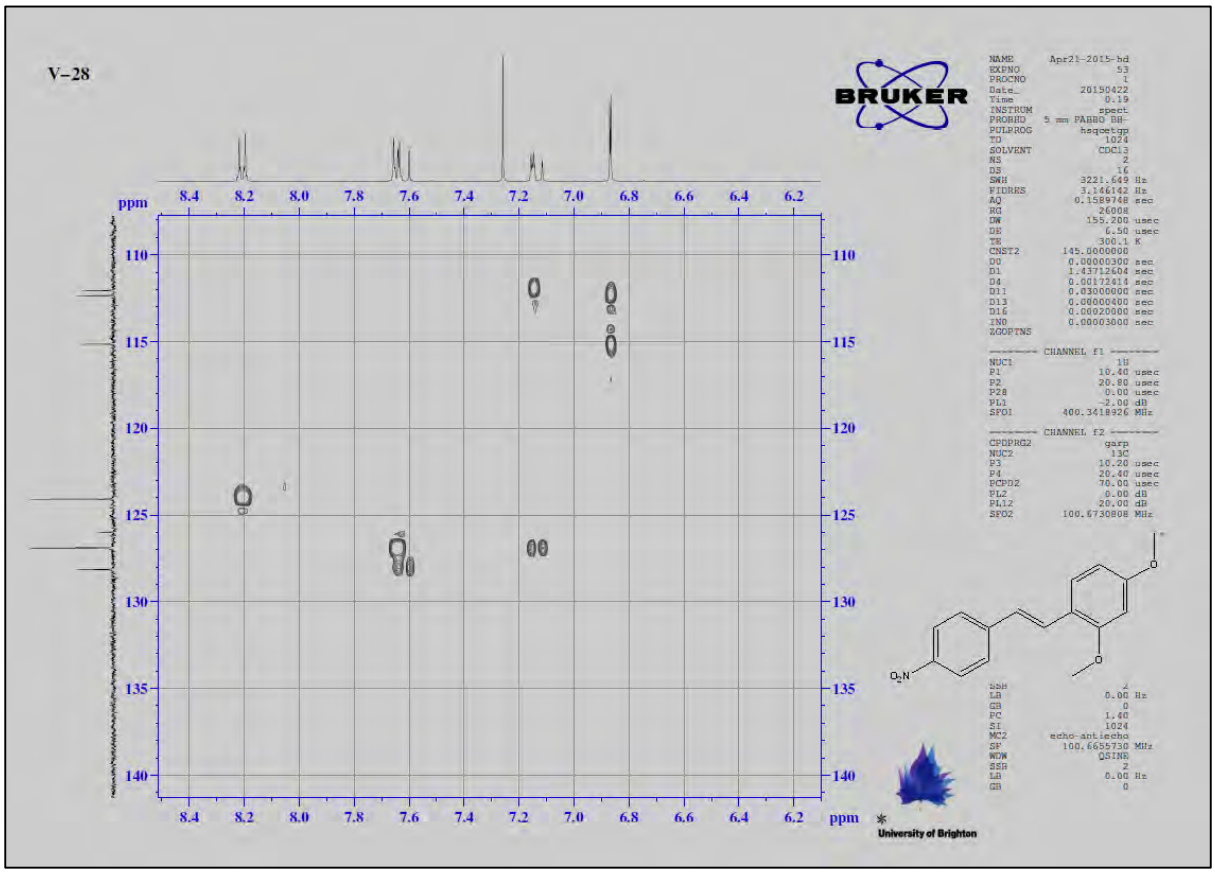

2D COSY spectra of V28

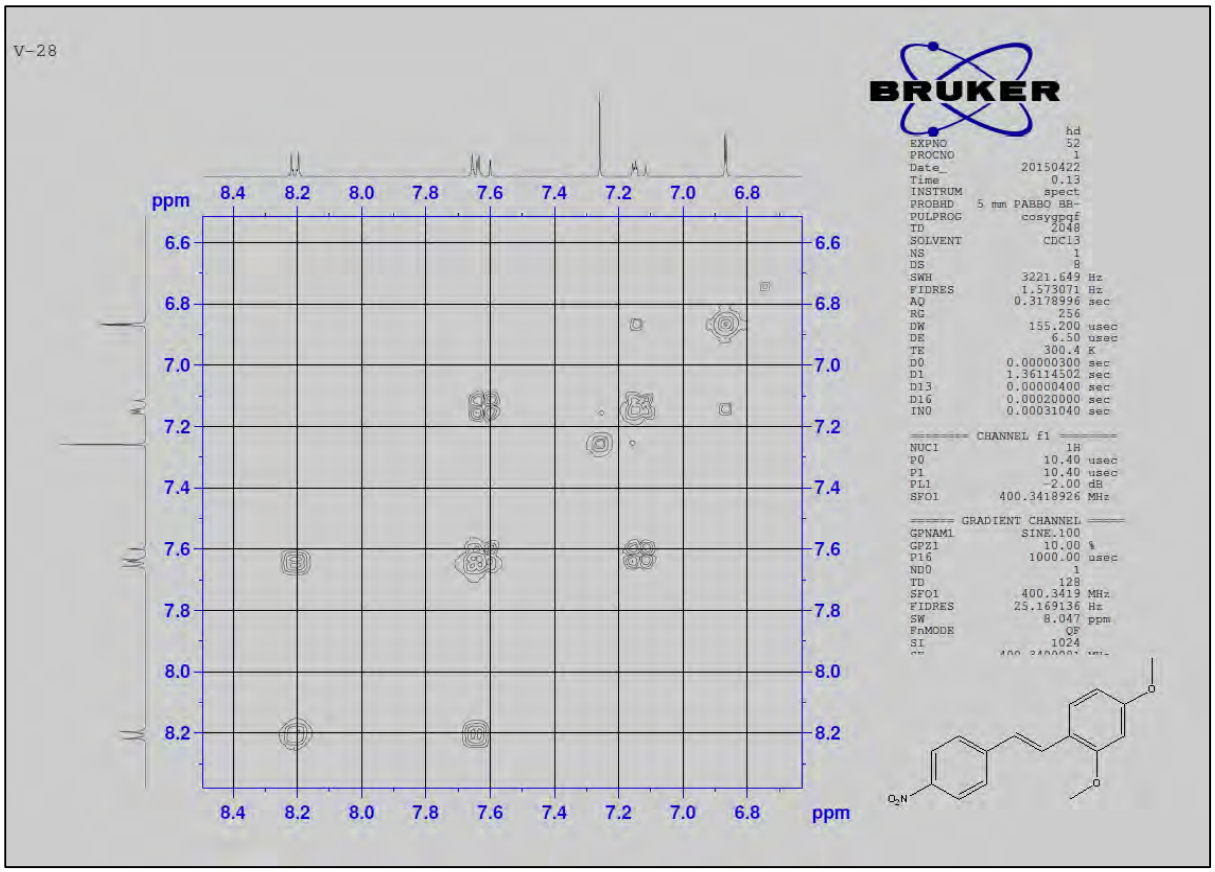

Mass spectra of V28

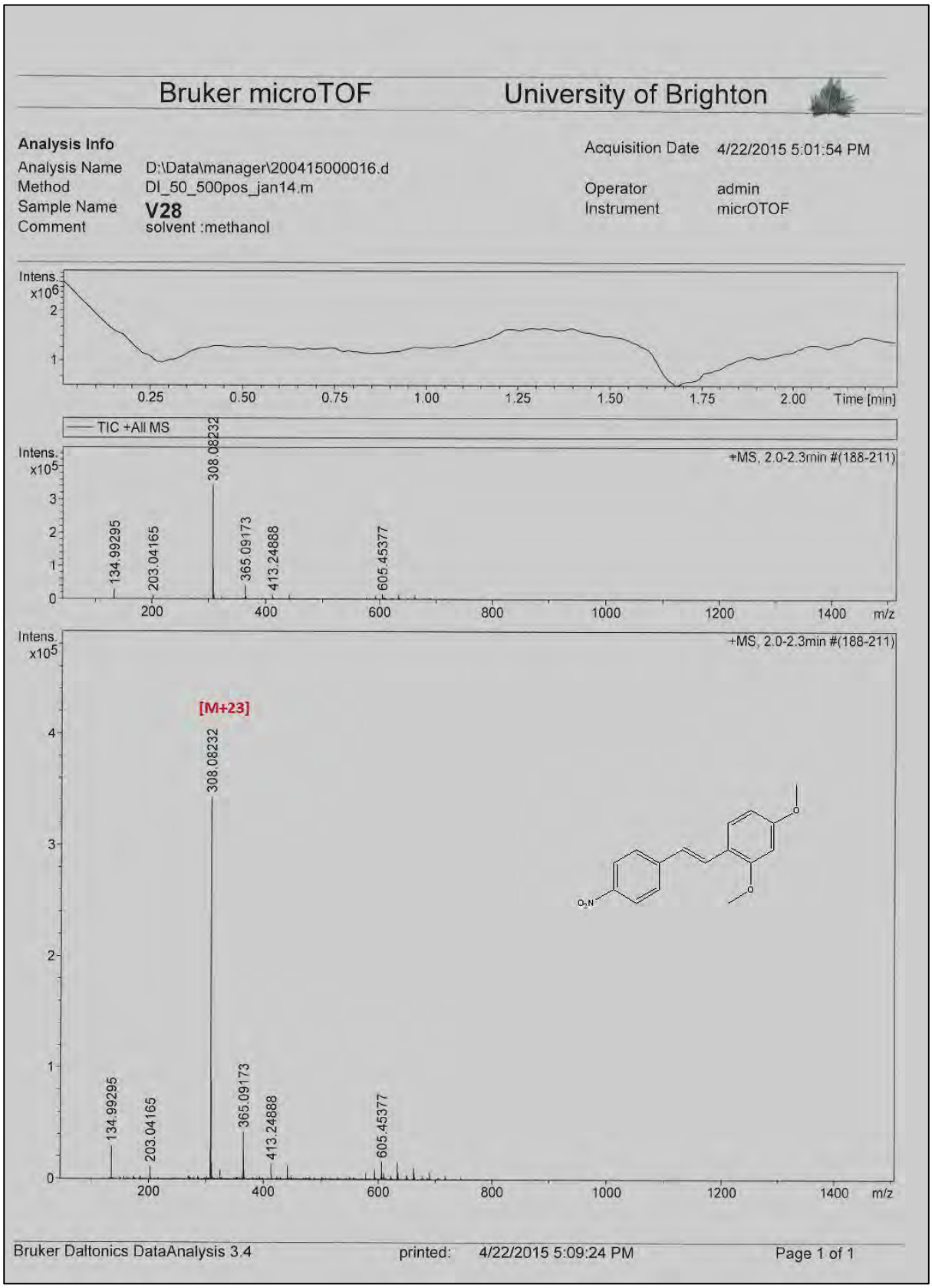

^{1}H NMR spectra of V29

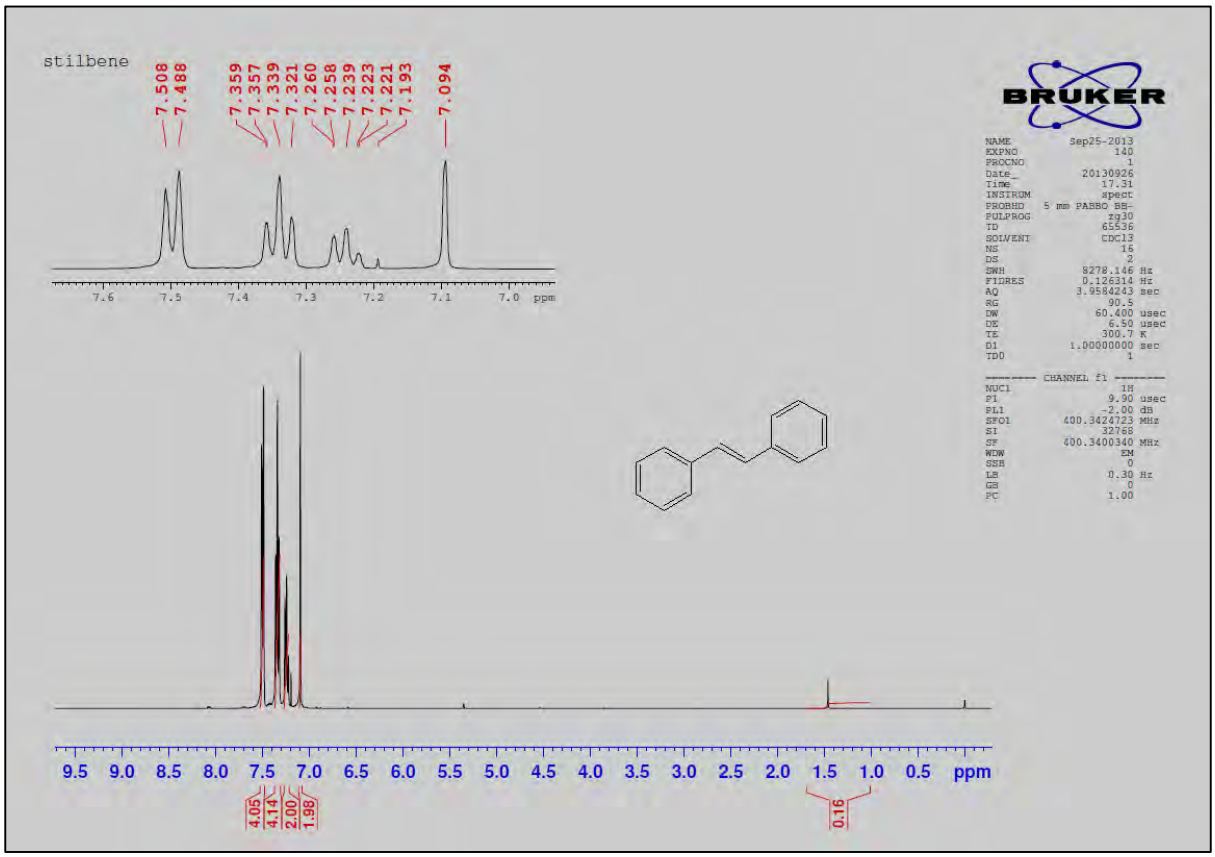

^{13}C NMR spectra of V29

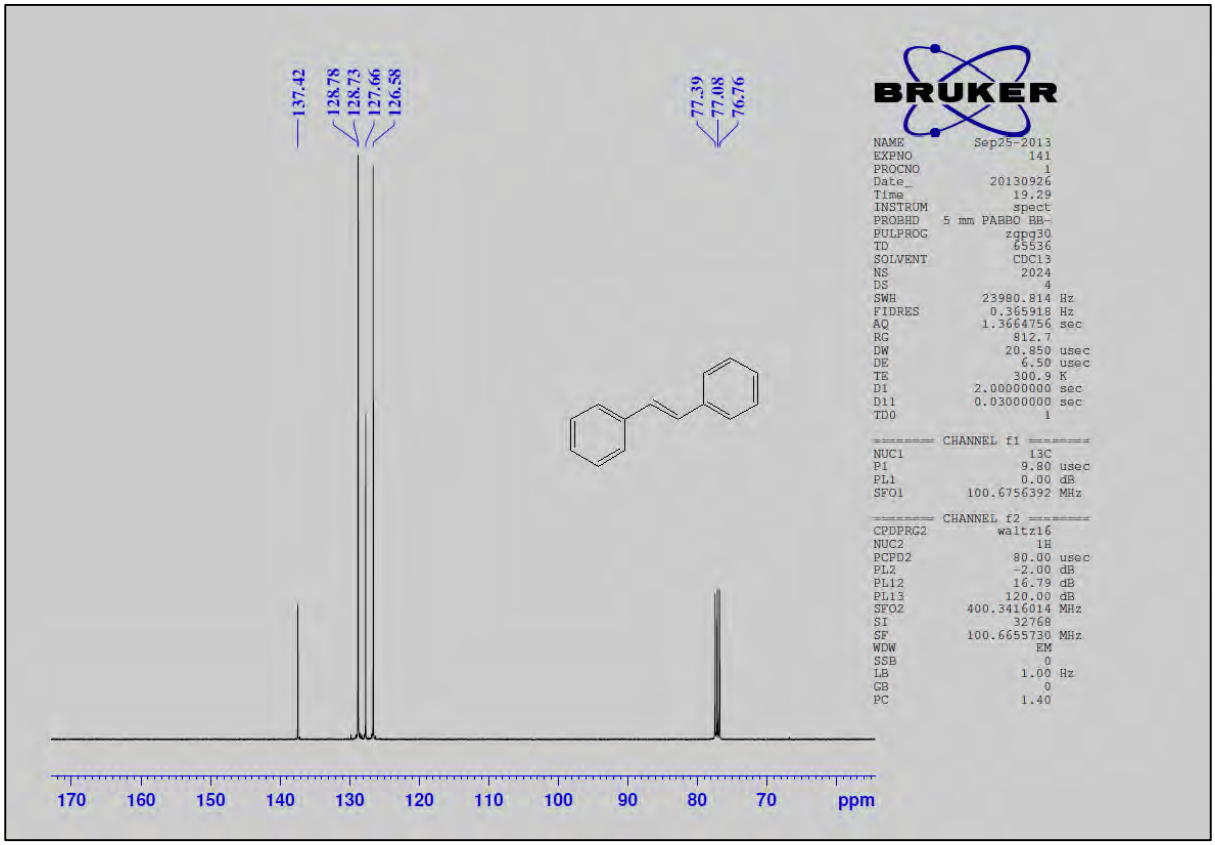

2D HSQC spectra of V29

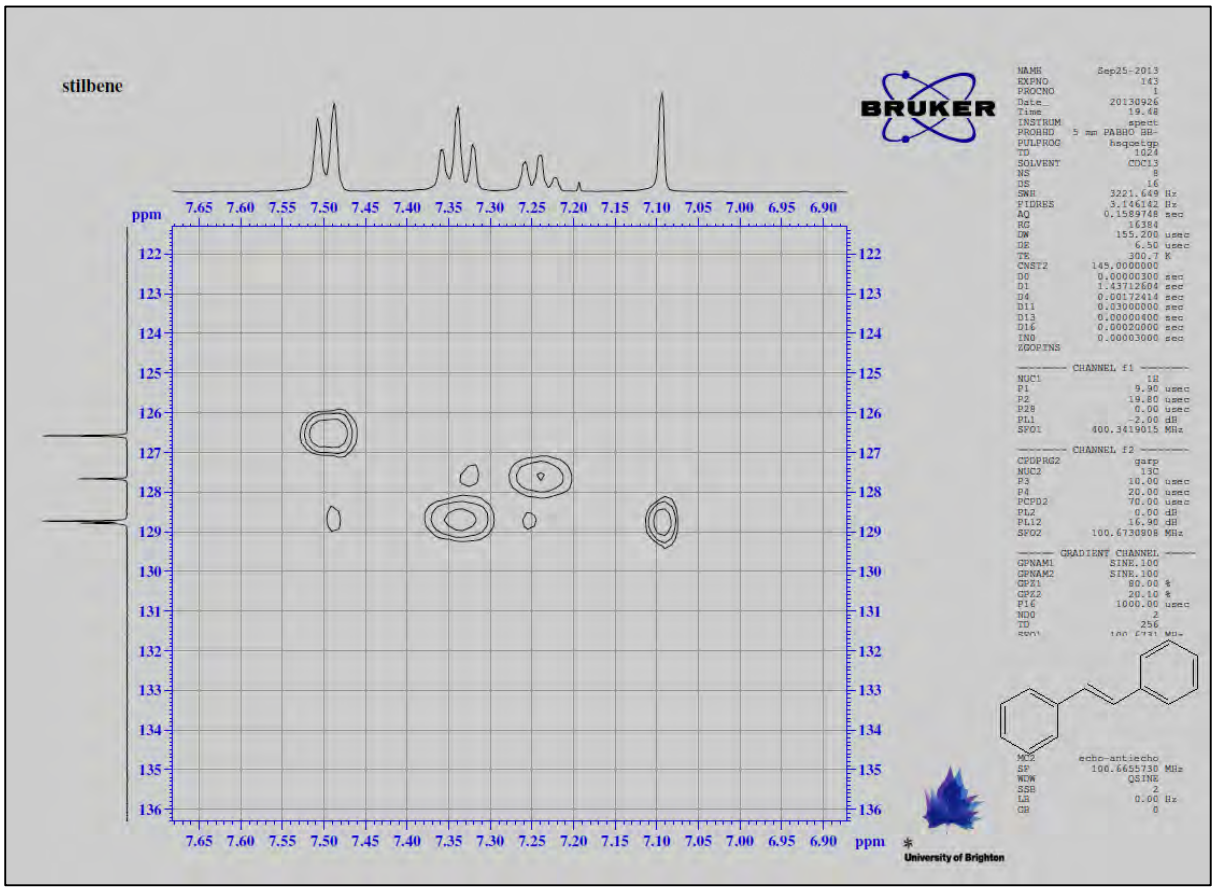

2D COSY spectra of V29

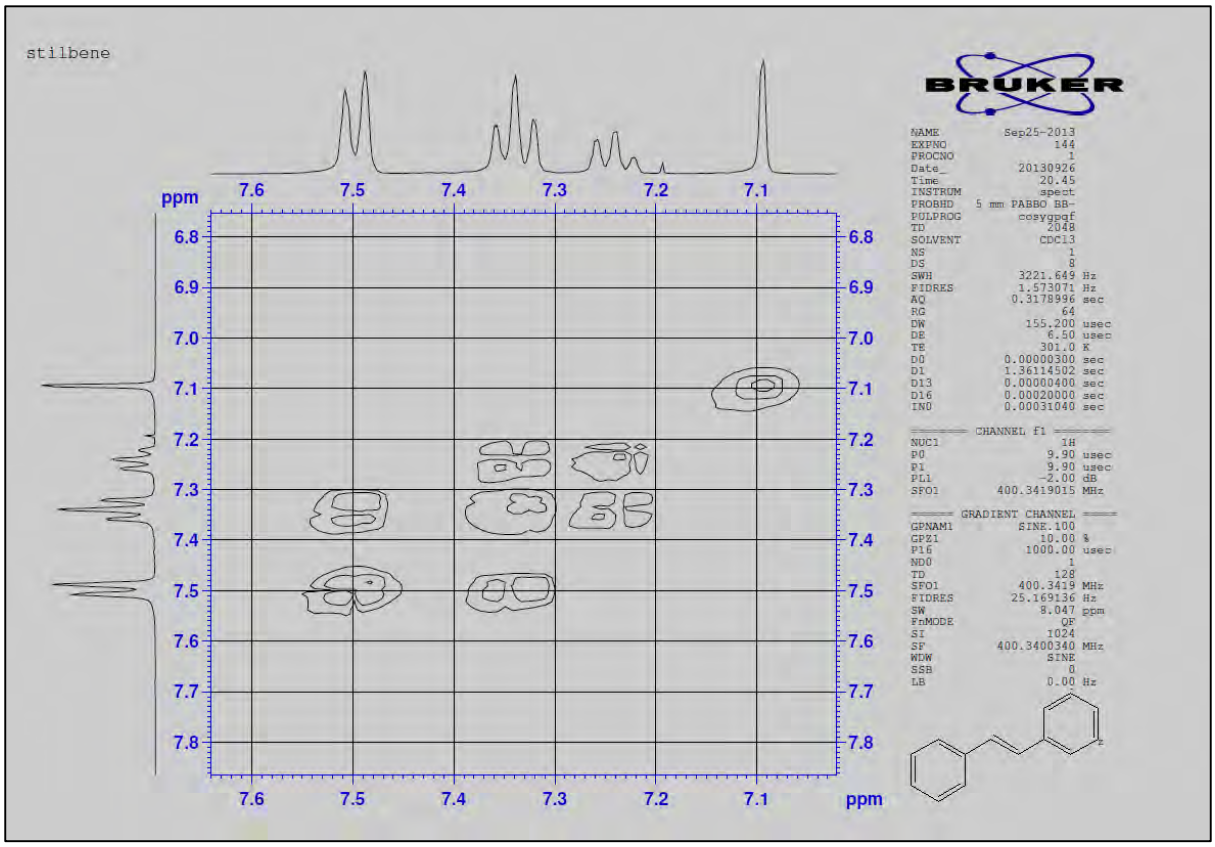

Mass spectra of V29

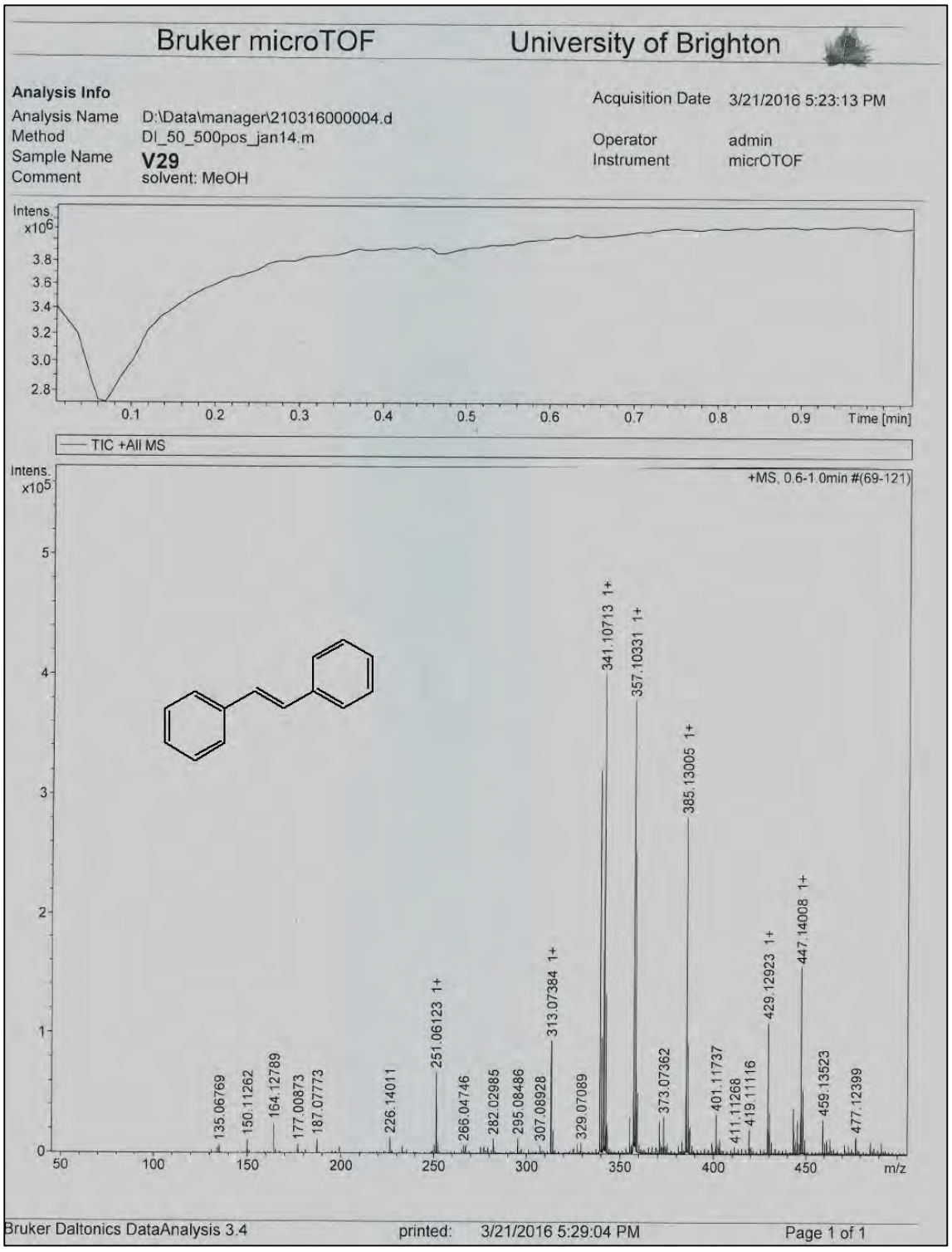

^{1}H NMR spectra of V30

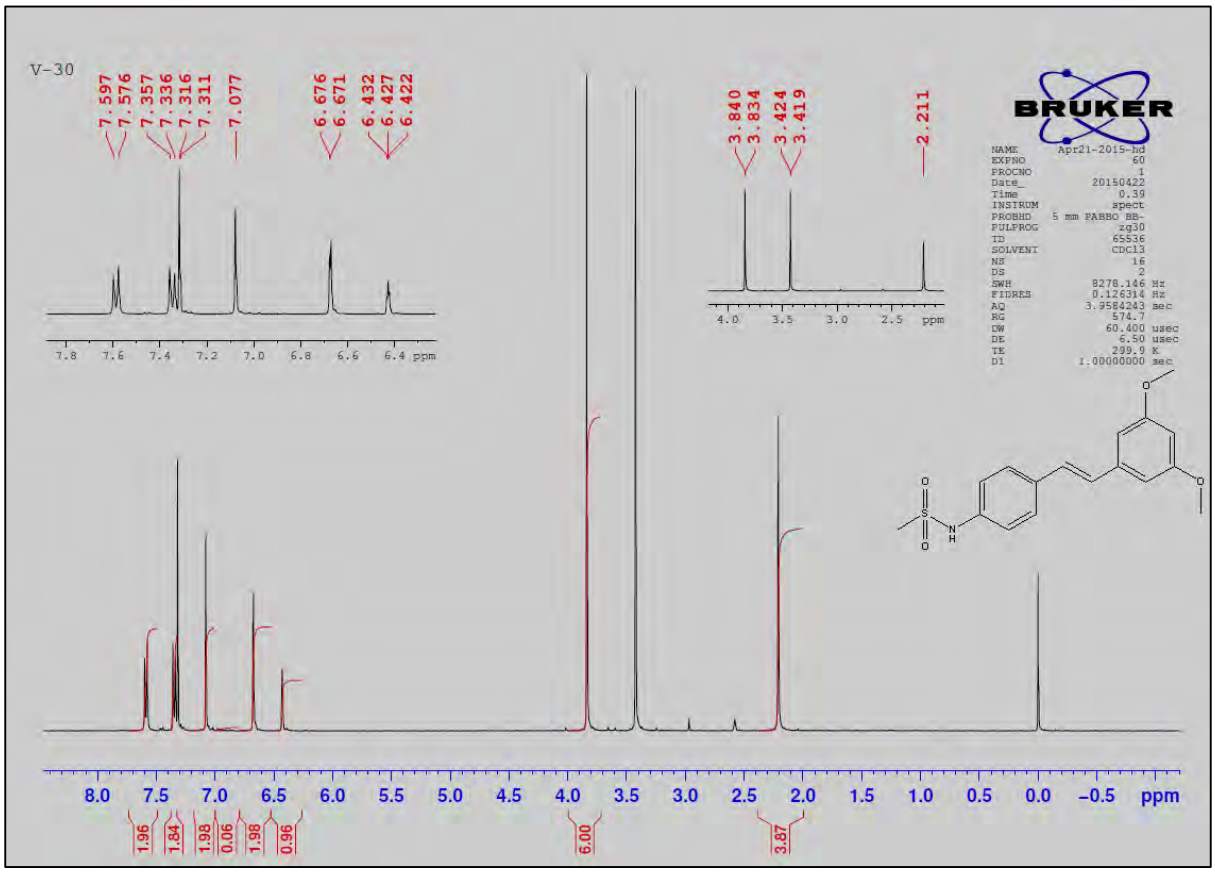

^{13}C NMR spectra of V30

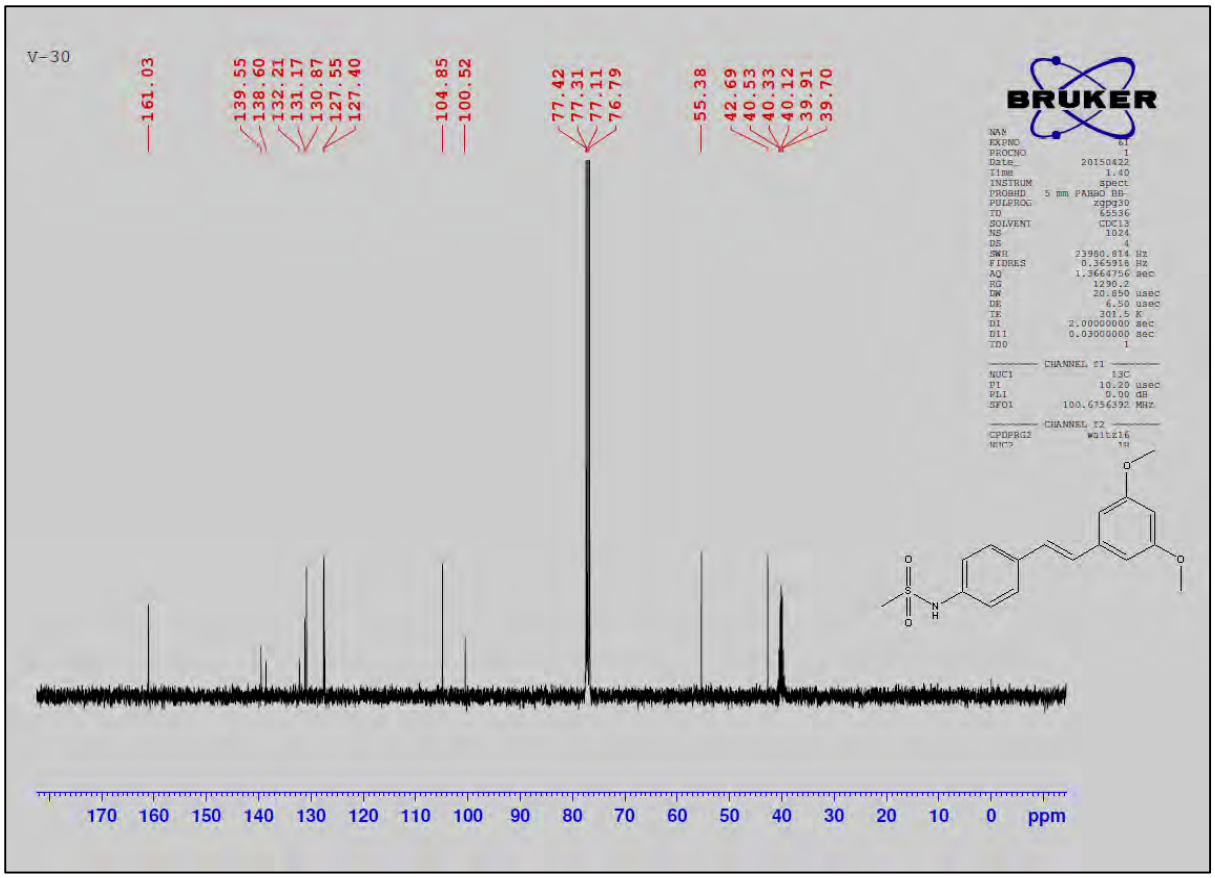

2D HSQC spectra of V30

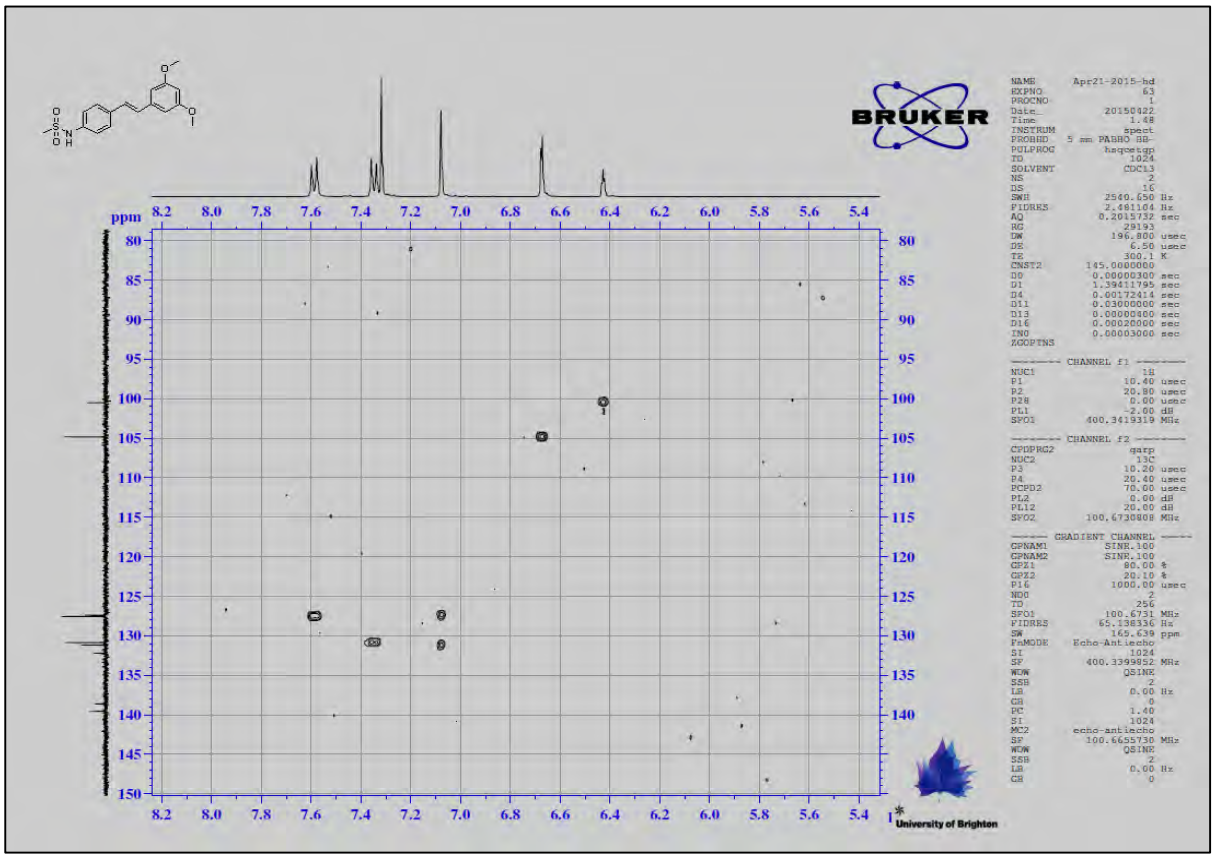

2D COSY spectra of V30

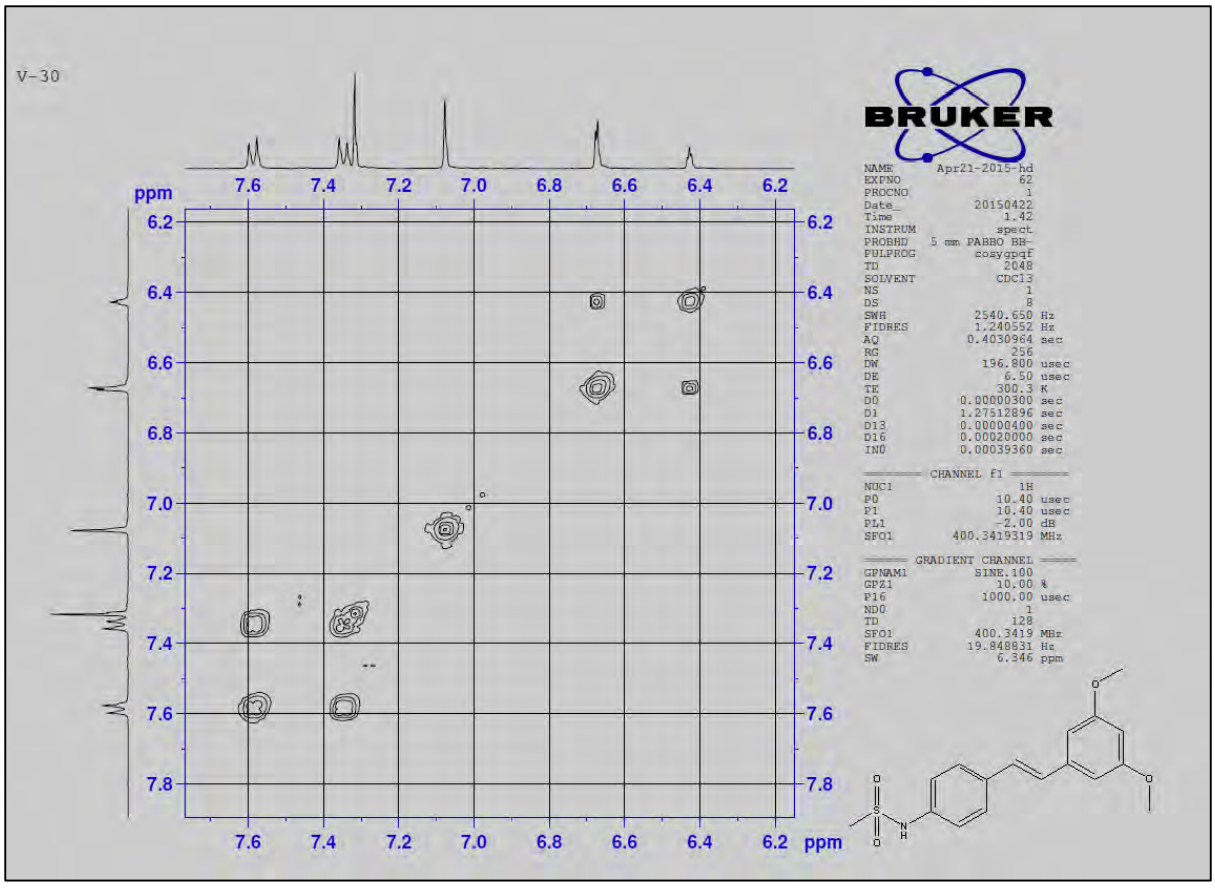

Mass spectra of V30

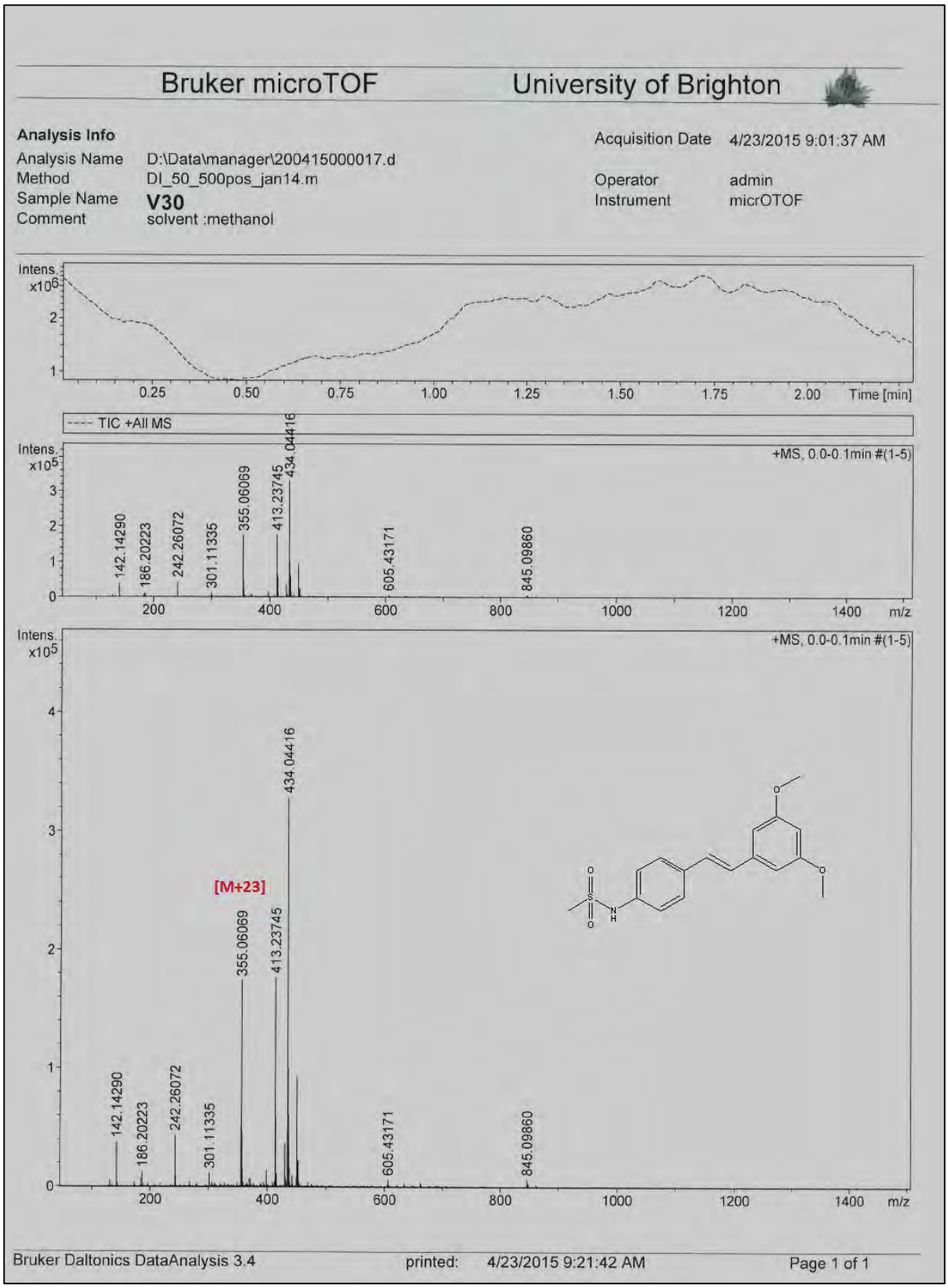

^{1}H NMR spectra of V31

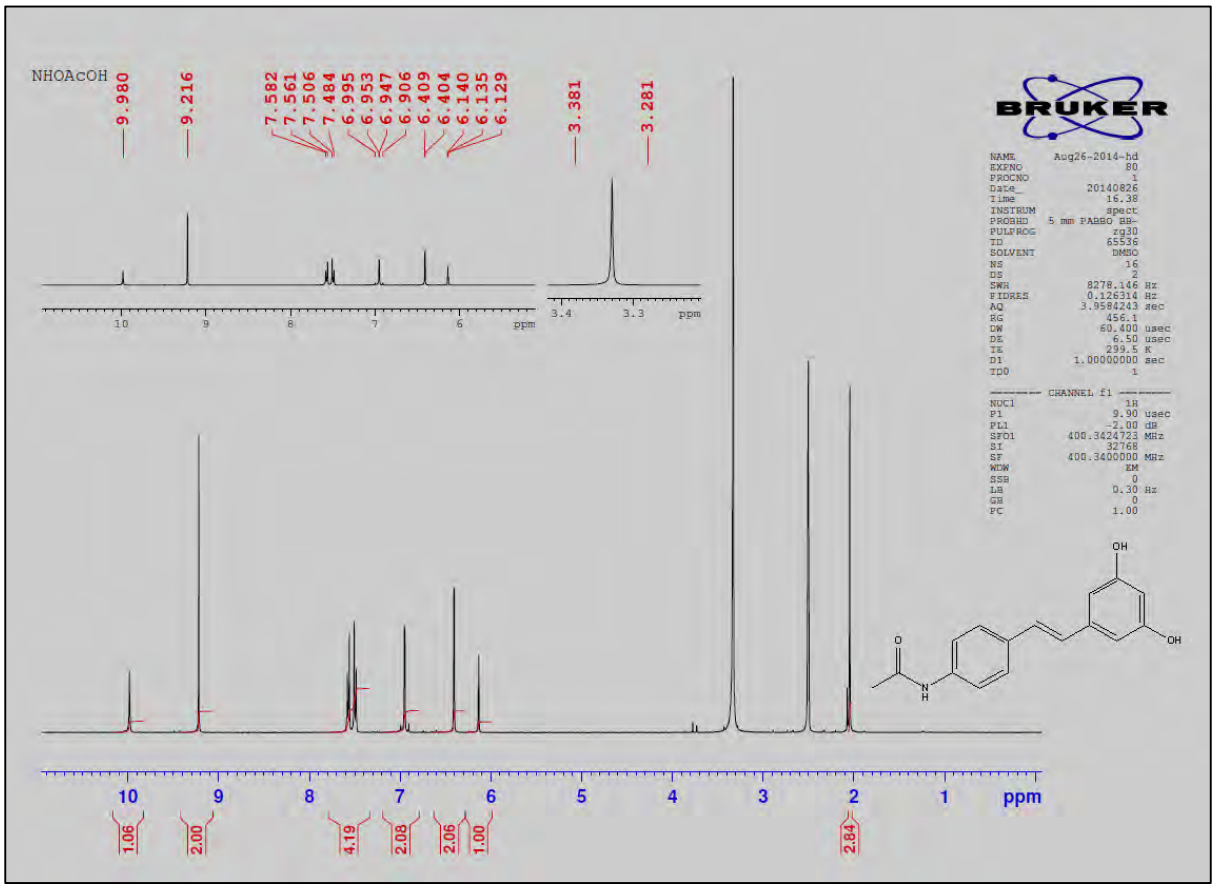

^{13}C NMR spectra of V31

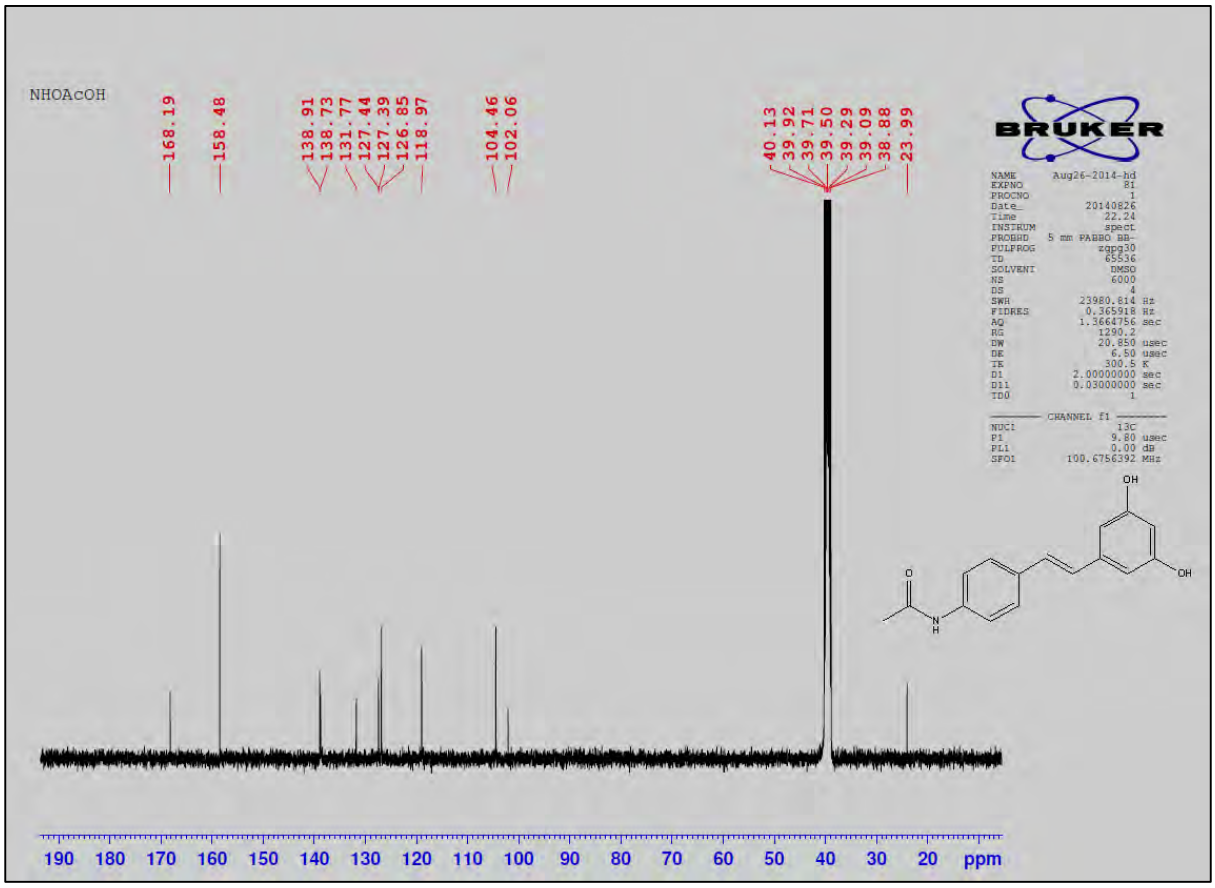

2D HSQC spectra of V31

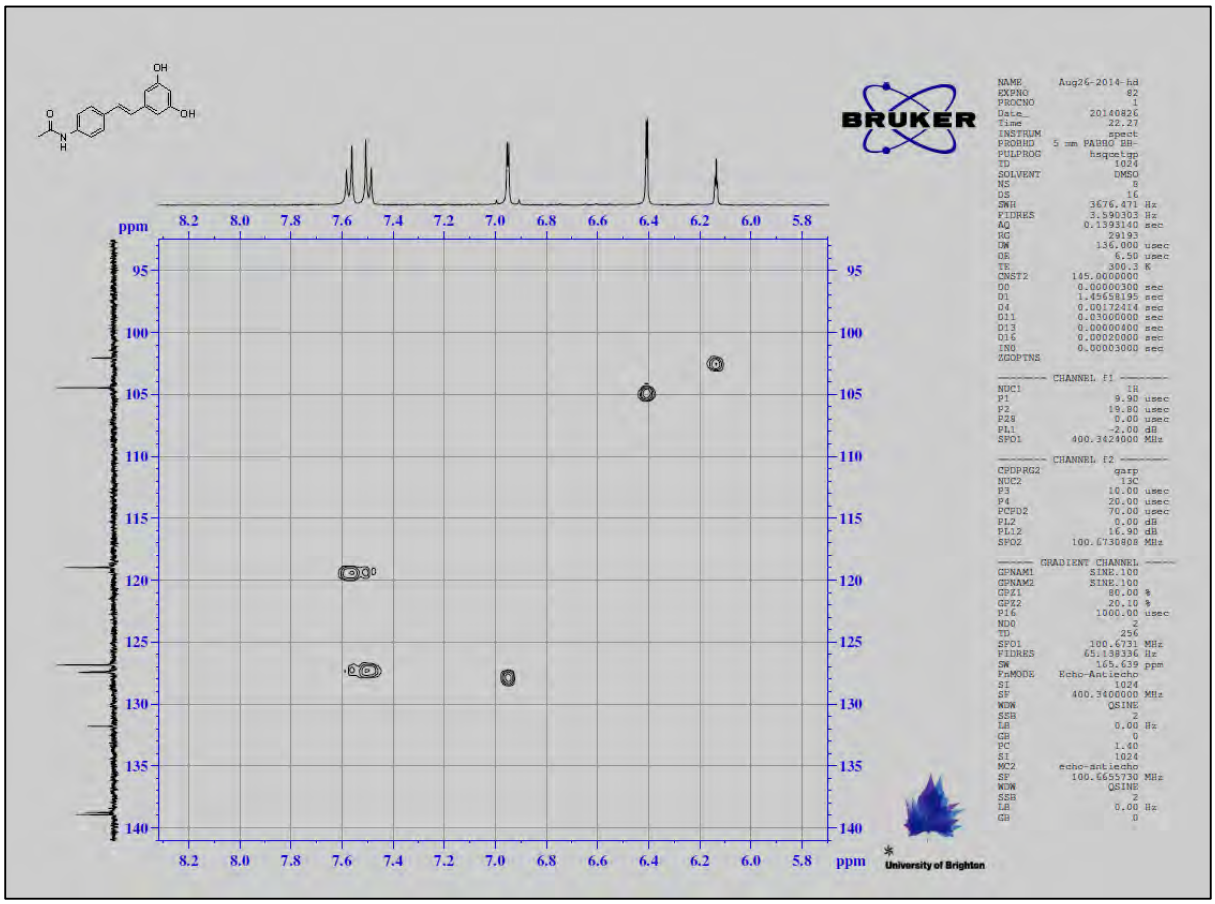

2D COSY spectra of V31

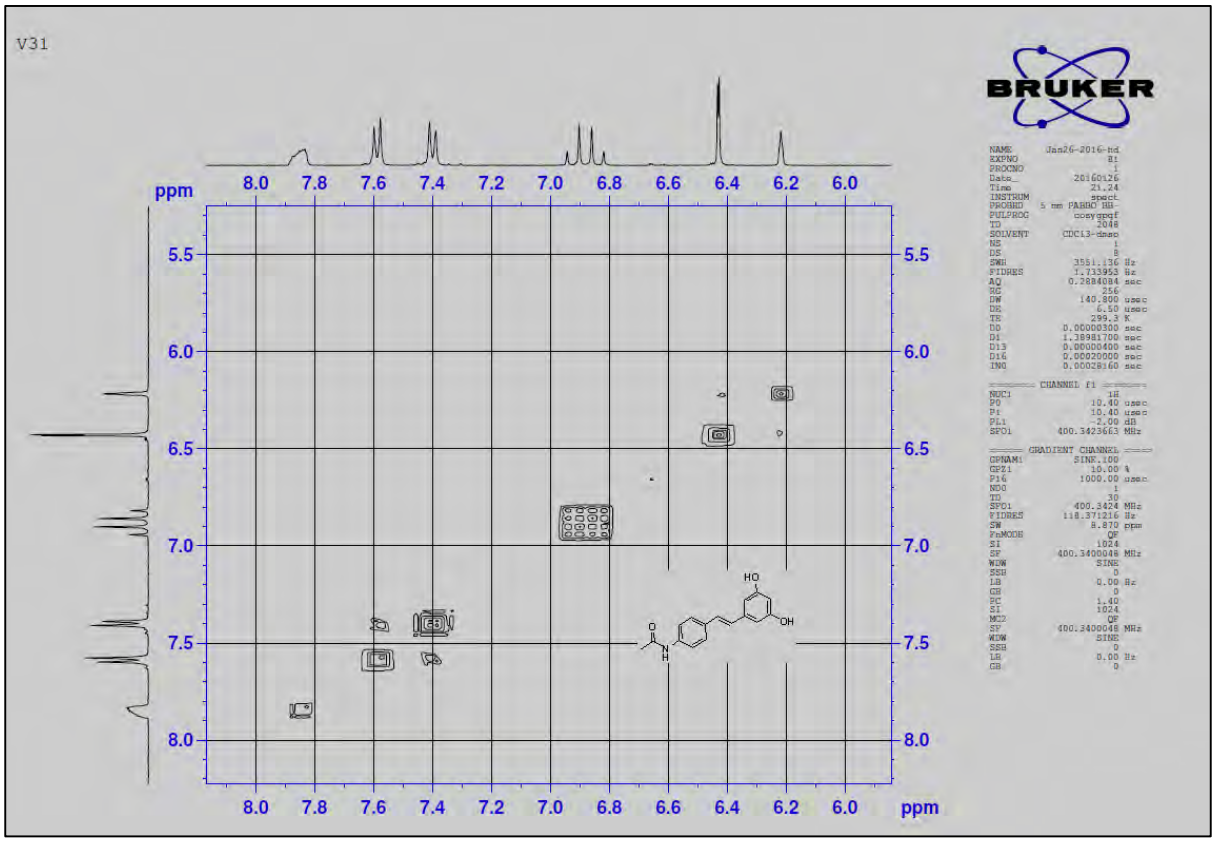

Mass spectra of V31

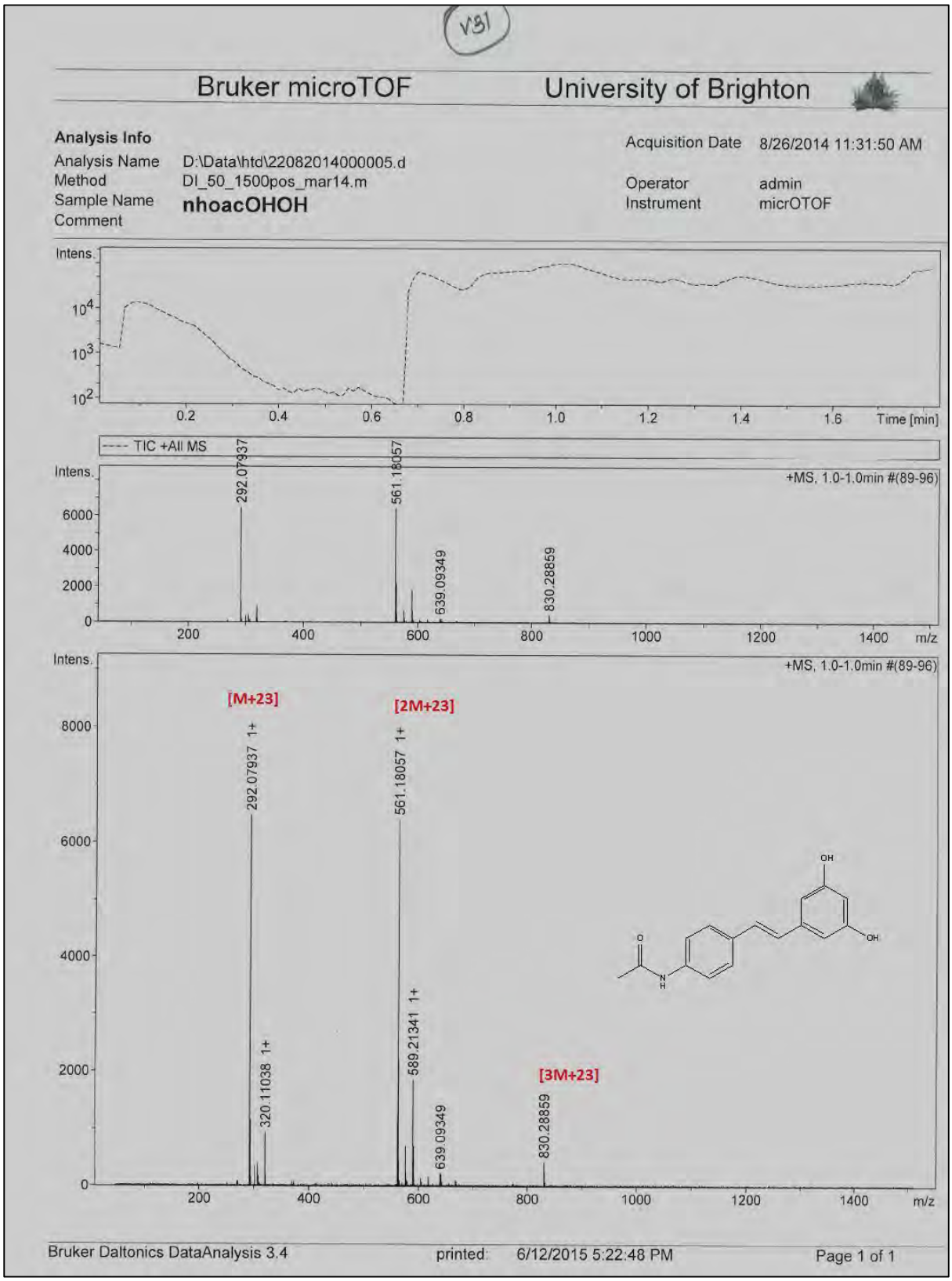

^{1}H NMR spectra of V32

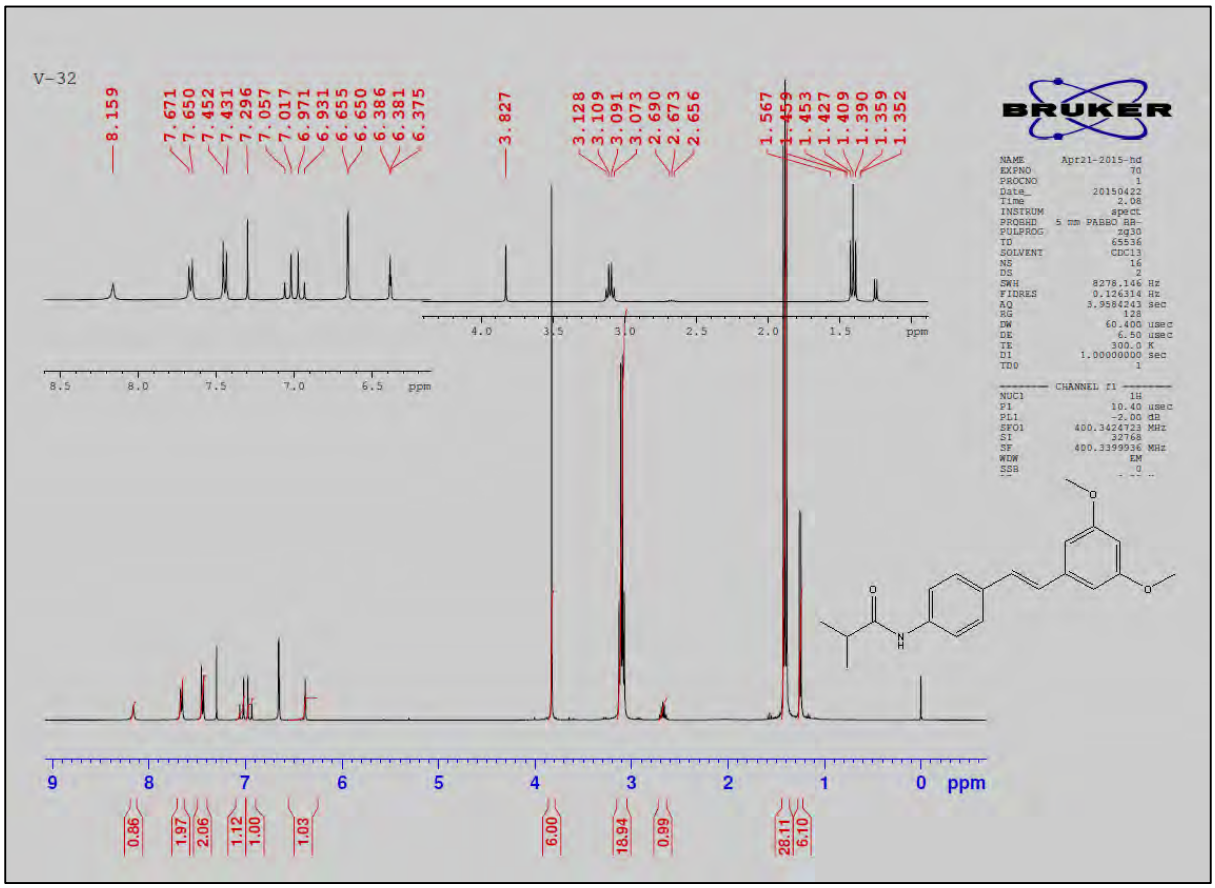

^{13}C NMR spectra of V32

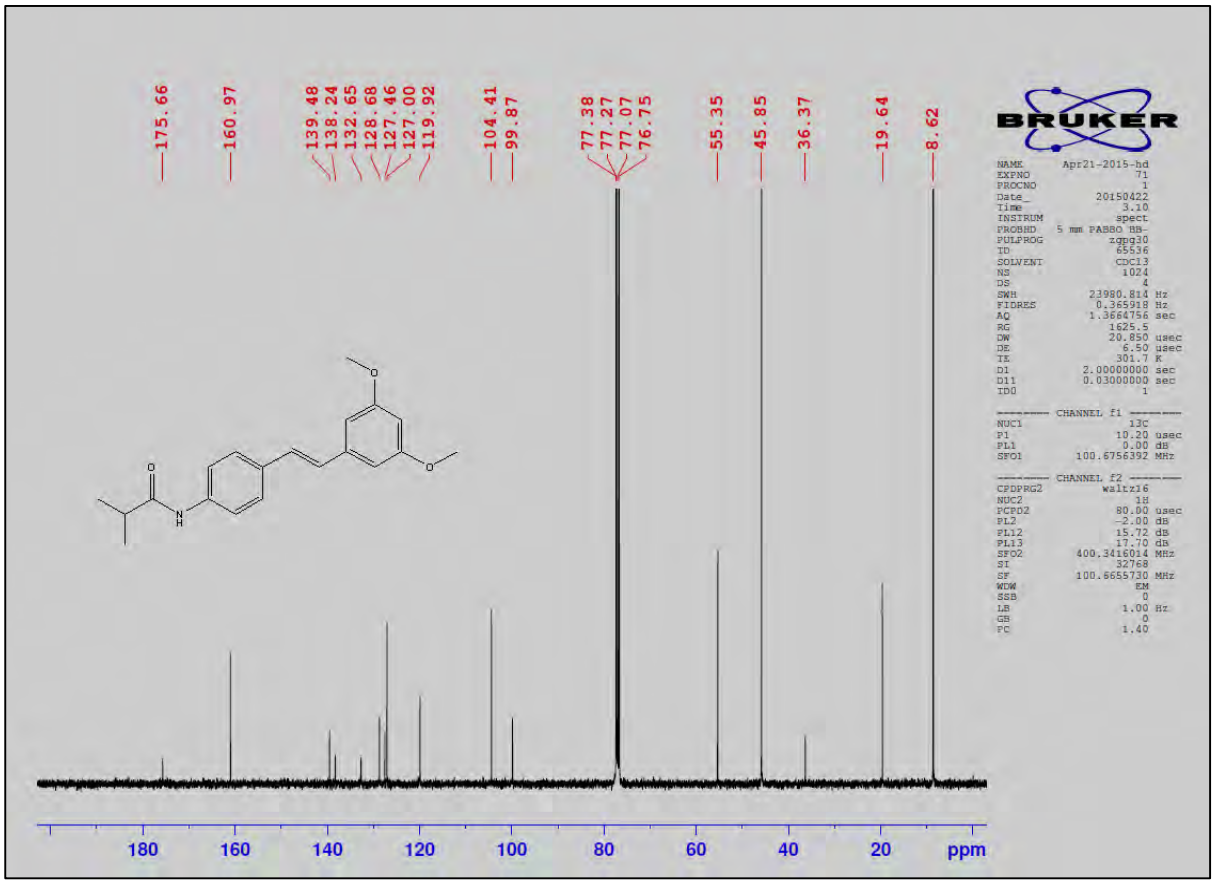

2D HSQC spectra of V32

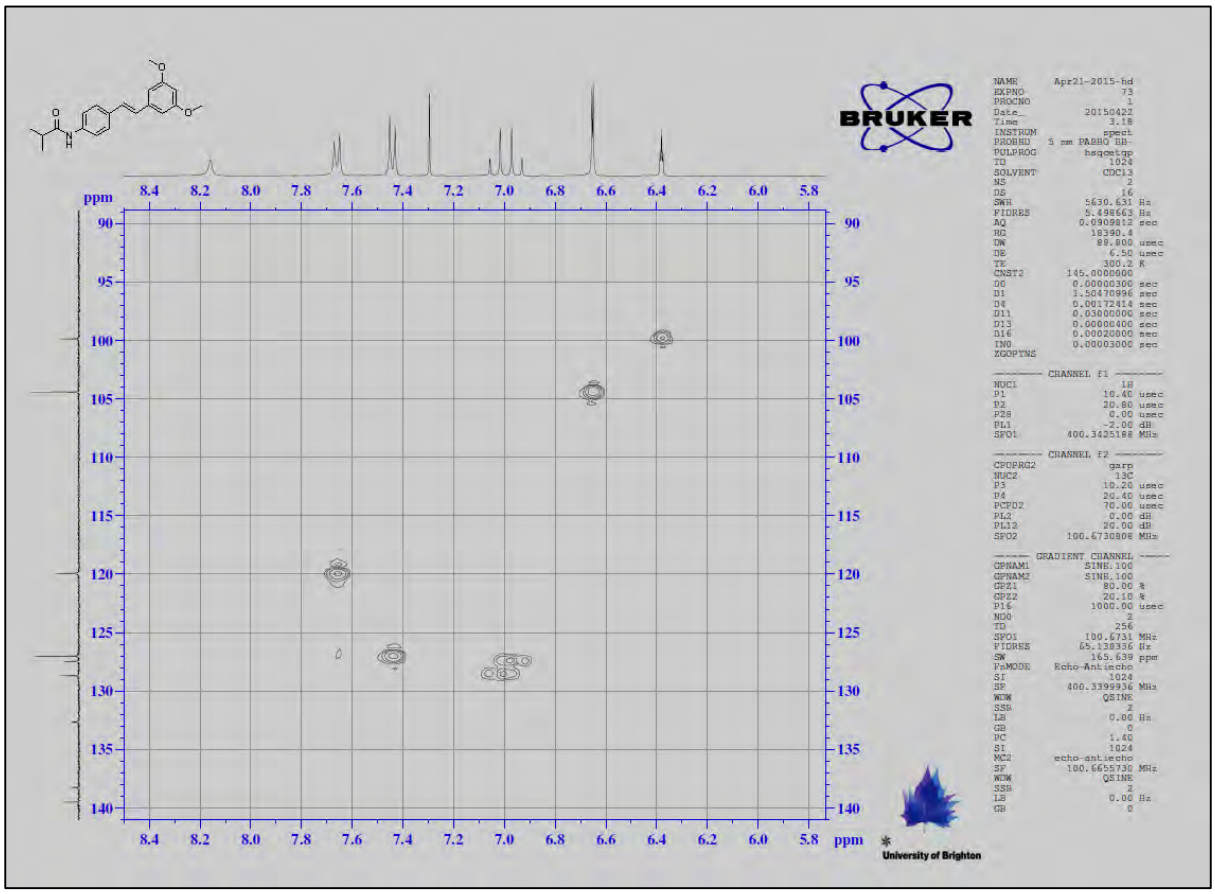

2D COSY spectra of V32

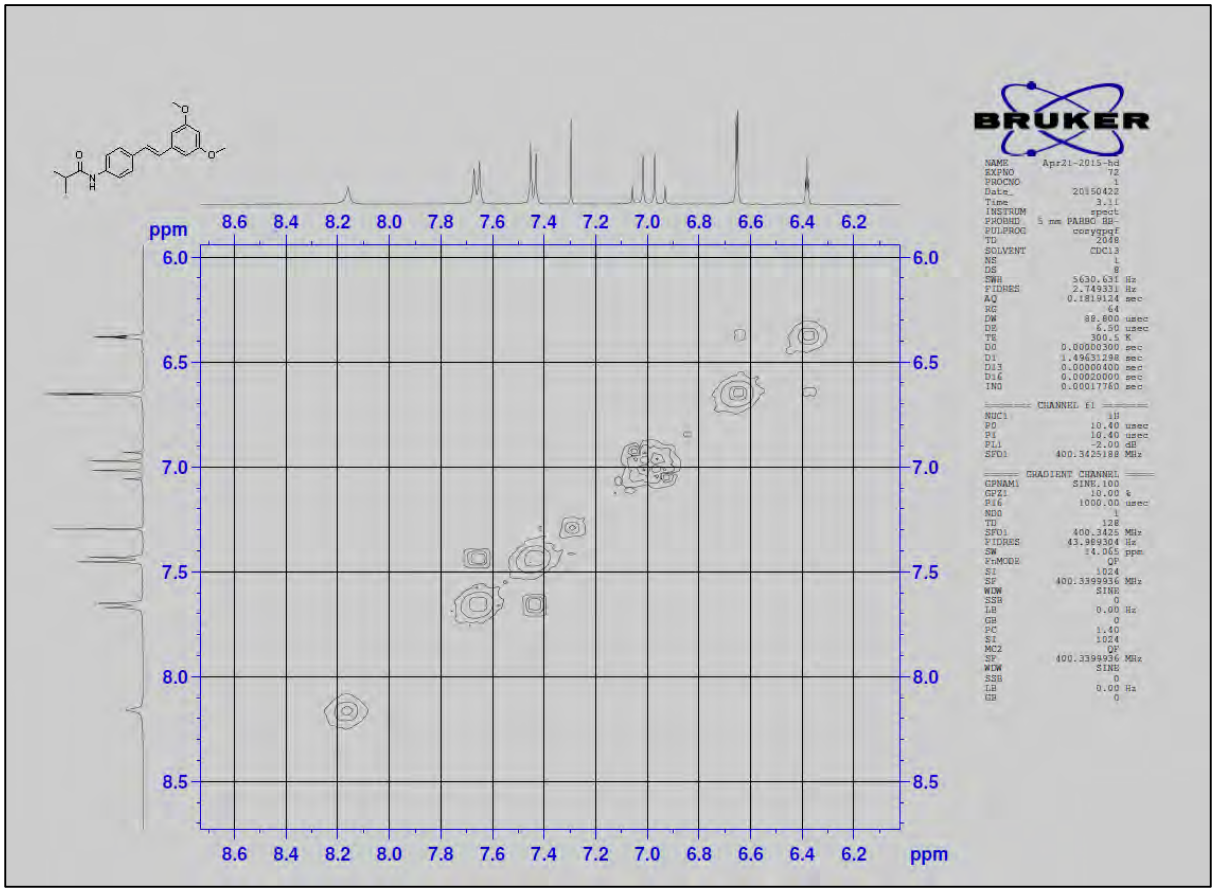

Mass spectra of V32

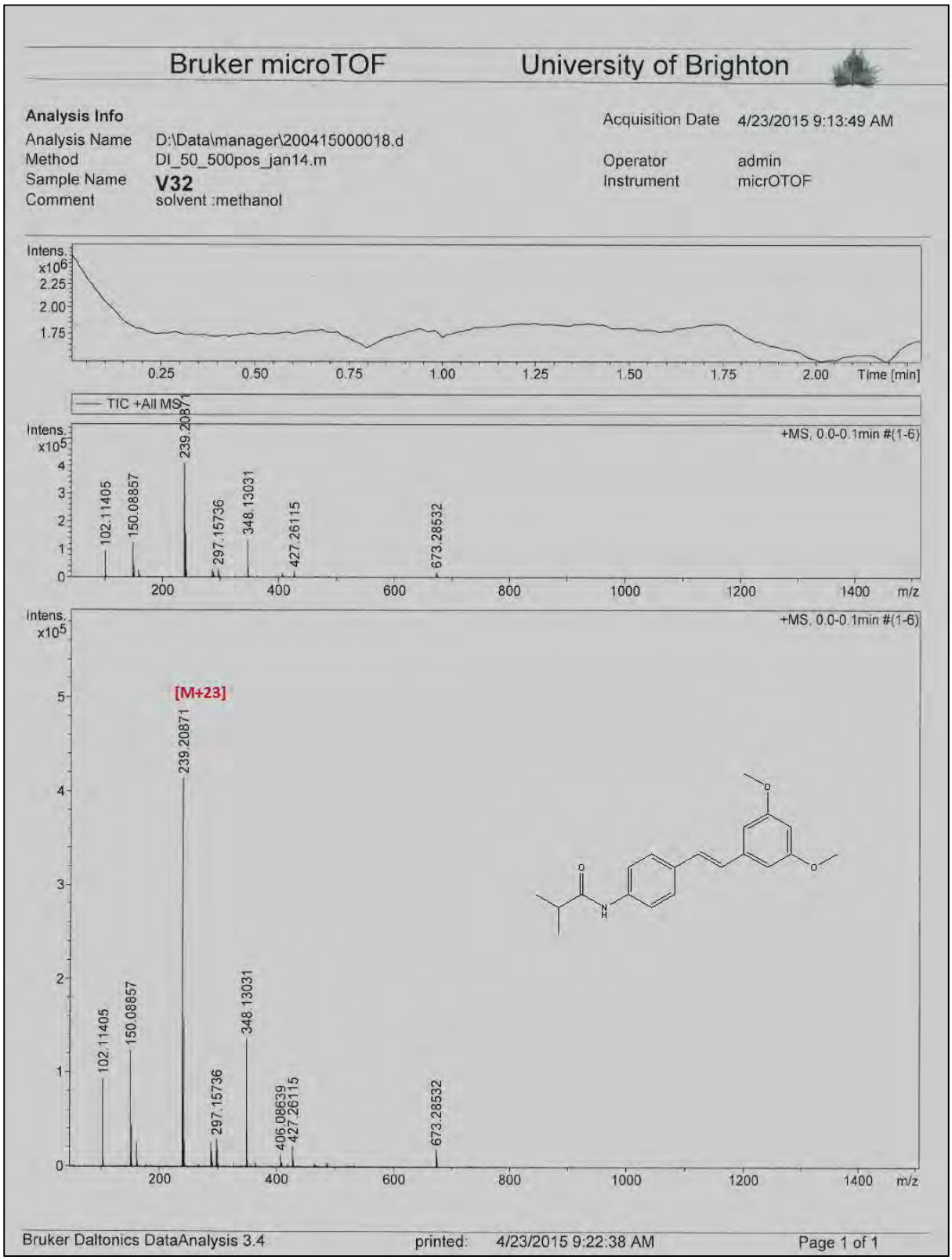

^{1}H NMR spectra of V33

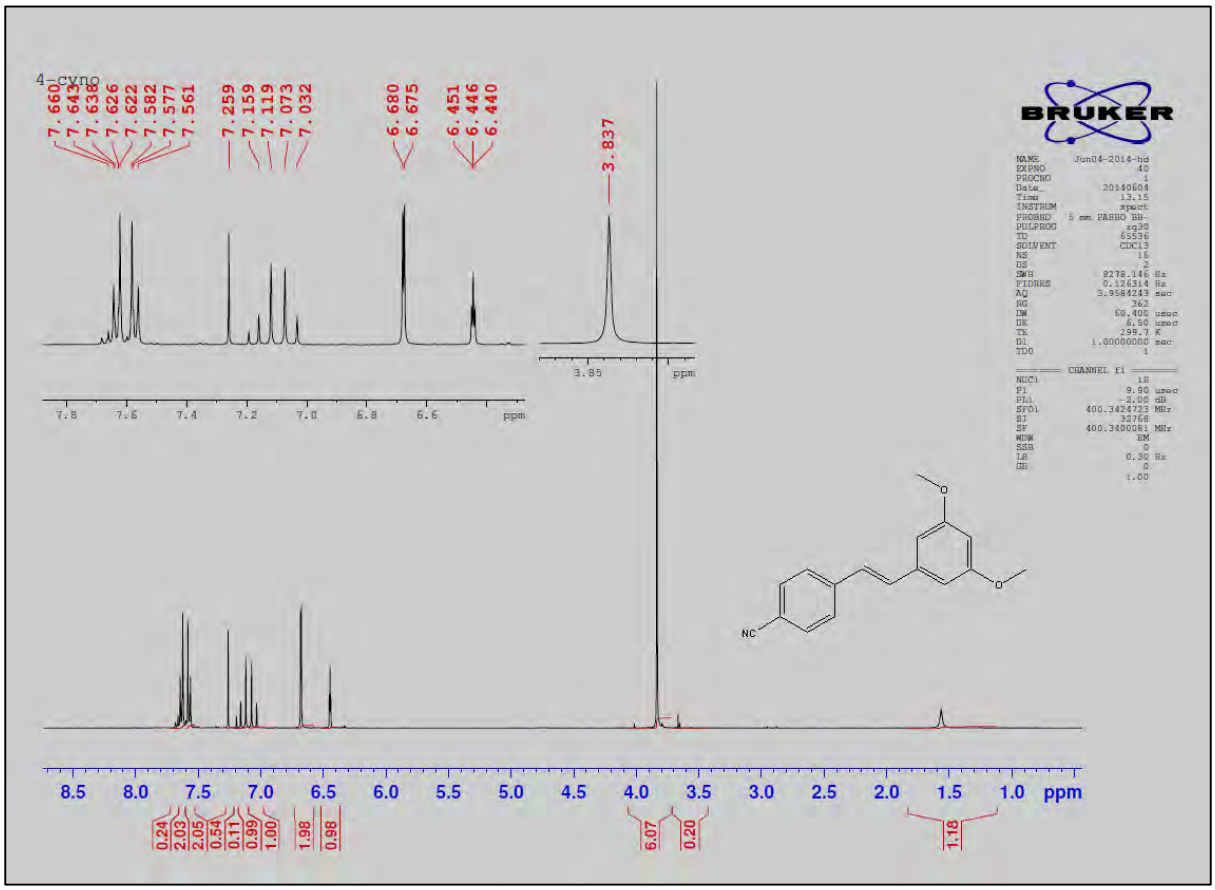

^{13}C NMR spectra of V33

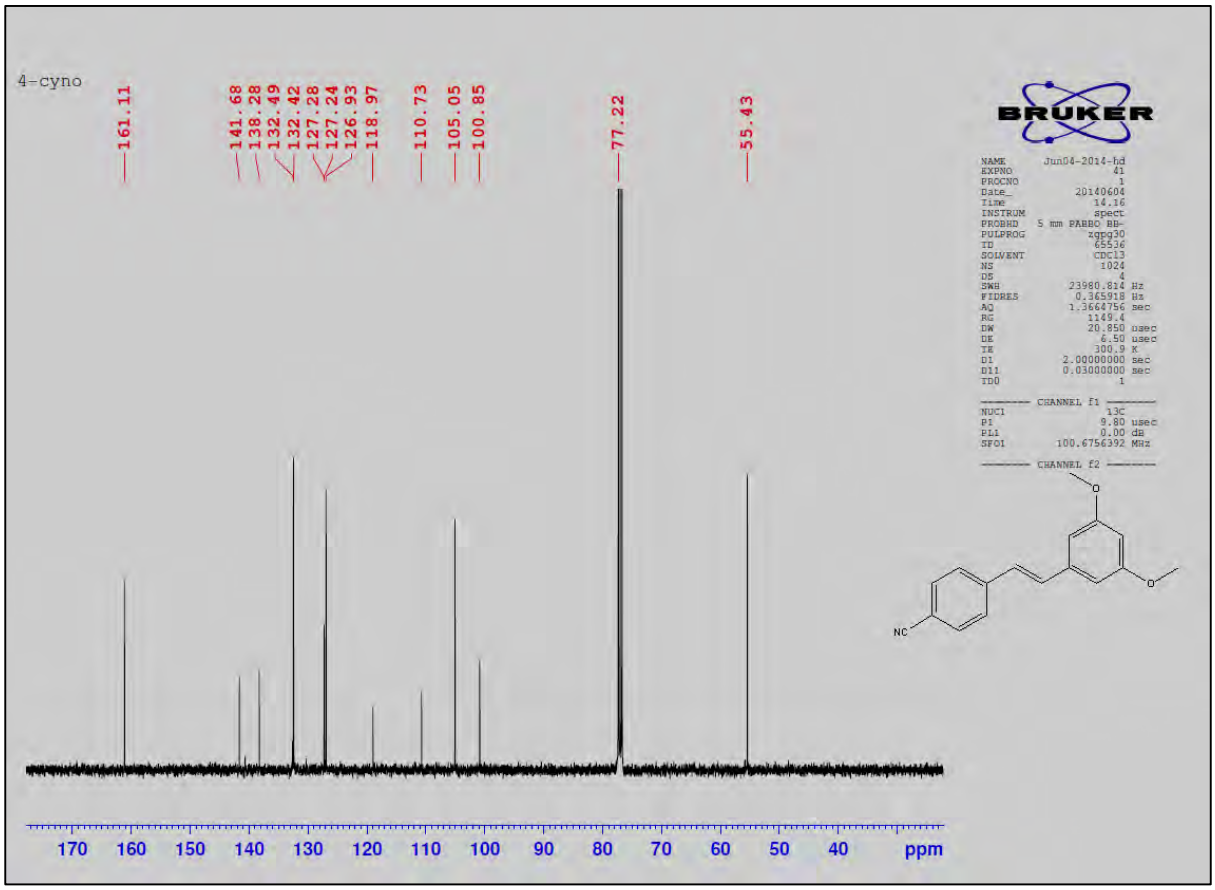

2D HSQC spectra of V33

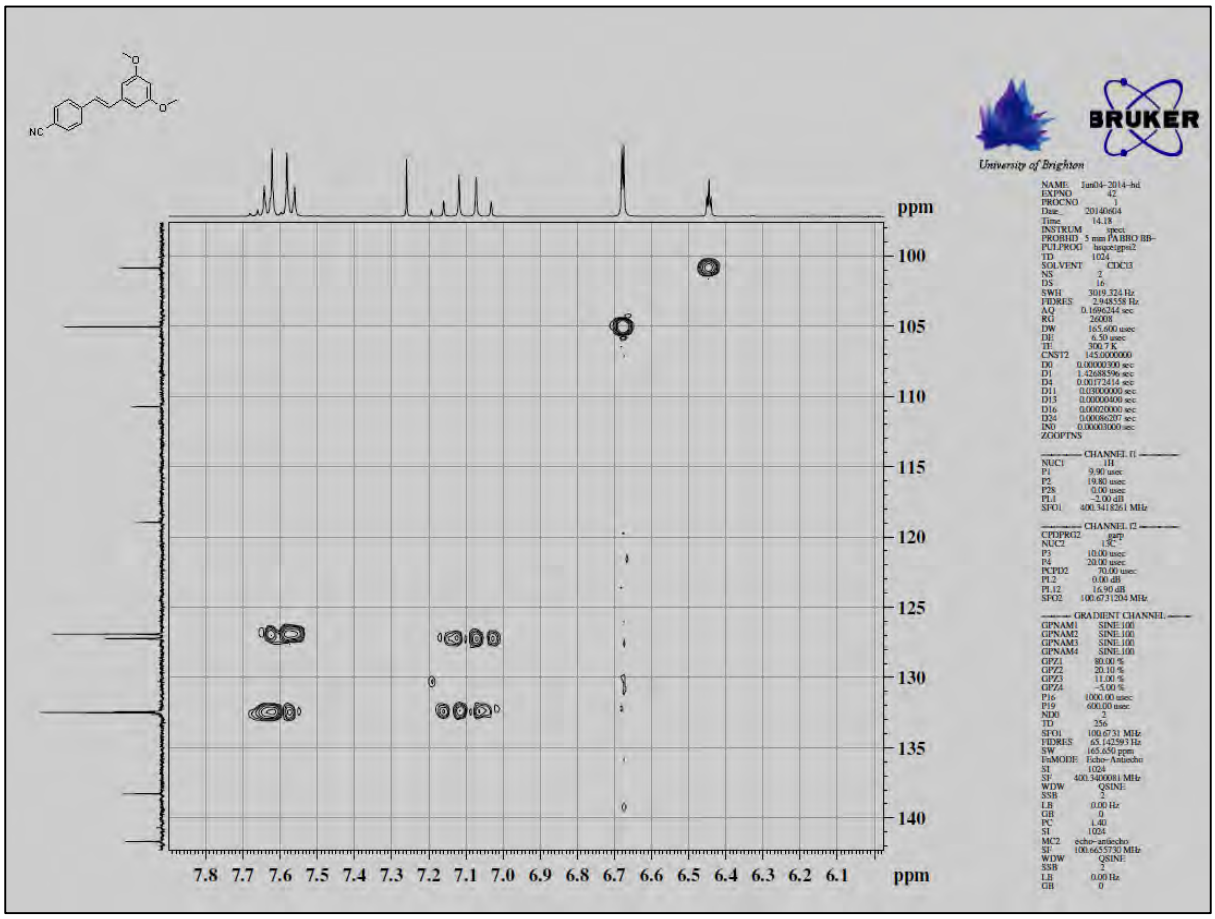

2D COSY spectra of V33

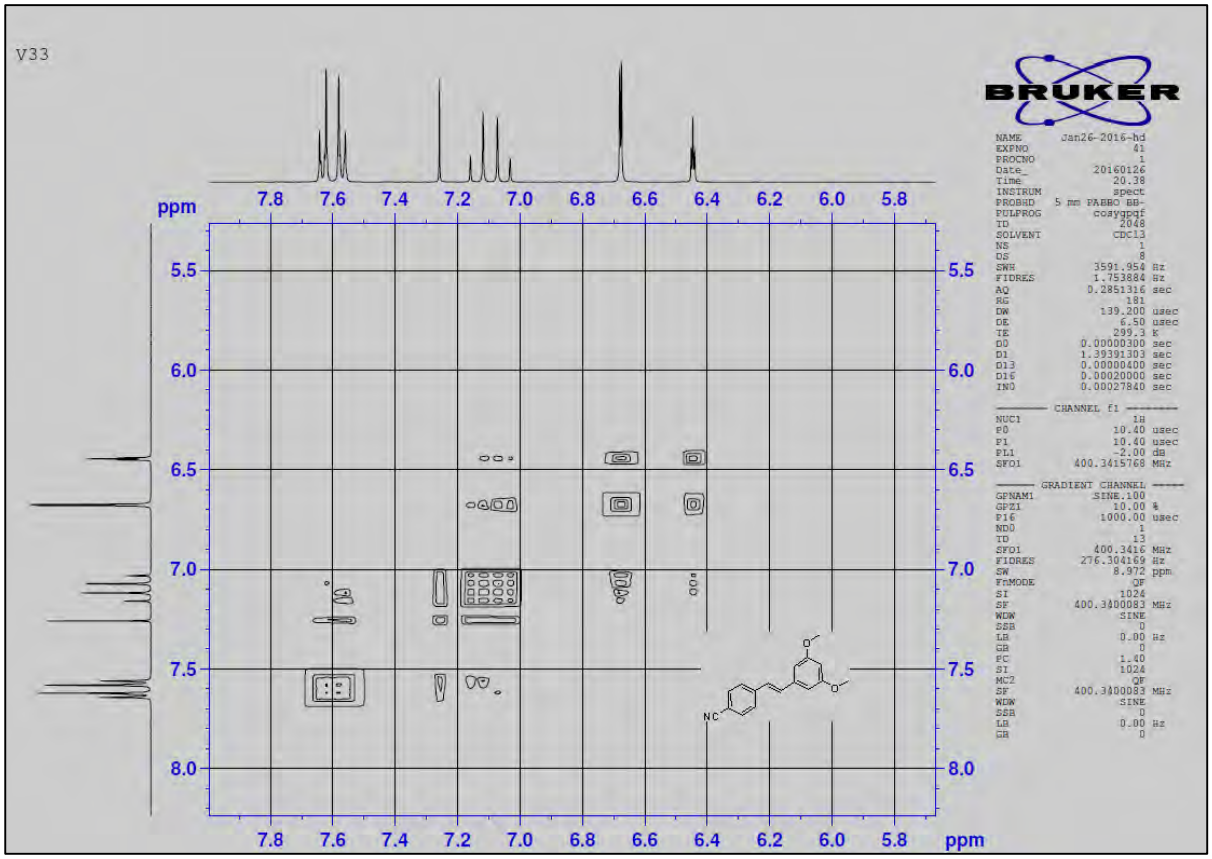

Mass spectra of V33

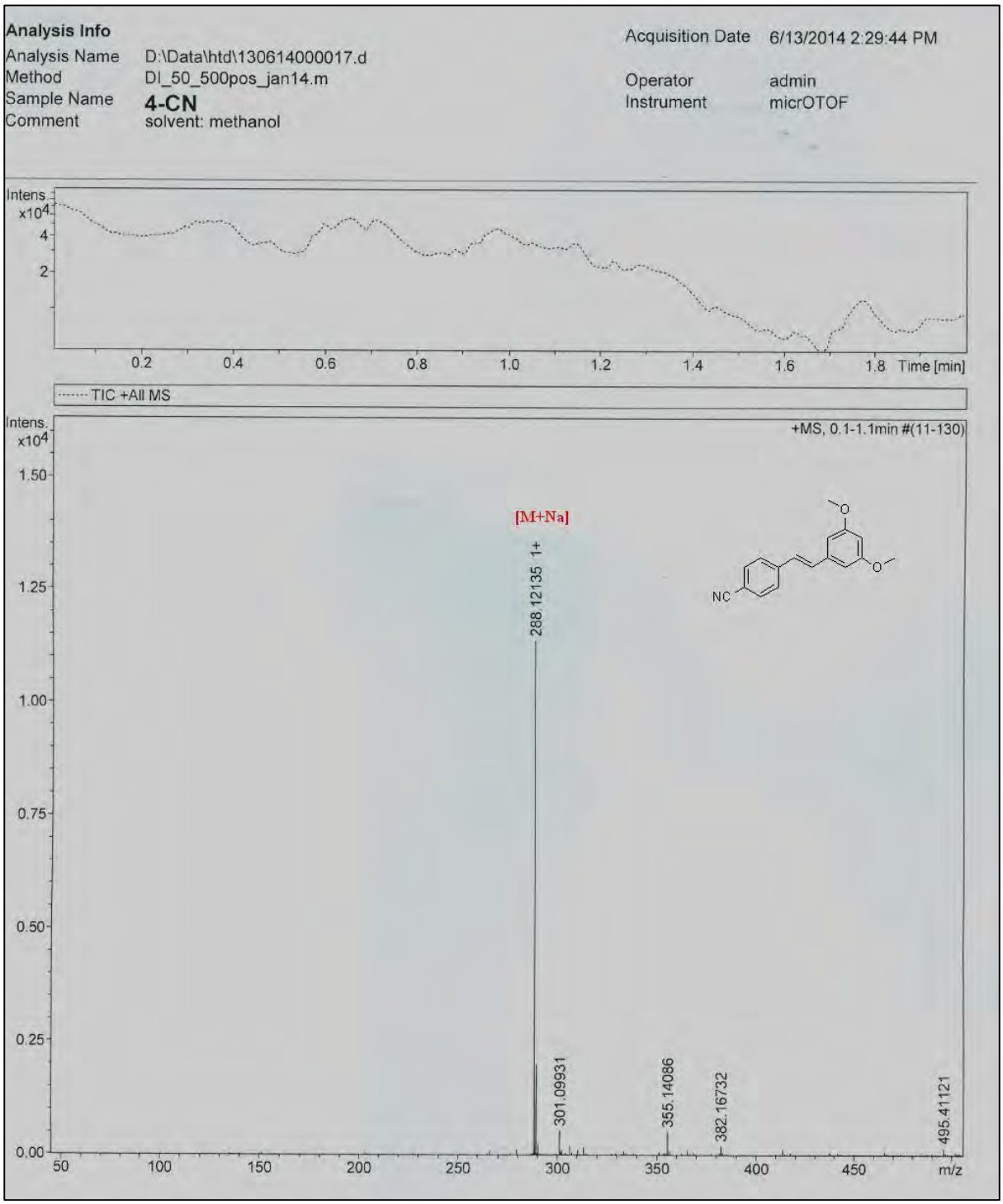

^{1}H NMR spectra of V 34

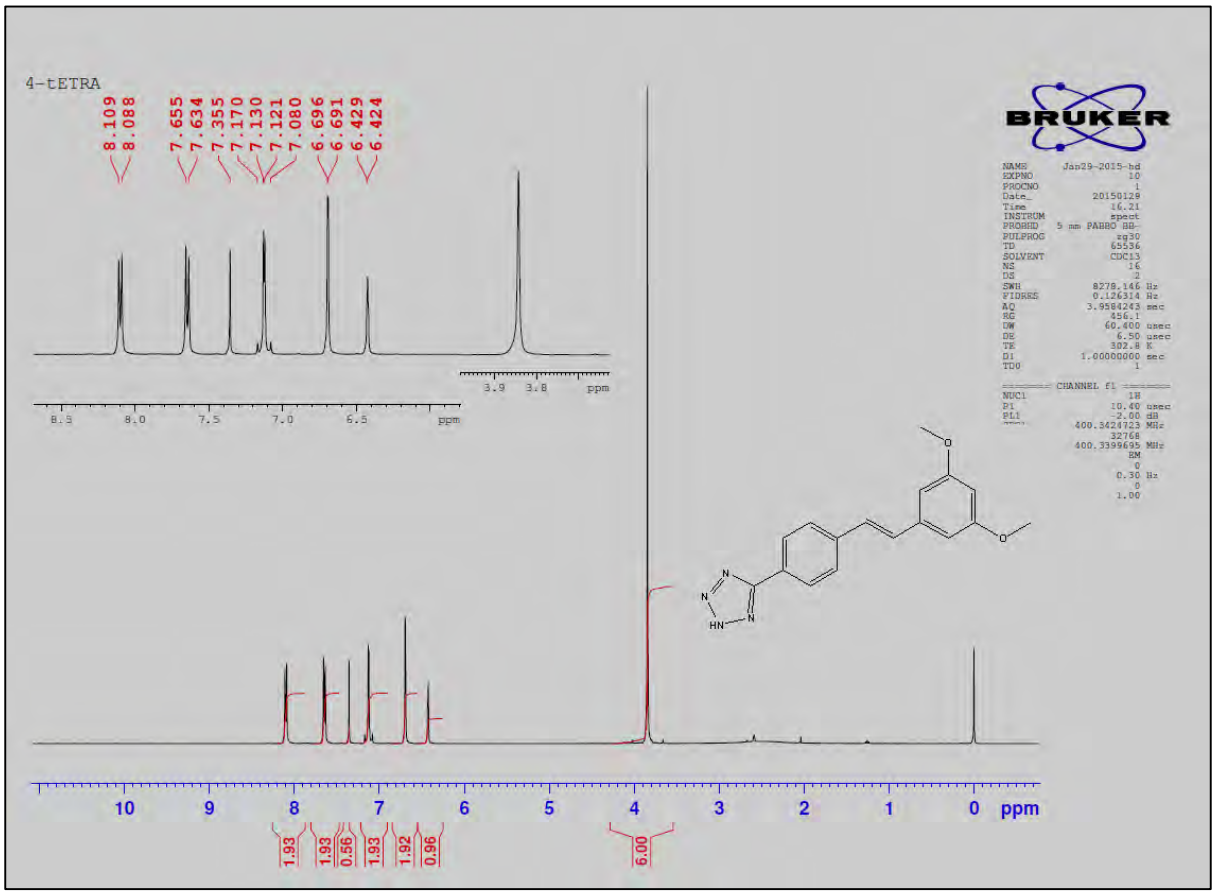

^{13}C NMR spectra of V34

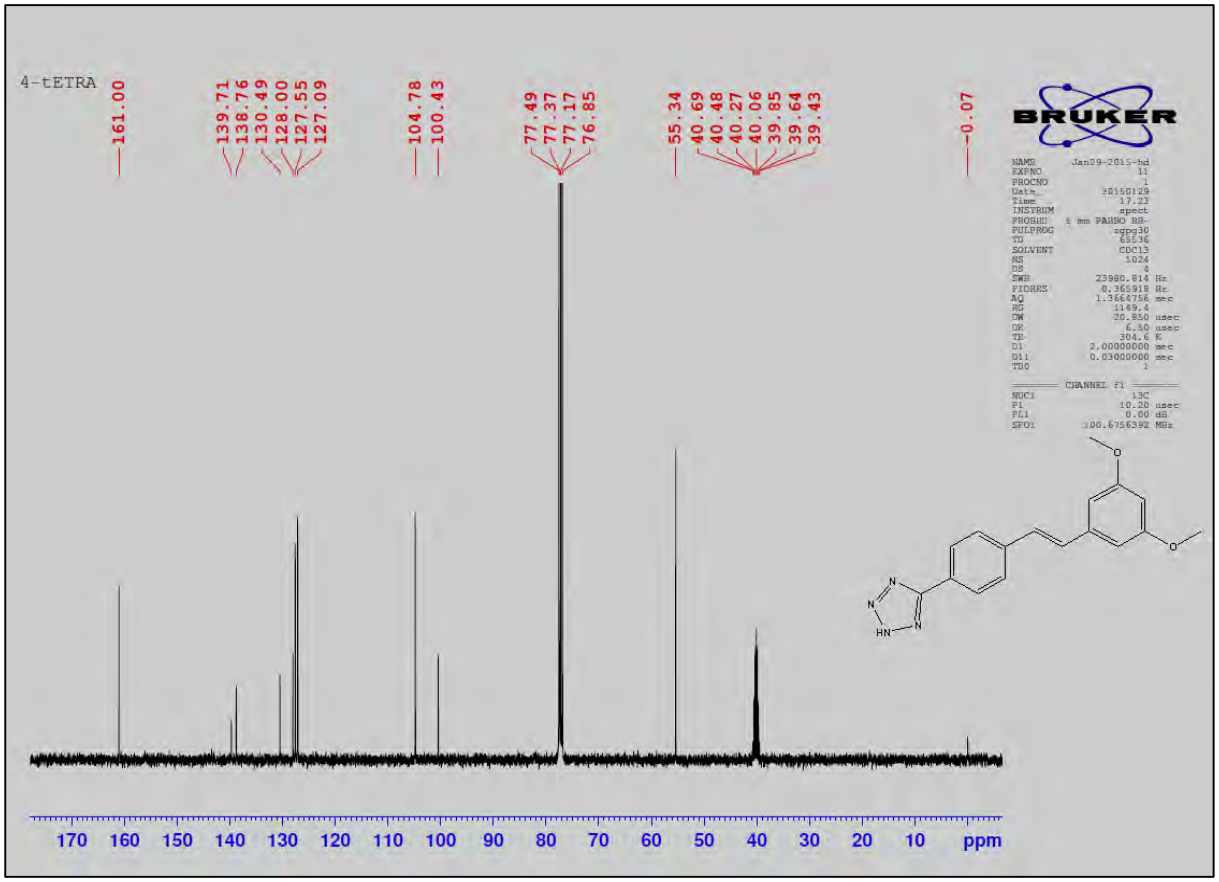

2D HSQC spectra of V34

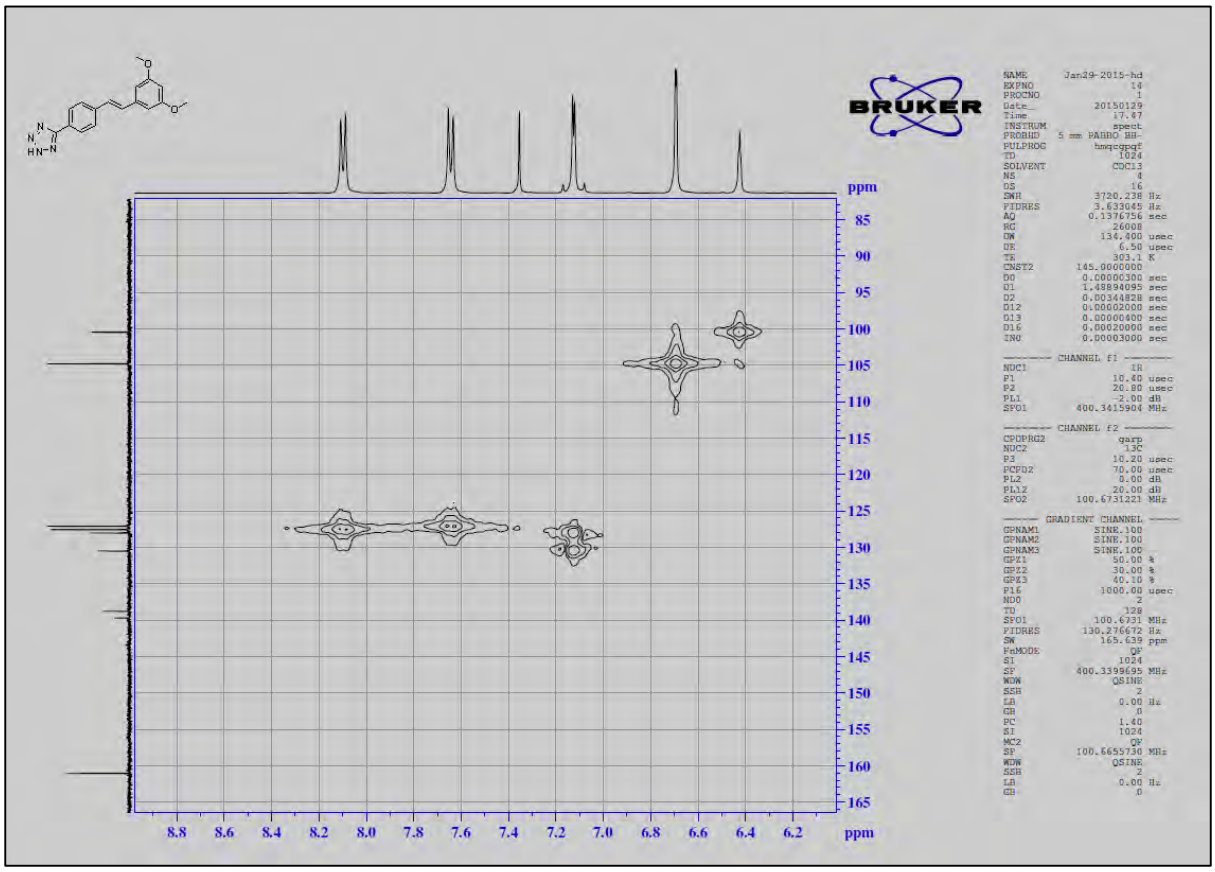

2D COSY spectra of V34

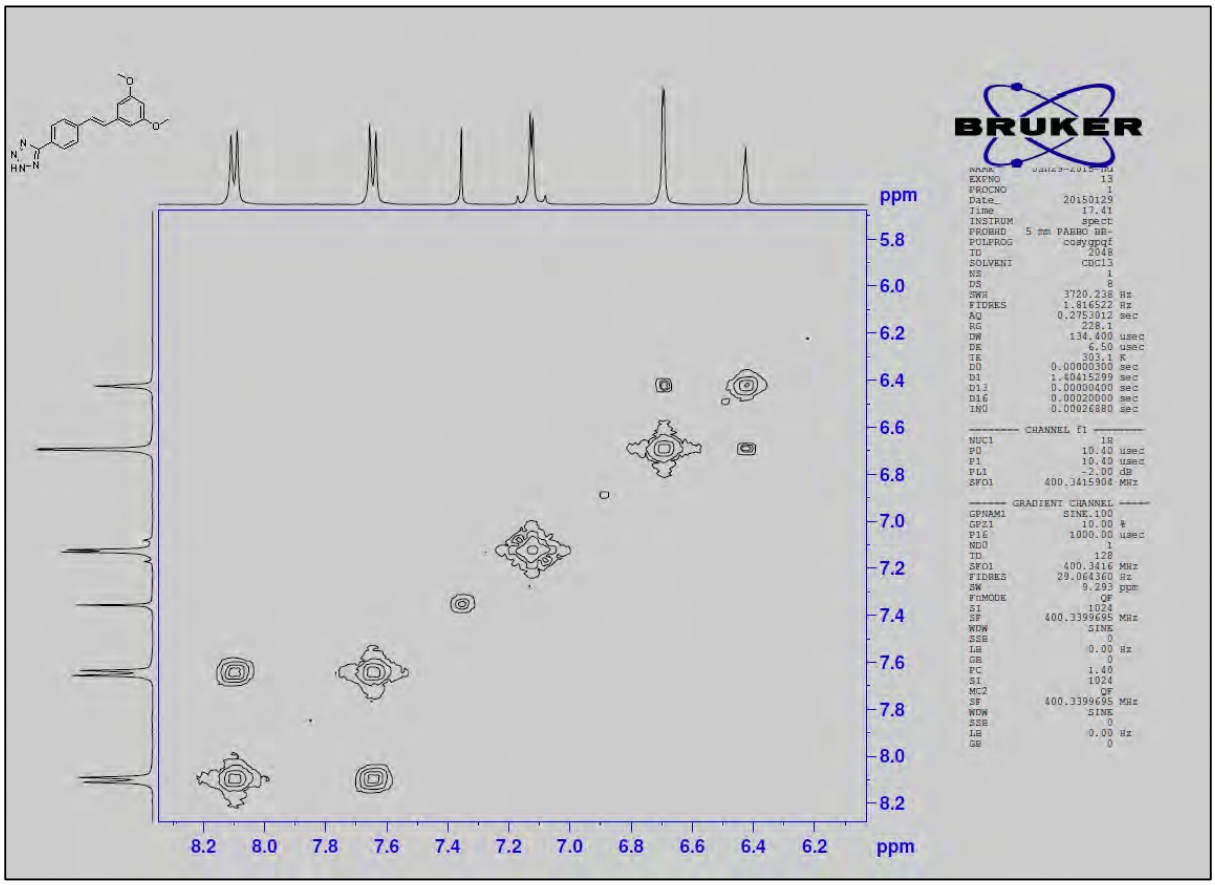

Mass spectra of V34

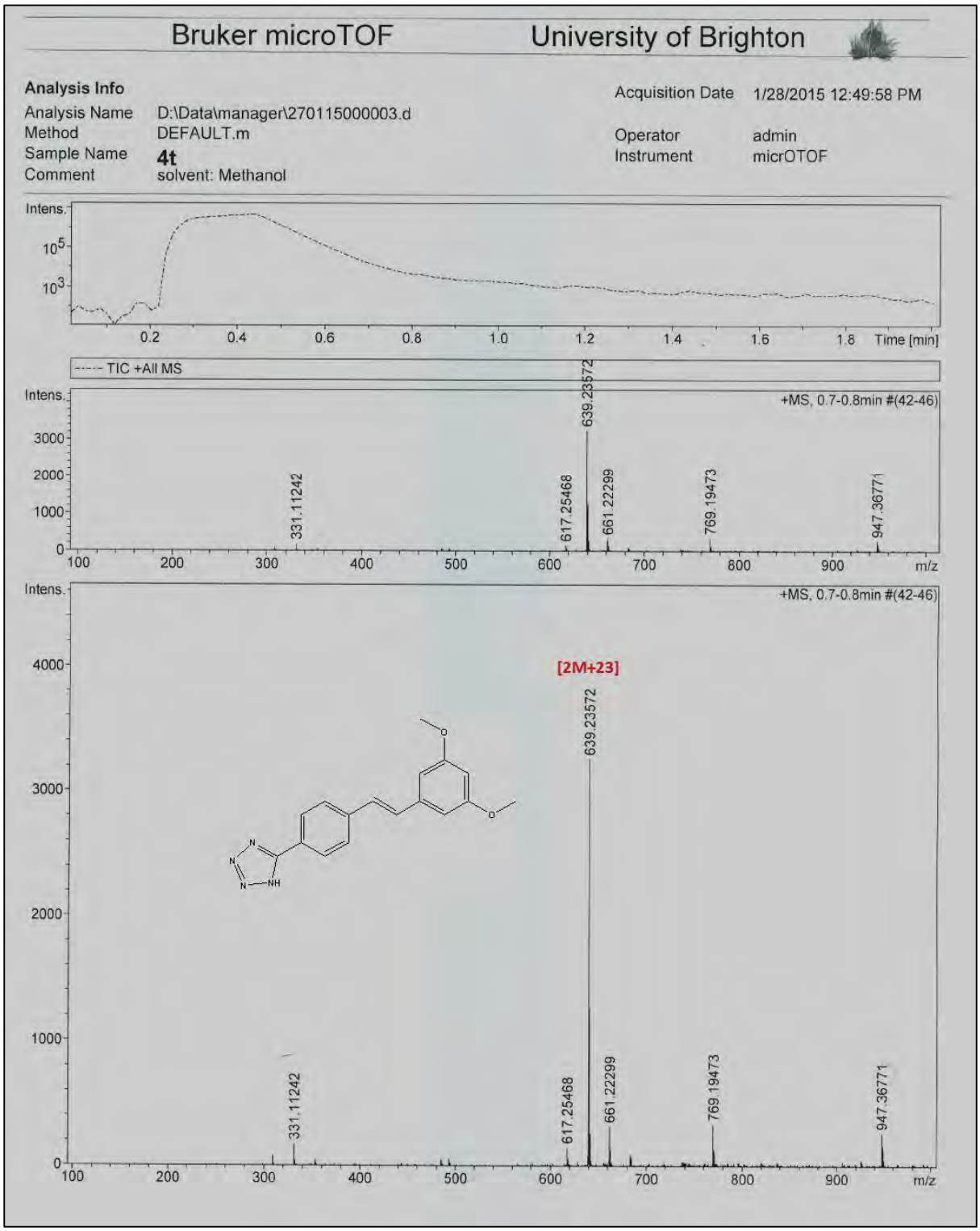

^{1}H NMR spectra of V36

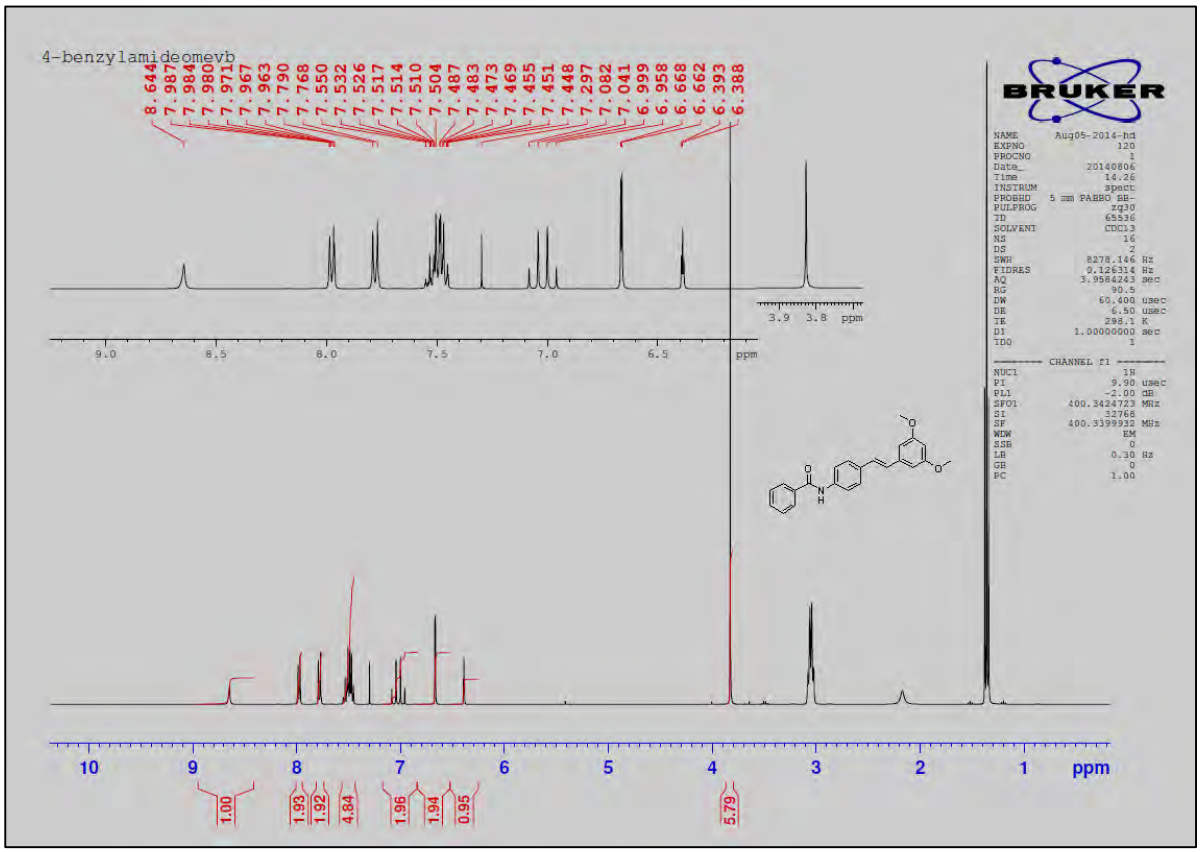

^{13}C NMR spectra of V36

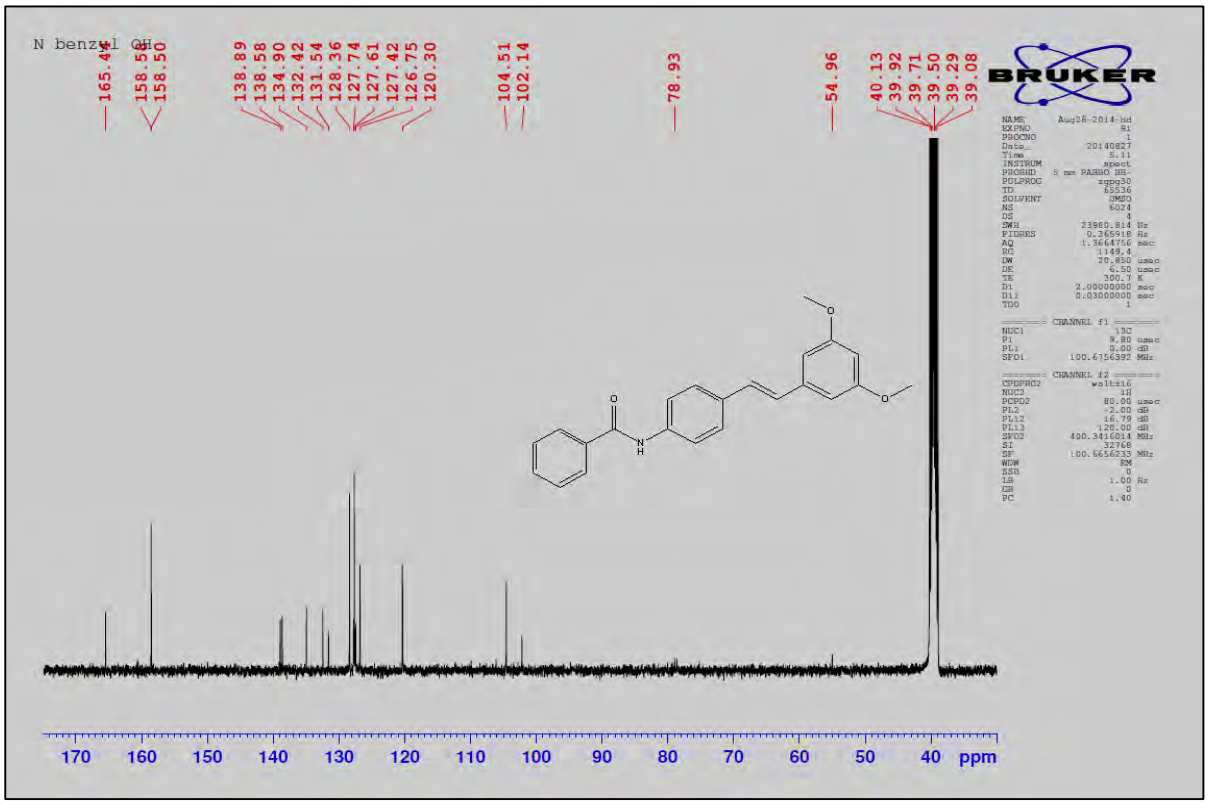

2D HSQC spectra of V36

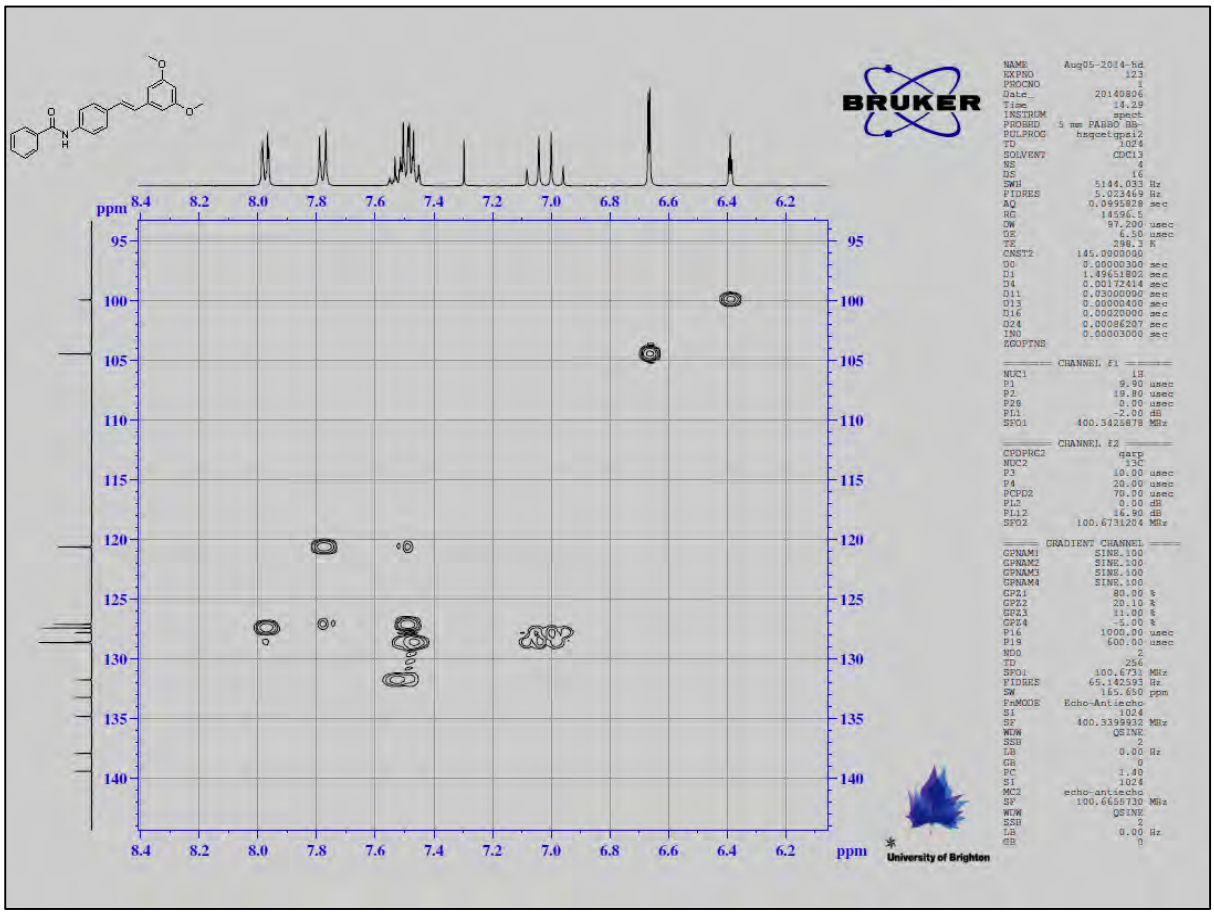

2D COSY spectra of V36

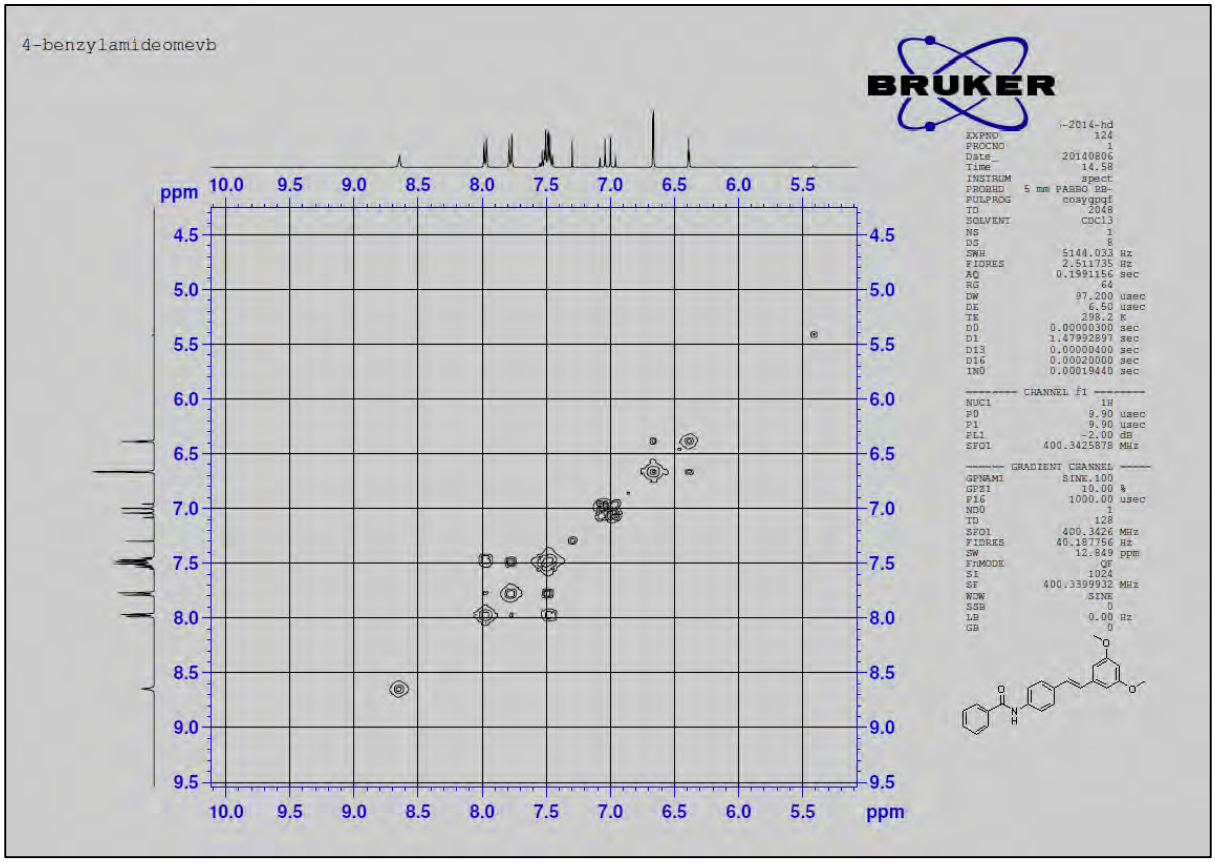

Mass spectra of V36

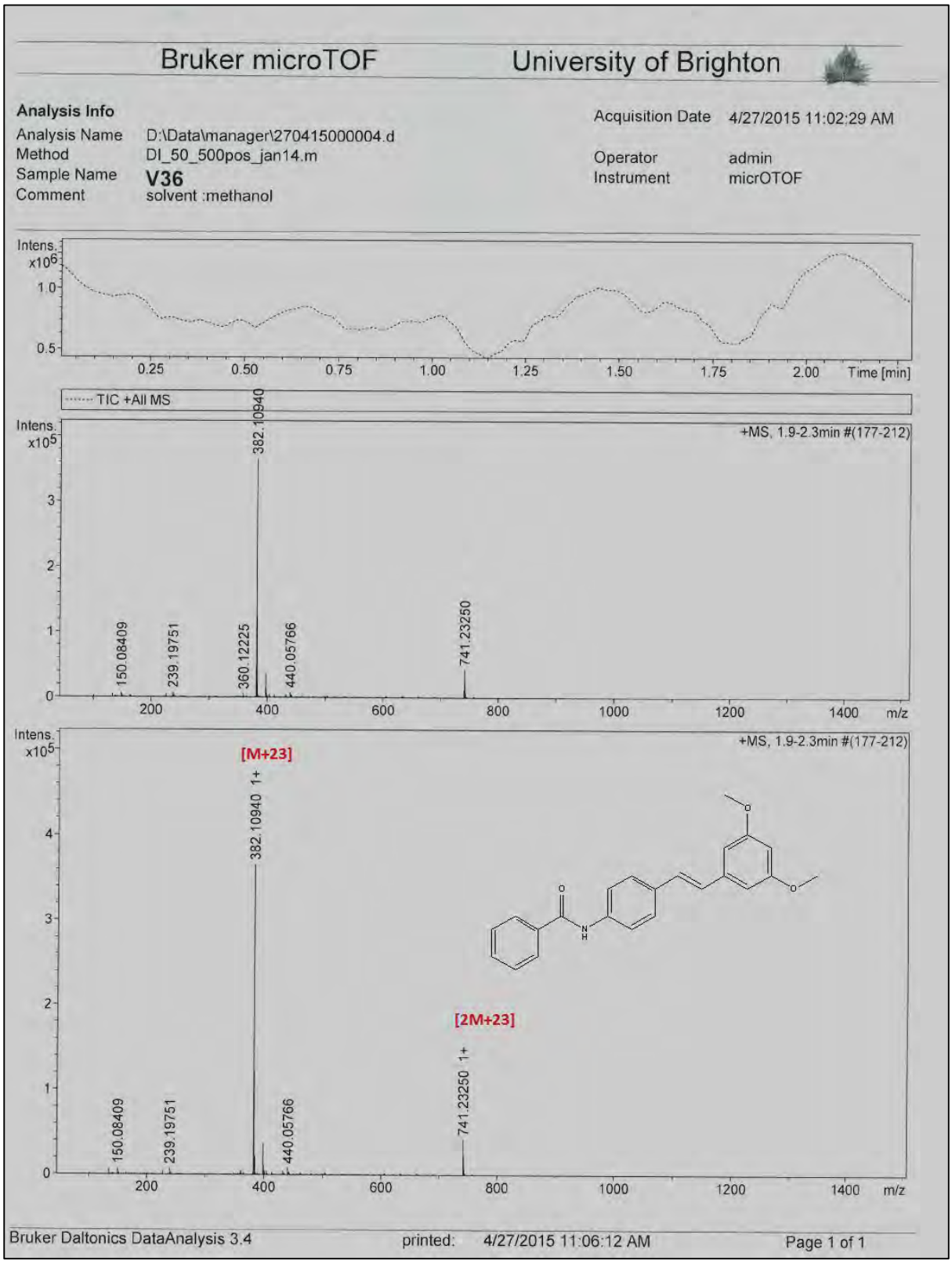

^{1}H NMR spectra of V37

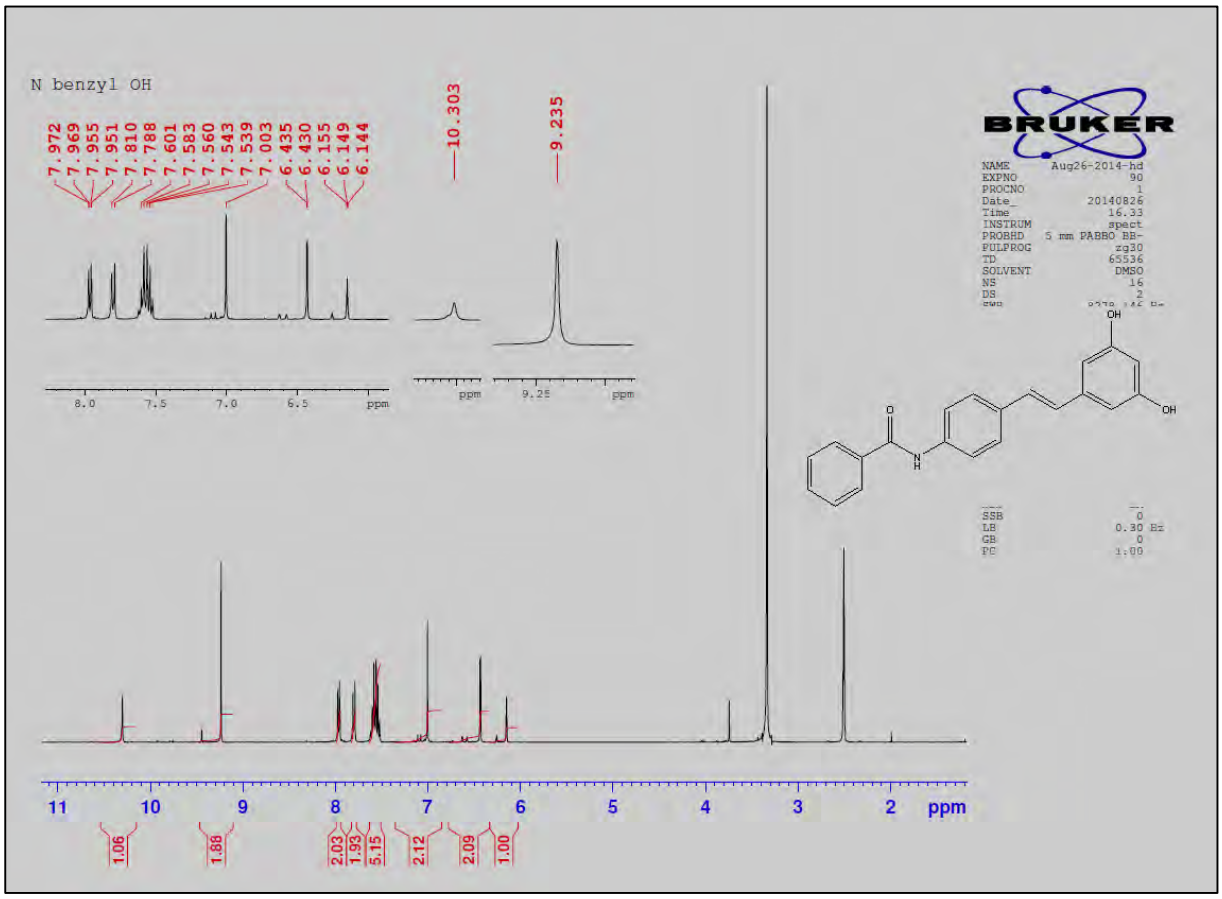

^{13}C NMR spectra of V37

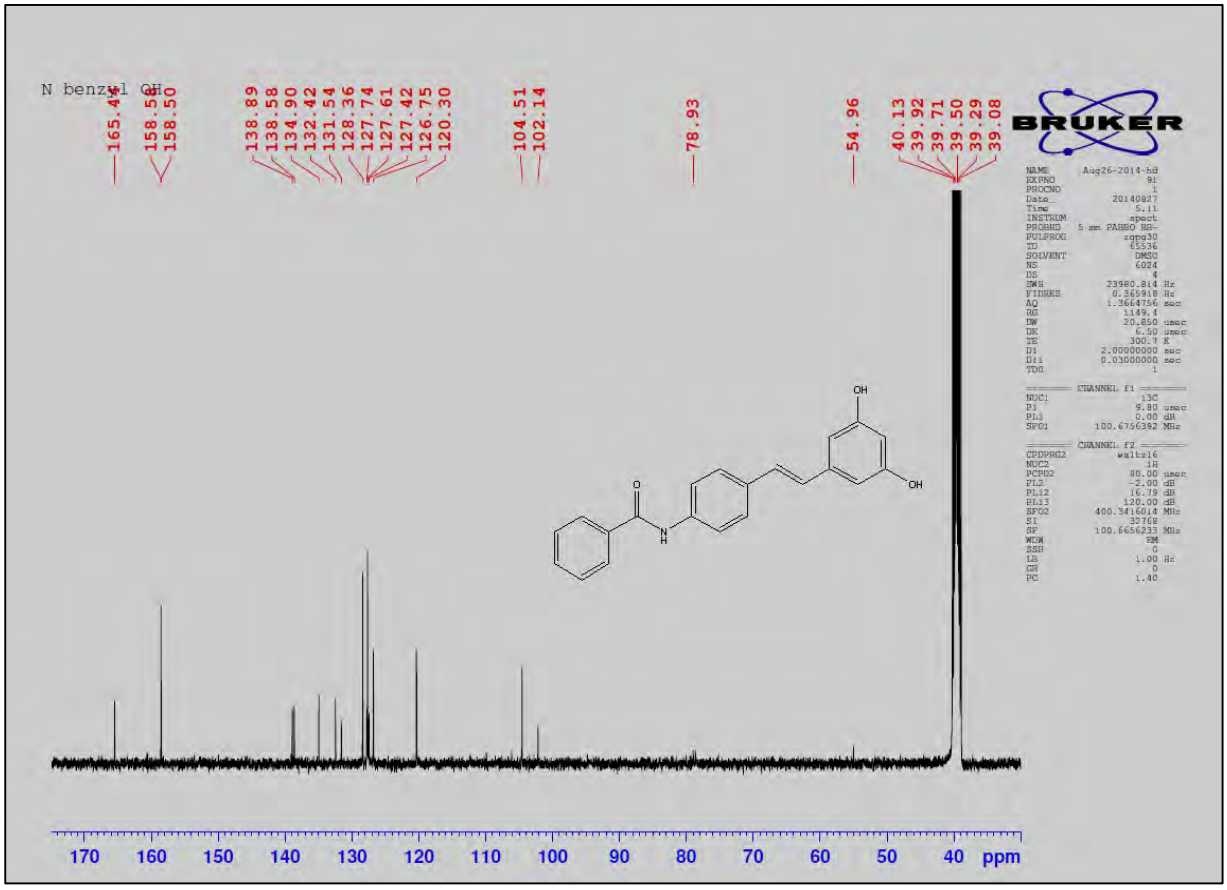

2D HSQC spectra of V37

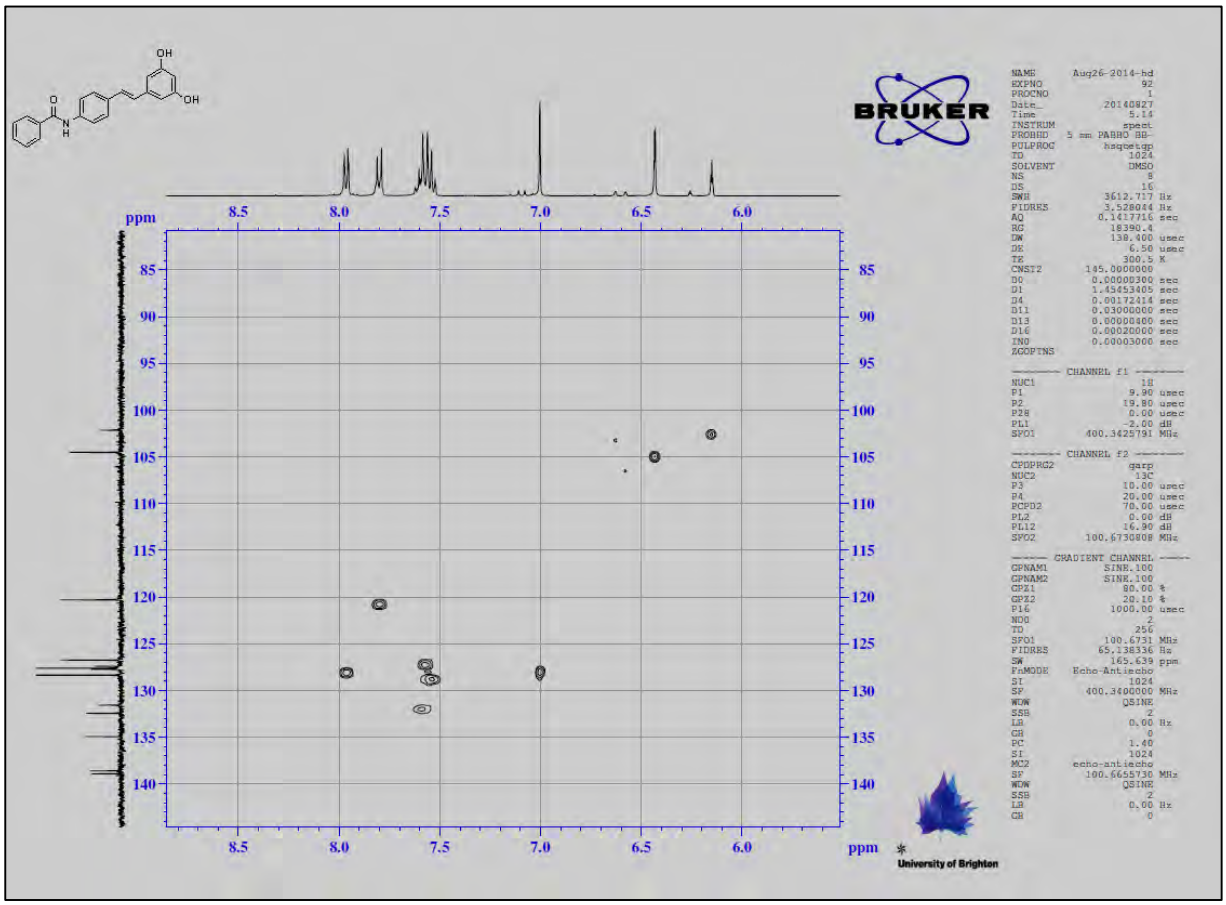

2D COSY spectra of V37

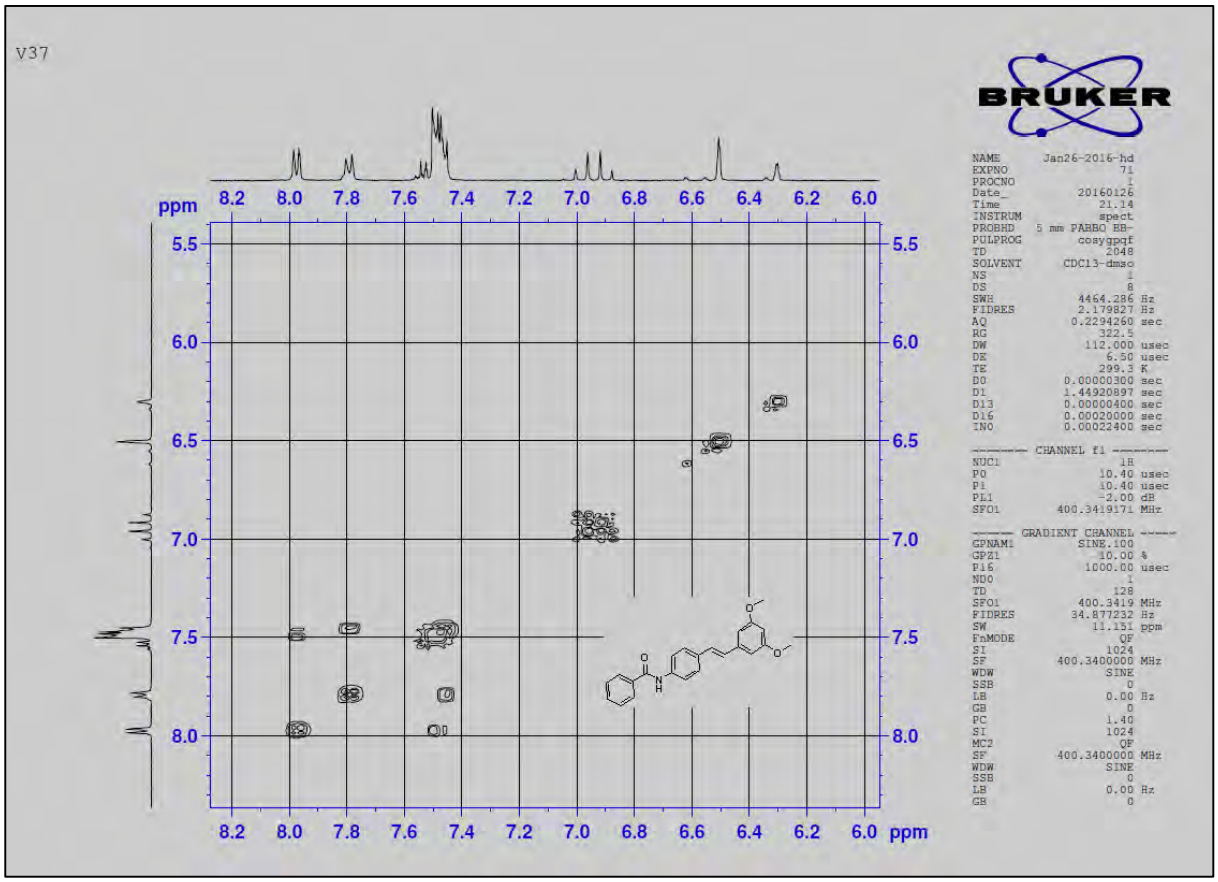

Mass spectra of V37

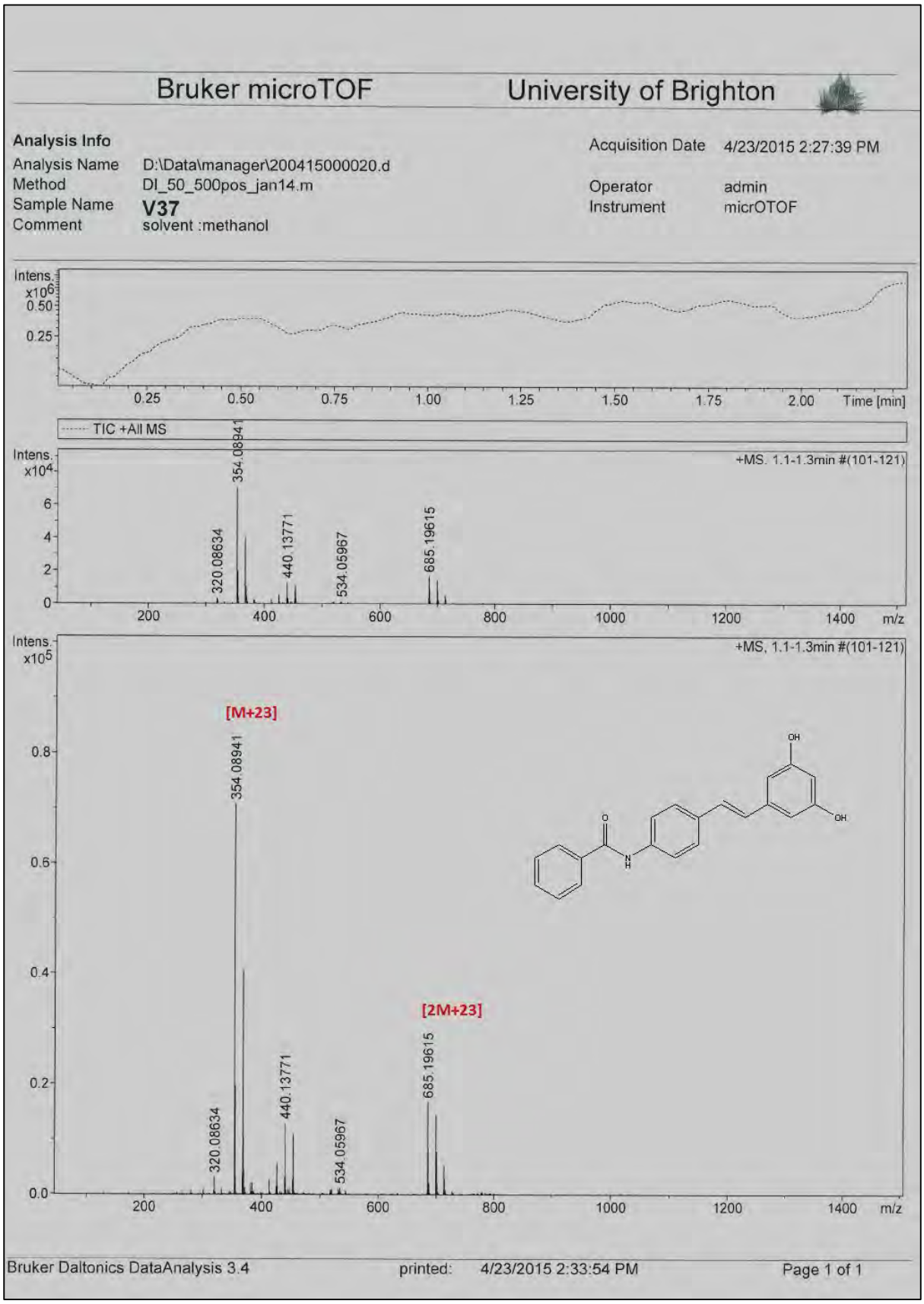

^{1}H NMR spectra of V38

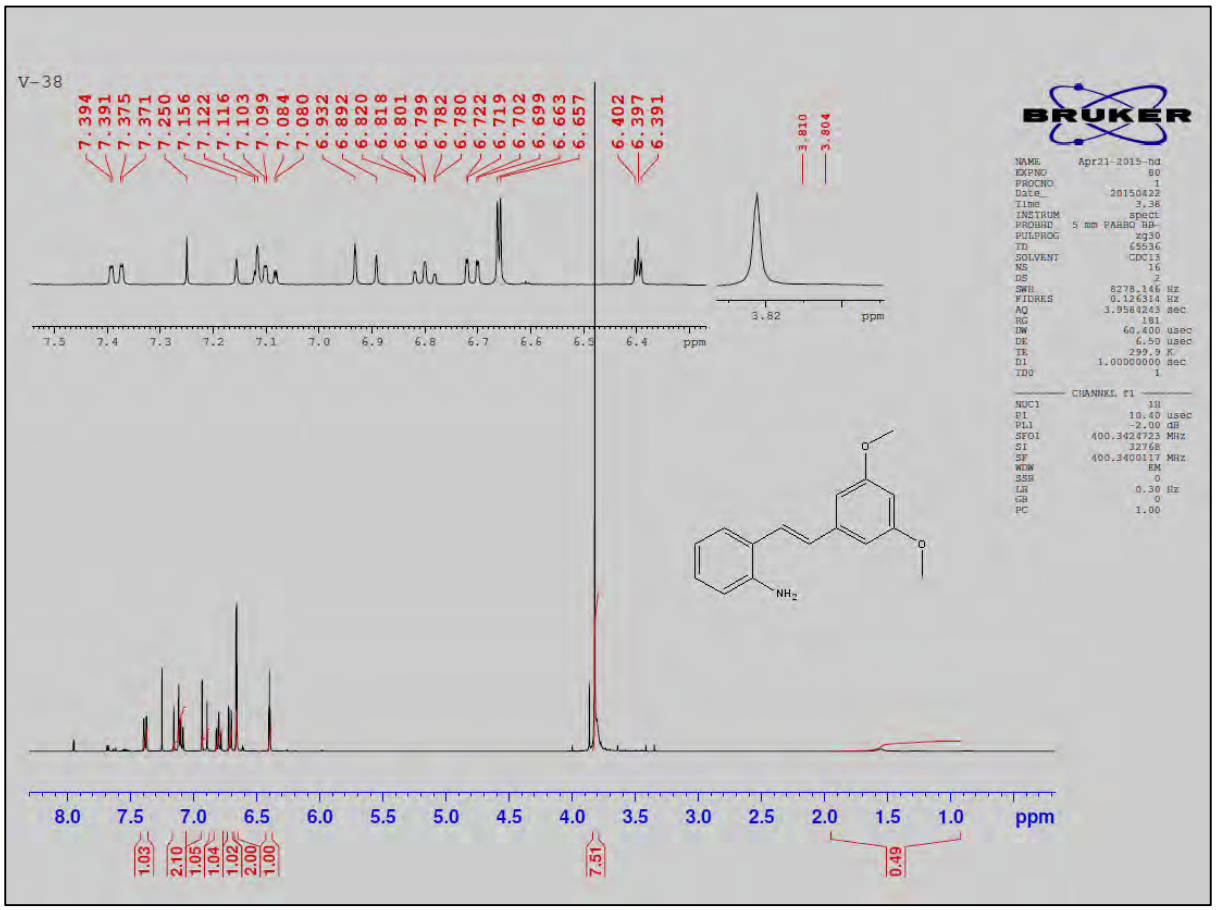

^{13}C NMR spectra of V38

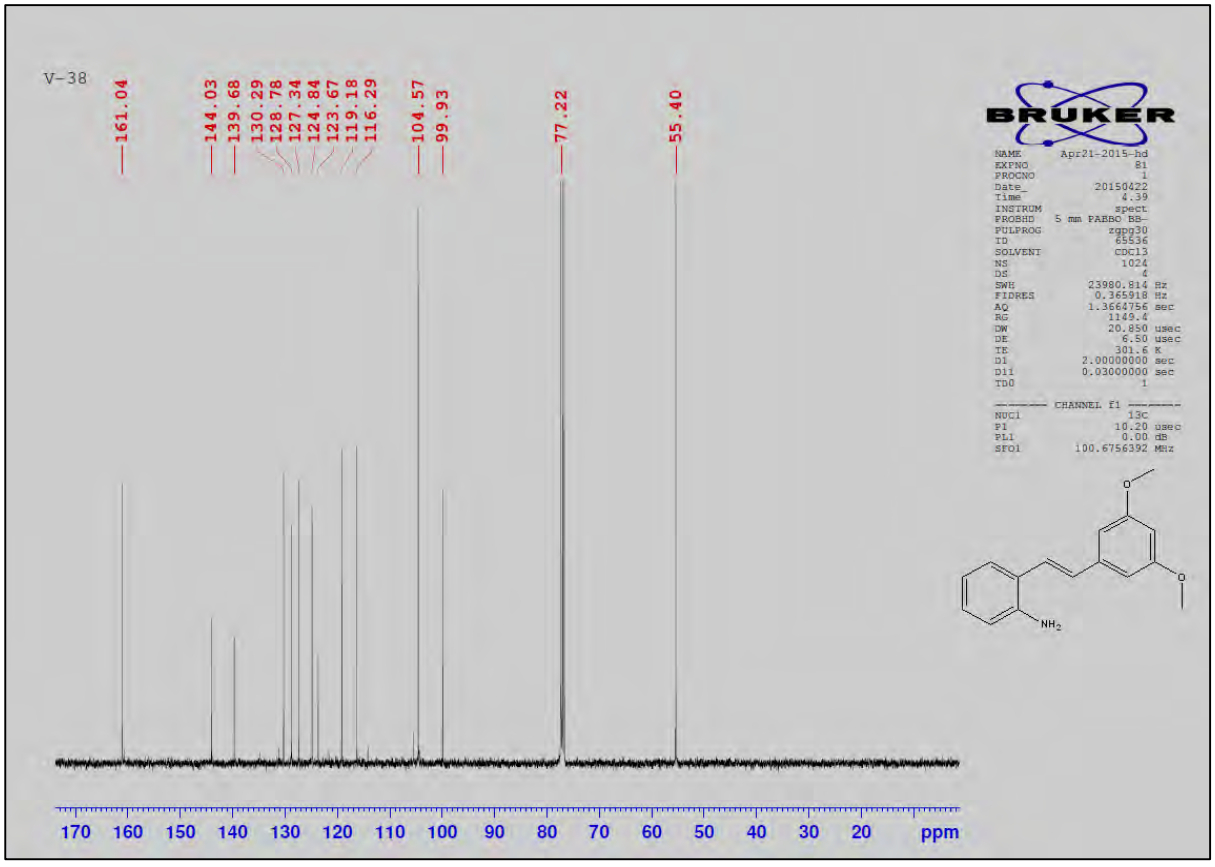

2D HSQC spectra of V38

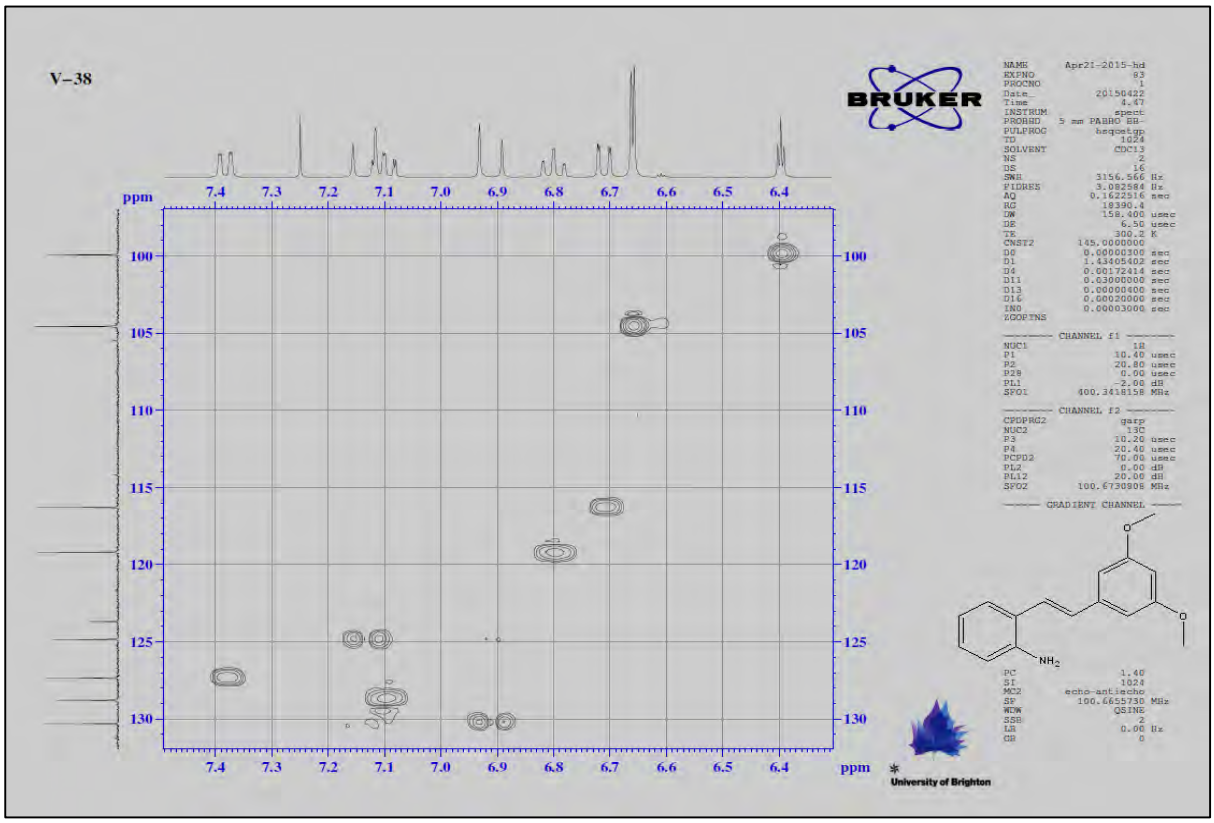

2D COSY spectra of V38

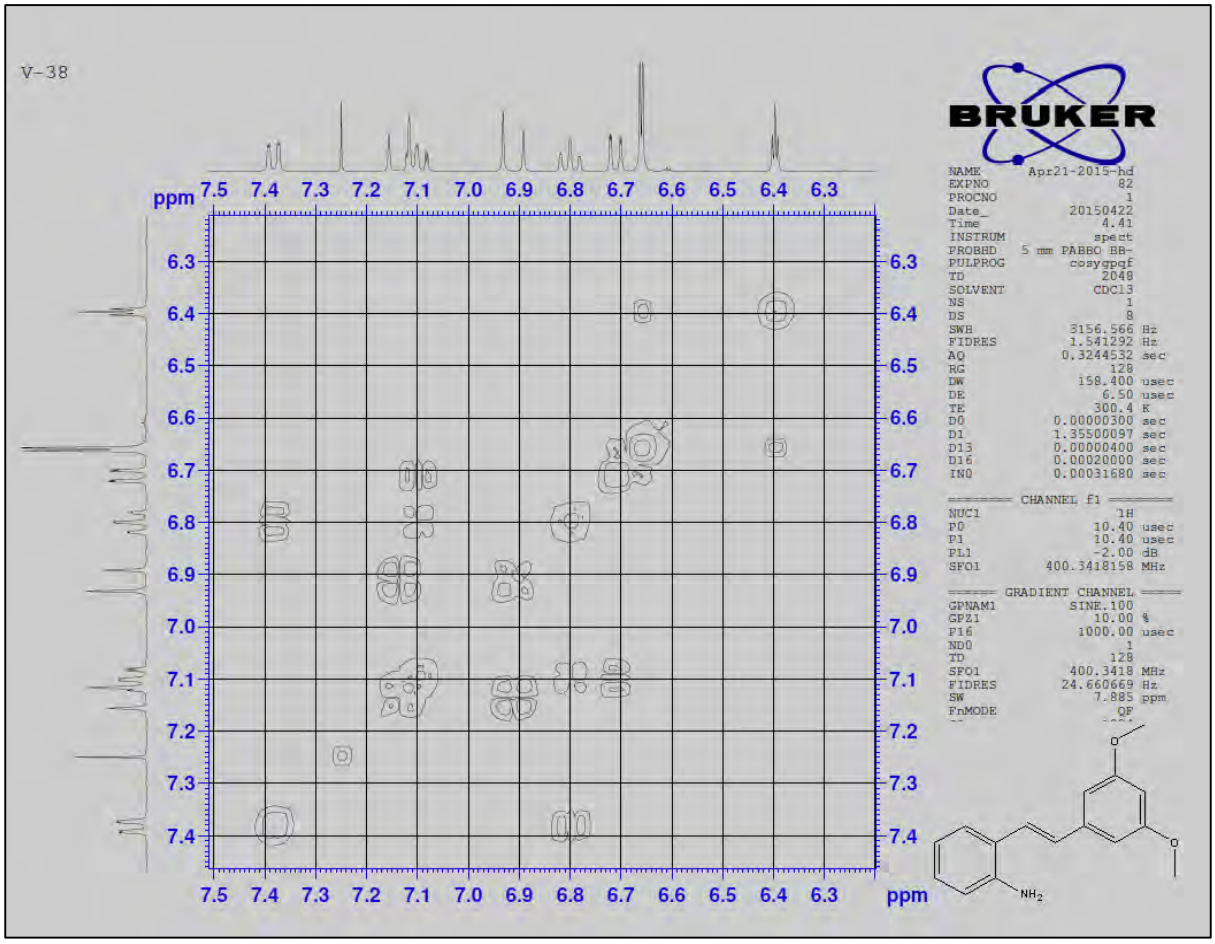

Mass spectra of V38

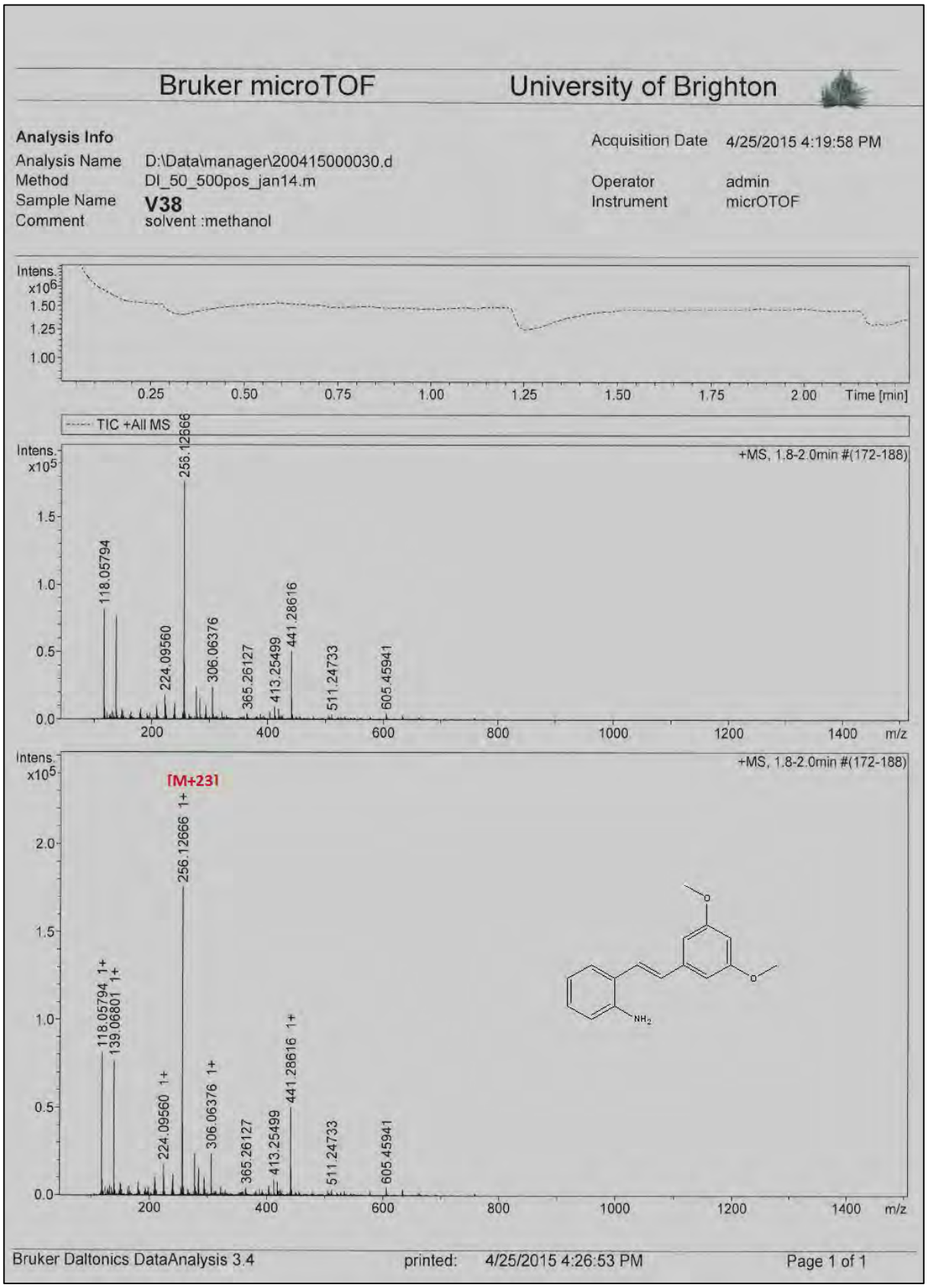

^{1}H NMR spectra of V39

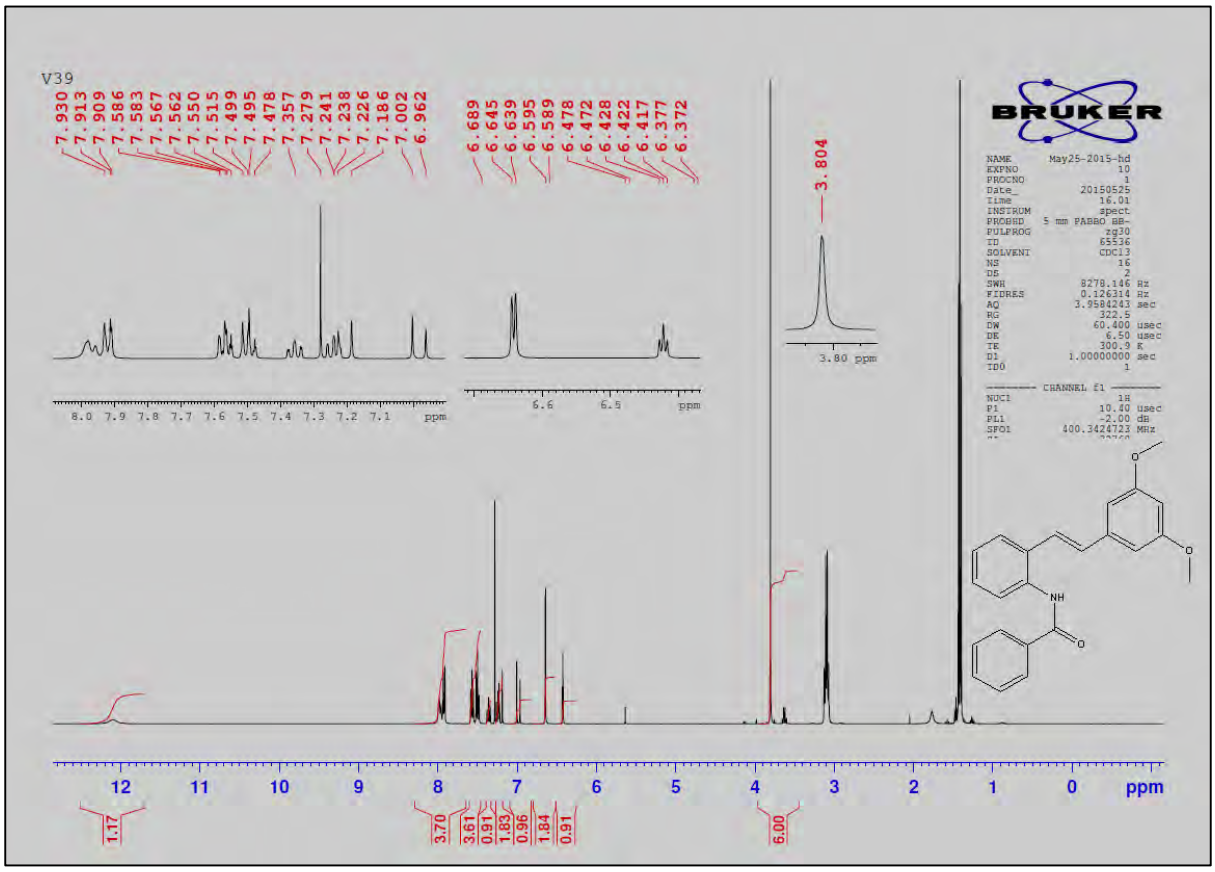

^{13}C NMR spectra of V39

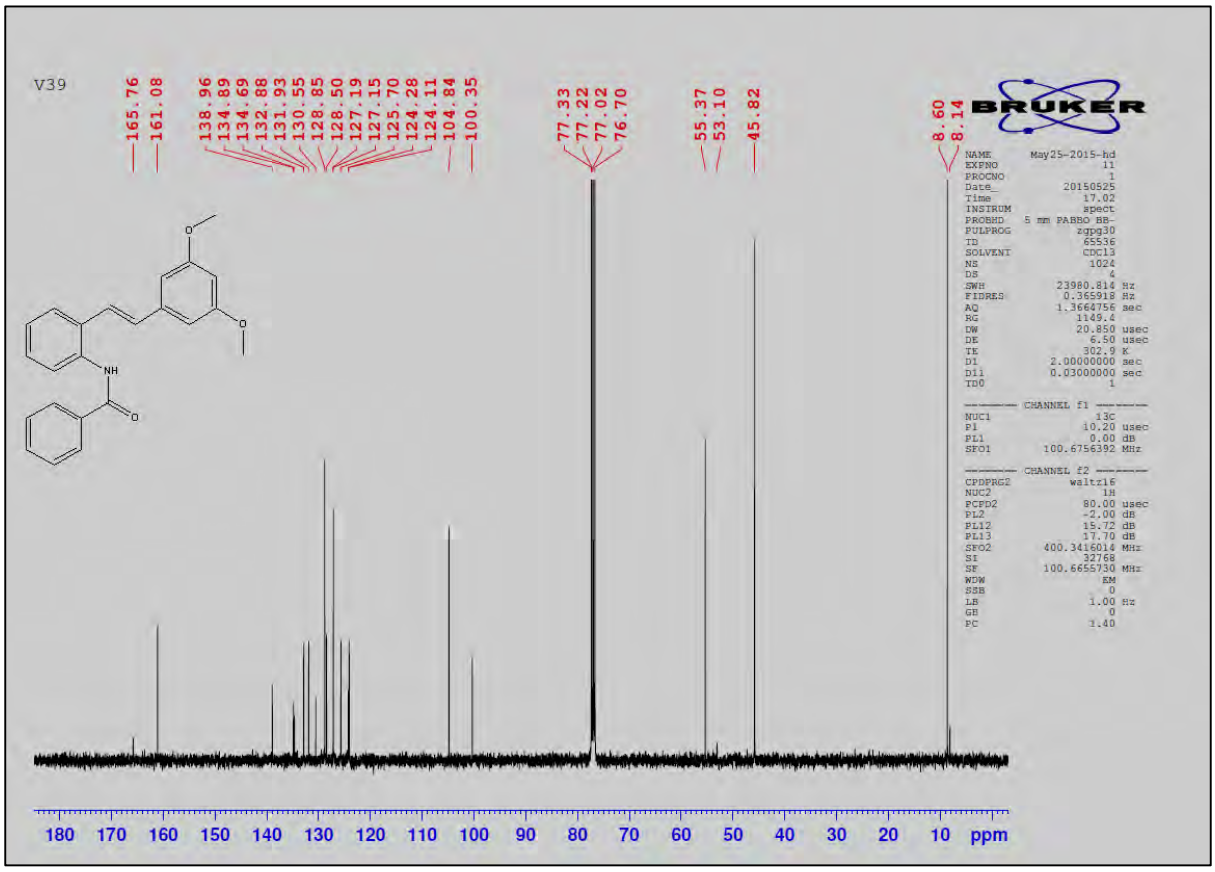

2D HSQC spectra of V39

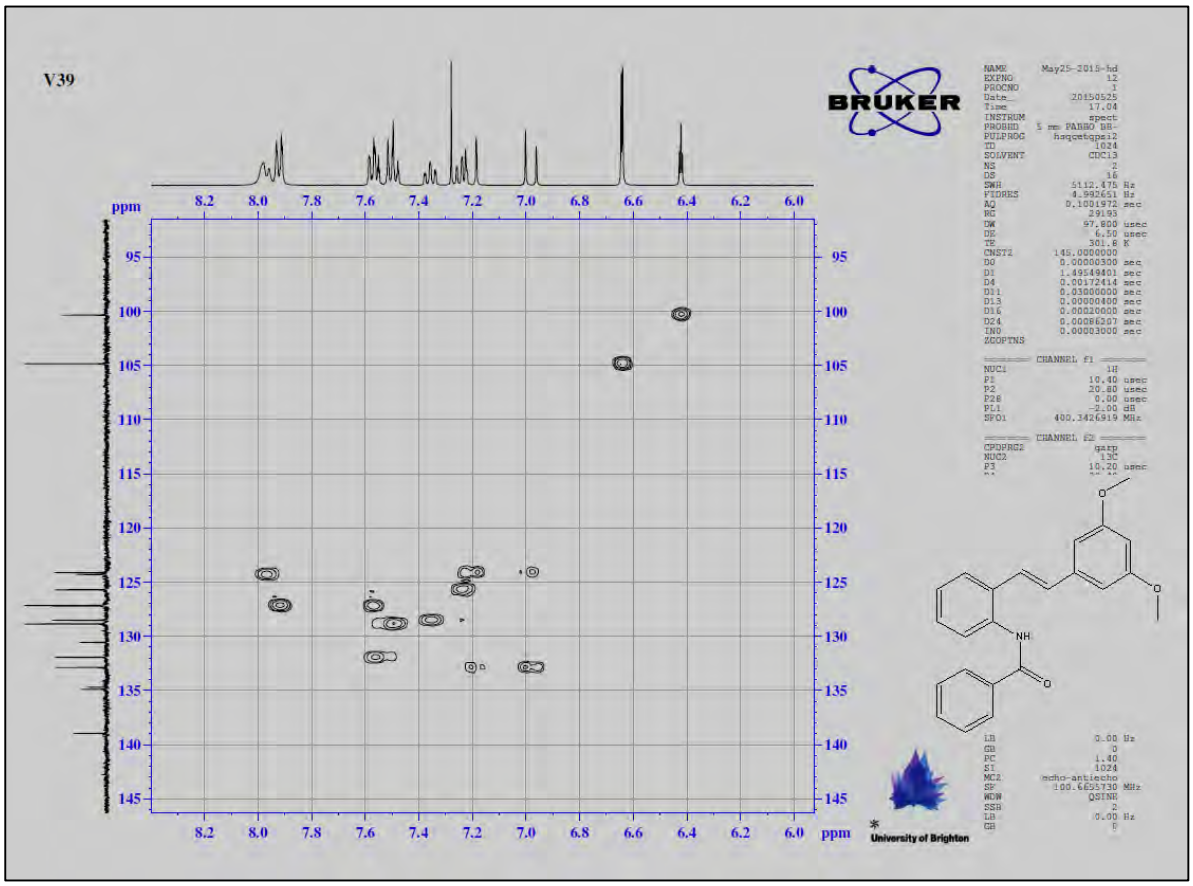

2D COSY spectra of V39

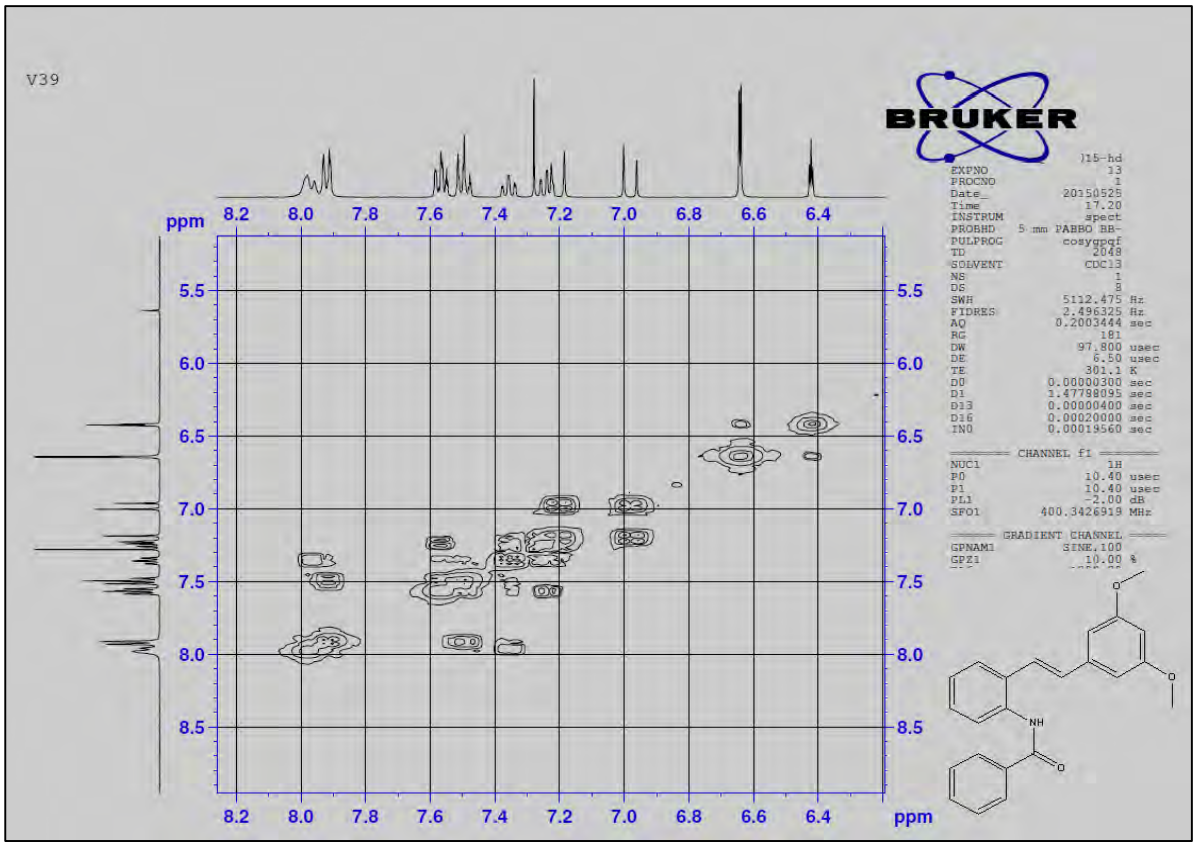

Mass spectra of V39

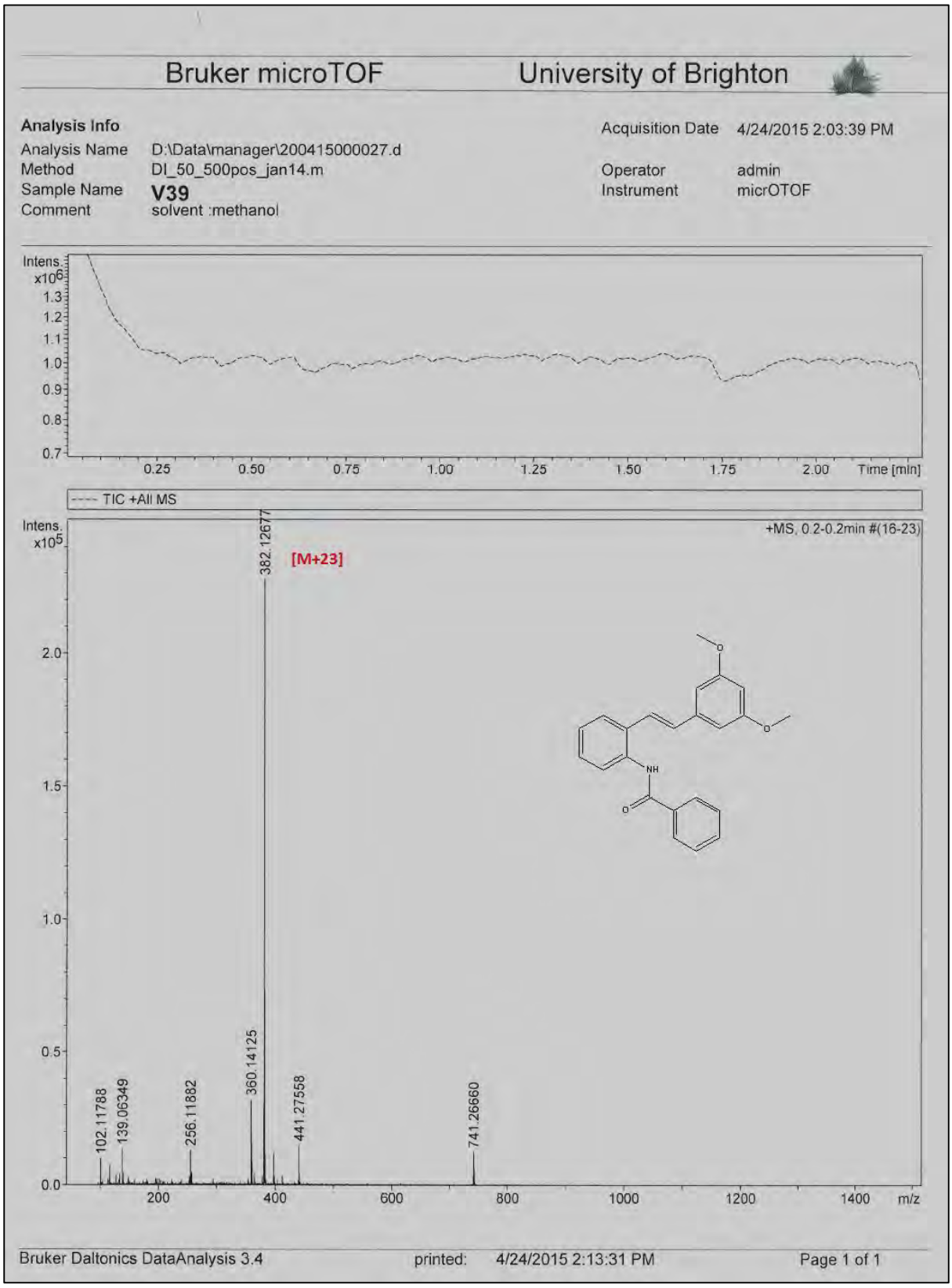

^{1}H NMR spectra of V40

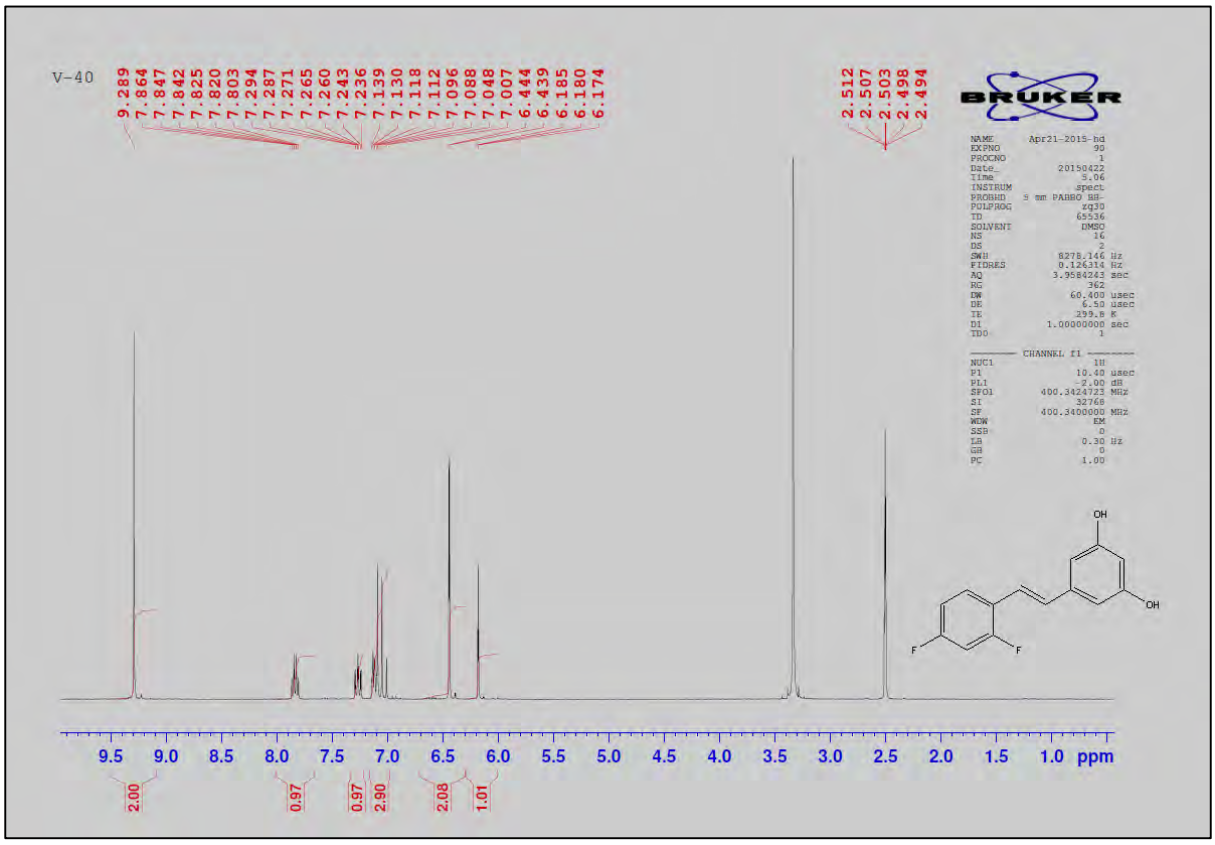

^{13}C NMR spectra of V40

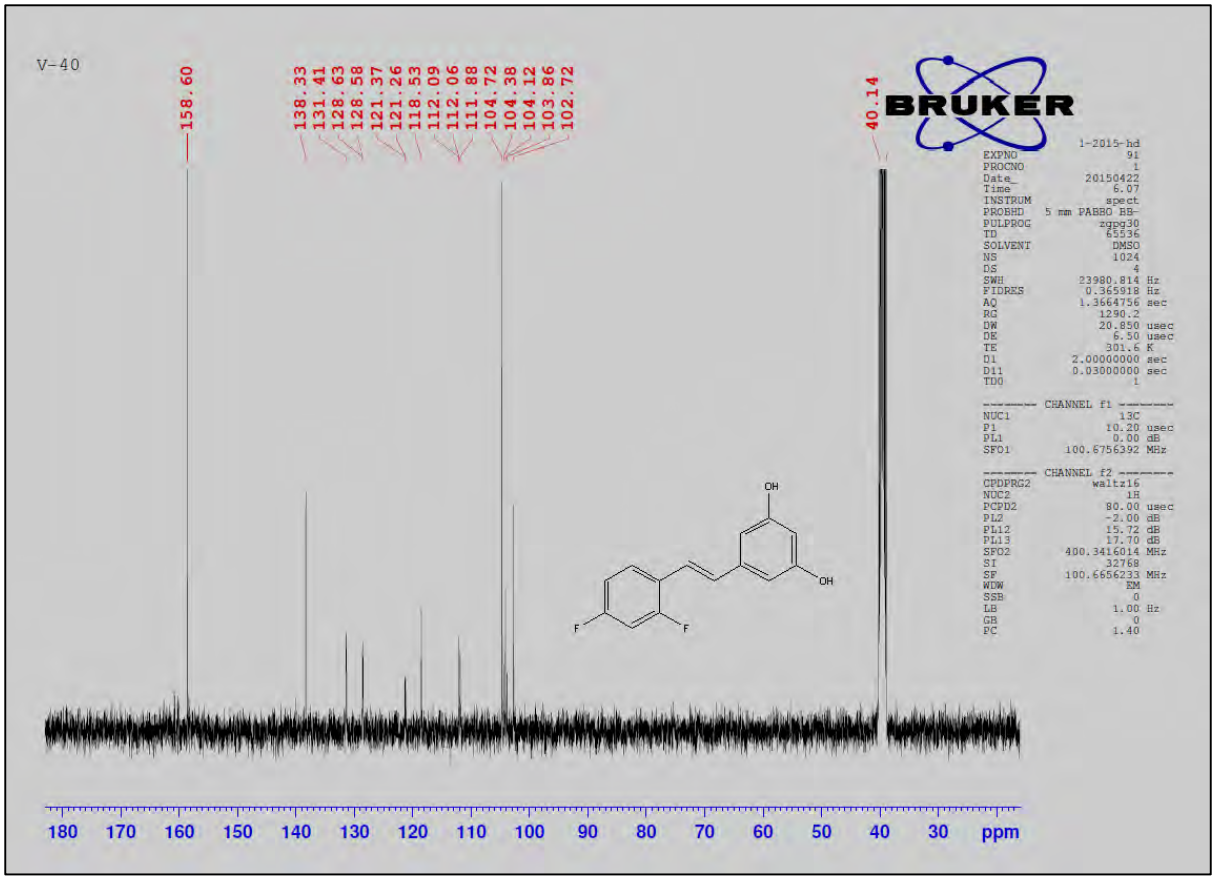

2D HSQC spectra of V40

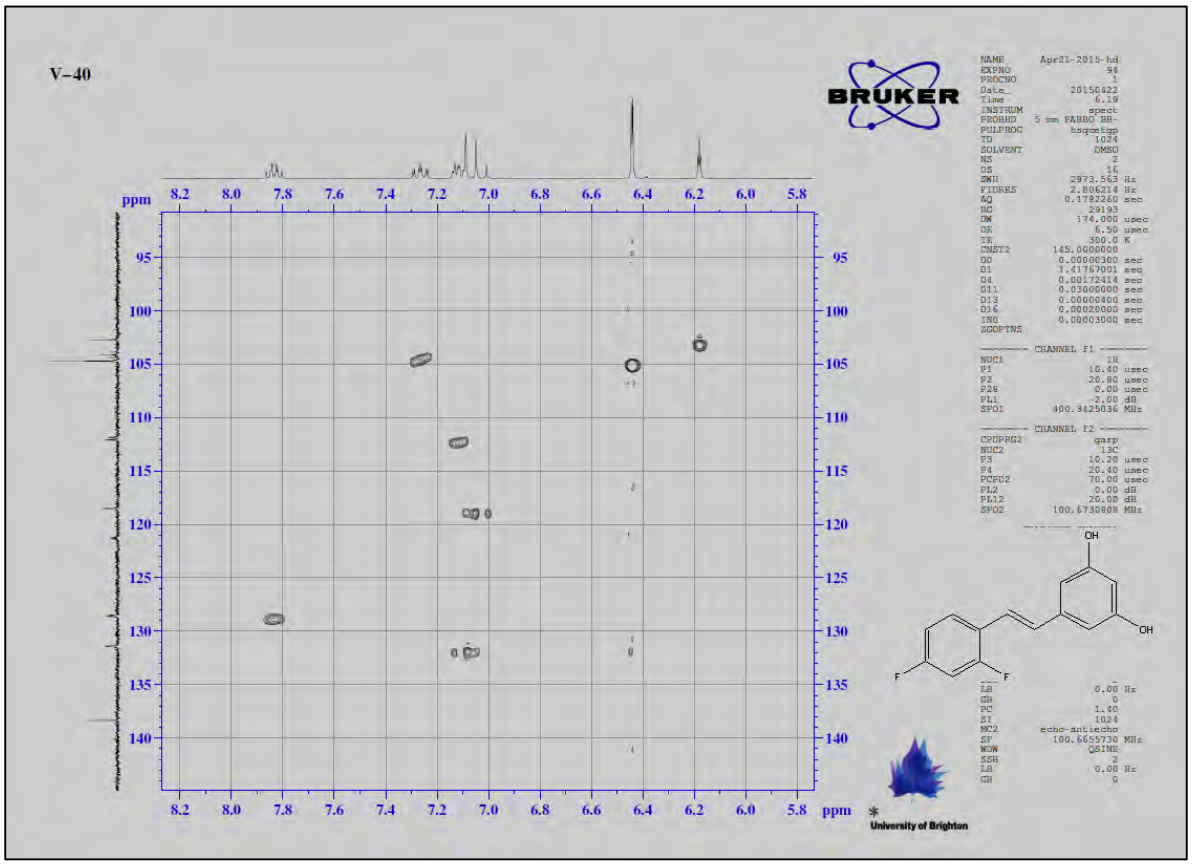

2D COSY spectra of V40

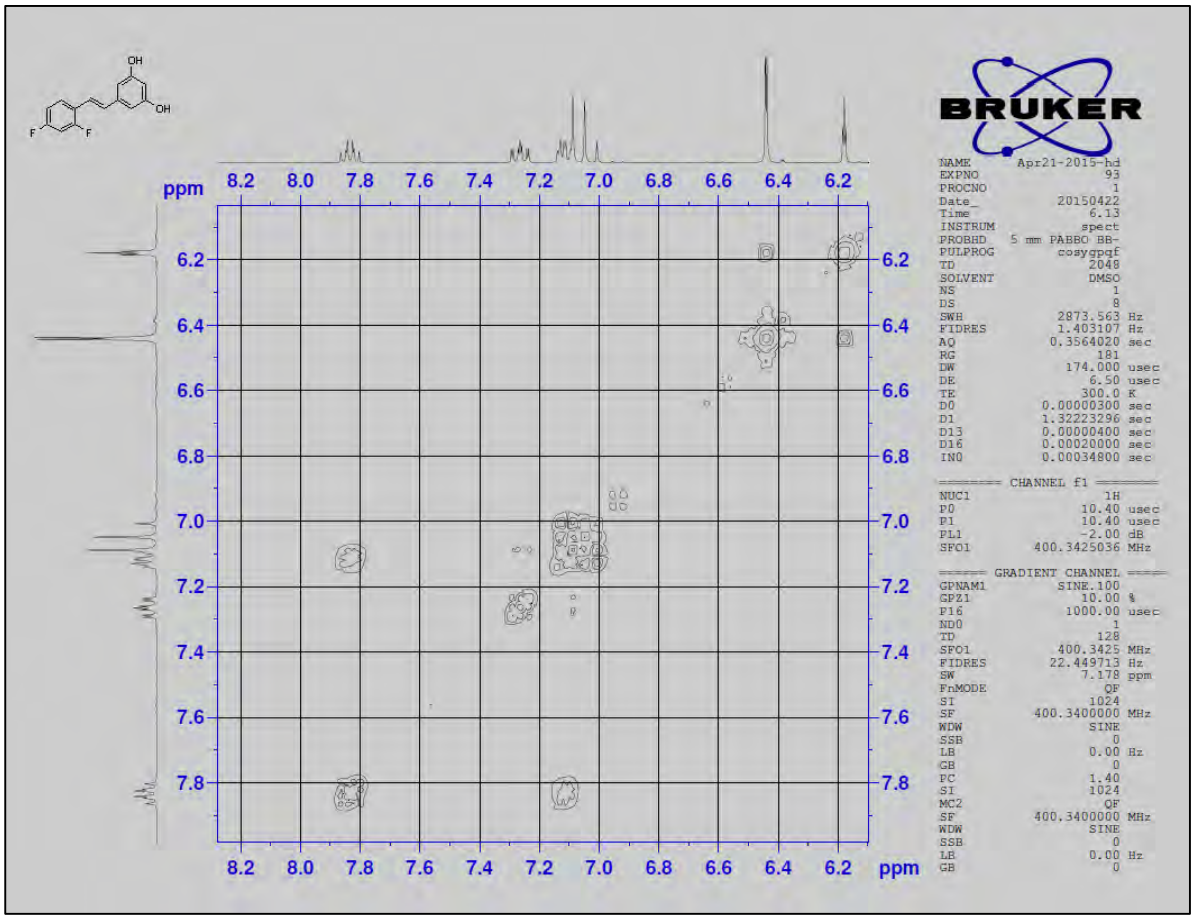

Mass spectra of V40

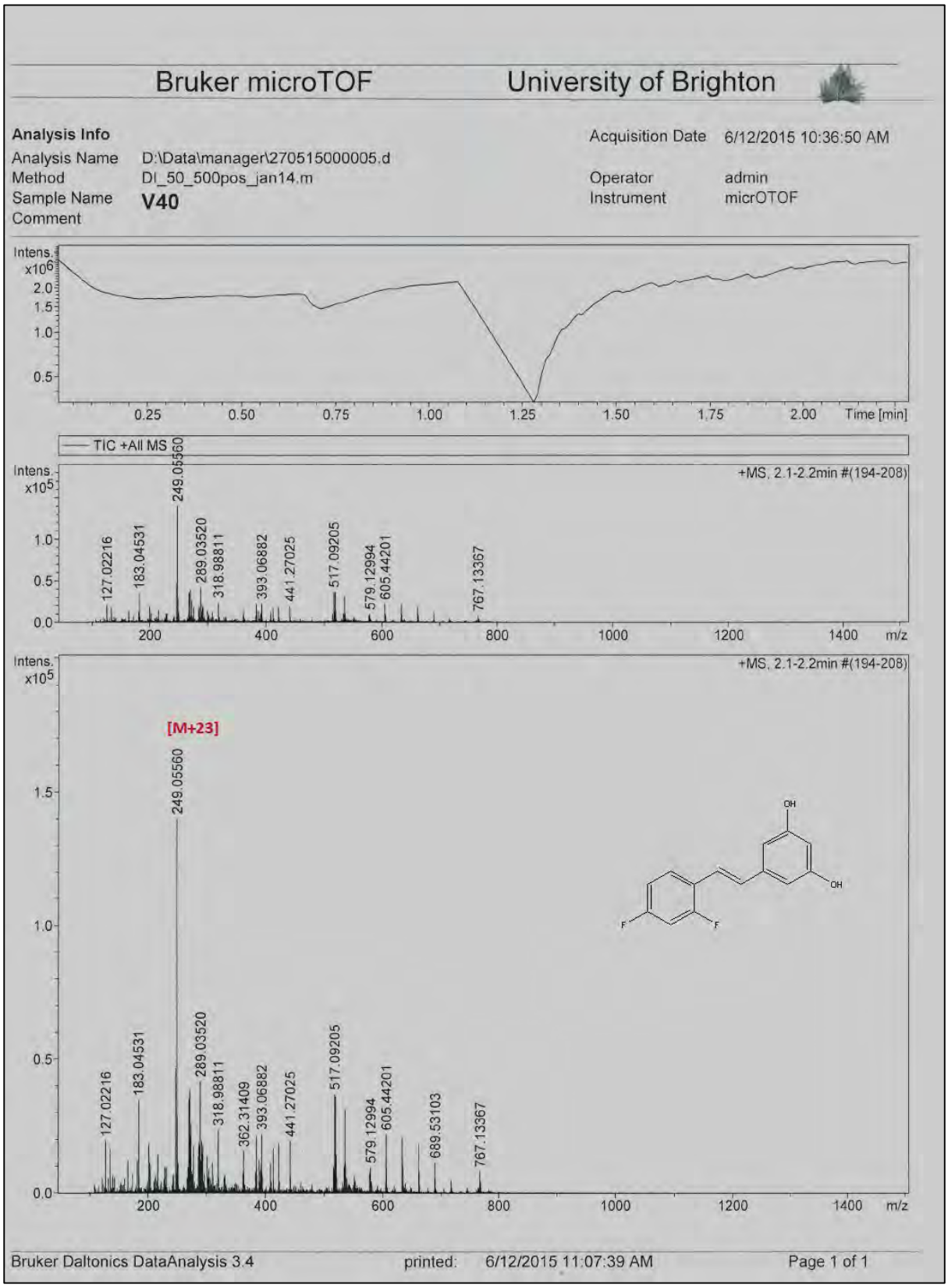

^{1}H NMR spectra of V41

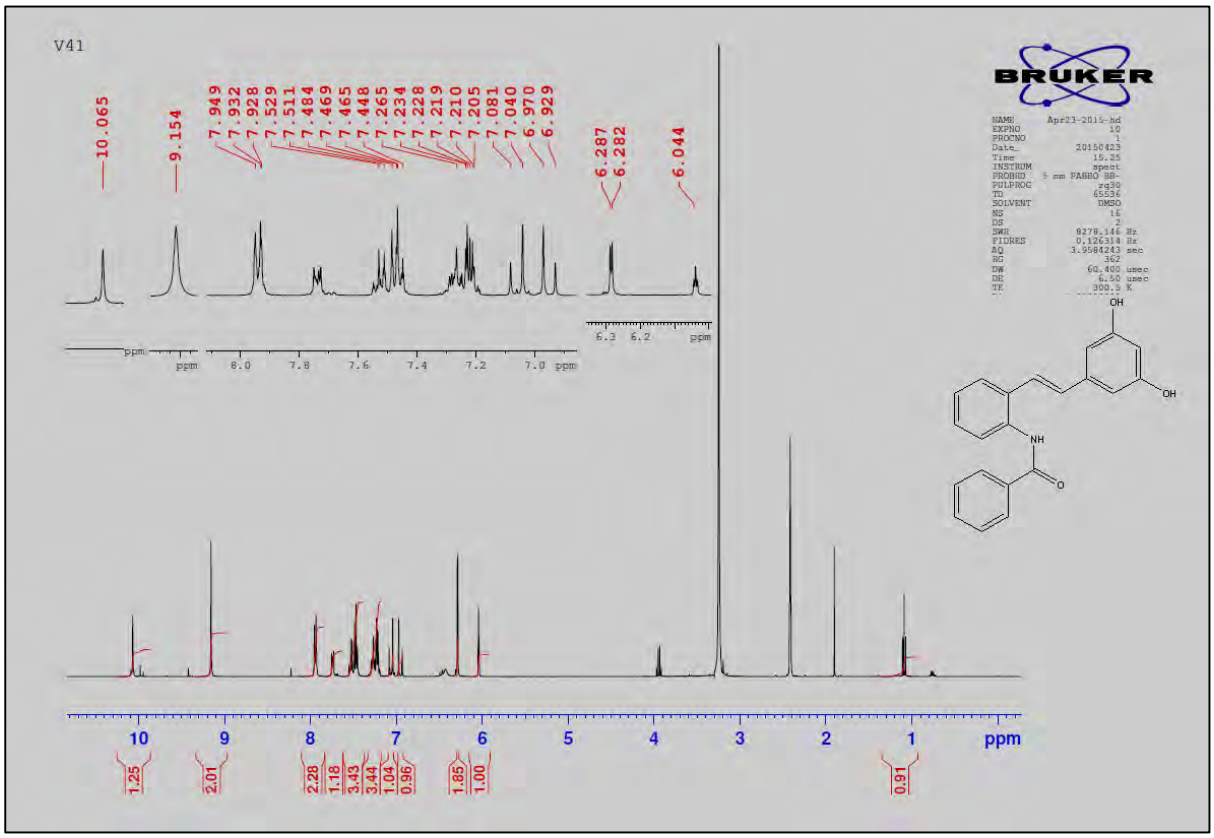

^{13}C NMR spectra of V41

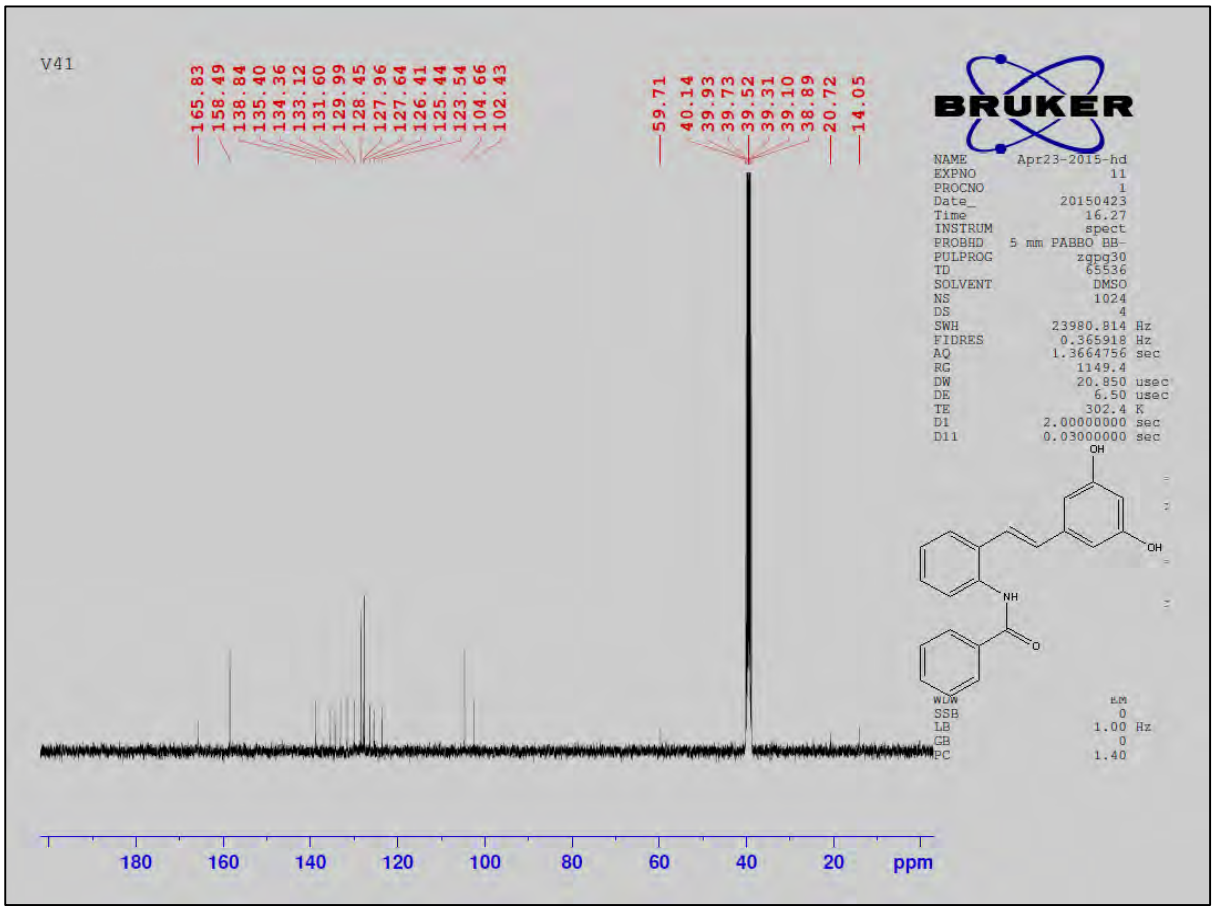

2D HSQC spectra of V41

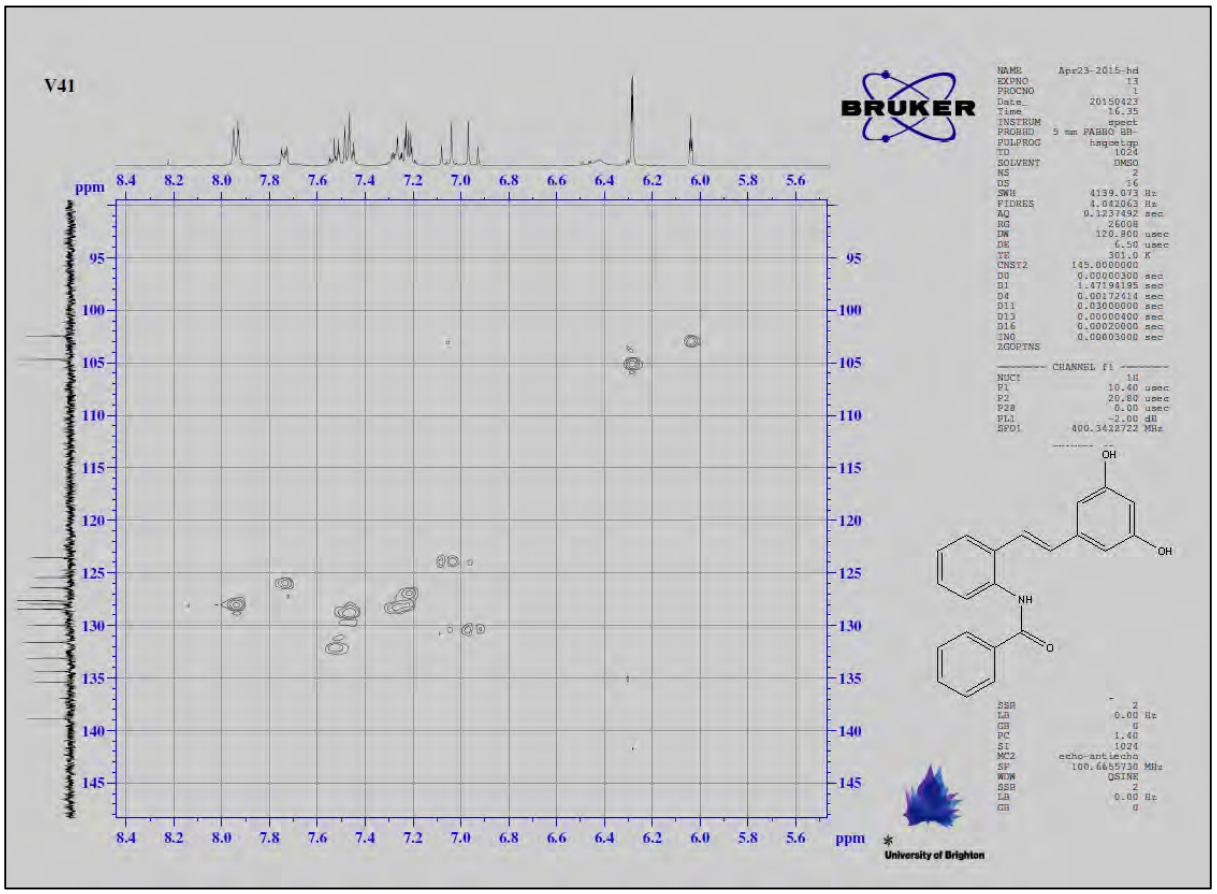

2D COSY spectra of V41

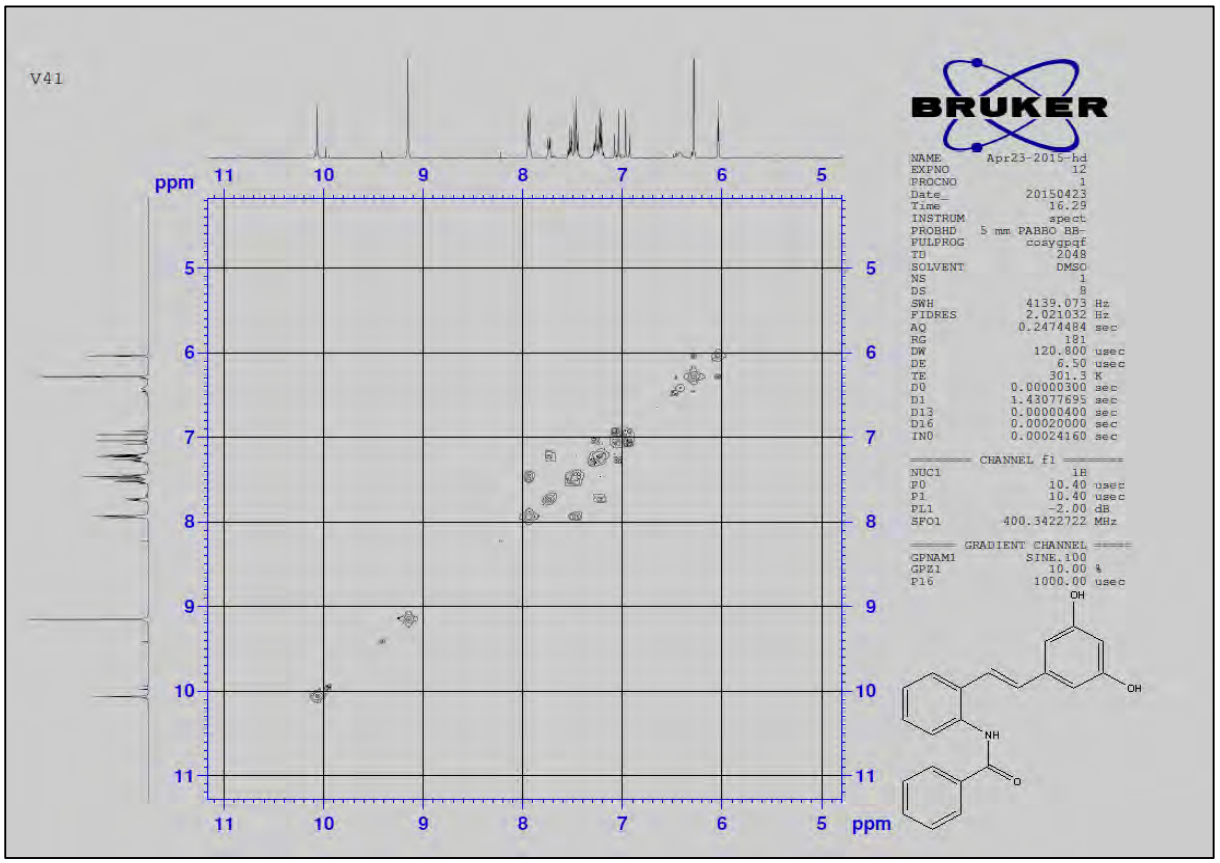

Mass spectra of V41

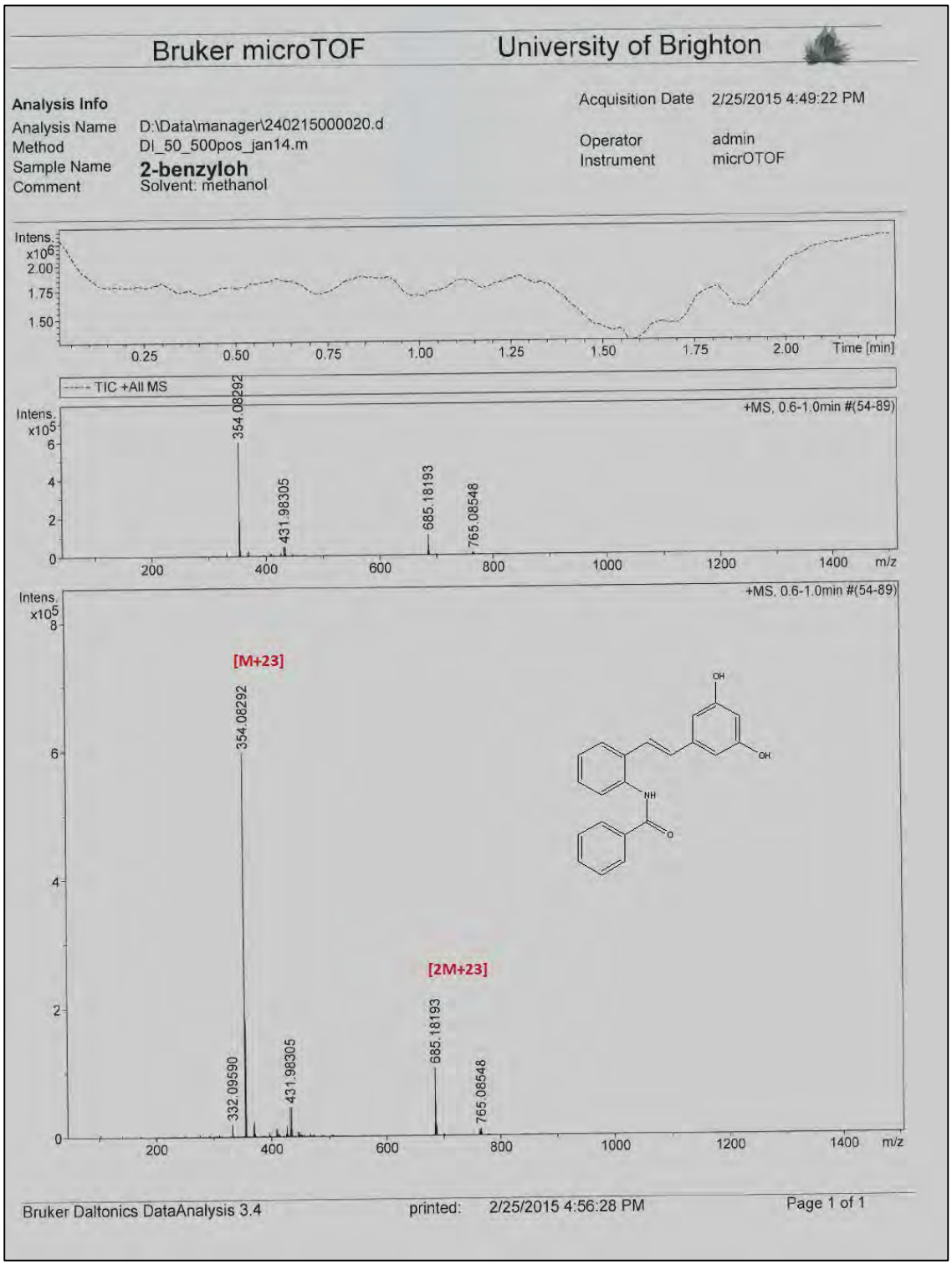

^{1}H NMR spectra of V42

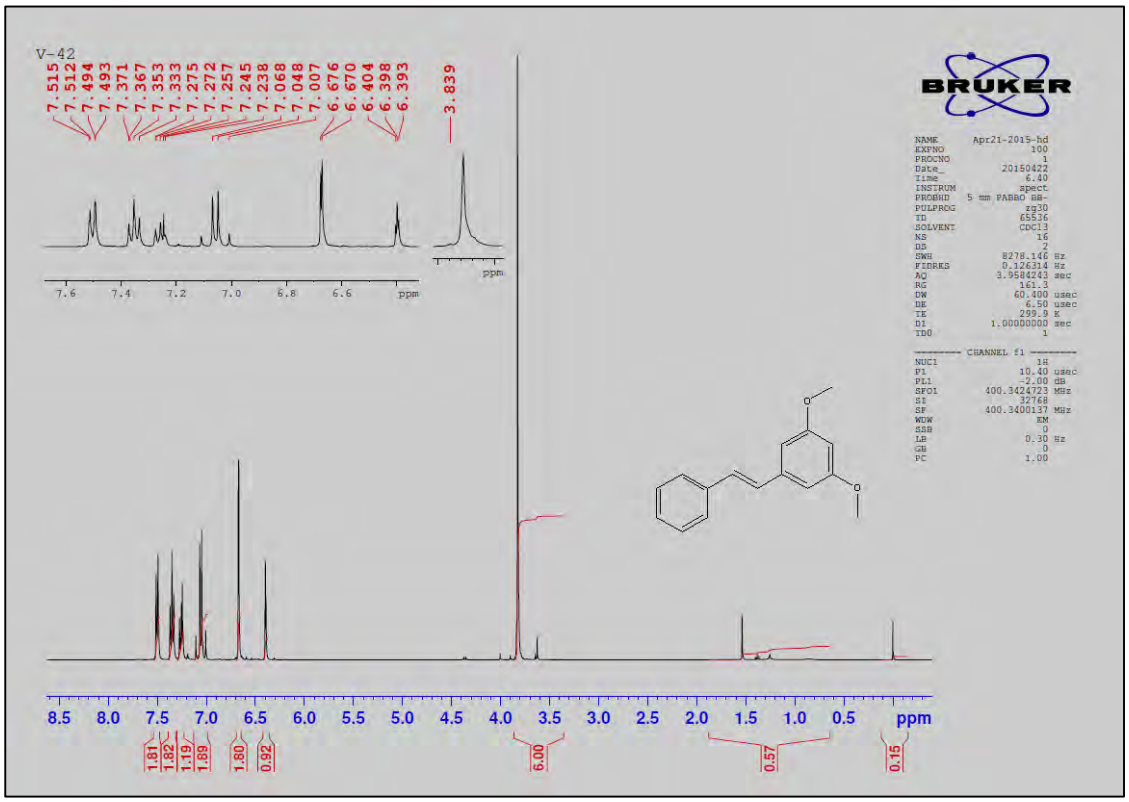

^{13}C NMR spectra of V42

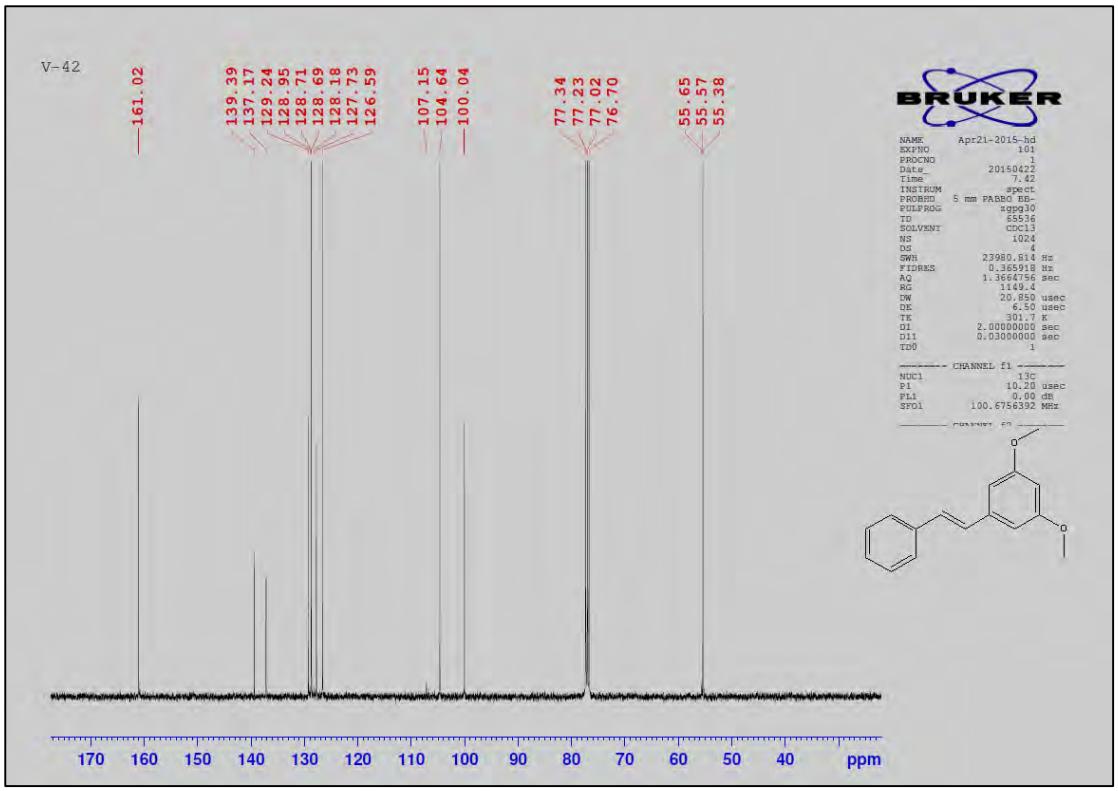

2D HSQC spectra of V42

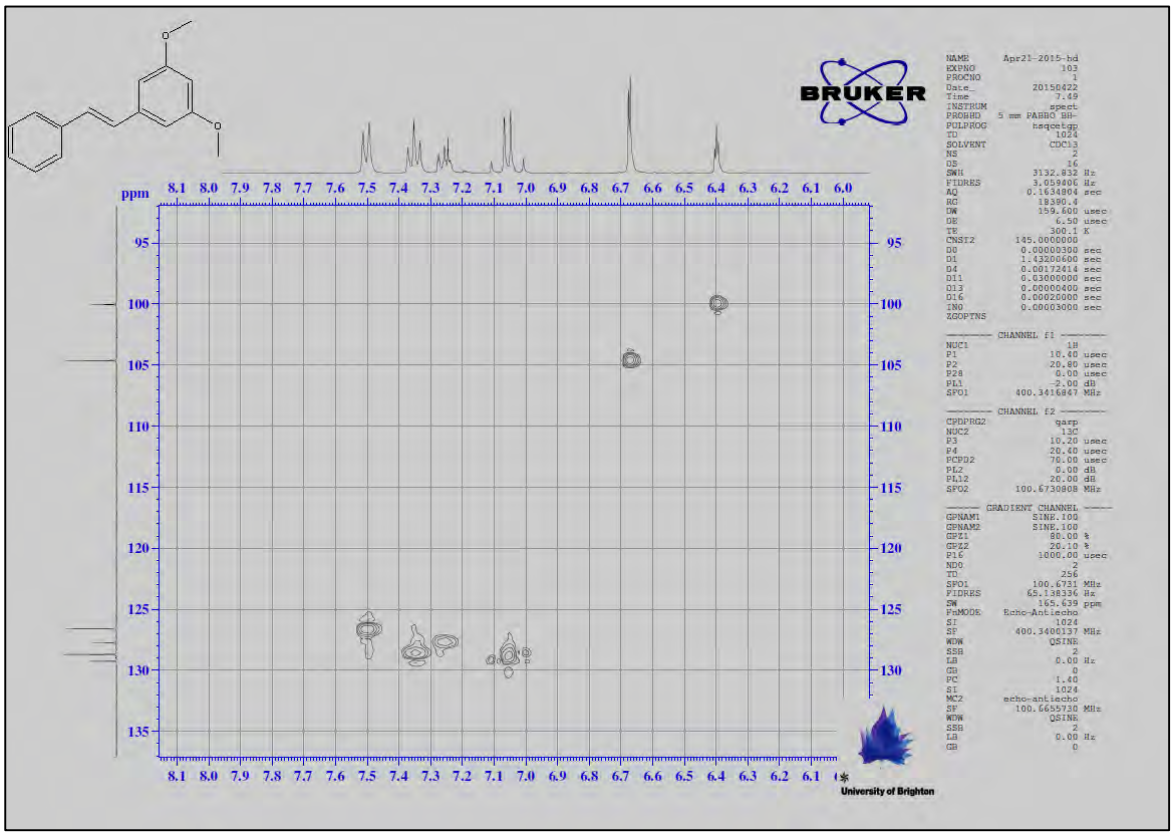

2D COSY spectra of V42

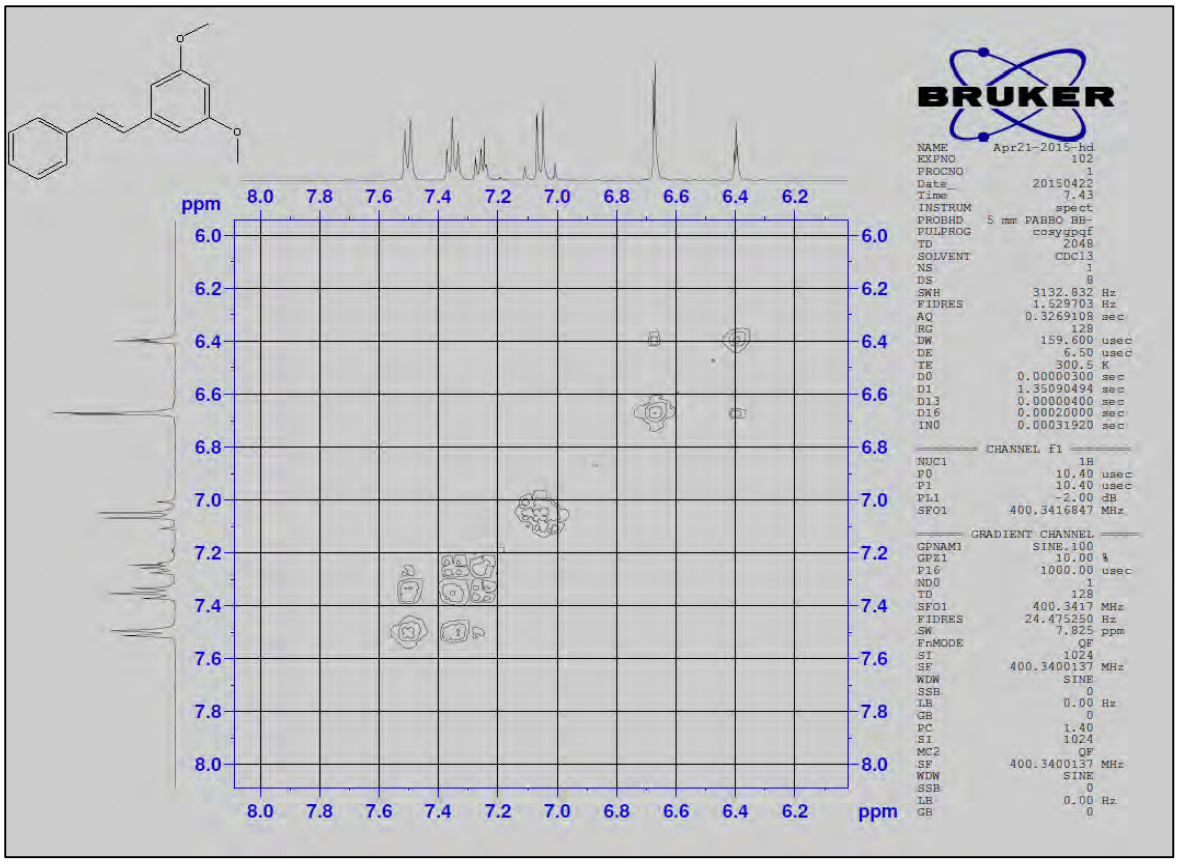

Mass spectra of V42

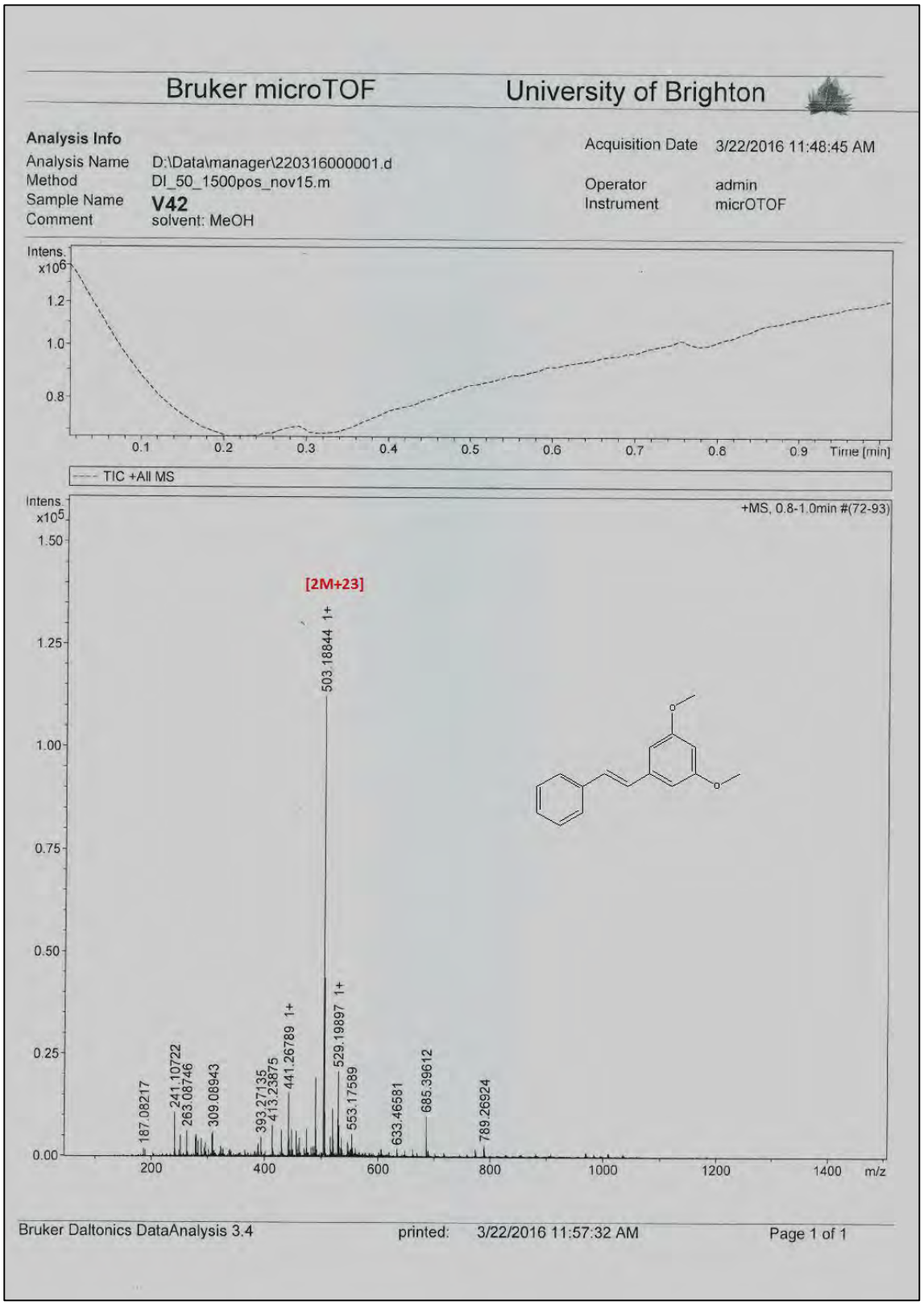

^{1}H NMR spectra of V43

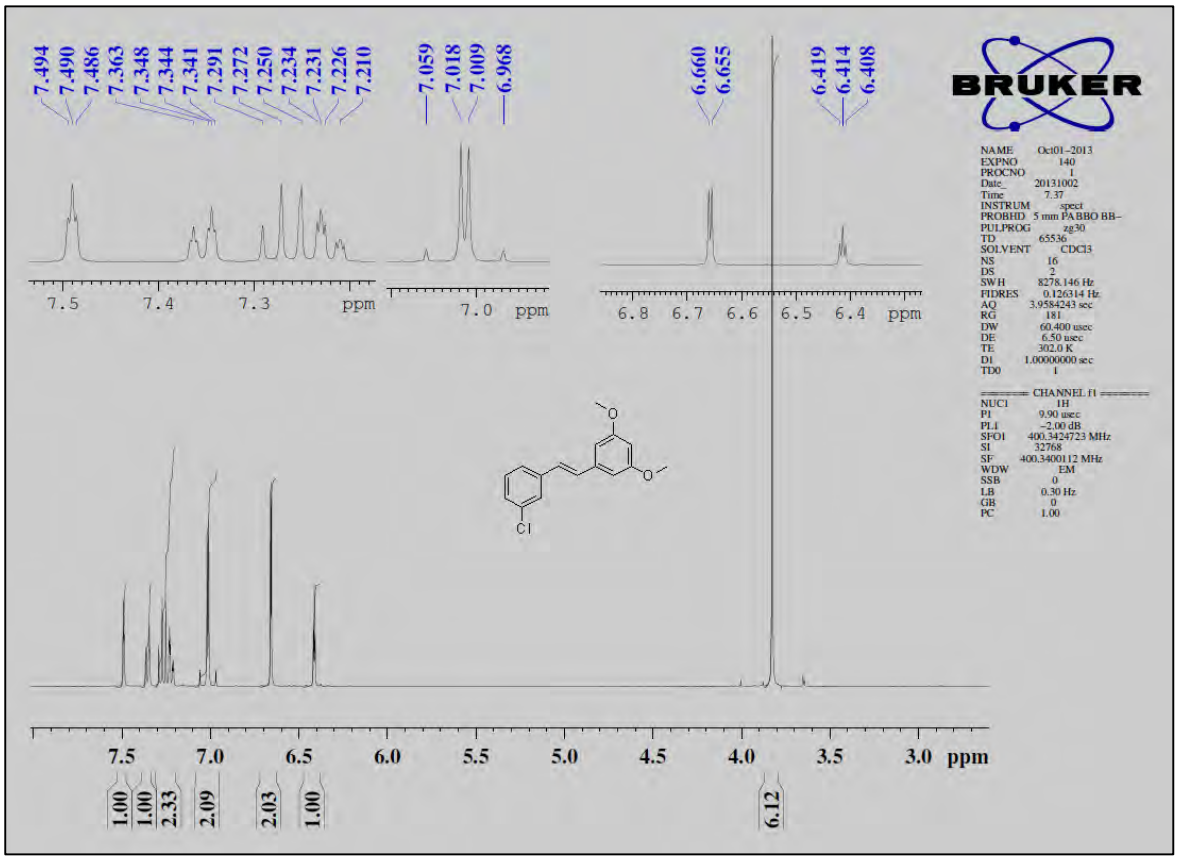

^{13}C NMR spectra of V43

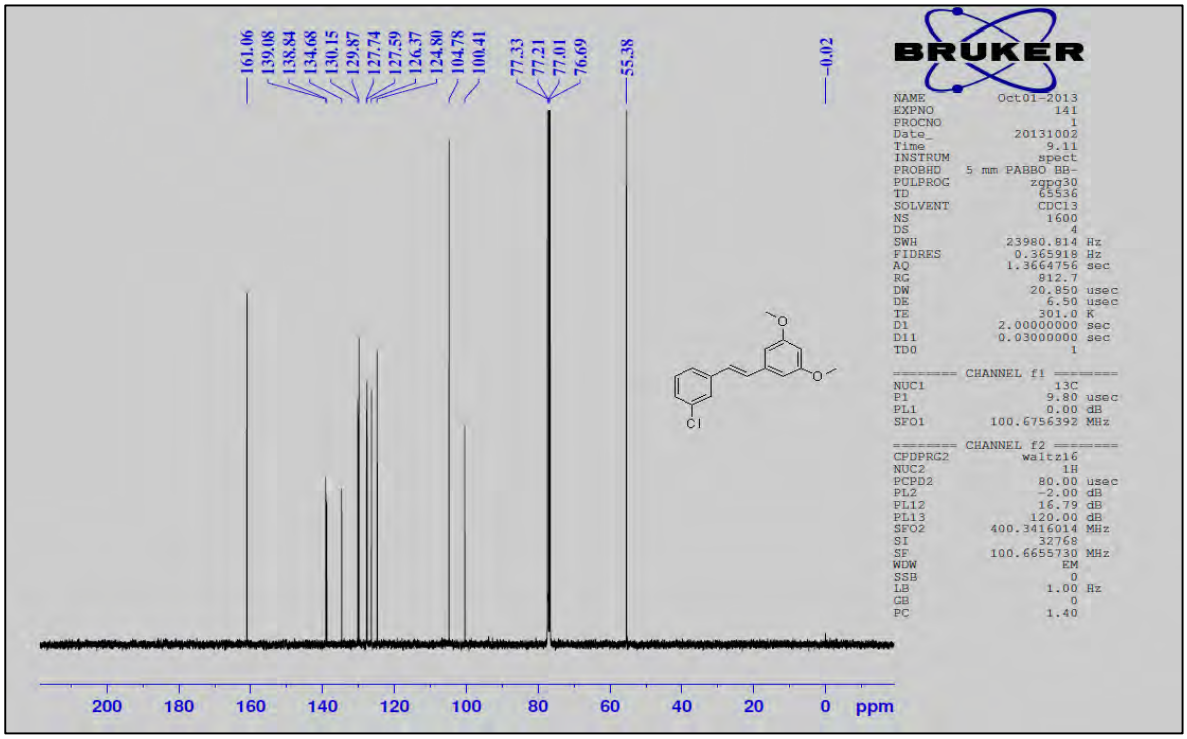

Mass spectra of V43

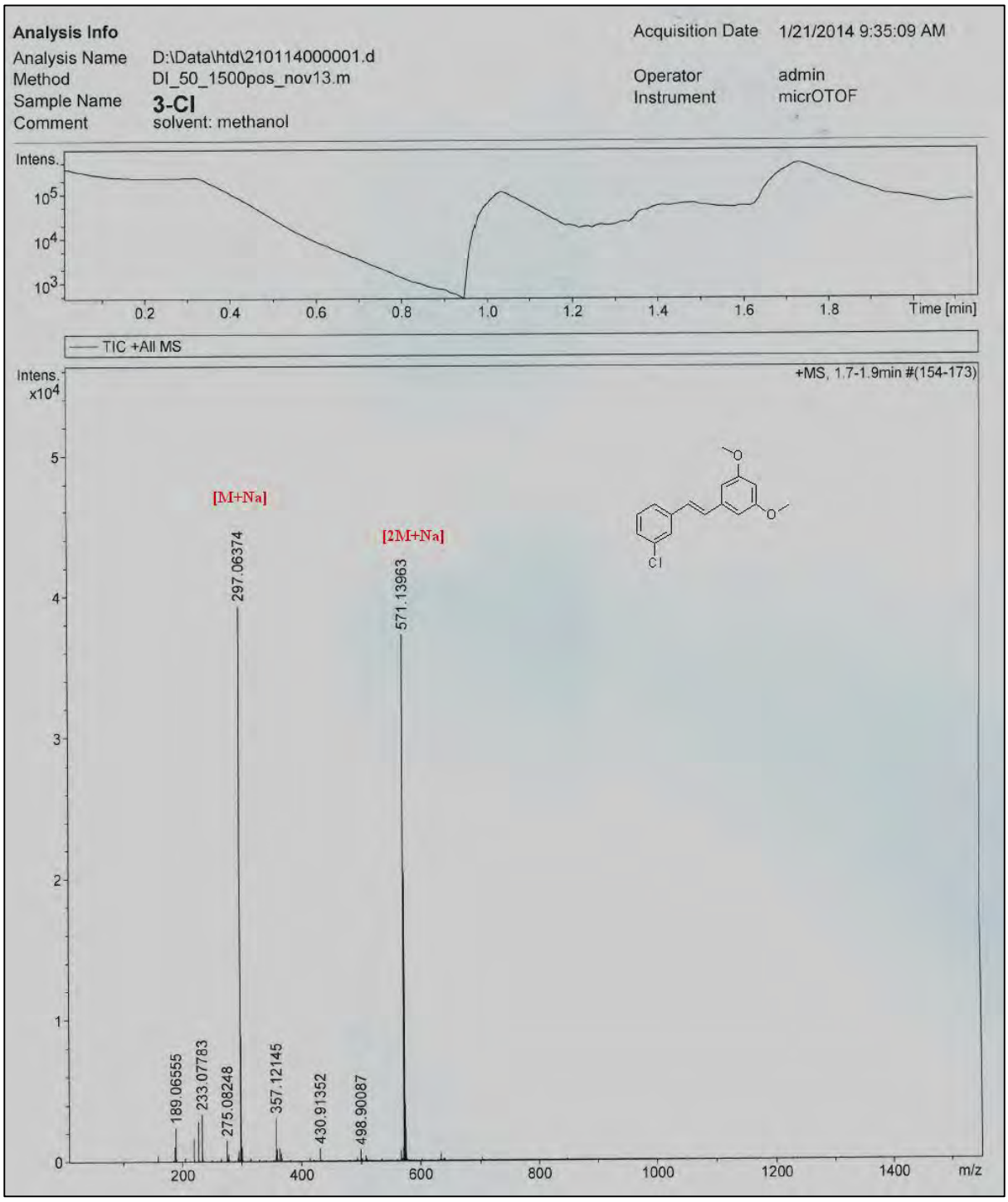

^{1}H NMR spectra of DHRSV

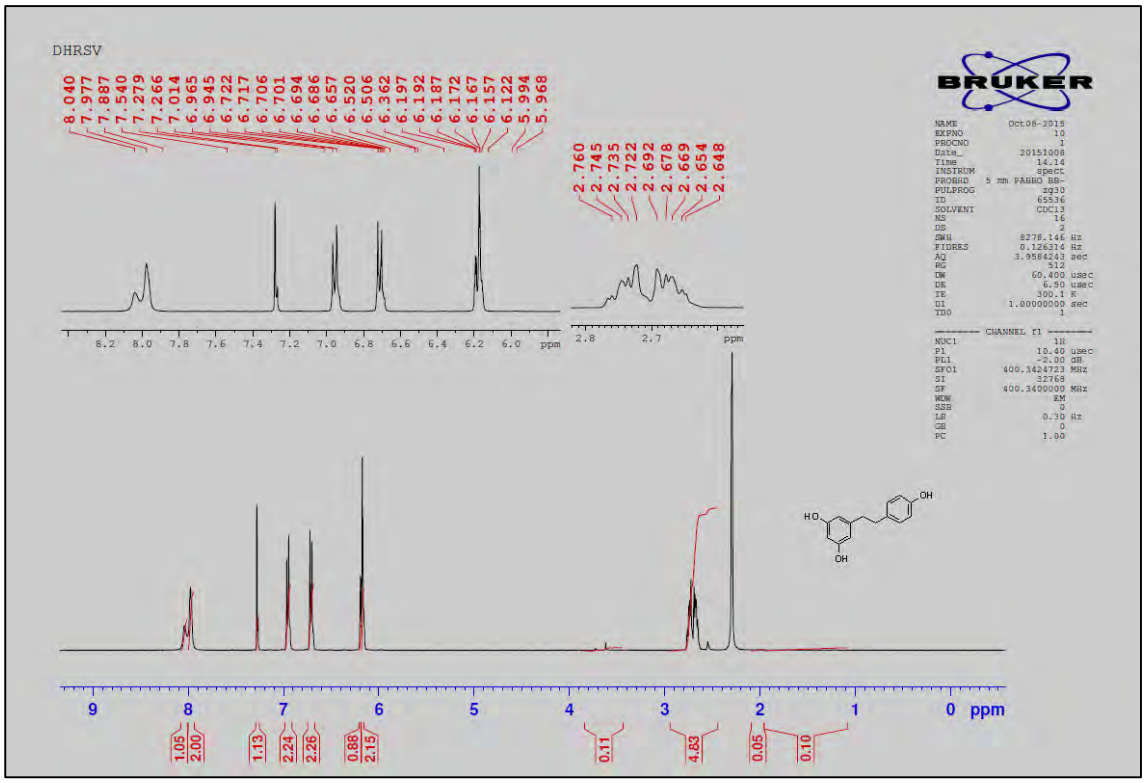

^{13}C NMR spectra of DHRSV

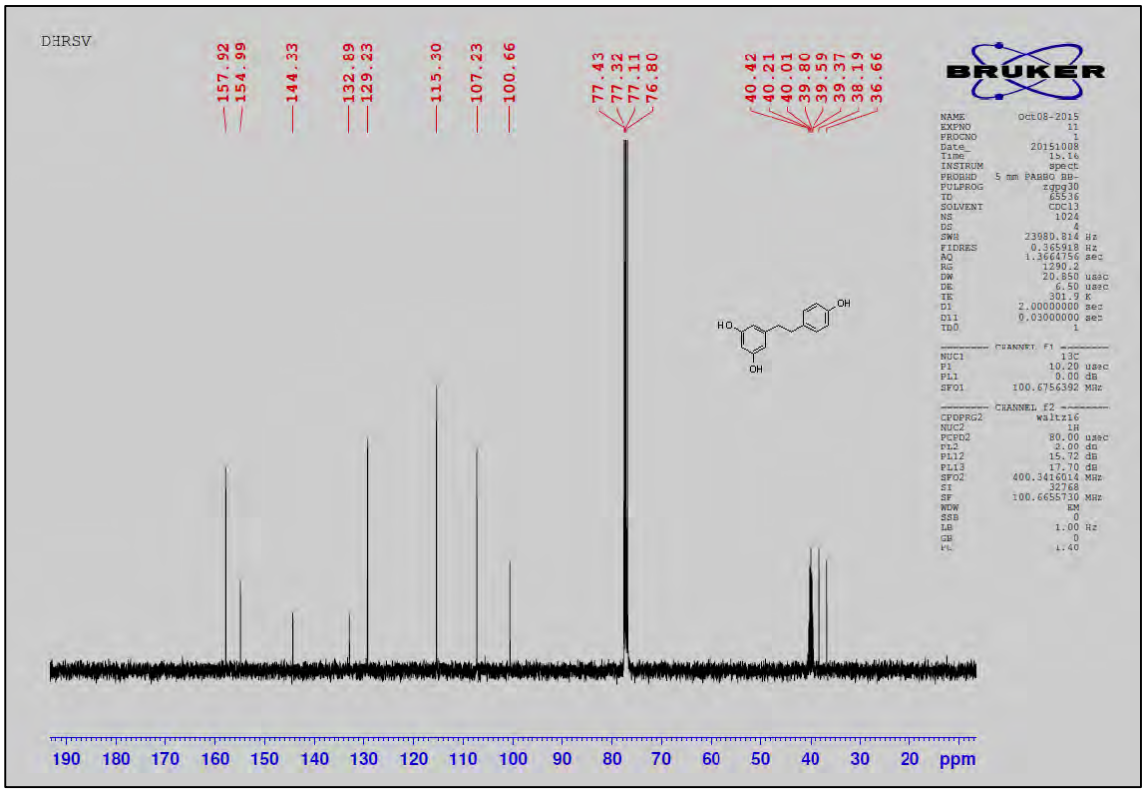

2D HSQC spectra of DHRSV

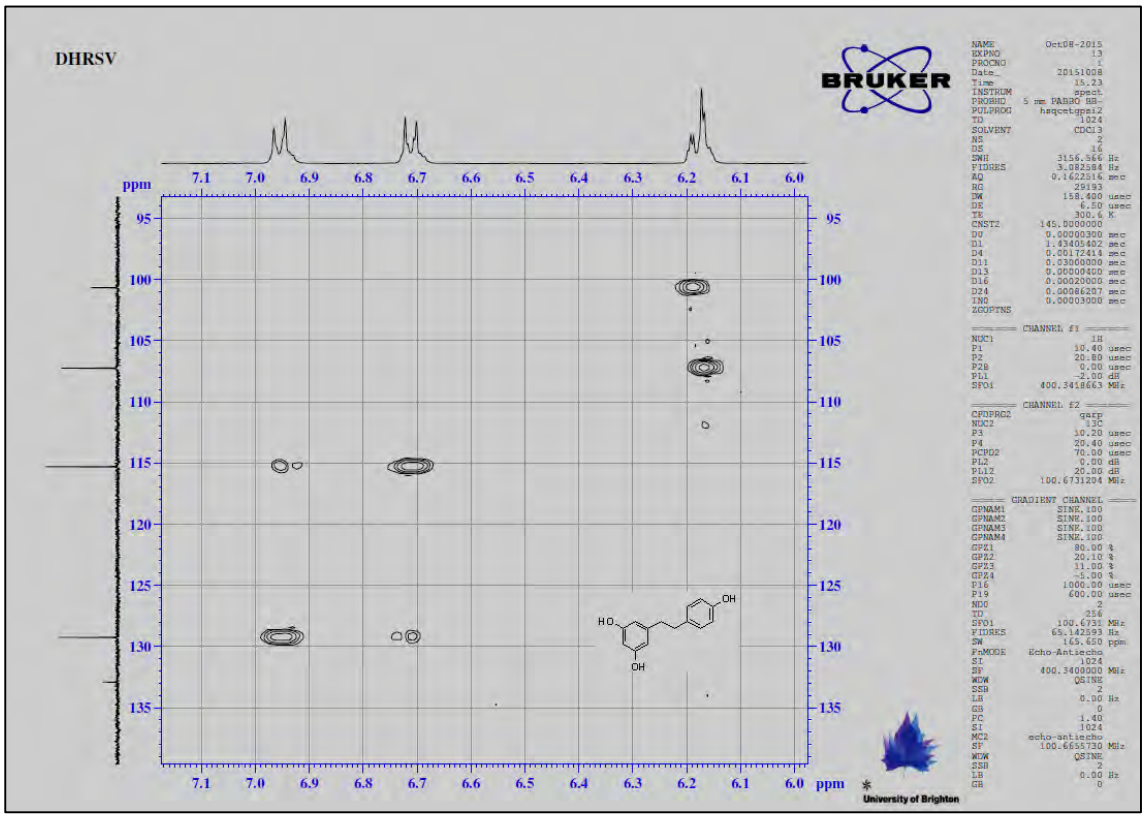

2D HSQC spectra of DHRSV

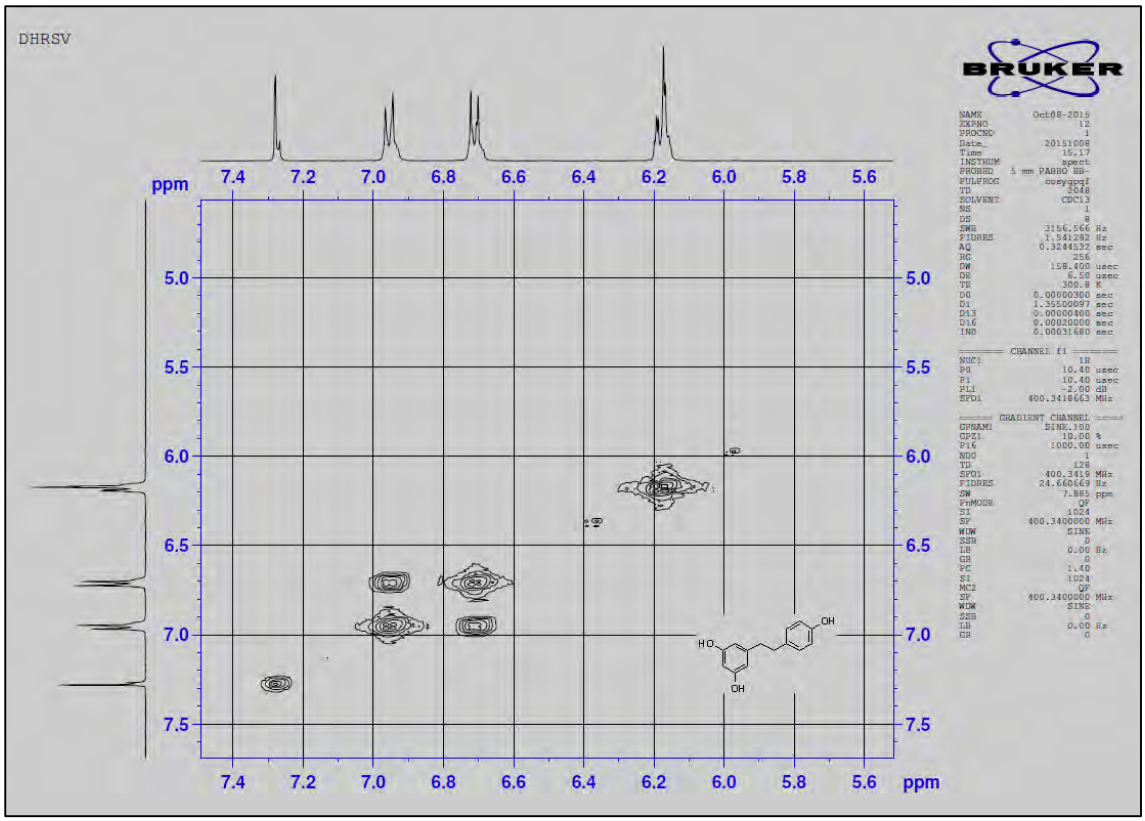

Mass spectra of DHRSV

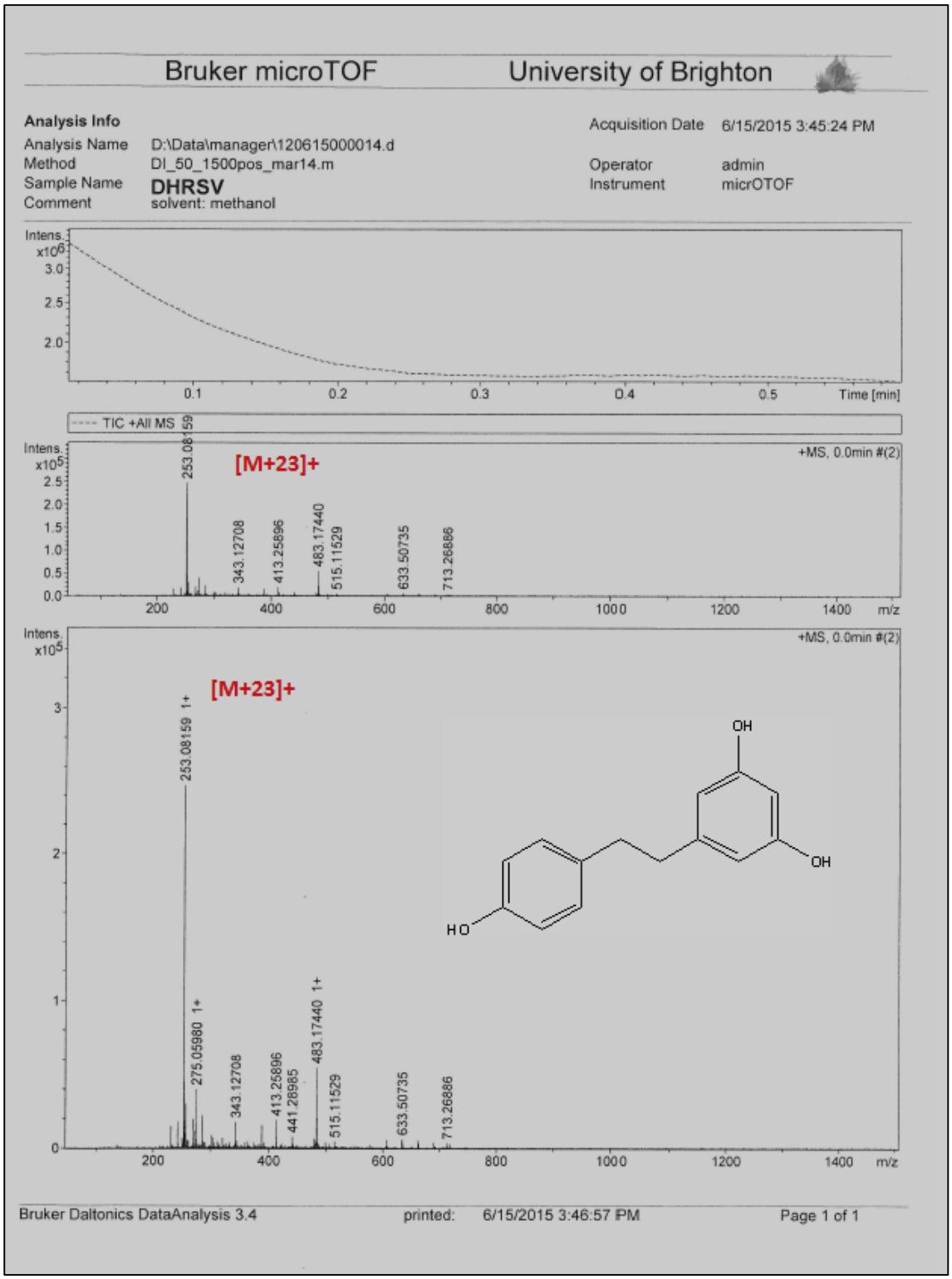

Appendix C

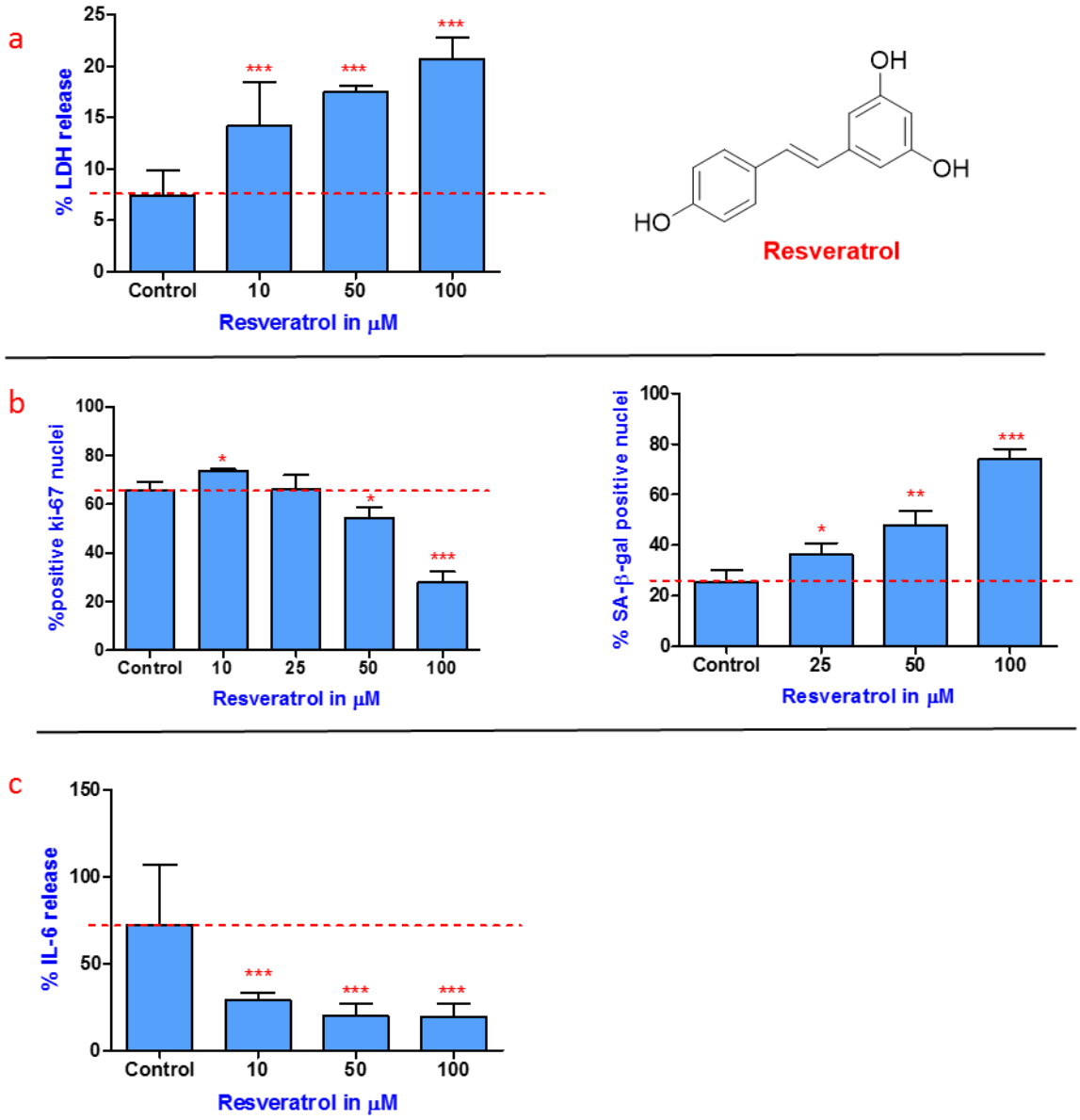

Figure C-1: Effect of resveratrol on a) LDH release b) proliferation fraction ki-67 and SA-β-galactosidase nuclei and c) effect on IL-6 release, where control represents vehicle only (DMSO treated MRC-5 cells) at (CPD36-39). All the experiments were carried out for n = 3 different biological experiments and error bar represents ±standard deviation. Statistical significance was analysed by using one way ANOVA followed by Dunnett's multiple comparison test: (*) $p<0.05$, (**) $p<0.01$, (***) $p<0.001$, versus control which represents vehicle only. Red line represents the changes observed when treated with various concentration of resveratrol.

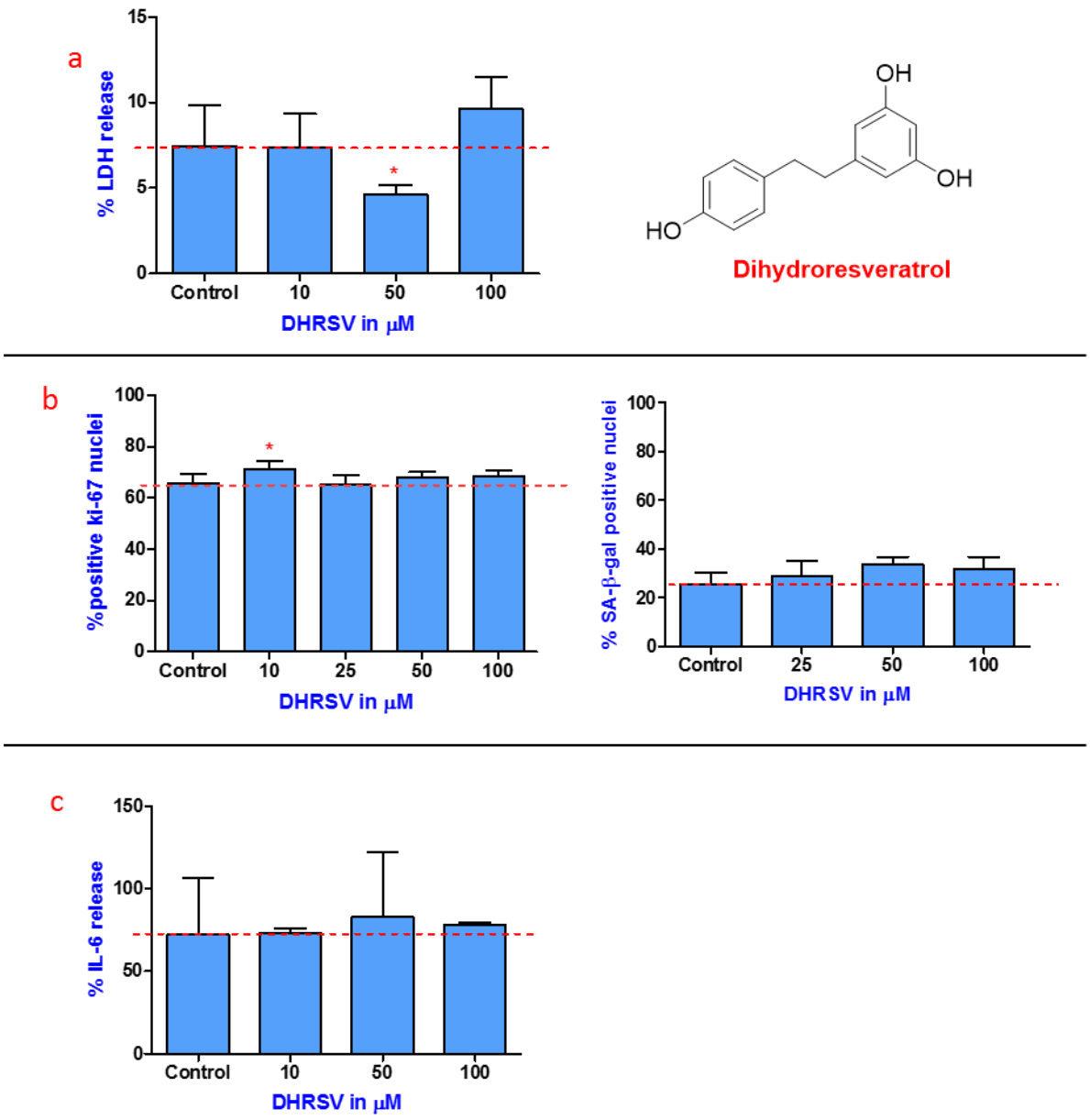

Figure C-2: Effect of dihydroresveratrol on a) LDH release b) proliferation fraction ki-67 and SA-β-galactosidase nuclei and c) effect on IL-6 release, where control represents vehicle only (DMSO treated MRC-5 cells) at (CPD36-39). All the experiments were carried out for n = 3 different biological experiments and error bar represents ±standard deviation. Statistical significance was analysed by using one way ANOVA followed by Dunnett's multiple comparison test: (*) $p<0.05$, (**) $p<0.01$, (***) $p<0.001$, versus control which represents vehicle only. Red line represents the changes observed when treated with various concentration of dihydroresveratrol.

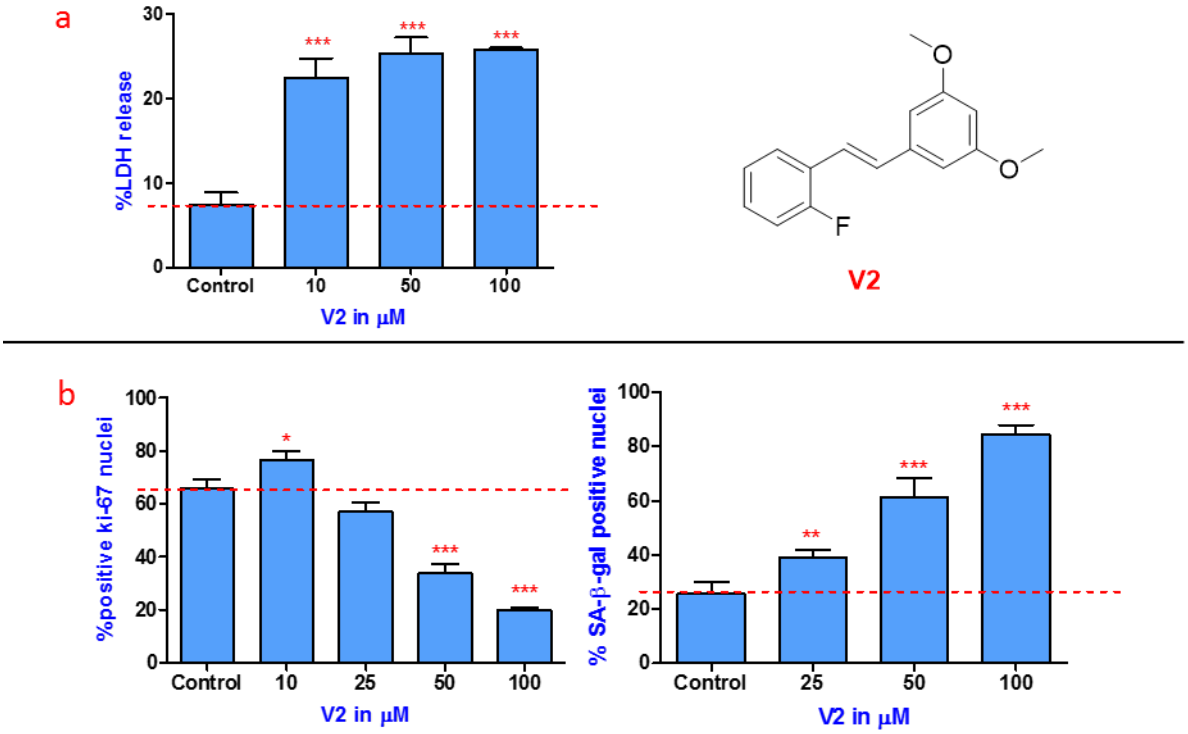

Figure C-3: Effect of V2 on a) LDH release b) proliferation fraction ki-67 and SA-β-galactosidase nuclei, where control represents vehicle only (DMSO treated MRC-5 cells) at (CPD36-39). All the experiments were carried out for n = 3 different biological experiments and error bar represents ±standard deviation. Statistical significance was analysed by using one way ANOVA followed by Dunnett's multiple comparison test: (*) p<0.05, (**) p<0.01, (***) p<0.001, versus control which represents vehicle only. Red line represents the changes observed when treated with various concentration of V2.

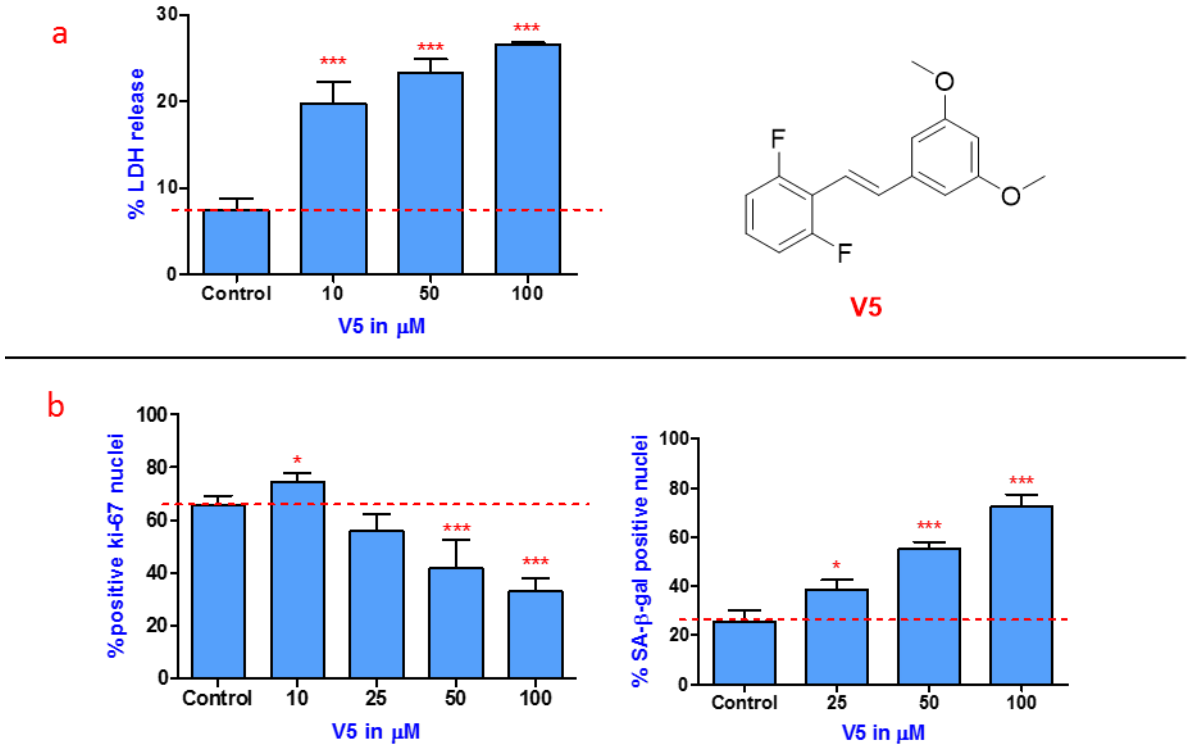

Figure C-4: Effect of V5 on a) LDH release b) proliferation fraction ki-67 and SA-β-galactosidase nuclei, where control represents vehicle only (DMSO treated MRC-5 cells) at (CPD36-39). All the experiments were carried out for n = 3 different biological experiments and error bar represents ±standard deviation. Statistical significance was analysed by using one way ANOVA followed by Dunnett's multiple comparison test: (*) $p<0.05$, (**) $p<0.01$, (***) $p<0.001$, versus control which represents vehicle only. Red line represents the changes observed when treated with various concentration of V5.

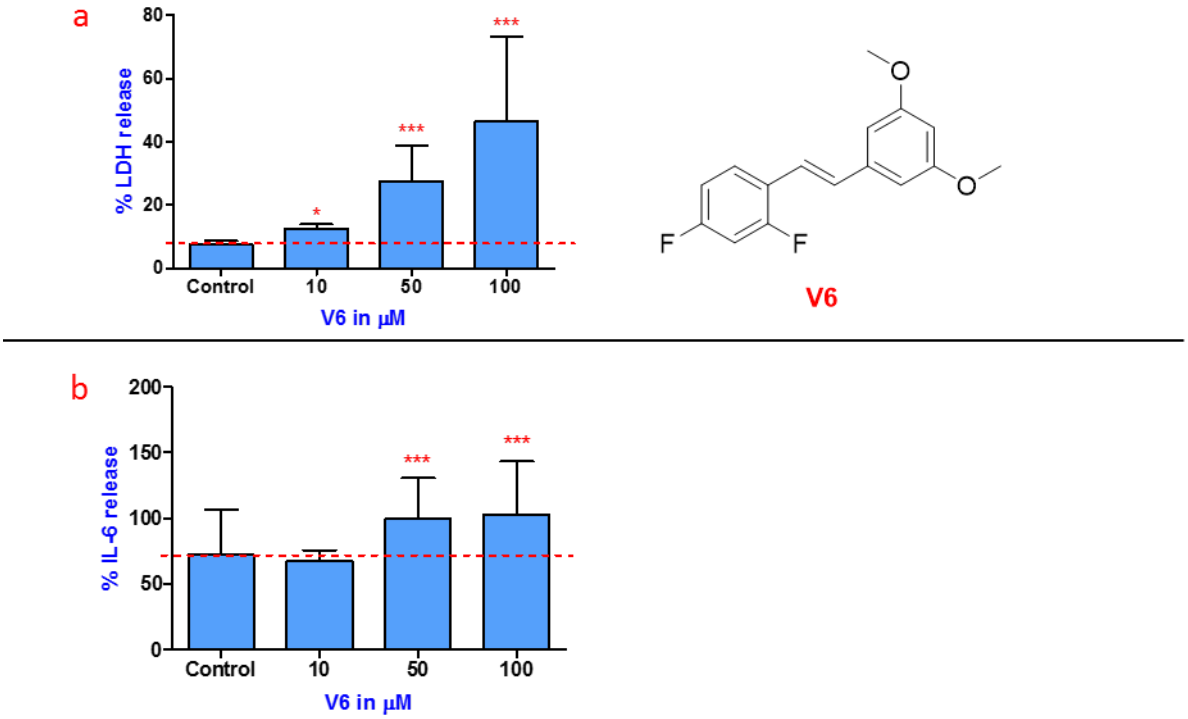

Figure C-5: Effect of V6 on a) LDH release b) effect on IL-6 release, where control represents vehicle only (DMSO treated MRC-5 cells) at (CPD36-39). All the experiments were carried out for n = 3 different biological experiments and error bar represents ±standard deviation. Statistical significance was analysed by using one way ANOVA followed by Dunnett's multiple comparison test: (*) $p<0.05$, (**) $p<0.01$, (***) $p<0.001$, versus control which represents vehicle only. Red line represents the changes observed when treated with various concentration of V6.

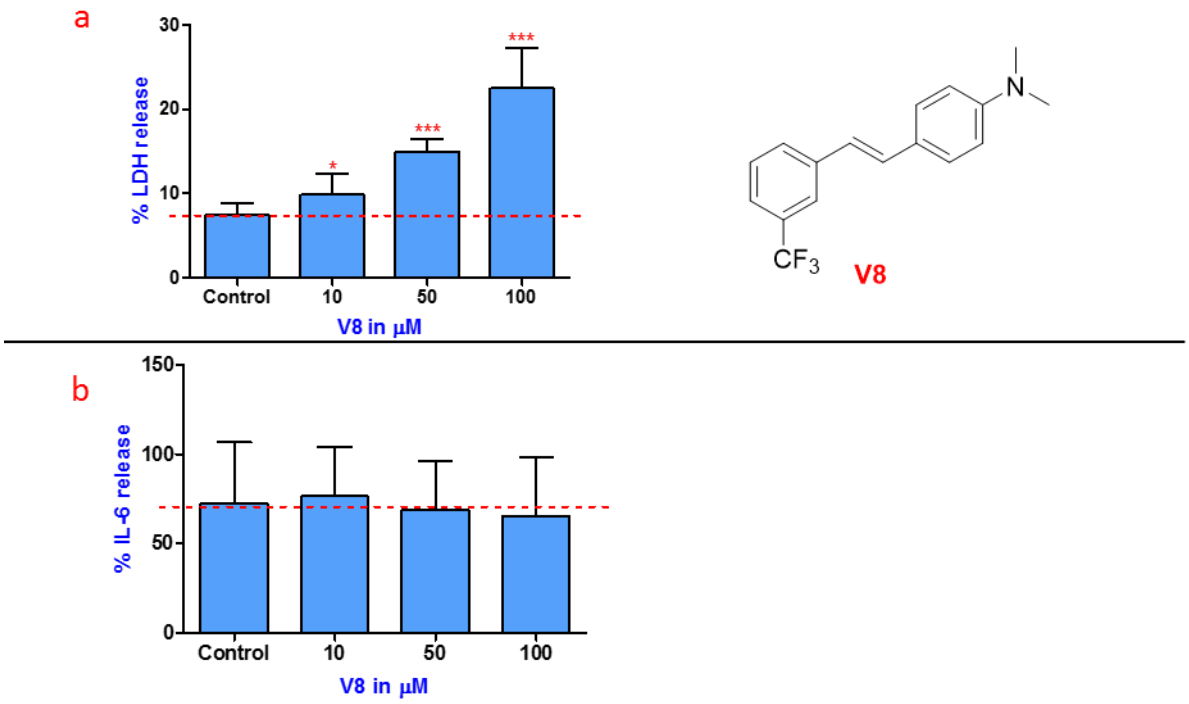

Figure C-6: Effect of V8 on a) LDH release b) effect on IL-6 release, where control represents vehicle only (DMSO treated MRC-5 cells) at (CPD36-39). All the experiments were carried out for n = 3 different biological experiments and error bar represents ±standard deviation. Statistical significance was analysed by using one way ANOVA followed by Dunnett's multiple comparison test: (*) $p<0.05$, (**) $p<0.01$, (***) $p<0.001$, versus control which represents vehicle only. Red line represents the changes observed when treated with various concentration of V8.

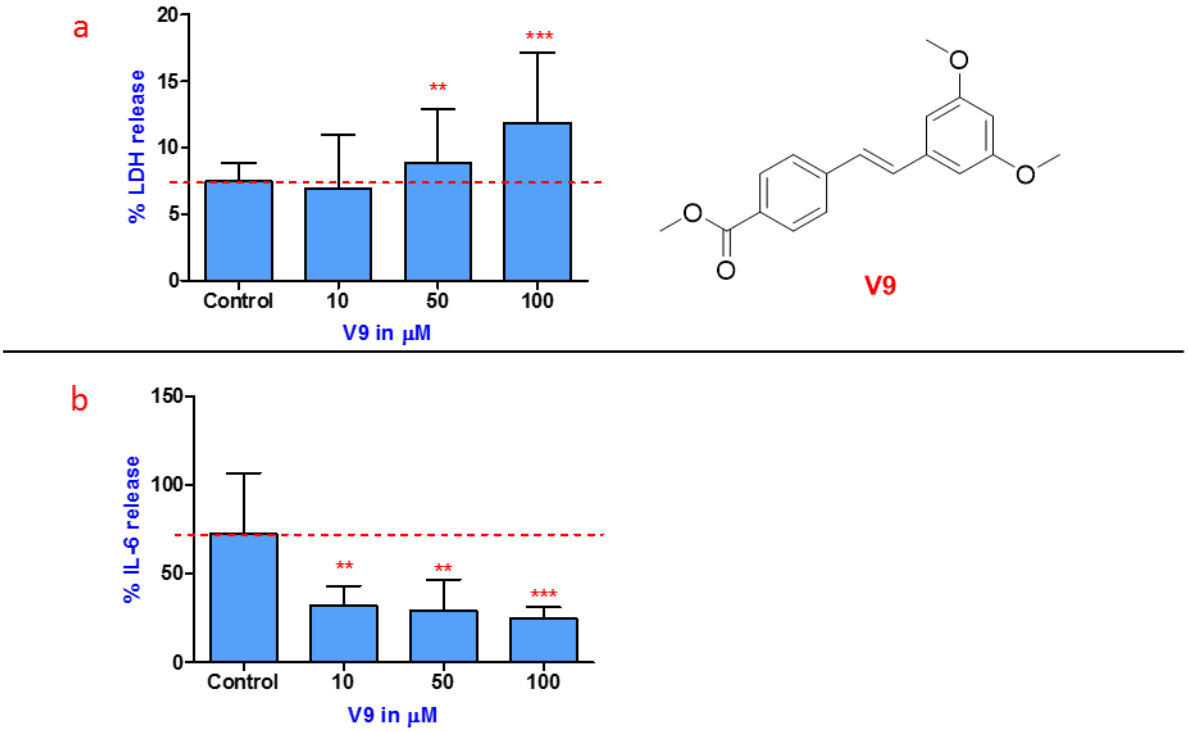

Figure C-7: Effect of V9 on a) LDH release b) effect on IL-6 release, where control represents vehicle only (DMSO treated MRC-5 cells) at (CPD36-39). All the experiments were carried out for n = 3 different biological experiments and error bar represents ±standard deviation. Statistical significance was analysed by using one way ANOVA followed by Dunnett's multiple comparison test: (*) $p<0.05$, (**) $p<0.01$, (***) $p<0.001$, versus control which represents vehicle only. Red line represents the changes observed when treated with various concentration of V9.

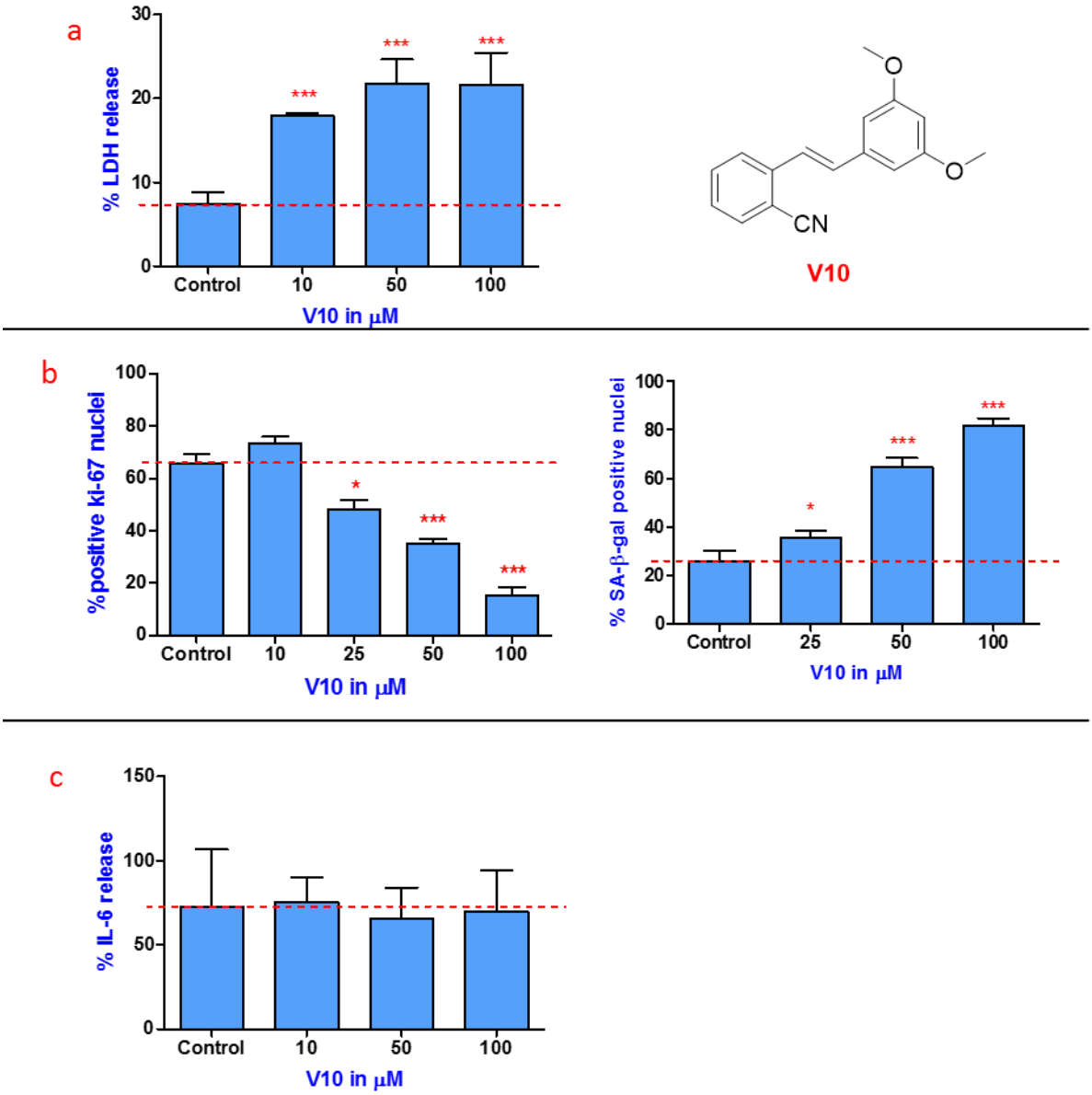

Figure C-8: Effect of V10 on a) LDH release b) proliferation fraction ki-67 and SA-β-galactosidase nuclei and c) effect on IL-6 release, where control represents vehicle only (DMSO treated MRC-5 cells) at (CPD36-39). All the experiments were carried out for n = 3 different biological experiments and error bar represents ±standard deviation. Statistical significance was analysed by using one way ANOVA followed by Dunnett's multiple comparison test: (*) $p<0.05$, (**) $p<0.01$, (***) $p<0.001$, versus control which represents vehicle only. Red line represents the changes observed when treated with various concentration of V10.

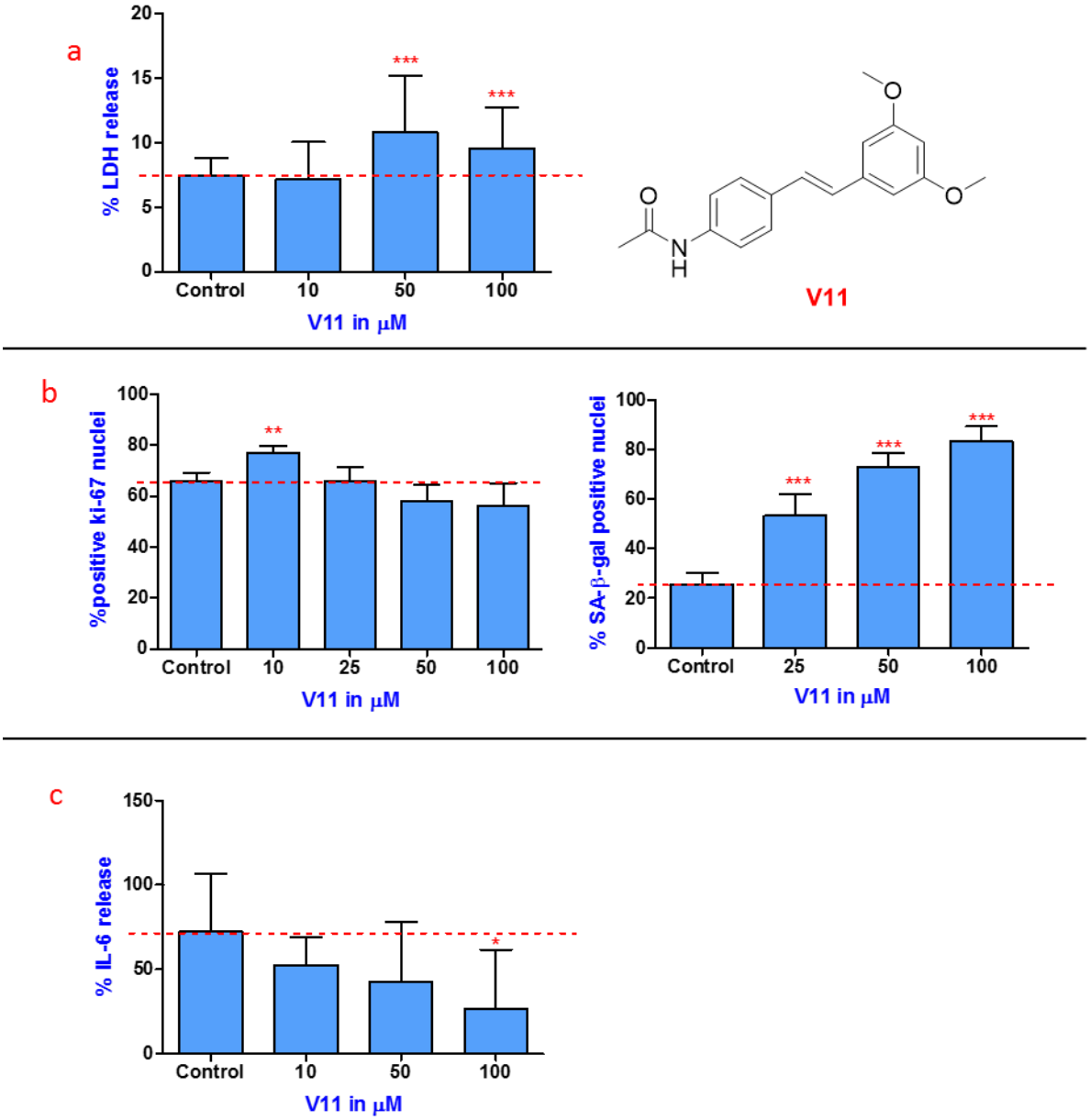

Figure C-9: Effect of V11 on a) LDH release b) proliferation fraction ki-67 and SA-β-galactosidase nuclei and c) effect on IL-6 release, where control represents vehicle only (DMSO treated MRC-5 cells) at (CPD36-39). All the experiments were carried out for n = 3 different biological experiments and error bar represents ±standard deviation. Statistical significance was analysed by using one way ANOVA followed by Dunnett's multiple comparison test: (*) $p<0.05$, (**) $p<0.01$, (***) $p<0.001$, versus control which represents vehicle only. Red line represents the changes observed when treated with various concentration of V11.

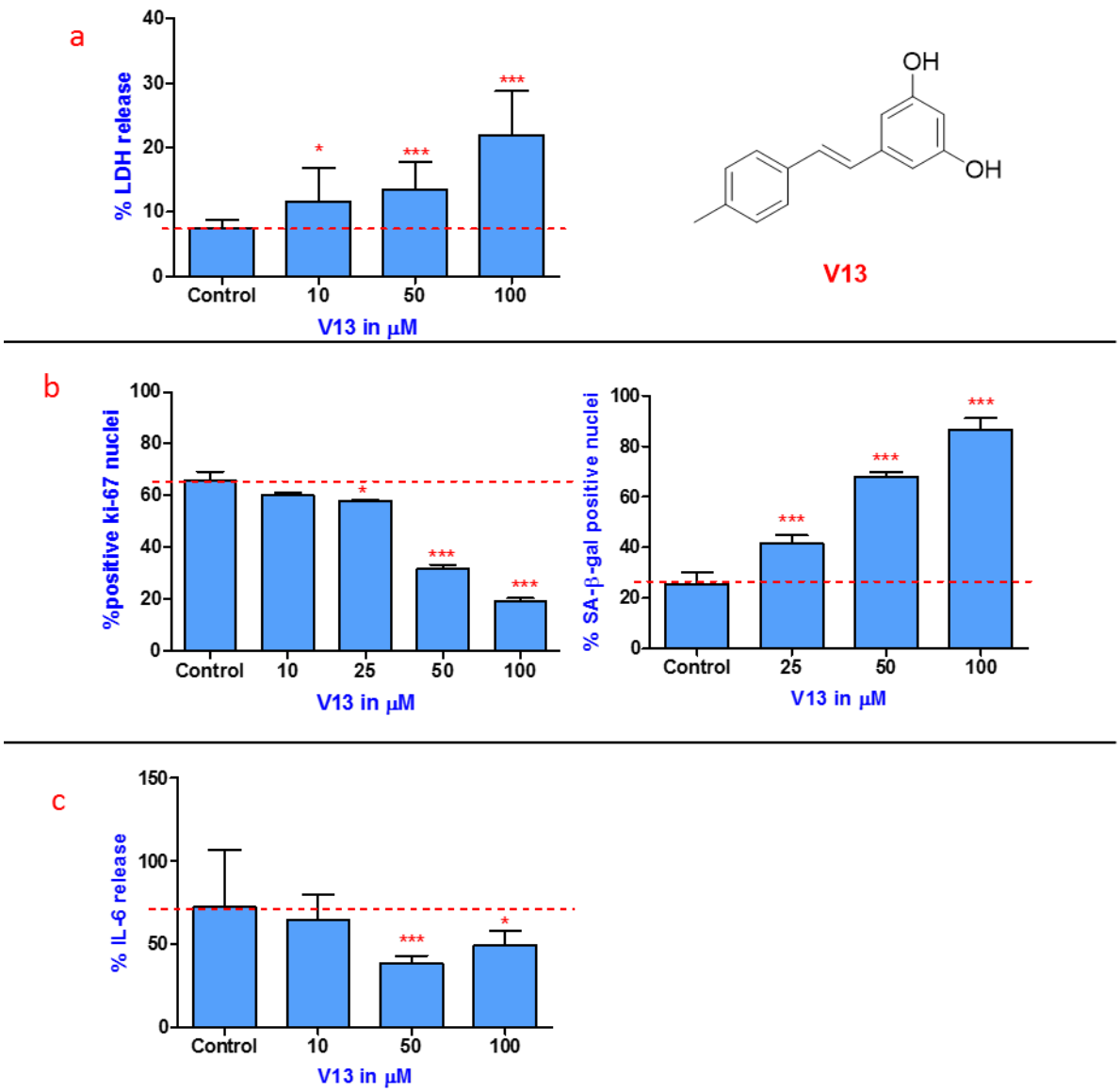

Figure C-10: Effect of V13 on a) LDH release b) proliferation fraction ki-67 and SA-β-galactosidase nuclei and c) effect on IL-6 release, where control represents vehicle only (DMSO treated MRC-5 cells) at (CPD36-39). All the experiments were carried out for n = 3 different biological experiments and error bar represents ±standard deviation. Statistical significance was analysed by using one way ANOVA followed by Dunnett's multiple comparison test: (*) $p<0.05$, (**) $p<0.01$, (***) $p<0.001$, versus control which represents vehicle only. Red line represents the changes observed when treated with various concentration of V13.

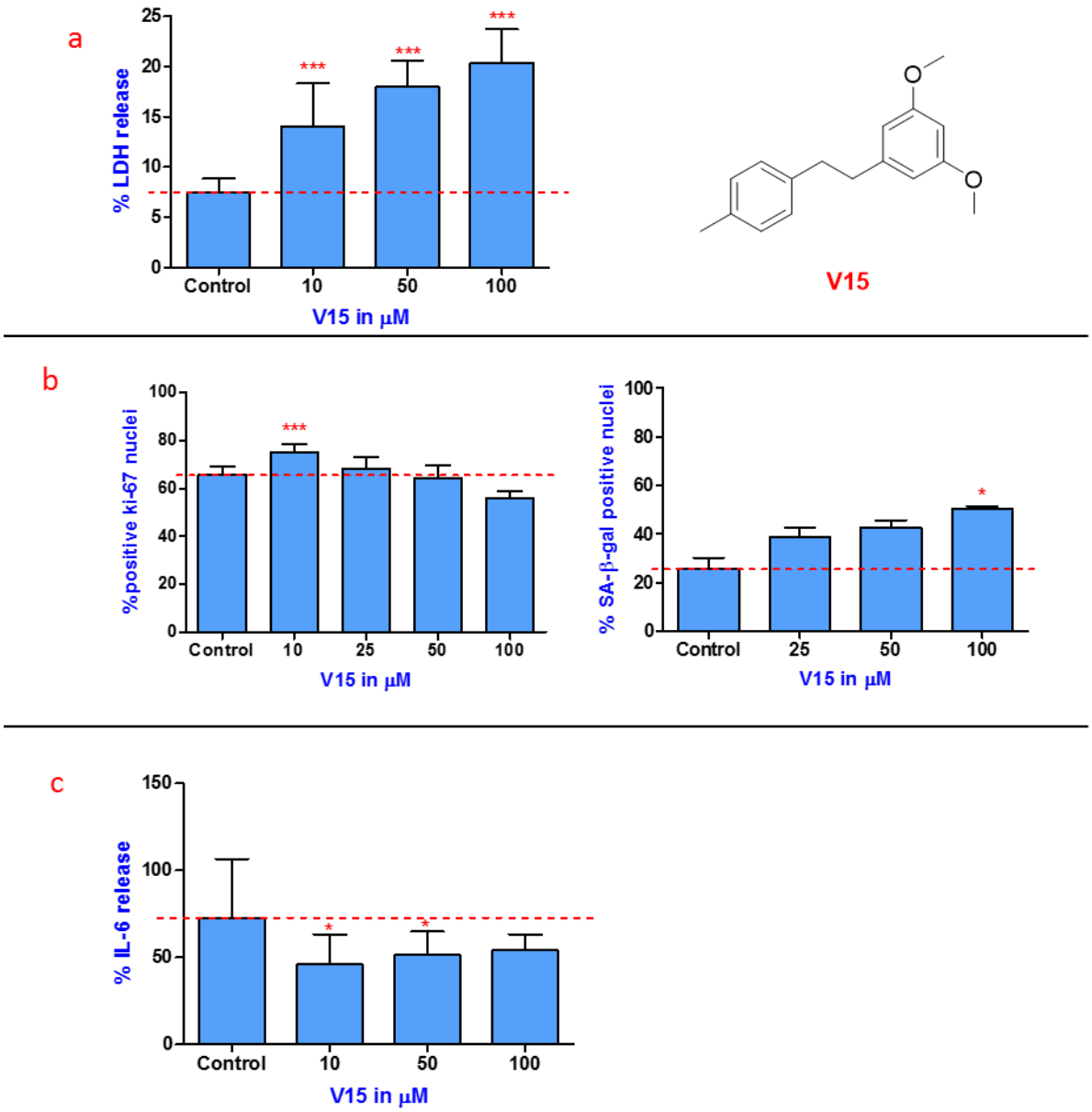

Figure C-11: Effect of V15 on a) LDH release b) proliferation fraction ki-67 and SA-β-galactosidase nuclei and c) effect on IL-6 release, where control represents vehicle only (DMSO treated MRC-5 cells) at (CPD36-39). All the experiments were carried out for n = 3 different biological experiments and error bar represents ±standard deviation. Statistical significance was analysed by using one way ANOVA followed by Dunnett's multiple comparison test: (*) $p<0.05$, (**) $p<0.01$, (***) $p<0.001$, versus control which represents vehicle only. Red line represents the changes observed when treated with various concentration of V15.

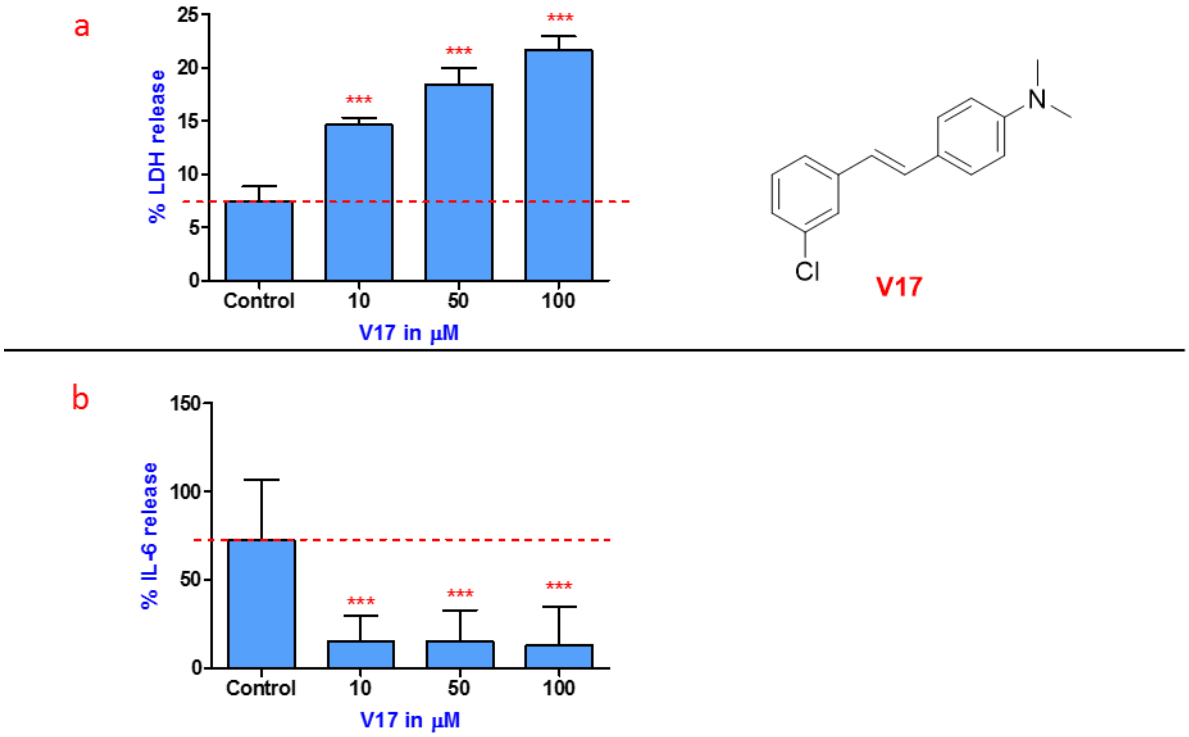

Figure C-12: Effect of V17 on a) LDH release b) effect on IL-6 release, where control represents vehicle only (DMSO treated MRC-5 cells) at (CPD36-39). All the experiments were carried out for n = 3 different biological experiments and error bar represents ±standard deviation. Statistical significance was analysed by using one way ANOVA followed by Dunnett's multiple comparison test: (*) $p<0.05$, (**) $p<0.01$, (***) $p<0.001$, versus control which represents vehicle only. Red line represents the changes observed when treated with various concentration of V17.

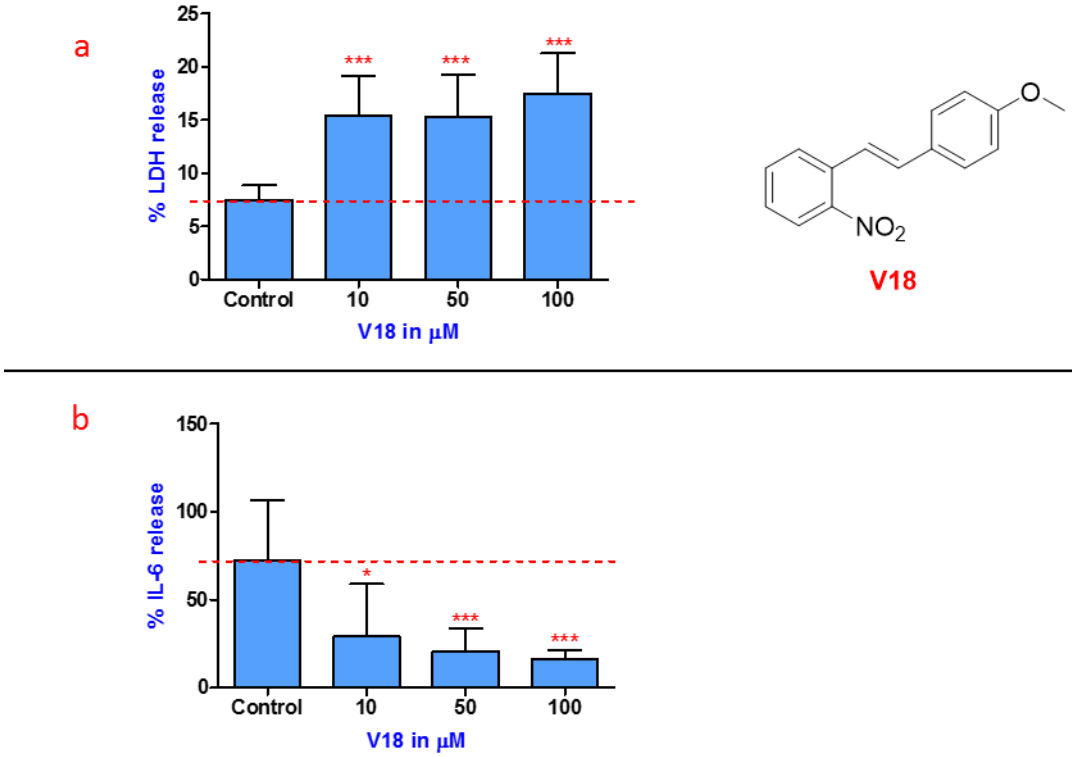

Figure C-13: Effect of V18 on a) LDH release b) effect on IL-6 release, where control represents vehicle only (DMSO treated MRC-5 cells) at (CPD36-39). All the experiments were carried out for n = 3 different biological experiments and error bar represents ±standard deviation. Statistical significance was analysed by using one way ANOVA followed by Dunnett's multiple comparison test: (*) $p<0.05$, (**) $p<0.01$, (***) $p<0.001$, versus control which represents vehicle only. Red line represents the changes observed when treated with various concentration of V18.

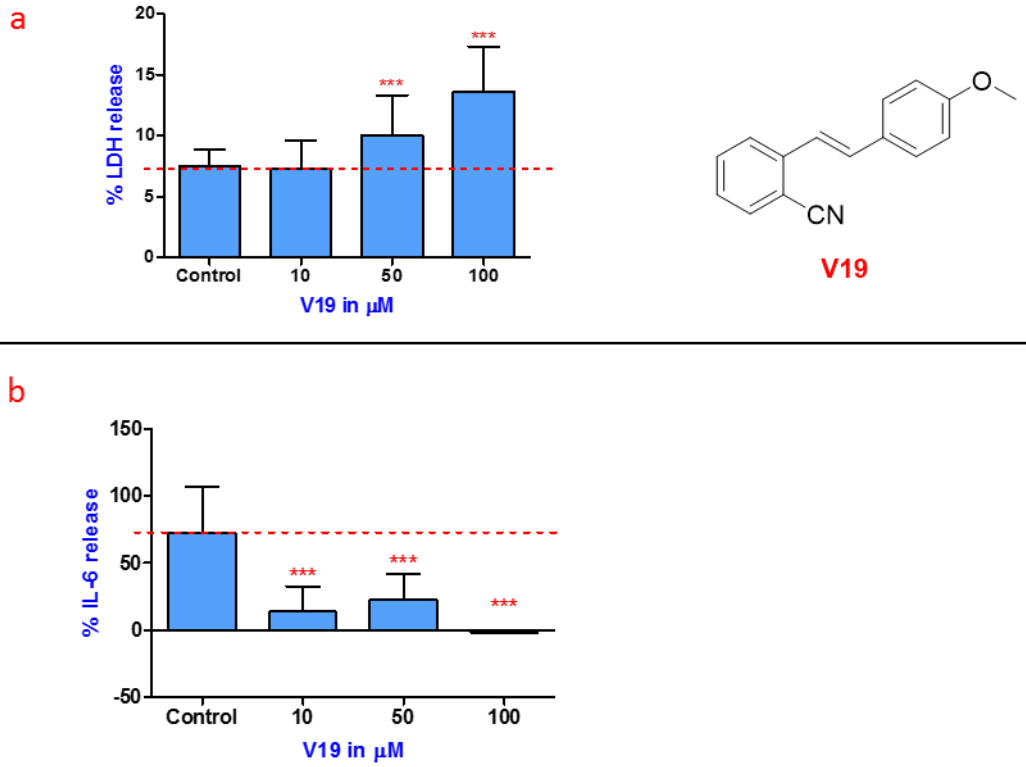

Figure C-14: Effect of V19 on a) LDH release b) effect on IL-6 release, where control represents vehicle only (DMSO treated MRC-5 cells) at (CPD36-39). All the experiments were carried out for n = 3 different biological experiments and error bar represents ±standard deviation. Statistical significance was analysed by using one way ANOVA followed by Dunnett's multiple comparison test: (*) $p<0.05$, (**) $p<0.01$, (***) $p<0.001$, versus control which represents vehicle only. Red line represents the changes observed when treated with various concentration of V19.

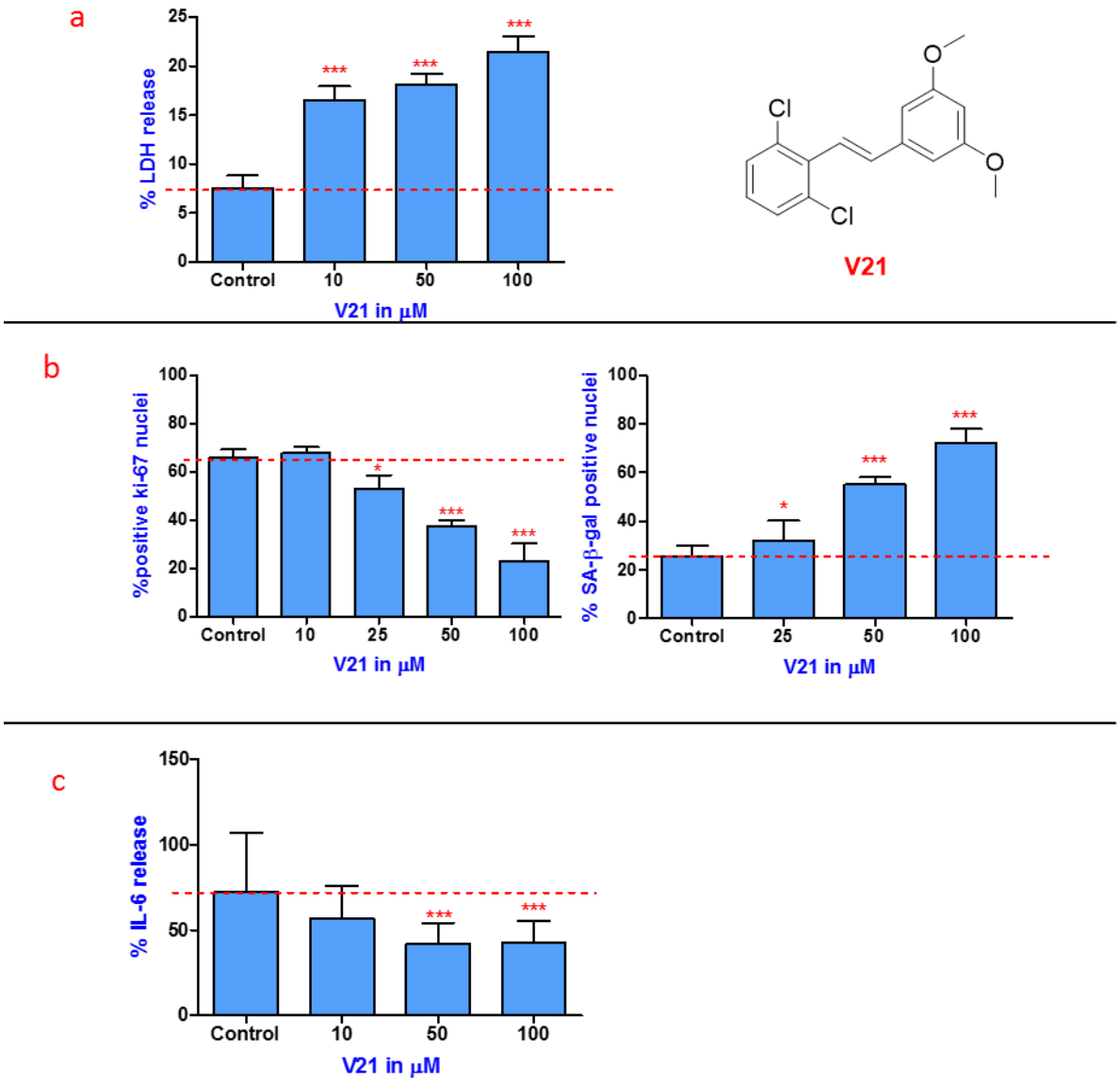

Figure C-15: Effect of V21 on a) LDH release b) proliferation fraction ki-67 and SA-β-galactosidase nuclei and c) effect on IL-6 release, where control represents vehicle only (DMSO treated MRC-5 cells) at (CPD36-39). All the experiments were carried out for n = 3 different biological experiments and error bar represents ±standard deviation. Statistical significance was analysed by using one way ANOVA followed by Dunnett's multiple comparison test: (*) p<0.05, (**) p<0.01, (***) p<0.001, versus control which represents vehicle only. Red line represents the changes observed when treated with various concentration of V21.

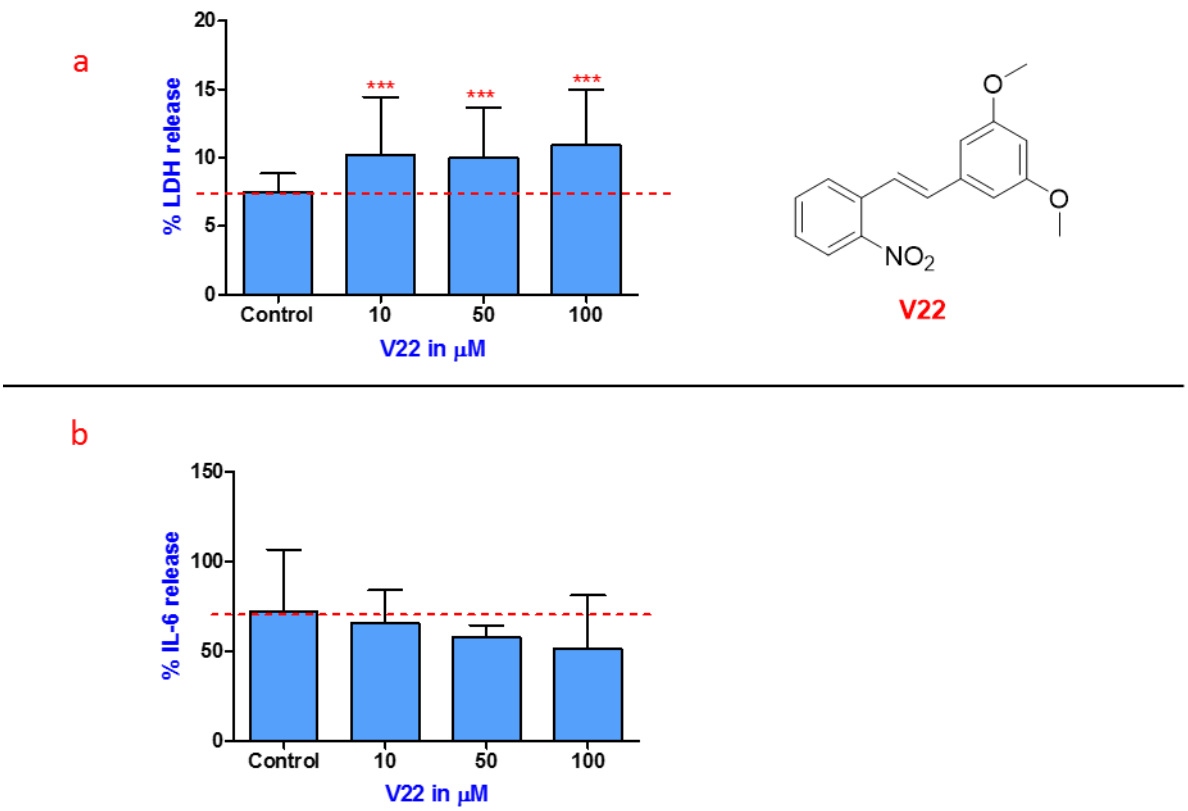

Figure C-16: Effect of V22 on a) LDH release b) effect on IL-6 release, where control represents vehicle only (DMSO treated MRC-5 cells) at (CPD36-39). All the experiments were carried out for n = 3 different biological experiments and error bar represents ±standard deviation. Statistical significance was analysed by using one way ANOVA followed by Dunnett's multiple comparison test: (*) $p<0.05$, (**) $p<0.01$, (***) $p<0.001$, versus control which represents vehicle only. Red line represents the changes observed when treated with various concentration of V22.

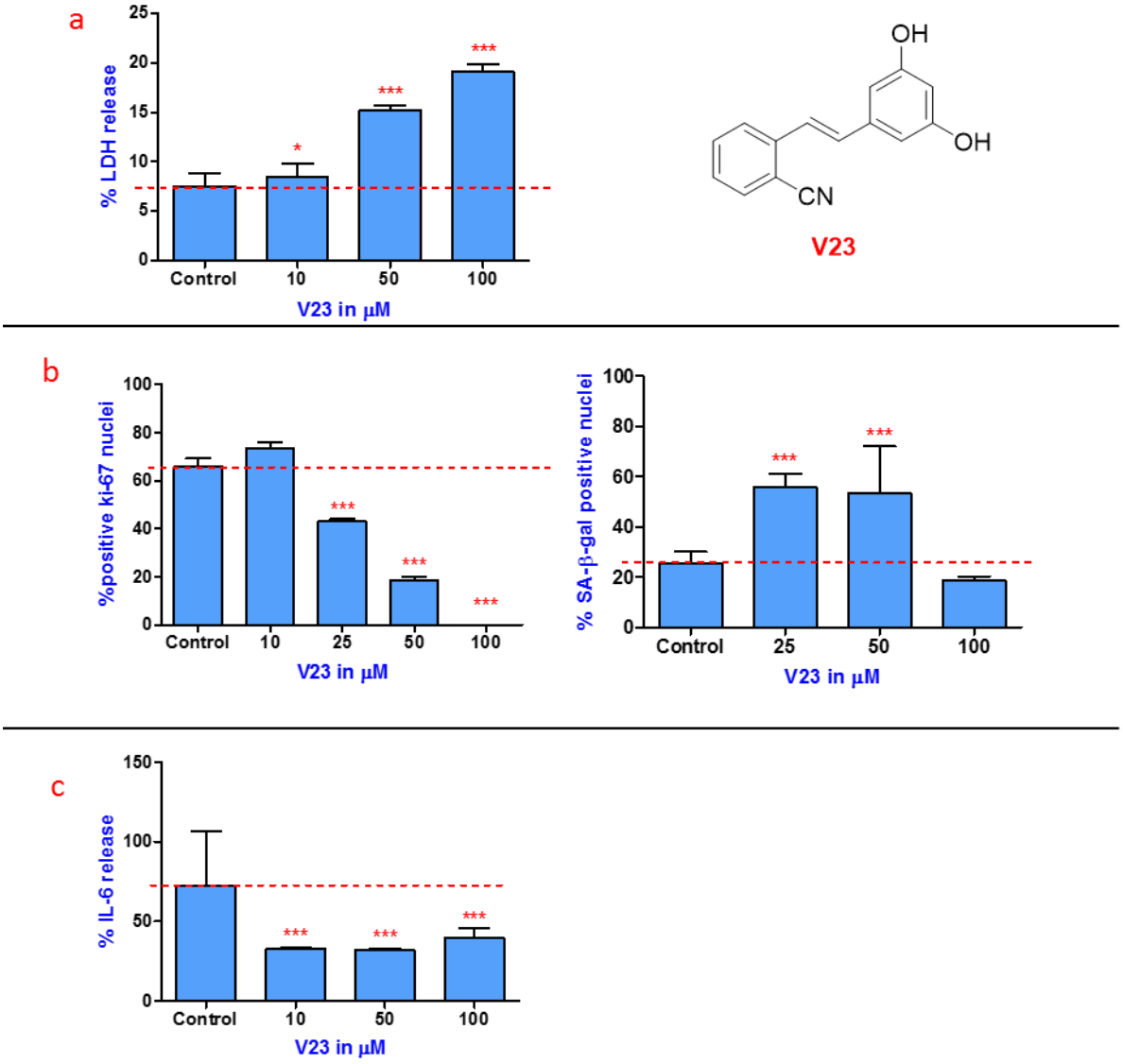

Figure C-17: Effect of V23 on a) LDH release b) proliferation fraction ki-67 and SA-β-galactosidase nuclei and c) effect on IL-6 release, where control represents vehicle only (DMSO treated MRC-5 cells) at (CPD36-39). All the experiments were carried out for n = 3 different biological experiments and error bar represents ±standard deviation. Statistical significance was analysed by using one way ANOVA followed by Dunnett's multiple comparison test: (*) $p<0.05$, (**) $p<0.01$, (***) $p<0.001$, versus control which represents vehicle only. Red line represents the changes observed when treated with various concentration of V23.

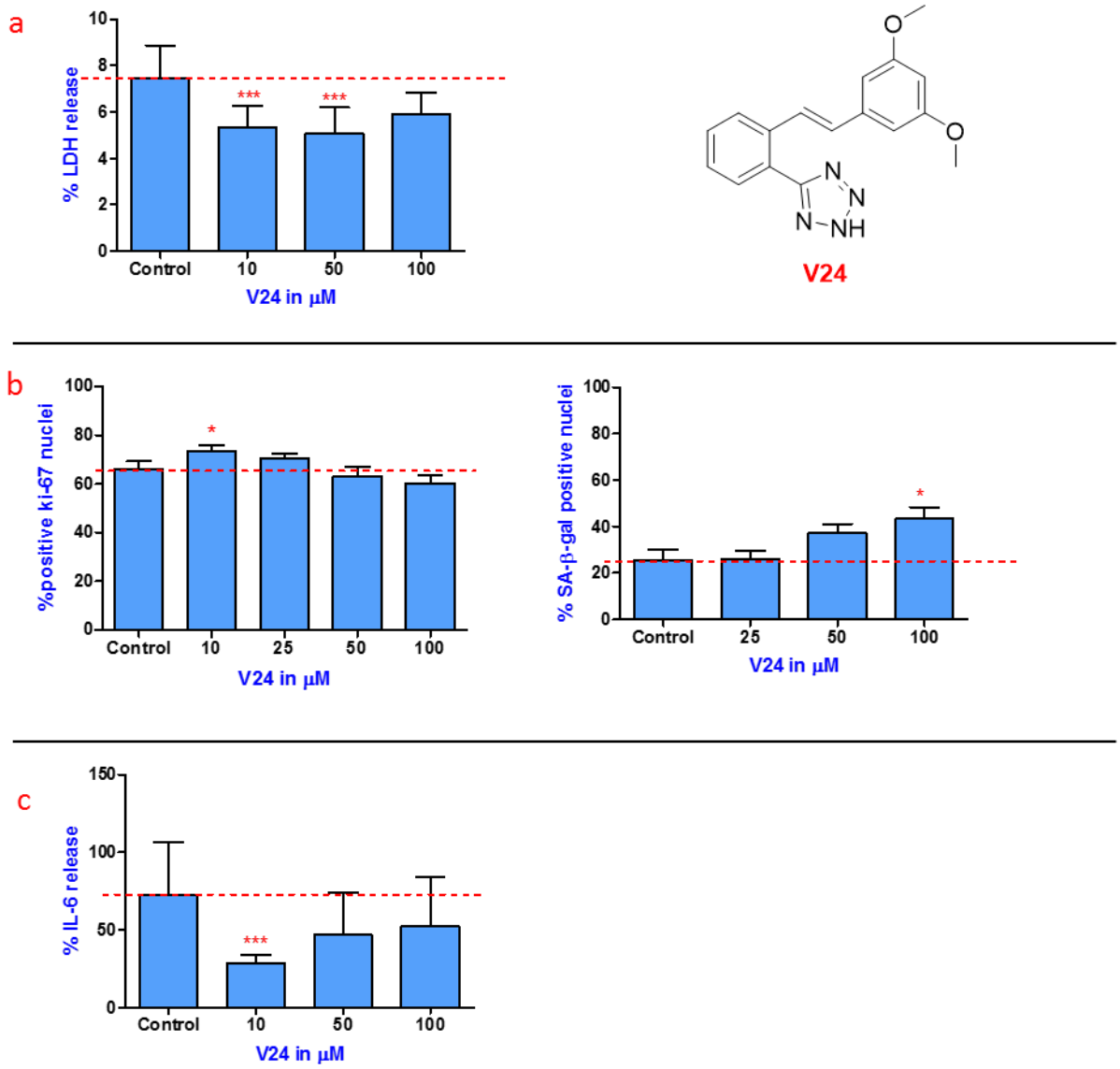

Figure C-18: Effect of V24 on a) LDH release b) proliferation fraction ki-67 and SA-β-galactosidase nuclei and c) effect on IL-6 release, where control represents vehicle only (DMSO treated MRC-5 cells) at (CPD36-39). All the experiments were carried out for n = 3 different biological experiments and error bar represents ±standard deviation. Statistical significance was analysed by using one-way ANOVA followed by Dennett's multiple comparison test: (*) $p<0.05$, (**) $p<0.01$, (***) $p<0.001$, versus control which represents vehicle only. Red line represents the changes observed when treated with various concentration of V24.

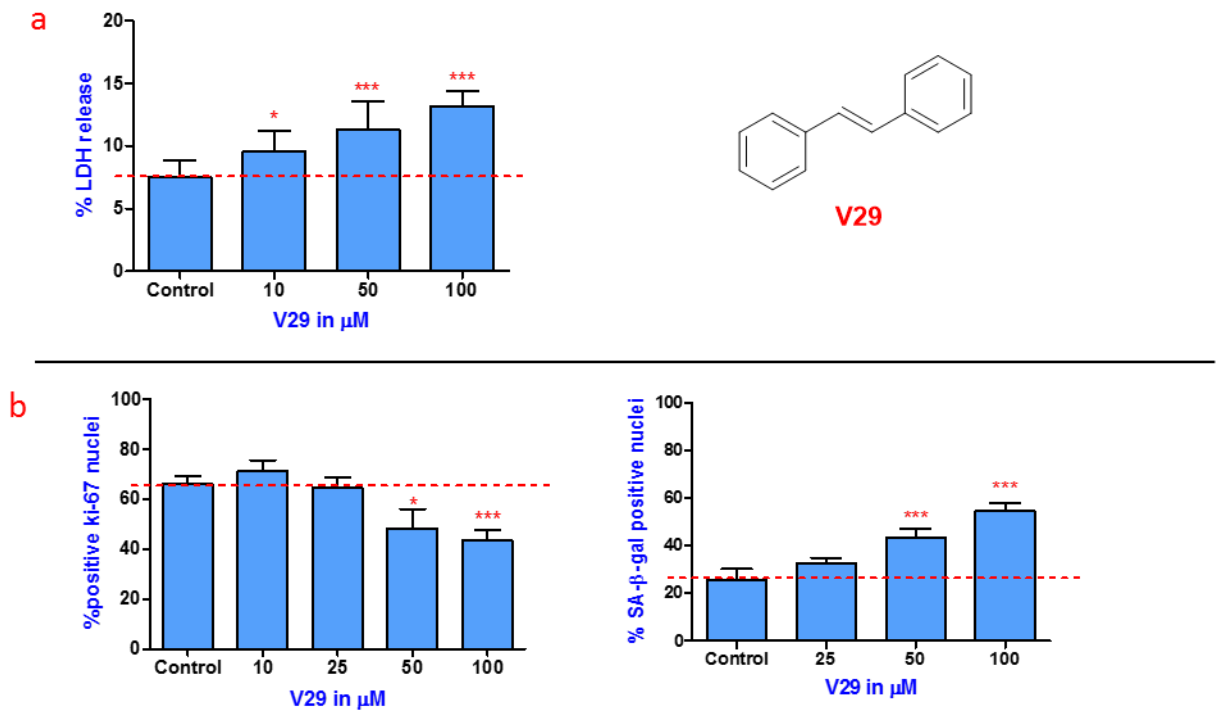

Figure C-19: Effect of V29 on a) LDH release b) proliferation fraction ki-67 and SA-β-galactosidase nuclei, where control represents vehicle only (DMSO treated MRC-5 cells) at (CPD36-39). All the experiments were carried out for n = 3 different biological experiments and error bar represents ±standard deviation. Statistical significance was analysed by using one-way ANOVA followed by Dennett's multiple comparison test: (*) $p<0.05$, (**) $p<0.01$, (***) $p<0.001$, versus control which represents vehicle only. Red line represents the changes observed when treated with various concentration of V29

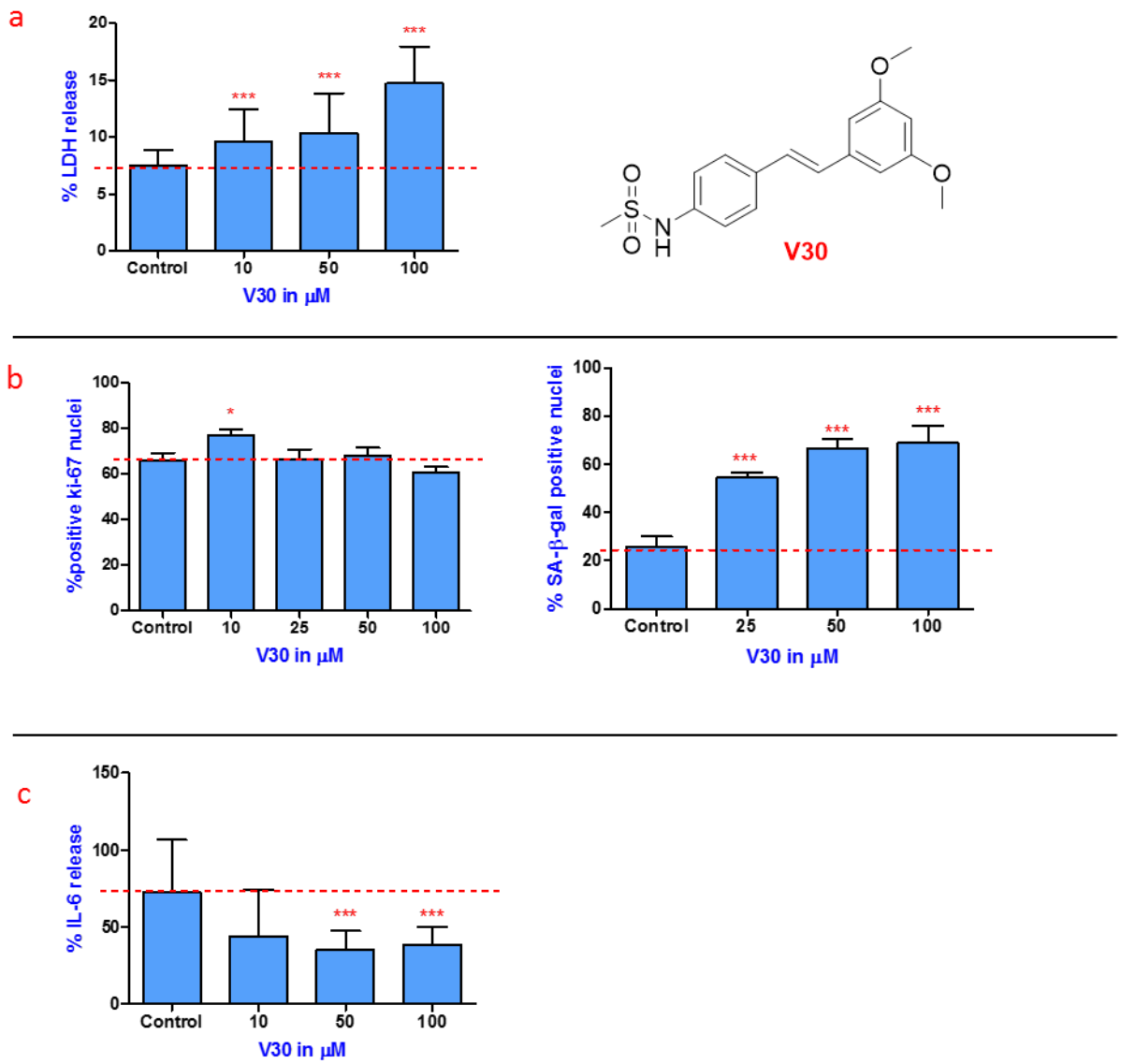

Figure C-20: Effect of V30 on a) LDH release b) proliferation fraction ki-67 and SA-β-galactosidase nuclei and c) effect on IL-6 release, where control represents vehicle only (DMSO treated MRC-5 cells) at (CPD36-39). All the experiments were carried out for n = 3 different biological experiments and error bar represents ±standard deviation. Statistical significance was analysed by using one-way ANOVA followed by Dennett's multiple comparison test: (*) $p<0.05$, (**) $p<0.01$, (***) $p<0.001$, versus control which represents vehicle only. Red line represents the changes observed when treated with various concentration of V30.

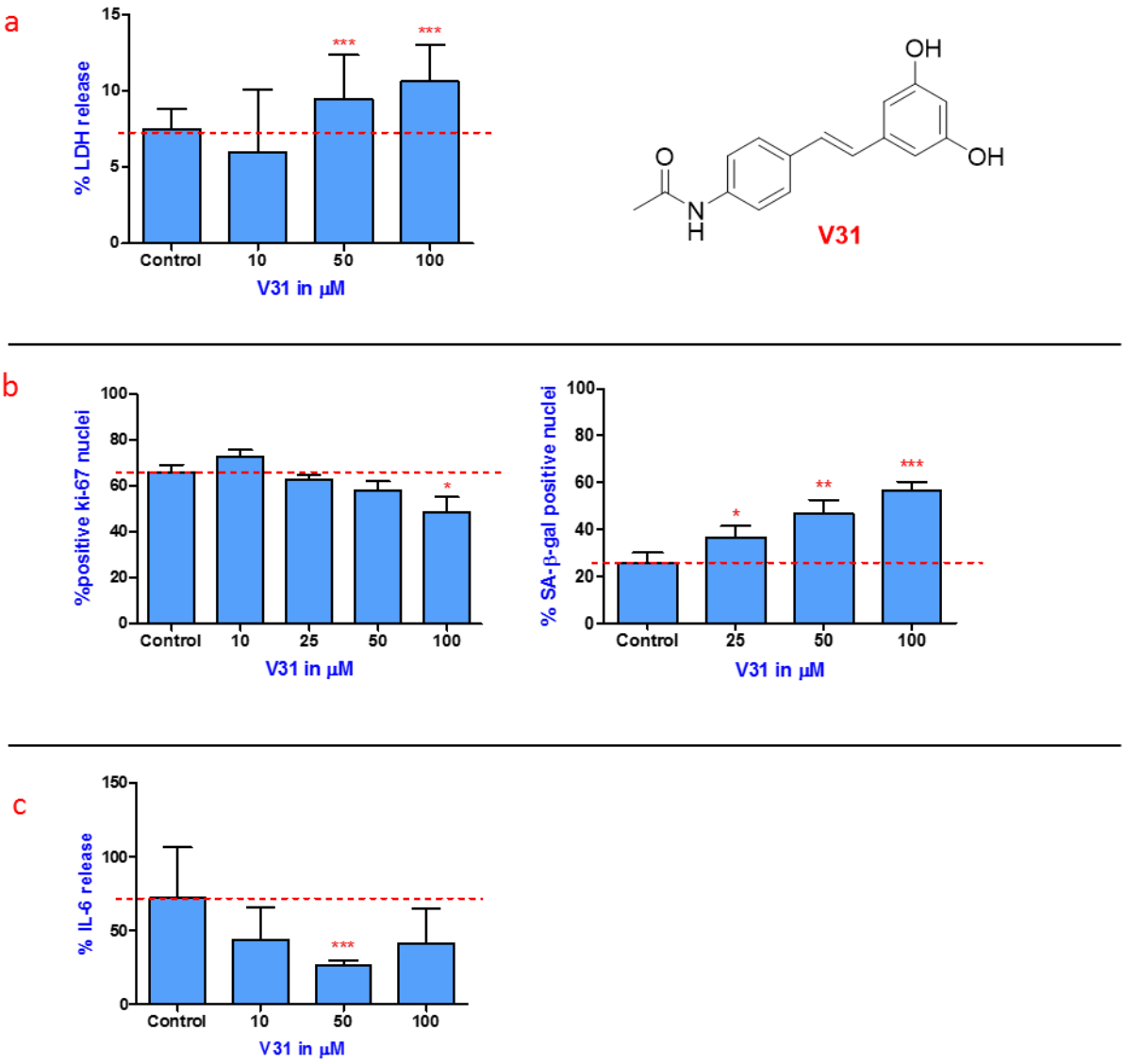

Figure C-21: Effect of V31 on a) LDH release b) proliferation fraction ki-67 and SA-β-galactosidase nuclei and c) effect on IL-6 release, where control represents vehicle only (DMSO treated MRC-5 cells) at (CPD36-39). All the experiments were carried out for n = 3 different biological experiments and error bar represents ±standard deviation. Statistical significance was analysed by using one-way ANOVA followed by Dennett's multiple comparison test: (*) $p<0.05$, (**) $p<0.01$, (***) $p<0.001$, versus control which represents vehicle only. Red line represents the changes observed when treated with various concentration of V31.

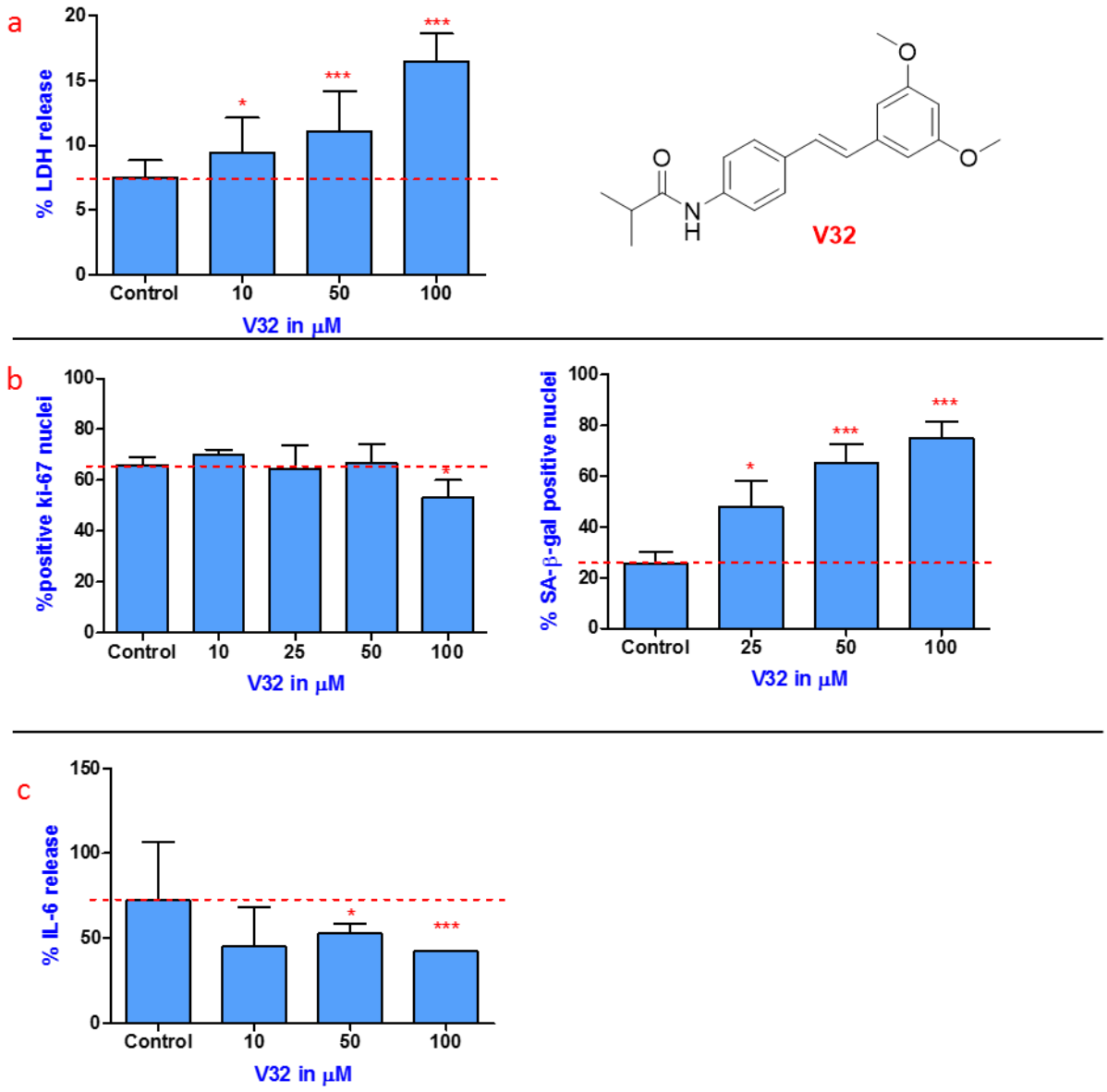

Figure C-22: Effect of V32 on a) LDH release b) proliferation fraction ki-67 and SA-β-galactosidase nuclei and c) effect on IL-6 release, where control represents vehicle only (DMSO treated MRC-5 cells) at (CPD36-39). All the experiments were carried out for n = 3 different biological experiments and error bar represents ±standard deviation. Statistical significance was analysed by using one-way ANOVA followed by Dennett's multiple comparison test: (*) $p<0.05$, (**) $p<0.01$, (***) $p<0.001$, versus control which represents vehicle only. Red line represents the changes observed when treated with various concentration of V32.

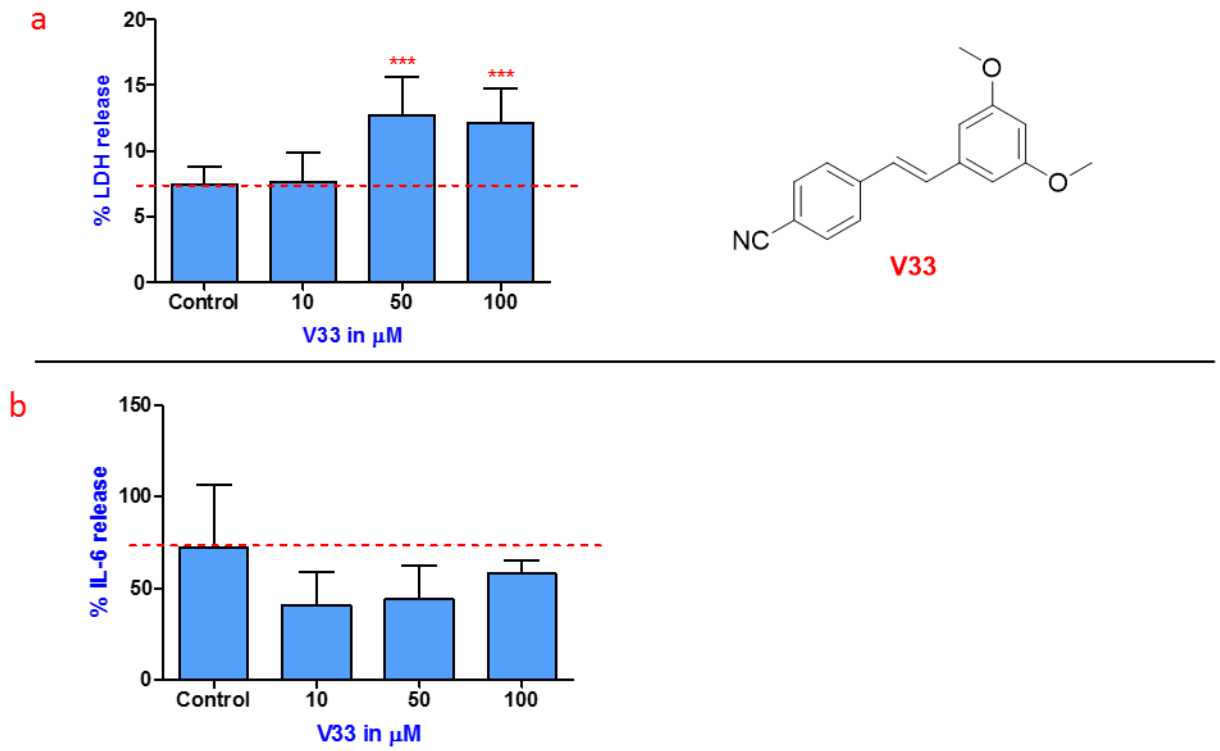

Figure C-23: Effect of V33 on a) LDH release b) effect on IL-6 release, where control represents vehicle only (DMSO treated MRC-5 cells) at (CPD36-39). All the experiments were carried out for n = 3 different biological experiments and error bar represents ±standard deviation. Statistical significance was analysed by using one-way ANOVA followed by Dennett's multiple comparison test: (*) $p<0.05$, (**) $p<0.01$, (***) $p<0.001$, versus control which represents vehicle only. Red line represents the changes observed when treated with various concentration of V33.

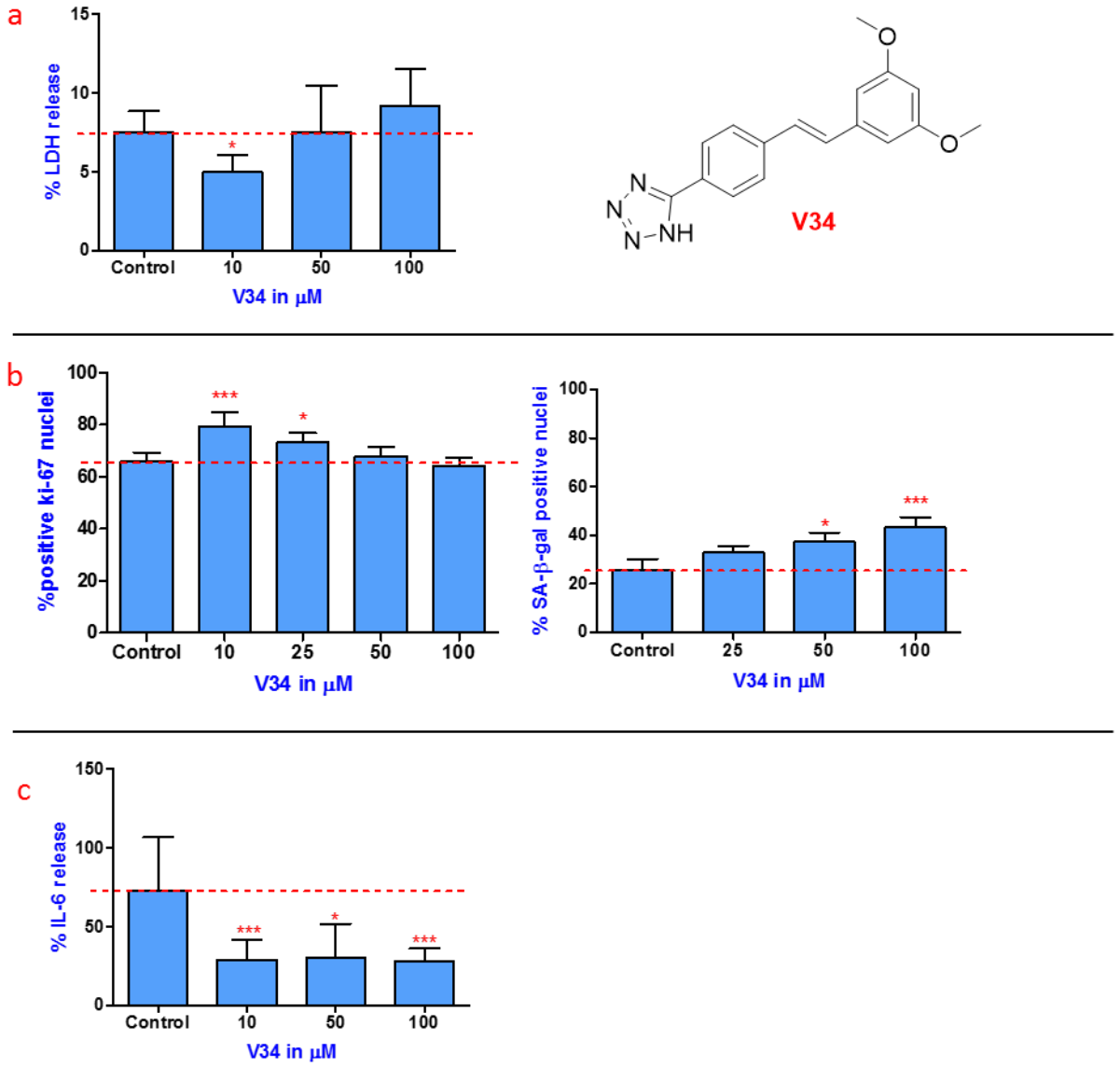

Figure C-24: Effect of V34 on a) LDH release b) proliferation fraction ki-67 and SA-β-galactosidase nuclei and c) effect on IL-6 release, where control represents vehicle only (DMSO treated MRC-5 cells) at (CPD36-39). All the experiments were carried out for n = 3 different biological experiments and error bar represents ±standard deviation. Statistical significance was analysed by using one-way ANOVA followed by Dennett's multiple comparison test: (*) $p<0.05$, (**) $p<0.01$, (***) $p<0.001$, versus control which represents vehicle only. Red line represents the changes observed when treated with various concentration of V34.

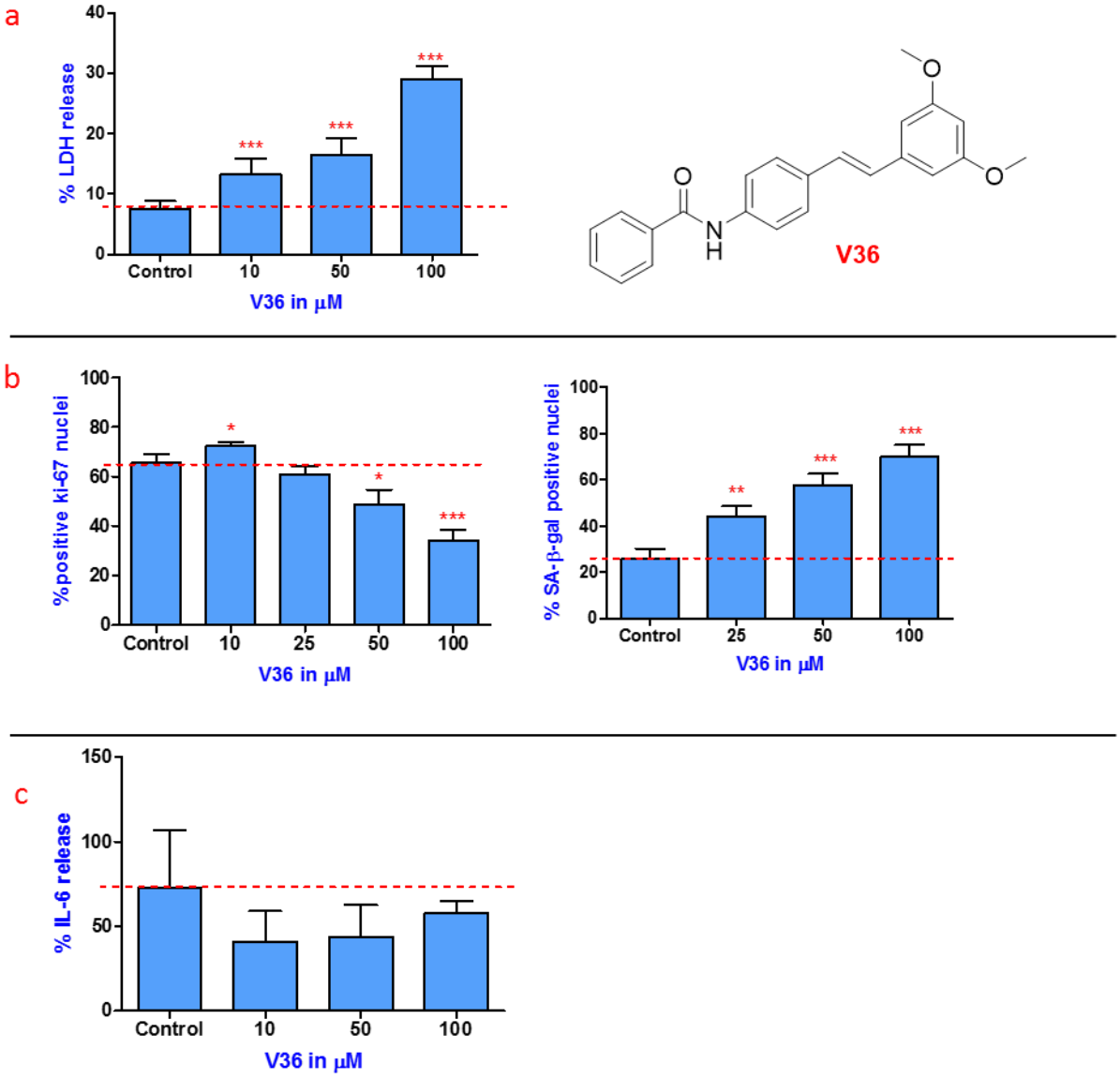

Figure C-25: Effect of V36 on a) LDH release b) proliferation fraction ki-67 and SA-β-galactosidase nuclei and c) effect on IL-6 release, where control represents vehicle only (DMSO treated MRC-5 cells) at (CPD36-39). All the experiments were carried out for n = 3 different biological experiments and error bar represents ±standard deviation. Statistical significance was analysed by using one-way ANOVA followed by Dennett's multiple comparison test: (*) $p<0.05$, (**) $p<0.01$, (***) $p<0.001$, versus control which represents vehicle only. Red line represents the changes observed when treated with various concentration of V36.

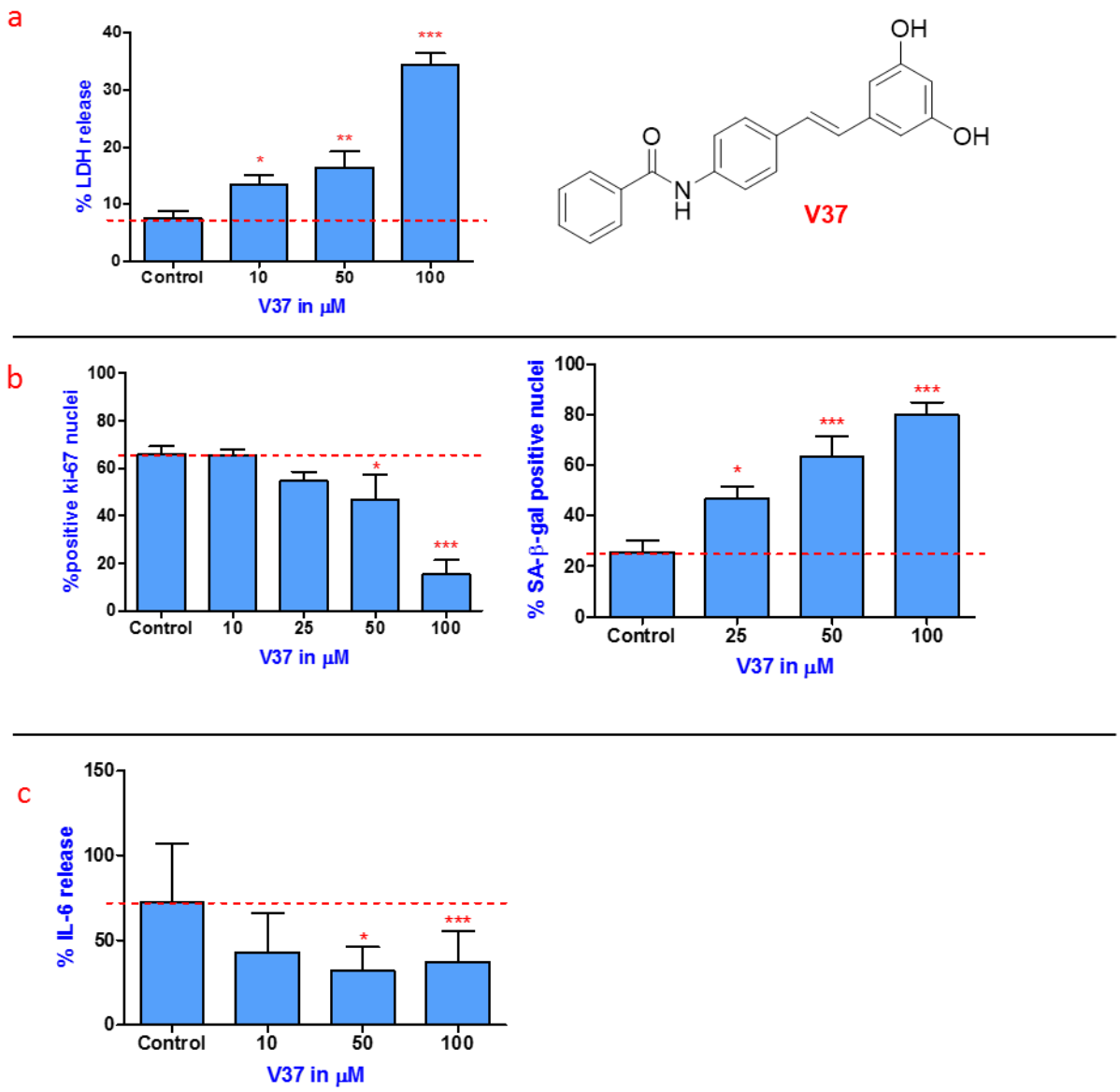

Figure C-26: Effect of V37 on a) LDH release b) proliferation fraction ki-67 and SA-β-galactosidase nuclei and c) effect on IL-6 release, where control represents vehicle only (DMSO treated MRC-5 cells) at (CPD36-39). All the experiments were carried out for n = 3 different biological experiments and error bar represents ±standard deviation. Statistical significance was analysed by using one-way ANOVA followed by Dennett's multiple comparison test: (*) $p<0.05$, (**) $p<0.01$, (***) $p<0.001$, versus control which represents vehicle only. Red line represents the changes observed when treated with various concentration of V37.

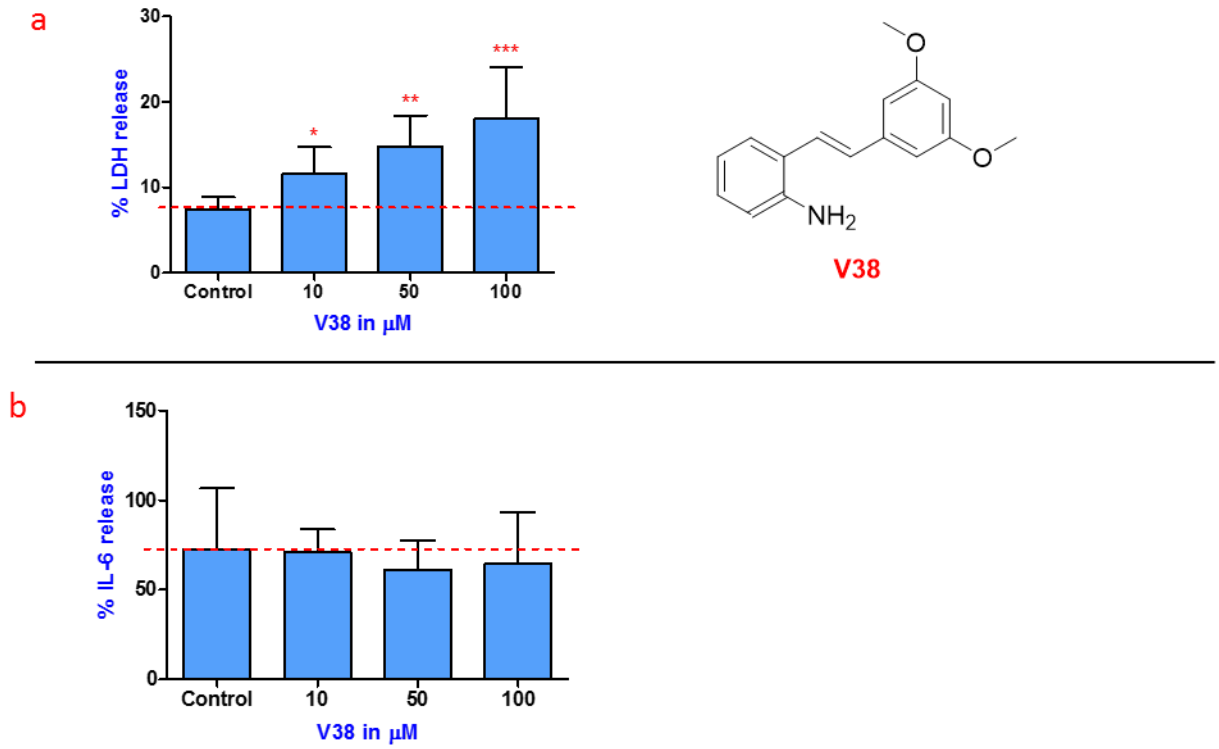

Figure C-27: Effect of V38 on a) LDH release b) effect on IL-6 release, where control represents vehicle only (DMSO treated MRC-5 cells) at (CPD36-39). All the experiments were carried out for n = 3 different biological experiments and error bar represents ±standard deviation. Statistical significance was analysed by using one-way ANOVA followed by Dennett's multiple comparison test: (*) $p<0.05$, (**) $p<0.01$, (***) $p<0.001$, versus control which represents vehicle only. Red line represents the changes observed when treated with various concentration of V38.

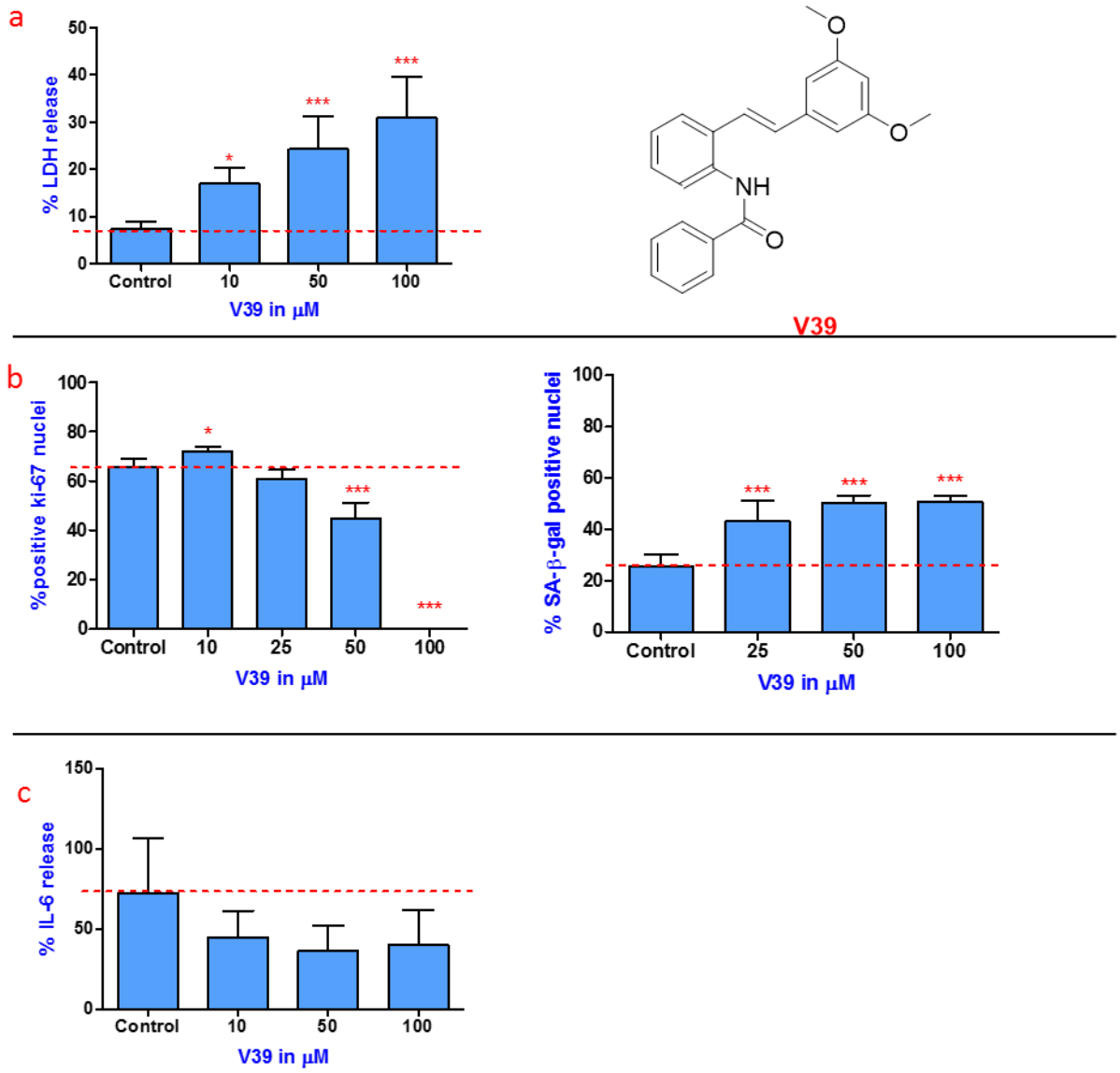

Figure C-28: Effect of V39 on a) LDH release b) proliferation fraction ki-67 and SA-β-galactosidase nuclei and c) effect on IL-6 release, where control represents vehicle only (DMSO treated MRC-5 cells) at (CPD36-39). All the experiments were carried out for n = 3 different biological experiments and error bar represents ±standard deviation. Statistical significance was analysed by using one-way ANOVA followed by Dennett's multiple comparison test: (*) $p<0.05$, (**) $p<0.01$, (***) $p<0.001$, versus control which represents vehicle only. Red line represents the changes observed when treated with various concentration of V39.

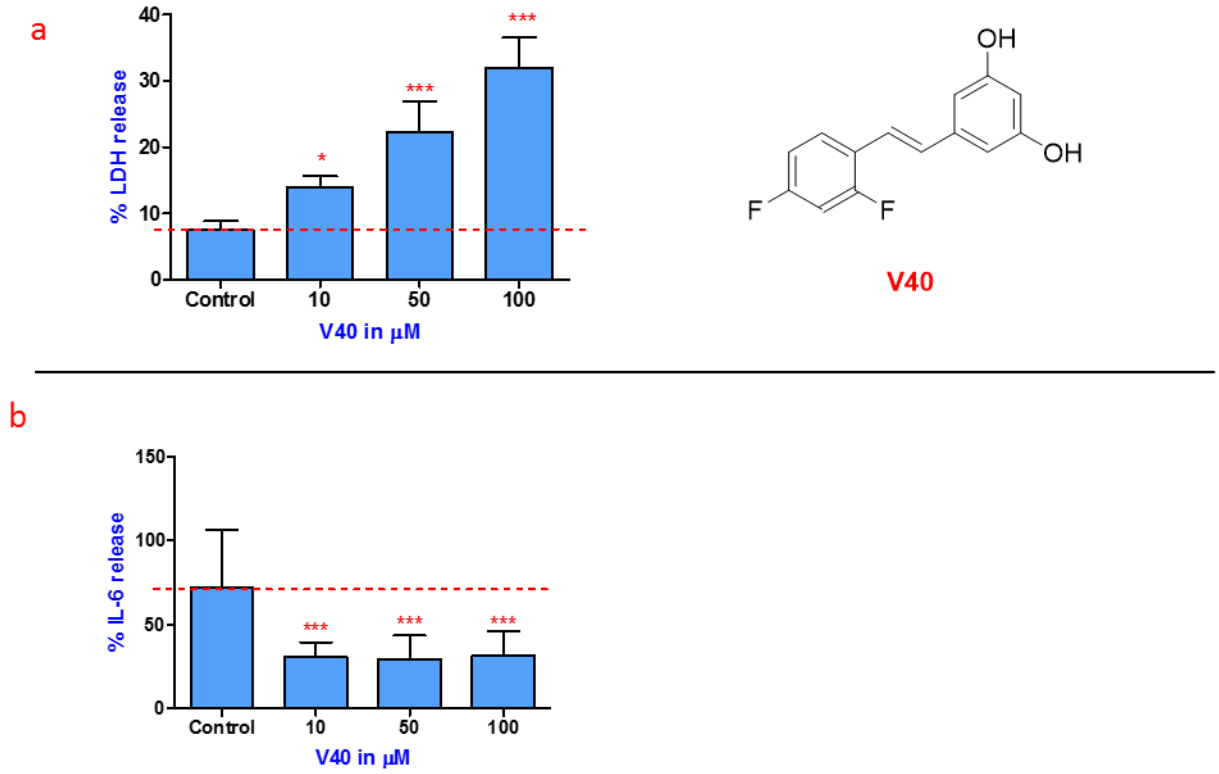

Figure C-29: Effect of V40 on a) LDH release b) effect on IL-6 release, where control represents vehicle only (DMSO treated MRC-5 cells) at (CPD36-39). All the experiments were carried out for n = 3 different biological experiments and error bar represents ±standard deviation. Statistical significance was analysed by using one-way ANOVA followed by Dennett's multiple comparison test: (*) $p<0.05$, (**) $p<0.01$, (***) $p<0.001$, versus control which represents vehicle only. Red line represents the changes observed when treated with various concentration of V40.

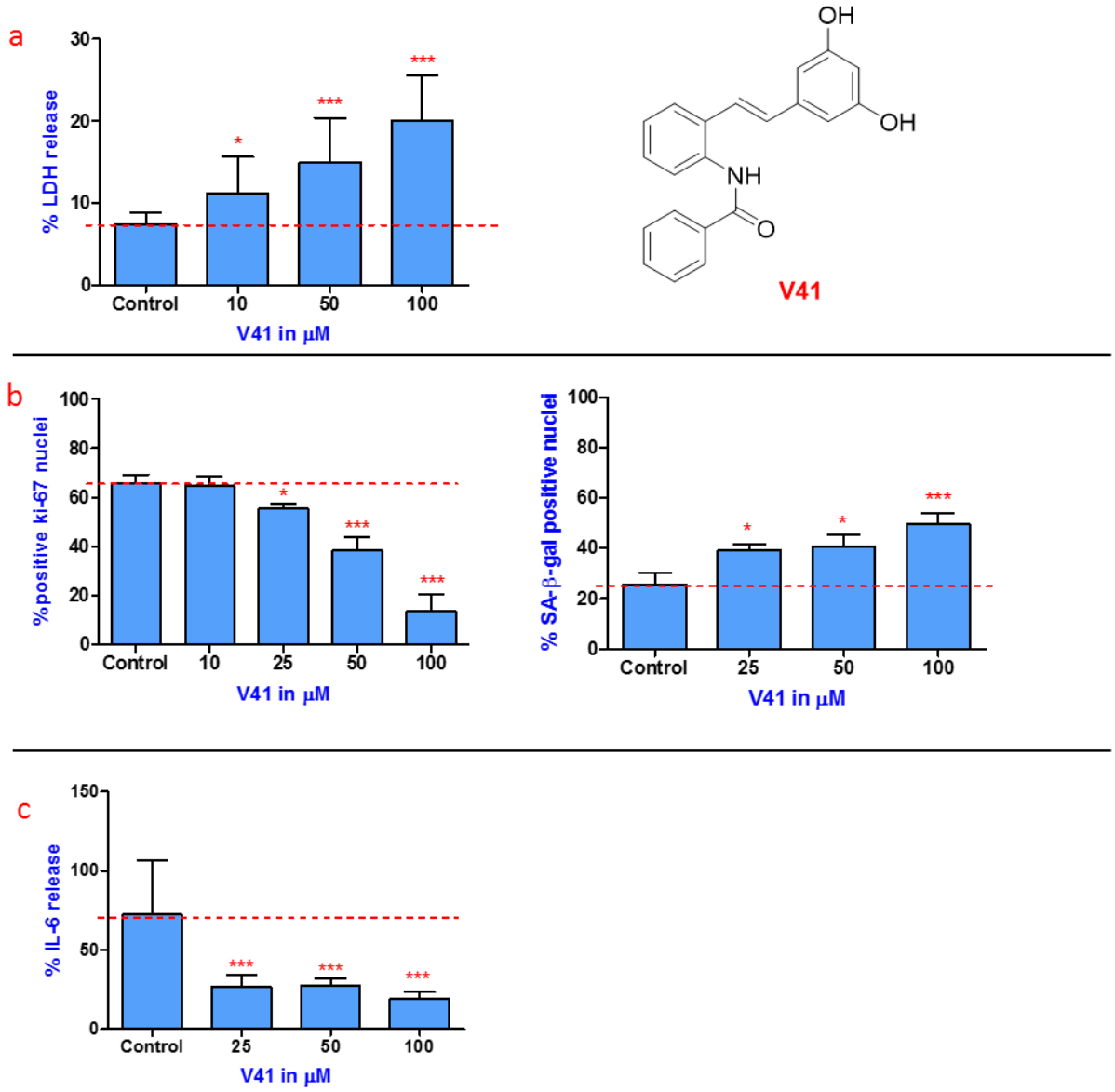

Figure C-30: Effect of V41 on a) LDH release b) proliferation fraction ki-67 and SA-β-galactosidase nuclei and c) effect on IL-6 release, where control represents vehicle only (DMSO treated MRC-5 cells) at (CPD36-39). All the experiments were carried out for n = 3 different biological experiments and error bar represents ±standard deviation. Statistical significance was analysed by using one-way ANOVA followed by Dennett's multiple comparison test: (*) $p<0.05$, (**) $p<0.01$, (***) $p<0.001$, versus control which represents vehicle only. Red line represents the changes observed when treated with various concentration of V41.

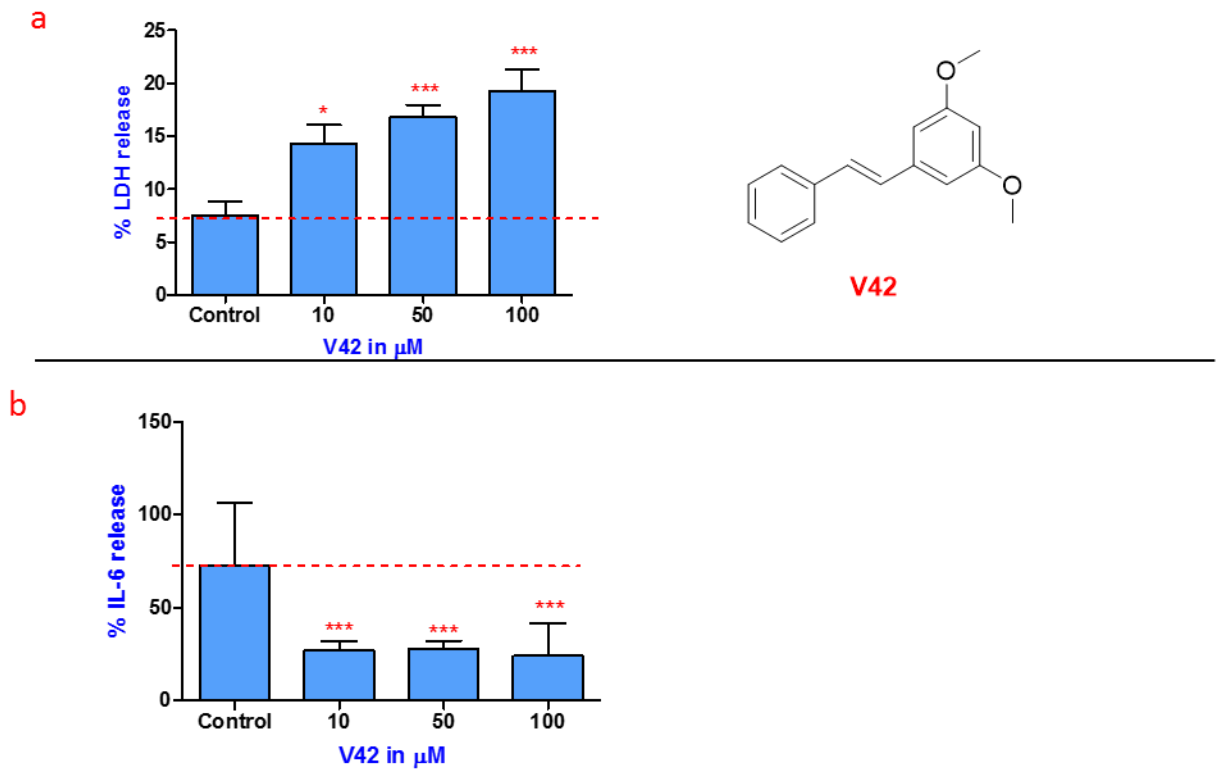

Figure C-31: Effect of V40 on a) LDH release b) effect on IL-6 release, where control represents vehicle only (DMSO treated MRC-5 cells) at (CPD36-39). All the experiments were carried out for n = 3 different biological experiments and error bar represents ±standard deviation. Statistical significance was analysed by using one-way ANOVA followed by Dennett's multiple comparison test: (*) $p<0.05$, (**) $p<0.01$, (***) $p<0.001$, versus control which represents vehicle only. Red line represents the changes observed when treated with various concentration of V31.